# MODELING THE PLANKTON–ENHANCING THE INTEGRATION OF BIOLOGICAL KNOWLEDGE AND MECHANISTIC UNDERSTANDING

**EDITED BY:** Christian Lindemann, Dag L. Aksnes, Kevin J. Flynn and Susanne Menden-Deuer

**PUBLISHED IN:** Frontiers in Marine Science and Frontiers in Ecology and Evolution

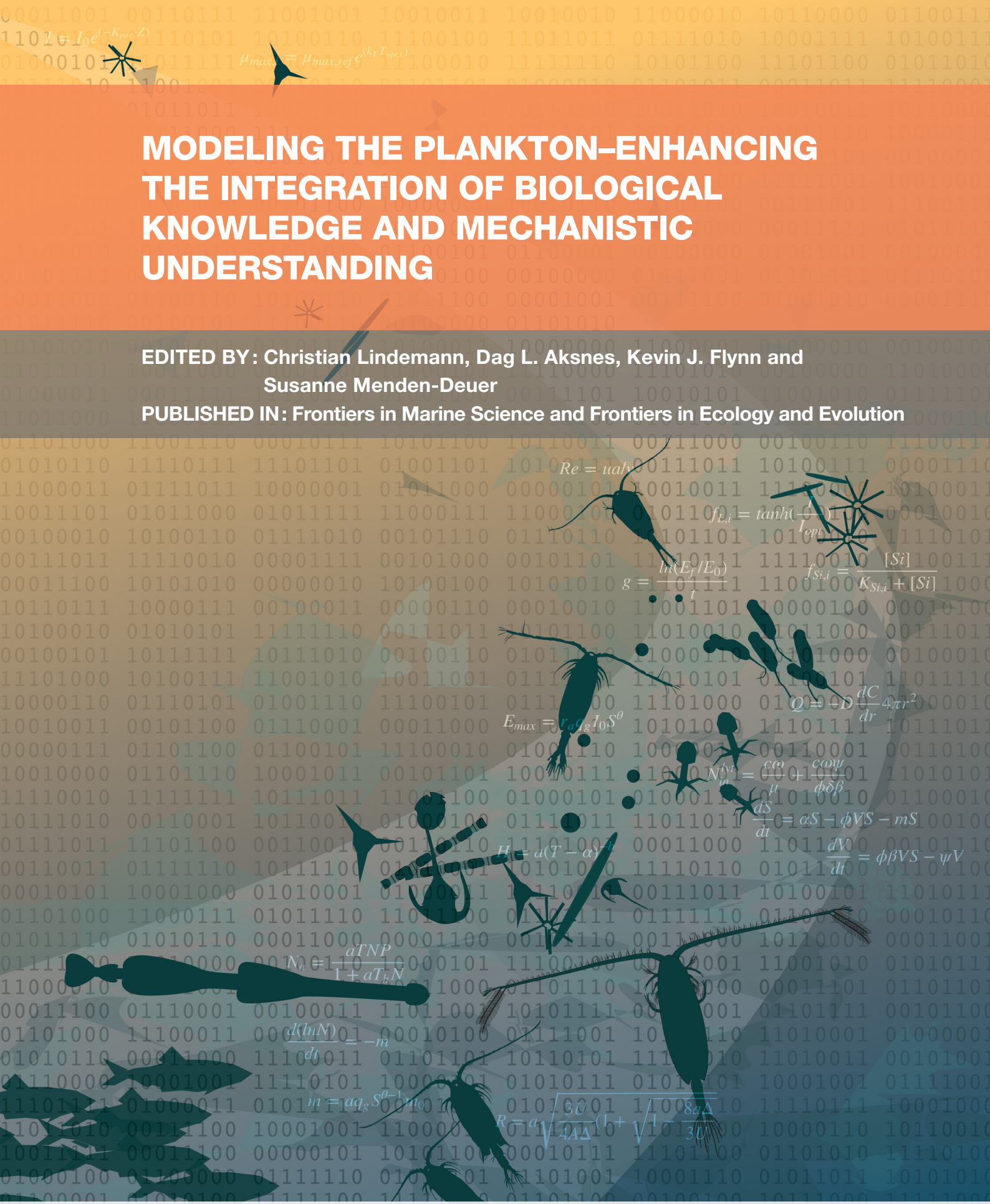


frontiers Research Topics

# frontiers



**ISSN 1664-8714**
**ISBN 978-2-88945-365-8**
**DOI 10.3389/978-2-88945-365-8**

## About Frontiers

Frontiers is more than just an open-access publisher of scholarly articles: it is a pioneering approach to the world of academia, radically improving the way scholarly research is managed. The grand vision of Frontiers is a world where all people have an equal opportunity to seek, share and generate knowledge. Frontiers provides immediate and permanent online open access to all its publications, but this alone is not enough to realize our grand goals.

## Frontiers Journal Series

The Frontiers Journal Series is a multi-tier and interdisciplinary set of open-access, online journals, promising a paradigm shift from the current review, selection and dissemination processes in academic publishing. All Frontiers journals are driven by researchers for researchers; therefore, they constitute a service to the scholarly community. At the same time, the Frontiers Journal Series operates on a revolutionary invention, the tiered publishing system, initially addressing specific communities of scholars, and gradually climbing up to broader public understanding, thus serving the interests of the lay society, too.

## Dedication to Quality

Each Frontiers article is a landmark of the highest quality, thanks to genuinely collaborative interactions between authors and review editors, who include some of the world's best academicians. Research must be certified by peers before entering a stream of knowledge that may eventually reach the public - and shape society; therefore, Frontiers only applies the most rigorous and unbiased reviews.
Frontiers revolutionizes research publishing by freely delivering the most outstanding research, evaluated with no bias from both the academic and social point of view.
By applying the most advanced information technologies, Frontiers is catapulting scholarly publishing into a new generation.

## What are Frontiers Research Topics?

Frontiers Research Topics are very popular trademarks of the Frontiers Journals Series: they are collections of at least ten articles, all centered on a particular subject. With their unique mix of varied contributions from Original Research to Review Articles, Frontiers Research Topics unify the most influential researchers, the latest key findings and historical advances in a hot research area! Find out more on how to host your own Frontiers Research Topic or contribute to one as an author by contacting the Frontiers Editorial Office: **researchtopics@frontiersin.org**

# MODELING THE PLANKTON–ENHANCING THE INTEGRATION OF BIOLOGICAL KNOWLEDGE AND MECHANISTIC UNDERSTANDING

Topic Editors:
**Christian Lindemann,** University of Bergen, Norway
**Dag L. Aksnes,** University of Bergen, Norway
**Kevin J. Flynn,** Swansea University, United Kingdom
**Susanne Menden-Deuer,** University of Rhode Island, United States

'Plankton recoded' by Jan Heuschele

In light of climate change and allied changes to marine ecosystems, mathematical models have become an important tool to examine processes and predict phenomena from local through to global scales. In recent years model studies, laboratory experiments and a better ecological

understanding of the pelagic ecosystem have enabled advancements on fundamental challenges in oceanography, including marine production, biodiversity and anticipation of future conditions in the ocean.

This research topic presents a number of studies that investigate functionally diverse organism in a dynamic ocean through diverse and novel modeling approaches.

**Citation:** Lindemann, C., Aksnes, D. L., Flynn, K. J., Menden-Deuer, S., eds. (2017). Modeling the Plankton–Enhancing the Integration of Biological Knowledge and Mechanistic Understanding. Lausanne: Frontiers Media. doi: 10.3389/978-2-88945-365-8

# Table of Contents

## Resolving trophic details



## From physics to biology

frontiers in Marine Science

EDITORIAL
published: 07 November 2017
doi: 10.3389/fmars.2017.00358

# Editorial: Modeling the Plankton–Enhancing the Integration of Biological Knowledge and Mechanistic Understanding

*Christian Lindemann*[1]*, *Dag L. Aksnes*[1], *Kevin J. Flynn*[2] and *Susanne Menden-Deuer*[3]

[1] Department of Biology, University of Bergen, Bergen, Norway, [2] Department of Biosciences, Swansea University, Swansea, United Kingdom, [3] Graduate School of Oceanography, University of Rhode Island, Narragansett, RI, United States

**Keywords: planktonic food web, ecosystem, biogeochemistry, functional diversity, Climate change simulation**

## Editorial on the Research Topic

## Modeling the Plankton–Enhancing the Integration of Biological Knowledge and Mechanistic Understanding

In marine science numerical models, and especially ecosystem models, have developed into an important tool for policy advice and environmental management applications (Rose et al., 2010; Holt et al., 2014; Robson, 2014; Lynam et al., 2016). The predictive capabilities of these models, in particular under changing environmental conditions, naturally rely strongly on the model formulation, including choice of functional groups and the form of their representation, i.e., their parameterisation.

In recent years, new knowledge generated regarding organism physiology; ecosystem functioning; new data types and increased resolution of data acquisition, particularly those collected by satellites, autonomous platforms and through genetic analyses; as well as new approaches to model marine systems have emerged, altering the way we think about modeling the plankton.

Mechanistic descriptions which can reflect physiological, behavioral and life-history traits (Baklouti et al., 2006), can improve the individual representation and thus provide a more robust platform, valid for a wider range of circumstances. Trait-based modeling and size-based scaling approaches have emerged as fruitful approaches, in some marine systems, to categorizes biological entities by their ecological meaningful characteristic (Litchman and Klausmeier, 2008). This can be done by using certain defining characteristics, such as cell size (Andersen et al., 2016), to scale related processes and functions.

Papers in this research topic provide insights into novel developments in the representation of plankton groups and how these improvements affect model outcomes. The scope of articles covers a wide range of different aspects, from viruses to fish larvae, from single cell mechanisms to improved description of community structure, from purely theoretical approaches to data heavy applications.

Though viruses have been recognized as an important player in the marine food web (Suttle, 2005) their inclusion in models remains rare. In a combination of review and modeling study, Record et al., assess key characteristics of marine viruses and the trade-offs between lysogenic and lytic strategies, particularly as a function of nutrient inputs to the system.

Similarly the ability of many phytoplankton and microzooplankton species to be mixotrophic, which has been known for decades with some attempts made to provide a conceptual basis for models (reviewed by Stoecker, 1998), is only now becoming mainstream. Ghyoot et al. tackle the challenge of modeling mixotrophy, proposing modifications to one of the classic approaches to modeling plankton, the Shuter approach (Shuter, 1979), that enables the simulation of the two main groups of mixotrophs, namely of the constitutives ("phytoplankton that eat") and non-constitutives ("microzooplankton that photosynthesizes") growing in the North Sea.

Using bulk nutrient uptake observations in combination with allometric scaling predictions, Atkins et al. suggest that net nitrogen dynamics can be quantified at an assemblage

OPEN ACCESS

***Edited and reviewed by:***
*Angel Borja,*
*AZTI Pasaia, Spain*

***Correspondence:**
*Christian Lindemann*
*chris.lindemann@uib.no*

***Specialty section:***
*This article was submitted to Marine Ecosystem Ecology, a section of the journal Frontiers in Marine Science*

***Received:*** *13 October 2017*
***Accepted:*** *25 October 2017*
***Published:*** *07 November 2017*

***Citation:***
*Lindemann C, Aksnes DL, Flynn KJ and Menden-Deuer S (2017) Editorial: Modeling the Plankton–Enhancing the Integration of Biological Knowledge and Mechanistic Understanding. Front. Mar. Sci. 4:358. doi: 10.3389/fmars.2017.00358*

scale using size dependencies of Michaelis-Menten uptake parameters and that their method can be applied to particle size distributions that have been routinely measured in eutrophic systems.

Exploiting a statistical approach, Stawiarski et al. compare different strains of picokaryotes in relation to Eppley's empirical relationships of temperature dependent growth (Eppley, 1972). Their results indicate that, when compared to picoeukaryotes, prokaryotic picoplankton have lower growth temperatures and a narrower temperature range. Interestingly they also find that the temperature tolerance range follows a unimodal function of cell size, with the $Q_{10}$ values for picoeukaryotes and picoprokaryotes being 2.3 and of 4.9, respectivly.

Sourisseau et al. explore the usefulness of a trait-trade-off approach to help improve descriptions of the success of the harmful algae bloom dinoflagellate *Alexandrium minutum* under conditions of changing temperature and the hydrographic conditions of the estuary.

Based on recent experimental data published on evolutionary change in a coccolithophore, Denman provides evidence that genetic mutations alone do not suffice to explain rapid thermal adaptation. This study contributes significant new knowledge to the field of organismal adaptation in the face of global warming.

Satellites have long been an important tool in oceanography as their measurement capacity is uniquely suited to transcend the large spatial scales of the global and dynamic ocean. Gregg and Rousseaux incorporate key characteristics of radiative transfer into a biogeochemical model and identified quantifiable trade-offs between nutrient concentration, phytoplankton type and directionality and attenuation wavelength that could affect net primary production and chlorophyll-a concentration from negligible to over 25%.

Laiolo et al. examine the seasonal plankton dynamics of cyclonic and anticyclonic eddies using satellite data, in situ observations and assimilating chlorophyll-a data into biogeochemical models of different complexity. Due to the shallower mixed layer, model simulations of cyclonic eddies show higher chlorophyll-a concentrations and higher concentration of large phytoplankton driven by higher light availability due to the mixed layer shoaling.

Increasing data and information use have been suggested as a step toward improving management applications (Dyble et al., 2008; Lynam et al., 2016). Everett et al. present a review on the current practices in zooplankton observation and modeling. They detail two ways that zooplankton biomass/abundance observations can be used to assess models: data wrangling that transforms observations to be more similar to model output; and observation models that transform model outputs to be more like observations.

Resolving zooplankton feeding traits to a sufficient degree can provide important insights into zooplankton dynamics and the dynamics of marine ecosystems. Wilson et al. use a trait-structured modeling approach to understand possible causes of differences between the *C. finmarchicus* and *C. helgolandicus* biogeographies. Based on their analyses they hypothesize that food quality is a key influence on the population dynamics and distribution of the two species.

Dufour et al. quantified intra-guild predation on copepod eggs by two dominant arctic species, *Calanus hyperboreus* and *Metridia longa* as a function of temperature, egg and alternative prey concentration. Incorporating these remarkably variable empirical data in a model simulation showed that *M. longa* predation had minimal impact on *C. hyperboreus* recruitment, but did benefit *M. longa*'s metabolic demands.

In size-spectrum models smaller zooplankton are often lumped together with phytoplankton, whereas larger (meso) zooplankton are categorized as fish. In the study by Heneghan et al. resolving zooplankton feeding traits explicitly led to an overall increase in fish biomass but also to a trade-off between productivity and stability. While herbivorous zooplankton supported more productive fish communities with higher resilience to fishing pressure, carnivorous zooplankton had a stabilzing effect on fish communities.

Life history can play an important role in the survival strategy of marine plankton, nevertheless it is often ignored in marine ecosystem models (Rose et al., 2010). Exemplified with species of the *Calanus* genus, Banas et al. modeled copepod life history traits and adaptation in seasonal environments. Their modeling experiments demonstrate that patterns in copepod community composition and productivity may be predicted from only a few key constraints on the individual energy budget.

Coupling ocean circulation models with Individual-Based-Models, Mayorga-Adame et al. investigated the effects of larval life-history on the connectivity of different organisms in between east African coral reefs. Long pelagic larval duration with active migration abilities, such as fish, had a much higher settling probability (>20%) than passive species like coral larvae (<1%).

Clearly, this research topic has attracted a varied range of modeling types, investigating functionally diverse organisms and probing a multitude of processes, from individual life histories to ecosystem nutrient dynamics and biophysical interactions driving the abundance, distribution and ultimately the biogeochemical footprint of plankton. Our ability to model key processes in plankton ecology and oceanography still lags behind the highly species-specific physiologies and behaviors of phylogenetically diverse plankton in a dynamic ocean (Menden-Deuer and Kiørboe, 2016). The contributions compiled here take important steps forward in demonstrating how modeling plankton yields important insights. Moreover, this compilation hopefully inspires others to integrate their empirical and analytical approaches with modeling, for equally fruitful outcomes.

## AUTHOR CONTRIBUTIONS

All authors wrote a summary for the articles they edited. CL wrote the initial draft of the editorial. All editors commented on the editorial.

## FUNDING

SM received support from the National Science Foundation Biological-Oceanography award 1736635.

## REFERENCES


Andersen, K. H., Berge, T., Gonçalves, R. J., Hartvig, M., Heuschele, J., Hylander, S., et al. (2016). Characteristic sizes of life in the Oceans, from Bacteria to Whales. *Annu. Rev. Mar. Sci.* 8, 217–241. doi: 10.1146/annurev-marine-122414-034144

Baklouti, M., Diaz, F., Pinazo, C., Faure, V., and Quéguiner, B. (2006). Investigation of mechanistic formulations depicting phytoplankton dynamics for models of marine pelagic ecosystems and description of a new model. *Progr. Oceanogr.* 71, 1–33. doi: 10.1016/j.pocean.2006.05.002

Dyble, J., Bienfang, P., Dusek, E., Hitchcock, G., Holland, F., Laws, E., et al. (2008). Environmental controls, oceanography and population dynamics of pathogens and harmful algal blooms: connecting sources to human exposure. *Environ. Health* 7(Suppl 2):S5. doi: 10.1186/1476-069X-7-S2-S5

Eppley, R. W. (1972). Temperature and Phytoplankton Growth in the Sea. *Fish. Bullet.* 70, 1063–1085.

Holt, J., Allen, J. I., Anderson, T. R., Brewin, R., Butenschön, M., Harle, J., et al. (2014). Challenges in integrative approaches to modelling the marine ecosystems of the North Atlantic: physics to fish and coasts to ocean. *Progr. Oceanogr.* 129, 285–313. doi: 10.1016/j.pocean.2014.04.024

Litchman, E., and Klausmeier, C. A. (2008). Trait-based community ecology of phytoplankton. *Annu. Rev. Ecol. Evol. Syst.* 39, 615–639. doi: 10.1146/annurev.ecolsys.39.110707.173549

Lynam, C. P., Uusitalo, L., Patrício, J., Piroddi, C., Queirós, A. M., Teixeira, H., et al. (2016). Uses of Innovative Modeling Tools within the Implementation of the Marine Strategy Framework Directive. *Front. Marine Sci.* 3:182. doi: 10.3389/fmars.2016.00182

Menden-Deuer, S., and Kiørboe, T. (2016). Small bugs with a big impact : linking plankton ecology with ecosystem processes. *J. Plankton Res.* 38, 1036–1043. doi: 10.1093/plankt/fbw049

Robson, B. J. (2014). When do aquatic systems models provide useful predictions, what is changing, and what is next? *Environ. Model. Softw.* 61, 287–296. doi: 10.1016/j.envsoft.2014.01.009

Rose, K. A., Allen, J. I., Artioli, Y., Barange, M., Blackford, J., Carlotti, F., et al. (2010). End-to-end models for the analysis of marine ecosystems: challenges, issues, and next steps. *Marine Coast. Fish.* 2, 115–130. doi: 10.1577/C09-059.1

Shuter, B. (1979). A model of physiological adaptation in unicellular algae. *J. Theor. Biol.* 78, 519–552. doi: 10.1016/0022-5193(79)90189-9

Stoecker, D. K. (1998). Conceptual models of mixotrophy in planktonic protists and some ecological and evolutionary implications. *Eur. J. Protistol.* 34, 281–290. doi: 10.1016/S0932-4739(98)80055-2

Suttle, C. A. (2005). Viruses in the Sea. *Nature* 437, 356–361. doi: 10.1038/nature04160


**Conflict of Interest Statement:** The authors declare that the research was conducted in the absence of any commercial or financial relationships that could be construed as a potential conflict of interest.

frontiers in Marine Science

ORIGINAL RESEARCH
published: 09 September 2016
doi: 10.3389/fmars.2016.00164

# The Physiological Response of Picophytoplankton to Temperature and Its Model Representation

*Beate Stawiarski *†, Erik T. Buitenhuis and Corinne Le Quéré*

*Tyndall Centre for Climate Change Research, School of Environmental Sciences, University of East Anglia, Norwich, UK*

Picophytoplankton account for most of the marine (sub-)tropical phytoplankton biomass and primary productivity. The contribution to biomass among plankton functional types (PFTs) could shift with climate warming, in part as a result of different physiological responses to temperature. To model these responses, Eppley's empirical relationships have been well established. However, they have not yet been statistically validated for individual PFTs. Here, we examine the physiological response of nine strains of picophytoplankton to temperature; three strains of picoprokaryotes and six strains of picoeukaryotes. We conduct laboratory experiments at 13 temperatures between –0.5 and 33°C and measure the maximum growth rates and the chlorophyll *a* to carbon ratios. We then statistically validate two hypotheses formulated by Eppley in 1972: The response of maximum growth rates to temperature (1) of individual strains can be represented by an optimum function, and (2) of the whole phytoplankton group can be represented by an exponential function Eppley (1972). We also quantify the temperature-related parameters. We find that the temperature span at which growth is positive is more constrained for picoprokaryotes (13.7–27°C), than for picoeukaryotes (2.8–32.4°C). However, the modeled temperature tolerance range (ΔT) follows an unimodal function of cell size for the strains examined here. Thus, the temperature tolerance range may act in conjunction with the maximum growth rate to explain the picophytoplankton community size structure in correlation with ocean temperature. The maximum growth rates obtained by a 99th quantile regression for the group of picophytoplankton or picoprokaryotes are generally lower than the rates estimated by Eppley. However, we find temperature-dependencies ($Q_{10}$) of 2.3 and of 4.9 for the two groups, respectively. Both of these values are higher than the $Q_{10}$ of 1.88 estimated by Eppley and could have substantial influence on the biomass distribution in models, in particular if picoprokaryotes were considered an independent PFT. We also quantify the increase of the chlorophyll *a* to carbon ratios with increasing temperature due to acclimation. These parameters provide essential and validated physiological information to explore the response of marine ecosystems to a warming climate using ocean biogeochemistry models.

**Keywords: picophytoplankton, picoeukaryotes, Eppley, phytoplankton growth rates, temperature tolerance, phytoplankton size scaling, physiological parameterization, chlorophyll *a* to carbon ratio**

OPEN ACCESS

***Edited by:***
*Christian Lindemann, University of Bergen, Norway*

***Reviewed by:***
*Aleksandra M. Lewandowska, University of Oldenburg, Germany*
*Gemma Kulk, University of Groningen, Netherlands*

****Correspondence:***
*Beate Stawiarski*
*beate.stawiarski@io-warnemuende.de*

***†Present Address:***
*Beate Stawiarski, Leibniz Institute for Baltic Sea Research Warnemünde, Rostock-Warnemünde, Germany*

***Specialty section:***
*This article was submitted to Marine Ecosystem Ecology, a section of the journal Frontiers in Marine Science*

***Received:*** *25 May 2016*
***Accepted:*** *24 August 2016*
***Published:*** *09 September 2016*

***Citation:***
*Stawiarski B, Buitenhuis ET and Le Quéré C (2016) The Physiological Response of Picophytoplankton to Temperature and Its Model Representation. Front. Mar. Sci. 3:164. doi: 10.3389/fmars.2016.00164*

## INTRODUCTION

Picophytoplankton contribute 26–56% to the global phytoplankton biomass (Buitenhuis et al., 2013) and about half of the global ocean primary productivity (Grossman et al., 2010). They dominate over wideocean areas, such as the oligotrophic subtropical gyres, and decrease polewards relative to other phytoplankton (Alvain et al., 2008; Buitenhuis et al., 2012). They play a significant role in the recycling of organic matter within the microbial loop of the surface ocean (Azam et al., 1983; Fenchel, 2008), but contribute little to the sinking of particulate matter to the intermediate and deep ocean (Michaels and Silver, 1988). With the projected extension of the oligotrophic subtropical gyres as a consequence of climate warming (Polovina et al., 2008), the recycling of nutrients within the microbial loop and consequently the contribution of picophytoplankton to the phytoplankton community may gain more importance in the marine biogeochemical cycles (Morán et al., 2010).

Temperature is an important environmental variable that determines, directly or indirectly, the biomass, productivity, and cell composition of all phytoplankton groups, single species and even ecotypes (Eppley, 1972; Sarmiento, 2004; Zinser et al., 2007). In particular, temperature directly affects the physiological processes that regulate the growth rates, the temperature span at which growth rates are positive, and the chlorophyll *a* to carbon ratios, among others (Eppley, 1972; Raven and Geider, 1988). In the field, temperature also influences the physical dynamics of the water column and the availability of nutrients and light (Eppley, 1972; Behrenfeld et al., 2006; Johnson et al., 2006), making it difficult to isolate the specific effect of temperature.

The contribution of picophytoplankton to the phytoplankton biomass was shown to correlate with *in situ* temperature (Agawin et al., 2000; Morán et al., 2010). Also a direct effect of temperature on the phytoplankton community size structure was found in the global ocean (Mousing et al., 2014; López-Urrutia and Morán, 2015). However, Marañón et al. (2014) argue that the correlation between temperature and size structure is due to an indirect effect through nutrient supply as they did not find a direct effect of temperature when data from similar nutrient supply regimes were used.

To isolate the specific effect of temperature on the physiology of different phytoplankton groups, representative laboratory strains must be used under controlled nutrient conditions. Furthermore, physiological temperature relevant parameters need to be defined and quantified to identify groups with common traits. It is well established that the maximum growth rate of phytoplankton at optimum conditions is correlated with the cell size and can be represented by a unimodal function of cell size, with decreasing maximum growth rates above and below 2 μm (Chisholm et al., 1992; Bec et al., 2008). This correlation has been shown to be independent of the optimum temperature (Chen et al., 2014) or nutrient supply (Bec et al., 2008), but other temperature-related parameters, such as the temperature tolerance range, have not yet been tested against cell size. It is essential to gain a detailed understanding of the effect of temperature on the physiology to constrain all relevant parameters in ocean biogeochemistry models. These models explicitly represent different phytoplankton and zooplankton groups with common traits, namely PFTs, to make projections about the implications of a warming climate on the marine ecosystem and its biogeochemical cycles (Le Quéré et al., 2005).

Ocean biogeochemistry models use the generalized equation proposed by Eppley (1972) for modeling the response of maximum growth rates of a phytoplankton community to temperature. Eppley formulated two major hypotheses: First, the maximum growth rates of individual species can be represented by an optimum function in response to temperature, and second, the maximum growth rates of a phytoplankton community can be represented by an exponential function in response to temperature. In addition, he formulated an equation which describes the exponential fit to the upper limit of the maximum growth rates of a phytoplankton community in response to temperature (Equation 1 in Eppley, 1972). Neither of these two hypotheses was statistically verified in Eppley (1972). Montagnes et al. (2003) showed that the maximum growth rates of most individual species are better represented by a linear fit than an exponential fit, but they did not consider an optimum fit, nor did they test the whole phytoplankton community. Bissinger et al. (2008) showed that the upper 99th quantile of the maximum growth rates of a mixed phytoplankton community can be represented by an exponential fit in response to temperature, with a $Q_{10}$ value similar to Eppley (1972), but with a higher maximum growth rate at 0°C. However, Bissinger et al. (2008) did not test other functions.

Temperature also affects the chlorophyll *a* to carbon ratio ($\theta$) of phytoplankton (Geider, 1987). This effect needs to be quantified when using chlorophyll *a* from field observation to estimate biomass, growth rates, or the community composition. For example, its divinyl derivatives are measured by satellites to identify the picoprokaryote *Prochlorococcus* sp. within a phytoplankton assemblage in the field (Chisholm et al., 1992; Alvain et al., 2005). However, the chlorophyll *a* to carbon ratio is a variable component within the cell. Generally, it decreases with temperature due to low temperature chlorosis, slower metabolic reactions or the increase in lipids to maintain membrane fluidity (Geider, 1987). The variability of the chlorophyll *a* to carbon ratio can be amplified by exposure to high light intensities (Geider, 1987). A positive effect of temperature on light-harvesting components and a negative effect on photoprotective components has previously been found between 16 and 24°C for picoprokaryotes and picoeukaryotes (Kulk et al., 2012). However, more data over a wide range of temperatures need to be collected to identify and quantify significant relationships.

The present study will investigate the influence of temperature on the physiology of nine picophytoplankton strains, with the aim of informing the representation of picophytoplankton in ocean biogeochemistry models. It will specifically: (a) quantify the response of maximum growth rates to temperature; (b) evaluate the two hypotheses of Eppley (1972); (c) extract the temperature-related parameters, separately for individual strains and the group of picoprokaryotes, picoeukaryotes, and picophytoplankton; and investigate the relationship (d) between cell size and the temperature-related parameters, and (e) between the chlorophyll *a* to carbon ratio and temperature.

# MATERIALS AND METHODS

## Cultures and Experimental Setup

Representative strains of picophytoplankton from diverse taxonomic classes were obtained from the Roscoff culture collection (RCC, Vaulot et al., 2004), to investigate the effect of temperature on the maximum growth rates of picophytoplankton. They include three picoprokaryotes, represented by *Synechococcus* sp. (RCC 30), a high light (HL), and a low light (LL) ecotype of *Prochlorococcus* sp. (RCC 296 and 162, respectively), as well as the picoeukaryotes *Bolidomonas pacifica* (RCC 212), which was recently renamed as *Triparma eleuthera* (Ichinomiya et al., 2016), *Micromonas pusilla* (RCC 1677), *Picochlorum* sp. (RCC 289), *Nannochloropsis granulata* (RCC 438), *Imantonia rotunda* (RCC 361), and *Phaeomonas* sp. (RCC 503) (**Table 1**). All strains were grown in artificial seawater medium (ESAW) (Berges et al., 2001) with ammonium [882 μM $(NH_4)_2SO_4$] as the nitrogen source and addition of 10 nM selenium ($Na_2SeO_3$). The physiological experiments in response to temperature were conducted in 55 ml tubes (Pyrex Brand 9826), which were placed into a temperature gradient bar The temperature gradient bar was built with space for 65 culture tubes in 13 rows and 5 columns. A temperature gradient is generated by heating one of the short ends and cooling the other end to achieve a gradient between −0.5 and 33°C. Each tube is lighted by an individual ultrabright LED (Winger WEPW1-S1 1W, 95 Lumen, white), achieving a light intensity of up to 480 μmol photons $m^{-2}$ $s^{-1}$ inside the tubes. The LED drivers are connected to mains electricity through a timer in the control unit, running on a 14:10 h light-dark cycle. Light was measured with a Radiometer (Biospherical Instruments Inc. QSL-2101) to be 291 ± 18 μmol photons $m^{-2}$ $s^{-1}$ for 8 strains and 81 ± 5 μmol photons $m^{-2}$ $s^{-1}$ for the low light *Prochlorococcus* sp. strain. These values are consistent with the average species specific light saturation levels (Stawiarski, 2014). To exclude any effect of light limitation or light inhibition, near optimum light conditions were chosen for each strain. A separate study with incubations at light intensities between 10 and 720 μmol photons $m^{-2}$ $s^{-1}$ has been conducted beforehand. The low light Prochlorococcus strain reached its highest growth rates with light saturation between 64 and 120 μmol photons $m^{-2}$ $s^{-1}$, but was light inhibited at light intensities > 120 μmol photons $m^{-2}$ $s^{-1}$. All other strains reached light saturation between 120 and 330 $m^{-2}$ $s^{-1}$. No light inhibition occurred at light intensities < 330 μmol photons $m^{-2}$ $s^{-1}$.

Temperatures were measured with a Grant Squirrel 1000. Thanks to the insulation at the sides and top of the temperature gradient bar, the average temperature gradient is linear (linear regression of temperature difference between adjacent sets of tubes, $p = 0.9$). However, the middle tubes in each column tend to be slightly colder at the cold end (up to 0.5°C), and as a consequence the standard deviation of the temperature in the five tubes is higher ($p = 0.002$). To prevent this from biasing the results, measurements are reported at the temperature measured in each tube.

## Analyses

For measuring the maximum growth rates, cultures of each strain were acclimated at 13 different temperatures for at least four divisions to reach balanced growth before daily *in vivo* fluorescence measurements were taken with a Turner Design Fluorometer (10 AU) (Anderson, 2005). Samples were placed in the dark prior to measurements and were measured until the signal stabilized. Only acclimated cultures were used within the present study, hence the fluorescence signal is considered as proportional to the low cell densities which were used (Anderson, 2005). The benefit of using this method instead of collecting cell counts was that the culture tube from the temperature gradient bar fits into the sample slot of the Fluorometer. Thus, no volume needed to be removed from the culture tube. The average cell size of the picophytoplankton strains was either provided by the RCC or obtained from the literature for *T. eleuthera* (Guillou et al., 1999).

To obtain chlorophyll *a* to carbon ratios, samples of particulate organic carbon (POC) and chlorophyll *a* were collected while the culture was still in exponential growth phase. POC was sampled on pre-combusted 13 mm GF/F filters for all strains. A layer of 3 filters was used for both *Prochlorococcus* sp. strains, because preliminary tests showed that their cells did not pass through, but were too small to remain on a single filter. Medium blanks were collected for each number of filter

**TABLE 1 | Picophytoplankton strains examined within this study, including three strains of picoprokaryotes and six strains of picoeukaryotes, their Roscoff culture collection number (RCC), stain, average cell size (diameter), and location and depth of isolation.**

| | Species | RCC | Strain | Size (μm) | Location of isolation | Depth of isolation (m) |
|---|---|---|---|---|---|---|
| Picoprokaryotes | *Prochlorococcus* sp.*(HL)* | 296 | GP2 | 0.6 | 8°32.5′N, 136°31.8′E | 150 |
| | *Prochlorococcus* sp. *(LL)* | 162 | NATL2-M98 | 0.6 | 38°59′N, 40°33′W | 10 |
| | *Synechococcus* sp. | 30 | MAX42Syn | 1 | 26°18′N, 63°26′W | 120 |
| Picoeukaryotes | *Triparma eleuthera* | 212 | OLI 41 SA-A | 1.2 | 2°30′N, 150°0′W | 15 |
| | *Micromonas pusilla* | 1677 | MICROVIR 17CR_2 | 1.5 | 54°24′N, 4°3′E | 10 |
| | *Picochlorum* sp. | 289 | OLI 26 SA | 2 | 7°0′S, 150°0′W | 15 |
| | *Nannochloropsis granulata* | 438 | BL_39 | 2 | 41°40′N, 2°48′E | 0 |
| | *Imantonia rotunda* | 361 | RA000609-17-10 | 2.5 | 48°45′N, 3°57′W | 0 |
| | *Phaeomonas* sp. | 503 | BL_149-10 | 3 | 41°40′N, 2°48′E | 0 |

layers. Samples of chlorophyll *a* were collected on pre-combusted 25 mm GF/F filters for 7 strains, but on 25 mm polycarbonate filters (0.2 μm) for both *Prochlorococcus* sp. strains. Both filter types were shown to lead to comparable chlorophyll a results using phytoplankton samples (Hashimoto and Shiomoto, 2000). Depending on the cell density of the culture, between 5 and 20 ml per sample were filtered and rinsed with Milli-Q water. After sampling all filters were frozen in liquid nitrogen immediately, and stored at −80°C until analyses. The cell numbers were measured by flow cytometry (BD Biosciences FACSCalibur, flow cytometer) and the flow rate was calibrated using the method of Marie et al. (2005).

For analysis, the POC samples were dried at 40°C for 24 h, placed into pre-combusted tin capsules and analyzed with an elemental analyser (Exeter Analytical, CE-440 Elemental Analyser), which was calibrated with acetanilide (Exeter Analytical). The chlorophyll *a* samples were extracted in 10 ml acetone (Fisher Scientific, 99.8+ %) in 15 ml centrifuge tubes and disintegrated by shaking and vortexing. The tubes were then wrapped in aluminum foil and stored at 4°C for 24 h. Prior to analysis, the samples were centrifuged and the supernatant was analyzed in a Fluorescence Spectrometer (PerkinElmer LS 45 Luminescence Spectrometer). After reading a sample, 3 drops of 8% HCl were added into the cuvette to measure the background signal caused by chlorophyll degradation products such as phaeopigments. The concentration of the calibration standard (SIGMA product No C5753) was also obtained prior to analyses (Parson et al., 1984).

## Calculations

The maximum growth rates of all strains were calculated by linear regression through at least three consecutive measurements of the log-transformed *in vivo* fluorescence measurements during the exponential growth phase. To test for the best representation of the response of the maximum growth rates to temperature, a linear, an exponential, and an optimum fit (Equations 1–3) were applied to the maximum growth rate measurements of each strain, of each of the two groups (picoprokaryotes or picoeukaryotes) and also of all strains combined, representative for a group of picophytoplankton.

$$\text{linear:} \qquad \mu_{max} = \mu_{max,0°C} + \text{slope} \times T \tag{1}$$

$$\text{exponential:} \qquad \mu_{max} = \mu_{max,0°C} \times Q_{10}^{\frac{T}{10}} \tag{2}$$

$$\text{optimum:} \qquad \mu_{max} = \mu_{Opt} \times \exp\left(-\frac{\left(T - T_{Opt}\right)^2}{\triangle T^2}\right) \tag{3}$$

where $\mu_{max}$ is the maximum growth rate, $\mu_{max,0°C}$ is the maximum growth rate at $0°C$, T is the temperature, $Q_{10}$ is the temperature dependence, which is a measure for the increase of the maximum growth rate with the increase of temperature by 10°C, $\mu_{Opt}$ is the optimum growth rate, $T_{Opt}$ is the optimum temperature, and $\triangle T$ is half the width of the temperature range at $\mu_{Opt} \times \exp(-1)$, which will be referred to as temperature tolerance range, not to be confused with $T_{max} - T_{min}$, which will be referred to as the temperature span.

The temperature-related parameters and their standard errors were estimated by minimizing the sum of squares between the fits and the measurements using the Gauss-Newton method in Mystat 12 (Systat software). The obtained parameters were not unique for the optimum fit to the combined data of all strains, because the optimum temperature was indefinite. For this reason, the sum of squares between the model and the data were calculated 15 times with varying starting values and it was found, that there was only a minor variability in the residual sum of squares (< 0.03%) and the parameters.

The relative quality of the three fits to equations 1–3 was compared using the Akaike's Information Criterion (AIC), which compares fits with different numbers of parameters (Equation 4, Burnham and Anderson, 1998).

$$\text{Akaike}'\text{s Information Criterion} \qquad AIC = n_{obs} log\left(\sigma^2\right) + 2n_{param} \tag{4}$$

where $n_{obs}$ is the number of observations, $\sigma^2$ is the standard deviation and $n_{param}$ is the number of parameters given in the equation of the fit. The lowest AIC value indicates the best fit. Although there is no formally defined significance level associated with the value of AIC, we have used the definition in Burnham and Anderson (1998), who state that if an AIC differs by less than 2 from the lowest value, this fit is also appropriate.

The data were also compared to the exponential fit presented in Eppley (1972) to the upper limit of the maximum growth rates of a mixed group of phytoplankton, which will be referred to as the absolute maximum growth rates, in response to temperature (Equation 5).

$$\text{Eppley (1972)} \qquad \mu_{max} = 0.59 \times 1.88^{\frac{T}{10}} \tag{5}$$

where the first constant is $\mu_{max,0°C}$ and the second constant is the $Q_{10}$.

To calculate the absolute maximum growth rates for a group of picophytoplankton and picoprokaryotes in response to temperature, we followed the method used by Bissinger et al. (2008). For this, we calculated the upper 99th quantile of the maximum growth rates for both groups by applying a linear quantile regression through the log-transformed maximum growth rates. The Software R with the software package quantreg was used (Koenker, 2006) with a significance level of $p < 0.001$. The resulting coefficients were then exponentially converted and the fit was compared to the fit presented in Eppley (1972). As an alternative means of showing the absolute maximum growth rates of a picophytoplankton community, we also calculated the linear, exponential and optimum fitthrough the optimum temperatures vs. optimum growth rates of the nine strains only.

## Statistical Analysis

To test for significant differences in the maximum growth rates or in the obtained temperature related parameters between the two picophytoplankton groups, the Wilcoxon-Mann–Whitney-*U*-test was used ($p \leq 0.05$, df = 1).To test for cell size related trends of the temperature related parameters, the Mitchell-Olds and Shaw test was used ($p \leq 0.05$) (Mitchell-Olds and Shaw,

1987). It tests for an intermediate maximum, in contrast to a monotonic relationship with extreme values at each end. For the linear trends in the response of the chlorophyll *a* to carbon ratios to temperature, a linear regression was applied and the obtained coefficients were analyzed by one-way ANOVA ($p \leq 0.05$).

# RESULTS

## Temperature-Response of Individual Picophytoplankton Strains

The maximum growth rates of picoprokaryotes range from 0.07 to 0.82 $d^{-1}$ and of picoeukaryotes from 0.005 to 2.04 $d^{-1}$ over the full range of tested temperatures (**Figure 1**). These rates generally increase with temperature up to an optimum temperature ($T_{Opt}$), above which they decrease (**Figure 1**) for all individual picophytoplankton strains. The AIC values are also smallest for the optimum fit (Equation 3) for seven of the nine individual strains (**Table 2**; **Figure 1**) compared to the linear (Equation 1) or exponential fit (Equation 2). For the two remaining strains, the AIC values for the optimum fit are within the range of an acceptable representation. *M. pusilla* did not grow at all above the optimum temperature. Therefore, there was no acclimated growth rate above the optimum temperature that would have been needed to get a good fit to the optimum function, and its growth rates are better represented by a linear fit. *T. eleuthera* grew at only four temperatures, thus the available data for this strain were insufficient to distinguish between the fits. The generally best agreement with the optimum fit suggests that three temperature-related parameters need to be quantified for the representation of the response of growth rates of individual strains to temperature: $\mu_{Opt}$, $T_{Opt,}$ and $\Delta T$ (**Table 3**).

The derived optimum growth rates ($\mu_{Opt}$) differ significantly ($p = 0.04$, df $= 1$) between the two groups, the average for picoprokaryotes is $0.47 \pm 0.17$ $d^{-1}$ and for picoeukaryotes it is $1.05 \pm 0.47$ $d^{-1}$. The average optimum temperature ($T_{Opt}$) of the individual strains is $23.3 \pm 2.7$°C and the temperature tolerance range ($\Delta T$) is $8.2 \pm 3.3$°C, with no significant difference in these two temperature-related parameters ($p_{T\mathrm{Opt}} = 0.8$; $p_{\Delta T} = 0.12$, df $= 1$) between picoprokaryotes and picoeukaryotes. None of the three temperature-related parameters was correlated with the latitude of isolation of the strains (**Figure 2**), i.e., tropical strains did not have a significantly higher $T_{Opt}$ than temperate strains. However, the overall temperature span at which the growth rates are positive is narrower for the three investigated strains of picoprokaryotes (13.7–27°C, **Table 3**) than for the six strains of picoeukaryotes (2.8–32.4°C). *Nannochloropsis granulata*, *M. pusilla* and *Picochlorum* sp., the three intermediate sized picoeukaryotes, grow at the most measured temperatures spanning up to 27°C, which is reflected in their higher $\Delta T$ values. Cell size has an effect on the temperature-related parameters for the individual picophytoplankton strains tested within this study. A significant unimodal relationship was found between the temperature tolerance range ($\Delta T$) and cell size ($R^2 = 0.73$, $p = 0.018$), but not between $\mu_{Opt}$ ($R^2 = 0.49$, $p = 0.17$), or $T_{Opt}$ ($R^2 = 0.25$, $p = 0.43$) and cell size. The cell size at which $\Delta T$ is maximal is 1.8 µm (**Figure 2**). There is also statistical support ($p < 0.01$, Mitchell-Olds and Shaw test) for a maximum of $\mu_{Opt}$ at the higher end of measured values of $\Delta T$, although $\mu_{Opt}$ does not increase significantly with $\Delta T$ ($p = 0.1$, linear regression, one-way ANOVA).

## Temperature-Response of Picophytoplankton

The maximum growth rates for the picoprokaryotes in response to temperature can be described equally well by all three fits (similar AIC values; **Table 2**), but the maximum growth rates for the picoeukaryotes are best described by either the linear or the optimum fit. Finally, the maximum growth rates for the group of picophytoplankton are best described by the exponential fit (**Figure 3**) and can be quantified by the two temperature-related parameters $\mu_{max,0°C}$ and $Q_{10}$ (**Table 3**).

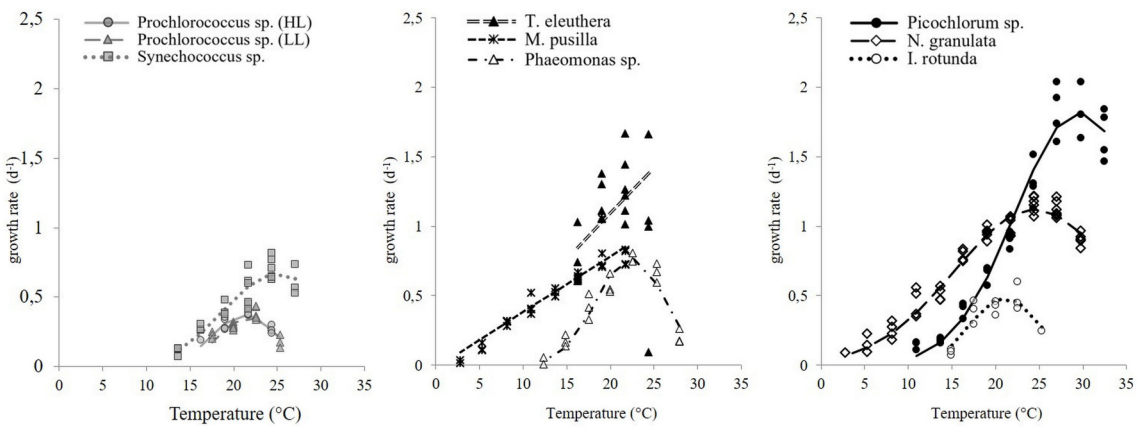


**FIGURE 1 | The response of maximum growth rates of picophytoplankton to temperature, including three strains of picoprokaryotes (gray symbols) and six strains of picoeukaryotes (black or white symbols).** The lines indicate the best fit chosen by AIC values.

In order to compare the temperature response of the group of picophytoplankton or of picoprokaryotes to the parameters obtained by Eppley (1972) and Bissinger et al. (2008), a fit to the upper exponential 99th quantile of the maximum growth rates was calculated (**Figure 3**). For the group of picophytoplankton ($\mu_{pic}$) the calculated $Q_{10}$ is 2.3 (Equation 6) but of picoprokaryotes ($\mu_{pro}$) the temperature response is stronger and results in a much higher $Q_{10}$ of 4.9 (Equation 7). For the picoeukaryotes ($\mu_{euk}$) the $Q_{10}$ would be 2.8 (Equation 8), but the AIC does not give support for an exponential fit as an acceptable representation of the maximum growth rates in response to temperature for this group (**Table 2**). Hence we will exclude this fit from the further discussion.

**TABLE 2 | AIC values for the linear, exponential and optimum fits for individual picophytoplankton strains, both groups of picoprokaryotes and picoeukaryotes, and picophytoplankton.**

| Strain | Linear | Exponential | Optimum |
|---|---|---|---|
| *Prochlorococcus* sp.(HL) | −33.6 | −33.7 | **−42.7** |
| *Prochlorococcus* sp.(LL) | −37.7 | −37.8 | **−43.6** |
| *Synechococcus* sp. | −42.9 | −39.2 | **−44.9** |
| *Triparma eleuthera* | **−19.3** | −18.7 | −18.6 |
| *Micromonas pusilla* | **−59.4** | −49.9 | −58.9 |
| *Picochlorum* sp. | −42.5 | −32.2 | **−52.7** |
| *Nannochloropsis granulata* | −74.7 | −64.1 | **−107.9** |
| *Imantonia rotunda* | −18.5 | −17.7 | **−22.0** |
| *Phaeomonas* sp. | −20.3 | −19.8 | **−37.3** |
| Picoprokaryotes | **−95.1** | −94.3 | −94.0 |
| Picoeukaryotes | **−162.6** | −158.9 | −161.2 |
| Picophytoplankton | −200.8 | **−205.7** | −203.3 |

*The lowest values are shown in bold print, other appropriate values (ΔAIC < 2) are underlined.*

$$\mu_{pic} = 0.22 \times 2.3^{\frac{T}{10}} \quad (6)$$

$$\mu_{pro} = 0.023 \times 4.9^{\frac{T}{10}} \quad (7)$$

$$\mu_{euk} = 0.19 \times 2.8^{\frac{T}{10}} \quad (8)$$

The corresponding coefficients for the linear regression to the logarithmically transformed data are presented in **Table 4**.

A different method to represent the response of the absolute maximum growth rates of the group of picophytoplankton to temperature is to test the fits through the optimum values of the nine strains (**Figures 3**, **4**). With this method, the AIC value is lowest for the linear fit (−5.41), is also appropriate for the exponential fit (−5.3), but clearly better than for the optimum fit (−2.68).

## Chlorophyll *a* to Carbon Ratios

The chlorophyll *a* to carbon ratio (θ) for the group of picophytoplankton increases significantly with temperature between 0.004 and 0.037 g Chl $g^{-1}$ C ($R^2 = 0.42$, $p < 0.001$, **Figure 5**), and can be described by Equation (9).

$$\theta = 1.01 * 10^{-3} + 9.38 * 10^{-4} T \quad (9)$$

This relationship is also significant ($p \leq 0.05$) for individual strains (see Supplementary Material), unless a strain grew only over a narrow temperature range (both *Prochlorococcus* sp. strains and *Imantonia rotunda*), or there was a high variability in the data over a low range of chlorophyll *a* to carbon ratios (*Micromonas pusilla*). Four strains show a drop in chlorophyll *a* to carbon ratio above $T_{Opt}$ (both *Prochlorococcus* sp. strains, *Picochlorum* sp., and *Nannochloropsis granulata*).

The cellular chlorophyll a concentration increases significantly ($p < 0.05$) with temperature for seven strains

**TABLE 3 | Temperature-related parameters for a linear, exponential, and optimum fit to represent the response of the maximum growth rates to temperature for individual picophytoplankton strains, both groups of picoprokaryotes and picoeukaryotes, and picophytoplankton.**

| Strain | *n* | Linear | | Exponential | | Optimum | | | Measured | |
|---|---|---|---|---|---|---|---|---|---|---|
| | | $\mu_{max,0°C}$ | Slope | $\mu_{max,0°C}$ | $Q_{10}$ | $\mu_{opt}$ | $T_{Opt}$ | $\Delta T$ | $T_{min}$ | $T_{max}$ |
| *Prochlorococcus* sp. (HL) | 16 | 0.30 (± 0.15) | 0.001 (± 0.007) | 0.30 (± 0.15) | 1.02 (± 0.23) | 0.38 (± 0.01) | 21.3 (± 0.2) | 5.3 (± 0.4) | 16.3 | 24.4 |
| *Prochlorococcus* sp. (LL) | 19 | 0.35 (± 0.17) | –0.003 (± 0.008) | 0.35 (± 0.20) | 0.92 (± 0.25) | 0.36 (± 0.02) | 21.7 (± 0.2) | 4.8 (± 0.5) | 17.5 | 25.3 |
| *Synechococcus* sp. | 24 | –0.38 (± 0.13) | 0.042 (± 0.006) | 0.10 (± 0.04) | 2.08 (± 0.31) | 0.67 (± 0.03) | 25.0 (± 0.7) | 8.6 (± 1.1) | 13.7 | 27.0 |
| *Triparma eleuthera* | 18 | –0.22 (± 0.44) | 0.066 (± 0.021) | 0.38 (± 0.16) | 1.70 (± 0.33) | 1.32 (± 0.07) | 22.8 (± 1.1) | 8.3 (± 2.1) | 16.3 | 24.4 |
| *Micromonas pusilla* | 29 | –0.02 (± 0.06) | 0.040 (± 0.003) | 0.21 (± 0.03) | 1.92 (± 0.16) | 0.80 (± 0.03) | 21.5 (± 1.5) | 12.9 (± 1.7) | 2.8 | 21.7 |
| *Picochlorum* sp. | 35 | –0.90 (± 0.16) | 0.087 (± 0.006) | 0.22 (± 0.05) | 1.96 (± 0.17) | 1.82 (± 0.04) | 29.6 (± 0.4) | 10.3 (± 0.6) | 10.9 | 32.4 |
| *Nannochloropsis granulata* | 50 | 0.19 (± 0.08) | 0.033 (± 0.004) | 0.43 (± 0.06) | 1.39 (± 0.07) | 1.12 (± 0.02) | 24.5 (± 0.3) | 13.0 (± 0.5) | 2.8 | 29.8 |
| *Imantonia rotunda* | 13 | –0.12 (± 0.24) | 0.024 (± 0.012) | 0.13 (± 0.10) | 1.67 (± 0.59) | 0.49 (± 0.04) | 21.1 (± 0.5) | 5.5 (± 0.7) | 14.9 | 25.3 |
| *Phaeomonas* sp. | 20 | 0.17 (± 0.26) | 0.013 (± 0.012) | 0.29 (± 0.18) | 1.22 (± 0.33) | 0.78 (± 0.04) | 22.3 (± 0.2) | 5.5 (± 0.3) | 12.3 | 27.9 |
| Picoprokaryotes | 59 | –0.23 (± 0.14) | 0.029 (± 0.006) | 0.08 (± 0.03) | 2.02 (± 0.36) | 0.51 (± 0.08) | 27.7 (± 5.0) | 12.7 (± 5.6) | 13.7 | 27.0 |
| Picoeukaryotes | 165 | –0.28 (± 0.10) | 0.054 (± 0.005) | 0.23 (± 0.03) | 1.83 (± 0.11) | 1.51 (± 0.28) | 37.7 (± 6.8) | 21.8 (± 5.2) | 2.8 | 32.4 |
| Picophytoplankton | 224 | –0.35 (± 0.10) | 0.050 (± 0.005) | 0.14 (± 0.02) | 2.09 (± 0.14) | 33.93 (± 1.1) | 125.5 (± 0.4) | 52.7 (± 0.2) | 2.8 | 32.4 |

*The asymptotic standard error is shown in brackets. The number of measured maximum growth rates is n, the measured minimum temperature ($T_{min}$), and maximum temperature ($T_{max}$), define the temperature span at which growth rates were positive.*

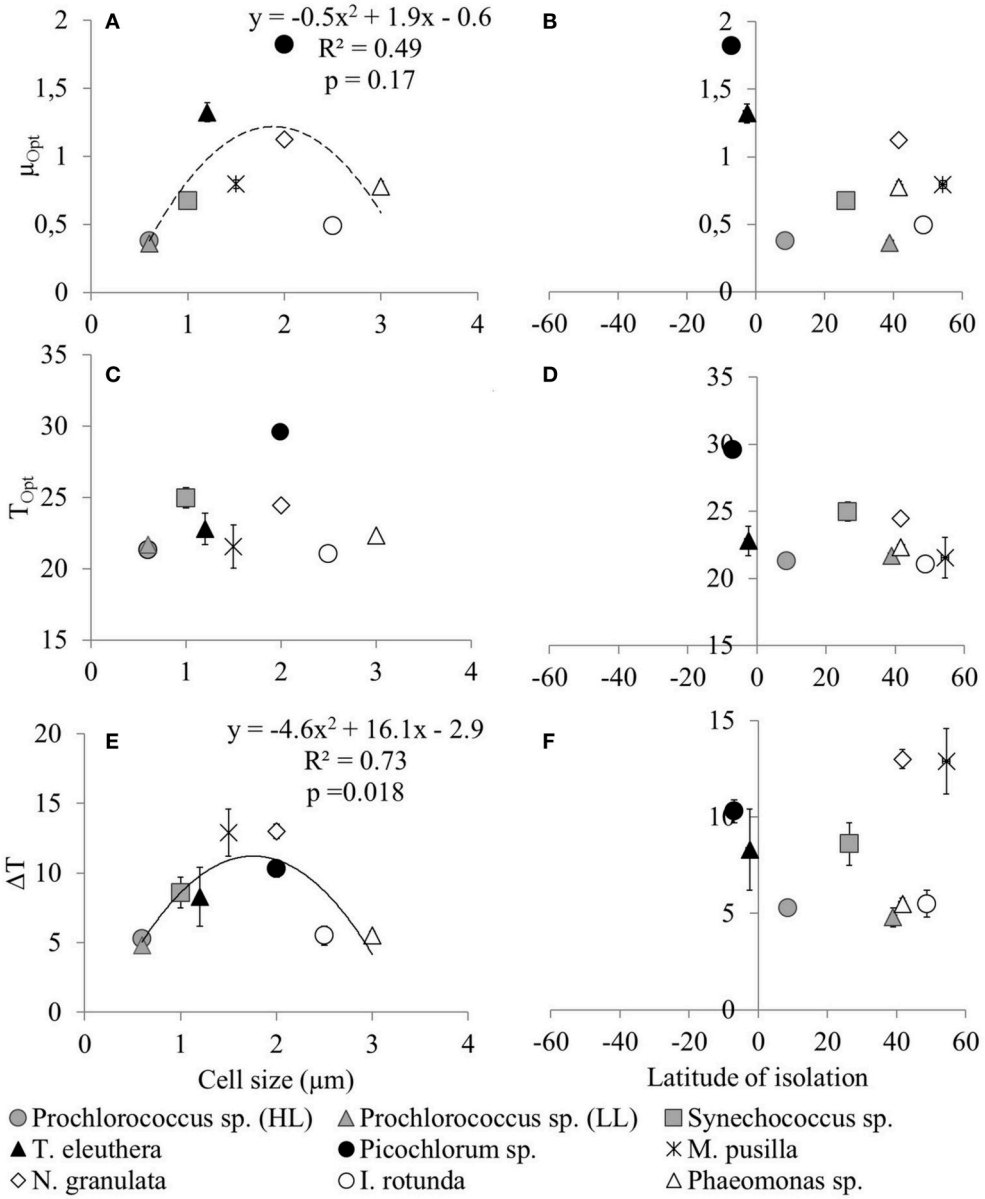


**FIGURE 2 | Temperature-related parameters of individual picophytoplankton strains ($\mu_{opt}$, $T_{opt}$ and $\Delta T$) as a function of cell size (A,C,E) or latitude of isolation (B,D,F).** The temperature-related parameters were obtained from an optimum fit (Equation 3) to the measured maximum growth rates of individual picophytoplankton strains for the representation of the response of maximum growth rates to temperature and are shown in **Table 3**. Error bars are asymptotic standard errors. Lines indicate unimodal functions [continuous line: Significant, $p = 0.018$, $r^2 = 0.728$; dotted line: Not significant, $p = 0.17$, $r^2 = 0.485$, but included because a significant trend was found by Bec et al. (2008)].

(see Supplementary Material). For *M. pusilla* it becomes significant ($p = 0.005$) if the four highest outliers over the whole temperature range are excluded. For *I. rotunda* a significant ($p = 0.038$) increase in chlorophyll a is found up to its optimum temperature. There is also a stronger significance ($p < 0.001$) for *N. granulata* up to its optimum and a decrease, however not significant above its optimum temperature. No significant trend was found for the high light *Prochlorococcus* sp. strain. *Phaeomonas* sp. shows a significantly ($p = 0.037$) decreasing trend with increasing temperature.

The cellular carbon concentration increases significantly with temperature for the low light *Prochlorococcus* sp. strain ($p = 0.004$). It decreases significantly for the three picoeukaryotes *N. granulata* ($p < 0.001$), *Phaeomonas* sp. ($p = 0.001$), and for *Picochlorum* sp. between 14 and 27°C ($p = 0.016$). No significant trends were established for the other strains.

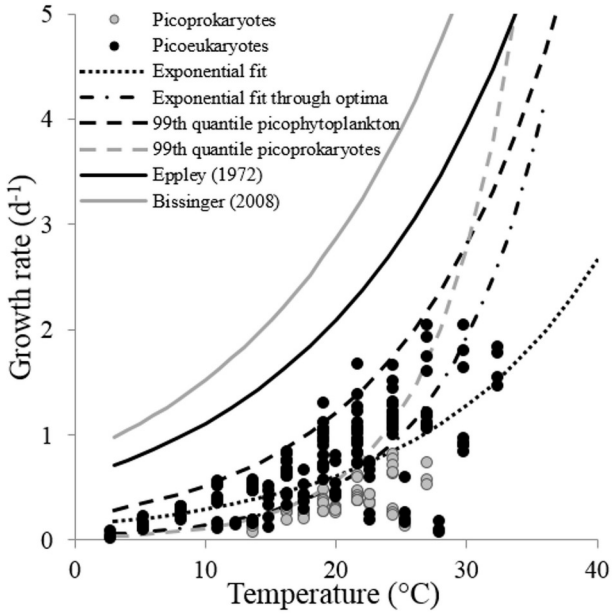


**FIGURE 3 | The response of the maximum growth rates of a group of picophytoplankton to temperature.** The lines indicate different fits discussed within this study: The exponential fit obtained from Equation (2) (exponential fit), the exponential fit through optimum growth rates at optimum temperatures of individual strains (exponential fit through optima), the exponential fit obtained from a 99th quantile regression to maximum growth rates of both, a group of picophytoplankton (99th quantile picophytoplankton), and a group of picoprokaryotes (99th quantile picoprokaryotes) and the fits presented in Eppley (1972) and Bissinger et al. (2008).

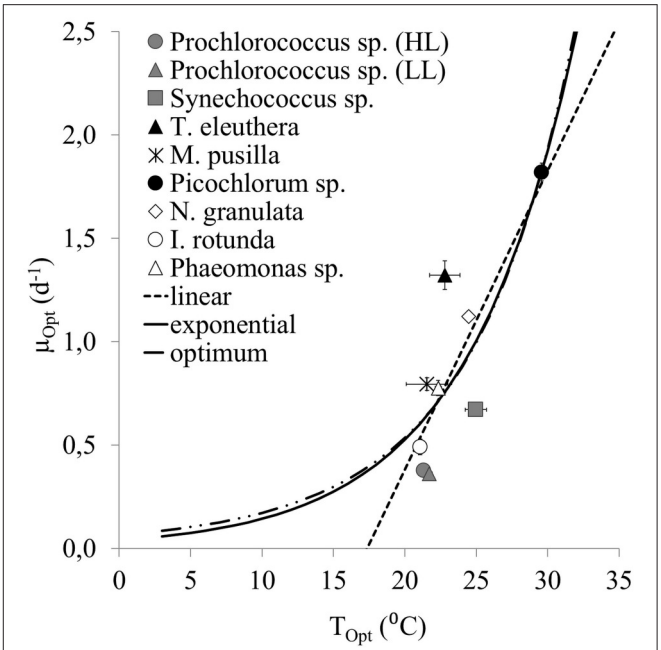


**FIGURE 4 | A linear, exponential and optimum fit through optimum growth rates at optimum temperatures of the individual strains examined within this study.** Error bars represent the standard error.

**TABLE 4 | Coefficients obtained from a linear 99th quantile regression to the log-transformed maximum growth rates of a group consisting of picoprokaryotes, and of picophytoplankton, using strains examined within this study with standard errors.**

| | Intercept | Standard error | Slope | Standard error |
|---|---|---|---|---|
| Picoprokaryotes | −3.774 | 0.076 | 0.160 | 0.004 |
| Picophytoplankton | −1.496 | 0.012 | 0.084 | 0.001 |
| Picoeukaryotes | (−1.680) | (0.186) | (0.101) | (0.009) |

*Coefficients for picoeukaryotes are provided for completeness.*

# DISCUSSION

## Temperature-Response of Individual Picophytoplankton Strains

In agreement with the first hypothesis formulated by Eppley (1972), our results show strong evidence that the maximum growth rates of individual picophytoplankton strains in response to temperature are best represented by an optimum function. Thus, the best way to parameterize this response is to describe their optimum growth rates, optimum temperatures, and temperature tolerance ranges.

The optimum growth rates, which were obtained for the individual strains of picoprokaryotes are lower than of picoeukaryotes. This confirms theoretical assumptions concerning the deviation of picophytoplankton from the classical allometric relationship with decreasing maximum growth rate with cell size in this group (Raven, 1998; Bec et al., 2008). The optimum temperatures, are slightly lower for *Prochlorococcus* sp. than for *Synechococcus* sp., which is also in agreement with previous studies (Moore et al., 1995; Johnson et al., 2006; Zinser et al., 2007). However, our estimated values are both lower than previously reported values of 24–25 and 28°C, respectively for the two species. There are different reasons which may cause this discrepancy. A possible reason is that none of these studies applied an optimum fit to their results. Instead $T_{Opt}$ was only described as the temperature at which the highest growth rate ($\mu_{Opt}$) was measured, even though $T_{Opt}$ and $\mu_{Opt}$ may be achieved between the tested temperatures. We have shown that the optimum function gives the best fit of the response of growth rates of individual picophytoplankton strains to temperature. We therefore conclude that our technique is more accurate in defining $T_{Opt}$, because it is able to interpolate between data points and provide error intervals. Another potential reason could be the change of photophysiological properties with temperature. We show that the increase in chlorophyll *a* to carbon ratio is due to the significant increase in cellular chlorophyll *a* concentration for most strains. This is in agreement with the expected increase of light harvesting compounds with increasing temperature and is also associated with the decrease of photoprotective compounds (Geider, 1987). This effect may also contribute to the shift of the optimum temperature with light intensity (Geider, 1987). The strains used by Moore et al. (1995) and those in the present study were

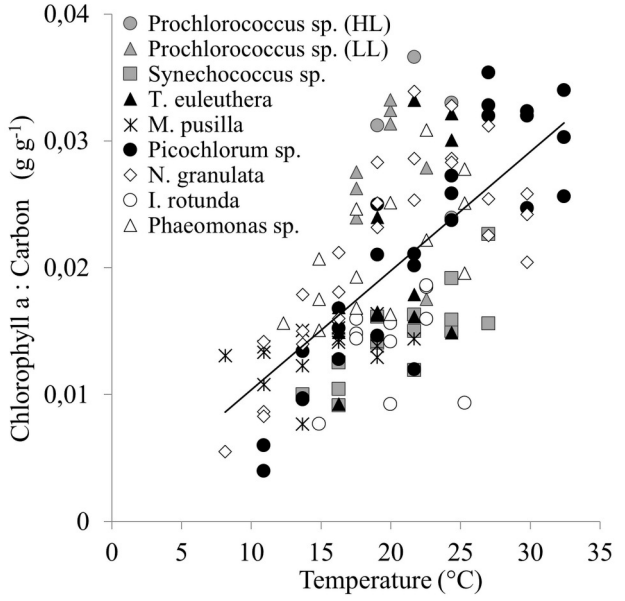


**FIGURE 5 | The response of the chlorophyll *a* to carbon ratios of a group of picophytoplankton to temperature.** The line indicates a linear regression including data for all 9 species (Equation 9, $r^2 = 0.42$, $p < 0.001$).

grown under light saturation. For this an extensive series of light experiments has been conducted for the strains examined here beforehand (Stawiarski, 2014). However, these different strains also have different light optima. Hence, the differences in temperature optima may also be attributed to the natural variability of ecotypes, which may be linked to the adaptation to different light conditions (Johnson et al., 2006; Zinser et al., 2007). The optimum temperatures for picoeukaryotes obtained within the present study are similar to those presented in previous studies (20–25°C) (Throndsen, 1976; Cho et al., 2007). A full description of the light response at constant temperature of some of these strains will be published in a separate paper (Stawiarski et al., in prep.).

$T_{Opt}$ is a common temperature-related parameter, which is used for modeling the distribution of different phytoplankton groups. Our results demonstrate that there are no significant differences in $T_{Opt}$ between picoprokaryotes and picoeukaryotes. Also there is no relationship between optimum temperature or latitude of isolation for the strains examined here, but both groups have been shown to occupy different thermal niches in the field (Buitenhuis et al., 2012). One could argue that culturing conditions may have led to a genetic adaptation and a shift in $T_{Opt}$, but we found that *Picochlorum* sp., the tropical strain which has been in culture the longest, shows the strongest deviation (>9°C) from its permanent culturing temperature. Contrary to our results, a study, in which an optimum function was used to obtain temperature-related parameters for 194 different strains of phytoplankton, found that $T_{Opt}$ follows an unimodal function of latitude and annual mean temperature of isolation (Thomas et al., 2012). We may not have found this trend in our data because of the much smaller number of data points we could obtain. However, they also find that $T_{Opt}$ shows considerable deviations from the annual mean temperature in polar and temperate waters, which suggests that $T_{Opt}$ is not the ultimate parameter controlling the distribution. Peak *in situ* abundances of different phytoplankton groups are not found at optimum temperatures, because of the combination of fluctuations in local temperature and the sharp drop in growth rates above $T_{Opt}$.

The temperature span at which growth was positive for individual strains in our study is comparable to their *in situ* distribution. Peak *in situ* abundances of *Prochlorococcus* sp. were reported at both lower (19°C) and higher temperatures (25–28°C) than their optimum temperature (Zinser et al., 2007) with strong inhibition above 28°C (Moore et al., 1995). The upper limit of the temperature span for the *Prochlorococcus* sp. strains presented here is consistent with those results, and the lower limit of the temperature span is consistent with the results of Kulk et al. (2012). We show that some picoeukaryotes grow over a wider span of temperatures than the smaller picoprokaryotes. However, we do not find a direct correlation between $\Delta T$ and latitude of isolation, which is in agreement with the study by Thomas et al. (2012). Instead, we find evidence that $\Delta T$, is significantly correlated with picophytoplankton cell size and can be represented by a unimodal function. The bigger picoprokaryote *Synechococcus* sp. grew over a wider span of temperatures than the smaller *Prochlorococcus* sp., consistent with earlier studies (Moore et al., 1995; Malinsky-Rushansky et al., 2002; Mackey et al., 2013). Also, the picoeukaryotes of an intermediate size ($\sim 2\,\mu m$) had a higher $\Delta T$ than other-sized members of the group. Together with the higher maximum growth rates of this intermediate size class (Bec et al., 2008) we suggest that their relatively high temperature tolerance range may contribute to their ubiquitous distribution. However, cell size and its variability would explicitly need to be measured over the full range of temperatures to gain a better understanding of this relationship.

We also find that a higher optimum growth rate is achieved by picophytoplankton strains with a high temperature tolerance range. In practice this would favor generalists in the field rather than allowing the coexistence of several specialist strains in different niche spaces. A field study has shown that 90% of analyzed gene sequences of picoeukaryotes can be attributed to Prasinophyceae, of which *M. pusilla*, an intermediate sized picoeukaryote, is an important member, with higher contributions in temperate and polar areas (Vaulot et al., 2008). In agreement with these results, we show that *M. pusilla* has a relatively high temperature tolerance range and a relatively high optimum growth rate. However, the study by Vaulot et al. (2008) was biased toward coastal areas and other factors such as light, nutrients, and water column stratification also need to be considered, especially in the open and oligotrophic ocean when investigating the community structure (Johnson et al., 2006; Bouman et al., 2011).

## Temperature-Response of Picophytoplankton

In agreement with the second hypothesis formulated by Eppley (1972), our results show that the maximum growth rates for the group of picophytoplankton in response to temperature are best represented by an exponential function (**Table 2**,

**Figure 3**). This representation is also appropriate for the group of picoprokaryotes alone (**Table 2**). Hence, for the calculation of the absolute maximum growth rates of these two groups we follow the approach by Bissinger et al. (2008), who confirmed the $Q_{10}$ (1.88) estimated by Eppley (1972) for a mixed phytoplankton group. Our results show that for a group of picophytoplankton the temperature-dependence is higher and for a group of picoprokaryotes more than twice as high (**Table 4**, **Figure 3**, Equations 6, 7) as for this group of mixed phytoplankton. These results are in agreement with recent studies on picophytoplankton, which found a higher $Q_{10}$ value for picophytoplankton compared to larger species (Chen et al., 2014) and also higher values for picoprokaryotes (3.6–4.4) than for picoeukaryotes (1.7–2) (Kulk et al., 2012). It should be noted that the variance in the data increases with temperature, which could bias the statistical results at small sample size. We found that the main contributor to the increase in variance is the interspecific variation of $\mu_{opt}$. However, the average squared residuals have a quite similar distribution as a function of temperature for the three functions. In addition, our sample size of 224 growth rates is large, so that the increase in variance would not bias the results, and we conclude that the comparison of Delta AIC to decide which function fits the data best seems valid despite the increase in variance with temperature in the observations.

The fit to the absolute maximum growth rates of the group of picophytoplankton in response to temperature presented in our study is lower than the fit presented in Eppley (1972). This can be explained by the generally lower maximum growth rates of picophytoplankton compared to those of other phytoplankton groups, e.g., diatoms (Furnas, 1990). The study by Eppley (1972) contained various groups of faster-growing phytoplankton and a substantial number of diatoms (43%). However, Bissinger et al. (2008) showed that a higher proportion of diatoms (68%) would not affect the fit. It is unclear, though, how high the proportion of picophytoplankton was in the database used in Bissinger et al. (2008). The lower absolute maximum growth rates and the higher $Q_{10}$ of the picophytoplankton examined here compared to mixed phytoplankton highlight the importance of quantifying the response of different phytoplankton groups to temperature individually. Especially in ocean regions where picoprokaryotes dominate the phytoplankton biomass, the influence of their higher $Q_{10}$ must be considered when modeling the response of the phytoplankton community to increased temperature as a consequence of climate warming.

We find that the group of picoeukaryotes grow over a wider span of temperatures than the smaller picoprokaryotes. Although our sample size of picoeukaryote species is larger than of picoprokaryote species, and we therefore have to be cautious about the interpretation of the wider temperature span of the picoeukaryotes as a group, these sample sizes reflect the diversity in the ocean of the two groups of picophytoplankton. Picoeukaryotes are spread across 12 classes in 4 divisions while there is only one class of picoprokaryotes (Vaulot et al., 2008). In addition, it is well established that picoeukaryotes dominate picophytoplankton biomass in colder waters at latitudes above 40° and have similar biomass at lower latitudes, but the smaller picoprokaryotes are more restricted toward warmer (sub-)tropical ocean waters (Buitenhuis et al., 2012). We therefore suggest that the difference in temperature span between the two groups could be real.

Our results further show that the exponential fit to the optimum growth rates only of all examined strains is lower than the fit to the upper 99th quantile of their maximum growth rates. This is because the maximum growth rates of faster-growing species at sub-optimum temperatures are higher than the optima of slower growing species. The fit through the optima was initially presented as an alternative method for representing the response of the absolute maximum growth rates of a phytoplankton community to temperature by Eppley (1972, Figure 2). However, more data of picophytoplankton strains with optima at lower temperatures would need to be included to distinguish better between these two methods of deriving the absolute maximum growth rates of a phytoplankton community.

## Temperature and the Chlorophyll *a* to Carbon Ratio

Phytoplankton acclimate to the prevailing environmental conditions by changing their cell composition. The chlorophyll *a* to carbon ratio is an important variable for measuring biomass and primary production and varies between different phytoplankton groups, e.g., diatoms have higher chlorophyll *a* to carbon ratios compared to picophytoplankton (Geider et al., 1997). In agreement with previous studies (Eppley, 1972; Geider, 1987) we show that with increasing temperature the chlorophyll *a* to carbon ratio also increases for the group of picophytoplankton. We also show that this effect on the chlorophyll *a* to carbon ratio is caused by the increase in chlorophyll a concentration with temperature, rather than by a potential decrease of cellular carbon.

We also indicate a drop above the optimum temperature for some individual strains. This reduction in photosynthetic machinery at supra-optimal temperatures is comparable to the effect caused by photoinhibition at high light levels to reduce damage (Geider, 1987) and is thus consistent with the photosynthetic model of Baumert and Petzoldt (2008), which attributes the decrease of growth rate above $T_{Opt}$ to an increase in light inhibition with temperature.

## Picophytoplankton and Climate Warming

Picophytoplankton, including both groups of picoprokaryotes and picoeukaryotes, is treated as a single plankton functional type in ocean biogeochemical models (Le Quéré et al., 2015). Hence, the assumption is that it can be represented with a common set of physiological traits. Generally, there is some support for this assumption, as both groups of picophytoplankton are adapted to low nutrient and light conditions because of their high nutrient uptake and light harvesting efficiency compared to other phytoplankton groups (Raven, 1998). Both adaptations could help to explain their better success in oligotrophic (Alvain et al., 2008) and deep mixed water columns (Veldhuis et al., 2005). However, the distribution of picoprokaryotes is inversely related to that of picoeukaryotes in the natural environment (Buitenhuis et al., 2012), and these distributions are correlated with nitrogen concentration and depth of the euphotic layer

(Bouman et al., 2011). In addition, temperature was also shown to be an important predictor for the realized ecological niche space of diverse phytoplankton groups (Brun et al., 2015). The temperature span at which growth was positive for *Prochlorococcus* sp. presented in our study is consistent with the quartile temperature span of the realized ecological niche (16–25°C) in the study by Brun et al. (2015) which uses observations from MAREDAT (Buitenhuis et al., 2013). Unfortunately, they were not yet able to specifically separate the realized ecological niche of picophytoplankton due to the lack of available data on a broader range of species. Our study highlights the importance of quantifying the direct impact of each temperature-related parameter for a large variety of phytoplankton strains to define fundamental ecological niches, which are required for the formulation of ocean biogeochemistry models (Le Quéré et al., 2005), and which aim to represent realized ecological niches as emergent properties (Follows et al., 2007).

With ongoing climate warming, the biomass and productivity of picophytoplankton relative to other phytoplankton could increase due to enhanced water column stratification and lower nutrient availability (Behrenfeld et al., 2006; Morán et al., 2010). The results presented here support a potential advantage for picophytoplankton as a consequence of the higher temperature dependence of their maximum growth rates compared to other phytoplankton groups. Picophytoplankton shows a stronger increase in absolute maximum growth rates with temperature with a $Q_{10}$ of 2.3 compared to coccolithophores with a $Q_{10}$ of 1.7 (Buitenhuis et al., 2008), and a mixed phytoplankton community with a $Q_{10}$ of 1.88 (Eppley, 1972). However, the relative advantage of the temperature dependence of the absolute maximum growth rates of picophytoplankton also needs to be considered within an ecosystem with trophic interactions in a warming climate, where the effect of temperature on the top down control by zooplankton may also alter the phytoplankton community structure.

In addition, we suggest that climate warming may also change the composition of the picophytoplankton community itself. Even though picoprokaryotes may show a stronger increase in biomass in specific regions due to their higher $Q_{10}$, they are restricted by a narrower temperature tolerance range. The sharp decrease of maximum growth rates above the optimum temperature suggest that the temperature tolerance range is also an influential parameter for the distribution of phytoplankton species and its change with climate warming. We therefore assume that picoprokaryotes will be shifted to higher latitudes or depth. This shift has already been suggested using a neural network model which defines niches of two picoprokaryotes based on temperature, PAR and nutrient availability (Flombaum et al., 2013). However, we also suggest that picoeukaryotes, in particular those of an intermediate size around 2 μm, will be able to increase their contribution to phytoplankton biomass over a wider temperature span.

## AUTHORS CONTRIBUTIONS

BS conducted the laboratory experiments, analyzed the data, and is the lead author on this paper. EB and CL wrote the project proposal, acquired funding, and put forward some of the hypotheses. All authors co-wrote the manuscript.

## FUNDING

The research leading to these results has received funding from the European Community's Seventh Framework Programme (FP7 2007-2013) under grant agreements n° 238366 (Greencycles II) and 282672 (EMBRACE), and the Natural Environment Research Council grant n° NE/K001302/1(i-MarNet).

## SUPPLEMENTARY MATERIAL

The Supplementary Material for this article can be found online at: http://journal.frontiersin.org/article/10.3389/fmars.2016.00164

## REFERENCES

Agawin, N., Duarte, C. M., and Agustí, S. (2000). Nutrient and temperature control of the contribution of picoplankton to phytoplankton biomass and production. *Limnol. Oceanogr.* 45, 591–600. doi: 10.4319/lo.2000.45.3.0591

Alvain, S., Moulin, C., Dandonneau, Y., and Breon, F. (2005). Remote sensing of phytoplankton groups in case 1 waters from global seaWiFS imagery. *Deep Sea Res. Part I Oceanogr. Res. Pap.* 52, 1989–2004. doi: 10.1016/j.dsr.2005.06.015

Alvain, S., Moulin, C., Dandonneau, Y., and Loisel, H. (2008). Seasonal distribution and succession of dominant phytoplankton groups in the global ocean: a satellite view. *Glob. Biogeochem. Cycles* 22, 1–15. doi: 10.1029/2007GB003154

Anderson, R. A. (2005). *Algal Culturing Techniques*. San Diego, CA: Elsevier Academic Press.

Azam, F., Fenchel, T., Field, J. G., Gra, J. S., and Thingstad, F. (1983). The ecological role of water-column microbes in the sea. *Mar. Ecol. Prog. Ser.* 10, 257–263.

Baumert, H. Z., and Petzoldt, T. (2008). The role of temperature, cellular quota and nutrient concentrations for photosynthesis, growth and light–dark acclimation in phytoplankton. *Limnologica Ecol. Manag. Inland Waters* 38, 313–326. doi: 10.1016/j.limno.2008.06.002

Bec, B., Collos, Y., Vaquer, A., Mouillot, D., and Souchu, P. (2008). Growth rate peaks at intermediate cell size in marine photosynthetic picoeukaryotes. *Limnol. Oceanogr.* 53, 863–867. doi: 10.4319/lo.2008.53.2.0823

Behrenfeld, M. J., O'Malley, R. T., Siegel, D. A., McClain, C. R., Sarmiento, J. L., Feldman, G. C., et al. (2006). Climate-driven trends in contemporary ocean productivity. *Nature* 444, 752–755. doi: 10.1038/nature05317

Berges, J. A., Franklin, D., and Harrison, P. J. (2001). Evolution of an artificial seawater medium: improvements in enriched seawater, artificial water over the last two decades. *J. Phycol.* 37, 1138–1145. doi: 10.1046/j.1529-8817.2001.01052.x

Bissinger, J. E., Montagnes, D. J. S., Sharples, J., and Atkinson, D. (2008). Predicting marine phytoplankton maximum growth rates from temperature: improving on the eppley curve using quantile regression. *Limnol. Oceanogr.* 53, 487–493. doi: 10.4319/lo.2008.53.2.0487

Bouman, H., Ulloa, O., Barlow, R., Li, W. K. W., Platt, T., Zwirglmaier, K., et al. (2011). Water-column stratification governs the community structure of subtropical marine picophytoplankton. *Environ. Microbiol. Rep.* 241, 1–10. doi: 10.1111/j.1758-2229.2011.00241.x

Brun, P., Vogt, M., Payne, M. R., Gruber, N., O'Brien, C. J., Buitenhuis, E. T., et al. (2015). Ecological niches of open ocean phytoplankton taxa. *Limnol. Oceanogr.* 60, 1020–1038. doi: 10.1002/lno.10074

Buitenhuis, E. T., Li, W. K. W., Vaulot, D., Lomas, M. W., Landry, M. R., Partensky, F., et al. (2012). Picophytoplankton biomass distribution in the Global Ocean. *Earth Syst. Sci. Data* 4, 37–46. doi: 10.5194/essd-4-37-2012

Buitenhuis, E. T., Pangerc, T., Franklin, D., Le Quéré, C., and Malin, G. (2008). Growth rates of six coccolithophorid strains as a function of temperature. *Limnol. Oceanogr*. 53, 1181–1185. doi: 10.4319/lo.2008.53.3.1181

Buitenhuis, E. T., Vogt, M., Moriarty, R., Bednaršek, N., Doney, S. C., Leblanc, K., et al. (2013). MAREDAT: towards a world atlas of MARine ecosystem DATa. *Earth Syst. Sci. Data* 5, 227–239. doi: 10.5194/essd-5-227-2013

Burnham, K. P., and Anderson, D. R. (1998). "Akaike's information criterion," in *Model Selection and Multimodel Inference: A Practical Information-Theoretic Approach,* (New York, NY: Springer Verlag), 42–49. doi: 10.1007/978-1-4757-2917-7_1

Chen, B., Liu, H., Huang, B., and Wang, J. (2014). Temperature effects on the growth rate of marine picoplankton. *Mar. Ecol. Prog. Ser*. 505, 37–47. doi: 10.3354/meps10773

Chisholm, S. W., Frankel, S. L., Goericke, R., Olson, R., Palenik, B., Waterbury, J. B., et al. (1992). *Prochlorococcus marinus* Nov. Gen. Nov. Sp.: an oxyphototrophic marine prokaryote containing divinyl chlorophyll a and b. *Arch. Microbiol*. 157, 297–300. doi: 10.1007/BF00245165

Cho, S. H., Ji, S.-C., Hur, S. B., Bae, J., Park, I.-S., and Song, Y.-C. (2007). Optimum temperature and salinity conditions for growth of green algae chlorella ellipsoidea and nannochloris oculata. *Fish. Sci*. 73, 1050–1056. doi: 10.1111/j.1444-2906.2007.01435.x

Eppley, R. (1972). Temperature and phytoplankton growth in the sea. *Fish. Bull.* 70, 1063–1085.

Fenchel, T. (2008). The microbial loop – 25 years later. *J. Exp. Mar. Biol. Ecol*. 366, 99–103. doi: 10.1016/j.jembe.2008.07.013

Flombaum, P., Gallegos, J. L., Gordillo, R. A., Rincón, J., Zabala, L. L., and Jiao, N. (2013). Present and future global distributions of the marine cyanobacteria *Prochlorococcus* and *Synechococcus*. *Proc. Natl. Acad. Sci. U.S.A.* 110, 9824–9829. doi: 10.1073/pnas.1307701110

Follows, M. J., Dutkiewicz, S., Grant, S., and Chisholm, S. W. (2007). Emergent biogeography of microbial communities in a Model Ocean. *Science* 315, 1843–1846. doi: 10.1126/science.1138544

Furnas, M. J. (1990). *In situ* growth rates of marine phytoplankton: approaches to measurement, community and species growth rates. *J. Plankton Res*. 12, 1117–1151. doi: 10.1093/plankt/12.6.1117

Geider, R. J. (1987). Light and temperature dependence of the carbon to chlorophyll a ratio in microalgae and cyanobacteria: implications for physiology and growth of phytoplankton. *New Phytol*. 106, 1–34. doi: 10.1111/j.1469-8137.1987.tb04788.x

Geider, R. J., MacIntyre, H. L., and Kana, T. M. (1997). Dynamic model of phytoplankton growth and acclimation:responses of the balanced growth rate and the chlorophyll a:carbon ratio to light, nutrient-limitation and temperature. *Mar. Ecol. Prog. Ser*. 148, 187–200. doi: 10.3354/meps148187

Grossman, A. R., Mackey, K. R. M., and Bailey, S. (2010). A perspective on photosynthesis in the oligotrophic oceans: hypotheses concerning alternate routes of electron flow1. *J. Phycol.* 46, 629–634. doi: 10.1111/j.1529-8817.2010.00852.x

Guillou, L., Chrétiennot-Dinet, M. J., Medlin, L. K., Claustre, H., Loiseaux-de Goer, S., and Vaulot, D. (1999). Bolidomonas: a new genus with two species belonging to a new algal class, the Bolidophyceae (Heterokonta). *J. Phycol.* 35, 368–381.

Hashimoto, S., and Shiomoto, A. (2000). Comparison of GF/F filters and 0.2 and 0.6 μM nuclepore filters on the chlorophyll a retention. *Bull. Nat. Res. Inst. Far Seas Fish.* 37, 45–48.

Ichinomiya, M., dos Santos, A. L., Gourvil, P., Yoshikawa, S., Kamiya, M., Ohki, K., et al. (2016). Diversity and oceanic distribution of the parmales (Bolidophyceae), a picoplanktonic group closely related to diatoms. *ISME J. Int. Soc. Microb. Ecol.* doi: 10.1038/ismej.2016.38. [Epub ahead of print].

Johnson, Z. I., Zinser, E. R., Coe, A., McNulty, N. P., Woodward, E. M. S., and Chisholm, S. W. (2006). Niche partitioning among Prochlorococcus ecotypes along ocean-scale environmental gradients. *Science* 311, 1737–1740. doi: 10.1126/science.1118052

Koenker, R. (2006). *Quantreg: Quantile Regression R Software Version 4.02.*

Kulk, G., de Vries, P., van de Poll, W., Visser, R., and Buma, A. (2012). Temperature-dependent growth and photophysiology of prokaryotic and eukaryotic oceanic picophytoplankton. *Mar. Ecol. Prog. Ser*. 466, 43–55. doi: 10.3354/meps09898

Le Quéré, C., Buitenhuis, E. T., Moriarty, R., Alvain, S., Aumont, O., Bopp, L., et al. (2015). Role of zooplankton dynamics for southern ocean phytoplankton biomass and global biogeochemical cycles. *Biogeosci. Discuss.* 12, 11935–11985. doi: 10.5194/bgd-12-11935-2015

Le Quéré, C., Harrison, S., Prentice, C., Buitenhuis, E. T., Aumont, O., Bopp, L., et al. (2005). Ecosystem dynamics based on plankton functional types for global ocean biogeochemistry models. *Glob. Change Biol.* 11, 2016–2040. doi: 10.1111/j.1365-2486.2005.01004.x

López-Urrutia, Á., and Morán, X. A. G. (2015). Temperature affects the size-structure of phytoplankton communities in the ocean. *Limnol. Oceanogr.* 60, 733–738. doi: 10.1002/lno.10049

Mackey, K. R. M., Paytan, A., Caldeira, K. R., Grossman, A., Moran, D., McIlvin, M., et al. (2013). Effect of temperature on photosynthesis and growth in marine Synechococcus Spp. *Plant Physiol.* 163, 815–829. doi: 10.1104/pp.113.221937

Malinsky-Rushansky, N., Berman, T., Berner, T., Yacobi, Y. Z., and Dubinsky, Z. (2002). Physiological characteristics of picophytoplankton, isolated from lake kinneret: responses to light and temperature. *J. Plankton Res.* 24, 1173–1183. doi: 10.1093/plankt/24.11.1173

Marañón, E., Cermeño, P., Huete-Ortega, M., López-Sandoval, D. C., Mouriño-Carballido, B., and Rodríguez-Ramos, T. (2014). Resource supply overrides temperature as a controlling factor of marine phytoplankton growth. *PLoS ONE* 9:e99312. doi: 10.1371/journal.pone.0099312

Marie, D., Simon, N., and Vaulot, D. (2005). "Phytoplankton cell counting by flow cytometry," in *Algal Culturing Techniques, edited by Robert Andersen and Provasoli-Guillard,* ed R. A. Andersen (West Boothbay Harbor, ME: Elsevier/Academic Press), 253–556.

Michaels, A. F., and Silver, M. W. (1988). Primary production, sinking fluxes and the microbial food web. *Deep Sea Res.* 35, 473–490. doi: 10.1016/0198-0149(88)90126-4

Mitchell-Olds, A. T., and Shaw, R. G. (1987). Regression analysis of natural selection: statistical inference and biological interpretation. *Evolution* 41, 1149–61.

Montagnes, D. J. S., Kimmance, S. A., and Atkinson, D. (2003). Using Q 10: can growth rates increase linearly with temperature? *Aquat. Microb. Ecol.* 32, 307–313. doi: 10.3354/ame032307

Moore, L. R., Goericke, R., and Chisholm, S. W. (1995). Comparative physiology of Synechococcus and Prochlorococcus: influence of light and temperature on growth, pigments, fluorescence and absorptive properties. *Mar. Ecol. Prog. Ser.* 116, 259–275. doi: 10.3354/meps116259

Morán, X. A. G., López-Urrutia, Á., Calvo-Díaz, A., and Li, W. K. W. (2010). Increasing importance of small phytoplankton in a Warmer Ocean. *Glob. Change Biol.* 16, 1137–1144. doi: 10.1111/j.1365-2486.2009.01960.x

Mousing, E. A., Ellegaard, M., and Richardson, K. (2014). Global patterns in phytoplankton community size structure—evidence for a direct temperature effect. *Mar. Ecol. Prog. Ser.* 497, 25–38. doi: 10.3354/meps10583

Parson, T. R., Maita, Y., and Lalli, C. M. (1984). *A Manual of Chemical and Biological Methods for Seawater Analysis. Chapter 4 Plant Pigments*. Oxford: Pergamon Press.

Polovina, J. J., Howell, E. A., and Abecassis, M. (2008). Ocean's least productive waters are expanding. *Geophys. Res. Lett.* 35, L03618. doi: 10.1029/2007GL031745

Raven, J. (1998). The twelfth tansley lecture. small is beautiful: the picophytoplankton. *Funct. Ecol.* 12, 503–513. doi: 10.1046/j.1365-2435.1998.00233.x

Raven, J., and Geider, R. J. (1988). Temperature and algal growth. *New Phytol.* 110, 441–461. doi: 10.1111/j.1469-8137.1988.tb00282.x

Sarmiento, J. L. (2004). Response of ocean ecosystems to climate warming. *Glob. Biogeochem. Cycles* 18:3003. doi: 10.1029/2003GB002134

Stawiarski, B. (2014). *The Physiological Response of 7 strains of Picophytoplankton to Light, Temperature and Nutrients, Including Climate Change Model Simulations.* Ph.D. thesis, University of East Anglia. Available online at: http://ethos.bl.uk/OrderDetails.do?uin=uk.bl.ethos.656091

Thomas, M. K., Kremer, C. T., Klausmeier, C. A., and Litchman, E. (2012). A global pattern of thermal adaptation in marine phytoplankton. *Science* 338, 1085–1088. doi: 10.1126/science.1224836

Throndsen, J. (1976). Occurance and productivity of small marine flagellates. *Nor. J. Bot.* 23, 269–293.

Vaulot, D., Eikrem, W., Viprey, M., and Moreau, H. (2008). The diversity of small eukaryotic phytoplankton ($< 3\,\mu m$) in marine ecosystems. *FEMS Microbiol. Rev.* 32, 795–820. doi: 10.1111/j.1574-6976.2008.00121.x

Vaulot, D., Le Gall, F., Marie, D., Guillou, L., and Partensky, F. (2004). The Roscoff Culture Collection (RCC): a collection dedicated to marine picoplankton. *Nova Hedwigia* 79, 49–70. doi: 10.1127/0029-5035/2004/0079-0049

Veldhuis, M., Timmermans, K., Croot, P., and Vanderwagt, B. (2005). Picophytoplankton; a Comparative study of their biochemical composition and photosynthetic properties. *J. Sea Res.* 53, 7–24. doi: 10.1016/j.seares.2004.01.006

Zinser, E. R., Johnson, Z. I., Coe, A., Karaca, E., Veneziano, D., and Chisholm, S. W. (2007). Influence of light and temperature on Prochlorococcus ecotype distributions in the Atlantic Ocean. *Limnol. Oceanogr.* 52, 2205–2220. doi: 10.4319/lo.2007.52.5.2205

**Conflict of Interest Statement:** The authors declare that the research was conducted in the absence of any commercial or financial relationships that could be construed as a potential conflict of interest.

frontiers in Marine Science

ORIGINAL RESEARCH
published: 14 October 2016
doi: 10.3389/fmars.2016.00194

# *In situ* Measurements and Model Estimates of $NO_3$ and $NH_4$ Uptake by Different Phytoplankton Size Fractions in the Southern Benguela Upwelling System

*J. Ffion Atkins*[1]*, *Coleen L. Moloney*[2], *Trevor A. Probyn*[3] and *Stewart Bernard*[1,4]

[1] Department of Oceanography, Marine Research Institute, University of Cape Town, Cape Town, South Africa, [2] Department of Biological Sciences, Marine Research Institute, University of Cape Town, Cape Town, South Africa, [3] Department of Agriculture, Forestry and Fisheries, Cape Town, South Africa, [4] Council for Scientific and Industrial Research, Cape Town, South Africa

Bulk measurements can be made of phytoplankton standing stocks on a quasi-synoptic scale but it is more difficult to measure rates of production and nutrient uptake. We present a method to estimate nitrogen uptake rates in productive coastal environments. We use observed phytoplankton cell size distributions and ambient nitrogen concentrations to calculate uptake rates of nitrate, ammonium and total nitrogen by different size fractions of diverse phytoplankton communities in a coastal upwelling system. The data are disaggregated into size categories, uptake rates are calculated and these uptake rates are reaggregated to obtain bulk estimates. The calculations are applied to 72 natural assemblages for which nitrogen uptake rates and particle size distributions were measured *in situ*. The calculated values of total N uptake integrated across all size classes are similar to those of *in situ* bulk measurements (N slope = 0.90), ($NH_4$ slope = 0.96) indicating dependence of $NH_4$ and total N uptake on ambient N concentrations and cell size distributions of the phytoplankton assemblages. $NO_3$ uptake was less well explained by cell size and ambient concentrations, but regressions between measured and estimated rates were still significant. The results suggest that net nitrogen dynamics can be quantified at an assemblage scale using size dependencies of Michaelis-Menten uptake parameters. These methods can be applied to particle size distributions that have been routinely measured in eutrophic systems to estimate and subsequently analyse variability in nitrogen uptake.

**Keywords: phytoplankton, diversity, allometry, nitrogen uptake, particle size distributions**

OPEN ACCESS

***Edited by:***
*Dag Lorents Aksnes, University of Bergen, Norway*

***Reviewed by:***
*Kyle Edwards, University of Hawaii at Manoa, USA*
*S. Lan Smith, Japan Agency for Marine-Earth Science and Technology, Japan*

***Correspondence:**
*Ffion Atkins*
*ffion.atkins@gmail.com*

***Specialty section:***
*This article was submitted to Marine Ecosystem Ecology, a section of the journal Frontiers in Marine Science*

***Received:*** *30 July 2016*
***Accepted:*** *23 September 2016*
***Published:*** *14 October 2016*

***Citation:***
*Atkins JF, Moloney CL, Probyn TA and Bernard S (2016) In situ Measurements and Model Estimates of $NO_3$ and $NH_4$ Uptake by Different Phytoplankton Size Fractions in the Southern Benguela Upwelling System Front. Mar. Sci. 3:194. doi: 10.3389/fmars.2016.00194*

## 1. INTRODUCTION

The diversity of phytoplankton communities influences the flows of carbon, nitrogen and other important elements through the marine environment. Marine ecosystem models that aim to capture this relationship represent phytoplankton diversity either by different functional groups (Follows and Dutkiewicz, 2011), cell size (e.g., Moloney et al., 1991; Baird and Suthers, 2007; Banas, 2011; Ward et al., 2012) or by both (Le Quéré et al., 2005). Our understanding of the

consequences of this diversity on global biogeochemistry is still limited (Lomas et al., 2014). In a broad ecological context, in addition to taxonomic distinction, the term diversity currently includes functionality within an environment (Tilman, 2001; McGill et al., 2006; Westoby and Wright, 2006; Litchman et al., 2007). A challenge in biogeochemical modeling is to try account for diversity among organisms and its role in nutrient flux (Follows and Dutkiewicz, 2011), plasticity in organism traits (Pahlow and Oschlies, 2009), trade-offs in energy expenditure and the relationships between physiological traits and environmental forcing (Aksnes and Cao, 2011). The most commonly used function to model nutrient uptake is the Michaelis-Menten equation and parameter values for maximum uptake rates ($V_{max}$) and half saturation constants ($K_s$) are widely available in the literature (see Litchman et al., 2015), often resolved at the species level in batch/continuous cultures (e.g., Eppley et al., 1969) and see Edwards et al. (2014) and typically at a genus level from natural populations (see Collos et al., 2005). The variation in $V_{max}$ and $K_s$ within phytoplankton groups and in relation to cell size were extensively reviewed by Litchman et al. (2007) and Edwards et al. (2012), where large variation was evident between and within phylogenetic groups. $K_s$ values, for example, were found to vary over two orders of magnitude for a given group (Collos et al., 2005; Franks, 2009; Seeyave et al., 2009; Aksnes and Cao, 2011). Collos et al. (2005) found strong genus-specific differences in $K_s$ between *Thalassiosira* and *Chaetoceros*, both diatoms, under similar nutrient levels. Absolute values of $V_{max}$ and their range are highest in diatoms, whereas $K_s$ values are highest in dinoflagellates (Litchman et al., 2007; Edwards et al., 2012). The paucity of $K_s$ values to account for all genotypic diversity in natural assemblages, under variable environmental conditions, as well as computational costs, has meant that $K_s$ is often regarded a constant. The assumption that these parameter values are invariant within phylogenetic groups has been highlighted as a potential source of error when parameterizing nutrient uptake by Michaelis-Menten kinetics (Franks, 2009).

Several studies have aimed to quantify the dynamic physiological response of phytoplankton cells to changing environmental conditions (e.g., Smith and Yamanaka, 2007; Pahlow et al., 2008; Bonachela et al., 2011; Smith et al., 2011) and have improved our conceptual understanding of cellular constraints on nutrient uptake and growth. Such dynamic trait-based approaches have been incorporated into large-scale modeling studies (Arteaga et al., 2014), with improved agreement between *in situ* values and model output (Smith et al., 2015). In many situations, the necessary *in situ* data are not available to constrain the dynamic response of a diverse, natural assemblage within a realistic, local context. Relatively simple size-based models can adequately replicate large scale dynamics of nitrogen in the marine environment (Ward et al., 2012; Acevedo-Trejos et al., 2014) with the advantage of reducing the number of free parameters, and thus model uncertainty, by using size-scaling exponents (Baird and Suthers, 2007; Banas, 2011; Ward et al., 2012). The size structure of plankton assemblages and the dominant size fraction will dictate, to some degree, the pathways of nutrients and how they are transferred to higher trophic levels (Probyn et al., 1990; Moloney et al., 1991; Chisholm, 1992; van der Lingen et al., 2006). Litchman et al. (2007) found strong empirical relationships between organism size and physiological rates ($V_{max}$ and $K_s$) and considered cell size a master trait. Our understanding of the variability in uptake kinetic parameters in relation to community composition and environmental variability is poor, and there is a need for field-based and laboratory studies of physiological processes of phytoplankton groups (Gregg et al., 2003; Litchman et al., 2007; Allen and Fulton, 2010).

This study hypothesized that some of the variance in Michaelis-Menten parameter values can be accounted for by considering the size spectra of the phytoplankton populations. To test such an hypothesis, we used measured particle size distributions (from Beckman Coulter Counter data) to calculate sets of theoretical, size-based biomass and Michaelis-Menten parameters for different field samples. We applied ambient nitrogen concentrations from each sample to Michaelis-Menten models to estimate size-based nitrogen uptake rates and integrated these across all sizes for the sample. These calculated rates were subsequently compared to measured *in situ* bulk uptake rates to estimated uptake rates of $NO_3$, $NH_4$ and total N (total N = $NO_3$ + $NH_4$ ). This research offers a tool to extend the application of pre-existing particle cell size distributions, relying on robust assumptions of the size dependence of nitrogen metabolism.

# 2. METHODS

## 2.1. *In situ* Data Collection

Data from three separate case studies were used, data from Lamberts Bay were taken from a fixed station (32°05.020′S, 18°16.010′E) at 0 m, 3.5 km off Lamberts Bay, as daily samples during the periods 25 February–11 March 2004 and 15 March–6 April 2005. In Saldanha Bay, sampling took place at a fixed station (33°01.748′ S, 18°00.888′ E) from 0, 3, 6, and 9 m, every 2 months for a period of 3 days from January 2012 to January 2013. Water samples were collected using a 5 L Niskin water sampler and stored in 20 L black buckets, which were then transported to the laboratory within 1–2 h of collection for the determinations of particle size distributions, nutrient concentrations, $^{15}N$ uptake and particulate nitrogen calculations. Methods employed in all three case studies were consistent, unless stipulated otherwise. Data from the different systems within the Benguela ecosystem were chosen to try obtain a good spread in biomass and uptake rate values.

### 2.1.1. Cell Size Distributions and Community Structure

Particle size distributions (PSDs) of samples were measured using a Beckman Multisizer 4 Coulter Counter. A discrete sample volume of 40 mL was used to count particles per size class and was blank corrected by 0.2 $\mu$m filtered seawater. An aperture size of 140 $\mu$m was used, with a capacity to measure particles from 2 to 86 $\mu$m. Confidence in measurements below 5 $\mu$m is significantly reduced, and thus such values are omitted from

particle size spectra. Dominant species were identified using inverted microscopy following Utermohl (1958).

#### 2.1.2. $^{15}$N Uptake

One liter from each sample was spiked with $^{15}$N-labeled $NH_4Cl$ or $NaNO_3$ (BOC Limited, isotope assay 99%) in acid-cleaned polycarbonate bottles. Spike concentrations were approximately 0.1 $\mu$mol $^{15}$N $L^{-1}$ for $NH_4$ and varied between 0.04 and 2 $\mu$mol $^{15}$N $L^{-1}$ for $NO_3$, depending on estimations of *in situ* $NO_3$ concentrations from temperature. Incubations were carried out *in situ* at the corresponding depth of collection, using a custom-made rig for 4 h in Lamberts Bay and for 24 h in Saldanha Bay. The differences between the two incubation times has been accounted for by scaling the 4 h incubations to 24 h. The assumption was made that daylight was 14 h and that uptake during the night was 55% of daylight rate for $NH_4$ and 12% of daylight rate of $NO_3$ uptake, as measured at in-shore locations in Probyn et al. (1996). Incubations were terminated by filtration onto Whatman GF/F filters approximately 30 min after retrieval. Filters were rinsed with artificial seawater and Milli-Q to flush dissolved isotopes from the filter matrix and dried at 75°C overnight before storage. Nitrogen uptake rates were calculated using post-incubation particulate N concentrations, which accounts for uptake of unlabeled nutrient sources (Dugdale and Wilkerson, 1986). Ammonium uptake rates are not corrected for isotope dilution and thus represent an underestimate. Incubations were terminated by filtration on 47 mm ashed GF/F filters, which were washed with artificial sea water and Milli-Q and then dried at 60°C overnight. Samples were punched out of each filter (disc size depending on organic coverage) and particulate $^{15}$N concentrations were measured on a Finnigan MAT mass spectrometer (Department of Archeometry, University of Cape Town). The filtrate was used for nutrient analysis of ambient concentrations at the end of the incubation.

#### 2.1.3. Nutrient Analyses

Nitrogenous nutrient concentrations were measured manually after filtration through Whatman GF/F filters. All nutrient analyses were initiated immediately on return to the shore within 1.5 h of collection. Ammonium ($NH_4$) was analyzed according to the methods described in Koroleff (1983) scaled down to 5 mL samples, and nitrate ($NO_3$) following the procedure of Nydahl (1976).

### 2.2. Model Setup

Theoretical uptake rates were calculated from measured *in situ* PSDs and ambient nitrogen concentrations. Details of each step are discussed further below. In brief,

1. Measured PSDs were converted to a biomass per size bin by assuming spherical shapes and a volume to nitrogen conversion (Moloney and Field, 1989; Menden-Deuer and Lessard, 2000). The sum of the estimated biomasses per size bin was compared to a corresponding *in situ* measurement of particulate nitrogen (PN).
2. Uptake parameters ($V_{max}$ and $K_s$) were calculated per size bin, using published relationships in Ward et al. (2012). A Michaelis-Menten model was used to estimate absolute uptake rates ($\rho$) of $NO_3$ and $NH_4$ in $\mu$ mol $L^{-1}$ $h^{-1}$ for each size bin, using ambient nutrient concentrations.
3. The sums of the estimated uptake rates per size bin ($\rho$ $NO_3$ and $\rho$ $NH_3$) were compared to corresponding *in situ* uptake measurements. The implications of the assumptions of each step are evaluated in the discussion.

#### 2.2.1. Conversions to Biomass

Measured biomass of particulate nitrogen ($\mu$mol $L^{-1}$) includes all particulate matter down to a cut-off nominal size of 0.7 $\mu$m (GF filter), whereas Coulter Counter measurements have a lower limit of 3 $\mu$m. A comparison between a linear (Moloney and Field, 1989) and non-linear (Menden-Deuer and Lessard, 2000) conversion from cell volume to biomass was carried out. Cellular nitrogen content was calculated per size bin and total biomass per size bin was calculated by multiplying by cell abundance (N) within each size bin. Carbon biomass was also calculated using (Moloney and Field, 1989), as a carbon biomass is required in addition to nitrogen biomass to solve for size-dependent uptake parameters. The non-linear equation follows that of Menden-Deuer and Lessard (2000):

$$logpgNcell^{-1} = -0.928 + 0.849 * logVol \quad (1)$$

Linear conversion follows (Moloney and Field, 1989) where 1 $\mu m^3 = 0.071$ pgC (dry) and 1 $\mu m^3 = 0.0185$ pgN (dry).

#### 2.2.2. Uptake Parameters

Size-dependent uptake parameters, $V_{max}$ ($\mu$molN $\mu$molC$^{-1}$ $h^{-1}$) and $K_s$ ($\mu$molN $L^{-1}$), were calculated per size bin using general allometric equations (aVol$^b$) with values $a$ and $b$ from Ward et al. (2012) (**Table 1** and **Figure 1**). Conversions of units were carried out by normalizing to carbon, calculated using the linear conversion to carbon (Moloney and Field, 1989).

#### 2.2.3. Estimating Uptake Rates

The size-dependent parameters were applied to the Michaelis-Menten equation to calculate nitrogen uptake rate for each size bin, using nitrogen biomass per size bin and ambient nitrogen concentrations. The $NO_3$ taken up by the assemblage was calculated by summing across all size bins:

$$\rho NO_3 = \sum^{size} \left( \frac{V_{max} * PN * NO_3}{NO_3 + K_s} \right) \quad (2)$$

where PN is the nitrogen biomass of the cells per size bin and $NO_3$ to ambient concentration. The corresponding equation was used to calculate $NH_4$ uptake. Estimated uptake rates are compared to the relative measured *in situ* N uptake. The inhibition of $NO_3$ by ambient $NH_4$ concentrations was also incorporated into separate estimations of $\rho NO_3$:

$$\rho NO_3 = \sum^{size} \left( V_{max_{NO_3}} \left( \frac{NO_3}{NO_3 + K_{s_{NO_3}}} \cdot e^{\psi NH_4} \right) \right) \quad (3)$$

Total nitrogen uptake was calculated both with and without an inhibition term, Equation (4) details total N uptake with inhibition:

**TABLE 1 | Parameters and their units used to estimate biomass and uptake rates from measured particle size distributions.**

| Parameter | Symbol | Unit | *a* | *b* | Value |
|---|---|---|---|---|---|
| Cell volume | Vol | $\mu m^3$ | | | |
| Cell abundance per size class | N | cells $L^{-1}$ | | | |
| Mass $cell^{-1}$ per size class | | $\mu$molN $cell^{-1}$ | | | |
| $\sum$ assemblage biomas | | $\mu$molN $L^{-1}$ | | | |
| Maximum uptake rate | $V_{maxNO3}$ | mmol N $mmolC^{-1}$ $h^{-1}$ | 0.51 | −0.27 | |
| | $V_{maxNH4}$ | mmol N $mmolC^{-1}$ $h^{-1}$ | 0.26 | −0.27 | |
| Half saturation constant | $K_{sNO}$ | mmol N $m^{-3}$ | 0.17 | 0.27 | |
| | $K_{sNH4}$ | mmol N $m^{-3}$ | 0.085 | 0.27 | |
| $\sum$ assemblage uptake rate of total N | ρN | $\mu$molN $L^{-1}$ $h^{-1}$ | | | |
| $\sum$ assemblage uptake rate of total $NO_3$ | ρ$NO_3$ | $\mu$molN $L^{-1}$ $h^{-1}$ | | | |
| $\sum$ assemblage uptake rate of total $NH_4$ | ρ$NH_4$ | $\mu$molN $L^{-1}$ $h^{-1}$& | | | |
| Ambient nutrient concentration | $NO_3$, $NH_4$ | $\mu$molN $L^{-1}$ | | | |
| $NH_4$ inhibition parameter | ψ | $\mu$mol $N^{-1}$ | | | 1.99 |

*Where appropriate size-dependent uptake parameters, $V_{max}$ and $K_s$ are calculated as $aVol^b$.*

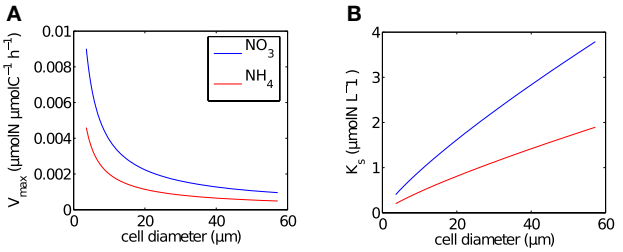


**FIGURE 1 | Size dependence of Michaelis-Menten uptake parameters.** **(A)** Mass-specific maximum uptake rate ($V_{max}$) and **(B)** half saturation constant ($K_S$), calculated using the formulations of Ward et al. (2012) per cell in each size bin for $NO_3$ (blue line ) and $NH_4$ (red line).

$$\rho N = \sum^{size} \left( V_{max_{NO_3}} \left( \frac{NO_3}{NO_3 + K_{s_{NO_3}}} \cdot e^{\psi NH_4} \right) + V_{max_{NH_4}} \left( \frac{NH_4}{NH_4 + K_{s_{NH_4}}} \right) \right) \quad (4)$$

Further comparisons were made between measured, mass-specific uptake rates (v) and non-allometric rates. Mass-specific uptake rates were calculated by dividing the bulk absolute rate by the corresponding measured nitrogen biomass (PN). The non-allometric rates were calculated using a fixed $V_{max}$ and $K_s$ value for all bins along the size spectrum. Sensitivity of the parameter values was tested by comparing the outcome of 9 combinations of realistic values for $NO_3$: $V_{max}$ = [0.1, 0.5, 1] , $K_{max}$ = [0.5, 2, 15]; and $NH_4$: $V_{max}$ = [0.1, 0.5, 1] and $K_s$ = [0.1, 1, 10]. All parameter units and values used are detailed in **Table 1**. Assessments were made between measured and estimated values of uptake rates of $NO_3$, $NH_4$ and total N by using an absolute percentage difference and bias estimates (Zibordi et al., 2004).

# 3. RESULTS

## 3.1. *In situ*

The range of values for measured particulate nitrogen, ambient nitrogen concentrations and uptake rates vary among the three case studies (**Figure 2**). This variability reflects distinct assemblages observed in each case study. Highest values of particulate nitrogen (PN) were observed in Lamberts Bay (LB04 and LB05) relative to Saldanha Bay. LB05 was dominated by a dinoflagellate *Prorocentrum triestinum* with maximum particulate nitrogen reaching 146 $\mu$mol N $L^{-1}$, in association with lowest ambient nitrogen concentrations. SB samples had relatively low biomass (average 10.3 $\mu$mol N $L^{-1}$), almost completely dominated by diatoms. Highest field-measured uptake rates of total nitrogen (**Figure 3A**) and nitrates (**Figure 3B**) were seen in LB04, corresponding to an assemblage dominated by a ciliate (*Myrionecta rubra*) and a diatom (*Skeletonema* spp.) with a maximum of 0.67 $\mu$mol N $L^{-1}h^{-1}$. Rates of $NH_4$ uptake were lower on average than $NO_3$ uptake in all case studies (**Figure 3C**). The size spectra measured were highly variable per sample. **Figures 4A,C,E** show typical size distributions of a low biomass range, and **Figures 4B,D,F** show samples of high biomass, illustrating distributions of bimodality.

## 3.2. Conversions to Biomass

The two methods of conversion from cell volume to mass gave estimates of particulate nitrogen that were significantly correlated with measured *in situ* values (**Figure 5**). For the combined data set (SB and LB), the correlation for the non-linear conversion was $r = 0.78$, $p < 0.005$ and for the linear conversion $r = 0.76$, $p < 0.005$. The two regressions comparing measured *in situ* and estimated particulate nitrogen using the linear and non-linear conversion methods were assessed by testing $H_0$: slope = 1 (**Table 2**). The regression slopes for the linear and non-linear conversions were greater than one, but were not significantly different; linear ($t_{0.05,\ 72} = 3.65, p = 0.99$) and non-linear ($t_{0.05,\ 72} = 3.33$, $p = 0.99$). Both slopes provided good predictions of

biomass from particle size distributions and both conversion methods. The non-linear conversion of Menden-Deuer and Lessard (2000) was used in further estimates of uptake rates.

## 3.3. Estimating Nitrogen Uptake

The ranges of estimated N uptake rates were similar to those measured *in situ* (**Figure 6**). Predictions of nitrogen uptake rates were significantly correlated with respective measured uptake rates: $NO_3$ ($r = 0.60$, $p < 0.005$); $NH_4$ ($r = 0.61$, $p < 0.005$) and total N ($r = 0.67$, $p < 0.005$). The slopes of the relationship between measured and estimated uptake rate values were also assessed testing $H_0$:slope = 1 (**Table 2**). The regression slopes were not statistically different from 1 for $NH_4$ ($t_{0.05,\ 67} = -0.26$ =, $p = 0.30$) and total N ($t_{0.05,\ 72} = -0.26$, $p = 0.40$); this was not the case for $NO_3$($t_{0.05,\ 72} = -3.06$, $p = 0.00$). An inhibition term ($\psi$) of 1.99 $\mu$mol $N^{-1}$ was estimated for $NO_3$ uptake. The resulting predictions for $\rho NO_3$ were similar to those of $\rho NO_3$ with no inhibition, with a increase in bias when inhibition is included (bias $\rho NO_3 = 0.03$, bias $\rho NO_3{}^{\psi} = -0.72$). Predictions of total N uptake do not differ greatly when an inhibition term is applied; $\rho N$ (slope = 0.97), $\rho N^{\psi}$ (slope = 1.05) (**Table 2**) but more bias is introduce with an inhibition term ($\rho N^{\psi} = -0.89$, bias $\rho N = -1.10$). Estimations for $\rho NO_3$ (both with and without an inhibition term) did not match those measured *in situ* (**Table 2**). The comparisons between measured and calculated mass-specific rates showed poor agreement, and no statistical similarity was observed between the two data sets (**Table 2**). The relationships between estimated and measured $\rho NH_4$, $\rho N$ and $\rho N^{\psi}$ are not statistically different (**Table 2**) and are thus considered good predictions of the uptake of $NH_4$ and total N. The non-allometric rates were also compared with each other and a hypothetical 1:1 slope (**Figure 7**). Of the 9 different combinations of uptake parameters tested ($H_0$ slope = 1), one set was close to 1 but not statistically significant (slope = 0.96, $p < 0.00$) for $NO_3$, and 2 sets for $NH_4$, the closest being significantly similar to 1 (slope = 1.2, $p = 0.78$) (**Table 3**).

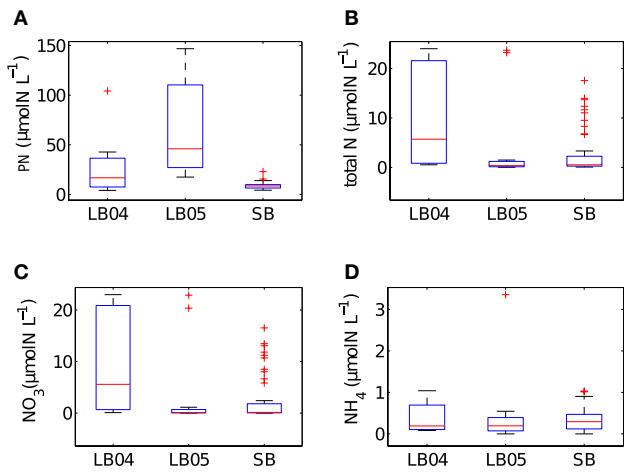


**FIGURE 2 | Summary box plots of the *in situ* data from Lamberts Bay 2004 and 2005 (LB04, LB05) and Saldanha Bay (SB) for (A) particulate nitrogen, (B) total N ($NO_3$ + $NH_4$), (C) $NO_3$ (D) $NH_4$ concentrations.** Boxes are medians, 25th and 75th quartiles and whiskers are extreme values not considered outliers, which are shown as crosses. SB ($n = 52$), LB04 ($n = 9$), LB05 ($n = 11$).

# 4. DISCUSSION

Predictions of biomass and nitrogen uptake rates were made using measured particle size distributions of natural assemblages, volume to biomass conversions (Menden-Deuer and Lessard, 2000) and size-dependent Michaelis-Menten uptake parameters (Ward et al., 2012). The *in situ* values used to validate the modeled values had a large range and thus a large spread existed in the data. There were good correlations between estimated and measured particulate N. This strong correlation gave necessary confidence in using particle size distributions derived from the Beckman Coulter Counter to predict the uptake rates of $NH_4$, total N and to a lesser extent $NO_3$. Significant correlations were found between modeled and *in situ* measured uptake rates and the values predicted for the uptake of $NH_4$ and total N were statistically similar to values measured *in situ*.

## 4.1. Conversions to Biomass

Both conversion models used to derive particulate nitrogen from particle size distributions (via non-linear or linear functions) yield similar results with a good correlation between estimated

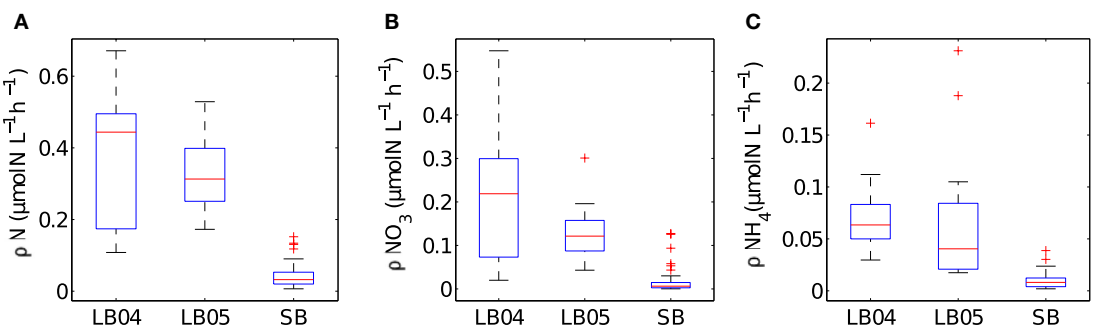


**FIGURE 3 | Summary plots of *in situ* measured uptake rates for (A) total nitrogen (B) $NO_3$ and (C) $NH_4$ for the different case studies (LB04, LB05, SB).** Boxes are medians, 25th and 75th quartiles and whiskers are extreme values not considered outliers, which are shown as crosses. SB ($n = 52$), LB04 ($n = 9$), LB05 ($n = 11$).

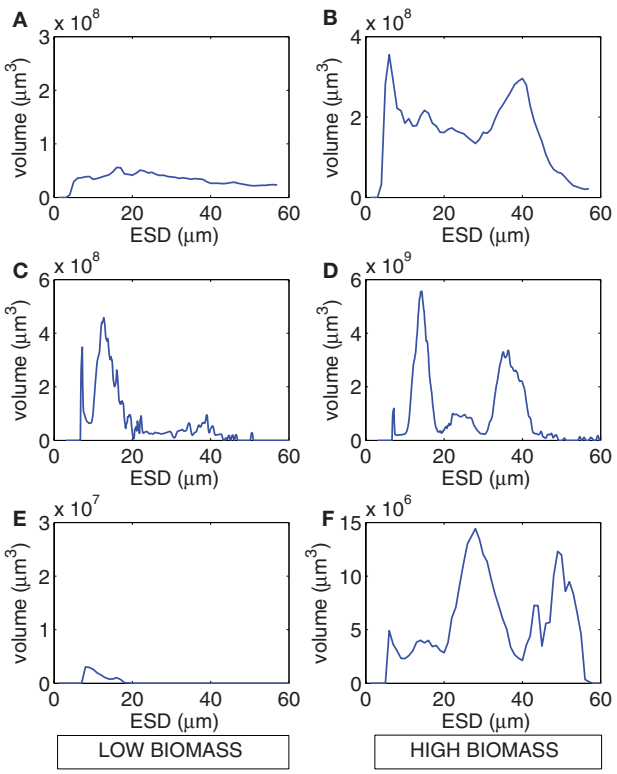


**FIGURE 4 | Example size spectra from the Coulter Counter for low biomass (left panels) and high biomass (right panels) for (A,B) LB04, (C,D) LB05, and (E,F) SB sample periods.**

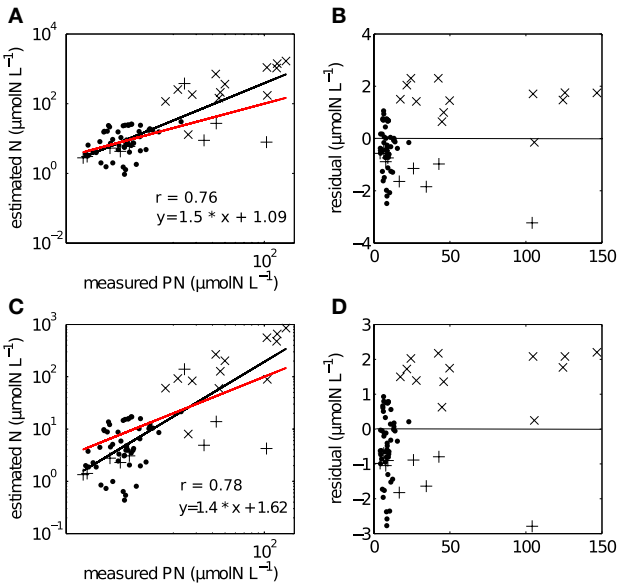


**FIGURE 5 | Regression analysis showing the relationships between measured and estimated particulate nitrogen using (A) non-linear conversion, with (B) corresponding log residuals, (C) linear conversion with (D) corresponding log residuals.** Black line refers to fitted regression line, red line has a hypothetical slope of 1:1 such that measured = estimated values. (• SB), (+ LB04), (x LB05).

and measured values. The regression equations used to estimate biomass were applied to all assemblages, which were most often mixed assemblages, i.e., containing dinoflagellates (LB05), ciliates (LB04), and diatoms (SB). LB05 had a high percentage of the dinoflagellate *Prorocentrum triestinum* at very high biomass (max. 146 $\mu$mol N $L^{-1}$), and the correlation coefficients for this particular data set are strongest. Even so, when applied to assemblages containing different taxa (ciliates or diatoms), overall the conversion factors performed well and the regression fit is close to a 1:1 relationship between measured and estimated nitrogen biomass. An even better fit may have resulted if group-specific conversion factors were used, but such empirical relationships for volume:nitrogen of the groups measured in this study were not found in the literature. It is noted that diatoms, for example, contain less carbon per unit volume than other groups, attributed to their significantly higher vacuole volume (Strathmann, 1967; Sicko-Goad et al., 1984). Cellular nitrogen content or nitrogen stores have also been observed to vary considerably between different species of phytoplankton (Parsons et al., 1961; Dortch et al., 1984).

Further errors could have been introduced by the assumptions made in deriving particle size distributions via a Coulter Counter, which assumes sphericity of cells. This could lead to underlying bias because of non-spherical groups (e.g., dinoflagellates) or particles of elongate shape, e.g., chain-forming diatoms, which are known to introduce error and can lead to an under/overestimation of total volume (Boyd and Johnson, 1995). Furthermore, the Coulter Counter measures down to 2 $\mu$m diameter (with confidence from 5 $\mu$m) and thus omits the submicron range due to limitations in technical capabilities. Nevertheless, the Coulter Counter has been used in several studies to successfully derive volume to carbon ratios (Mullin et al., 1966; Strathmann, 1967; Montagnes et al., 1994) and the presented results provide confidence that such data can adequately represent the particulate biomass of the nitrogen inventory in natural, diverse assemblages in eutrophic systems, characterized by large cells and high biomass.

The data presented here show that particle size distributions convert well to a measure of biomass, despite the broad scale application of a dinoflagellate volume:nitrogen conversion to mixed assemblages, the exclusion of submicron size ranges, and the assumptions of sphericity when using the Coulter counter. It has been noted that quantitative measurements of particulate carbon/nitrogen are in general lacking (Behrenfeld and Boss, 2006), and we suggest tha Coulter Counter derived PSDs can provide adequate measures of nitrogen biomass, most notably, when examining communities in eutrophic systems. Such conversions may not be as successful in oligotrophic areas, where cell size distributions are characteristically dominated by pico/nano plankton (<2 $\mu$m), but would need further investigation.

## 4.2. Estimating Uptake Rates

A significant correlation exists between the estimated and measured uptake rates of $NO_3$, $NH_4$ and total N, for natural

**TABLE 2 | Comparison of the strength of the correlation and *t*-test values between *in situ* measured and calculated uptake rates of $NO_3$, $NH_4$ and total N.**

| | *a* (slope) | SE | *b* (intercept) | $r^2$ | *t*(df = 72) | *p*-value |
|---|---|---|---|---|---|---|
| **PARTICULATE NITROGEN** | | | | | | |
| Measured vs. non-linear estimate | 1.5 | 0.141 | −1.09 | 0.61 | 3.33 | 0.99 |
| Measured vs. linear estimate | 1.4 | 0.144 | −1.62 | 0.59 | 3.65 | 0.99 |
| **ABSOLUTE UPTAKE RATES** | | | | | | |
| Measured vs. estimated $\rho NO_3$ | 0.68 | 0.10 | −1.36 | 0.37 | −3.06 | 0.00 |
| Measured vs. estimated $\rho NO_3(\psi = 1.99)$ | 0.65 | 0.11 | −2.25 | 0.32 | −3.20 | 0.00 |
| Measured vs. estimated $\rho NH_4$ | 0.92 | 0.15 | −0.60 | 0.36 | $0.51_{df = 67}$ | 0.30 |
| Measured vs. estimated $\rho N$ | 0.97 | 0.13 | −0.90 | 0.42 | −0.26 | 0.40 |
| Measured vs. estimated $\rho N$ ($\psi = 1.99$) | 1.05 | 0.14 | −0.88 | 0.44 | 0.34 | 0.63 |
| **MASS SPECIFIC UPTAKE RATES** | | | | | | |
| Measured vs. estimated $vNO_3$ | −0.26 | 0.11 | −2.44 | 0.07 | −11.13 | 0.00 |
| Measured vs. estimated $vNH_4$ | 0.44 | 0.09 | 0.27 | 0.28 | −6.48 | 0.00 |
| Measured vs. estimated vN | 0.38 | 0.26 | −3.85 | 0.03 | −2.33 | 0.01 |

*$t = a - 1/$Standard Error (SE) where $H_o$: slope = 1. DF = 72, critical value of* t *(1.66) and alpha ($\alpha = 0.05$).*

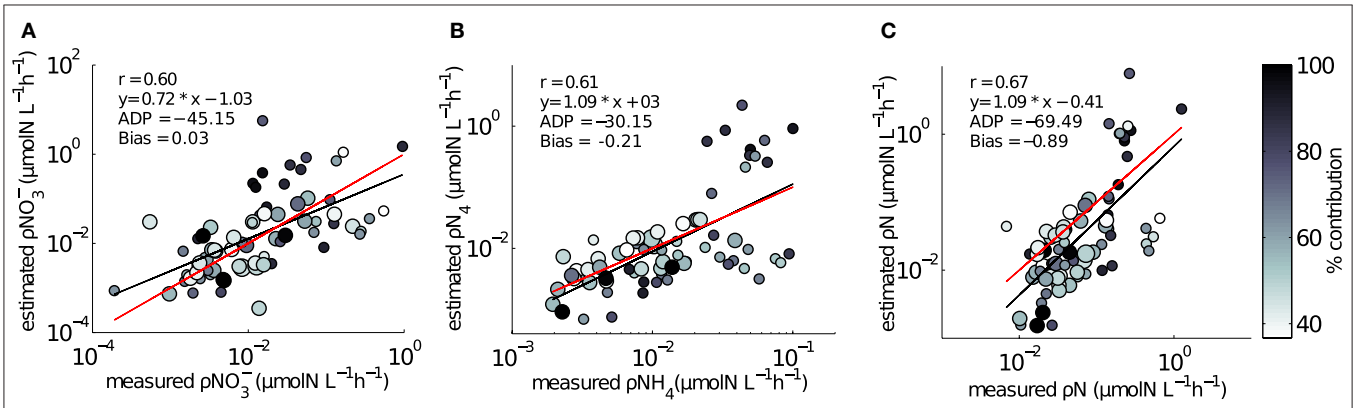


**FIGURE 6 | Comparisons between *in situ* measured and model estimated uptake rates using size dependent $V_{max}$ and $K_s$ from Ward et al. (2012). (A)** $\rho NO_3$ **(B)** $\rho NH_4$, **(C)** $\rho N$. Symbol size is representative of two size groups: small circle is <15$\mu$m; large circle is 15–30 $\mu$m . The third, largest size group of 30–60 $\mu$m did not dominate uptake rates in any of the samples. Colorbar represents the percentage contribution to the bulk uptake rate by the dominant size group. Red line is a hypothetical 1:1 slope, black line is the regression between measured and model uptake rates.

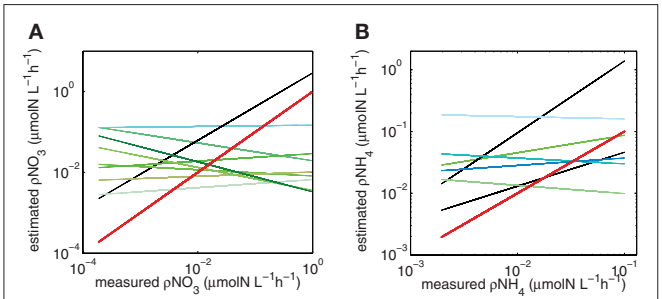


**FIGURE 7 | Trendlines for each combination of $V_{max}$ and $K_S$ for (A) $NO_3$ and (B) $NH_4$.** Red line is the hypothetical 1:1 slope, black lines represent slopes that are closest to 1 (see **Table 3**).

assemblages. The slopes of the regressions for the estimated vs. measured values of $NH_4$ and total N uptake were close to 1, indicating statistical similarity to what was measured *in situ*. The size-dependence of the Michaelis-Menten uptake parameters, $V_{max}$ and $K_s$, used by Ward et al. (2012) proved to be adequate values and yielded comparable results of nitrogen uptake to what had been measured *in situ*. Several studies have called into question the adequacy of the Michaelis-Menten kinetics equation to describe nutrient uptake in phytoplankton (Droop, 1974; Pasciak and Gavis, 1974; Aksnes and Egge, 1991). These criticisms are based on the premise that the equation does not account for differences in uptake rates in limiting or non-limiting conditions (Rhee, 1974; Grover, 1991), or that internal stores of nutrients can dictate uptake based on simple diffusion limitation (Droop, 1974). Both Michaelis-Menten uptake parameters are subject to variability, not only in different species but due to differences in nutrient availability and varying environmental conditions (Lomas and Glibert, 1999; Collos et al., 2005 and references therein). Smith et al. (2009) suggest that optimal uptake kinetics, which accounts for physiological acclimation to fluctuating environmental conditions, is a superior alternative

**TABLE 3 | The combination of uptake parameters ($V_{max}$ and $K_s$) that resulted in the regression slope closest to 1.**

| | $K_s$ | $V_{max}$ | *a* (slope) | *t* ($df_{NO3}$ = 72, $df_{NH4}$ = 69) | *p*-value |
|---|---|---|---|---|---|
| $NO_3$ | 0.5 | 1 | 0.96 | −3.72 | 0.00 |
| $NH_4$ | 0.01 | 1 | 1.2 | 0.79 | 0.78 |
| $NH_4$ | 0.5 | 1 | 0.4 | −2.30 | 0.01 |

*t = a − 1/Standard Error (SE) where $H_o$: slope = 1. Critical value of t (1.66) and alpha ($\alpha = 0.05$).*

to standard Michaelis-Menten descriptions of $V_{max}$ and $K_s$. A flexible phytoplankton functional type (FlexPFT) model (Smith et al., 2015), which resolves the dynamic response of phytoplankton communities, which was able to reproduce productivity and chlorophyll values of two contrasting time series better than when no flexible response was included. Thus, the limitations of Michaelis-Menten are recognized, more particularly in its assumption that parameter values are constant during environmental fluctuations. However, its use will most likely remain popular due its simplicity and the availability of parameter values in the literature. The variability of *in situ* measured uptake rates of $NH_4$ and total N is statistically matched by the variability in what was estimated using size-scaled parameters, which implies that much of the variability in Michaelis-Menten parameters, when applied at an assemblage scale, can be accounted for by simple size scaling of $V_{max}$ and $K_s$. The results also imply that net community rates of $NH_4$ and total nitrogen uptake are driven by ambient concentrations and cell size.

As expected, the case for $NO_3$ was more complex. Although the slope of the estimated $\rho NO_3$ was positive and close to 1, statistically it was not significant and reveals the potential importance of other influencing factors, in addition to cell size and ambient concentration. The suppression of $NO_3$ uptake by $NH_4$ may explain some of the variability observed in *in situ* measured values that is not accounted for in the model estimates. Numerous studies have shown an interaction between $NH_4$ and $NO_3$ uptake (e.g., McCarthy et al., 1975; Muggli and Smith, 1993; Harrison et al., 1996). $NH_4$ is generally considered to suppress the uptake of $NO_3$ (Dortch, 1990) but this is observed to be a highly variable process, where $NH_4$ can have little to no effect on $NO_3$ uptake (Kokkinakis and Wheeler, 1987) or can enhance rather than inhibit $NO_3$ uptake (Dortch, 1990). The extent to which $NH_4$ will affect $NO_3$ uptake is not just species-dependent, but is also affected by physiological state and the preconditioning nutrient concentrations (Varela and Harrison, 1999; L'Helguen et al., 2008). Equally, the concentration of $NH_4$ at which suppression of $NO_3$ uptake occurs varies between systems (Dortch, 1990; Dugdale et al., 2006, 2007; Probyn et al., 2015). The effect of incorporating an inhibition term, in this case, made little difference to the estimates of $\rho NO_3$ and $\rho N$. A range of inhibition parameter values used in other studies were also investigated, ranging from 1.5 (Kishi et al., 2007) to 4.6 (Dutkiewicz et al., 2009), with little significant change in statistical comparisons. The value of 1.99, the outcome of a best fit model to the $NO_3$ uptake values for this study, was deemed optimal for the range of values measured. Another suggestion to explain the deviations from Michaelis-Menten kinetics for $NO_3$ uptake, is the potential for "shift-up" kinetics described in Dugdale et al. (1990, 2006). It was observed that $NO_3$ uptake may not follow Michaelis-Menten kinetics consistently along the upwelling timeframe, where initial (highest) concentrations of $NO_3$ will not equate to highest uptake rates, as communities take time to respond to new injections of $NO_3$.

The predictions did not work when measured and calculated biomass-specific rates ($h^{-1}$) were compared (**Table 2**). This is not surprising. The measured uptake rates result from an interplay between ambient nitrogen concentrations, total particulate nitrogen and the structure (size and taxa) of the phytoplankton assemblage, which will affect mass-specific rates as well as affinity for nitrogen. Mass-specific values influence physiological efficiency, with small cells having faster mass-specific rates and greater affinity for nitrogen at low concentrations than large cells. These influences of assemblage structure cannot be accounted for when dividing uptake rates by measured particulate nitrogen. Much of the uptake signal is dominated by the small fractions (<15 um) of the size spectra (**Figure 6**) and highest uptake rates are observed when the small size fractions dominate and thus biomass is low, illustrating that the successful predictions of uptake rates is not driven by high biomass. Absolute uptake rates can be considered an ecosystem metric of nitrogen dynamics, and this study shows that, in a eutrophic environment, size-scaled MM parameters can be used to predict $NH_4$ and total N uptake, keeping the numbers of parameters to a minimum and thus minimizing uncertainty associated with each parameter. Data to constrain added parameters are not available from the *in situ* experiments. The non-allometric predictions, which use constant $V_{max}$ and $K_s$ values across the entire spectrum resulted in a variety of regression slopes, with few matching a 1:1 relationship. The kinetic parameter values used all fall within a realistic range observed in the region, and of the nine combinations tested (**Figure 7**), no significant prediction was made for $NO_3$ (although the slope was close to 1) and one successful prediction was made for $NH_4$. However, it would be difficult to know in advance which parameter values to use, whereas the allometric calculations produced good matches to the observations.

To conclude, a large proportion of the variability observed in uptake rates of nitrogen measured *in situ*, in various assemblages, was explained by ambient nutrient concentrations and cell size, in spite of several simplifications and sources of error. The case for $NO_3$ uptake was not as strong as $NH_4$ and is suggested to be due to the complex suppressive behavior of $NH_4$ on $NO_3$ uptake as well potential "shift-up" effects observed in upwelling systems. In addition, accounting for the internal storage of $NO_3$ may have improved estimations of $\rho NO_3$, but are beyond the scope of these data. Nevertheless, realistic approximations of nitrogen uptake, and thus new production (Dugdale and Goering, 1967) are achieved when using size-scaled Michaelis-Menten uptake parameters and particle size distributions. The strength of this study lies in its application to *in situ* measurements of cell size distributions and ambient nutrient concentration, to derive approximations of nitrogen uptake. Further research is recommended to include Dissolved Organic Nitrogen uptake

rates into approximations of total N uptake, given its significant contribution to total production (Harrison et al., 1985; Probyn, 1988). This is no menial task however, given its complex kinetic behavior (Eppley et al., 1971; Bronk et al., 2004; Solomon et al., 2010) and current lack of size-scaling relationships in the literature. New production, considered to be the portion of primary production with the highest implications for carbon export or the flow of energy to higher trophic levels (Hutchings, 1992; Probyn, 1992; Dugdale et al., 2006), is a useful measurement in studies of ecosystem dynamics. In the absence of laborious and expensive $^{15}$N data, the use of particle size distributions to estimate nitrogen uptake can be a useful tool in assemblage scale studies of nitrogen dynamics in productive coastal upwelling systems.

## AUTHOR CONTRIBUTIONS

2004/2005 *in situ* data were collected and analyzed by TP ($^{15}$N, nutrient analyses) and SB (particle size distributions). 2012/2013 data were collected by both TP ($^{15}$N, nutrient analyses) and FA ($^{15}$N, nutrient analyses, particle size distributions). FA designed the study, performed analyses, made the figures and wrote the manuscript. CM contributed to model implementation and validating of methods used, discussions of the results and edited the manuscript. TP also contributed to discussions of research and edited the manuscript. SB contributed to discussions of research.

## FUNDING

This work is based on research supported in part by the National Research Foundation of South Africa (Grant Number 98967). Additional funds were from the Ma-Re Institute of the University of Cape Town, 7701, Cape Town, South Africa and the Council for Scientific and Industrial Research (CSIR), Rosebank, 7700, Cape Town, South Africa.

## ACKNOWLEDGMENTS

The authors would like to thank André du Randt and Lisa Mansfield of the Department of Agriculture, Forestry and Fisheries as well Marie Smith from the University of Cape Town for help with data collection during the several sampling periods.

## REFERENCES

Acevedo-Trejos, E., Brandt, G., Steinacher, M., and Merico, A. (2014). A glimpse into the future composition of marine phytoplankton communities. *Front. Mar. Sci.* 1:15. doi: 10.3389/fmars.2014.00015

Aksnes, D., and Egge, J. (1991). A theoretical model for nutrient uptake in phytoplankton. *Mar. Ecol. Prog. Ser.* 70, 65–72. doi: 10.3354/meps070065

Aksnes, D. L., and Cao, F. J. (2011). Inherent and apparent traits in microbial nutrient uptake. *Mar. Ecol. Prog. Ser.* 440, 41–51. doi: 10.3354/meps09355

Allen, J. I., and Fulton, E. (2010). Top-down, bottom-up or middle-out? Avoiding extraneous detail and over-generality in marine ecosystem models. *Prog. Oceanogr.* 84, 129–133. doi: 10.1016/j.pocean.2009.09.016

Arteaga, L., Pahlow, M., and Oschlies, A. (2014). Global patterns of phytoplankton nutrient and light colimitation inferred from an optimality-based model. *Glob. Biogeochem. Cycles* 28, 648–661. doi: 10.1002/2013GB004668

Baird, M. E., and Suthers, I. M. (2007). A size-resolved pelagic ecosystem model. *Ecol. Model.* 203, 185–203. doi: 10.1016/j.ecolmodel.2006.11.025

Banas, N. S. (2011). Adding complex trophic interactions to a size-spectral plankton model: emergent diversity patterns and limits on predictability. *Ecol. Model.* 222, 2663–2675. doi: 10.1016/j.ecolmodel.2011.05.018

Behrenfeld, M. J., and Boss, E. (2006). Beam attenuation and chlorophyll concentration as alternative optical indices of phytoplankton biomass. *J. Mar. Res.* 64, 431–451.

Bonachela, J. A., Raghib, M., and Levin, S. A. (2011). Dynamic model of flexible phytoplankton nutrient uptake. *Proc. Natl. Acad. Sci. U.S.A.* 108, 20633–20638. doi: 10.1073/pnas.1118012108

Boyd, C. M., and Johnson, G. (1995). Precision of size determination of resistive electronic counters. *J. Plankt. Res.* 17, 41–58. doi: 10.1093/plankt/17.1.41

Bronk, D. A., Sanderson, M. P., Mulholland, M. R., Heil, C. A., and Neil, J. M. (2004). "Organic and inorganic nitrogen uptake kinetics in field populations dominated by Karenia brevis," in *Harmful Algae*, Vol. 1, eds K. A. Steidinger, J. J. Landsberg, C. R. Tomas, and G. A. Vargo (Florida Fish and Wildlife Conservation Commission, Florida Institute of Oceanography, and Intergovernmental Oceanographic Commission of UNESCO), 3–5.

Chisholm, S. W. (1992). *Primary Productivity and Biogeochemical Cycles in the Sea*. Springer US.

Collos, Y., Vaquer, A., and Souchu, P. (2005). Acclimation of nitrate uptake by phytoplankton to high substrate levels. *J. Phycol.* 41, 466–478. doi: 10.1111/j.1529-8817.2005.00067.x

Dortch, Q. (1990). The interaction between ammonium and nitrate uptake in phytoplankton. *Mar. Ecol. Prog. Ser.* 61, 183–201. doi: 10.3354/meps061183

Dortch, Q., Clayton, J. R., Thoresen, S. S., and Ahmed, S. I. (1984). Species differences in accumulation of nitrogen pools in phytoplankton. *Mar. Biol.* 81, 237–250. doi: 10.1007/BF00393218

Droop, M. R. (1974). The nutrient status of algal cells in continuous culture. *J. Mar. Biol. Assoc. UK* 54, 825–855. doi: 10.1017/S002531540005760X

Dugdale, R. C., and Goering, J. J. (1967). Uptake of new and regenerated forms of nitrogen in primary productivity. *Limnol. Oceanogr.* 12, 196–206.

Dugdale, R. C., and Wilkerson, F. P. (1986). The use of 15N to measure nitrogen uptake in eutrophic ocean. Experimental considerations. *Limnol. Oceanogr.* 31, 673–689. doi: 10.4319/lo.1986.31.4.0673

Dugdale, R. C., Wilkerson, F. P., Hogue, V. E., and Marchi, A. (2006). Nutrient controls on new production in the Bodega Bay, California, coastal upwelling plume. *Deep Sea Res. II Top. Stud. Oceanogr.* 53, 3049–3062. doi: 10.1016/j.dsr2.2006.07.009

Dugdale, R. C., Wilkerson, F. P., Hogue, V. E., and Marchi, A. (2007). The role of ammonium and nitrate in spring bloom development in San Francisco Bay. *Estuarine Coast. Shelf Sci.* 73, 17–29. doi: 10.1016/j.ecss.2006.12.008

Dugdale, R. C., Wilkerson, F. P., Morel, A., and Physique, L. D. (1990). Realization of new production in coastal upwelling: a means to compare relative performance areas. 35, 822–829. doi: 10.4319/lo.1990.35.4.0822

Dutkiewicz, S., Follows, M. J., and Bragg, J. G. (2009). Modeling the coupling of ocean ecology and biogeochemistry. *Global Biogeochem. Cycles* 23, 1–15. doi: 10.1029/2008GB003405

Edwards, K. F., Klausmeier, C. A., and Litchman, E. (2014). Evidence for a three-way trade-off between nitrogen and phosphorus competitive abilities and cell size in phytoplankton. *Ecol. Soc. Am.* 92, 2085–2095. doi: 10.1890/11-0395.1

Edwards, K. F., Thomas, M. K., Klausmeier, C., and Litchman, E. (2012). Allometric scaling and taxonomic variation in nutrient utilization traits and maximum growth rate of phytoplankton. *Limnol. Oceanogr.* 57, 554–566. doi: 10.4319/lo.2012.57.2.0554

Eppley, R. W., Carlucci, A. F., Kiefer, D., Mccarthy, J. J., Venrick, E., and Williams, P. M. (1971). Phytoplankton growth and composition in shipboard cultures

supplied with nitrate, ammonium, or urea as the nitrogen source. *Limnol. Oceanogr.* 16, 741–751. doi: 10.4319/lo.1971.16.5.0741

Eppley, R. W., Rogers, J. N., and Mccarthy, J. J. (1969). Half-saturation constants for uptake of nitrate and ammonium by marine phytoplankton. *Limnol. Oceanogr.* 14, 912–920. doi: 10.4319/lo.1969.14.6.0912

Follows, M. J., and Dutkiewicz, S. (2011). Modeling diverse communities of marine microbes. *Annu. Rev. Mar. Sci.* 3, 427–451. doi: 10.1146/annurev-marine-120709-142848

Franks, P. J. S. (2009). Planktonic ecosystem models: perplexing parameterizations and a failure to fail. *J. Plankt. Res.* 31, 1299–1306. doi: 10.1093/plankt/fbp069

Gregg, W. W., Ginoux, P., Schopf, P. S., and Casey, N. W. (2003). Phytoplankton and iron: validation of a global three-dimensional ocean biogeochemical model. *Deep-Sea Res. Part II Top. Stud. Oceanogr.* 50, 3143–3169. doi: 10.1016/j.dsr2.2003.07.013

Grover, J. P. (1991). Resource competition in a variable environment: phytoplankton growing according to the variable-internal-stores model. *Am. Nat.* 138, 811–835.

Harrison, W. G., Harris, L. R., and Irwin, B. D. (1996). The kinetics of nitrogen utilization in the oceanic mixed layer: nitrate and ammonium interactions at nanomolar concentrations. *Limnol. Oceanogr.* 41, 16–32. doi: 10.4319/lo.1996.41.1.0016

Harrison, W., Head, E., Conover, R., Longhurst, A., and Sameoto, D. (1985). The distribution and metabolism of urea in the eastern Canadian Arctic. *Deep-Sea Res. Part A Oceanogr. Res. Papers* 32, 23–42. doi: 10.1016/0198-0149(85)90015-9

Hutchings, L. (1992). Fish harvesting in a variable, productive environment. Searching for rules or searching for exceptions? *South African J. Mar. Sci.* 12, 297–318. doi: 10.2989/02577619209504708

Kishi, M., Kashiwai, M., Ware, M., Megrey, B. A., Eslinger, D. L., Werner, F. E., et al. (2007). NEMURO a lower trophic level model for the North Pacific marine ecosystem. *Ecol. Model.* 202, 12–25. doi: 10.1016/j.ecolmodel.2006.08.021

Kokkinakis, S., and Wheeler, P. (1987). Nitrogen uptake and phytoplankton growth in coastal upwelling regions. *Limnol. Oceanogr.* 32, 1112–1123. doi: 10.4319/lo.1987.32.5.1112

Koroleff, F. (1983). "Determination of ammonia," in *Methods of Seawater Analysis, 2nd Edn.*, eds K. Grasshoff, E. Ehrhardt, and K. Kremling (Weinheim: Verlag Chemie), 150–157.

Le Quéré, C. L., Harrison, S. P., Colin Prentice, I., Buitenhuis, E. T., Aumont, O., Bopp, L., et al. (2005). Ecosystem dynamics based on plankton functional types for global ocean biogeochemistry models. *Global Change Biol.* 11, 2016–2040. doi: 10.1111/j.1365-2486.2005.01004.x

L'Helguen, S., Maguer, J. F., and Caradec, J. (2008). Inhibition kinetics of nitrate uptake by ammonium in size-fractionated oceanic phytoplankton communities: implications for new production and f-ratio estimates. *J. Plankt. Res.* 30, 1179–1188. doi: 10.1093/plankt/fbn072

Litchman, E., Edwards, K. F., and Klausmeier, C. A. (2015). Microbial resource utilization traits and trade-offs: implications for community structure, functioning, and biogeochemical impacts at present and in the future. *Front. Microbiol.* 6:254. doi: 10.3389/fmicb.2015.00254

Litchman, E., Klausmeier, C. A., Schofield, O. M., and Falkowski, P. G. (2007). The role of functional traits and trade-offs in structuring phytoplankton communities: scaling from cellular to ecosystem level. *Ecol. Lett.* 10, 1170–1181. doi: 10.1111/j.1461-0248.2007.01117.x

Lomas, M. W., Bonachela, J. A., Levin, S. A., and Martiny, A. C. (2014). Impact of ocean phytoplankton diversity on phosphate uptake. *In Review* 111, 17540–17545. doi: 10.1073/pnas.1420760111

Lomas, M. W., and Glibert, P. M. (1999). Temperature regulation of nitrate uptake: a novel hypothesis about nitrate uptake and reduction in cool-water diatoms. *Limnol. Oceanogr.* 44, 556–572. doi: 10.4319/lo.1999.44.3.0556

McCarthy, J. J., Taylor, W. L., and Taft, J. (1975). "The dynamics of nitrogen and phosphorous cycling in the open waters of the chesapeake bay," in *Marine Chemistry in Coastal Environment*, ed T. M. Church (American Chemical Society), 664–681.

McGill, B. J., Enquist, B. J., Weiher, E., and Westoby, M. (2006). Rebuilding community ecology from functional traits. *Trends Ecol. Evol.* 21, 178–185. doi: 10.1016/j.tree.2006.02.002

Menden-Deuer, S., and Lessard, E. J. (2000). Carbon to volume relationships for dinoflagellates, diatoms, and other protist plankton. *Limnol. Oceanogr.* 45, 569–579. doi: 10.4319/lo.2000.45.3.0569

Moloney, C. L., Field, J., and Lucas, M. (1991). The size-based dynamics of plankton food webs. II. Simulations of three contrasting southern Benguela food webs. *J. Plankt. Res.* 13, 1039–1092. doi: 10.1093/plankt/13.5.1039

Moloney, C. L., and Field, J. G. (1989). General allometric equations for rates of nutrient uptake, ingestion, and respiration in plankton organisms. *Limnol. Oceanogr.* 34, 1290–1299. doi: 10.4319/lo.1989.34.7.1290

Montagnes, D., Berges, J., Harrison, P., and Taylor, F. (1994). Estimating carbon, nitrogen, protein and chlorophyll a from volume in marine phytoplankton. *Limnol. Oceanogr.* 39, 1044–1060. doi: 10.4319/lo.1994.39.5.1044

Muggli, D., and Smith, W. J. (1993). Regulation of nitrate and ammonium uptake in the Greenland Sea. *Mar. Biol.* 208, 199–208. doi: 10.1007/BF00346336

Mullin, M., Sloan, P., and Eppley, R. (1966). Relationship between carbon content, cell volume and area in phytoplankton. *Limnol. Oceanogr.* 11, 307–311. doi: 10.4319/lo.1966.11.2.0307

Nydahl, F. (1976). On the optimum conditions for the reduction of nitrate to nitrite by cadmium. *Talanta* 23, 349–357. doi: 10.1016/0039-9140(76)80047-1

Pahlow, M., and Oschlies, A. (2009). Chain model of phytoplankton P, N and light colimitation. *Mar. Ecol. Prog. Ser.* 376, 69–83. doi: 10.3354/meps07748

Pahlow, M., Vézina, A. F., Casault, B., Maass, H., Malloch, L., Wright, D. G., et al. (2008). Adaptive model of plankton dynamics for the North Atlantic. *Prog. Oceanogr.* 76, 151–191. doi: 10.1016/j.pocean.2007.11.001

Parsons, T. R., Stephens, K., and Strickland, J. D. H. (1961). On the Chemical Composition of Eleven Species of Marine Phytoplankters. *J. Fish. Res. Board Canada* 18, 1001–1016. doi: 10.1139/f61-063

Pasciak, W. J., and Gavis, J. (1974). Transport limitation of nutrient uptake in phytoplankton. *Limnol. Oceanogr.* 19, 881–888.

Probyn, T. (1988). Nitrogen utilization by phytoplankton in the Namibian upwelling region during an austral spring. *Deep-Sea Res. Part A Oceanogr. Res. Papers* 35, 1387–1404. doi: 10.1016/0198-0149(88)90090-8

Probyn, T. A. (1992). The inorganic nitrogen nutrition of phytoplankton in the southern Benguela: new production, phytoplankton size and implications for pelagic foodwebs. *South Afr. J. Mar. Sci.* 12, 411–420. doi: 10.2989/02577619209504715

Probyn, T. A., Atkins, J. F., and Pitcher, G. C. (2015). Saldanha Bay, South Africa III: new production and carrying capacity for bivalve aquaculture. *South Afr. J. Mar. Sci.* 37, 521–531. doi: 10.2989/1814232X.2015.1113203

Probyn, T. A., Waldron, H. N., and James, A. G. (1990). Size-fractionated measurements of nitrogen uptake in aged upwelled waters: implications for pelagic food webs. *Limnol. Oceanogr.* 35, 202–210. doi: 10.4319/lo.1990.35.1.0202

Probyn, T. A., Waldron, H. N., Searson, S., and Owens, N. J. P. (1996). Diel variability in nitrogenous nutrient uptake at photic and subphotic depths. *J. Plankt. Res.* 18, 2063–2079. doi: 10.1093/plankt/18.11.2063

Rhee, G.-Y. (1974). Phosphate uptake under nitrate limitation by Scenedesmus sp. and its ecological implications. *J. Phycol.* 10, 470–475. doi: 10.1111/j.1529-8817.1974.tb02742.x

Seeyave, S., Probyn, T. A., Pitcher, G. C., Lucas, M. I., and Purdie, D. A. (2009). Nitrogen nutrition in assemblages dominated by Pseudo-nitzschia spp., *Alexandrium catenella* and *Dinophysis acuminata* off the west coast of South Africa. *Mar. Ecol. Prog. Ser.* 379, 91–107. doi: 10.3354/meps07898

Sicko-Goad, L. M., Schelske, C. L., and Stoermer, E. F. (1984). Estimation of intracellular carbon and silica content of diatoms from natural assemblages using morphometric techniques. *Limnol. Oceanogr.* 29, 1170–1178. doi: 10.4319/lo.1984.29.6.1170

Smith, S. L., Pahlow, M., Merico, A., Acevedo-Trejos, E., Sasai, Y., Yoshikawa, C., et al. (2015). Flexible phytoplankton functional type (FlexPFT) model: size-scaling of traits and optimal growth. *J. Plankt. Res.* 1–16. doi: 10.1093/plankt/fbv038

Smith, S. L., Pahlow, M., Merico, A., and Wirtz, K. W. (2011). Optimality-based modeling of planktonic organisms. *Limnol. Oceanogr.* 56, 2080–2094. doi: 10.4319/lo.2011.56.6.2080

Smith, S. L., and Yamanaka, Y. (2007). Optimization-based model of multinutrient uptake kinetics. *Limnol. Oceanogr.* 52, 1545–1558. doi: 10.4319/lo.2007.52.4.1545

Smith, S. L., Yamanaka, Y., Pahlow, M., and Oschlies, A. (2009). Optimal uptake kinetics: physiological acclimation explains the pattern of nitrate uptake by phytoplankton in the ocean. *Mar. Ecol. Prog. Ser.* 384, 1–12. doi: 10.3354/meps08022

Solomon, C. M., Collier, J. L., Berg, G. M., and Glibert, P. M. (2010). Role of urea in microbial metabolism in aquatic systems: a biochemical and molecular review. *Aquat. Microb. Ecol.* 59, 67–88. doi: 10.3354/ame01390

Strathmann, R. R. (1967). Estimating the organic carbon content of phytoplankton from cell volume or plasma volume. *Limnol. Oceanogr.* 12, 411–418. doi: 10.4319/lo.1967.12.3.0411

Tilman, D. (2001). Functional diversity. *Encyclopedia Biodivers.* 3, 109–120. doi: 10.1006/rwbd.1999.0154

Utermohl, H. (1958). Zur vervollkommnung der quantitativen Phytoplankton Methodik. *Mitt. Int. Ver. Theor. Angew. Limnol.* 9, 1–38.

van der Lingen, C., Hutchings, L., and Field, J. (2006). in the southern Benguela: are species alternations between small pelagic fish trophodynamically mediated? *Afr. J. Mar. Sci.* 28, 465–477. doi: 10.2989/18142320609504199

Varela, D. E., and Harrison, P. J. (1999). Effect of ammonium on nitrate utilization by *Emiliania huxleyi*, a coccolithophore from the oceanic northeastern Pacific. *Mar. Ecol. Prog. Ser.* 186, 67–74. doi: 10.3354/meps186067

Ward, B. A., Dutkiewicz, S., Jahn, O., and Follows, M. J. (2012). A size-structured food-web model for the global ocean. *Limnol. Oceanogr.* 57, 1877–1891. doi: 10.4319/lo.2012.57.6.1877

Westoby, M., and Wright, I. J. (2006). Land-plant ecology on the basis of functional traits. *Trends Ecol. Evol.* 21, 261–268. doi: 10.1016/j.tree.2006.02.004

Zibordi, G., Mélin, F., Hooker, S. B., D'Alimonte, D., and Holben, B. (2004). An autonomous above-water system for the validation of ocean color radiance data. *IEEE Trans. Geosci. Remote Sens.* 42, 401–415. doi: 10.1109/TGRS.2003.821064

**Conflict of Interest Statement:** The authors declare that the research was conducted in the absence of any commercial or financial relationships that could be construed as a potential conflict of interest.

frontiers in Marine Science

ORIGINAL RESEARCH
published: 11 January 2017
doi: 10.3389/fmars.2016.00286

# A Model Simulation of the Adaptive Evolution through Mutation of the Coccolithophore *Emiliania huxleyi* Based on a Published Laboratory Study

*Kenneth L. Denman* *

*Canadian Centre for Climate Modelling and Analysis, Bob Wright Centre, School of Earth and Ocean Sciences, University of Victoria, Victoria, BC, Canada*

We expect the structure and functioning of marine ecosystems to change over this century in response to changes in key ocean variables associated with a changing climate. Organisms with generation times from years to decades have the capacity to adapt to changing environmental conditions over a few generations by selecting from existing genotypes/phenotypes, but it is unlikely that evolution through mutation will be a major factor for organisms with generation times of years to decades. However, phytoplankton and other microbes, with generation times of days or less, experience hundreds of generations each year, allowing the possibility for favorable mutations (i.e., those that produce organisms with fitness maxima nearer to the environmental conditions at that time) to dominate existing genotypes and survive in a changing climate. Several laboratories have grown phytoplankton cultures for hundreds to thousands of generations and demonstrated that they have changed genetic makeup. In particular Schlüter et al. (2014) grew replicates derived from a single cell of *Emiliania huxleyi*, a coccolithophorid with broad geographical and thermal range, for 3 years (~1250 generations) at 15°C, and then for a year at 26.3°C, near their upper thermal limit. During the last year the intrinsic growth rate increased more or less linearly, which the authors attribute to genetic mutation. Here we simulate genetic mutation of a single trait (intrinsic growth rate), both for the control phase and the warm phase of their study. We consider sensitivities to frequency of mutation, changes with temperature in intrinsic growth rate, and use the experimental setup and results to place constraints on the way mutations occur. In particular, all numerical experiments with mutation result in a lag time ~30–140 generations before a significant increase in realized growth rate occurs. This lag after a favorable mutation results from the number of generations required for a single favorable mutant cell to reach a significant fraction of the $\sim 10^5$ cells in the culture. A numerical experiment that includes a simple plastic response formulation shows that plasticity could remove this lag and yield results more in agreement with those observed in the laboratory study.

**Keywords: climate change, phytoplankton, adaptive modeling, traits, genetic mutation, plasticity**

OPEN ACCESS

***Edited by:***
*Dag Lorents Aksnes, University of Bergen, Norway*

***Reviewed by:***
*Thorsten Reusch, GEOMAR Kiel, Germany*
*Chris J. Daniels, Independent Researcher, UK*

***Correspondence:**
*Kenneth L. Denman*
*denmank@uvic.ca*

***Specialty section:***
*This article was submitted to Marine Ecosystem Ecology, a section of the journal Frontiers in Marine Science*

***Received:*** *09 June 2016*
***Accepted:*** *19 December 2016*
***Published:*** *11 January 2017*

***Citation:***
*Denman KL (2017) A Model Simulation of the Adaptive Evolution through Mutation of the Coccolithophore Emiliania huxleyi Based on a Published Laboratory Study. Front. Mar. Sci. 3:286. doi: 10.3389/fmars.2016.00286*

## INTRODUCTION

The climate has been changing and is expected to continue to change—and possibly at an increasing rate (Collins et al., 2013; Rhein et al., 2013) The oceans are intimately involved in both regulating and responding to that change, and marine ecosystems are and will continue to change in response to changes associated with a changing climate (Hoegh-Guldberg et al., 2014; Pörtner et al., 2014; Wong et al., 2014). However, coupled climate-ecosystem models that predict future changes in marine ecosystems, for the most part use fixed compartment model structures for ecosystems with minimally-adaptive parameters: mainly variable C:N ratios and a temperature dependence of some intrinsic rates such as phytoplankton growth rate (e.g., Chust et al., 2014). While we use these models to predict the future structure and function of marine ecosystems, considerable skepticism remains (e.g., Planque, 2015).

Increasing temperature is the first order environmental change affecting marine species. In response, the ranges of most species are shifting poleward, nearly 2° latitude per decade, ∼190 km ± 20%(SE) (e.g., Sorte et al., 2010). In particular, *Emiliania huxleyi* blooms in polar regions became more frequent and of greater extent in SeaWiFS satellite imagery (1997-2007) compared with CZCS imagery (1978-1986) (Winter et al., 2014). The large variability in rates of poleward shift for different species means, for example, that the species assemblage (of fishes) in a fixed region is changing (Simpson et al., 2011). Other documented changes in response to warming are in phenology: for example, open ocean and coastal zooplankton reaching their biomass maximum ∼1 month earlier over 40 years, correlated with the total number of "degree-days" above 6°C over the spring months of March-April-May (Mackas et al., 2007).

There are three other main mechanisms of adaptation to climate-related, multi-decadal change in the ocean environment. First, there is evolutionary adaptation within existing genotypic/phenotypic variability. Guppies removed from one stream to another for several years exhibit a rate of evolution in age and size at maturity many orders of magnitude higher than rates inferred from the geological record (e.g., Reznick et al., 1997). Second, there is evolutionary adaptation through mutation that changes genotypes. Evolution by mutation in phytoplankton reared in laboratory conditions over hundreds to thousands of generations has been documented in several studies (Collins and Bell, 2004; Collins et al., 2006; Collins, 2011; Lohbeck et al., 2012; Schlüter et al., 2014). The speed of evolutionary adaptation is expected to be inversely proportional to generation time: most microbes in the ocean have generation times of a day or less, so experience thousands of generations in a decade. Hence, evolutionary adaptation would be expected to be important for these organisms on decadal and longer timescales. The third adaptive response is phenotypic plasticity: "...the capacity of a single genotype to exhibit variable phenotypes in different environments" (Whitman and Agrawal, 2009). There is still much uncertainty about the mechanisms, magnitudes, limits, heretability, and tradeoffs of plasticity, and how to distinguish it from evolutionary adaptation (e.g., Collins et al., 2014; Reusch, 2014).

The objective of this paper is to develop a model at the trait level of genetic mutation by the coccolithophorid *Emiliania huxleyi* based on observations taken over 4 years of laboratory culture experiments (Schlüter et al., 2014). Litchman and Klausmeier (2008) and Litchman et al. (2012) described a framework for a trait-based approach to investigate the evolutionary responses of phytoplankton to global environmental change. In a series of original papers, Norberg has explored the application of complex adaptive modeling concepts to examples of evolutionary adaptation to environmental change within existing phenotypic variability (Norberg et al., 2001, 2012; Norberg, 2004). Here, as in Norberg (2004), the single trait is the maximum growth rate of phytoplankton as a function of the environmental variable temperature. As in the laboratory experiments, the model simulates the growth of *E. huxleyi* at 15°C for 3 years, and then for 1 year after the temperature is increased to 26.3°C. The simulations explore first the response of random mutations that are equally probable across the trait space (a "flat" probability distribution function—pdf), and then of infinitesimal or incremental random mutations centered on the existing mean of the genotype distribution for various widths of a Gaussian normal pdf of mutation magnitudes. Finally, the effect of a simple formulation for phenotypic plasticity of the original genotype grown at 15°C, then warmed abruptly to 26.3°C, will be presented.

## MODEL DESCRIPTION

### The Coccolithophore *Emiliania huxleyi*

The coccolithophore *E. huxleyi* is widely distributed over the global ocean (e.g., Hagino et al., 2011), viable over a temperature range from 4 to 28°C (e.g., Watabe and Wilbur, 1966; Fielding, 2013), with maximum growth rates in the temperature range 18–25°C (Watabe and Wilbur, 1966; Zhang et al., 2014). In general, growth rates increase with temperature, with clear differences between Arctic and Atlantic strains (Daniels et al., 2014; Zhang et al., 2014). Zhang et al. developed thermal reaction norms (TRNs) for six *E. huxleyi* isolates originating from the central Atlantic near the Azores, Portugal (38°34′N; monthly SST range 16–22°C), and five isolates originating from coastal waters near Bergen, Norway (60°18'N; monthly SST range 6–16°C), all kept at 15°C in culture. The fitted growth rates for the Bergen isolates were higher in the range 7–22°C; they were higher for the Azores isolates in the range 26–28°C, with a crossover point near 24°C.

While isolates of *E. huxleyi* from various regions around the globe have a core set of common genes, there is considerable genetic variability across its global distribution (Hagino et al., 2011; Read et al., 2013). According to Read et al., "*Genome variability within this species complex seems to underpin its capacity both to thrive in habitats ranging from the equator to the subarctic and to form large-scale episodic blooms under a wide variety of environmental conditions*." Thus, the cultures in Schlüter et al. (2014), originating from a single cell take from waters (∼10°C) near Bergen, Norway, would not necessarily be expected to grow at the maximum rate observed for the species at 15°C, even though they were apparently growing in an exponential manner.

## Experimental Background

The model is formulated to simulate, as closely as possible, the experimental protocol followed during the laboratory studies (Schlüter et al., 2014). The main trait is the growth rate ($d^{-1}$), which is a function of a single environmental variable/stressor—temperature. The cultures were grown at three different $pCO_2$ levels: 400, 1100, and 2200 μatm, but in this model only the experiments at the "ambient" level, 400 μatm, are simulated. The maximum growth rate as a function of temperature has long been considered to be an important predictor of the rate of primary production, along with incoming irradiance and nutrient availability (Eppley, 1972; Bissinger et al., 2008). A recent analysis of observations of growth rate as a function of temperature specifically for *E. huxleyi* has been published (Fielding, 2013): non-zero growth rates have been observed over the range of temperatures from 2 to 27°C, with a very sharp decline at ~27°C as also observed by Schlüter et al. (2014). The most dense range of observations are for standard temperatures 10 and 15°C, where growth rates from near zero to the maximum at that temperature have been observed (Figure 2A from Fielding, 2013). Several fits to the 99th quantile of the data (i.e., 1% of the data points exceeded the fitted function) were carried out. We adopted the power law fit, which is the best fit according to the criteria used by Fielding. **Figure 1** shows the dependence of growth rate on temperature for the power law fit (Fielding, 2013). The red line shows the power law fit that passes through the growth rate at 15°C observed by Schlüter et al. (2014) (1.15 $d^{-1}$, black diamond), and the vertical dashed red line shows its rapid drop off near 27°C. The dashed black line shows the dependence on temperature of the maximum growth rate observed for *E. huxleyi*, according to Fielding (2013).

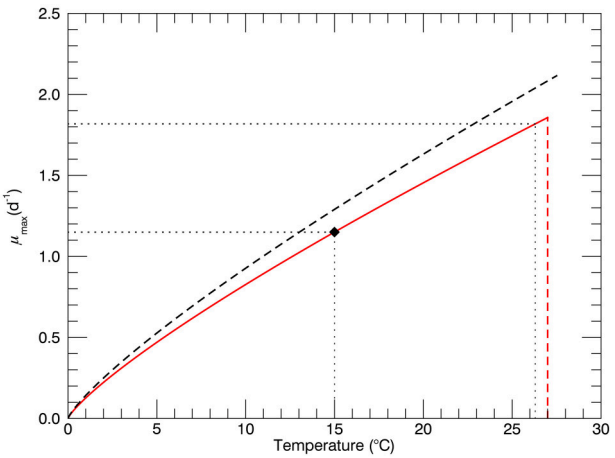


**FIGURE 1 | The black dashed line represents the dependence of maximum possible growth rate $\mu_{max}$ on temperature for the power law fit (Fielding, 2013).** The solid red line represents power law fit through the observed growth rate of for the genotype at 15°C (1.15 $d^{-1}$, solid diamond ♦). The red dashed line represents the sharp drop off near 27°C observed in culture experiments (Schlüter et al., 2014). Horizontal dotted lines show values of the growth rate for temperatures 15 and 26.3°C.

## Model Setup

In the model, genotypes are formulated in equal intervals along the trait axis, the growth rate $\mu$(T) ($d^{-1}$), where T is the temperature. Thus, there are potential genotypes along the trait axis from $\mu_{max} = 0$ to $\mu_{max} \approx 2$ $d^{-1}$ [corresponding to a temperature ~27°C, where the growth rate drops precipitously to zero (Fielding, 2013; Schlüter et al., 2014, Supplementary Information)].

The model is a simple exponential growth equation for each genotype i:

$$\frac{dN_i}{dt} = \mu_i(T)N_i \quad (1)$$

where: $N_i$ is the number of cells in genotype *i*, and $\mu^i$(T) is the growth rate of genotype *i*. At 15°C the maximum possible growth rate is $\mu_{max} = 1.29$ $d^{-1}$ (**Figure 1**, Fielding, 2013) and, as shown by the solid diamond in **Figure 1**, the realized growth rate was 1.15 $d^{-1}$ (Schlüter et al., 2014).

During the laboratory experiments, $10^5$ cells were transferred every 5 days from the existing batch cultures into fresh culture medium to initiate the next batch culture. In the model, the total number of cells across all genotypes $N_T$ ($= \sum_i N_i$) is "normalized" to $10^5$ every timestep (0.2 d) with the same normalization factor applied to each genotype. In the standard simulations, random mutation was allowed once each day: at 15°C the growth rate was 1.15 $d^{-1}$, so that a mutation occurred slightly more often than 1 per generation. Each mutation produced a single cell (in $10^5$ cells). Mutations were allowed at genotypes with growth rates less than and equal to 1.15 $d^{-1}$. Those mutant genotypes with growth rates less than 1.15 $d^{-1}$ grew less quickly than the original genotype—so were not "fixed." Because of the normalization each timestep, those mutants consisted of less than 1 cell, so were set to zero (i.e., not fixed) when they dropped to 0.1 cells. When multiple non-zero genotypes exist, the mean realized growth rate across all non-zero genotypes is given as $\mu_{mean} = (\sum_i N_i \mu_i)/N_T$.

According to Huertas et al. (2011), *"Experimental measures of mutation rates in phytoplankton range from $10^{-5}$ to $10^{-7}$ mutations per cell per generation."* So the rate of one mutation per 1.15 generations in a culture of $10^5$ cells is at the high end of the published rates. We carried out sensitivity studies with mutations occurring both more or less frequently than 1 per day: generally the simulations at lower rates resulted in a slowing down of the increase in biomass of favorable mutations but without any material change in the final results.

The magnitude of each mutation (distance of mutant genotype along the growth rate trait axis from its parent genotype) was determined from a random number generator. Two cases were simulated. First, with a "flat" pdf where the new genotype was equally probable anywhere from the lowest to highest allowed growth rate for that temperature, and, second with a Gaussian normal pdf, where the width of the distribution across genotypes was changed for different simulations. The original genotype and genotypes resulting from mutations were tracked separately. For a flat pdf, only mutations from the original genotype were allowed, since the origin was not important. For the Gaussian pdf, mutations were allowed from the original genotype or from the mutant genotypes (with a probability proportional to their relative biomasses). In both cases, only one

mutation was allowed per day; sensitivity simulations with more or fewer mutations per day did not materially affect the results.

To illustrate the description above without explanation until the Results section, **Figure 2A** shows an initial genotype at the start of a simulation at 15°C, and **Figure 2B** shows a histogram of the distribution (on a logarithmic axis) of total cell biomass in each genotype—after 3 years of simulation at 15°C. The blue bars represent the relative biomass in all non-zero genotypes; "extinct" or not "fixed" genotypes were set to $10^{-7}$ as explained above.

This model considers only one trait, the maximum growth rate at a given temperature. However, two other traits were considered. First, the mortality rate $\mu_{\mathrm{mort}}$ is considered to follow a power law scaling increasing as a function of temperature (Brown et al., 2004; McCoy and Gillooly, 2008; and, specifically for phytoplankton, Regaudie-de-Gioux and Duarte, 2013). However, the observations do not show any sudden drop in realized growth rate when the cultures were warmed from 15 to 26.3°C, suggesting that this scaling is inappropriate for short term changes and more appropriate for asymptotic "steady state" conditions. Second, cell size is also a function of temperature, but calculations based on the experimental results suggest that it is a minor effect. Hence, neither mortality nor cell size are considered further.

The other important environmental variable in the study of Schlüter et al. (2014) is $pCO_2$. While only the 400 μatm case is considered here, it is likely that higher concentrations of $CO_2$ result in a reduction in the height of the "fitness window," in analogy with the "thermal window" concept for animals (Pörtner and Farrell, 2008; Denman et al., 2011).

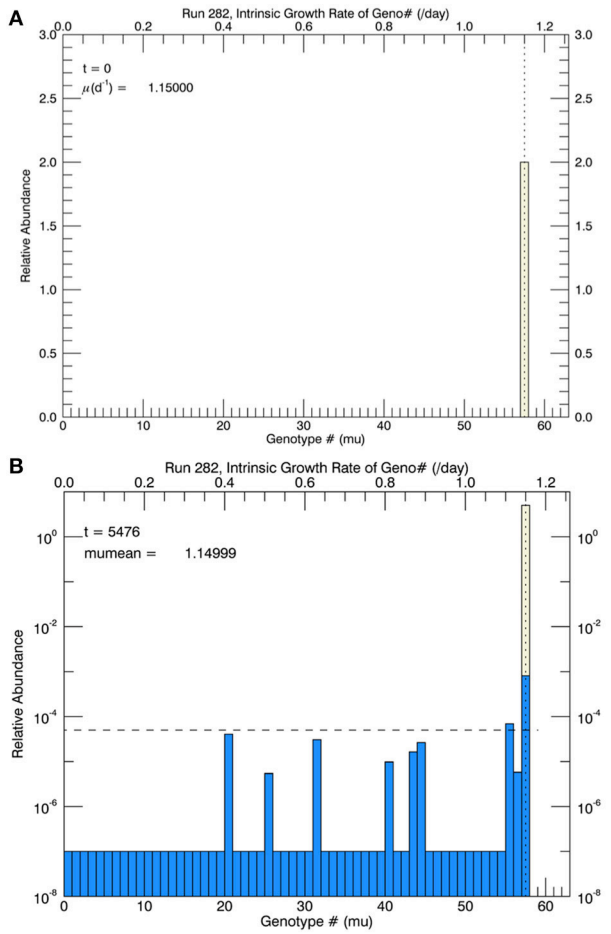


**FIGURE 2 | For the first set of simulations, at 15°C, there were 58 genotypes (#0–#57) spaced evenly in 0.02 $d^{-1}$ intervals along the growth rate/trait axis $\mu$ spanning the range from 0 to 1.16 $d^{-1}$. (A)** Shows the initial genotype with $\mu = 1.15$ $d^{-1}$ (the center value of the highest genotype). **(B)** Shows (for one particular simulation) the relative biomass (logarithmic scale) in each genotype after 3 years of mutations, where the probability of mutation was equal ("flat") across all genotypes. After 3 years, all genotypes except #57 (and #55, which would soon become extinct) were extinct (or not "fixed") since their simulated concentrations had become less than 1 cell (horizontal dashed line) in a culture of $10^5$ cells. When low fitness genotypes reached 1/10 of a cell, they were determined to be extinct and set to a value of $10^{-7}$.

## Simulations

For the first 3 years, five replicates of the coccolithophore *Emiliania huxleyi* were grown in culture at 15°C for each of three $pCO_2$ levels: 400, 1100, and 2200 μatm. At the end of 3 years, the temperature of the cultures was raised in intervals of 1°C $d^{-1}$ to a final temperature of 26.3°C at which they were grown for an additional 1 year. Model simulations of the laboratory experiments with $pCO_2$ concentration of 400 μatm were performed as follows:

(1) *Simulations at 15°C.* These simulations started with a single genotype of $10^5$ cells centered on a growth rate of 1.15 $d^{-1}$, representing the mean observed growth rate of the five replicate cultures. Random mutation of a single cell occurred each day with a flat pdf over the growth rate trait between 0 and the maximum (for 15°C) shown by the solid red curve in **Figure 1** (from Fielding, 2013). Initially there were 58 genotypes, each 0.02 $d^{-1}$ wide, with growth rates ranging from 0 to 1.16 $d^{-1}$, the maximum growth rate under the solid red curve in **Figure 1**. We assume that this clone/genotype was growing (during the first 3 years in culture) at its optimal rate, dependent on its original *in situ* temperature and location, and was not capable, under any conditions, of growing at the maximum rate observed for *E. huxleyi* from all locations (in Fielding, 2013).

(2) *Simulations at 26.3°C, flat pdf for mutations.* These simulations also started with a single genotype of $10^5$ cells centered on a growth rate of 1.15 $d^{-1}$, representing the mean observed growth rate of the cultures grown at 15°C for 3 years (over 1500 generations). Now there were 92 possible genotypes, with maximum growth rates ranging from 0 to 1.84 $d^{-1}$ (the maximum growth rate under the solid curve in **Figure 1** at 26.3°C).

(3) *Simulations at 26.3°C, Gaussian normal pdf for mutations.* The setup was the same as in study 2, but now the magnitude of each random mutation, relative to the center of the parent genotype, followed a Gaussian normal pdf with a width *s,* in units of 0.02 $d^{-1}$ (i.e., the width of one genotype interval), which was specified at the start of the simulation.

(4) *Simulations at 26.3°C, addition of a plastic response.* In all simulations in study 3, for the different values of $s$, there was a lag of at least 60 days or generations before $\mu_{\text{mean}}$, the mean growth rate of the five "replicate" simulations began to increase, contrary to the laboratory results where $\mu_{\text{mean}}$ increased linearly throughout year 4 without any noticeable lag or offset when the temperature was raised from 15 to 26.3°C (Schlüter et al., 2014). To remove this lag, a simple, but plausible, formulation of a plastic response (to be described later) was implemented.

# RESULTS

## Simulations at 15°C

Based on arguments (Orr, 1998, 2005) critical of the concept that adaptive evolution proceeds according "micromutationism" or infinitesimal mutations as first postulated by Fisher (1930), the first set of simulations (for 3 years at 15°C) allowed for the random mutations to obey a flat pdf over the growth rate from 0 to 1.16 $d^{-1}$, the approximate observed growth rate $\mu_{\text{mean}}$ at 15°C (**Figure 1**). There were 58 equally wide genotypes over this space (numbered from 0 to 57). Initially they were all zero except for genotype #57, representing the measured mean growth rate 1.15 $d^{-1}$, shown as the solid diamond in **Figure 1**. The initial biomass of genotype #57 in each simulation is shown as the height of the pale yellow bar in **Figure 2A**.

In the simulations at 15°C, genotype #57 outcompeted all other mutant genotypes, all of which had lower growth rates (and hence lower fitness) than genotype #57. [We take the fitness of a mutant genotype $m$ relative to the parent genotype $p$ to be the ratio of their realized growth rates: $W_{mp} = \mu_m/\mu_p$, and of the relative fitness of mutant genotype $i$ relative to mutant genotype $j$ to be $W_{ij} = \mu_i/\mu_j$ (Lenski et al., 1991; Schlüter et al., 2014). If $W_{mp}$ ($W_{ij}$) is greater than 1, then genotype $m$ ($i$) has a higher fitness than genotype $p$ ($j$).] Therefore, after 3 years, in all five replicate simulations the most abundant genotype was #57 (**Figure 2B**), with its realized growth rate of 1.15 $d^{-1}$. The horizontal dashed line represents $10^{-5}$ of the total biomass, i.e., 1 cell. So by the end of the simulation, almost all genotypes except that with the highest realized growth rate (i.e., genotype #57) had biomass less than 1 cell and were effectively extinct. In the particular simulation shown in **Figure 2B** (one of 5 replicates) genotype #55 also had barely more than 1 cell, but it was a very recent mutation and its biomass would have quickly dropped below 1 cell, as can be seen in **Figure 3**. **Figure 3A** shows the magnitude of all the mutations over the 3 years: they are randomly distributed evenly over all genotypes between #0 and #57.

**Figure 3B** shows the time paths of the logarithm of the biomass of genotypes 20, 55, 56, and 57. Whenever there is a mutation to genotype # 20 (blue dashed line), it quickly dies out because its fitness relative to the parent genotype #57 is small, $W_{20\ 57} \sim 0.36$. Genotype #55 (green) dies out more slowly, $W_{55\ 57} \sim 0.97$, and genotype #56 dies out even more slowly, $W_{56\ 57} \sim 0.98$. The solid red line shows the total biomass of genotype #57, consisting mostly of the original genotype (pale yellow portion in **Figure 2B**) plus mutations to that genotype (lower blue portion), which is also shown by the solid black line in **Figure 3B**. Note that

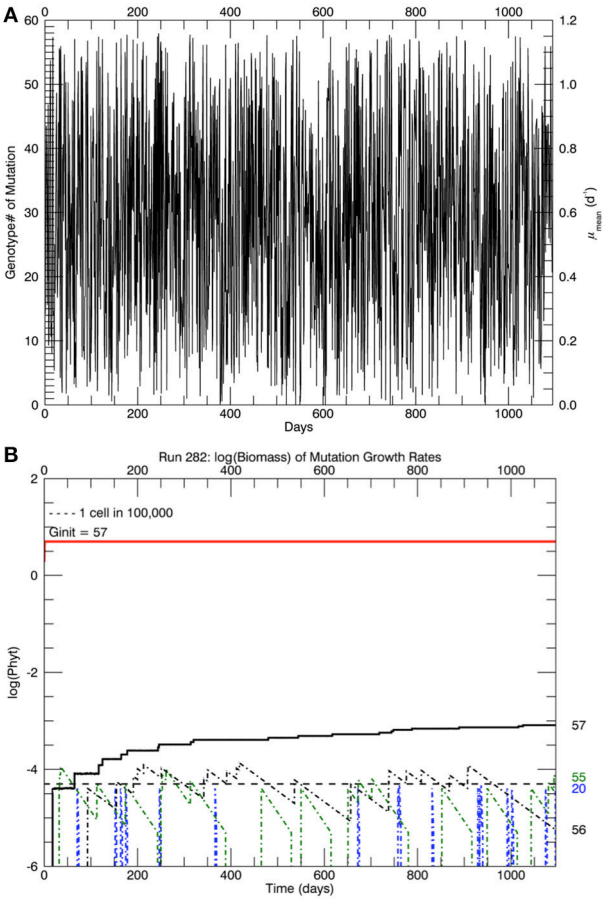


**FIGURE 3 | For the same simulation as in Figure 2B. (A)** Shows the magnitude of the mutations over the 3 years of the simulation. **(B)** Shows the time history of the logarithm of the biomass for the original clone plus mutations to that same growth rate (red line), the proportion of that biomass which was from mutations (black line) and the other three mutant genotypes with the most biomass after 3 years: #20, #55, and #56.

the vertical scale in **Figures 2B**, **3B** is the logarithm of biomass, so actually only 0.016% of the biomass in genotype #57 consisted of mutant cells after 3 years (all 5 replicate simulations had a similar fraction of biomass in genotype #57 ~0.02%. These cells have growth rates equal to the original clone, but they may have other genes that differ from the original clone, as pointed out by Schlüter et al. (2014). However, the simulations in the next section started with $10^5$ cells of what is assumed to be the original genotype #57, which were then warmed instantaneously (in the model) to a temperature of 26.3°C.

## Simulations at 26.3°C with a Flat Pdf for Mutations

In the simulations described here, there are 92 genotypes (numbered 0 to 91) between a growth rate of 0 $d^{-1}$ and the maximum growth rate $\mu_{\text{max}}$ at 26.3°C (solid red line in **Figure 1**), with each genotype interval being 0.02 $d^{-1}$ wide as before. Thus, the highest genotype #91 is centered at 1.83 $d^{-1}$ with its upper

limit being $\mu_{max}(26.3°C) = 1.84\ d^{-1}$. Similarly, $\mu_{max}(15°C) = 1.15\ d^{-1}$ occurs at the center of genotype #57.

Five replicate simulations at 26.3°C with a flat pdf of the magnitudes of random mutations all quickly ended up with mutant genotypes with the highest growth rate or relative fitness eventually dominating the culture. **Figure 4** tracks the time history of the biomass of the four highest genotypes: 88, 89, 90, and 91 for one of the 5 simulations. A mutation to #89 occurred first (on day 31), followed by one to #88 (on day 59), then one to #91 (on day 72), and lastly one to #90 (on day 219), with the four jumps afterwards indicating subsequent mutations to this genotype. These are not the only mutations to these genotypes then, just the first ones during this simulation. Note that #88 grew more slowly than #89 (because the fitness of #89 was relatively higher, but #91 outpaced them both, for the same reason. They all outcompeted the original clone #57 because of their significantly higher relative fitness. This coexistence of four mutant clones is an example of clonal interference observed in asexual populations (e.g., Muller, 1932; Gerrish and Lenski, 1998; Imhof and Schlötterer, 2001).

Given enough generations, the clone with the highest fitness will dominate the culture. Reducing the mutations from once a day (slightly greater than one generation) to every other day did not affect the end result, only marginally the rate of getting there. **Figure 5** shows time series of the growth rate for the five replicate simulations, each with a new "seed" for the random mutations. The timing and nature of the increase in growth rate also depends on how soon mutations at the higher genotypes occur. Regardless, in each of these simulations, there is no significant increase in growth rate in the first ~20 days, then it rapidly increases eventually to the growth rate of the highest mutant genotype. This behavior does not follow the linear increase in $\mu_{mean}$ from 1.15 $d^{-1}$ at the start of the year to 1.33 $d^{-1}$ (with no discernable initial lag) that was observed in the laboratory (Schlüter et al., 2014). Moreover, the asymptotic mean growth rate after 1 year in these simulations is much higher than the eventual observed mean growth rate in the laboratory experiments (shown by the blue dashed line).

## Simulations at 26.3°C with a Gaussian Normal Pdf of Random Mutations

In the simulations with a flat pdf for random mutations, the invariable domination by mutations near the maximum possible growth rate $\mu_{max}$ suggests that in the laboratory experiments mutations with infinitesimal magnitudes might have been more likely (as suggested by Fisher, 1930), rather than mutations with "large" magnitudes being as likely as infinitesimal mutations (as argued by Orr, 1998, 2005, and others).

In these simulations, the magnitudes of mutations follow a Gaussian normal random pdf about the parent genotype. The width of the Gaussian normal pdf of mutation magnitude about the genotype undergoing a mutation is given by $s$ (measured in genotype intervals of 0.02 $d^{-1}$). Hence, for $s = 1$ the distance from the center of the parent genotype interval to the outsides of the two adjacent genotypes is $\pm 1.5s$, i.e., the probability of a mutation occurring in the parent genotype or the adjoining genotypes is 86.6%. For $s = 2$ the distance from the center of the parent genotype interval to the outsides of the two adjacent genotypes is $\pm 0.75s$, i.e., the probability of a mutation occurring in the parent genotype or the adjoining genotypes is reduced to 54.7%.

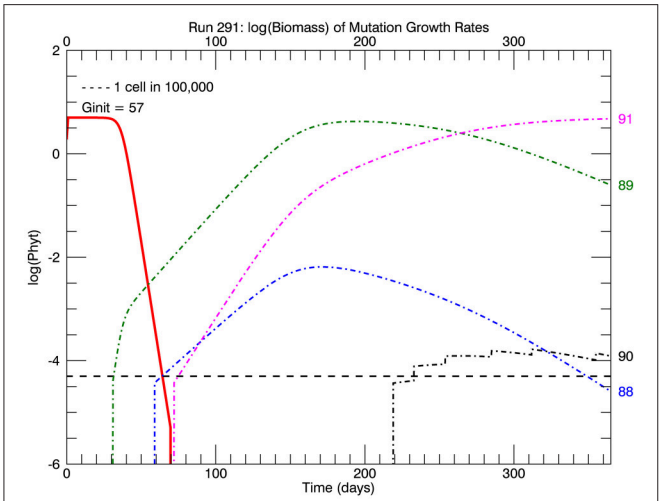


**FIGURE 4 | Time history of relative biomasses (logarithmic scale) for different genotypes for one replicate simulation after abrupt warming from 15 to 26.3°C.** There are now 92 genotypes (#0–#91) spanning the trait range from 0 to 1.84 $d^{-1}$, the latter being the maximum growth rate at 26.3°C (solid red line, **Figure 1**). As before a mutation was equally probable to all genotypes ("flat" pdf). The initial genotype (representative of the culture at 15°C) was now #57 with a growth rate of 1.15 $d^{-1}$. The first large magnitude mutation, to genotype #89 on day 31, rapidly replaced the original genotype #57 because of its much greater relative fitness 1.56. However, the mutant genotype #91(magenta line) eventually replaced earlier genotypes #89 (green line) and #88 (blue line) because it had the highest relative fitness of all mutants.

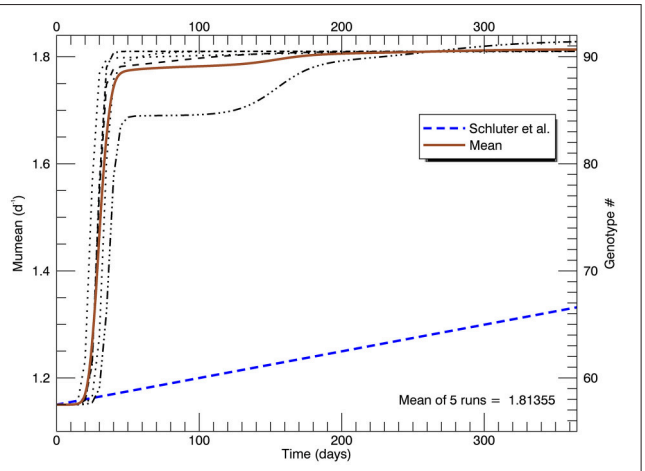


**FIGURE 5 | Time series of five replicate simulations at 26.3°C, including that in Figure 4, each with a different random seed (with a flat pdf for random mutations).** The vertical axis on the left shows the growth rate (for each genotype shown on the right). The heavy brown curve shows the time history of the mean of the five replicate simulations. The heavy blue dashed line is the fitted line to the measured mean growth rate (of five replicate cultures) in the experiments (Schlüter et al., 2014).

Three sets of five replicate simulations were performed, with $s = 1$, 2, and 3. For $s = 1$, the growth rates after 1 year were well below those observed and these results are not discussed further. In **Figure 6A**, for $s = 2$, we show the distribution of biomass among genotypes after 1 year on a logarithmic scale for the replicate with the median mean growth rate. Although there appear to be about 20 genotypes in play, a linear plot of these genotypes (**Figure 6B**) shows that only about 4 or 5 genotypes account for almost all (at least 99%) of the biomass. We have therefore allowed only the 10 highest biomass mutant genotypes to undergo mutations themselves, with a probability inversely proportional to their relative biomass. Thus, from **Figure 6B**, on the next day, a mutation would be most likely be from #63, next most likely from #61, next most likely from #64 and so on, with the magnitude of each mutation determined randomly from a Gaussian normal pdf with $s = 2$. **Figure 7A** shows, for the same replicate simulation as in **Figure 6**, the time evolution of the biomasses of the original clone (#57, red) as well as the five mutant genotypes with the most biomass after 1 year: 61, 63, 64, 65, and 66, again demonstrating clonal interference, especially with #63 outcompeting #61, and with the higher fitness genotypes 64, 65, and 66 increasing each at a greater rate. **Figure 7B** shows the realized growth rate for the same simulation (heavy solid line), the mutations each day (jagged light solid line), and ± the standard deviation of the distribution of the biomasses of the active genotypes (see **Figure 6A**), along the trait or genotype axes (light dashed lines)

In this set of five replicate simulations with $s = 2$, the mean growth rate increased from 1.15 to 1.27 $d^{-1}$ after 1 year. In addition, the growth rate did not begin to increase until after ∼110 days, roughly 125 generations (**Figure 8**). In the laboratory study (Schlüter et al., 2014), the realized growth rate increased, more or less linearly without discernible lag, to a value (from their fitted line) of 1.33 $d^{-1}$ at the end of 1 year. Thus, the increase in realized growth rate in these

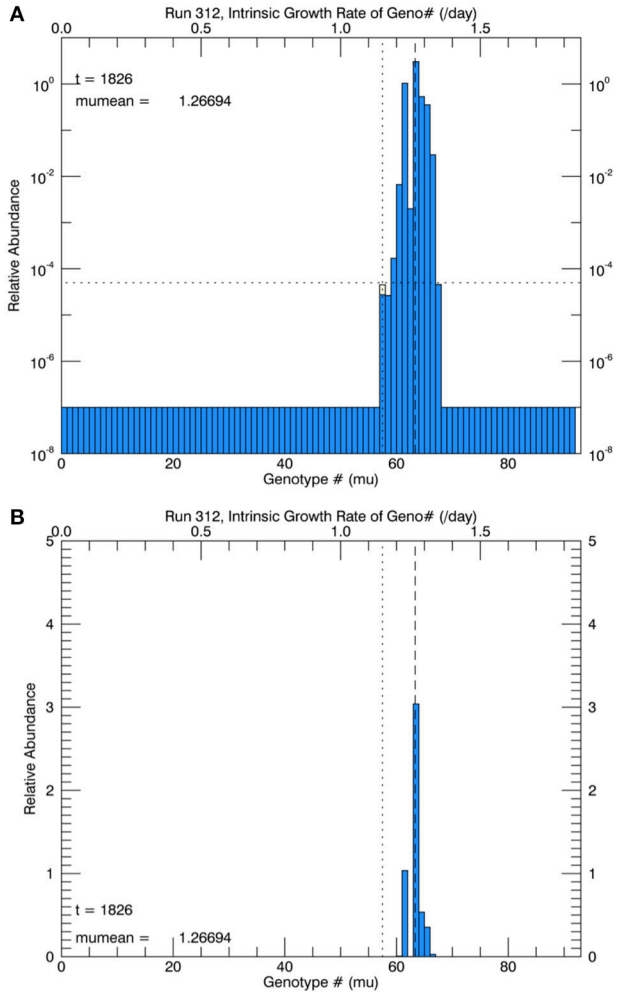


**FIGURE 6 | Results at the end of 1 year for one of five replicate simulations at 26.3°C with a Gaussian normal pdf for random mutations, with a width $s = 2$ genotype intervals of 0.02 $d^{-1}$. (A)** Shows the relative biomass (on a logarithmic axis) of mutations in all genotypes after 1 year. The horizontal dotted line represents 1 cell in $10^5$ cells, and the vertical dashed line is the mean realized growth rate of the distribution. **(B)** Shows the same information, but for a linear biomass axis.

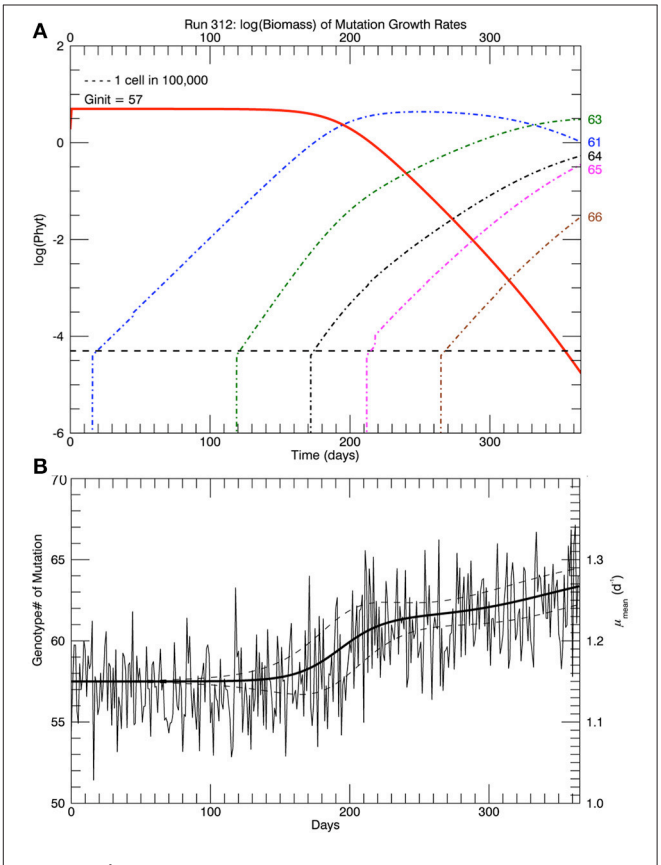


**FIGURE 7 | (A)** Shows, for the same replicate simulation as in **Figure 6**, the time history of relative biomasses for the original genotype #57 and for the five most abundant mutant genotypes (61, 63, 64, 65, and 66) 1 year after abrupt warming from 15 to 26.3°C (similar to **Figure 4**). **(B)** Shows the time history of the mutations (light solid jagged line) about the growth rate (heavy solid line). Light dashed lines show ± one standard deviation of the distribution of biomass (**Figure 6**) about the growth rate/trait axis. When there are more genotypes with significant biomass, the standard deviation will be larger.

simulations was too small and the initial lag of ~110 days was unrealistic.

Another set of five simulations was performed with $s = 3$. **Figure 9** shows the time path of the mean growth rate for each of the five replicate simulations (light lines), the overall mean growth rate (brown solid line) and the fitted linear increase in growth rate from the experiments (blue dashed line, Schlüter et al., 2014). After 1 year, the mean growth rate was 1.47 $d^{-1}$ (range 1.39–1.69 $d^{-1}$), exceeding that in the laboratory experiment. These simulations tend to exhibit lags of ~70–130 days followed by plateaus, especially the simulation with the highest growth rate after 1 year. In that simulation, after ~70 days the growth rate increased steeply to a plateau ~1.33 $d^{-1}$ (genotype #66), then at ~200 days it increased again to a plateau ~1.55 $d^{-1}$ (genotype #77) followed by another steep rise starting at ~320 days. **Figure 10A** shows the distribution of genotypes after 1 year for this simulation: here there were 12 genotypes with biomasses greater than 1 cell. **Figure 10B** tracks the time history of the simulation for genotypes 66, 77, 81, 82, and 85. The first large magnitude mutation from the parent genotype #57 to genotype #66 (on day 15) is rare (3$s$) but possible for a Gaussian normal pdf with $s = 3$; the second from #66 to #77 (on day 149) is also rare but possible. **Figure 10B** again shows clonal interference, as mutants with higher relative fitness eventually out-compete less fit mutants (cf. Figures 8, 9 in Gerrish and Lenski, 1998).

To summarize the results of this set of simulations, the overall mean growth rate increased roughly linearly after about 70 days, but again among the replicate simulations there was a lag of

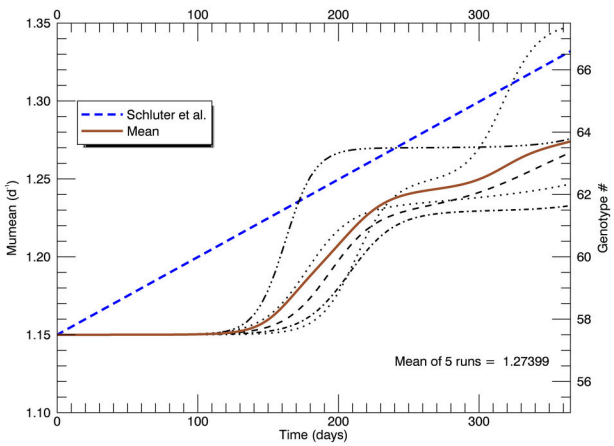


**FIGURE 8 | Time series of all five replicate simulations at 26.3°C with a Gaussian normal pfd (with $s = 2$) for mutations about the mean growth rate Note that the realized growth rate did not increase significantly in any simulation until after ~110 days.** The blue dashed line is as in **Figure 5** (note change of scale on the vertical axis).

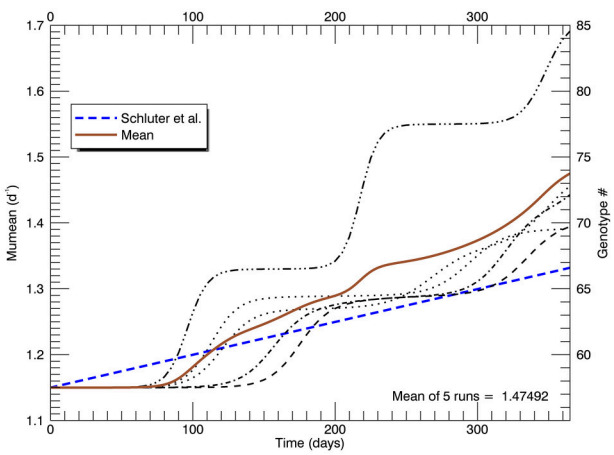


**FIGURE 9 | Time series of the realized growth rates for all five replicate simulations with $s = 3$ (light broken lines), the mean growth rate for the five simulations (solid brown line), and the fitted (dashed blue) line to the experimental results as in Figures 5, 8 (again note the change of scale on the vertical axis).**

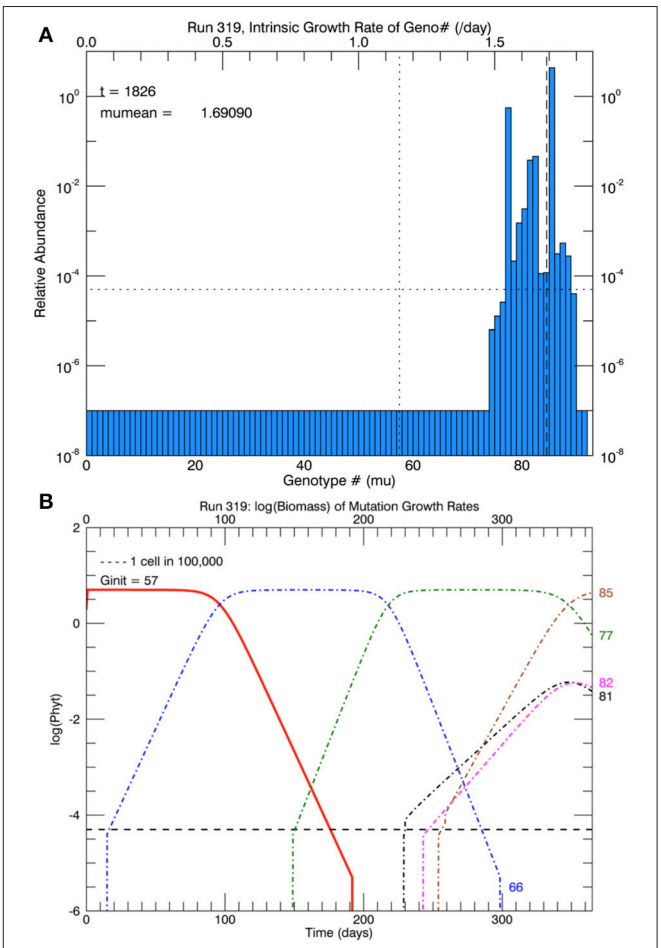


**FIGURE 10 | Results for one of five replicate simulations with $s = 3$, the one with the highest growth rate (1.69 $d^{-1}$) at the end of 1 year.** All other parameters are the same as in **Figures 6–8**. **(A)** Shows the relative biomass of mutations in all genotypes after 1 year. **(B)** Shows the time history of the original genotype #57 (solid red line) and five other genotypes (66, 77, 81, 82, and 85). Mutations with large magnitude to #66 and later to #77 each became dominant, resulting in plateaus lasting ~60 days (see **Figure 9**).

∼70–130 days before the growth rate(s) start to increase, contrary to the experimental data (Schlüter et al., 2014).

# DISCUSSION

## Three-Year Simulations at 15°C

Initially, the model was set up with 58 genotypes (each 0.02 $d^{-1}$ wide) spanning the range of possible growth rates at 15°C from 0 to ∼1.16 $d^{-1}$ (Figure 2 and Fielding, 2013). Mutations were equally probable (a "flat" pdf) to all 58 genotypes (#0 to #57) under the assumption that the original genotype #57 was the genotype with the highest possible growth rate and hence the maximum relative fitness. So only mutations to that same genotype survived or were "fixed," while mutations to other genotypes (#0 to #56), all with lower relative fitness, became extinct (or failed to be "fixed"), as shown in **Figures 2**, **3**. At the end of the 3 years, in all five replicate simulations, mutations to genotype #57 contributed ∼0.02% to the total biomass shown in that genotype. Although these cells had the same growth rate as the original clones, they presumably possessed other genes that apparently did not affect their growth rate at 15°C.

## Time Lag in Growth Rate Response to Mutations

Simulations at 26.3°C had 92 possible genotypes, each of width 0.02 $d^{-1}$, spanning the growth rates between 0 and 1.84 $d^{-1}$, the maximum possible growth rate for this clone (the value of the red line in **Figure 1** at 26.3°C). The initial genotype was still #57, assumed to be the single genotype existing after 3 years of growing at 15°C, ignoring the ∼0.02% of the cells that were mutants in the simulations but with the same growth rate at 15°C. All simulations exhibited a time lag after the temperature shift from 15°C before there was any significant increase in the realized growth rate, which was not observed in the laboratory experiments of Schlüter et al. (2014).

For a flat pdf of random mutations, the genotype created from the largest magnitude favorable mutation eventually dominated and replaced the original genotype. Usually, after 1 year the dominant genotype is #90 or #91 (**Figures 4**, **5**). **Figure 5** shows that there is typically a lag of ∼15–30 days (∼17–34 generations) before the realized growth rate starts to increase significantly. Then very quickly (over ∼20 days) the growth rate climbs rapidly to that for the highest mutant genotype, where it remains for the rest of the year unless there is a subsequent mutation to a higher genotype. This behavior, two plateaus separated by an abrupt increase from the first to the second, is completely inconsistent with, and with a much larger final growth rate than, the final fitted growth rate from the laboratory experiments.

For the flat pdf, each mutation has a 62% chance of having a relative fitness less than that of the original clone (57 of 92 possible genotypes). If the rate of mutations were to decrease by a factor of 10, then the lag time would be 10 times longer, but the time for a given favorable mutation to increase would be the same because it is a function of the generation time or growth rate.

It was concluded from these simulations that an initial lag followed by an abrupt increase in growth rate results from allowing mutations of the largest magnitude to have the same probability as mutations of the smallest magnitude. If small magnitude mutations were to have a much higher probability than large magnitude mutations, then possibly the transition to higher grow rates after increasing the temperature to 26.3°C would be more gradual and continuous. To allow for mutations of very small magnitude, in subsequent simulations the magnitude of each mutation along the trait axis was chosen randomly from a Gaussian normal pdf, N($\mu_{max}$, $s$) in statistical notation, centered on the growth rate of the parent genotype, with a width along the trait axis scaled by the standard deviation s (in genotype intervals).

The first set of five simulations shown here, with $s = 2$ genotypes wide, generated a much too small increase in mean growth rate $\mu_{mean}$, reaching only 1.27 $d^{-1}$ compared with the fitted value of 1.33 $d^{-1}$ from the laboratory experiments. Again, the simulations show a long lag of ∼110 days before any significant increase occurred (**Figure 8**). A second set of five simulations with $s = 3$ was then performed (**Figure 9**). A larger number of genotypes were generated from mutations, with many of them still viable (1 cell or more) at the end of 1 year (**Figure 10**). The mean growth rate of the five replicate simulations increased more or less linearly for the latter two thirds of the year, with a slope roughly double that observed. But there still remained a lag of ∼70 days before the mean growth rate started to increase. Overall, for a larger $s$, i.e., larger magnitude mutations, the lag time was shorter. For $s = 1$, 2, and 3, the lag time was respectively ∼150, ∼120, and ∼70 days. Clearly, adaptive evolution by genetic mutations, modeled in the manner described here, cannot alone explain the laboratory results (Schlüter et al., 2014) because all simulations were characterized by initial lags upon warming to 26.3°C.

## A "Plastic" Response to Abrupt Temperature Change?

A possible explanation for the immediate continuous increase in observed growth rate after increasing the temperature from 15 to 26.3°C is that it was a "plastic" response of the cells to their changing environment. The idea of plasticity "buying time" for genetic adaptation to take place is central to the concept of "plastic rescue" avoiding extinction (e.g., Lande, 2009; Chevin et al., 2010; Kopp and Matuszewski, 2014). There are many definitions of plasticity: Whitman and Agrawal (2009) list 11, but perhaps their simplest is "Phenotypic plasticity" is "the capacity of a single genotype to exhibit variable phenotypes in different environments ...." According to Reusch (2014), reviewing evidence of plasticity in marine animals and plants: "Phenotypic plasticity broadly defines the adjustment of phenotypic values of genotypes depending on the environment, without genetic changes."

Most studies of plasticity compare different phenotypes of the same genotype in different environments. More relevant in our case would be studies that consider the temporal change in phenotypic properties of a given genotype in response to a change (continuous or abrupt) in its environment, but such studies are rare. And different species generally have different plastic responses to the same change in environment (different "reaction

norms," (e.g., Pigliucci, 2005; Whitman and Agrawal, 2009; Reusch, 2014). There is no clear information on how plasticity might be modeled in this case, especially what ultimately limits the rate and magnitude of plastic response. Currently, both the energetic costs and limits of plasticity are research questions of considerable interest (e.g., DeWitt et al., 1998; Pigliucci, 2005).

Given that the generation time of *E. huxleyi* in the laboratory experiments was less than 1 day, a plastic response would have to be "transgenerational" or heritable, for which there is mounting evidence in animals (Munday, 2014; Walsh et al., 2014), in clonal plants (e.g., Latzel and Klimešová, 2010), and in phytoplankton (Schaum et al., 2013; Schaum and Collins, 2014). For asexual reproduction the hypothesized mechanism is "epigenetic inheritance" whereby an environmental change causes genes to be expressed, which continue to be expressed in succeeding generations if the environmental change continues (Latzel and Klimešová, 2010; Schaum et al., 2013; Schaum and Collins, 2014; van Oppen et al., 2015). In the laboratory experiments of Schlüter et al. (2014), it is assumed that the change in temperature from 15 to 26.3°C caused the expression of an existing gene in essentially all cells in the culture in the first and succeeding generations which mediated a slow increase in growth rate, without the lag that would result from the favorable mutation of a single cell dividing sufficiently often to start to compete with the original population.

Here we assume that the plasticity is heritable, and model it as a first order restoring function without lag:

$$\frac{d\mu_i(t)}{dt} = (\mu_{\max}(i) - \mu_i(t))/T \tag{2}$$

where $\mu_i(t)$ is the realized growth rate and $\mu_{\max}(i)$ is the maximum growth rate, both for the initial genotype $i$, according to the power law fit (Fielding, 2013) through the original growth rate at 15°C (solid red line in **Figure 1**). $T$ (or $\tau$) is the "e-folding" time for the response. The assumed mechanism is that because of energy costs the plastic response of a given genotype $i$ cannot exceed its $\mu_{\max}(i)$ value for 15°C, even though it is now at a higher temperature. The rate at which $\mu_i(t)$ approaches $\mu_{\max}(i)$ decreases as it gets closer, the logic being that the larger the plastic response, the more energy that is required.

The solution to the ordinary differential Equation (2) is standard:

$$\mu_i(t) = (\mu_i(0) - \mu_{\max}(i))\mathrm{e}^{-t/T} + \mu_{\max}(i) \tag{3}$$

This function has the form shown **Figure 11**, where the dashed curve shows the full function to its asymptote. The solid curve has a $T$ value set to 281 d, so that the initial slope of Equation (3) at small $t$ is equal to the slope of the linear fit to the observations over 1 year (Figure 1A in Schlüter et al., 2014). For the initial genotype, $\mu_{\max} = 1.29$ d$^{-1}$, so that the observed (fitted) growth rate after 1 year of 1.33 d$^{-1}$ could not be reached by means of plasticity alone. In fact for the value chosen for $T$, the plastic response at the end of 1 year would result in a mean growth rate of only 1.25 d$^{-1}$ (solid curve, **Figure 11**).

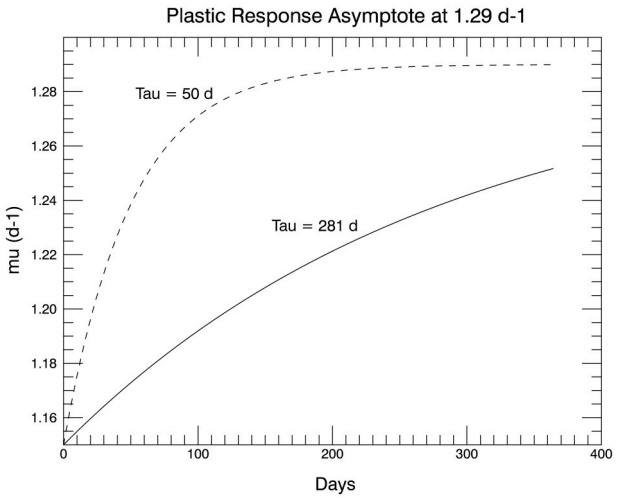


**FIGURE 11 | The proposed plastic response over time of genotype #57 to the temperature change from 15 to 26.3°C.** The asymptote is $\mu_{\max}$ for 15°C (shown in the dashed curve). The initial slope in the solid curve (used in the simulations) is set to match the slope of the line fitted to the 1 year of measured growth rates from the laboratory experiments in Schlüter et al. (2014).

Three sets of five replicate simulations were then performed at 26.3°C with $s = 2$, 2.5, and 3, but with a plastic response of the original genotype. Now the growth rate of the initial genotype (initially $\mu_i(0) = 1.15$ d$^{-1}$) increased with time according to Equation (3). As its growth rate increased, the biomass of the original genotype was added to any in the appropriate growth rate interval that had accumulated from mutations. Due to the plastic response, the original genotype had moved from #57 to #62 on the growth rate axis after 1 year. **Figure 12A** shows the results of 1 replicate simulation with $s = 2.5$; in all five replicate simulations with $s = 2.5$, the original genotype represented most of the biomass in that interval. **Figure 12B** shows the time evolution of the five other genotypes with the most biomass after 1 year: clonal interference between genotypes 63, 64, and 66. Genotype #66, because it had the highest relative fitness, outcompeted genotypes 63, and 64, even though they had mutated earlier. **Figure 13A** shows the time history of the growth rates for all five replicate simulations, the ensemble mean growth rate (solid brown line), and the (dashed blue) line fitted to the laboratory results. The plastic response eliminated the initial lag in the increase of the growth rate, consistent with the observations. The ensemble growth rate after 1 year was 1.34 d$^{-1}$ (slightly greater than that of the observations, 1.33 d$^{-1}$). In **Figure 13B**, simulated random measurement error has been added to the simulated overall mean growth rate, for comparison with the observations (Figure 1A in Schlüter et al., 2014). Thus, the plastic response, as formulated, removed the lag in response present in all previous simulations, giving time for mutations to new genotypes eventually to dominate the culture toward the end of the year. In addition to the maximum growth rate, the only other trait reported on by Schlüter et al. (2014) was cell diameter. The

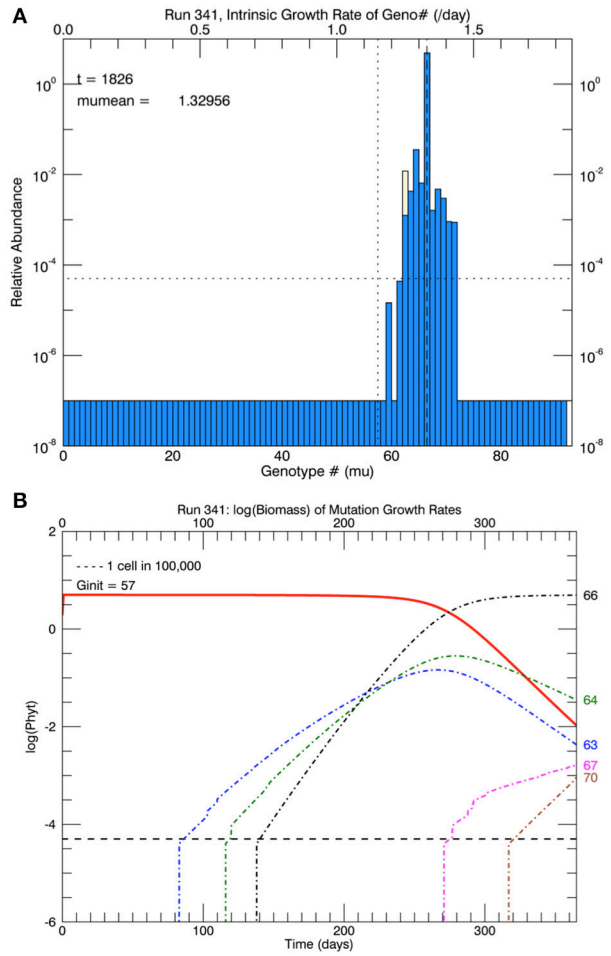


**FIGURE 12 | Results for one simulation (with $s = 2.5$) that includes the plastic response (Figure 11).** In **(A)**, the vertical dotted line shows the growth rate of the original genotype and the position on the x-axis of the light yellow bar shows where the growth rate of the initial genotype (#57) has reached (genotype #62) with the growth rates shown on the upper x-axis. **(B)** Shows the time series of the relative biomass of the different genotypes: the original genotype (#57, solid red line), and the five most abundant genotypes at the end of 1 year (63, 64, 66, 67, and 70). Genotype #66 has become the dominant genotype (highest peak in **A**) due to its higher fitness relative to #57, although eventually the mutant genotype #70 would replace #66.

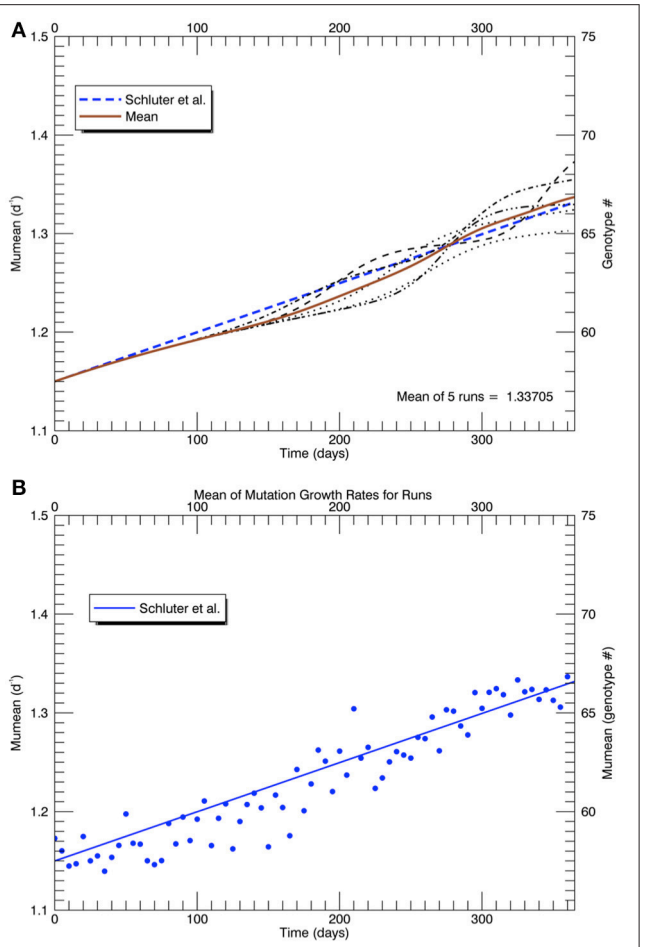


**FIGURE 13 | Similar to Figure 10, (A)** shows the time series of all five replicate simulations ($s = 2.5$) with the plastic response implemented as in **Figure 11** (light curves), the mean realized growth rate for the five replicate simulations (solid brown curve), and (as in **Figures 5**, **8**, **10**) the (dashed blue) line fitted to the experimental results (Schlüter et al., 2014). **(B)** shows (blue) points along the mean (brown) curve with simulated random "measurement errors," and the fit to the experimental results (solid blue line), for comparison with Figure 1A in Schlüter et al. (2014).

cell diameter was significantly smaller (∼10%) at 26.3°C, but only for the cultures grown at the "ambient" level of $pCO_2$: 400 μatm.

## Effects of Multiple Stressors

Schlüter et al. (2014) maintained cultures of *Emiliania huxleyi*, all originating from the same single cell, at three different $pCO_2$ levels for 4 years, increasing the temperature from 15 to 26.3°C at the end of the third year. Although the growth rate at 15°C decreased with increasing $pCO_2$, the growth rate increase over the last year (at 26.3°C) was greater at successive higher $pCO_2$ levels, such that the growth rates at the end of the experiment were closer together than during the first 3 years, suggesting that at the higher temperature, the cells were affected less by $CO_2$ concentration. Without some information about energy costs of adaptation, it is not clear how to model either the effects of mutation (or of plasticity) in response to two simultaneous stressors.

## CONCLUSIONS

Modeling even the adaptive response to abrupt change in a single environmental variable in an asexual phytoplankton population of a single trait led to unexpected results. If this model is a valid representation of the experimental results of Schlüter et al. (2014), then several conclusions pertain:

(1) The largely linear increase over 1 year in measured growth rate without an initial lag after an abrupt increase in temperature cannot be explained on the basis of genetic mutation alone. The caveat (mentioned by Schlüter et al., 2014) is that there were cells in the culture at 15°C after 3 years, which were mutants with the same growth rate 1.15 $d^{-1}$ but with some different genes that would possibly allow

them to respond differently to the increase in temperature to 26.3°C. In the model simulations at 15°C, after 3 years these cells comprised only ∼0.02% of the culture, suggesting that some lag would still occur after the switch to a warmer temperature.

(2) Mutation may occur frequently, i.e., close to every generation, but not all mutations are favorable, i.e., have a higher relative greater fitness than the original culture, and all mutations with a relative fitness less than the original culture are not "fixed" and hence become extinct.

(3) Future models of plasticity and effects of multiple stressors require some knowledge and formulation of "costs vs. benefits" in order to determine rates and ultimate limits in plastic response (e.g., Sokolova, 2013).

## AUTHOR CONTRIBUTIONS

All research and manuscript writing and preparation were carried out by the author.

## FUNDING

The author received no research funds for this work. The Canadian Centre for Climate Modelling and Analysis of Environment and Climate Change Canada and the University of Victoria provided office space and network support.

## ACKNOWLEDGMENTS

The author benefitted from discussions with other participants at the 2014 and 2016 Gordon Research Conferences on Ocean Global Change Biology, and from discussions with J. R. Christian. Y. Zhang, U. Riebesell, and T. Reusch provided their growth rate vs. temperature data and fitted thermal response functions from Zhang et al. (2014). The author wishes to thank the two reviewers for their constructive and helpful comments, which improved the manuscript immeasurably.

## REFERENCES

Bissinger, J. E., Montagnes, D. J. S., Sharples, J., and Atkinson, D. (2008). Predicting marine phytoplankton maximum growth rates from temperature: improving on the Eppley curve using quantile regression. *Limnol. Oceanogr.* 53, 487–493. doi: 10.4319/lo.2008.53.2.0487

Brown, J. H., Gillooly, J. F., Allen, A. P., Savage, V. M., and West, G. B. (2004). Toward a metabolic theory of ecology. *Ecology* 85, 1771–1789. doi: 10.1890/03-9000

Chevin, L.-M., Lande, R., and Mace, G. M. (2010). Adaptation, plasticity, and extinction in a changing environment: towards a predictive theory. *PLoS Biol.* 8:e1000357. doi: 10.1371/journal.pbio.1000357

Chust, G., Allen, J. I., Bopp, L., Schrum, C., Holt, J., Tsiaras, K., et al. (2014). Biomass changes and trophic amplification of plankton in a warmer ocean. *Glob. Chang. Biol.* 20, 2124–2139. doi: 10.1111/gcb.12562

Collins, M., Knutti, R., Arblaster, J., Dufresne, J.-L., Fichefet, T., Friedlingstein, P., et al. (2013). "Long-term climate change: projections, commitments and irreversibility," in *Climate Change 2013: The Physical Science Basis. Contribution of Working Group I to the Fifth Assessment Report of the Intergovernmental Panel on Climate Change*, eds T. F. Stocker, D. Qin, G.-K. Plattner, M. Tignor, S. K. Allen, J. Boschung, et al. (Cambridge; New York, NY: Cambridge University Press), 1029–1136.

Collins, S. (2011). Many possible worlds: expanding the ecological scenarios in experimental evolution. *Evol. Biol.* 38, 3–14. doi: 10.1007/s11692-010-9106-3

Collins, S., and Bell, G. (2004). Phenotypic consequences of 1,000 generations of selection at elevated $CO_2$ in a green alga. *Nature* 431, 566–569. doi: 10.1038/nature02945

Collins, S., Sültemeyer D., Bell, G. (2006). Rewinding the tape: selection of algae adapted to high $CO_2$ at current and pleistocene levels of $CO_2$. *Evolution* 60, 1392–1401. doi: 10.1111/j.0014-3820.2006.tb01218.x

Collins, S., Rost, B., and Rynearson, T. A. (2014). Evolutionary potential of marine phytoplankton under ocean acidification. *Evol. Appl.* 7, 140–155. doi: 10.1111/eva.12120

Daniels, C. J., Sheward, R. M., and Poulton, A. J. (2014). Biogeochemical implications of comparative growth rates of *Emiliania huxleyi* and *Coccolithus* species. *Biogeosciences* 11, 6915–6925. doi: 10.5194/bg-11-6915-2014

Denman, K., Christian, J. R., Steiner, N., Poertner, H.-O., and Nojiri, Y. (2011). Potential impacts of future ocean acidification on marine ecosystems and fisheries: current knowledge and recommendations for future research. *ICES J. Mar. Sci.* 68, 1019–1029. doi: 10.1093/icesjms/fsr074

DeWitt, T. J., Sih, A., and Wilson, D. S. (1998). Costs and limits of phenotypic plasticity. *Trends Ecol. Evol. (Amst).* 13, 77–81. doi: 10.1016/S0169-5347(97)01274-3

Eppley, R. W. (1972). Temperature and phytoplankton growth in the sea. *Fish. Bull.* 70, 1063–1085.

Gerrish, P. J., and Lenski, R. E. (1998). The fate of competing beneficial mutations in an asexual population. *Genetica* 102–103, 127–144. doi: 10.1023/A:1017067816551

Fielding, S. R. (2013). *Emiliania huxleyi* specific growth rate dependence on temperature. *Limnol. Oceanogr.* 58, 663–666. doi: 10.4319/lo.2013.58.2.0663

Fisher, R. A. (1930). *The Genetical Theory of Natural Selection*. Oxford: Oxford University Press.

Hagino, K., Bendif, E. M., Young, J. R., Kogame, K., Probert, I., Takano, Y., et al. (2011). New evidence for morphological and genetic variation in the cosmopolitan coccolithophore *Emiliania huxleyi* (prymnesiophyceae) from the cox1b-atp4 genes1. *J. Phycol.* 47, 1164–1176. doi: 10.1111/j.1529-8817.2011.01053.x

Hoegh-Guldberg, O., Cai, R., Poloczanska, E. S., Brewer, P. G., Sundby, S., Hilmi, K., et al. (2014). "The ocean," in *Climate Change 2014: Impacts, Adaptation, and Vulnerability. Part B: Regional Aspects. Contribution of Working Group II to the Fifth Assessment Report of the Intergovernmental Panel of Climate Change*, eds V. R. Barros, C. B. Field, D. J. Dokken, M. D. Mastrandrea, K. J. Mach, T. E. Bilir, et al. (Cambridge; New York, NY: Cambridge University Press), 1655–1731.

Huertas, I. E., Rouco, M., López-Rodas, V., and Costas, E. (2011). Warming will affect phytoplankton differently: evidence through a mechanistic approach. *Proc. Biol. Sci.* 278, 3534–3543. doi: 10.1098/rspb.2011.0160

Imhof, M., and Schlötterer, C. (2001). Fitness effects of advantageous mutations in evolving *Escherichia coli* populations. *Proc. Natl. Acad. Sci. U.S.A.* 98, 1113–1117. doi: 10.1073/pnas.98.3.1113

Kopp, M., and Matuszewski, S. (2014). Rapid evolution of quantitative traits: theoretical perspectives. *Evol. Appl.* 7, 169–191. doi: 10.1111/eva.12127

Lande, R. (2009). Adaptation to an extraordinary environment by evolution of phenotypic plasticity and genetic assimilation. *J. Evol. Biol.* 22, 1435–1446. doi: 10.1111/j.1420-9101.2009.01754.x

Latzel, V., and Klimešová, J. (2010). Transgenerational plasticity in clonal plants. *Evol. Ecol.* 24, 1537–1543. doi: 10.1007/s10682-010-9385-2

Lenski, R., Rose, M., Simpson, S., and Tadler, S. (1991). Long-term experimental evolution in *Escherichia-coli*. 1. Adaptation and divergence during 2,000 generations. *Am. Nat.* 138, 1315–1341. doi: 10.1086/285289

Litchman, E., Edwards, K. F., Klausmeier, C. A., and Thomas, M. K. (2012). Phytoplankton niches, traits and eco-evolutionary responses to global environmental change. *Mar. Ecol. Prog. Ser.* 470, 235–248. doi: 10.3354/meps09912

Litchman, E., and Klausmeier, C. A. (2008). Trait-based community ecology of phytoplankton. *Annu. Rev. Ecol. Evol. Syst.* 39, 615–639. doi: 10.1146/annurev.ecolsys.39.110707.173549

Lohbeck, K. T., Riebesell, U., and Reusch, T. B. H. (2012). Adaptive evolution of a key phytoplankton species to ocean acidification. *Nat. Geosci.* 5, 346–351. doi: 10.1038/ngeo1441

Mackas, D. L., Batten, S., and Trudel, M. (2007). Effects on zooplankton of a warmer ocean: recent evidence from the Northeast Pacific. *Prog. Oceanogr.* 75, 223–252. doi: 10.1016/j.pocean.2007.08.010

McCoy, M. W., and Gillooly, J. F. (2008). Predicting natural mortality rates of plants and animals. *Ecol. Lett.* 11, 710–716. doi: 10.1111/j.1461-0248.2008.01190.x

Muller, H. J. (1932). Some genetic aspects of sex. *Am. Nat.* 66, 118–138. doi: 10.1086/280418

Munday, P. L. (2014). Transgenerational acclimation of fishes to climate change and ocean acidification. *F100Prime Rep.* 6:99. doi: 10.12703/P6-99

Norberg, J. (2004). Biodiversity and ecosystem functioning: a complex adaptive systems approach. *Limnol. Oceanogr.* 49, 1269–1277. doi: 10.4319/lo.2004.49.4_part_2.1269

Norberg, J., Swaney, D. P., Dushoff, J., Lin, J., Casagrandi, R., and Levin, S. A. (2001). Phenotypic diversity and ecosystem functioning in changing environments: a theoretical framework. *Proc. Natl. Acad. Sci. U.S.A.* 98, 11376–11381. doi: 10.1073/pnas.171315998

Norberg, J., Urban, M. C., Vellend, M., Klausmeier, C. A., and Loeuille, N. (2012). Eco-evolutionary responses of biodiversity to climate change. *Nat. Clim. Chang.* 2, 747–751. doi: 10.1038/nclimate1588

Orr, H. A. (1998). The population genetics of adaptation: the distribution of factors fixed during adaptive evolution. *Evolution* 52, 935–949. doi: 10.2307/2411226

Orr, H. A. (2005). The genetic theory of adaptation: a brief history. *Nat. Rev. Genet.* 6, 119–127. doi: 10.1038/nrg1523

Pigliucci, M. (2005). Evolution of phenotypic plasticity: where are we going now? *Trends Ecol. Evol.* 20, 481–486. doi: 10.1016/j.tree.2005.06.001

Planque, B. (2015). Projecting the future state of marine ecosystems, "la grande illusion"? *IICES J. Mar. Sci.* 73, 204–208. doi: 10.1093/icesjms/fsv155

Pörtner, H. O., and Farrell, A. P. (2008). Physiology and climate change. *Science* 322, 690–692. doi: 10.1126/science.1163156

Pörtner, H.-O., Karl, D., Boyd, P. W., Cheung, W., Lluch-Cota, S. E., Nojiri, Y., et al. (2014). "Ocean systems," in *Climate Change 2014: Impacts, Adaptation, and Vulnerability. Part A: Global and Sectoral Aspects. Contribution of Working Group II to the Fifth Assessment Report of the Intergovernmental Panel of Climate Change*, eds C. B. Field, V. R. Barros, D. J. Dokken, K. J. Mach, M. D. Mastrandrea, T. E. Bilir, et al. (Cambridge; New York, NY: Cambridge University Press), 411–484.

Read, B. A., Kegel, J., Klute, M. J., Kuo, A., Lefebvre, S. C., Maumus, F., et al. (2013). Pan genome of the phytoplankton *Emiliania* underpins its global distribution. *Nature* 499, 209–213. doi: 10.1038/nature12221

Regaudie-de-Gioux, A., and Duarte, C. M. (2013). Global patterns in oceanic planktonic metabolism. *Limnol. Oceanogr.* 58, 977–986. doi: 10.4319/lo.2013.58.3.0977

Reusch, T. B. H. (2014). Climate change in the oceans: evolutionary versus phenotypically plastic responses of marine animals and plants. *Evol. Appl.* 7, 104–122. doi: 10.1111/eva.12109

Reznick, D. N., Shaw, F. H., Rodd, F. H., and Shaw, R. G. (1997). Evaluation of the rate of evolution in natural populations of guppies (*Poecilia reticulata*). *Science* 275, 1934–1937. doi: 10.1126/science.275.5308.1934

Rhein, M., Rintoul, S. R., Aoki, S., Campos, E., Chambers, D., Feely, R. A., et al. (2013). "Observations: ocean," in *Climate Change 2013: The Physical Science Basis. Contribution of Working Group I to the Fifth Assessment Report of the Intergovernmental Panel on Climate Change*, eds T. F. Stocker, D. Qin, G.-K. Plattner, M. Tignor, S. K. Allen, J. Boschung, et al. (Cambridge; New York, NY: Cambridge University Press), 255–316.

Schaum, C. E., and Collins, S. (2014). Plasticity predicts evolution in a marine alga. *Proc. R. Soc. B* 281:20141486. doi: 10.1098/rspb.2014.1486

Schaum, E., Rost, B., Millar, A. J., and Collins, S. (2013). Variation in plastic responses of a globally distributed picoplankton species to ocean acidification. *Nat. Clim. Chang.* 3, 298–302. doi: 10.1038/nclimate1774

Schlüter, L., Lohbeck, K. T., Gutowska, M. A., Groger, J. P., Riebesell, U., and Reusch, T. B. H. (2014). Adaptation of a globally important coccolithophore to ocean warming and acidification. *Nat. Clim. Change* 4, 1024–1030. doi: 10.1038/nclimate2379

Simpson, S. D., Jennings, S., Johnson, M. P., Blanchard, J. L., Schön, P.-J., Sims, D. W., et al. (2011). Continental shelf-wide response of a fish assemblage to rapid warming of the sea. *Curr. Biol.* 21, 1565–1570. doi: 10.1016/j.cub.2011.08.016

Sokolova, I. M. (2013). Energy-limited tolerance to stress as a conceptual framework to integrate the effects of multiple stressors. *Integr. Comp. Biol.* 53, 597–608. doi: 10.1093/icb/ict028

Sorte, C. J. B., Williams, S. L., and Carlton, J. T. (2010). Marine range shifts and species introductions: comparative spread rates and community impacts. *Glob. Ecol. Biogeogr.* 19, 303–316. doi: 10.1111/j.1466-8238.2009.00519.x

van Oppen, M. J. H., Oliver, J. K., Putnam, H. M., and Gates, R. D. (2015). Building coral reef resilience through assisted evolution. *Proc. Natl. Acad. Sci. U.S.A.* 112, 2307–2313. doi: 10.1073/pnas.1422301112

Walsh, M. R., Whittington, D., and Funkhouser, C. (2014). Thermal transgenerational plasticity in natural populations of *Daphnia*. *Integr. Comp. Biol.* 54, 822–829. doi: 10.1093/icb/icu078

Watabe, N., and Wilbur, K. (1966). Effects of temperature on growth calcification and coccolith form in *Coccolithus huxleyi* (coccolithineae). *Limnol. Oceanogr.* 11, 567–575. doi: 10.4319/lo.1966.11.4.0567

Whitman, D. W., and Agrawal, A. A. (2009). "What is phenotypic plasticity and why is it important?" in *Phenotypic Plasticity of Insects : Mechanisms and Consequences*, eds D. W. Whitman, and T. N. Ananthakrishnan (Enfield, NH: Science Publishers), 1–63.

Winter, A., Henderiks, J., Beaufort, L., Rickaby, R. E. M., and Brown, C. W. (2014). Poleward expansion of the coccolithophore *Emiliania huxleyi*. *J. Plankton Res.* 36, 316–325. doi: 10.1093/plankt/fbt110

Wong, P. P., Losada, I. J., Gattuso, J.-P., Hinkel, J., Khattabi, A., McInnes, K. L., et al. (2014). "Coastal systems and low-lying areas," in *Climate Change 2014: Impacts, Adaptation, and Vulnerability. Part A: Global and Sectoral Aspects. Contribution of Working Group II to the Fifth Assessment Report of the Intergovernmental Panel of Climate Change*, eds C. B. Field, V. R. Barros, D. J. Dokken, K. J. Mach, M. D. Mastrandrea, T. E. Bilir, et al. (Cambridge; New York, NY: Cambridge University Press), 361–409.

Zhang, Y., Klapper, R., Lohbeck, K. T., Bach, L. T., Schulz, K. G., Reusch, T. B. H., et al. (2014). Between- and within-population variations in thermal reaction norms of the coccolithophore *Emiliania huxleyi*. *Limnol. Oceanogr.* 59, 1570–1580. doi: 10.4319/lo.2014.59.5.1570

**Conflict of Interest Statement:** The author declares that the research was conducted in the absence of any commercial or financial relationships that could be construed as a potential conflict of interest.

frontiers in Marine Science

REVIEW
published: 15 December 2016
doi: 10.3389/fmars.2016.00251

# Quantifying Tradeoffs for Marine Viruses

*Nicholas R. Record*[1]*, *David Talmy*[2] *and Selina Våge*[3]

[1] Bigelow Laboratory for Ocean Sciences, East Boothbay, ME, USA, [2] Department of Earth, Atmosphere and Planetary Sciences, Massachusetts Institute of Technology, Cambridge, MA, USA, [3] Department of Biology, Hjort Centre for Marine Ecosystem Dynamics, University of Bergen, Bergen, Norway

The effects of viruses on marine microbial communities are myriad. The high biodiversity of viruses and their complex interactions with diverse hosts makes it a challenge to link modeling work with experimental work. In various trophic groups, trait-based approaches have helped to simplify this complexity, as traits describe organism properties in terms of taxon-transcending units, allowing for easier identification of generic, underlying principles. By predicting large-scale biogeography of different plankton functional types based on key sets of traits and their associated tradeoffs, these approaches have made major contributions to our understanding of global biogeochemistry and ecology. This review addresses the question of how a trait-based approach can make contributions toward understanding marine virus ecology. We review and synthesize current knowledge on virus traits with a focus on quantifying the associated tradeoffs. We use three case studies—virulence, host range, and cost of resistance—to illustrate how quantification of tradeoffs can help to explain observed patterns, generate hypotheses, and improve our theoretical understanding of virus ecology. Using a nutrient-susceptible-infected-virus model as a framework, we discuss tradeoffs as a link between model building (theory) and experimental design (practice). Finally, we address how insights from virus ecology can contribute back to the trait-based ecology community.

**Keywords: marine virus, host, tradeoff, trait, model**

OPEN ACCESS

***Edited by:***
*Susanne Menden-Deuer, University of Rhode Island, USA*

***Reviewed by:***
*Kristina Dee Anne Mojica, Oregon State Univeristy, USA*
*Urania Christaki, Ministry of Research and Higher Education, France*

***Correspondence:**
*Nicholas R. Record*
*nrecord@bigelow.org*

***Specialty section:***
*This article was submitted to Marine Ecosystem Ecology, a section of the journal Frontiers in Marine Science*

***Received:*** *31 July 2016*
***Accepted:*** *18 November 2016*
***Published:*** *15 December 2016*

***Citation:***
*Record NR, Talmy D and Våge S (2016) Quantifying Tradeoffs for Marine Viruses. Front. Mar. Sci. 3:251. doi: 10.3389/fmars.2016.00251*

## 1. INTRODUCTION

*"We live in a dancing matrix of viruses"*

– Thomas and Parker (1974).

Linking modeling and experimental work is an ongoing challenge in ecology. For marine viruses, ecologists are beginning to model the role of viruses in shaping biogeography, biogeochemistry, macroecology, and climate in the oceans. As bearers of life and death, viruses influence growth and mortality rates within microbial communities, mediating biogeochemical processes, and driving adaptation and evolution (Fuhrman, 1999; Brussaard, 2004; Suttle, 2007; Weitz and Wilhelm, 2012). Lytic viruses may account for up to 50% of bacterial mortality in the pelagic ecosystem (Suttle, 1994; Fuhrman and Noble, 1995; Fuhrman, 1999), and they can abruptly terminate eukaryotic algae blooms (Bratbak et al., 1993; Nagasaki et al., 1994). Lysogenic viruses, embedded in the host genome, may on the other hand have effects on hosts ranging from parasitic to mutualistic (Weinbauer, 2004). Viruses contribute to both top-down and bottom-up control of the microbial community (Weitz et al., 2016). They are thus key components of ocean ecosystem models.

Virus-mediated mortality has multiple, often contrasting, and globally significant biogeochemical effects. For example, there are competing hypotheses on whether viral lysis increases or decreases carbon export from the euphotic zone. If dissolved matter from lysis is typically remineralized, this would lead to increased regenerate production in the euphotic zone (Fuhrman, 1999; Wilhelm and Suttle, 1999; Weinbauer, 2004) and reduce export by shortcutting transfer to higher trophic levels and sinking fecal pellets (De La Rocha and Passow, 2007). On the other hand, transparent exopolymeric particles released during lysis may actually enhance particle aggregation and sinking (Proctor and Fuhrman, 1991). Furthermore, by stimulating regenerate production, viruses may sustain higher microbial biomass (Weinbauer, 2004), which may affect export. Virus infection can also alter cell stoichiometry and uptake rates, thereby altering biogeochemical pathways (Weitz and Wilhelm, 2012; Jover et al., 2014).

Viruses are also important drivers of microbial diversity (Thingstad, 2000; Weinbauer, 2004; Thingstad et al., 2015). A consequence of the strong top-down control by viruses on the microbial community is selection for host cell structures and functions rendering resistance. Such structural adaptations may be physiologically costly, which allows coexistence of both susceptible and resistant hosts. Typically, structural changes are such that virus-host interactions become highly specific (Lima-Mendez et al., 2015). The result is that viruses can regulate strain diversity within species (Thingstad et al., 2014), or species diversity within microbial communities, depending on the specificity of the virus-host interactions. In a dynamic world, co-evolutionary arms races—where hosts try to escape virus infections and viruses evolve to infect resistant hosts—provide an important mechanism to build and maintain microbial diversity (Martiny et al., 2014).

The increasing recognition of the importance of viruses has motivated work to incorporate them into ecosystem models—particularly those representing biogeochemical processes (Weitz et al., 2015; Middleton et al., in press). Virus ecology is complex, however, and representing the diversity of processes and interactions described above remains a challenge for modelers. Most ecosystem models approach ecological problems either at the species level or at the level of trophic groups. This strategy is reasonable, given the fundamental importance of species as a taxonomic unit and of trophic interactions. However, this approach has limitations when it comes to certain objectives. Challenges include: (1) connecting community structure with ecological function, (2) drawing causal links between organism properties and macroecological patterns, and (3) making diversity tractable in ecosystem models. Each of these challenges is key both to understanding basic ecology as well as to predicting the ocean's response to changing climate and other pressures.

An alternative to species-centric models is the trait-based approach to ecology, which has seen a recent resurgence in marine ecology (Barton et al., 2016). The trait-based approach to ecology has some early roots in marine systems (Sheldon et al., 1972), but much of the foundational work comes from terrestrial ecosystems, where global trait databases have facilitated breakthroughs (Wright et al., 2005; Violle et al., 2007; Kattge et al., 2011). The approach has gained traction in marine ecosystems over the past 10 years, primarily for phytoplankton (Follows et al., 2007; Litchman et al., 2007; Litchman and Klausmeier, 2008; Edwards et al., 2012; Barton et al., 2013), but also for zooplankton (Kiørboe et al., 2010; Litchman et al., 2013; Record et al., 2013b) and fish (Claudet et al., 2010; Marras et al., 2013; Opdal and Jørgensen, 2015; Pimentel et al., 2016). While ecologists have not agreed upon a single rigorous definition of "trait," the objective is to define characteristics of organisms that link processes at the individual level to population-, community-, or ecosystem-level processes. Traits are typically taxon-transcending properties that describe growth, ontogeny, reproduction, and defense, and ultimately determine fitness (Litchman et al., 2013). When successful, the trait-based approach can explain mechanistically the organization and function of an ecosystem (Hansen et al., 1994; Follows et al., 2007; Rose et al., 2007; Banas, 2011; Record et al., 2012, 2013a; Zhang et al., 2013; Andersen and Beyer, 2015). The notion of a trait often goes hand-in-hand with modeling, as traits can be represented as parameters in systems of dynamical equations. As such, they provide a useful link between models, which require values for these parameters, and experiments, which measure them.

Many of the parameters found in virus models have been reviewed and described in the context of traits (Weitz et al., 2016, Ch. 2). To link traits with the underlying ecology, we also require an understanding of tradeoffs associated with sets of traits. Tradeoffs occur when an increase in fitness associated with one trait comes at a fitness cost associated with another trait. Identification of tradeoffs has recently been proposed as a key step toward linking the work of modelers and empiricists (Barton et al., 2016). The concept of tradeoffs is commonly invoked in the virus literature (Bohannan et al., 2002; De Paepe and Taddei, 2006; Jessup and Bohannan, 2008; Pradeep Ram and Sime-Ngando, 2010; Keen, 2014), and with the recent reemergence of the trait-based approach in marine ecology, it is timely to review our understanding of marine virus tradeoffs in order to help incorporate it into the broader trait-based dialogue. Here we provide a review of marine virus traits and attempt to characterize and quantify the tradeoffs associated with some of the most important traits. We include viruses that infect pelagic bacteria, archaea, and eukaryotes, though there is considerably more literature on bacteriophages. We use three case studies and simple illustrative model simulations to demonstrate how quantification of tradeoffs can help to explain observed patterns, generate hypotheses, and link modeling work and empirical work.

## 2. A FRAMEWORK FOR TRAIT-BASED VIRUS MODELS

The first step in a trait-based approach to the ecology of a group of organisms is to build a framework that includes the traits involved in important tradeoffs (Litchman et al., 2013). Here we use a dynamical systems model as the core of our framework. A recent review of marine virus-host models (Middleton et al.,

in press) found a wide variety in model equations and state variables used to describe marine virus-host interactions. While there was some commonality among models, nearly one third did not include a state variable tracking virion abundance (e.g., Beltrami and Carroll, 1994; Chattopadhyay and Pal, 2002; Singh et al., 2004; Rhodes and Martin, 2010). This follows the convention in biogeochemical models of using a linear mortality term to capture all background mortality including viral lysis. Other notable state variables in marine virus-host models included a separate infected host population (Bratbak et al., 1998), a virus population within host cells (Siekmann and Malchow, 2008), a virus inhibitor (Thyrhaug et al., 2003), and a resistant population (Middelboe, 2000). Model design is often dictated by available data or by hypotheses, or, for marine virus-host models, based on other standard forms such as susceptible-infected-removed (SIR) models of epidemics (Kermack and McKendrick, 1927).

Following Litchman et al. (2013), we have classified virus traits based on ecological function and trait type (**Table 1**). This exercise itself illustrates some of the challenges around building a general trait-based framework for marine pelagic ecology. Some of the trait categories in the Litchman classification needed to be changed to apply to viruses. Additionally, not all of these traits convert easily into model parameters. Some traits that have been studied and reviewed (Weitz et al., 2016) translate directly to model parameters (e.g., burst size). Those that do not (e.g., size) generally have one or more underlying relationships that translate indirectly into model parameters. We constructed a set of equations based on the common components in marine virus-host models (Middleton et al., in press) designed to incorporate the quantitative traits outlined in **Table 1**. The full model includes all traits discussed in this review so that the associated tradeoffs can be explored mathematically. The model can be reduced based on simplifying assumptions into various forms that are used in other modeling studies (detailed in Supplementary Material). A chemostat is simulated, where hosts are partitioned into those that are susceptible and those that are infected. Encounter between free living viruses and susceptible hosts creates infected hosts. The full model is a Nutrient-Susceptible-Infected-Virus (NSIV) model, representing virus infection of a generic host population. The equations are written:

$$\frac{dN}{dt} = \delta(N_{in} - N) - \mu(N)(S + \gamma I) \quad (1)$$

$$\frac{dS}{dt} = \frac{1}{c}\mu(N)S - \phi SV - \omega S \quad (2)$$

$$\frac{dI}{dt} = \gamma\frac{1}{c}\mu(N)I + \phi SV - (1-\gamma)\lambda I - \omega I \quad (3)$$

$$\frac{dV}{dt} = \beta(1-\gamma)\lambda I - \phi SV - \psi V \quad (4)$$

where $N$ is the nutrient concentration supplied at an input concentration $N_{in}$ and dilution rate $\delta$, $S$ is the population of susceptible hosts, $I$ is the population of infected hosts, and $V$ is the population of viruses (**Table 2**). The parameter $\phi$ represents an interaction kernel between viruses and hosts, $\mu$ is a growth function for hosts, and $c$ is the host nutrient quota. Host and virus losses, $\omega$ and $\psi$ respectively, include losses due to dilution, as well as other forms of mortality or decay. The parameter $\gamma$ determines the virulence strategy, representing the lysogenic proportion of the virus. Hosts are lysed at rate $\lambda$, and each lysis event results in $\beta$ free living virions. Each parameter represents a trait explicitly or can be expressed as a function of a trait. In some contexts, a parameter can combine multiple traits, such as the interaction kernel, which includes processes like encounter (dependent upon size) as well as structure or entry mechanism. In such cases, as we understand more about these traits, we can replace the parameter with a more refined function that captures multiple traits. We will use this model, or its reduced versions (detailed in Supplementary Material), to illustrate the tradeoffs associated with the reviewed traits.

## 3. IDENTIFYING AND QUANTIFYING TRADEOFFS

Each of the traits listed in **Table 1** is hypothetically involved in one or more tradeoffs. Here we focus on four traits and their associated tradeoffs: size, virulence, host range, and resistance. For the latter three cases, we use the NSIV model framework (Equations 1–4) to evaluate the tradeoff associated with the trait and compare predictions to observations. The fourth case—resistance—illustrates the interaction between virus traits and host traits.

### 3.1. Size

Ocean ecosystems are strongly size-structured. Organism size is a first-order determinant of many aspects of ecosystem structure and function, including production and metabolism (López-Urrutia et al., 2006), reproduction (Sheldon et al., 1972), predator-prey interactions (Banas, 2011; Golet et al., 2015), and species richness (Record et al., 2012) to name a few. As a trait, it is often viewed as a primary axis for describing marine ecosystems (Barton et al., 2013; Litchman et al., 2013), with a strong body of theory explaining how size structures marine ecosystems from bacteria to whales (Andersen et al., 2016). It is unknown whether these allometric relationships extend to the viruses.

#### 3.1.1. Survival

Important sources of virus loss include ultraviolet light (Murray and Jackson, 1993; Wilhelm et al., 2003), grazing (Deng et al., 2014), adsorption, and genome size and density (De Paepe and Taddei, 2006). These processes have strong allometric dependencies in general, but it is an open question whether virus loss in the marine environment is strongly size-dependent.

#### 3.1.2. Encounter and Infection

As non-motile entities, extracellular virus particles depend on Brownian motion for random encounter with hosts. As such, diffusive transport is likely to be a primary determinant of host-virus encounter. Larger virus particles diffuse more slowly, and are thus expected to be at a disadvantage in terms of contact rates (Murray and Jackson, 1992). Simple physical arguments may also be used to understand which hosts are more

**TABLE 1 | Overview of virus traits, following the classification scheme of Litchman et al. (2013).**

| Trait type | | Ecological function | | |
|---|---|---|---|---|
| | | **Survival** | **Replication and production (reproduction)** | **Encounter and infection (feeding)** |
| | **Morphology** | • **Size**<br>• Capsid (lipid-enveloped vs. naked protein) | • **Size** | • **Size**<br>• Structure (icosahedral, helical, complex) |
| | **Physiology** | • UV resistance<br>• **Latent period (λ)**<br>• Transcription control | • **Burst size ($\beta$)**<br>• **Latent period (λ)**<br>• Transcription control | • Genome type<br>• **Genome length** |
| | **Infection mechanism (behavior)** | | • Entry mechanism<br>• Release mechanism<br>• Replication site<br>• Assembly site | • **Host range ($\rho$)** |
| | **Infection strategy (life history)** | • **Virulence ($\gamma$)** | • **Virulence ($\gamma$)**<br>• Transcription control | |

*Where the category names have been changed, the original Litchman category name is given in parentheses. Bold text indicates quantitative trait; plain text indicates categorical trait. Parameter in parentheses corresponds to how the trait is represented in Equations (1–4) or (11, 12).*

**TABLE 2 | Parameter and variable descriptions and units.**

| Symbol | Description | Units |
|---|---|---|
| $N$ | Nutrient concentration | mM |
| $S$ | Susceptible host biomass | $L^{-1}$ |
| $I$ | Infected host biomass | $L^{-1}$ |
| $V$ | Free living phage biomass | $L^{-1}$ |
| $\delta$ | Dilution rate | $day^{-1}$ |
| $N_{in}$ | Nutrient concentration in input reservoir | mM |
| $\mu$ | Encounter rate between nutrient ions and host cells | L $(day)^{-1}$ |
| $c$ | Host nutrient quota | mmol |
| $\phi$ | Interaction kernel between susceptible hosts and free living phage | L $(day)^{-1}$ |
| $\gamma$ | Proportion of each phage population that are lysogenic | - |
| $\lambda$ | Lysis rate | $day^{-1}$ |
| $\beta$ | Burst size | - |
| $\omega$ | Host losses | $day^{-1}$ |
| $\psi$ | Virus losses | $day^{-1}$ |

susceptible to encounter with virus particles. Probability of virus attachment is greater for larger organisms with higher surface area. Furthermore, larger organisms generally swim faster, clearing a larger volume of water and enhancing the probability of virus encounter (Murray and Jackson, 1992). Simple physical controls on encounter do not necessarily manifest in clear relations between virus particle size and the size of the host it is able to infect. For example, coccolithoviruses with capsids ∼170–200 nm in diameter infect haptophyte *Emiliania huxleyi* (5–8 μm diameter) (Schroeder et al., 2002), while the significantly smaller *Rhizosolenia setigera*-virus (∼30 nm diameter) infects the much larger diatom *R. setigera* (2–50 μm diameter and 0.1–1 mm length) (Nagasaki et al., 2004). Furthermore, the sizes of virus and host genomes appear to be unrelated (Brown et al., 2006). While these examples do not point toward a simple, canonical virus:host size ratio, to the best of our knowledge, no one has systematically addressed this question in a broad range of marine virus-host systems.

### 3.1.3. Virus Production

Over sufficiently large ranges, growth rate tends to decline with organism size in eukaryotes, while the opposite is true for prokaryotes (Kempes et al., 2012). Very little is known about the relation between virus particle size and production rate. Since viruses utilize host metabolic machinery for replication, virus production rate generally follows growth rates of the host and varies depending on host growth conditions and physiology (Van Etten et al., 1983; Moebus, 1996; Bratbak et al., 1998; Middelboe, 2000; Baudoux and Brussaard, 2008). On the other hand, replication rate may depend more directly on virus particle size. Virus replication rate is also likely to depend on morphological variation across diverse phylogenies. A proxy often used to infer virus accumulation rate is burst size. There is evidence that burst size is related to the ratio between host and virus genome lengths (Weitz et al., 2015), and that number of base pairs is related to capsid size (Jover et al., 2014), suggesting that a smaller virus can make more copies of itself than a large virus, all other factors being equal. However, burst size is not a direct reflection of the metabolic efficiency of virus replication. It says nothing about the time required for replication, which in part may be reflected in the duration of latent period. Few direct measurements of virus replication rates are available, making it difficult to know the allometric scaling of virus production.

## 3.2. Virulence: Tradeoffs with Lysogeny and Lysis

Pathogenic virulence influences microbial fitness in complex and interesting ways. Lysogenic viruses can enhance host fitness by increasing the growth of infected hosts (Edlin et al., 1975), and providing protection against closely related viruses (Ptashne,

1967). Lysogeny is associated with horizontal gene transfer (Chiura, 1997; Lawrence and Ochman, 1998; Ochman et al., 2000), and bacterial genomes contain a high portion of dormant or repurposed phage genes (Casjens et al., 2000; Ochman et al., 2000; Hayashi et al., 2001; Daubin et al., 2003). Due to its importance for public health and epidemiology, there is a sizeable literature on factors controlling the switch from lysogeny to lysis (Brüssow et al., 2004; Ptashne, 2004), as well as some marine examples (Paul and Jiang, 2001; Brum et al., 2016). The switch may be related to molecular interactions between host and virus (Ptashne, 2004; Zeng et al., 2010), or environmental cues that relate, for example, to host production (Koudelka et al., 1988; Wilson and Mann, 1997; Williamson et al., 2002; Weinbauer et al., 2003). Relatively few studies (Levin and Lenski, 1983; Stewart and Levin, 1984; Koudelka et al., 1988; Williamson et al., 2002; Weinbauer et al., 2003) have explored the ecological factors that may ultimately govern when and where lysogenic vs. lytic replication modes are selected. Here, we briefly review observed relationships between environmental variables and prevalence of lysogeny. We then use Equations (1–4) to explore a tradeoff that may govern observed trends.

### 3.2.1. Temperature

Wilson and Mann (1997) concluded that the only studies relating temperature to the switch between lysogeny and lysis were with enteric hosts (Edgar and Lielausis, 1964; Gough, 1968), and that evidence in marine systems was limited. Since then, correlations between temperature and lysogeny have been found in a range of environments (Cochran and Paul, 1998; Williamson et al., 2002; Maurice et al., 2010; Payet and Suttle, 2013). The general pattern shows low temperatures favoring lysogenic phages, and high temperatures favoring lytic phages. Temperature has been used to provoke prophage induction in natural seawater samples (Jiang and Paul, 1996), but laboratory experiments testing the dependence of the switch on temperature have been equivocal (Williamson and Paul, 2006). Early in their experiments, Williamson and Paul (2006) observed elevated temperature leading to higher production rates and reduced lysogeny. Later in the experiments however, high temperature cultures reduced overall production of free phage by both lytic and lysogenic infections.

### 3.2.2. Light

Tests of the influence of light intensity on the switch between lysogeny and lysis can be divided into those that tested effects of UV radiation, and those that tested whether direct sunlight could induce lysis. In general, the results evidence that induction response to light varies among host species (possibly even at the strain level) and specific lysogens. For example, *Vibrio* lysogens could be induced by sunlight (Faruque et al., 2000) and *Synechococcus* phages could be induced by continuous, high light (McDaniel et al., 2006). In contrast, other studies failed to induce natural assemblages with sunlight (Wilcox and Fuhrman, 1994; Jiang and Paul, 1996) while UV radiation has been proven effective to revert lysogenic to lytic infections within natural assemblages (Jiang and Paul, 1996; Weinbauer and Suttle, 1996).

### 3.2.3. Nutrients

Field and laboratory observations suggest nutrient status is likely to influence the prevalence of lysogeny. There is ample evidence, from a range of studies in different oceanic regions, that the proportion of hosts in natural assemblages carrying inducible prophages varies as a function of trophic status. The abundance of hosts with lysogenic infections is often lower in more productive than in less productive waters and also lower in highly productive summer months than in low productive winter months (Jiang and Paul, 1994; McDaniel et al., 2002; Weinbauer et al., 2003; Lymer and Lindström, 2010; Payet and Suttle, 2013). Additionally, it has been empirically shown that nutrient enrichment of natural samples may induce lysogens in some bacterial assemblages (Wilson et al., 1998; Williamson et al., 2002), but not in others, e.g., *Synechococcus* populations (McDaniel and Paul, 2005), while nutrient starvation can lead to the establishment of lysogeny in the heterotrophic bacteria *Pseudomonas aeruginosa* (Kokjohn et al., 1991). Similarly, phosphate depletion in cultures of the photoautotrophic bacteria *Synechococcus* sp. (Wilson et al., 1996) has been shown to decrease burst size and lysis rate of infected host populations, suggesting cyanophages entered a lysogenic state in response to nutrient starvation.

### 3.2.4. The Virulence Tradeoff

There must be a tradeoff associated with the switch between lysis and lysogeny, otherwise one would always be favored over the other. In low productive systems, encounter between hosts and extracellular virus particles may be low, and insufficient to overcome losses, rendering lysogeny the favorable strategy for production. In relatively productive systems, when encounter is high, virus replication could be maximized by frequently lysing hosts. This amounts to a tradeoff with the maximum host production potential. The above literature review suggests increases in light, temperature, and nutrients are all correlated with diminished lysogeny, with arguably the strongest support for nutrient related control. We can examine this hypothesized tradeoff using the NSIV model (Equations 1–4), where the parameter $\gamma$ determines the virulence strategy of the virus. When $\gamma = 1$, the virus is lysogenic. Infected hosts grow at the same rate as susceptible hosts (a simplifying assumption that can potentially be relaxed), and there is no lysis. When $\gamma = 0$, infected hosts do not grow, and lysis proceeds at rate $\lambda$. With the system solved in steady state (see Supplementary Material), we can explore two scenarios exemplifying contrasting virulence strategies. The following two expressions are the total equilibrium virus biomass when $\gamma = 1$ and when $\gamma = 0$, respectively.

$$V_{lys}^{tot} = \frac{\beta\delta}{c\omega} N_{in} - \frac{\beta\delta}{\mu} \tag{5}$$

$$V_{lyt}^{tot} = \frac{\beta\delta\mu}{c(\beta\delta\phi + \psi\mu)} N_{in} - \frac{\omega}{\phi} \tag{6}$$

Note that these expressions assume the rate of lysis, $\lambda$, is significantly greater than other parameters in the model (Supplementary Material). The above expressions are both linear

functions of the nutrient input concentration $N_{in}$ (**Figure 1A**), and give a guide to when lytic replication may be favorable over lysogeny. Interestingly, the minimal nutrient input required for lytic viruses to exist is always greater than the nutrient input required for lysogenic viruses to exist:

$$N_{in}^{lys} = \frac{c\omega}{\mu} \tag{7}$$

$$N_{in}^{lyt} = \frac{c\omega}{\mu} + \frac{c\omega\psi}{\phi\delta\beta} \tag{8}$$

Since $c$, $\omega$, $\psi$, $\phi$, $\delta$, and $\beta$ are all positive, we have $N_{in}^{lys} < N_{in}^{lyt}$. The prediction is that lytic viruses may only be present at a nutrient input concentration that is higher than that required to sustain host biomass. Thus, low nutrient supply may naturally favor lysogenic viruses, since lytic viruses may not survive as free-existing entities. If viruses are assumed to switch from lysogeny to lysis once nutrient supply is sufficient to support a free living population of viruses, then the overall prevalence of lysogeny would decrease as a function of nutrient enrichment, perhaps replaced by predominately lytic viruses (**Figure 1B**). Thus, lysogeny may be favored under low nutrient conditions, and lytic production favored under relatively high nutrient conditions (Knowles et al., 2016; Weitz et al., 2016, cf).

The analysis presented here examines the potential for lytic viruses to exist in a range of nutrient conditions, but says nothing about the biological mechanisms that directly control virus replication strategy. Host metabolic state is associated with changes in replication strategy (Ptashne, 2004; Ghosh et al., 2009), and is expected to improve as nutrient supply increases. Host metabolic state may therefore provide a direct, mechanistic link between environmental conditions and virus replication strategy. Better understanding of the transition from lysogeny to lysis thus depends on our mechanistic understanding of metabolic cues, as well as the trade-offs governing feasibility of the different strategies, shown here to include host-virus encounter, burst, virus replication rate, host, and virus mortality (Equations 5, 6, **Figure 1**).

## 3.3. Host Range: Tradeoffs with Specificity and Generality

The prevalent view of high host specificity among marine viruses has been changing recently as wide and variable host ranges are observed among marine viruses (Holmfeldt et al., 2007; Flores et al., 2011). Host ranges can be variable across host strains (DePaola et al., 1998; Liu et al., 2001; Allen et al., 2007; Holmfeldt et al., 2007; Stenholm et al., 2008; Martínez et al., 2015) as well as across host phyla (Malki et al., 2015). A broad host range (generalist) must come with some cost; otherwise we would expect no host specialists. Coexistence between generalists and specialists is a topic of broader interest in ecology (Egas et al., 2004; Ma and Levin, 2006). In other ecological contexts, tradeoffs associated with generalism versus specialism are associated with foraging strategy (Wilson, 1994), scale of temporal variability in environment or resource (Gilchrist, 1995), and habitat fragmentation (Marvier et al., 2004) to name a few. For viruses, there has been some analytical work examining possible tradeoffs (Jover et al., 2013). By revisiting data in published studies, we found evidence for possible tradeoffs with host range size, including virus genome size, burst size, and morphology (**Table 3**, data shown in Supplementary Material). There are other sources of information that suggest possible tradeoffs but without sufficient measurements to show statistical significance (e.g., Mojica and Brussaard, 2014).

### 3.3.1. Genome Size

A broader host range could imply that the virus strain has some increased ability to overcome a wider range of host defenses. The hypothesized tradeoff would be that this requires a longer genome with larger functional potential, which requires more cell resources to assemble, ultimately slowing virus population increase rates. In a diverse host community, access to a greater number of hosts would outweigh this cost for a generalist, and in less diverse host communities, the more rapid population increase rate of specialists would be favored. There is some evidence that host range size correlates positively with genome size for lytic viruses (**Table 3**). These relationships are driven by the extremes (i.e., generalists and specialists), with higher variance for intermediate host ranges. The relationship is also reversed for lysogenic viruses (**Table 3**) (e.g., Stenholm et al., 2008). In some cases there is no relationship (Comeau et al., 2006).

### 3.3.2. Burst Size

There is at least one example of evidence for a strong relationship between host range and burst size, though this relationship is based on a small sample size (**Table 3**) (Stenholm et al., 2008). The relationship is also in the reverse direction from what one would expect from a tradeoff: a higher host range is associated with a higher burst size, so generalists would hypothetically have an advantage over specialists in both cases. However, greater burst size is also associated with greater latency period (Wang, 2006), and greater burst size, as with host range, is associated with larger genomes (Brown et al., 2006; Weitz et al., 2016). A tradeoff might therefore involve more than two traits, with a greater host range requiring extra genetic machinery and longer latency time, producing a cost with the potential to offset the advantages of generalism.

### 3.3.3. Morphology

A number of morphological traits associated with size relate positively with host range size, namely head length, head diameter, and tail diameter (**Table 3**). Additionally, DePaola et al. (1998) found among *Vibrio* phages a distinct short-tailed, long capsid morphotype that had a markedly wider host range than the other phages examined. Again, the tradeoff would likely have to do with the extra resources required for larger sizes.

### 3.3.4. Interaction Networks

The host range trait can be categorized into generalists, specialists, and intermediate cases, and the overall prevalence of these different strategies manifest in distinct network structures (Proulx et al., 2005). Nestedness—that is, the specialist virus

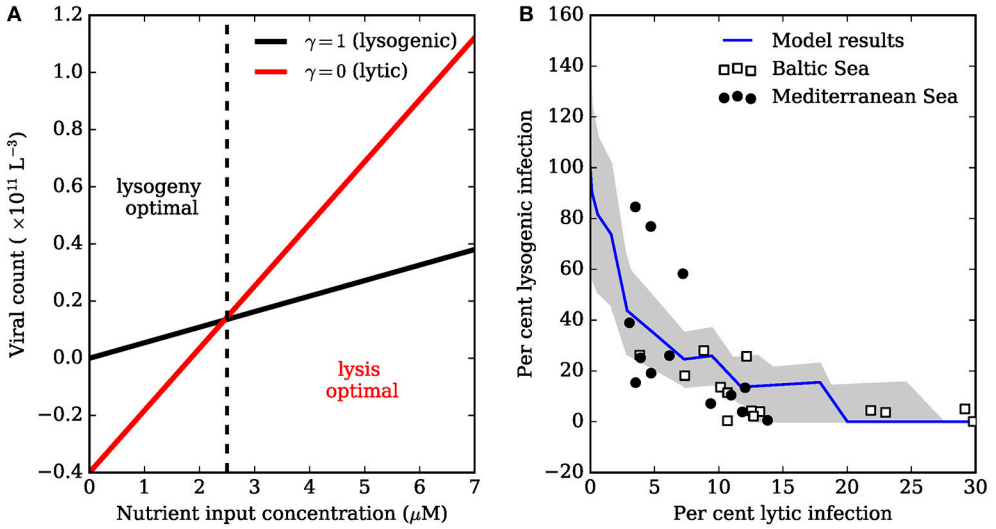


**FIGURE 1 | Tradeoff between lysogenic and lytic infection. (A)** Lines were generated using Equations (5) and (6) with $\delta$, $\mu$, $c$, $\beta$, $\phi$, $\omega$, and $\psi$ equal to 0.1, $1\times10^{-9}$, $2.3\times10^{-12}$, 50, $1\times10^{-11}$, 0.4, 0.1, respectively. The lysogenic and lytic populations can sustain non-negative biomass when $N_{in} = N_{in}^{lys}$, and $N_{in} = N_{in}^{lyt}$, respectively (Equations 7, 8). Low nutrient input enables lysogeny to survive when the lytic strategy would fail. High nutrient input can lead to survival of free-existing lytic phage. **(B)** The model in **(A)** can be used to explain the relationship between fraction of hosts that are lysogenic (FLC), and fraction of hosts with lytic infections (FIC). Data are of bacterial assemblages in a range of trophic conditions, ranging from the relatively oligotrophic Mediterranean Sea, to the more productive Baltic Sea (Weinbauer et al., 2003). Total lysogenic infection was inferred by treatment with mitomycin C. The decline in FLC as a function of FIC is thought to be due to nutrient enrichment. The jagged blue line averages total lysogenic (FIC) and lytic infection (FLC) for a community of phages, each modeled with Equations (1–4) where parameters $\beta$ and $\phi$ were drawn randomly from uniform distributions ±50% of the values in **(A)**, and no tradeoffs were imposed between parameters. Each virus in the community was assumed to switch from lysis to lysogeny when $N_{in} = N_{in}^{lyt}$. The jagged line arises because each community member has a unique $N_{in}^{lyt}$ determined by the randomly drawn $\beta$ and $\phi$. The gray shaded region is one standard deviation from the mean for FLC and FIC.

infects the host that is infected most commonly—appears to be common among closely related host-virus groups, though other configurations occur (Flores et al., 2011). Interestingly, these network structures appear limited to more closely related phylogentic host-virus networks. Broad phylogenetic groups are characterized by a nested-modular network structure, whereby nestedness only occurs in modules, and viruses within each module are generally unable to infect more distantly related hosts belonging to separate modules (Beckett and Williams, 2013). Marine viruses follow these patterns as well, though an aggregation of the reviewed data shows a disproportionately high number of generalists and specialists as compared to intermediate cases (**Figure 2A**).

### 3.3.5. The Host Range Tradeoff

To examine the potential tradeoffs associated with host range, we use a simplified version of the NSIV model (Equations 1–4), where we consider only the lytic case without an explicit population of infected hosts (Supplementary Material Section 1.3). If we assume a nutrient replete environment, we can approximate host population growth rate with a constant $\alpha$, and write the system as two equations:

$$\frac{dS}{dt} = \alpha S - \phi VS - mS \tag{9}$$

$$\frac{dV}{dt} = \phi\beta VS - \psi V \tag{10}$$

Simplifications like this allow for focusing on a single tradeoff. To understand the host range dimension, we include multiple hosts and viruses, with different combinations of infection:

$$\frac{dS_j}{dt} = \alpha_j S_j - \sum_i \phi_{ij} V_i S_j \left[\frac{\rho_{ij} S_j}{\sum_k \rho_{ik} S_k}\right] - m_j S_j \tag{11}$$

$$\frac{dV_i}{dt} = \sum_j \phi_{ij}\beta_{ij} V_i S_j \left[\frac{\rho_{ij} S_j}{\sum_k \rho_{ik} S_k}\right] - \psi_i V_i \tag{12}$$

where $i$ and $j$ subscripts represent hosts and viruses respectively, and $\rho_{ij}$ is a binary parameter that describes whether virus $j$ infects host $i$. In this configuration, different host-virus interaction matrices (Flores et al., 2011) can be input as binary matrices of $\rho$ values.

In this system, a diversity of viruses and hosts can coexist if host range trades off with $\phi_i\beta_i/\psi_i$ (Jover et al., 2013). We tested a tradeoff between host range and the interaction kernel $\phi$, which encapsulates the above reviewed traits that likely tradeoff with host range. We ran an ensemble of simulations with varying numbers of hosts and viruses, nested host range structures, and a forced tradeoff between host range and $\phi$ (**Figure 2B**). The simulation reproduced the observed bimodal pattern of higher abundance of generalists and specialists as compared to the intermediate cases (**Figure 2C**) when two conditions were met: the interaction network has a nested structure, and the tradeoff relationship (**Figure 2B**) is

**TABLE 3 | Evidence for tradeoffs with host range.**

| Trait related to host range | Direction | $r^2$ | $p$ | Note | References |
|---|---|---|---|---|---|
| Genome size (kb) | + | 0.40 | 0.001 | | Holmfeldt et al., 2007 |
| | − | 0.57 | 0.01 | Two bands | Holmfeldt et al., 2007 |
| | − | 0.79 | 0.001 | Two bands | Holmfeldt et al., 2007 |
| | + | 0.42 | 0.001 | Lytic | Stenholm et al., 2008 |
| | − | 0.55 | 0.001 | Lysogenic | Stenholm et al., 2008 |
| | − | | | Lytic | Baudoux and Brussard, 2005 |
| Burst size | + | 0.96 | 0.02 | | Stenholm et al., 2008 |
| | + | | | Lytic | Baudoux and Brussard, 2005 |
| Latent period | + | | | Lytic | Baudoux and Brussard, 2005 |
| Head diameter | + | 0.79 | 0.01 | Lysogenic | Stenholm et al., 2008 |
| | − | 0.31 | 0.03 | Lytic | Comeau et al., 2006 |
| Head length | + | 0.71 | 0.02 | Lysogenic | Stenholm et al., 2008 |
| | + | N/A | 0.001 | | DePaola et al., 1998 |
| Tail diameter | + | 0.58 | 0.05 | Lysogenic | Stenholm et al., 2008 |

*The scatter plots for these correlation analyses are in the Supplement.*

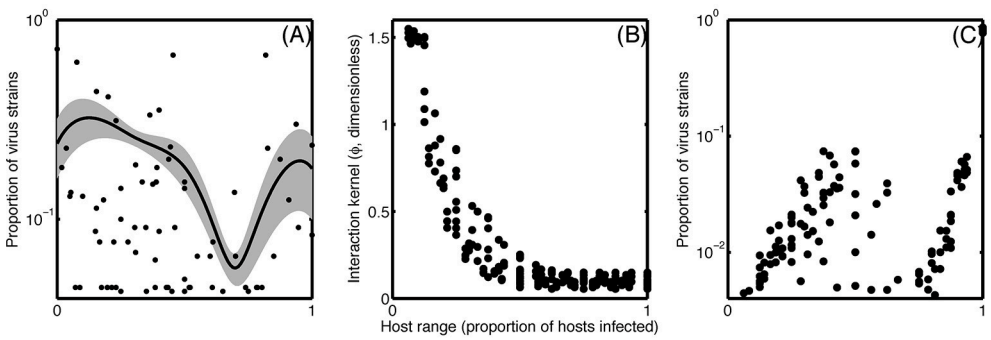


**FIGURE 2 | (A)** Smoothed histogram showing the proportion of virus strains with each host range strategy from 0 (infecting no tested hosts) to 1 (infecting all tested hosts), averaged across 11 published experiments (Suttle and Chan, 1993; DePaola et al., 1998; Wichels et al., 1998; Sullivan et al., 2003; Comeau et al., 2005, 2006; Allen et al., 2007; Holmfeldt et al., 2007; Stenholm et al., 2008; Middelboe et al., 2009; Martínez et al., 2015). Gray shading shows variance around the mean. **(B)** Input relationship between host range and interaction kernel, representing a hypothetical tradeoff. **(C)** Resulting output, after convergence, from simulation examining a tradeoff associated with host range using the tradeoff depicted in **(B)**.

concave up. If the tradeoff is concave down, then increasing host range toward the extreme comes at a very high cost in terms of the interaction kernel (and vice versa), shifting the resulting distribution to a unimodal one with an intermediate host range. This example shows how the trait-based approach gives us a quantitative hypothesis about the shape of a tradeoff and its ability to describe observed patterns.

Host range is not just a function of virus traits, however. Defense mechanisms of hosts can vary across strains as well. Because the life histories of viruses and hosts are intimately coupled, tradeoffs with host range can occur across the virus-host relationship. We discuss this idea more generally in the next section.

## 3.4. Resistance to Infection: Tradeoffs Relating to Host Traits

Because viruses rely on hosts for their genetic material, tradeoffs associated with virus traits can be intimately tied to host traits as well. Tradeoffs around competitive and defensive traits in hosts (in the following referred to as cost of resistance, COR) are an intriguing example of such a link between virus and host traits.

### 3.4.1. COR in Natural Communities

Natural virus-host communities provide indirect evidence for COR. The apparent paradox between laboratory experiments, where host resistance readily evolves and eventually excludes viruses, and the large abundance of viruses in the pelagic environment (Weinbauer, 2004) gets resolved when considering

COR. Specifically, resource limitation in natural environments may render expensive defense less viable. There is ample evidence of coexistence of susceptible and resistant hosts in natural communities (Waterbury and Valois, 1993; Tarutani et al., 2000; Holmfeldt et al., 2007; Middelboe et al., 2009), supporting the idea that COR prevents resistant types to outcompete susceptible types. Further support for COR is found in the observation that dominant host types tend to be both resistant (Rosenzweig, 1973; Lenski and Levin, 1985; Suttle and Chan, 1993; Waterbury and Valois, 1993; Malmstrom et al., 2004; Suttle, 2007; Middelboe et al., 2009; Campbell et al., 2011; Våge et al., 2013; Thingstad et al., 2014) and slow growing (Malmstrom et al., 2004; Suttle, 2007; Campbell et al., 2011; Samo et al., 2014; Thingstad et al., 2014). Finally, it appears that nested infection networks are widespread in natural communities (Chao et al., 1977; Flores et al., 2011; Jover et al., 2013; Koskella and Brockhurst, 2014; Martiny et al., 2014). In these networks, COR prevents defense-specialized hosts infected by generalist viruses only to outcompete competition-specialized hosts that are infected by most viruses. Supporting this idea, there is evidence that hosts infected by specialist viruses have faster growth rates than hosts infected by generalist viruses (Chao et al., 1977).

### 3.4.2. COR in Experimental Communities

Observing COR directly in experiments can be difficult, since COR may be small and dependent on the environment (Bohannan et al., 2002). Nevertheless, a number of studies have measured COR. The most prevalent expression of COR is a reduced growth rate in resistant types, as observed experimentally in prokaryotes including *Escherichia coli* (Lenski and Levin, 1985; Lenski, 1988; Bohannan et al., 1999; Bohannan and Lenski, 2000; Harcombe and Bull, 2005), *Pseudomonas* (Lythgoe and Chao, 2003), *Synechococcus* (Waterbury and Valois, 1993; Lennon et al., 2007), *Flavobacteria* (Middelboe et al., 2009), *Prochlorococcus* (Avrani et al., 2011) and eukaryotic *Phaeocystis pouchetti* (Haaber and Middelboe, 2009) and *Ochromonas tauri* (Thomas et al., 2011). Besides reduced growth rates, increased susceptibility to other viruses (Avrani et al., 2011, *Prochlorococcus*) and reduced abilities to form biofilms (Buckling and Rainey, 2002; Brockhurst et al., 2005, *Pseudomonas*) are other known expressions of COR.

### 3.4.3. Defense Mechanisms with Varying COR

Besides environmental conditions that may influence the expression of COR (Lennon et al., 2007), different defense mechanisms probably have varying COR, both in quality and quantity. Changes in surface receptors that hamper virus adsorption (Middelboe, 2000; Middelboe et al., 2001; Buckling and Rainey, 2002; Mizoguchi et al., 2003; Stoddard et al., 2007; Middelboe et al., 2009; Pagarete et al., 2009; Avrani et al., 2011; Bidle and Vardi, 2011) often hamper uptake of limiting nutrients as well, which can explain reduced growth rates in resistant hosts. On the other hand, internal defense mechanisms such as the CRISPR-Cas (Barrangou et al., 2007; Sorek et al., 2008; Levin, 2010; Makarova et al., 2011) and restriction enzymes (Wilson and Murray, 1991; Labrie et al., 2010) prevent take-over of the host by the virus after adsorption, which does not influence nutrient uptake dynamics directly. Instead, costs for these internal defense systems may arise from resource allocation and maintenance of the enzymatic machinery. It is conceivable that extending resistance to new viruses with these internal defense systems (e.g., by adding an additional recognition sequence in the CRISPR system) may be relatively inexpensive, but we lack quantitative evidence. Other mechanisms rendering resistance to various degrees, whose specific COR are poorly understood, include prophage incorporation (Stoddard et al., 2007; Martiny et al., 2014), chronic infection (Fuhrman, 1999; Thomas et al., 2011), immunization through viral lysate (Bidle and Vardi, 2011) and quorum sensing allowing a regulated expression of surface receptors (Høyland-Kroghsbo et al., 2013). The most drastic defense is abortive infection leading to induced cell death (Bidle and Vardi, 2011; Berngruber et al., 2013; Refardt et al., 2013).

### 3.4.4. Linking Host and Virus Traits through COR

An intriguing aspect of virus ecology is the strong link between virus and host traits. A resistance trait in the host leads to adaptive and evolutionary changes in the virus to sustain infectivity. Interestingly, however, COR also affects viruses in a more direct way. In a review on marine viruses, Suttle (2007) hypothesized inverse rank-abundance distributions of hosts and their associated viruses, where the most abundant hosts are low-active and infected by rare and low virulent viruses, while the rare hosts are active and infected by abundant and highly virulent viruses. Findings of abundant low-active and defensive hosts (Rosenzweig, 1973; Lenski and Levin, 1985; Suttle and Chan, 1993; Waterbury and Valois, 1993; Malmstrom et al., 2004; Suttle, 2007; Middelboe et al., 2009; Campbell et al., 2011; Våge et al., 2013; Samo et al., 2014; Thingstad et al., 2014) and inverse rank-abundance distributions emerging in virus-host interaction models when assuming COR (Våge et al., 2013; Thingstad et al., 2014) support Suttle's hypothesis. The positive correlation between host activity and virulence in this scenario provides a direct link between COR and viral infectivity.

Inverse rank abundance distributions also impose a tradeoff between host abundance and virulence, which becomes apparent when considering the model for host infection rates used earlier:

$$R = \phi_{ij} V_i S_j \tag{13}$$

where $R$ is the infection rate for $S_j$ by $V_i$. Given inverse rank-abundance distributions as described by Suttle (2007), infection rates for highly competitive hosts should be reduced due to the low host abundance, despite high adsorption coefficients of their viruses, whereas infection rates for highly defensive hosts should be reduced due to the low adsorption coefficient of their viruses, despite the high host abundance. The consequence is that highest infection rates may occur at intermediate virulence and host defensiveness (**Figure 3**). This tradeoff between host abundance and virulence of the virus can only be corroborated once we overcome the major challenge of quantifying abundances of viruses associated with defensive vs. competitive hosts (Jover et al., 2013). A step in that direction can be made through methods that identify single virus-host pairs in natural communities, such as phageFish (e.g., Martiny et al., 2014).

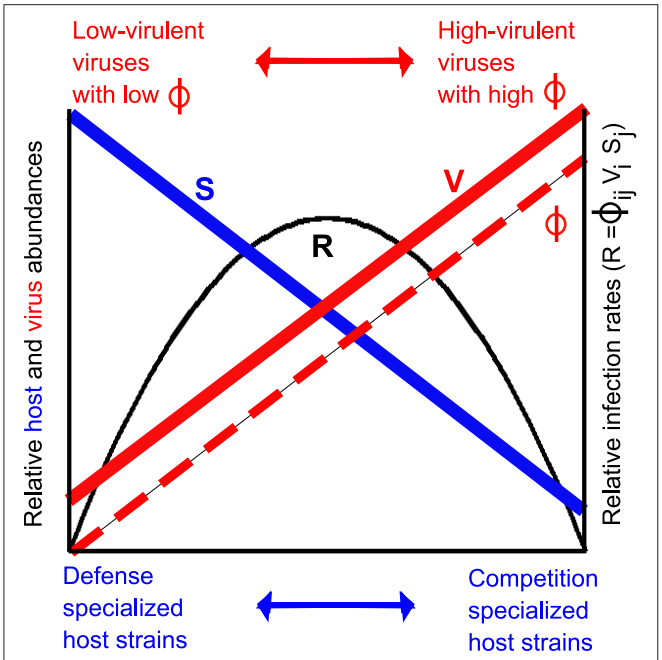


**FIGURE 3 | Illustration of virus tradeoff in inverse rank-abundance scenario.** Defense specialized host strains are more abundant than competition specialized host strains (blue line), whereas low-virulent viruses (here illustrated by small interaction kernel $\phi$) associated with defense specialists are less abundant than high-virulent viruses (large interaction kernel $\phi$) associated with competition specialists (red line). Relative interaction kernel for pairs of host and associated viruses are shown in dashed red line. Relative infection rate $R$ (Equation 13) is shown in black.

We also note that "host abundance" needs to be treated with care, as analysis of SSU rRNA used to quantify host abundances in the field resolves "species" level diversity, whereas virus-host interactions typically take place on the more strain-specific level. Investigations of virus-host interactions in natural communities will therefore rely on refinements in sequence-based methods, such as CRISPR spacer similarities and single-cell sequencing (Roux et al., 2016).

## 3.5. Summary

In this section, we have reviewed different virus traits and discussed quantification of potential tradeoffs by means of a dynamic NSIV model framework. We have shown that tradeoffs fundamentally influence community structure, and we have pointed out areas where more knowledge regarding tradeoffs would better inform our understanding. In the case studies we have discussed, we used trait-based tradeoffs to generate hypotheses, to explain observed patterns, and to link empirical and modeling work. In the virulence example, a steady-state analysis provided a hypothesized relationship between nutrient concentration and the fractions of hosts that are lytic and lysogenic. This hypothesis held up well to a small dataset of field measurements, and with additional support of field measurements could have important implications for the biogeography of lysogeny and lysis at basin and global scales. In the host range example, we explored a particular tradeoff between host range and interaction kernel. The simulation provided an explanation for the observed pattern where host range tends toward the extremes. Because host range can tradeoff with other traits as well (Jover et al., 2013), this is just one candidate explanation for the observed pattern, and it could be that the host range tradeoff involves multiple traits. Our review of the literature data (**Table 3**, Supplementary Material) provides strong evidence for host range tradeoffs, but no clear single trait involved in this tradeoff. In this case, analysis shows how a tradeoff can explain an observed pattern, and more experimental work is required to resolve the specifics of tradeoff and the traits involved. In these examples, the close interaction between virus traits and host traits is inescapable. Both the lysis-lysogeny switch and the host range tradeoff depend on traits such as $\mu$-the host growth rate. The interaction between virus traits and host traits is perhaps most pronounced with COR, where this interaction can drive evolutionary dynamics and shape the rank-abundance structure of the community. Understanding these interactions and their dynamics would have value beyond virus ecology, to the field of trait-based ecology as a whole.

# 4. FUTURE DIRECTIONS

> *"The best theory is inspired by practice. The best practice is inspired by theory."*
>
> Knuth (1991).

One of the current challenges identified by the trait-based ecology community is bridging the gap between empiricists (i.e., practice) and modelers (i.e., theory) (Barton et al., 2016). This challenge is a common vein that runs through much of the history of science (Knuth, 1991), but has become particularly pronounced with the increased specialization required in both ecological modeling and experimentation. The quantification of ecological tradeoffs, as we have presented in this review, is an objective that provides a useful nexus of modeling and experimental work and an avenue that can cut across subdisciplines. The use of traits and tradeoffs to organize ecological information has the potential to offer a robust theory for understanding a system. Here we briefly discuss a few of the central questions in marine virus ecology, with an eye toward how the study of tradeoffs can inform these questions. We also emphasize points where the study of virus ecology can contribute new insights to trait-based ecology in general.

## 4.1. What Portion of Primary and Bacterial Production Goes to Viruses vs. to Grazers?

In some ways, viruses and grazers compete for the same resource. Additionally, virus infection could alter grazing rates. This question is key to understanding when and under what conditions production is exported or recycled (Fuhrman, 1999; Brussaard, 2004; Suttle, 2007; Weitz and Wilhelm, 2012). It is a major challenge and one for which models are indispensable (Weitz et al., 2015). To tackle this problem with models, traits that control consumption of bacteria and phytoplankton must be understood, but there is currently a lack of clarity on how to compare zooplankton traits with virus traits. For decades, zooplankton ecologists have evaluated grazing competitiveness

by comparing parameters that control the shape of the curve defining zooplankton consumption as a function of prey concentration (Holling, 1959; Gentleman et al., 2003; Jeschke et al., 2004; Kiørboe, 2008; Prowe et al., 2012).

Typically, zooplankton consumption increases linearly with prey density at low prey concentrations and saturates toward a handling time limit—for example,

$$\frac{g_{max}H}{K_g + H} \tag{14}$$

where $H$ is the total prey concentration and $K_g$ is the prey concentration at which predator consumption rate is half the maximal value, $g_{max}$. The parameters that define the shape of this curve, $g_{max}$ and $K_g$, can be a useful guide for zooplankton ecologists to evaluate consumption of prey biomass. This raises the question of whether virus consumption of prey biomass can be described in a comparable way and, if so, how do the different rate constants compare.

If we assume that the total concentration of prey can be approximated by the total concentration of susceptible hosts, we can write an analogous expression in terms of virus abundance and traits (Supplementary Material),

$$\frac{\lambda H}{\frac{\lambda}{\phi} + H} \tag{15}$$

Evaluating the parameters that control curve shapes may be a useful way to understand competition between viruses and grazers. To the best of our knowledge, very little work has been done to standardize and compare virus and zooplankton Holling curve parameters. Most virus models that explicitly resolve free-existing viruses assume a linear relation between virus production and host density, where the slope of the line is defined by adsorption and burst size (Thingstad, 2000; Beckett and Williams, 2013; Weitz et al., 2015). Yet, it is conceivable that at a sufficiently high host density, the burst becomes independent of encounter, and depends instead on the duration of the latent phase. Understanding tradeoffs among key parameters $\lambda$ and $\phi$ will help evaluate whether losses due to viral infection saturate as a function of host cell density, with implications for transfer to higher trophic levels.

## 4.2. What Regulates Virus to Host Ratios?

Virus to host ratios have been measured as a proxy for the importance of viruses in aquatic systems for over two decades (Ogunseitan et al., 1990; Wommack and Colwell, 2000; Wigington et al., 2016). Numbers vary greatly (Wigington et al., 2016), but the ratio is typically considered to be roughly 10:1. What regulates this number still remains an important question, as the ratio has far reaching biogeochemical consequences (Fuhrman, 1999; Weinbauer, 2004; Suttle, 2007). A recent analysis of an idealized microbial food web model revealed intricate links between mechanisms within the bacterial host community and between different plankton functional types, providing a framework for how virus to host ratios may emerge in the bacterial community (Våge et al., 2016). Briefly, assuming total host abundance to be controlled by micrograzers as a result of their quick response to bacterial production (Azam et al., 1983) and assuming grazing to be non-selective, viral lysis compensates for differences in growth rates of the host strains. Virus abundance is thus positively correlated to the width of the growth rate spectrum in the host community. Interestingly, the width of the host growth rate spectrum and thus virus to bacteria ratios as well as food web structure at the level of plankton functional types are highly sensitive to COR. This suggests that mechanistically understanding and quantifying COR will be key to better understand aquatic microbial ecology and evolutionary dynamics. In trait-based ecology in general, the emphasis has been on tradeoffs within a species or trophic group, so an understanding of how traits can tradeoff between viruses and hosts has the potential to bring new knowledge to how traits can tradeoff across trophic groups more generally.

## 4.3. How Can the Trait-Based Approach Better Inform us on the Role of Marine Viruses in Regulating Climate?

Understanding climate and the cycling of carbon is one of the most pressing earth science challenges of the day. The role of marine viruses is complex and nuanced, and answering this question relies on incorporating knowledge of virus ecology into climate system models. Global and ocean scale climate models are state variable limited because of computational costs. Adding the level of complexity required to resolve food web dynamics, let alone virus ecology, is often too computationally burdensome at the global scale. Particular ecological components, if they are included at all, are typically simplified to a single state variable with fixed parameters. As computational restrictions are gradually overcome, tradeoffs offer one potentially useful technique for capturing some of the ecological complexity while minimizing state variable increases. If we relax the notion that parameter values (or traits) are fixed for species, but rather change and respond to other traits, we can capture some aspects of adaptation and diversity within modeled ecosystems. For example, virus infections can drive changes in host traits, such as growth rate, rapidly (Avrani and Lindell, 2015). By allowing parameter values to be flexible and depend on each other based on tradeoffs, we can capture some of the community dynamics without adding state variables. Virus-host dynamics are rapid enough to allow for studying these dynamics in detail and for revealing their underlying principles. Incorporating this information into climate models is a promising approach both to answer questions about the role of marine viruses in climate and to introduce ecological processes more generally into climate models.

# 5. CONCLUSION

Virus ecology and trait-based ocean ecology have new insights to offer each other. There are some ways in which trait-based approaches to ocean life can inform virus ecology. For example, the strongly size structured character of the ocean ecosystem has been explored in depth across trophic levels (cf. Andersen et al., 2016), but there is limited work on the allometry of marine viruses. A detailed investigation of the marine virus size

spectrum could facilitate the incorporation of virus ecology into models. However, as we have discussed, there are ways in which virus allometry might deviate from pelagic food web allometry in general. Because of differences like this, the exchange of knowledge works in both directions: the study of virus ecology can also provide new insights to trait-based ecology. For example, the role of adaptation and evolution in altering traits dynamically has been a challenge to measure at higher trophic levels. This type of dynamic has been explored in models (Record et al., 2013a; Sauterey et al., 2014), but it is difficult to link with empirical work. The short time scales at which virus-host interactions take place makes it possible to quantify and study these dynamics, and the insights gained can help guide ecology at higher trophic levels. Along a similar vein, trait-based studies typically focus on the traits of the focal taxa, while ignoring the traits of adjacent trophic groups. The intimate interaction between virus replication and host reproduction at the genetic level forces us to consider both virus and host traits together. Because of these perspectives, virus ecology is uniquely poised to offer new insights to the broader field of trait-based ecology.

## AUTHOR CONTRIBUTIONS

NR, DT, and SV contributed equally to this manuscript.

## FUNDING

This publication was supported by the Ocean Carbon and Biogeochemistry program (NSF, NASA). NR was supported by Bigelow Laboratory institutional funds. DT was supported by NSF grant OCE-1536521 and the Gordon and Betty Moore Foundation through grant GBMF3778 to M.J. Follows. SV was supported by the University of Bergen.

## ACKNOWLEDGMENTS

This manuscript is a product of a collaboration at the "Trait-based Approaches to Ocean Life" Scoping Workshop, which was supported by the Ocean Carbon and Biogeochemistry group (NSF, NASA), the Simons Foundation, and the Gordon and Betty Moore Foundation. We thank two reviewers for their input and Joaquín Martínez Martínez for valuable comments that greatly improved the manuscript.

## SUPPLEMENTARY MATERIAL

The Supplementary Material for this article can be found online at: http://journal.frontiersin.org/article/10.3389/fmars.2016.00251/full#supplementary-material

## REFERENCES

Allen, J., Somerfield, P., and Gilbert, F. (2007). Quantifying uncertainty in high-resolution coupled hydrodynamic-ecosystem models. *J. Mar. Syst.* 64, 3–14. doi: 10.1016/j.jmarsys.2006.02.010

Andersen, K. H., Berge, T., Gonçalves, R. J., Hartvig, M., Heuschele, J., Hylander, S., et al. (2016). Characteristic sizes of life in the oceans, from bacteria to whales. *Mar. Sci.* 8, 217–241. doi: 10.1146/annurev-marine-122414-034144

Andersen, K. H., and Beyer, J. E. (2015). Size structure, not metabolic scaling rules, determines fisheries reference points. *Fish Fish.* 16, 1–22. doi: 10.1111/faf.12042

Avrani, S., and Lindell, D. (2015). Convergent evolution toward an improved growth rate and a reduced resistance range in prochlorococcus strains resistant to phage. *Proc. Natl. Acad. Sci. U.S.A.* 112, E2191–E2200. doi: 10.1073/pnas.1420347112

Avrani, S., Wurtzel, O., Sharon, I., Sorek, R., and Lindell, D. (2011). Genomic island variability facilitates Prochlorococcus-virus coexistence. *Nature* 474, 604–608. doi: 10.1038/nature10172

Azam, F., Fenchel, T., Field, J., Gray, J., Meyer-Reil, L., and Thingstad, F. (1983). The ecological role of water-column microbes in the sea. *Mar. Ecol. Prog. Ser.* 10, 257–263. doi: 10.3354/meps010257

Banas, N. S. (2011). Adding complex trophic interactions to a size-spectral plankton model: emergent diversity patterns and limits on predictability. *Ecol. Model.* 222, 2663–2675. doi: 10.1016/j.ecolmodel.2011.05.018

Barrangou, R., Fremaux, C., Deveau, H., Richards, M., Boyaval, P., Moineau, S., et al. (2007). Crispr provides acquired resistance against viruses in prokaryotes. *Science* 315, 1709–1712. doi: 10.1126/science.1138140

Barton, A., Finkel, Z., Ward, B., Johns, D., and Follows, M. (2013). On the roles of cell size and trophic strategy in North Atlantic diatom and dinoflagellate communities. *Limnol. Oceanogr.* 58, 254–266. doi: 10.4319/lo.2013.58.1.0254

Barton, A. D., Dutkiewicz, S., Andersen, K. H., Fiksen, Ø. Ø., Follows, M. J., Mouw, C. B., et al. (2016). *Report on the "Trait-Based Approaches to Ocean Life" Scoping Workshop*. Waterville Valley, NH: U.S. Ocean Carbon and Biogeochemistry Program, p. 35. doi: 10.1575/1912/8017

Baudoux, A.-C., and Brussaard, C. P. D. (2008). Influence of irradiance on virus-algal host interactions. *J. Phycol.* 44, 902–908. doi: 10.1111/j.1529-8817.2008.00543.x

Baudoux, A.-C., and Brussard, C. P. D. (2005). Characterization of different viruses infecting the marine harmful algal bloom species phaeocystis globosa. *Virology* 341, 80–90. doi: 10.1016/j.virol.2005.07.002

Beckett, S., and Williams, H. (2013). Coevolutionary diversification creates nested-modular structure in phage bacteria interaction networks. *Interface Focus* 3:20130033. doi: 10.1098/rsfs.2013.0033

Beltrami, E., and Carroll, T. (1994). Modeling the role of viral disease in recurrent phytoplankton blooms. *J. Math. Biol.* 32, 857–863. doi: 10.1007/BF00168802

Berngruber, T. W., Lion, S., and Gandon, S. (2013). Evolution of suicide as a defence strategy against pathogens in a spatially structured environment. *Ecol. Lett.* 16, 446–453. doi: 10.1111/ele.12064

Bidle, K., and Vardi, A. (2011). A chemical arms race at sea mediates algal host-virus interactions. *Curr. Opin. Microbiol.* 14, 449–457. doi: 10.1016/j.mib.2011.07.013

Bohannan, B., and Lenski, R. (2000). Linking genetic change to community evolution: insights from studies of bacteria and bacteriophage. *Ecol. Lett.* 3, 362–377. doi: 10.1046/j.1461-0248.2000.00161.x

Bohannan, B. J., Kerr, B., Jessup, C. M., Hughes, J. B., and Sandvik, G. (2002). Trade-offs and coexistence in microbial microcosms. *Antonie Van Leeuwenhoek* 81, 107–115. doi: 10.1023/A:1020585711378

Bohannan, B. J. M., Travisano, M., and Lenski, R. E. (1999). Epistatic interactions can lower the cost of resistance to multiple consumers. *Evolution* 53, 292–295.

Bratbak, G., Egge, J., and Heldal, M. (1993). Viral mortality of the marine alga *Emiliania huxleyi* ( Haptophyceae ) and termination of algal blooms. *Mar. Ecol. Prog. Ser.* 93, 39–48.

Bratbak, G., Jacobsen, A., Heldal, M., Nagasaki, K., and Thingstad, F. (1998). Virus production in *Phaeocystis pouchetii* and its relation to host cell growth and nutrition. *Aquat. Microb. Ecol.* 16, 1–9.

Brockhurst, M. A., Buckling, A., and Rainey, P. B. (2005). The effect of a bacteriophage on diversification of the opportunistic bacterial pathogen, *Pseudomonas aeruginosa*. *Proc. Biol. Sci.* 272, 1385–1391. doi: 10.1098/rspb.2005.3086

Brown, C., Lawrence, J., and Campbell, D. (2006). Are phytoplankton population density maxima predictable through analysis of host and viral genomic DNA content? *J. Mar. Biol. Assoc. U.K.* 86:491. doi: 10.1017/s0025315406013397

Brum, J. R., Hurwitz, B. L., Schofield, O., Ducklow, H. W., and Sullivan, M. B. (2016). Seasonal time bombs: dominant temperate viruses affect Southern Ocean microbial dynamics. *ISME J.* 10, 437–449. doi: 10.1038/ismej.2015.125

Brussaard, C. (2004). Viral control of phytoplankton populations - A review. *J. Eukaryot. Microbiol.* 51, 125–138. doi: 10.1111/j.1550-7408.2004.tb00537.x

Brüssow, H., Canchaya, C., and Hardt, W. D. (2004). Phages and the evolution of bacterial pathogens : from genomic rearrangements to lysogenic conversion phages and the evolution of bacterial pathogens : from genomic rearrangements to lysogenic conversion. *Microbiol. Mol. Biol. Rev.* 68, 560–602. doi: 10.1128/MMBR.68.3.560-602.2004

Buckling, A., and Rainey, P. B. (2002). Antagonistic coevolution between a bacterium and a bacteriophage. *Proc. Biol. Sci.* 269, 931–936. doi: 10.1098/rspb.2001.1945

Campbell, B. J., Yu, L., Heidelberg, J. F., and Kirchman, D. L. (2011). Activity of abundant and rare bacteria in a coastal ocean. *Proc. Natl. Acad. Sci. U.S.A.* 108, 12776–12781. doi: 10.1073/pnas.1101405108

Casjens, S., Palmer, N., Van Vugt, R., Huang, W. M., Stevenson, B., Rosa, P., et al. (2000). A bacterial genome in flux: the twelve linear and nine circular extrachromosomal DNAs in an infectious isolate of the Lyme disease spirochete *Borrelia burgdorferi*. *Mol. Microbiol.* 35, 490–516. doi: 10.1046/j.1365-2958.2000.01698.x

Chao, L., Levin, B. R., and Stewart, F. M. (1977). A complex community in a simple habitat: an experimental study with bacteria and phage. *Ecology* 58, 369–378. doi: 10.2307/1935611

Chattopadhyay, J., and Pal, S. (2002). Viral infection on phytoplankton-zooplankton system - a mathematical model. *Ecol. Model.* 151, 15–28. doi: 10.1016/S0304-3800(01)00415-X

Chiura, H. X. (1997). Generalized gene transfer by virus-like particles from marine bacteria. *Aquat. Microb. Ecol.* 13, 75–83.

Claudet, J., Osenberg, C. W., Domenici, P., Badalamenti, F., Milazzo, M., Falcón, J., et al. (2010). Marine reserves: fish life history and ecological traits matter. *Ecol. Appl.* 20, 830–839. doi: 10.1890/08-2131.1

Cochran, P. K., and Paul, J. H. (1998). Seasonal abundance of lysogenic bacteria in a subtropical estuary. *Appl. Environ. Microbiol.* 64, 2308–2312.

Comeau, A. M., Buenaventura, E., and Suttle, C. A. (2005). A persistent, productive, and seasonally dynamic vibriophage population within pacific oysters (*Crassostrea gigas*). *Appl. Environ. Microbiol.* 71, 5324–5331. doi: 10.1128/AEM.71.9.5324-5331.2005

Comeau, A. M., Chan, A. M., and Suttle, C. A. (2006). Genetic richness of vibriophages isolated in a coastal environment. *Environ. Microbiol.* 8, 1164–1176. doi: 10.1111/j.1462-2920.2006.01006.x

Daubin, V., Lerat, E., and Perrière, G. (2003). The source of laterally transferred genes in bacterial genomes. *Genome Biol.* 4:R57. doi: 10.1186/gb-2003-4-9-r57

De La Rocha, C., and Passow, U. (2007). Factors influencing the sinking of POC and the efficiency of the biological carbon pump. *Deep Sea Res. II* 54, 639–658. doi: 10.1016/j.dsr2.2007.01.004

De Paepe, M., and Taddei, F. (2006). Viruses' life history: towards a mechanistic basis of a trade-off between survival and reproduction among phages. *PLoS Biol.* 4:e193. doi: 10.1371/journal.pbio.0040193

Deng, L., Krauss, S., Feichtmayer, J., Hofmann, R., Arndt, H., and Griebler, C. (2014). Grazing of heterotrophic flagellates on viruses is driven by feeding behaviour. *Environ. Microbiol. Rep.* 6, 325–330. doi: 10.1111/1758-2229.12119

DePaola, A., Motes, M. L., Chan, A. M., and Suttle, C. A. (1998). Phages infecting vibrio vulnificus are abundant and diverse in oysters (*Crassostrea virginica*) collected from the gulf of mexico. *Appl. Environ. Microbiol.* 64, 346–351.

Edgar, R., and Lielausis, I. (1964). Temperature-sensitive mutants of bacteriophage T4D: their isolation and genetic characterization. *Genetics* 49, 649–662.

Edlin, G., Lin, L., and Kudrna, R. (1975). Lambda lysogens of *E. coli* reproduce more rapidly than non-lysogen. *Nature* 255, 735–737.

Edwards, K., Thomas, M., Klausmeier, C., and Litchman, E. (2012). Allometric scaling and taxonomic variation in nutrient utilization traits and maximum growth rate of phytoplankton. *Limnol. Oceanogr.* 57, 554–566. doi: 10.4319/lo.2012.57.2.0554

Egas, M., Dieckmann, U., and Sabelis, M. W. (2004). Evolution restricts the coexistence of specialists and generalists: the role of trade-off structure. *Am. Nat.* 163, 518–531. doi: 10.1086/382599

Faruque, S., Asadulghani, Rahman, M. M., Waldor, M. K., and Sack, D. A. (2000). Sunlight-induced propagation of the lysogenic phage encoding cholera toxin. *Infect. Immun.* 68, 4795–4801. doi: 10.1128/IAI.68.8.4795-4801.2000

Flores, C. O., Meyer, J. R., Valverde, S., Farr, L., and Weitz, J. S. (2011). Statistical structure of host-phage interactions. *Proc. Natl. Acad. Sci. U.S.A.* 108, 288–297. doi: 10.1073/pnas.1101595108

Follows, M., Dutkiewicz, S., Grant, S., and Chisholm, S. W. (2007). Emergent biogeography of microbial communities in a model ocean. *Science* 315, 1843–1846. doi: 10.1126/science.1138544

Fuhrman, J. (1999). Marine viruses and their biogeochemical and ecological effects. *Nature* 399, 541–548.

Fuhrman, J. A., and Noble, R. T. (1995). Viruses and protists cause similar bacterial mortality in coastal seawater. *Limnol. Oceanogr.* 40, 1236–1242.

Gentleman, W., Leising, A., Frost, B., Strom, S., and Murray, J. (2003). Functional responses for zooplankton feeding on multiple resources: a review of assumptions and biological dynamics. *Deep. Res. II Top. Stud. Oceanogr.* 50, 2847–2875. doi: 10.1016/j.dsr2.2003.07.001

Ghosh, D., Roy, K., Williamson, K. E., Srinivasiah, S., Wommack, K. E., and Radosevich, M. (2009). Acyl-homoserine lactones can induce virus production in lysogenic bacteria: an alternative paradigm for prophage induction. *Appl. Environ. Microbiol.* 75, 7142–7152. doi: 10.1128/AEM.00950-09

Gilchrist, G. W. (1995). Specialists and generalists in changing environments. I. fitness landscapes of thermal sensitivity. *Am. Nat.* 146, 252–270.

Golet, W. J., Record, N. R., Lehuta, S., Lutcavage, M., Galuardi, B., Cooper, A. B., et al. (2015). The paradox of the pelagics: why bluefin tuna can go hungry in a sea of plenty. *Mar. Ecol. Prog. Ser.* 527, 181–192. doi: 10.3354/meps11260

Gough, M. (1968). Second locus of bacteriophage P22 necessary for the maintenance of lysogeny. *J. Virol.* 2, 992–998.

Haaber, J., and Middelboe, M. (2009). Viral lysis of *Phaeocystis pouchetii*: implications for algal population dynamics and heterotrophic c, n and p cycling. *ISME J.* 3, 430–441. doi: 10.1038/ismej.2008.125

Hansen, B., Gaard, E., and Reinert, J. (1994). "Physical effects on recruitment of faroe plateau cod," in *ICES Marine Science Symposia. Copenhagen [ICES MAR. SCI. SYMP.]*., eds J. Jakobsson, O. Astthorsson, R. Beverton, B. Bjoernsson, N. Daan, K. Frank, J. Meincke, B. Rothschild, S. Sundby, and S. Tilseth, International Counc. for the Exploration of the Sea (Copenhagen).

Harcombe, W. R., and Bull, J. J. (2005). Impact of phages on two-species bacterial communities. *Appl. Environ. Microbiol.* 71, 5254–5259. doi: 10.1128/AEM.71.9.5254-5259.2005

Hayashi, T., Makino, K., Ohnishi, M., Kurokawa, K., Ishii, K., Yokoyama, K., et al. (2001). Complete genome sequence of enterohemorrhagic *Escherichia coli* O157:H7 and genomic comparison with a laboratory strain K-12. *DNA Res.* 8, 11–22. doi: 10.1093/dnares/8.1.11

Holling, C. (1959). The Components of predation as revealed by a study of small-mammal predation of the European pine sawfly. *Can. Entomol.* 91, 293–320.

Holmfeldt, K., Middelboe, M., Nybroe, O., and Riemann, L. (2007). Large variabilities in host strain susceptibility and phage host range govern interactions between lytic marine phages and their flavobacterium hosts. *Appl. Environ. Microbiol.* 73, 6730–6739. doi: 10.1128/AEM.01399-07

Høyland-Kroghsbo, N. M., Mærkedahl, R. B., and Svenningsen, S. L. (2013). A quorum-sensing-induced bacteriophage defense mechanism. *MBio* 4, e00362-e00312. doi: 10.1128/mBio.00362-12

Jeschke, J. M., Kopp, M., and Tollrian, R. (2004). Consumer-food systems: why type I functional responses are exclusive to filter feeders. *Biol. Rev.* 79, 337–349. doi: 10.1017/S1464793103006286

Jessup, C. M., and Bohannan, B. J. (2008). The shape of an ecological trade-off varies with environment. *Ecol. Lett.* 11, 947–959. doi: 10.1111/j.1461-0248.2008.01205.x

Jiang, S., and Paul, J. (1994). Seasonal and diel abundance of viruses and occurrence of lysogeny/bacteriocinogeny in the marine environment. *Mar. Ecol. Prog. Ser.* 104, 163–172.

Jiang, S., and Paul, J. (1996). Occurrence of lysogenic bacteria in marine microbial communities as determined by prophage induction. *Mar. Ecol. Prog. Ser.* 142, 27–38.

Jover, L. F., Effler, T. C., Buchan, A., Wilhelm, S. W., and Weitz, J. S. (2014). The elemental composition of virus particles: implications

for marine biogeochemical cycles. *Nat. Rev. Microbiol.* 12, 519–528. doi: 10.1038/nrmicro3289

Jover, L. F., Cortez, M. H., and Weitz, J. S. (2013). Mechanisms of multi-strain coexistence in host–phage systems with nested infection networks. *J. Theor. Biol.* 332, 65–77. doi: 10.1016/j.jtbi.2013.04.011

Kattge, J., Ogle, K., Bönisch, G., Díaz, S., Lavorel, S., Madin, J., et al. (2011). A generic structure for plant trait databases. *Methods Ecol. Evol.* 2, 202–213. doi: 10.1111/j.2041-210X.2010.00067.x

Keen, E. C. (2014). Tradeoffs in bacteriophage life histories. *Bacteriophage* 4:e28365. doi: 10.4161/bact.28365

Kempes, C. P., Dutkiewicz, S., and Follows, M. J. (2012). Growth, metabolic partitioning, and the size of microorganisms. *Proc. Natl. Acad. Sci. U.S.A.* 109, 495–500. doi: 10.1073/pnas.1115585109

Kermack, W. O., and McKendrick, A. G. (1927). A contribution to the mathematical theory of epidemics. *Proc. R. Soc. Lond. A* 115, 700–721.

Kiørboe, T. (2008). *A mechanistic Approach to Plankton Ecology*. Princeton, NJ: Princeton University Press.

Kiørboe, T., Andersen, A., Langlois, V. J., and Jakobsen, H. H. (2010). Unsteady motion: escape jumps in planktonic copepods, their kinematics and energetics. *J. R. Soc. Interface* 7, 1591–1602. doi: 10.1098/rsif.2010.0176

Knowles, B., Silveira, C. B., Bailey, B. A., Barott, K., Cantu, V. A., Cobián-Güemes, A., et al. (2016). Lytic to temperate switching of viral communities. *Nature* 531, 466–470. doi: 10.1038/nature17193

Knuth, N. (1991). Theory and practice. *Theor. Comput. Sci.* 90, 1–15.

Kokjohn, T., Sayler, G., and Miller, R. (1991). Attachment and replication of *Pseudomonas aeruginosa* bacteriophages under conditions simulating aquatic environments. *J. Gen. Microbiol.* 137, 661–666.

Koskella, B., and Brockhurst, M. A. (2014). Bacteria–phage coevolution as a driver of ecological and evolutionary processes in microbial communities. *FEMS Microbiol. Rev.* 38, 916–931. doi: 10.1111/1574-6976.12072

Koudelka, G. B., Harbury, P., Harrison, S. C., and Ptahsne, M. (1988). Dna twisting and the affinity of bacteriophage 434 operator for bacteriophage 434 represso. *Proc. Natl. Acad. Sci. U.S.A.* 85, 4633–4637.

Labrie, S. J., Samson, J. E., and Moineau, S. (2010). Bacteriophage resistance mechanisms. *Nat. Rev. Microbiol.* 8, 317–327. doi: 10.1038/nrmicro2315

Lawrence, J. G., and Ochman, H. (1998). Molecular archaeology of the *Escherichia coli* genome. *Proc. Natl. Acad. Sci. U.S.A.* 95, 9413–9417.

Lennon, J., Khatana, S., Marston, M., and Martiny, J. (2007). Is there a cost of virus resistance in marine cyanobacteria? *ISME J.* 1, 300–312. doi: 10.1038/ismej.2007.37

Lenski, R. E. (1988). Experimental studies of pleiotropy and epistasis in *Escherichia coli*. I. variation in competitive fitness among mutants resistant to virus T4. *Evolution* 42, 425–432.

Lenski, R. E., and Levin, B. R. (1985). Constraints on the coevolution of bacteria and virulent phage: a model, some experiments, and predictions for natural communities. *Am. Nat.* 125, 585–602.

Levin, B. R., and Lenski, R. E. (1983). "Coevolution in bacteria and their viruses and plasmids," in *Coevolution*, eds D. J. Futuyma and M. Slatkin (Sunderland, MA: Sinauer Associates Inc.), 99–127.

Levin, B. R. (2010). Nasty viruses, costly plasmids, population dynamics, and the conditions for establishing and maintaining crispr-mediated adaptive immunity in bacteria. *PLoS Genet.* 6:e1001171. doi: 10.1371/journal.pgen.1001171

Lima-Mendez, G., Faust, K., Henry, N., Decelle, J., Colin, S., Carcillo, F., et al. (2015). Determinants of community structure in the global plankton interactome. *Science* 348:1262073. doi: 10.1126/science.1262073

Litchman, E., and Klausmeier, C. (2008). Trait-based community ecology of phytoplankton. *Annu. Rev. Ecol. Evol. Syst.* 39, 615–639. doi: 10.1146/annurev.ecolsys.39.110707.173549

Litchman, E., Klausmeier, C. A., Schofield, O. M., and Falkowski, P. G. (2007). The role of functional traits and trade-offs in structuring phytoplankton communities: scaling from cellular to ecosystem level. *Ecol. Lett.* 10, 1170–1181. doi: 10.1111/j.1461-0248.2007.01117.x

Litchman, E., Ohman, M. D., and Kiørboe, T. (2013). Trait-based approaches to zooplankton communities. *J. Plankton Res.* 35, 473–484. doi: 10.1093/plankt/fbt019

Liu, H., Laws, E., Villareal, T., and Buskey, E. (2001). Nutrient-limited growth of *Aureoumbra lagunensis* (Pelagophyceae), with implications for its capability to outgrow other phytoplankton species in phosphate-limited environments. *J. Phycol.* 37, 500–508. doi: 10.1046/j.1529-8817.2001.037004500.x

López-Urrutia, Á., San Martin, E., Harris, R. P., and Irigoien, X. (2006). Scaling the metabolic balance of the oceans. *Proc. Nat. Acad. Sci. U.S.A.* 103, 8739–8744. doi: 10.1073/pnas.0601137103

Lymer, D., and Lindström, E. (2010). Changing phosphorus concentration and subsequent prophage induction alter composition of a freshwater viral assemblage. *Freshw. Biol.* 55, 1984–1996. doi: 10.1111/j.1365-2427.2010.02435.x

Lythgoe, K., and Chao, L. (2003). Mechanisms of coexistence of a bacteria and a bacteriophage in a spatially homogeneous environment. *Ecol. Lett.* 6, 326–334. doi: 10.1046/j.1461-0248.2003.00433.x

Ma, J., and Levin, S. A. (2006). The evolution of resource adaptation: how generalist and specialist consumers evolve. *Bull. Math. Biol.* 68, 1111–1123. doi: 10.1007/s11538-006-9096-6

Makarova, K. S., Wolf, Y. I., Snir, S., and Koonin, E. V. (2011). Defense islands in bacterial and archaeal genomes and prediction of novel defense systems. *J. Bacteriol.* 193, 6039–6056. doi: 10.1128/JB.05535-11

Malki, K., Kula, A., Bruder, K., Sible, E., Hatzopoulos, T., Steidel, S., et al. (2015). Bacteriophages isolated from lake michigan demonstrate broad host-range across several bacterial phyla. *Virol. J.* 12, 164. doi: 10.1186/s12985-015-0395-0

Malmstrom, R. R., Kiene, R. P., Cottrell, M. T., and Kirchman, D. L. (2004). Contribution of sar11 bacteria to dissolved dimethylsulfoniopropionate and amino acid uptake in the North Atlantic Ocean. *Appl. Environ. Microbiol.* 70, 4129–4135. doi: 10.1128/AEM.70.7.4129-4135.2004

Marras, S., Killen, S. S., Domenici, P., Claireaux, G., and McKenzie, D. J. (2013). Relationships among traits of aerobic and anaerobic swimming performance in individual european sea bass *Dicentrarchus labrax*. *PLoS ONE* 8:e72815. doi: 10.1371/journal.pone.0072815

Martínez, J. M., Boere, A., Gilg, I., van Lent, J. W., Witte, H. J., van Bleijswijk, J. D., et al. (2015). New lipid envelope-containing dsdna virus isolates infecting micromonas pusilla reveal a separate phylogenetic group. *Aquat. Microbiol. Ecol.* 74, 17–28. doi: 10.3354/ame01723

Martiny, J. B. H., Riemann, L., Marston, M. F., and Middelboe, M. (2014). Antagonistic coevolution of marine planktonic viruses and their hosts. *Mar. Sci.* 6, 393–414. doi: 10.1146/annurev-marine-010213-135108

Marvier, M., Kareiva, P., and Neubert, M. G. (2004). Habitat destruction, fragmentation, and disturbance promote invasion by habitat generalists in a multispecies metapopulation. *Risk Anal.* 24, 869–878. doi: 10.1111/j.0272-4332.2004.00485.x

Maurice, C. F., Bouvier, T., Comte, J., Guillemette, F., and Del Giorgio P. (2010). Seasonal variations of phage life strategies and bacterial physiological states in three northern temperate lakes. *Environ. Microbiol.* 12, 628–641. doi: 10.1111/j.1462-2920.2009.02103.x

McDaniel, L., DelaRosa, M., and Paul, J. (2006). Temperate and lytic cyanophages from the Gulf of Mexico. *J. Mar. Biol. Assoc. U.K.* 86, 517–527. doi: 10.1017/S0025315406013427

McDaniel, L., Houchin, L. A., Williamson, S. J., and Paul, J. H. (2002). Lysogeny in marine Synechococcus. *Nature* 415:496. doi: 10.1038/415496a

McDaniel, L., and Paul, J. (2005). Effect of nutrient addition and environmental factors on prophage induction in natural populations of marine Synechococcus species. *Appl. Environ. Microbiol.* 71, 842–850. doi: 10.1128/AEM.71.2.842-850.2005

Middelboe, M. (2000). Bacterial growth rate and marine virus–host dynamics. *Microb. Ecol.* 40, 114–124. doi: 10.1007/s00248-001-0012-1

Middelboe, M., Hagström, A., Blackburn, N., Sinn, B., Fischer, U., Borch, N., et al. (2001). Effects of bacteriophages on the population dynamics of four strains of pelagic marine bacteria. *Microb. Ecol.* 42, 395–406. doi: 10.1007/s00248-001-0012-1

Middelboe, M., Holmfeldt, K., Riemann, L., Nybroe, O., and Haaber, J. (2009). Bacteriophages drive strain diversification in a marine flavobacterium: implications for phage resistance and physiological properties. *Environ. Microbiol.* 11, 1971–1982. doi: 10.1111/j.1462-2920.2009.01920.x

Middleton, J., Martínez Martínez, J., Wilson, W., and Record, N. (in press). Functional dynamics of *Emiliania huxleyi* virus-host interactions across multiple spatial scales. *Limnol. Oceanogr.*

Mizoguchi, K., Morita, M., Fischer, C. R., Yoichi, M., Tanji, Y., and Unno, H. (2003). Coevolution of bacteriophage pp01 and *Escherichia coli* o157: H7 in continuous culture. *Appl. Environ. Microbiol.* 69, 170–176. doi: 10.1128/AEM.69.1.170-176.2003

Moebus, K. (1996). Marine bacteriophage reproduction under nutrient-limited growth of host bacteria. II. investigations with phage-host system [H3:H3/1]. *Mar. Ecol. Prog. Ser.* 144, 13–22.

Mojica, K. D., and Brussaard, C. P. (2014). Factors affecting virus dynamics and microbial host-virus interactions in marine environments. *FEMS Microbiol. Ecol.* 89, 495–515. doi: 10.1111/1574-6941.12343

Murray, A., and Jackson, G. (1992). Viral dynamics : a model of the effects of size , shape , motion and abundance of single-celled planktonic organisms and other particles. *Mar. Ecol. Prog. Ser.* 89, 103–116.

Murray, A. G., and Jackson, G. A. (1993). Viral dynamics II: a model of the interaction of ultraviolet light and mixing processes on virus survival in seawater. *Mar. Ecol. Prog. Ser.* 102, 105–114.

Nagasaki, K., Ando, M., Imai, I., Itakura, S., and Ishida, Y. (1994). Virus-like particles in *Heterosigma akashiwo* (raphidophyceae): a possible red tide disintegration mechanism. *Mar. Biol.* 119, 307–312.

Nagasaki, K., Tomaru, Y., Katanozaka, N., Nishida, K., Itakura, S., Shirai, Y., et al. (2004). Isolation and characterization of a novel single-stranded RNA virus infecting the bloom-forming diatom *Rhizosolenia setigera* isolation and characterization of a novel single-stranded RNA virus infecting the bloom-forming diatom *Rhizosolenia setigera*. *Appl. Environ. Microbiol.* 70, 704–711. doi: 10.1128/AEM.70.2.704-711.2004

Ochman, H., Lawrence, J. G., and Groisman, E. A. (2000). Lateral gene transfer and the nature of bacterial innovation. *Nature* 405, 299–304. doi: 10.1038/35012500

Ogunseitan, O. A., Sayler, G. S., and Miller, R. V. (1990). Dynamic interactions of *Pseudomonas aeruginosa* and bacteriophages in lake water. *Microb. Ecol.* 19, 171–185.

Opdal, A. F., and Jørgensen, C. (2015). Long-term change in a behavioural trait: truncated spawning distribution and demography in northeast arctic cod. *Glob. Change Biol.* 21, 1521–1530. doi: 10.1111/gcb.12773

Pagarete, A., Allen, M. J., Wilson, W. H., Kimmance, S. A., and de Vargas, C. (2009). Host-virus shift of the sphingolipid pathway along an *Emiliania huxleyi* bloom: survival of the fattest. *Environ. Microbiol.* 11, 2840–2848. doi: 10.1111/j.1462-2920.2009.02006.x

Paul, J. H., and Jiang, S. C. (2001). Lysogeny and transduction. *Method Microbiol.* 30, 105–125. doi: 10.1016/S0580-9517(01)30042-9

Payet, J., and Suttle, C. (2013). To kill or not to kill: the balance between lytic and lysogenic viral infection is driven by trophic status. *Limnol. Oceanogr.* 58, 465–474. doi: 10.4319/lo.2013.58.2.0465

Pimentel, M. S., Faleiro, F., Marques, T., Bispo, R., Dionísio, G., Faria, A. M., et al. (2016). Foraging behaviour, swimming performance and malformations of early stages of commercially important fishes under ocean acidification and warming. *Clim. Change* 137, 495–509. doi: 10.1007/s10584-016-1682-5

Pradeep Ram, A. S., and Sime-Ngando, T. (2010). Resources drive trade-off between viral lifestyles in the plankton: evidence from freshwater microbial microcosms. *Environ. Microbiol.* 12, 467–479. doi: 10.1111/j.1462-2920.2009.02088.x

Proctor, L., and Fuhrman, J. (1991). Roles of virus infection in organic particle flux. *Mar. Ecol. Prog. Ser.* 69, 133–142.

Proulx, S. R., Promislow, D. E., and Phillips, P. C. (2005). Network thinking in ecology and evolution. *Trends Ecol. Evol.* 20, 345–353. doi: 10.1016/j.tree.2005.04.004

Prowe, A., Pahlow, M., Dutkiewicz, S., Follows, M., and Oschlies, A. (2012). Top-down control of marine phytoplankton diversity in a global ecosystem model. *Prog. Oceanogr.* 101, 1–13. doi: 10.1016/j.pocean.2011.11.016

Ptashne, M. (1967). Specific binding of the lambda phage repressor to lambda DNA. *Nature* 214, 232–234.

Ptashne, M. (2004). *A Genetic Switch: Phage Lambda Revisited*. Palo Alto, CA: Cold Spring Harbour Laboratory Press.

Record, N., Pershing, A., and Maps, F. (2012). First principles of copepod development help explain global marine diversity pattern. *Oecologia* 170, 289–295. doi: 10.1007/s00442-012-2313-0

Record, N. R., Pershing, A. J., and Maps, F. (2013a). Emergent copepod communities in an adaptive trait-structured model. *Ecol. Model.* 260, 11–24. doi: 10.1016/j.ecolmodel.2013.03.018

Record, N. R., Pershing, A. J., and Maps, F. (2013b). The paradox of the "paradox of the plankton". *ICES J. Mar. Sci.* 71, 236–240. doi: 10.1093/icesjms/fst049

Refardt, D., Bergmiller, T., and Kümmerli, R. (2013). Altruism can evolve when relatedness is low: evidence from bacteria committing suicide upon phage infection. *Proc. R. Soc. Lond. B* 280:20123035. doi: 10.1098/rspb.2012.3035

Rhodes, C. J., and Martin, A. P. (2010). The influence of viral infection on a plankton ecosystem undergoing nutrient enrichment. *J. Theor. Biol.* 265, 225–237. doi: 10.1016/j.jtbi.2010.04.022

Rose, K. A., Megrey, B. A., Werner, F. E., and Ware, D. M. (2007). Calibration of the NEMURO nutrient-phytoplankton-zooplankton food web model to a coastal ecosystem: evaluation of an automated calibration approach. *Ecol. Model.* 202, 38–51. doi: 10.1016/j.ecolmodel.2006.08.016

Rosenzweig, M. L. (1973). Evolution of the predator isocline. *Evolution* 27, 84–94.

Roux, S., Brum, J. R., Dutilh, B. E., Sunagawa, S., Duhaime, M. B., Loy, A., et al. (2016). Ecogenomics and potential biogeochemical impacts of globally abundant ocean viruses. *Nature* 537, 689–693. doi: 10.1038/nature19366

Samo, T. J., Smriga, S., Malfatti, F., Sherwood, B. P., and Azam, F. (2014). Broad distribution and high proportion of protein synthesis active marine bacteria revealed by click chemistry at the single cell level. *Front. Mar. Sci.* 1:48. doi: 10.3389/fmars.2014.00048

Sauterey, B., Ward, B. A., Follows, M. J., Bowler, C., and Claessen, D. (2014). When everything is not everywhere but species evolve: an alternative method to model adaptive properties of marine ecosystems. *J. Plankton Res.* 37, 28–47. doi: 10.1093/plankt/fbu078

Schroeder, D. C., Oke, J., Malin, G., and Wilson, W. H. (2002). Coccolithovirus (Phycodnaviridae): characterisation of a new large dsDNA algal virus that infects *Emiliana huxleyi*. *Arch. Virol.* 147, 1685–1698. doi: 10.1007/s00705-002-0841-3

Sheldon, R., Prakash, A., and Sutcliffe, W. (1972). The size distribution of particles in the ocean. *Limnol. Oceanogr.* 17, 327–340.

Siekmann, I., and Malchow, H. (2008). An extension of the beretta-kuang model of viral disease. *Math. Biosci. Eng.* 5, 549–565. doi: 10.3934/mbe.2008.5.549

Singh, B. K., Chattopadhyay, J., and Sinha, S. (2004). The role of virus infection in a simple phytoplankton zooplankton system. *J. Theor. Biol.* 231, 153–166. doi: 10.1016/j.jtbi.2004.06.010

Sorek, R., Kunin, V., and Hugenholtz, P. (2008). Crispr—a widespread system that provides acquired resistance against phages in bacteria and archaea. *Nat. Rev. Microbiol.* 6, 181–186. doi: 10.1038/nrmicro1793

Stenholm, A. R., Dalsgaard, I., and Middelboe, M. (2008). Isolation and characterization of bacteriophages infecting the fish pathogen flavobacterium psychrophilum. *Appl. Environ. Microbiol.* 74, 4070–4078. doi: 10.1128/AEM.00428-08

Stewart, F. M., and Levin, B. R. (1984). The population biology of bacterial viruses: why be temperate. *Theor. Popul. Biol.* 26, 93–117.

Stoddard, L. I., Martiny, J. B., and Marston, M. F. (2007). Selection and characterization of cyanophage resistance in marine Synechococcus strains. *Appl. Environ. Microbiol.* 73, 5516–5522. doi: 10.1128/AEM.00356-07

Sullivan, M. B., Waterbury, J. B., and Chisholm, S. W. (2003). Cyanophages infecting the oceanic cyanobacterium Prochlorococcus. *Nature* 424, 1047–1051. doi: 10.1038/nature01929

Suttle, C. (2007). Marine viruses–major players in the global ecosystem. *Nat. Rev. Microbiol.* 5, 801–812. doi: 10.1038/nrmicro1750

Suttle, C., and Chan, A. (1993). Marine cyanophages infecting oceanic and coastal strains of Synechococcus: abundance, morphology, cross-infectivity and growth characteristics. *Mar. Ecol. Prog. Ser.* 92, 99–109.

Suttle, C. A. (1994). The significance of viruses to mortality in aquatic microbial communities. *Microb. Ecol.* 28, 237–243.

Tarutani, K., Nagasaki, K., and Yamaguchi, M. (2000). Viral impacts on total abundance and clonal composition of the harmful bloom-forming phytoplankton *Heterosigma akashiwo*. *Appl. Environ. Microbiol.* 66, 4916–4920. doi: 10.1128/AEM.66.11.4916-4920.2000

Thingstad, T. (2000). Elements of a theory for the mechanisms controlling abundance, diversity, and biogeochemical role of lytic bacterial viruses in aquatic systems. *Limnol. Oceanogr.* 45, 1320–1328. doi: 10.4319/lo.2000.45.6.1320

Thingstad, T. F., Våge, S., Storesund, J. E., Sandaa, R. A., and Giske, J. (2014). A theoretical analysis of how strain-specific viruses can control

microbial species diversity. *Proc. Natl. Acad. Sci. U.S.A.* 111, 7813–7818. doi: 10.1073/pnas.1400909111

Thingstad, T. F., Pree, B., Giske, J., and Våge, S. (2015). What difference does it make if viruses are strain-, rather than species-specific? *Front. Microbiol.* 6:320. doi: 10.3389/fmicb.2015.00320

Thomas, L., and Parker, T. (1974). *The Lives of a Cell*. New York, NY: Viking Books New York.

Thomas, R., Grimsley, N., Escande, M. L., Subirana, L., Derelle, E., and Moreau, H. (2011). Acquisition and maintenance of resistance to viruses in eukaryotic phytoplankton populations. *Environ. Microbiol.* 13, 1412–1420. doi: 10.1111/j.1462-2920.2011.02441.x

Thyrhaug, R., Larsen, A., Thingstad, T., and Bratbak, G. (2003). Stable coexistence in marine algal host-virus systems. *Mar. Ecol. Prog. Ser.* 254, 27–35. doi: 10.3354/meps254027

Våge, S., Pree, B., and Thingstad, T. F. (2016). Linking internal and external bacterial community control gives mechanistic framework for pelagic virus-to-bacteria ratios. *Environ. Microbiol.* 18, 3932–3948. doi: 10.1111/1462-2920.13391

Våge, S., Storesund, J. E., and Thingstad, T. F. (2013). Adding a cost of resistance description extends the ability of virus-host model to explain observed patterns in structure and function of pelagic microbial communities. *Environ. Microbiol.* 15, 1842–1852. doi: 10.1111/1462-2920.12077

Van Etten, J. L., Burbank, D. E., Kia, Y., and Meints, R. H. (1983). Growth cycle of a virus, PBCV-1, that infects clorella-like algae. *Virology* 126, 117–125.

Violle, C., Navas, M., Vile, D., Kazakou, E., Fortunel, C., Hummel, I., et al. (2007). Let the concept of trait be functional! *Oikos* 116, 882–892. doi: 10.1111/j.0030-1299.2007.15559.x

Wang, I.-N. (2006). Lysis timing and bacteriophage fitness. *Genetics* 172, 17–26. doi: 10.1534/genetics.105.045922

Waterbury, J. B., and Valois, F. W. (1993). Resistance to co-occurring phages enables marine Synechococcus communities to coexist with cyanophages abundant in seawater. *Appl. Environ. Microbiol.* 59, 3393–3399.

Weinbauer, M. (2004). Ecology of prokaryotic viruses. *FEMS Microbiol. Rev.* 28, 127–181. doi: 10.1016/j.femsre.2003.08.001

Weinbauer, M., Brettar, I., and Höfle, M. (2003). Lysogeny and virus-induced mortality of bacterioplankton in surface, deep, and anoxic marine waters. *Limnol. Oceanogr.* 48, 1457–1465. doi: 10.4319/lo.2003.48.4.1457

Weinbauer, M. G., and Suttle, C. A. (1996). Potential significance of lysogeny to bacteriophage production and bacterial mortality in coastal waters of the gulf of Mexico. *Appl. Environ. Microbiol.* 62, 4374–4380.

Weitz, J., Beckett, S., Brum, J., Cael, B., and Dushoff, J. (2016). Lysis, lysogeny, and virus-microbe ratios. *bioRxiv* 1–5. doi: 10.1101/051805

Weitz, J. S., and Wilhelm, S. W. (2012). Ocean viruses and their effects on microbial communities and biogeochemical cycles. *F1000 Biol. Rep.* 4:17. doi: 10.3410/b4-17

Weitz, J. S., Stock, C. A., Wilhelm, S. W., Bourouiba, L., Coleman, M. L., Buchan, A., et al. (2015). A multitrophic model to quantify the effects of marine viruses on microbial food webs and ecosystem processes. *ISME J.* 9, 1352–1364. doi: 10.1038/ismej.2014.220

Wichels, A., Biel, S. S., Gelderblom, H. R., Brinkhoff, T., Muyzer, G., and Schütt, C. (1998). Bacteriophage diversity in the north sea. *Appl. Environ. Microbiol.* 64, 4128–4133.

Wigington, C. H., Sonderegger, D., Brussard, C. P. D., Buchan, A., Finke, J. F., Fuhrman, J. A., et al. (2016). Re-examination of the relationship between marine virus and microbial cell abundances. *Nat. Microbiol.* 1:15024. doi: 10.1038/nmicrobiol.2015.24

Wilcox, R., and Fuhrman, J. (1994). Bacterial viruses in coastal seawater: lytic rather than lysogenic production. *Mar. Ecol. Prog. Ser.* 114, 35–46.

Wilhelm, S. W., and Suttle, C. A. (1999). Viruses and nutrient cycles in the sea viruses play critical roles in the structure and function of aquatic food webs. *Bioscience* 49, 781–788.

Wilhelm, S. W., Jefferey, W. H., Dean, A. L., Meador, J., Pakulski, J. D., and Mitchell, D. L. (2003). UV radiation induced DNA damage in marine viruses along a latitudinal gradient in the southereastern pacific ocean. *Aquat. Microb. Ecol.* 31, 1–8. doi: 10.3354/ame031001

Williamson, S. J., Houchin, L., McDaniel, L., and Paul, J. H. (2002). Seasonal variation in lysogeny as depicted by prophage induction in Tampa Bay, Florida. *Appl. Environ. Microbiol.* 68, 4307–4314. doi: 10.1128/AEM.68.9.4307-4314.2002

Williamson, S. J., and Paul, J. H. (2006). Environmental factors that influence the transition from lysogenic to lytic existence in the phiHSIC/Listonella pelagia marine phage-host system. *Microb. Ecol.* 52, 217–225. doi: 10.1007/s00248-006-9113-1

Wilson, E. O. (1994). Biodiversity: challenge, science, opportunity. *Am. Zool.* 34, 5–11.

Wilson, G. G., and Murray, N. E. (1991). Restriction and modification systems. *Annu. Rev. Genet.* 25, 585–627.

Wilson, W., Carr, N., and Mann, N. (1996). The effect of phosphate status on the kinetic of cyanophage infection in the oceanic cyanobacterium Synechococcus sp. WH7803. *J. Phycol.* 32, 506–516.

Wilson, W., and Mann, N. (1997). Lysogenic and lytic viral production in marine microbial communities. *Aquat. Microb. Ecol.* 13, 95–100.

Wilson, W., Turner, S., and Mann, N. (1998). Population dynamics of phytoplankton and viruses in a phosphate-limited mesocosm and their effect on DMSP and DMS production. *Estuar. Coast. Shelf Sci.* 46, 49–59.

Wommack, K. E., and Colwell, R. R. (2000). Virioplankton: viruses in aquatic ecosystems. *Microbiol. Mol. Biol. Rev.* 64, 69–114. doi: 10.1128/MMBR.64.1.69-114.2000

Wright, I. J., Reich, P. B., Cornelissen, J. H., Falster, D. S., Garnier, E., Hikosaka, K., et al. (2005). Assessing the generality of global leaf trait relationships. *New Phytol.* 166, 485–496. doi: 10.1111/j.1469-8137.2005.01349.x

Zeng, L., Skinner, S. O., Zong, C., Sippy, J., Feiss, M., and Golding, I. (2010). Decision making at a subcellular level determines the outcome of bacteriophage infection. *Cell* 141, 682–691. doi: 10.1016/j.cell.2010.03.034

Zhang, L., Thygesen, U. H., Knudsen, K., and Andersen, K. H. (2013). Trait diversity promotes stability of community dynamics. *Theor. Ecol.* 6, 57–69. doi: 10.1007/s12080-012-0160-6

**Conflict of Interest Statement:** The authors declare that the research was conducted in the absence of any commercial or financial relationships that could be construed as a potential conflict of interest.

frontiers in Marine Science

ORIGINAL RESEARCH
published: 22 November 2016
doi: 10.3389/fmars.2016.00240

# Directional and Spectral Irradiance in Ocean Models: Effects on Simulated Global Phytoplankton, Nutrients, and Primary Production

*Watson W. Gregg*[1]* *and Cécile S. Rousseaux*[1, 2]

[1] NASA Global Modeling and Assimilation Office, Greenbelt, MD, USA, [2] Goddard Earth Sciences Technology and Research, Universities Space Research Association (USRA), Greenbelt, MD, USA

The importance of including directional and spectral light in simulations of ocean radiative transfer was investigated using a coupled biogeochemical-circulation-radiative model of the global oceans. The effort focused on phytoplankton abundances, nutrient concentrations and vertically-integrated net primary production. The importance was approached by sequentially removing directional (i.e., direct vs. diffuse) and spectral irradiance and comparing results of the above variables to a fully directionally and spectrally-resolved model. In each case the total irradiance was kept constant; it was only the pathways and spectral nature that were changed. Assuming all irradiance was diffuse had negligible effect on global ocean primary production. Global nitrate and total chlorophyll concentrations declined by about 20% each. The largest changes occurred in the tropics and sub-tropics rather than the high latitudes, where most of the irradiance is already diffuse. Disregarding spectral irradiance had effects that depended upon the choice of attenuation wavelength. The wavelength closest to the spectrally-resolved model, 500 nm, produced lower nitrate (19%) and chlorophyll (8%) and higher primary production (2%) than the spectral model. Phytoplankton relative abundances were very sensitive to the choice of non-spectral wavelength transmittance. The combined effects of neglecting both directional and spectral irradiance exacerbated the differences, despite using attenuation at 500 nm. Global nitrate decreased 33% and chlorophyll decreased 24%. Changes in phytoplankton community structure were considerable, representing a change from chlorophytes to cyanobacteria and coccolithophores. This suggested a shift in community function, from light-limitation to nutrient limitation: lower demands for nutrients from cyanobacteria and coccolithophores favored them over the more nutrient-demanding chlorophytes. Although diatoms have the highest nutrient demands in the model, their relative abundances were generally unaffected because they only prosper in nutrient-rich regions, such as the high latitudes and upwelling regions, which showed the fewest effects from the changes in radiative simulations. The results showed that including directional and spectral irradiance when simulating the ocean light field can be important for ocean biology, but the magnitude varies with variables and regions. The quantitative results are intended to assist ocean modelers when considering improved irradiance representations relative to other processes or variables associated with the issues of interest.

**Keywords: spectral irradiance, directional irradiance, global phytoplankton, radiative transfer, global models**

OPEN ACCESS

***Edited by:***
*Susanne Menden-Deuer, University of Rhode Island, USA*

***Reviewed by:***
*Oliver Zielinski, University of Oldenburg, Germany*
*Colleen Mouw, University of Rhode Island, USA*

***Correspondence:**
*Watson W. Gregg*
*watson.gregg@nasa.gov*

***Specialty section:***
*This article was submitted to Marine Ecosystem Ecology, a section of the journal Frontiers in Marine Science*

***Received:*** *20 July 2016*
***Accepted:*** *04 November 2016*
***Published:*** *22 November 2016*

***Citation:***
*Gregg WW and Rousseaux CS (2016) Directional and Spectral Irradiance in Ocean Models: Effects on Simulated Global Phytoplankton, Nutrients, and Primary Production. Front. Mar. Sci. 3:240. doi: 10.3389/fmars.2016.00240*

## INTRODUCTION

Light is a critical physical influence on ocean biology. It initiates the process of photosynthesis, the first step supporting nearly all life in the oceans (Dickey et al., 2011), and altering the oxygen and carbon balances on the Earth. Light from the sun arrives at the top of the atmosphere with different intensities at different spectral bands. It comes entirely in a specific direction depending on the time of day and season, in a beam that is defined by the solar zenith angle. This beam is the direct irradiance. The atmosphere modulates this direct irradiance via spectral absorption by optically active gases and also introduces a second pathway to the oceans resulting from scattering by clouds, aerosols, and molecules. This latter process gives rise to diffuse irradiance, where the light now enters the ocean from a hemisphere encompassing the horizon to nadir. This "sky light" does not have direction specified and is in contrast to direct irradiance that arrives uninterrupted by the atmosphere. Irradiance reaching the surface is often a combination of the direct and diffuse components. The term directional refers to this difference in irradiance pathways.

Once the spectral and directional light enters the ocean, it continues its journey of absorption and scattering, now guided by optical constituents with different spectral absorption capabilities and sizes that determine their scattering effects. Now it encounters much more strongly absorbing constituents than in the atmosphere and finds its pathways blocked by a phalanx of life forms and associated byproducts, as well as inorganic substances, each of which with demands for light unheard of in the atmosphere. Its passage in the oceans differs by the constituents it encounters and the directions it is forced to take, which alters the availability and nature of light to be taken up by phytoplankton and initiate process of photosynthesis, further affecting the distribution of life at the surface and at depth.

Despite the directional and spectral nature of irradiance in the oceans, models that represent these aspects are uncommon. Most ocean biogeochemical models simulate surface bulk irradiance, typically as shortwave radiation (e.g., Maier-Reimer et al., 2005; Doney et al., 2006; Henson et al., 2010) or as photosynthetically available radiation (PAR) (Palmer and Totterdell, 2001; Zielinski et al., 2002; Marinov et al., 2010; Laufkötter et al., 2013), and then represent the transmission as a function of an attenuation term (e.g., Zhao et al., 2013). This is especially true for the global models. The attenuation term is sometimes divided into a component for water and another for phytoplankton (Jiang et al., 2003; Maier-Reimer et al., 2005; Manizza et al., 2005; Xiu and Chai, 2014), but can also represent an estimated average loss of light in the water column (e.g., Doney et al., 2006).

Recognition of the importance of directional and spectral irradiance for phytoplankton dates to Sathyendranath and Platt (1988, 1989) in investigations of phytoplankton *in situ* light absorption and estimates of *in situ* primary production. Spectral irradiance was explicitly included in a 1-dimensional regional model of the Sargasso Sea (Bissett et al., 1999), the West Florida Shelf (Bissett et al., 2005), and in 3-dimensional models of the eastern US continental shelf (Mobley et al., 2009) and North Pacific (Xiu and Chai, 2014). But spectral and especially directional irradiance have largely been ignored in global coupled biological-circulation models (with the exceptions of Gregg, 2000; Gregg et al., 2003; Gregg and Casey, 2007; Dutkiewicz et al., 2015). This is likely related to the computational load directional and spectral radiative transfer imposes on ocean models, especially globally resolved ones. But in an era of multi-parallel processing, perhaps the time has come to reconsider its inclusion. Light in the natural oceans is, after all, directionally and spectrally resolved and therefore including these characteristics would enhance the realism of simulated ocean transmittance and light availability.

Our purpose here is to evaluate the importance of directional and spectral irradiance in the global oceans using an established ocean biogeochemical model and an established radiative transfer model that incorporates these aspects of light in the atmosphere and through the oceans. We limit our focus here to the effects on biological processes, specifically phytoplankton abundance, nutrient distributions, and vertically-integrated primary production. Nutrients are indirectly related to irradiance via uptake by phytoplankton. Changes in heat transfer due to ocean light absorption is important for ocean modeling as well (e.g., Gnanadesikan and Anderson, 2009), but we will defer these evaluations in the interest of brevity. Quantitative assessments can assist global modelers on how to proceed with future model improvements by quantifying the importance of these aspects and enable rational choices.

## METHODS

### Global Ocean Physical-Biogeochemical Model Configuration

The underlying biogeochemical constituents are simulated by the NASA Ocean Biogeochemical Model (NOBM; Gregg and Casey, 2007; Gregg et al., 2013) which is coupled to a global ocean circulation model, Modular Ocean Model version 4 (MOM4; Griffies et al., 2004; Gnanadesikan et al., 2006). It spans the global ocean at 1° horizontal resolution, with 50 vertical levels and the shallowest level at 10 m bottom depth. NOBM incorporates global coupled physical-biological processes, including six phytoplankton groups (diatoms, chlorophytes, cyanobacteria, coccolithophores, dinoflagellates, and *Phaeocystis* spp.). The *Phaeocystis* genus only includes the high latitude species, specifically *Phaeocystis pouchetti* (northern high latitudes) and *Phaeocystis antarctica* (Southern Ocean). These phytoplankton groups span much of the functionality of the global oceans. Diatoms represent high growth, fast sinking, silicate-dependent phytoplankton that have high nutrient requirements. Cyanobacteria are the functional opposite, with slow maximum growth rates, slow sinking, low nutrient requirements, and a capability for nitrogen fixation. Coccolithophores are moderate growers that sink relatively quickly due to their calcium carbonate coccoliths. They are efficient users of nitrogen, enabling them to flourish in low nutrient regions (although not as efficient as cyanobacteria). *Phaeocystis* spp., at least as represented here, are high latitude nanoplankton that play a role in the Earth's sulfur cycle. Unlike

the other phytoplankton, they have a temperature optimum in maximum growth rate around 3°C (Schoemann et al., 2005). Dinoflagellates are large, slow-growing phytoplankton with high nutrient requirements, but sink slowly based on the limited motility provided by flagella. Finally, chlorophytes are intended to represent the diverse functionality associated with nanoplankton, with growth rates, sinking rates, and nutrient requirements between the functional extremes and the more specialized phytoplankton. Phytoplankton-specific physiological and physical parameters are shown in Appendix Table 1.

Diatoms and chlorophytes (Arrigo and Sullivan, 1994; Arrigo et al., 1995; Robinson et al., 1998) and *Phaeocystis* spp. (Tang et al., 2009; Arrigo et al., 2014) have the capability to grow in sea ice. We limit irradiance in sea ice to one-tenth its value at the surface (Gregg and Casey, 2007). Biological activities in ice are modified by the percentage of sea ice present in a model grid cell.

The model also contains four nutrients (nitrate, ammonium, silicate, and dissolved iron), three detrital components (particulate organic carbon, silicate, and iron), and five carbon components: dissolved organic and inorganic carbon (DOC and DIC), alkalinity, and two new variables, particulate inorganic carbon (PIC), and chromophoric dissolved organic carbon (CDOC).

Phytoplankton growth is a function of scalar quantum irradiance, which is a measure of the photons impacting phytoplankton cells from all directions, expressed as units of μmol photons $m^{-2}$ $s^{-1}$ (Kirk, 1992). Variable carbon to chlorophyll ratios are utilized, that depend on the light history (Gregg and Casey, 2007).

PIC is produced by coccolithophores as detached coccoliths and is lost via sinking and dissolution. PIC is produced as a fraction (25%) of the coccolithophore growth rate (Gregg and Casey, 2007) minus respiration. The PIC sinking rate is represented here as an exponential function of concentration, assuming that large concentrations of PIC are associated with larger coccolith size

$$w_s(\mathrm{PIC}) = a_o \exp(a_1 {}^{*}\mathrm{PIC}) \tag{1}$$

where $w_s$ is the PIC sinking rate (m $d^{-1}$), PIC is in units of μgC $l^{-1}$, $a_0 = 0.1$ m $d^{-1}$ and $a_1 = 1.0$ l μg$C^{-1}$. Dissolution follows Buitenhuis et al. (2001), except that no dissolution is allowed for depths shallower than the calcium carbonate compensation depth, which we define as 3500 m.

CDOC represents the biogeochemical constituent necessary for the simulation of absorption by $a_{CDOC}(\lambda)$, the absorption coefficient, which is an optical quantity. It has two sources in the model: phytoplankton excretion and river discharge. Phytoplankton excretion assumes a DOC:CDOC production ratio of 0.7. It is destroyed by the absorption of photons, assuming a quantum yield for CDOC

$$\varphi\,\mathrm{CDOC} = \frac{\mu\ \mathrm{mol\ CDOC\ destroyed}}{\mu\ \mathrm{mol\ photons\ absorbed}} \tag{2}$$

and the quantum absorption of available spectral irradiance in the water column by CDOC

$$Q_a = \int_{200}^{800} a_{CDOC}(\lambda)\left[Q_d(\lambda) + Q_s(\lambda) + Q_u(\lambda)\right] d\lambda \tag{3}$$

where $Q_a$ is the absorbed quanta by CDOC (μmol photons $m^{-3}$ $s^{-1}$). Q denotes irradiance expressed as quanta with subscripts d, s, and u representing direct downwelling, diffuse downwelling, and diffuse upwelling components (μmol photons $m^{-2}$ $s^{-1}$), respectively, and $a_{CDOC}$ is the absorption coefficient of CDOC ($m^{-1}$).

The photolysis of CDOC is then

$$\frac{dCDOC}{dt} = \mathrm{CDOC} - \varphi_{\mathrm{CDOC}} * \mathrm{Qa} \tag{4}$$

There is regional information on defining $\varphi_{CDOC}$ (e.g., Reader and Miller, 2012, 2014), but we seek a global spectrally integrated solution for computational reasons. In this case, we iterate model runs with various values of $\varphi_{CDOC}$, using global distributions of data from MODIS-Aqua (Maritorena et al., 2010) as a target. After several dozen model runs, we derive $\varphi_{CDOC}$ = 1.0E-6 (μM/μmol photons absorbed $m^{-3}$) for results in reasonable agreement with MODIS-Aqua data, which we use in this simulation.

This approach ignores photo-bleaching of CDOC, which is sometimes assumed to be an intermediate condition on the path to photolysis (photo-oxidation) (Del Vecchio et al., 2009). Photo-bleaching is a milder form of degradation, where the slope of the CDOC absorption curve, $S_{CDOC}$ (see Equation 18) declines (i.e., spectral-dependence becomes weaker) with exposure to irradiance. However, keeping track of various states of photo-bleaching is difficult for a prognostic tracer and requires multiple tracers with different absorption curve slopes to be realistic. Dutkiewicz et al. (2015) approach the problem by defining a CDOM-like tracer that is photo-bleached as a function of PAR. Like here, Xiu and Chai (2014) ignored variability of $S_{CDOC}$ (and thus photo-bleaching). Bissett et al. (1999) also photolyzed CDOC, bypassing photo-bleaching. However, photolysis degradation products were reverted to the DOC pool rather than the DIC pool. The spectral slope $S_{CDOC}$ may also change by water type (Stedmon et al., 2011) but is also not considered here.

River inputs of nutrients and some carbon components are included in the model, but amounts are not differentiated individually by river source. Nitrate and silicate concentrations at river mouths are assumed to be 10 μM, while dissolved iron is 1 nM. DOC is specified at 100 μM, while DIC and alkalinity are assumed to be the same as the nearby ocean discharge locations. CDOC is assumed to be 750 μM at the river mouths. Here we make an exception for northern high latitudes (>70°N) where concentrations are set to 300 μM because the higher concentrations led to complete irradiance extinction, which is not supported by data.

## OCEAN-ATMOSPHERE SPECTRAL IRRADIANCE MODEL

NOBM is coupled to the Ocean-Atmosphere Spectral Irradiance Model (OASIM; Gregg and Carder, 1990; Gregg, 2002; Gregg and Casey, 2009) to simulate the propagation of downward spectral irradiance in the atmosphere and oceans and the upwelling irradiance/radiance in the oceans. The irradiance pathways for OASIM are shown in **Figure 1**. The atmosphere and ocean portions of the irradiance are implemented at variable spectral resolution over the range 200 nm–4 mm, depending upon the major atmospheric and oceanic absorbing sources. There are 33 spectral bands, which account for >99% of the total solar extraterrestrial irradiance. For the PAR spectral region (defined here as 350–700 nm following historical precedent) the model utilizes 25 nm spectral resolution (**Figure 2**), with band centers located at the bands shown. The 350 nm band represents the beginning of the first band and 700 nm the end of the last band, making them approximately half the width of the other bands (Gregg, 2002).

The atmospheric component of OASIM tracks irradiance through cloudy and clear skies (see **Figure 1**), accounting for spectral absorption and scattering of atmospheric gases, clouds, and aerosols. Biases and uncertainties in the atmospheric component of OASIM have been characterized for clear sky high spectral resolution (1 nm; Gregg and Carder, 1990) and under mixed cloudy and clear skies for 25 nm spectral resolution (Gregg and Casey, 2009). We elaborate here on the ocean optical calculations.

Ocean radiative transfer uses a "three-stream" method based on the Aas (1987) two stream approximation, modified for an explicit direct downwelling component by Ackleson et al. (1994)

$$\frac{dE_d(\lambda)}{dz} = -C_d(\lambda)E_d(\lambda) \quad (5)$$

$$\frac{dE_s(\lambda)}{dz} = -C_s(\lambda)E_s(\lambda) + B_u(\lambda)E_u(\lambda) + F_d(\lambda)E_d(\lambda) \quad (6)$$

$$\frac{dE_u(\lambda)}{dz} = -C_u(\lambda)E_u(\lambda) - B_s(\lambda)E_s(\lambda) - B_d(\lambda)E_d(\lambda) \quad (7)$$

where $E_d(\lambda)$ is the spectral downwelling direct irradiance at the bottom of a model layer, $E_s(\lambda)$ is the downwelling diffuse irradiance, and $E_u(\lambda)$ is the upwelling diffuse irradiance. The attenuation terms $C_x$ (where x is an indicator for the irradiance pathway d for direct downwelling, s for diffuse downwelling, and u for diffuse upwelling), backscattering terms $B_x$, and forward scattering $F_x$ differ for each of the irradiance pathways because of different shape factors (Aas, 1987; Ackleson et al., 1994) and mean cosines

$$C_d(\lambda) = [a(\lambda) + b(\lambda)]/\underline{\mu}_d \quad (8)$$

$$C_s(\lambda) = [a(\lambda) + r_s b_b(\lambda)]/\underline{\mu}_s \quad (9)$$

$$C_u(\lambda) = [a(\lambda) + r_u b_b(\lambda)]/\underline{\mu}_u \quad (10)$$

$$B_d(\lambda) = b_b(\lambda)/\underline{\mu}_d \quad (11)$$

$$B_s(\lambda) = r_s b_b(\lambda)/\underline{\mu}_s \quad (12)$$

$$B_u(\lambda) = r_u b_b(\lambda)/\underline{\mu}_u \quad (13)$$

$$F_d(\lambda) = (1 - b'_b)b(\lambda)/\underline{\mu}_d \quad (14)$$

where a is the absorption coefficient, b is the total scattering coefficient, $b_b$ is the backscattering coefficient, $b'_b$ is the ratio of backscattering to total scattering, and $\underline{\mu}$ is the mean cosine (constant for diffuse irradiance, but varies with solar zenith angle for direct irradiance). The shape factors are indicated by the $r_x$ terms, and are specified as in Ackleson et al. (1994). Equation 5 can be solved a *priori*, which can then be used as a boundary condition, greatly simplifying the solution of the coupled Equations 6, 7.

OASIM is used in 5 different Ocean General Circulation Models (OGCM): NASA Global Modeling and Assimilation Office (GMAO) Poseidon (Gregg, 2000; Gregg and Casey, 2007; Rousseaux and Gregg, 2015), GMAO MOM4 (present effort), NASA Goddard Institute for Space Studies (GISS) HYCOM (Romanou et al., 2013, 2014), NASA GISS Russell (Romanou et al., 2014), and Massachusetts Institute of Technology (MIT) OGCM (Dutkiewicz et al., 2015). It is used in the coupled ocean-atmosphere models of NASA/GMAO-GEOS-5 and NASA/GISS ModelE-H and -R.

### Optical Properties of Ocean Constituents

The coupled NOBM-OASIM model includes optically active constituents, including water, phytoplankton, detritus, PIC, and CDOC each with unique spectral characteristics (**Figure 3**). All are prognostic state variables, with individual sources and sinks. The optical properties of each constituent are taken from various efforts in the peer reviewed literature.

#### Water

The spectral absorption and scattering properties of water have been re-evaluated several times in the past 3 decades. Originally

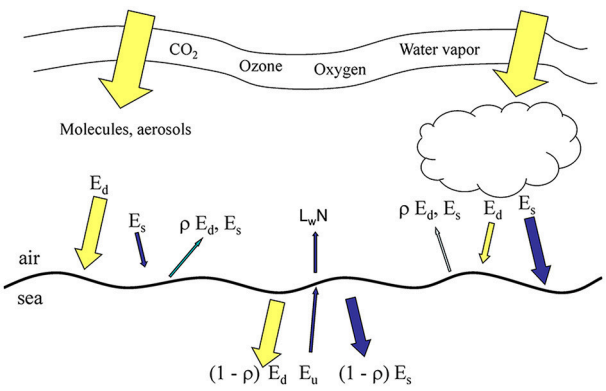


**FIGURE 1 | Irradiance pathways (directional irradiance) in OASIM.** $E_d$ is direct downwelling irradiance, $E_S$ is diffuse downwelling, $\rho$ is surface reflectance, $E_u$ is diffuse upwelling irradiance, and LwN is normalized water-leaving radiance. All irradiances and radiances are spectrally resolved at 25 nm for $E_d$, $E_S$, and $E_u$ for the range 350–700 nm, and at variable resolution for the remainder of the 200 nm–4 um. Size of arrows approximates relative contributions.

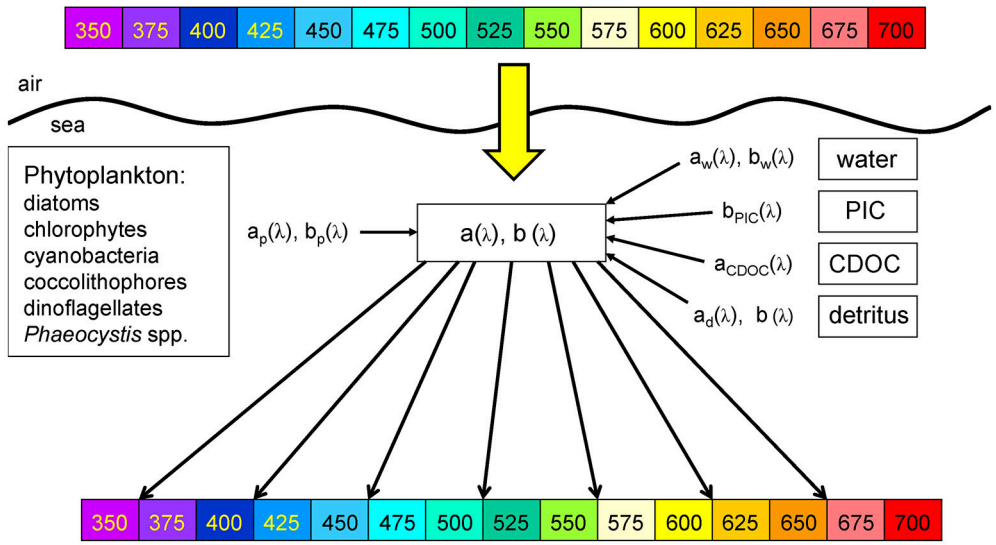


**FIGURE 2 | OASIM spectral downwelling radiance and dependencies in the ocean.** Shown are the visible bands. Inherent optical properties (spectral absorption coefficient a[λ], and spectral scattering coefficient b[λ]) are derived from spectral characteristics of water, phytoplankton groups, detritus, PIC, and CDOC. OASIM tracks spectral irradiance from the sun through the atmosphere into and through the oceans.

reported by Smith and Baker (1981) for the 200–800 nm spectral domain, the data was revised by Pope and Fry (1997) for the range 380–720 nm. Morel et al. (2007) derived new data for absorption and scattering for the spectral range 300–500 nm using information in the clearest ocean waters of the South Pacific. Finally, Lee et al. (2015) reported new absorption coefficients in the range 350–550 nm.

Water absorption data used here are from Smith and Baker (1981) for 200–300 nm and 730–800 nm, Morel et al. (2007) for 300–350 nm, Lee et al. (2015) for 350–550 nm, Pope and Fry (1997) for 550–720 nm, Circio and Petty (1951) for 800 nm–2.5 μm, and Maul (1985) for 2.5–4 μm. Water scattering are from Smith and Baker (1981) for the range 200–350 nm and 500–800 nm, and Morel et al. (2007) for the spectral range 350–500 nm. We assume no scattering by water for wavelengths longer than 850 nm. The backscattering-to-total scattering ratio $\tilde{b}_{bw}$ for water is 0.5.

## Phytoplankton

Phytoplankton optical properties are obtained from various sources. Chlorophyll-specific absorption coefficients $a_p^*(\lambda)$ are derived by taking reported spectra and normalizing to the absorption at 440 nm $[a_p^*(440)]$. Normalized specific absorption spectra $[a_p^*(\lambda)]N$ are computed for each of the five phytoplankton groups: diatom and chlorophyte $[a_p^*(\lambda)]N$ are taken from Sathyendranath et al. (1987), cyanobacteria from Bricaud et al. (1988), coccolithophores from Morel and Bricaud (1981), and dinoflagellates from Ahn et al. (1992). Then the specific spectral $a_p^*(\lambda)$ values are derived using mean values at 440 nm. Diatom $a_p^*(440)$ represents the mean of 5 observations containing 4 different spp., chlorophytes 6 observations from 4 spp., cyanobacteria 5 observations from 3 spp., coccolithophores 3 observations of 1 sp., and dinoflagellates 1 sp., all from the references listed above. *Phaeocystis* spp. specific spectral absorption coefficients are taken from Stuart et al. (2000) measurements for the Arctic species *Phaeocystis* pouchetti.

Phytoplankton specific scattering coefficients $b_p^*(\lambda)$ are obtained from measurements at 590 nm and extended to the entire spectrum from specific attenuation coefficients (Bricaud et al., 1988). Diatom and chlorophyte specific scattering coefficients at 590 nm, $b_p^*(590)$ and $b_p^*(590)$, are the mean of 5 observations and 6 observations, respectively, from Morel (1987), Bricaud and Morel (1986) and Bricaud et al. (1988). Cyanobacteria $b_p^*(590)$ is the mean of 8 observations from Morel (1987), Bricaud and Morel (1986), Bricaud et al. (1988) and Ahn et al. (1992). Coccolithophore $b_p^*(590)$ is derived from the mean of 3 observations from Bricaud and Morel (1986), Bricaud et al. (1988), and Ahn et al. (1992). Dinoflagellate $b_p^*(590)$ is derived from a single observation by Ahn et al. (1992). We have been unable to locate spectral scattering properties for *Phaeocystis* spp., so we assume the specific scattering coefficients are the same as diatoms.

We assume no spectral dependence in the backscattering-to-total scattering ratio $\tilde{b}_{bp}$. Ahn et al. (1992) suggested a spectral dependence for cyanobacteria but generally none for the other groups. Reported values for $\tilde{b}_{bp}$ are 0.002 for diatoms (Morel, 1988), 0.00071 for chlorophytes (Ahn et al., 1992), 0.0032 for cyanobacteria (Ahn et al., 1992), 0.00071 for coccolithophores, 0.0029 for dinoflagellates (both from Morel, 1988), and 0.002 for *Phaeocystis* spp. (assumed same as diatoms). Some of these values have been questioned based on non-sphericity of many natural phytoplankton populations (Vaillancourt et al., 2004; Whitmire et al., 2010). Based on these results, we increased $\tilde{b}_{bp}$

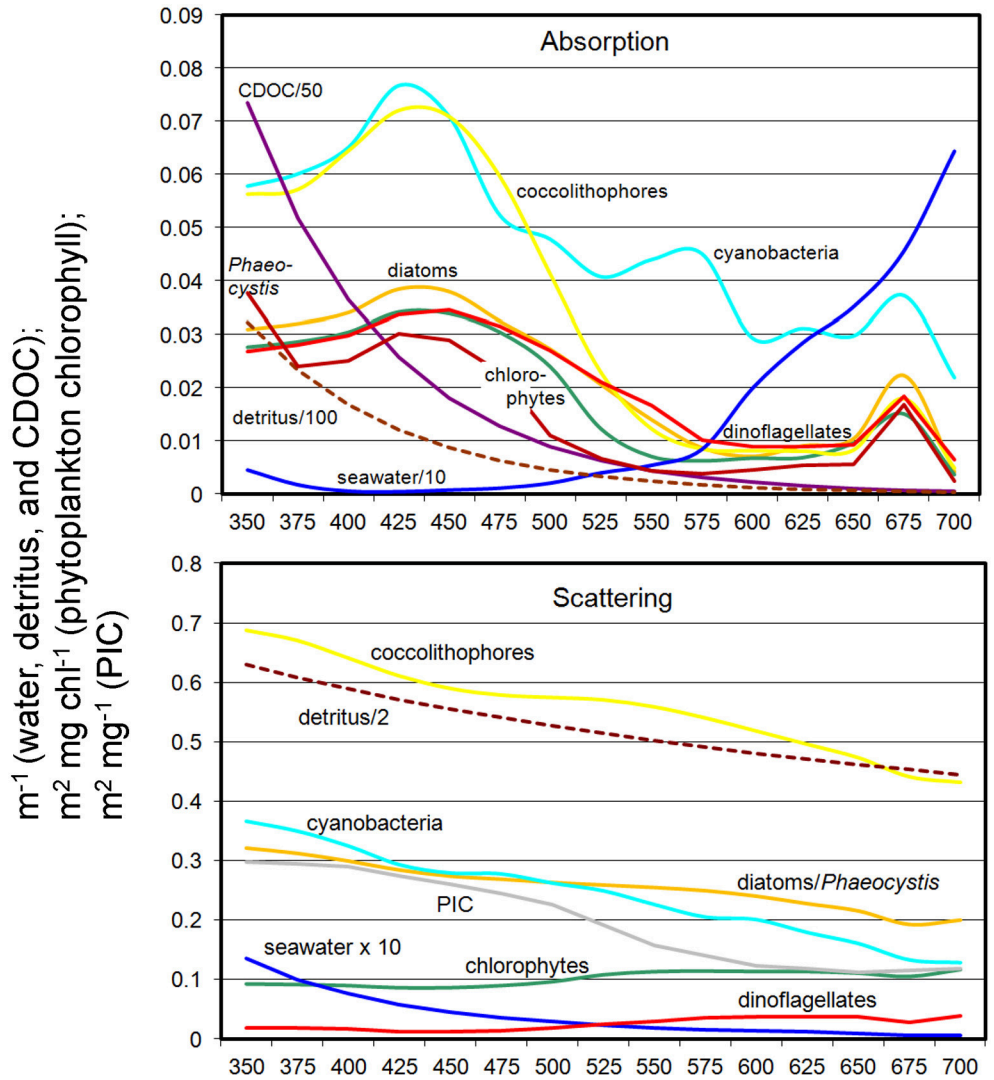


**FIGURE 3 | Spectral absorption and scattering coefficients of water, phytoplankton, detritus, PIC, and CDOC in OASIM.**

for chlorophytes and coccolithophores by a factor of 10, but kept them as reported for diatoms, cyanobacteria, dinoflagellates, and *Phaeocystis* spp.

## Detritus

Detritus both absorbs and scatters light (**Figures 2**, **3**). Absorption is typically considered an exponential function of wavelength (Roesler et al., 1989; Gallegos et al., 2011)

$$a_d(\lambda) = Da^*_d \exp[-S_d(\lambda - 440)] \quad (15)$$

where D is the concentration of detritus μg C $l^{-1}$, $a_d(\lambda)$ is the absorption coefficient of detritus ($m^{-1}$), $S_d = 0.013$ $nm^{-1}$ (Gallegos et al., 2011) and $a*_d$ is the mass-specific absorption coefficient of detritus, which is set to 8.0E-5 $m^2$ $mg^{-1}$ for small detritus as typically found in oceanic waters (Gallegos et al., 2011). Only organic carbon detritus in the model is used for detrital optics.

Detritus scattering is also taken from Gallegos et al. (2011)

$$b_d(\lambda) = Db^*_d(550/\lambda)^{0.5} \quad (16)$$

where $b_d$ is the total scattering coefficient, $b^*_d$ is the mass-specific scattering coefficient. The scattering coefficient is set as 0.00115 $m^2$ $mg^{-1}$ and the backscattering-to-total scattering ratio $\tilde{b}_{bd}$ is 0.005, as in Gallegos et al. (2011).

## PIC

PIC optical properties have been evaluated by Gordon et al. (2009). We adopt this formulation for our simulation. PIC scatters irradiance but does not absorb

$$b_{PIC}(\lambda) = \mathrm{PIC}\, b^*_{PIC}(\lambda) \quad (17)$$

where PIC is the concentration of PIC (mgC $m^{-3}$) and $b^*_{PIC}(\lambda)$ is PIC-specific spectral scattering coefficient from Gordon et al.

(2009) in units of $m^2$ $mgC^{-1}$. The backscattering-to-total scattering ratio $\tilde{b}_{bpic}$ is from Balch et al. (1996), using their lower bound of 0.01.

### CDOC

As a dissolved component, CDOC only absorbs and does not scatter. Its spectral absorption is similar to detritus but with a different slope

$$a_{CDOC}(\lambda) = a^*_{cdoc} \exp[-S_{CDOC}(\lambda - 443)] \quad (18)$$

where $a^*_{cdoc}$ is the mass-specific absorption coefficient of CDOC, $S_{CDOC} = 0.014\ nm^{-1}$ (Bricaud et al., 1981, 2010). $S_{CDOC}$ is in the low end range of observations in surface waters of the Equatorial Atlantic (Andrew et al., 2013) but only slightly lower than those observed in the Mediterranean Sea (Organelli et al., 2014). There are few reports of the mass-specific absorption coefficient of CDOC $a^*_{cdoc}$. We have found three observations in the literature (Carder et al., 1989; Yacobi et al., 2003; Tzortziou et al., 2007). The more recent two are in agreement at $2.98 \times 10^{-4}$ $m^2$ $mg^{-1}$ in 4 rivers in Georgia, USA (Yacobi et al., 2003) and $2.78 \times 10^{-4}$ $m^2$ $mg^{-1}$ as the mean of 4 stations in the Rhode River, Maryland, USA (Tzortziou et al., 2007). Carder et al. (1989) reported a mean over about nearly an order of magnitude lower in the Gulf of Mexico ($4.74 \times 10^{-5}$ $m^2$ $mg^{-1}$). We choose Yacobi et al. (2003) for our simulation.

## Model Setup

The model is integrated for 30 years from an initial state using climatological atmospheric forcing and atmospheric absorbing gases from Modern-Era Retrospective Analysis for Research and Applications (MERRA; Rienecker et al., 2011). The initial state for nitrate and silicate is taken from the National Centers for Environmental Information World Ocean Atlas (Conkright et al., 2002), dissolved iron is from Fung et al. (2000), and ammonium is arbitrarily set to 0.5 μM. All phytoplankton concentrations are initialized to 0.5 mg $m^{-3}$ and the new variables PIC and CDOC initialized to 0 Concentrations (μg $l^{-1}$ and μM, respectively). Alkalinity and dissolved inorganic carbon are initialized using Global Data Analysis Project (GLODAP; Key et al., 2004) and dissolved organic carbon is initialized as 0 μM. Cloud and aerosol optical properties for surface irradiance are obtained from MODIS-Aqua. Diurnal variability is represented at the model 30-min time step, but atmospheric optical components are monthly climatologies.

## Error Characterization of the Model

The biological and optical constituents of the NOBM-OASIM model are compared to *in situ* and/or satellite (MODIS) data where and when available, in order to quantify the bias and uncertainty. Satellite chlorophyll data are compared with the surface level of the model which is 10 m. Phytoplankton groups are compared to *in situ* data while total chlorophyll, PIC, and $a_{CDOC}$ are compared to satellite estimates. The statistics are aggregated over the 12 basins of the global oceans, mean differences (biases) computed, and then correlations computed over the basins. This provides an estimate of large scale correlations and is very stringent considering the low number of observations. The major ocean basins are divided into 3 main regions, high latitudes (poleward of 40° latitude): North Atlantic and Pacific and Southern Ocean, mid-latitudes (between 40° and 10° latitude): North Central Atlantic and Pacific, South Atlantic, Pacific and Indian, and North Indian, and tropical basins (between ±10° latitude): Equatorial Atlantic, Pacific, and Indian.

Phytoplankton groups are represented as relative abundances, and are compared to *in situ* data on relative abundances. The *in situ* data is a compilation described by Gregg and Casey (2007) and is available at http://gmao.gsfc.nasa.gov/research/oceanbiology/data.php. Some changes to the error characterization of Gregg and Casey (2007) include (1) removal of data obtained in the sub-polar tropical Pacific basins during El Niño-Southern Oscillation (ENSO) events and (2) removal of chlorophyte data poleward of 40° latitude. ENSO events change the phytoplankton relative abundances, sometimes drastically, as noted in *in situ* (Bidigare and Ondrusek, 1996; Karl et al., 2001), satellite (Uitz et al., 2010; Masotti et al., 2011; Bricaud et al., 2012), and satellite data assimilation studies (Rousseaux and Gregg, 2012). Regarding the removal of high latitude chlorophyte data, we note that little of the data in our data base have explicitly identified chlorophyte relative abundances. Instead, we assume that all reports of intermediate phytoplankton, e.g., nanoplankton, nano-eukaryotes, etc. are compatible with the role played by chlorophytes in the model. While this assumption still holds, it is likely that such a categorization includes *Phaeocystis* spp. in the high latitudes, which are common here. Since we now explicitly represent these polar species *Phaeocystis*, we do not need to use chlorophytes as a proxy for nanoplankton and can avoid the misrepresentations between data and model in the high latitudes that we previously accommodated.

We have been unable to find relative abundance data for *Phaeocystis* spp., so we use absolute abundances from the MARine Ecosytem DATa (MAREDAT) project (Vogt et al., 2012). The data are reported as μg C $l^{-1}$, which was converted to mg chl $m^{-3}$ as reported in the model using a carbon:chlorophyll ratio of 50 g $g^{-1}$. *Phaeocystis globosa* data are removed from the comparison because our characterization is strictly for polar species of *Phaeocystis*. We also remove data reported prior to 1975 due to suspect quality. Abundances are log-transformed prior to statistical analysis. We have not been able to obtain global data on dinoflagellate relative abundances and there is not yet a database from MAREDAT, so we are unable to quantify model error statistics on this phytoplankton group.

There is no available satellite data for CDOC that we are aware of, but a satellite product called $a_{CDM}$ (absorption coefficient of Chromophoric Dissolved and Particulate Organic Matter at 443 nm) is available (Garver and Siegel, 1997; Maritorena and Siegel, 2005; Maritorena et al., 2010). We use the products from MODIS-Aqua in this effort. This product represents the absorption of both CDOM and detritus (hence the usage of CDM to minimize confusion about its nature). Siegel et al. (2002) estimated the detrital contribution as (12%). This difference in

dissolved organic detrital representations contributes to the low model estimates relative to data reported here, as well as possibly inadequate phytoplankton production of CDOC and/or excessive photolysis. However, the regional correlation in **Table 1** is likely more robust.

Model total chlorophyll is also substantially lower than satellite data (**Table 1**). This is driven by the uneven seasonal sampling of satellites, resulting in little or no coverage in local winter, when chlorophyll concentrations are very low. By observing the oceans only in seasons of higher growth, satellite data overestimates global median chlorophyll.

Satellite primary production data is from the Vertically Generalized Production Model (Behrenfeld and Falkowski, 1997). Data shown in **Table 1** is a climatology from MODIS-Aqua from 2003–2013.

The atmospheric portion of OASIM has been quantitatively evaluated against *in situ* data (Gregg and Carder, 1990; Gregg and Casey, 2009), so no further analysis is done here. Spectrally-integrated surface irradiance from OASIM had root mean square (RMS) difference = 20.1 $Wm^{-2}$ (about 11%), bias = 1.6 W $m^{-2}$ (about 0.8%), regression slope = 1.01 and correlation coefficient = 0.89, when compared to 2322 *in situ* observations under mixed cloudy and clear skies (Gregg and Casey, 2009). Under clear skies the model has demonstrated a 6.6% RMS with *in situ* surface observations at 1 nm spectral resolution (Gregg and Carder, 1990).

**TABLE 1 | Bias and correlation of major model variables with data sources.**

| | Bias | Correlation (r) | Notes |
|---|---|---|---|
| Nitrate | 6.2% ($N = 12$) | 0.987 ($P < 0.05$) | *In situ* |
| Silicate | −35.4% ($N = 12$) | 0.885 ($P < 0.05$) | *In situ* |
| Dissolved Iron | 51.2% ($N = 12$) | 0.441 (NS) | *In situ* |
| Total chlorophyll | −13.4% ($N = 12$) | 0.717 ($P < 0.05$) | *In situ* |
| Total chlorophyll | −37.3% ($N = 12$) | 0.658 ($P < 0.05$) | Satellite (MODIS-Aqua) |
| Diatoms | 4.9% ($N = 11$) | 0.810 ($P < 0.05$) | *In situ*, relative abundance |
| Chlorophytes | 2.2% ($N = 6$) | 0.814 ($P < 0.05$) | *In situ*, relative abundance |
| Cyanobacteria | 15.0% ($N = 11$) | 0.951 ($P < 0.05$) | *In situ*, relative abundance |
| Coccolithophores | 6.5% ($N = 10$) | 0.722 ($P < 0.05$) | *In situ*, relative abundance |
| Dinoflagellates | −−− | −−− | NA |
| *Phaeocystis* | −5.6% ($N = 1899$) | 0.534 ($P < 0.05$) | *In situ*. Absolute abundance, not averaged over basins |
| Herbivores | −−− | −−− | NA |
| Detritus | −−− | −−− | NA |
| PIC | −1.2% ($N = 12$) | 0.566 (NS) | Satellite (MODIS-Aqua) |
| $a_{CDOC}$ | −65.1% ($N = 12$) | 0.919 ($P < 0.05$) | Satellite (MODIS-Aqua) |
| Primary Production | −6.0% ($N = 12$) | 0.604 ($P < 0.05$) | Satellite (MODIS-Aqua) |

*NS indicates non-significant correlation, $P < 0.05$ indicates statistical significance at 95% probability. Values are for basins, where data are averaged over each of the 12 basins prior to comparison, producing $N = 12$. Bias is model minus in situ/satellite data. NA indicates no data for comparison found.*

The ocean component of OASIM has been shown to improve the representation of the deep chlorophyll concentration maximum (Dutkiewicz et al., 2015). Dutkiewicz et al. (2015) also provided maps comparing computed upwelling radiances with some of the MODIS-Aqua bands. Here we present a quantitative comparison of global OASIM normalized upwelling spectral radiances compared to MODIS-Aqua accompanied by statistical characterization. In this evaluation we utilize a different global ocean model (Poseidon; Schopf and Loughe, 1995) with nearly identical NOBM configuration (i.e., not including dinoflagellates and *Phaeocystis* spp.), and assimilate total chlorophyll, PIC, and $a_{CDM}(443)$ (Maritorena et al., 2010) from MODIS-Aqua. This novel use of data assimilation ensures consistency in underlying optical constituents with observations. This enables us to isolate the OASIM calculations of spectral radiance. The simulation/assimilation/satellite data year for the comparison is 2007. The reason for the ocean circulation model switch is that data assimilation has not yet been developed for GEOS-5 MOM4-NOBM and it is essential for isolating the radiative transfer model evaluation. The normalized upwelling radiance calculation is described in Appendix 1. For this evaluation, we utilize 1 nm spectral resolution data for surface irradiance and ocean optical properties. The 1 nm bands chosen for comparison align with the band centers for MODIS-Aqua. This enables us to match to MODIS bands and reduce impacts of model/data band misalignment in the error characterization.

## Evaluation Scenarios for Spectral and Directional Irradiance

The model is run an additional 10 years of simulation after the initial spinup under different scenarios of irradiance treatment in the water column to evaluate the effects of spectral and directional irradiance. Ten years is sufficient to achieve stability for most of the scenarios (defined as <1% change in global nitrate, chlorophyll, and primary production per year), but the more different the scenario from the control, the longer it can take to achieve this level of stability. This extended run was required only for the test of direct irradiance, which required 20 years to stabilize.

All scenarios are evaluated against a control run, which is the spun-up model with full treatment of directional and spectral irradiance. Each scenario of directional and spectral irradiance is evaluated against this directionally and spectrally-resolved model. We focus here strictly on the changes in ocean biology, specifically nitrate, total chlorophyll, phytoplankton composition, and net primary production.

In all cases the surface irradiance enters the ocean as fully differentiated directionally and spectrally using the atmospheric component of OASIM, which accounts for absorption and scattering by atmospheric constituents (clouds, aerosols, gases) and penetration through the atmosphere-ocean boundary as a function of surface roughness (**Figure 1**). We evaluate the

importance of the irradiance nature in the oceans using the ocean component of OASIM (the three-stream model described above, Equations 5–14) by simulating irradiance transmittance involving one of the aspects of the irradiance at a time.

First, directional irradiance is evaluated. All of the surface irradiance, and its spectral quality is conserved. In this case, the light is transmitted through the oceans as purely direct irradiance. The surface diffuse irradiance is added into the direct path as

$$E_d(\lambda, 0^-) = E_d(\lambda, 0^-) + E_s(\lambda, 0^-) \quad (19)$$

and is then zeroed out

$$E_s(\lambda, 0^-) = 0 \quad (20)$$

The irradiance is tracked in the three-stream model as strictly direct irradiance (Equation 5). This enables us to understand the importance of the nature of the light and its effects if treated in the oceans strictly as direct irradiance, without changing the total irradiance entering.

The test of diffuse irradiance is similar, with the roles reversed, i.e., surface direct irradiance is added to the diffuse, and is then zeroed out

$$E_s(\lambda, 0^-) = E_d(\lambda, 0^-) + E_s(\lambda, 0^-) \quad (21)$$

$$E_d(\lambda, 0^-) = 0 \quad (22)$$

Now the radiative transfer is computed using Equations 6 and 7, where the terms containing $E_d$ are zero.

The scenarios thus treat the pathways of light in the oceans differently and are attenuated differently, despite containing the same total irradiance at the surface. The spectral nature of the irradiance is preserved in these scenarios so that we are strictly observing the effects of light direction.

The spectral irradiance scenarios preserve the directional nature of the surface irradiance, with direct and diffuse components explicitly computed in the water column by the OASIM three-stream model. This time, however, we compute only the attenuation (absorption and scattering) of a single spectral band. This is somewhat complex because it is difficult to decide which individual band to select a *priori*. Thus we test several wavelengths spanning the range of PAR individually. Specifically, we sum all of the irradiance in all the PAR bands into the 400 nm band, then use the attenuation characteristics of 400 nm, i.e., spectral absorption and scattering of water, phytoplankton, detritus, PIC, and CDOC at 400 nm

$$E_d(400) = \int_{350}^{700} Ed\,(\lambda)\ d\lambda \quad (23)$$

$$E_s(400) = \int_{350}^{700} Es\,(\lambda)\ d\lambda \quad (24)$$

Then we repeat the process at 450 nm, 500 nm, 550 nm, 600 nm, and finally 650 nm, again moving all the surface spectral irradiance into the band of interest and tracking attenuation in that band. We evaluate changes in ocean biology based on the individual band attenuation compared to the full spectral nature of natural irradiance. In this and the other spectral scenarios, directionality is treated as in the control, i.e., fully resolved from surface inputs including monthly climatological clouds and aerosols.

Finally we evaluate the combined effect of directional and spectral irradiance by choosing the band that most agrees with the control and assuming only diffuse irradiance. The total irradiance entering the ocean is conserved as in all the preceding scenarios.

# RESULTS

## Model Error Characterization

Comparisons of major constituents in NOBM with various *in situ* and satellite data sets are summarized in **Table 1**. *In situ* and satellite data sets were available for most of the model tracers, but some, like detritus and dinoflagellates, were not. Bias was represented by the global difference (model minus data, usually expressed as percent) and uncertainty was represented by correlation with significance testing. The model variables were taken from year 30 of the 30-year spinup.

OASIM normalized upwelling radiances were compared with the radiances available from MODIS-Aqua. This was a different circulation model coupled to NOBM in a configuration that has the capability to assimilate satellite data, but was otherwise nearly identical to NOBM used here with MOM4 (i.e., not including dinoflagellates and *Phaeocystis* spp.). The assimilation ensures that we have evaluated the radiative transfer model, rather than convolving differences in underlying optical constituents. We are characterizing the error of the radiative model here, and it is essential to utilize optical constituent distributions that more closely resemble nature than a free-run model does. We achieve this through a novel use of data assimilation. The global mean bias for the band composite was −0.6 mW $cm^{-2}$ $\mu m^{-1}$ $sr^{-1}$ (−8.0%) and the correlation was 0.68 ($P < 0.05$). Bias and correlation for normalized upwelling radiances compared to the 6 MODIS visible bands are provided in **Table 2**.

**TABLE 2 | Statistics on the comparison of global normalized water-leaving radiances $L_wN(\lambda)$ from the NOBM-OASIM model and radiances from MODIS-Aqua for 2007.**

| Wavelength | Median Difference | SIQR | Correlation (r) | N |
|---|---|---|---|---|
| 412 nm | −0.163 (−11.9%) | 0.160 | 0.948 ($P < 0.05$) | 418169 |
| 443 nm | −0.052 (−3.8%) | 0.106 | 0.934 ($P < 0.05$) | 418287 |
| 488 nm | −0.065 (−0.6%) | 0.076 | 0.841 ($P < 0.05$) | 418317 |
| 531 nm | −0.040 (−9.7%) | 0.054 | 0.449 ($P < 0.05$) | 418317 |
| 547 nm | −0.031 (−10.1%) | 0.048 | 0.460 ($P < 0.05$) | 418317 |
| 667 nm | −0.008 (−44.4%) | 0.005 | 0.445 ($P < 0.05$) | 418272 |
| Global Mean all bands | −0.060 (−8.0%) | 0.075 | 0.680 ($P < 0.05$) | 418280 |

*SIQR is the semi-interquartile range.*

## Directional Irradiance

When all surface irradiance was assumed to be direct, and light transmittance followed Equation 5, global nitrate concentrations increased >200% (**Table 3**). This was accompanied by a large decline in global net primary production of more than −80% compared to the directionally and spectrally resolved simulation (**Table 3**). Global annual median chlorophyll, however, was only modestly affected by the change in light stream, falling only by −8.3% (**Table 3**).

When all surface irradiance was assumed to be diffuse, and irradiance was computed using Equations 6, 7, global surface nitrate concentrations decreased by nearly 19% and global median chlorophyll concentrations decreased similarly, by 21% (**Table 3**). Regional distributions showed that the changes were largest in the sub-tropical and tropical regions, defined here as equator-ward of 40° latitude (**Figure 4**). Global net primary production increased slightly in a diffuse-only representation of irradiance (**Table 3**). Phytoplankton relative abundances changed considerably more than PP and nitrate for some groups (**Figure 5**). Chlorophyte relative abundance declined while cyanobacteria, coccolithophores, and dinoflagellates increased. Diatoms and *Phaeocystis* spp. remained nearly constant regardless of whether the irradiance was treated as directional or as diffuse only.

**TABLE 3 | Global annual mean nitrate concentrations, global annual median chlorophyll concentrations and global net primary production as a function of directional irradiance.**

| | Directional + Spectral | Direct Only | Diffuse Only |
|---|---|---|---|
| Nitrate (μM) | 5.59 | 20.02 (258.1%) | 4.54 (−18.8%) |
| Total Chlorophyll (mg $m^{-3}$) | 0.154 | 0.141 (−8.3%) | 0.121 (−21.2%) |
| Primary Production (Pg C $y^{-1}$) | 49.2 | 7.8 (−83.7%) | 50.1 (3.9%) |

*Shown are the fully directional (and spectral) model, transmittance in the oceans using only direct irradiance, and transmittance using only diffuse irradiance.*

## Spectral Irradiance

Treatment of irradiance attenuation as non-spectral produced differences with the full spectral model that depended upon the choice of attenuation band (**Figure 6**). Using 400 nm, mean global nitrate concentrations were much lower than the full spectral calculation, a pattern that persisted for the shorter wavelengths through 500 nm. For wavelengths >500 nm, nitrate concentrations were much higher, ranging from 104% at 550 nm to >200% for 600 nm and 650 nm. Global median chlorophyll concentrations tracked nitrate through 550 nm, with lower concentrations than the full spectral model for 400–500 nm, then higher at 550 nm (**Figure 6**). At longer attenuation wavelengths than 550 nm, global median chlorophyll and global mean nitrate diverged, with nitrate higher than control and chlorophyll lower than the control. Attenuation at 500 nm produced the closest

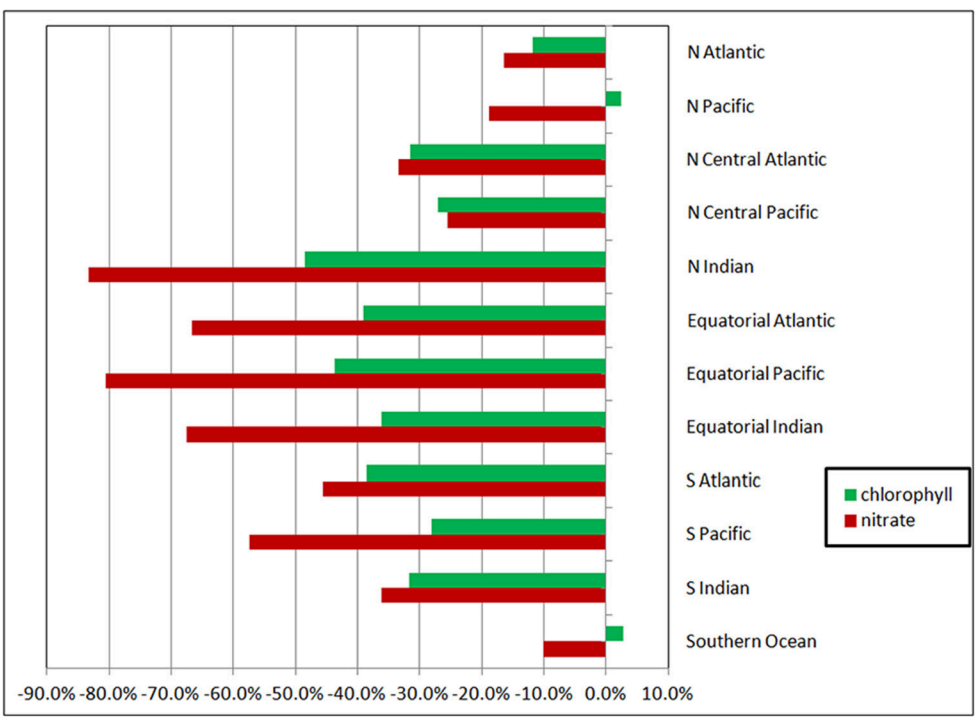


**FIGURE 4 | Changes in regional nitrate and chlorophyll as a function of radiative transfer in the oceans tracking only the diffuse component.** Changes are relative to the directionally-spectrally resolved model. The high latitudes are poleward of 40° latitude (i.e., the North Atlantic, North Pacific, and Southern Ocean). The tropical and sub-tropical basins are in the middle, with the tropical/sub-tropical delineation at 10°.

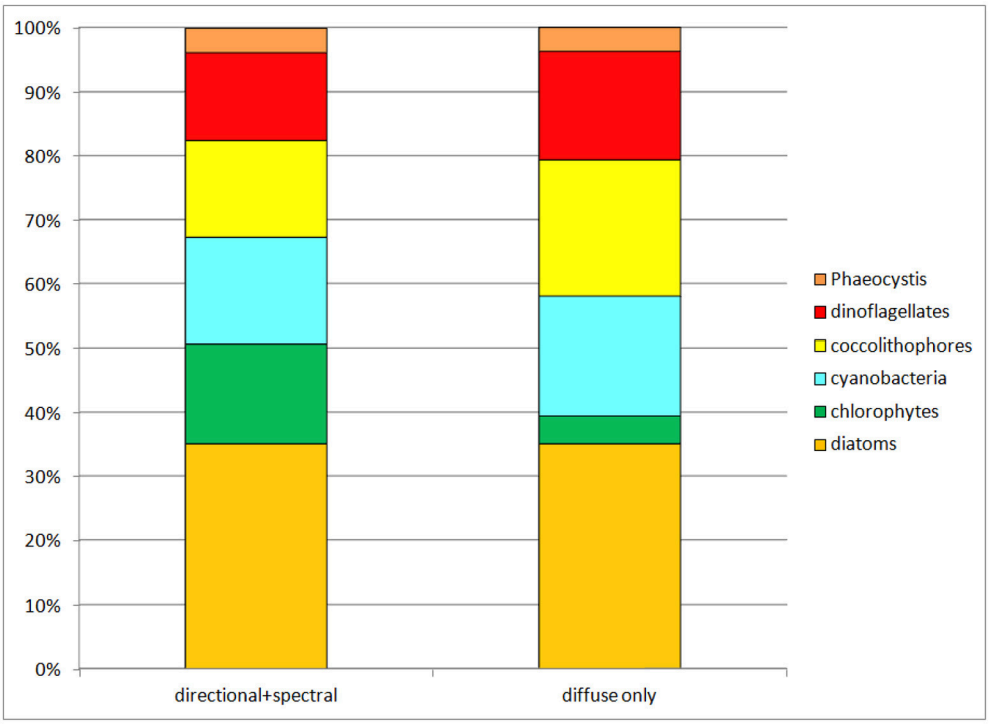


**FIGURE 5 | Phytoplankton group relative abundances in the directional and spectrally-resolved model and the diffuse-only simulation.** The direct-only simulation is not shown because it attenuates so much irradiance the results are clearly unrealistic.

approximation to full spectral treatment for both global nitrate and chlorophyll.

Phytoplankton relative abundances were also sensitive to non-spectral irradiance transmittance in the oceans (**Figure 7**). As with nitrate, chlorophyll and primary production, transmittance at 500 nm was closest to the spectral calculation. But even here there were departures from the spectrally-resolved model: chlorophytes were almost half their relative abundance in the full spectral solution, while coccolithophores and cyanobacteria increased their relative abundances by about 3% each. Diatoms were relatively steady in their proportion of the phytoplankton community regardless of the choice of attenuation. Other than diatoms there were major changes in phytoplankton for attenuation choices greater than 500 nm.

Global net primary production as a function of spectral transmittance exhibited inverse patterns to global annual median chlorophyll (**Figure 8**). Transmittance at 500 nm compared the most favorably to the spectral primary production. Transmittances at wavelengths shorter than 500 nm showed increased primary production, while those longer showed smaller production, with declines well over 50% for 600 nm and above.

## Combined Effect of Directional and Spectral Irradiance

The combined effect of utilizing only diffuse and non-spectral irradiance for estimation of the underwater light field was larger than the individual representations of diffuse only and transmittance at 500 nm (the best case for non-spectral attenuation). Global surface nitrate concentrations were lower (−33.6% compared to the directionally and spectrally-resolved model) as was global surface median chlorophyll (−16.4%) (data not shown). Comparisons with *in situ* and satellite data (**Figures 9**, **10**) reinforced these results as well. In contrast, total primary production was quite similar to the directionally and spectrally-resolved simulations. Global net primary production was within 2.4 Pg C $y^{-1}$ or about 5%, with the non-resolved model higher (data not shown).

# DISCUSSION

Here we have attempted to clarify the effects of neglecting directional and spectral irradiance in simulations of global ocean biological variables, specifically nitrate, total chlorophyll, phytoplankton relative abundances, and net primary production. Beginning with an ocean radiative transfer model that resolves both directional and spectral irradiances, and a companion atmospheric radiative transfer model that represents directional and spectral irradiance deriving from the sun and local atmospheric conditions, including absorbing gases, clouds, and aerosols, we sequentially remove the directional and spectral components, all the while ensuring that the exact same total irradiance begins at the surface, and then report the changes in the above described biological constituents in the oceans.

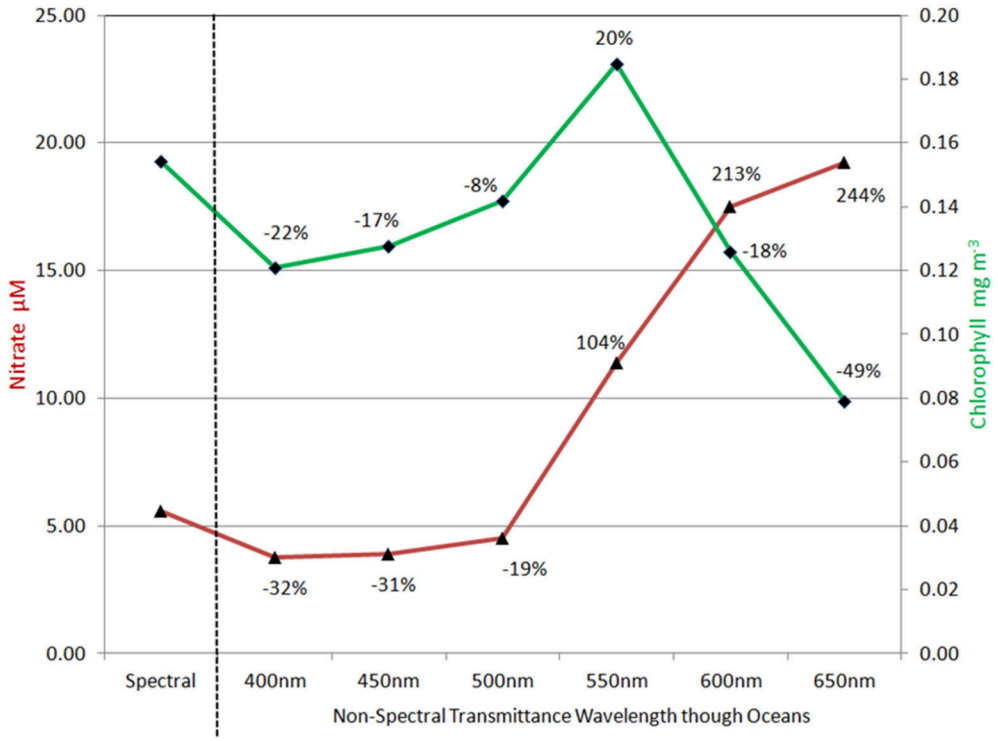


**FIGURE 6 | Global nitrate and chlorophyll concentrations using non-spectral transmittance of irradiance.** The non-spectral attenuation is shown for six different bands, each beginning with the same total surface irradiance as the spectrally resolved model. The percent change is relative to the spectrally-resolved model. Nitrate is shown in red and follows the left vertical axis.

The results show consequential, but not drastic changes in global ocean biology from not resolving directional irradiance and treating all irradiance as diffuse: approximately 20% reductions in global annual mean nitrate and global annual median chlorophyll. Global net primary production changes are essentially negligible at 4%. However, there are important changes in the phytoplankton relative abundances, with cyanobacteria and coccolithophores increasing their relative abundances from 31 to 40% of the total combined while chlorophytes fall from 16% of the community (second highest behind diatoms) to 4% (second lowest next to *Phaeocystis* spp.) (**Figure 5**).

The changes in nitrate and chlorophyll due to simulation of exclusively diffuse irradiance are much larger in the tropics (between −10° and 10° latitude) and sub-tropics than in the high latitudes (poleward of 40° latitude). For example, the changes in nitrate and total chlorophyll in the Equatorial Pacific are −80 and −43%, respectively, compared to the Southern Ocean, where changes of −10 and −3%, respectively, are found (**Figure 4**). This is because in the high latitudes surface irradiances is already dominated by diffuse irradiance due to the presence of persistent clouds. Treating all the irradiance as diffuse here has less effect than in the lower latitudes, since there is already less direct irradiance to begin with.

We note that nitrate and total chlorophyll decline (approximately −20% each) while primary production increases by 4% in the diffuse-only scenario (**Table 3**). Diffuse-only transmittance produces more total irradiance in the water column, which increases primary production and diminishes surface nitrate through uptake. These relationships have been noted by Kim et al. (2015) in a study on the effects on CDOM on biology in the global oceans. Higher total irradiance results in higher community metabolic activity in the surface, especially grazing, which has the net effect of reducing both nitrate (through increased uptake) and surface chlorophyll (through grazing). Higher irradiance also produces higher carbon:chlorophyll ratio, further depressing surface chlorophyll.

In this diffuse-only scenario the increase in primary production is partially due to the fact that in the merger of direct and diffuse solar irradiance (Equations 25, 26) the spectral quality of the direct irradiance is retained. This means the full solar spectrum, most relevantly the shorter (blue) wavelengths from the formerly direct irradiance are added to the diffuse stream in the interest of conserving total irradiance at the surface. These blue spectra (both from the diffuse and the additional direct converted to diffuse) photolyze CDOC, reducing its concentration, and consequently stimulate primary production by enhancing the availability of blue irradiance for photosynthesis. This also suggests that diffuse pathways in the oceans provide more ambient light than the multiple angles of the direct irradiance each day. Although this may seem counter-intuitive because clouds are the most important cause of diffuse irradiance, it is important to remember that clouds also cause a reduction in total irradiance, whereas here the full direct+diffuse irradiance is conserved in the simulation, with the

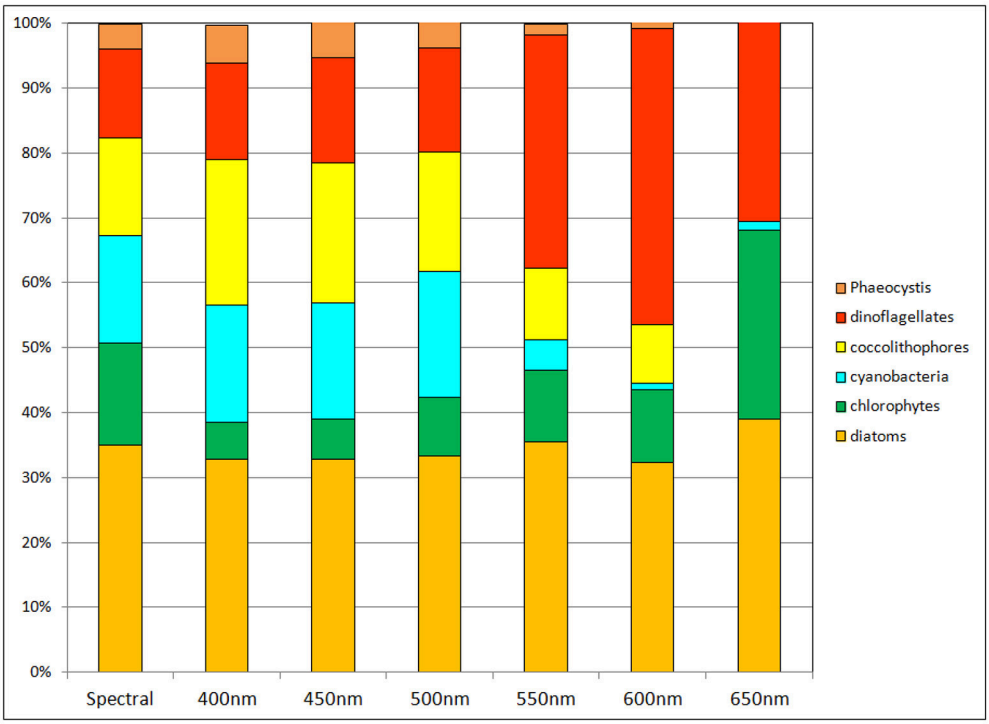


**FIGURE 7 | Phytoplankton group relative abundances using non-spectral transmittance of irradiance.** The non-spectral attenuation is shown for 6 different bands, each beginning with the same total surface irradiance as the spectrally-resolved model.

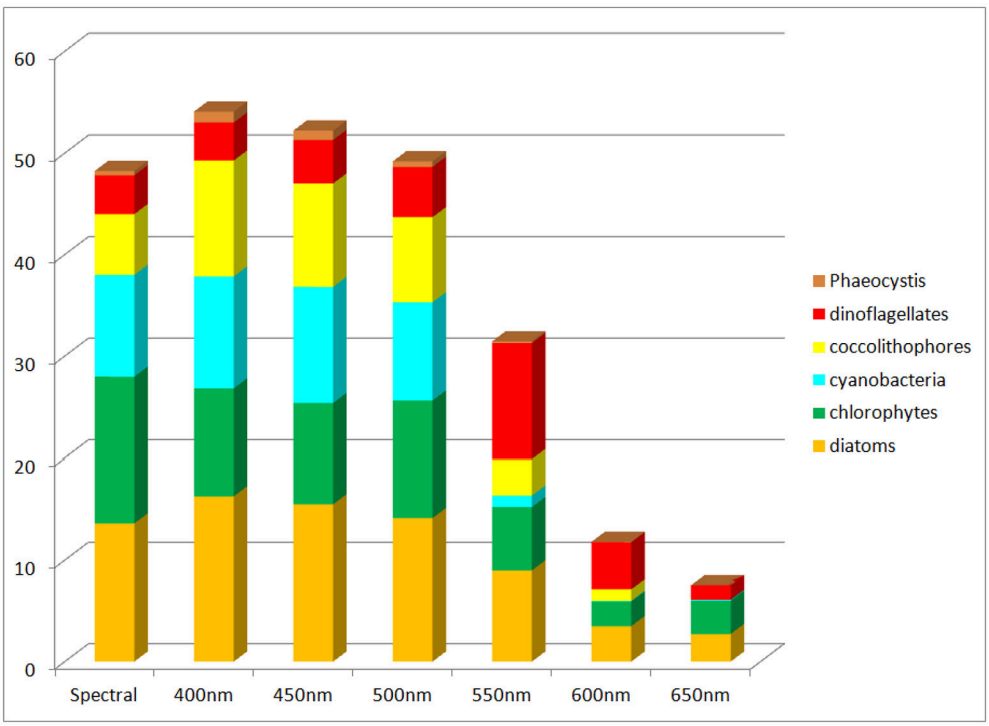


**FIGURE 8 | Global net primary production using non-spectral transmittance of irradiance compared to the spectrally-resolved model.** Included is the contribution of each phytoplankton component to the total.

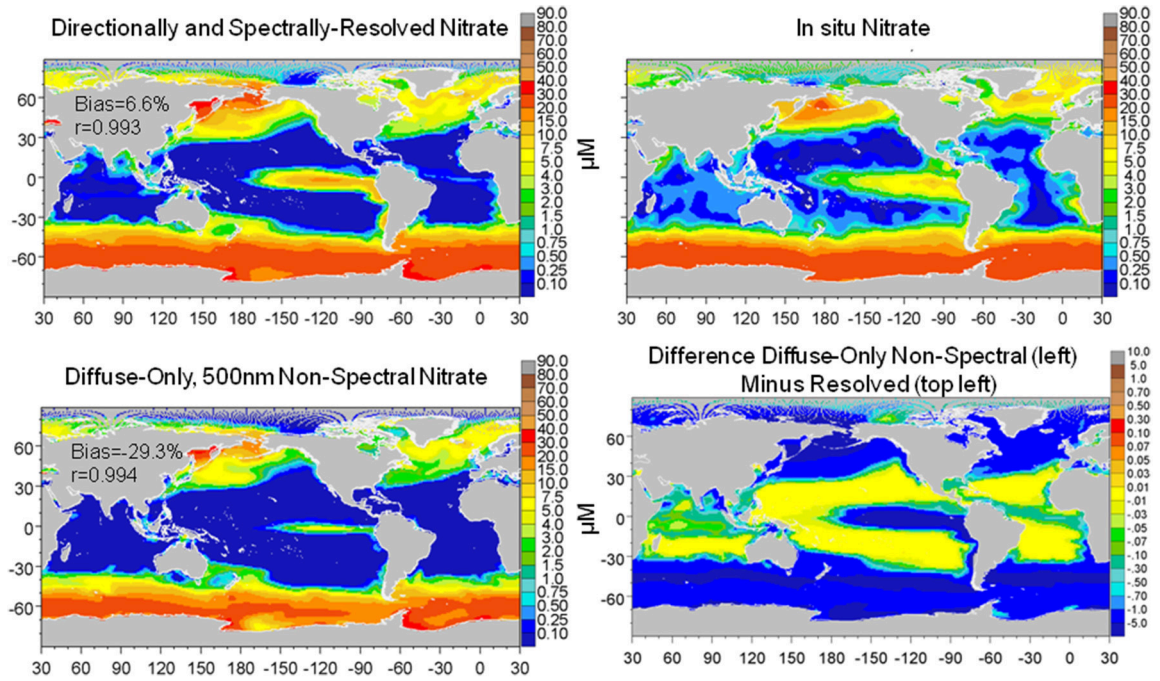


**FIGURE 9 | Global distribution of nitrate from the directionally and spectrally-resolved model, *in situ* data and the diffuse-only, 500 nm non-spectral simulation and the difference.** Statistics on global distributions compared to *in situ* data are shown in the plots. The correlation for both models is statistically significant at $P < 0.05$.

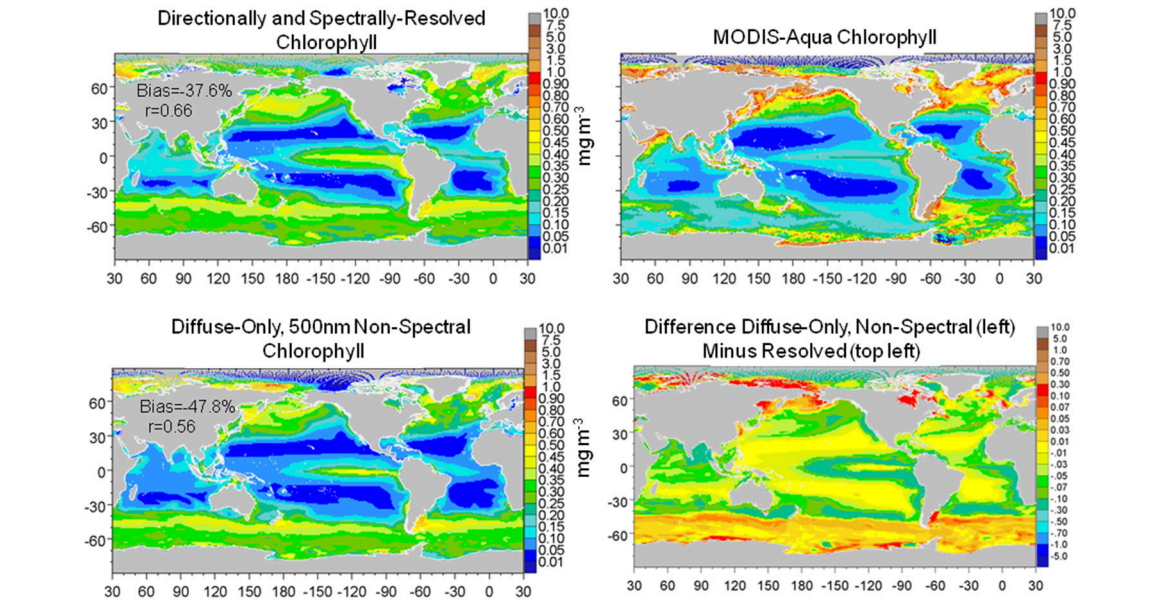


**FIGURE 10 | Global distribution of chlorophyll from the directionally and spectrally-resolved model, climatological satellite data, the diffuse-only, 500 nm non-spectral simulation and the ditierence.** Statistics on global distributions compared to satellite data are shown in the plots. The directionally-spectrally resolved correlation is statistically significant at $P < 0.05$; the ditiuse-only + non-spectral model is not.

clear-sky direct added to the cloudy and clear diffuse. This is clearly unreasonable in nature but here we are testing modeling approaches for representing the ocean light field. A model that does not consider irradiance directionality but is given the correct total surface irradiance would be susceptible to the scenario described here.

Ocean biological concentrations and primary production are sensitive to the nature of spectral irradiance. The magnitude of the behavior of ocean biology to simulations using non-spectral radiative transfer is dependent upon which wavelength is selected. The shorter (bluer) wavelengths are associated with higher primary production and consequently lower nitrate and chlorophyll (**Figure 6**). The changes to nitrate and chlorophyll track one another for non-spectral transmittance in these bands. The best comparison with the fully spectrally-resolved model occurs at 500 nm, but even here there are substantial changes in phytoplankton composition, with reductions in the relative abundance of chlorophytes compensated by increases in cyanobacteria and coccolithophores (**Figure 7**). This suggests, however, that there is potentially an optimal choice for non-spectral transmittance, at least for global representations, and it likely lies near 500 nm. This in turn suggests support for use of diffuse attenuation coefficient for PAR, which is derived from the attenuation coefficient at 490 nm ($K_d490$) (Morel et al., 2007) or using $K_d490$ itself (e.g., Lee et al., 2005).

Non-spectral radiative transfer using bands higher than 550 nm show much larger impacts on primary production, nitrate, and chlorophyll. Here the association between nitrate and chlorophyll diverges, with nitrate increasing with increasing wavelength and chlorophyll decreasing.

Relative abundances of phytoplankton are highly sensitive to non-spectral choices of transmittance wavelength (**Figure 7**). To understand why, we refer to **Figure 3**, which shows the spectral dependences of the ocean optical constituents. The shorter (blue) wavelengths are where CDOC absorption is strongest, and using these bands for non-spectral attenuation maximizes the absorption by this constituent. It also maximizes the photolysis of CDOC (Equations 3, 4, and **Figure 3**), which in turn leads to more blue light available for phytoplankton absorption and growth. CDOC global concentrations for the 400 nm transmittance scenario are 46% lower than the spectrally-resolved case (data not shown). This explains the elevated primary production observed in this spectral region (**Figure 8**). The remaining blue to green light available after absorption by CDOC favors cyanobacteria and coccolithophores, which have strong specific spectral absorption in this region (**Figure 3**), facilitating their growth and increased relative abundances compared to chlorophytes. This explains the changes observed in relative abundances (**Figure 7**). As we approach longer wavelengths, water absorption dominates, extinguishing available light for all phytoplankton and leading to high nutrient availability due to reduced primary production. Additionally, CDOC increases because it is a poor absorber in red light and consequently its photolysis is reduced, further exacerbating the irradiance deficit. In this case, the phytoplankton groups with the fastest growing capabilities in nutrient-replenished conditions are advantaged over the other types such as cyanobacteria and coccolithophores, which are better suited for utilizing nutrients at low concentrations.

The combined diffuse-only/non-spectral simulation with 500 nm as the attenuation wavelength does not show compensation, but rather exacerbation of the differences observed in the individual diffuse and spectral scenarios. Nitrate differences exceed −30% (non-directional/spectral low) and chlorophyll is lower by −16%. Global chlorophyll even loses significance in the correlation with satellite data, in contrast to the directionally-spectrally-resolved model (**Figure 10**). Primary production is only modestly higher at 5.1%. Chlorophytes are the most impacted, dropping their relative abundances from 15.6% in the resolved model to only 2.3%, while cyanobacteria and coccolithophores increase. This suggests that changes in irradiance simulation excluding diffuse/direct differentiation and full spectral behavior spur a community functional switch from light-limitation to nutrient limitation, shifting phytoplankton groups from the high nitrate users like chlorophytes to the efficient users like cyanobacteria and coccolithophores. Although diatoms are the most demanding for nitrate, they are relatively unaffected by changes in the light fields by omitting directional and spectral light, because they are most abundant in the nutrient-rich regions to begin with (e.g., high latitudes and upwelling regions).

We emphasize that the differences using non-directional and non-spectral simulations compared to the three-stream model and optical characterizations used here does not imply that the resolved model is correct. The OASIM model and characterizations have been evaluated in several contexts, as explained in the Methods, but we have not and most likely cannot evaluate the model in all scenarios. We do assert that it is more comprehensive in its representations of directional and spectral irradiance and therefore technically more realistic than models that do not incorporate these characteristics. Natural irradiance is directional and spectral. A model that accounts for these characteristics of light is therefore at least nominally representative. However, this does not necessarily mean the model here is accurate or even complete. There are several optical constituents in the real oceans that are not considered here, such as suspended sediments/minerals, viruses and bacteria (Balch et al., 2002; Stramski et al., 2004), suspended desert dust (Wozniak and Stramski, 2004), and mycosporine-like amino acids (Moisan and Mitchell, 2001), as well as unaccounted effects such as polarization, bi-directionality among others.

We are unable to directly compare the model described here with more typical PAR/shortwave-diffuse attenuation coefficient models because of our inclusion of CDOC. The majority of models using diffuse attenuation coefficient only represent attenuation by water and phytoplankton, which are sometimes taken as climatologies from satellite ocean color. There is growing recognition of the importance of CDOC for ocean biological modeling (e.g., Xiu and Chai, 2014; Dutkiewicz et al., 2015; Kim et al., 2015), building on the pioneering work of Bissett et al. (1999). In our representation, CDOC not only affects the irradiance availability but is also photolyzed by spectral irradiance. Any comparison with other types of models requires us to make significant assumptions about how to handle CDOC photolysis and production. The assumptions themselves would likely be a more important consideration than the presence or absence of directionally and spectrally-resolved radiative transfer.

Our purpose here is to assist modelers in understanding and quantifying the advantages and disadvantages of explicitly incorporating directional and spectral effects of radiative transfer

in models of ocean biology. Many models use a representation of PAR or shortwave radiation at the surface, and propagate irradiance as a function of an empirical or analytical diffuse attenuation coefficient using Beer-Lambert's law or another non-spectral, non-directional approach. This is especially true of the global models. It is true that many of these models also obtain very good representations of ocean biology and primary production (e.g., Moore et al., 2004; Dunne et al., 2013). It may be that the parameterization of the models and the radiative transfer implicitly incorporate the dominant effects required for simulation of ocean biology. However, it is also possible that missing explicit directional and spectral aspects of oceanic radiative transfer may impact our ability to simulate climate change scenarios where, for example, changes in clouds may lead to changes in direct and diffuse composition of surface irradiance, thereby affecting evaluations of future phytoplankton and carbon representations and feedbacks. This effort is intended to help modelers quantitatively evaluate the importance of the complexity of ocean radiative transfer and help inform decisions on future model developments.

## AUTHOR CONTRIBUTIONS

All authors listed, have made substantial, direct and intellectual contribution to the work, and approved it for publication.

## ACKNOWLEDGMENTS

We thank the NASA/MERRA Project, the MODIS Ocean Color and Atmosphere Processing Teams, the MAREDAT data project, and the algorithm developers for PIC and $a_{CDM}$. We thank Venetia Stuart, Bedford Institute of Oceanography, for providing *Phaeocystis* spp. spectral absorption coefficient data. We thank two reviewers for comments and suggestions. This work was supported by NASA PACE, S-NPP, and MAP Programs.

## SUPPLEMENTARY MATERIAL

The Supplementary Material for this article can be found online at: http://journal.frontiersin.org/article/10.3389/fmars.2016.00240/full#supplementary-material

## REFERENCES

Aas, E. (1987). Two-stream irradiance model for deep waters. *Appl. Opt.* 26, 2095–2101. doi: 10.1364/AO.26.002095

Ackleson, S. G., Balch, W. M., and Holligan, P. M. (1994). Response of water-leaving radiance to particulate calcite and chlorophyll a concentrations: a model for Gulf of Maine coccolithophore blooms. *J. Geophys. Res.* 99, 7483–7499. doi: 10.1029/93JC02150

Ahn, Y.-H., Bricaud, A., and Morel, A. (1992). Light backscattering efficiency and related properties of some phytoplankters. *Deep Sea Res.* 39, 1835–1855. doi: 10.1016/0198-0149(92)90002-B

Andrew, A. A., DelVecchio, R., Subramaniam, A., and Blough, N. V. (2013). Chromophoric dissolved organic matter (CDOM) in the Equatorial Atlantic Ocean: optical properties and their relation to CDOM structure and source. *Mar. Chem.* 148, 33–43. doi: 10.1016/j.marchem.2012.11.001

Arrigo, K., Dieckmann, G., Gosselin, M., Robinson, D., Fritsen, C., and Sullivan, C. (1995). High resolution study of the platelet ice ecosystem in McMurdo Sound, Antarctica: biomass, nutrient, and production profiles within a dense microalgal bloom. *Mar. Ecol. Prog. Ser.* 127, 255–268. doi: 10.3354/meps127255

Arrigo, K. R., Brown, Z. W., and Mills, M. M. (2014). Sea ice algal biomass and physiology in the Amundsen Sea, Antarctica. *Elementa Sci. Anthropocene* 2:000028. doi: 10.12952/journal.elementa.000028

Arrigo, K. R., and Sullivan, C. W. (1994). A high resolution bio-optical model of microalgal growth: tests using sea-ice algal community time-series data. *Limnol. Oceanogr.* 39, 609–631. doi: 10.4319/lo.1994.39.3.0609

Balch, W. M., Kilpatrick, K. A., and Trees, C. C. (1996). The 1991 coccolithophore bloom in the central North Atlantic. 1. Optical properties and factors affecting their distribution. *Limnol. Oceanogr.* 41, 1669–1683. doi: 10.4319/lo.1996.41.8.1669

Balch, W. M., Vaughn, J. M., Novotny, J. F., Drapeau, D. T., Goes, J. I., Booth, E., et al. (2002). Fundamental changes in light scattering associated with infection of marine bacteria by bacteriophage. *Limnol. Oceanogr.* 47, 1554–1561. doi: 10.4319/lo.2002.47.5.1554

Barlow, R. G., and Alberte, R. S. (1985). Photosynthetic characteristics of phycoerythrin-containing marine *Synechococcus* spp. *Mar. Biol.* 86, 63–74. doi: 10.1007/BF00392580

Bates, S. S., and Platt, T. (1984). Fluorescence induction as a measure of photosynthetic capacity in marine phytoplankton: response of *Thalassiosira pseudonana* (Bacillariophyceae) and *Dunaliella tertiolecta* (Chlorophyceae). *Mar. Ecol. Prog. Ser.* 18, 67–77. doi: 10.3354/meps018067

Behrenfeld, M. J., and Falkowski, P. G. (1997). Photosynthetic rates derived from satellite-based chlorophyll concentration. *Limnol. Oceanogr.* 42, 1–20. doi: 10.4319/lo.1997.42.1.0001

Ben-Amotz, A., and Gilboa, A. (1980). Cryptopreservation of marine unicellular algae. I. A survey of algae with regard to size, culture age, photosynthetic activity and chlorophyll - to - cell ratio. *Mar. Ecol. Prog. Ser.* 2, 157–161. doi: 10.3354/meps002157

Bidigare, R. R., and Ondrusek, M. E. (1996). Spatial and temporal variability of phytoplankton pigment distributions in the central equatorial Pacific Ocean. *Deep Sea Res. II* 43, 809–833. doi: 10.1016/0967-0645(96)00019-7

Bissett, W. P., Arnone, R., DeBra, S., Dieterle, D. A., Dye, D., Kirkpatrick, G. J., et al. (2005). Predicting the optical properties of the West Florida Shelf: resolving the potential impacts of a terrestrial boundary condition on the distribution of colored dissolved and particulate matter. *Mar. Chem.* 95, 199–233. doi: 10.1016/j.marchem.2004.09.007

Bissett, W. P., Carder, K. L., Walsh, J. J., and Dieterle, D. A. (1999). Carbon cycling in the upper waters of the Sargasso Sea: II. Numerical simulation of apparent and inherent optical properties. *Deep Sea Res. Part I Oceanogr. Res. Pap.* 46, 271–317. doi: 10.1016/S0967-0637(98)00063-6

Brand, L. E., Sunda, W. G., and Guillard, R. R. I. (1983). Limitation of marine phytoplankton reproductive rates by zinc, manganese, and iron. *Limnol. Oceanogr.* 28, 1182–1198. doi: 10.4319/lo.1983.28.6.1182

Brand, L. E., Sunda, W. G., and Guillard, R. R. L. (1986). Reductionof marine phytoplankton reproduction rates by copper and cadmium. *J. Exp. Mar. Biol. Ecol.* 96, 225–250. doi: 10.1016/0022-0981(86)90205-4

Bricaud, A., Ciotti, A. M., and Gentili, B. (2012). Spatial-temporal variations in phytoplankton size and colored detrital matter absorption at global and regional scales, as derived from twelve years of SeaWiFS data (1998–2009). *Global. Biogeochem. Cycles* 26, GB1010. doi: 10.1029/2010GB003952

Bricaud, A., Edhomme, A.-L., and Morel, A. (1988). Optical properties of diverse phytoplanktonic species: experimental results and theoretical interpretation. *J. Plankton Res.* 10, 851–873. doi: 10.1093/plankt/10.5.851

Bricaud, A., Babin, M., Claustre, H., Ras, J., and Tieche, F. (2010). Light absorption properties and absorption budget of Southeast Pacific waters. *J. Geophys. Res.* 115, C08009. doi: 10.1029/2009JC005517

Bricaud, A., and Morel, A. (1986). Light attenuation and scattering by phytoplanktonic cells: a theoretical modeling. *Appl. Opt.* 25, 571–580. doi: 10.1364/AO.25.000571

Bricaud, A., Morel, A., and Prieur, L. (1981). Absorption by dissolved organic matter of the sea (yellow substance) in the UV and visible domains. *Limnol. Oceanogr.* 26, 43–53. doi: 10.4319/lo.1981.26.1.0043

Buitenhuis, E. T., van der Wal, P., and de Baar, H. J. W. (2001). Blooms of Emiliana huxleyi are sinks of atmospheric carbon dioxide: a field and mesocosm study derived simulation. *Glob. Biogeochem. Cycles* 15, 577–587. doi: 10.1029/2000GB001292

Carder, K. L., Steward, R. G., Harvey, G. R., and Ortner, P. B. (1989). Marine humic and fulvic acids: their effects on remote sensing of ocean chlorophyll. *Limnol. Oceanogr.* 34, 68–81. doi: 10.4319/lo.1989.34.1.0068

Circio, J. A., and Petty, C. C. (1951). The near infrared absorption spectrum of liquid water. *J. Opt. Soc. Am.* 41, 302–308. doi: 10.1364/JOSA.41.000302

Coale, K. H., Wang, X., Tanner, S. J., and Johnson, K. S. (2003). Phytoplankton growth and biological response to iron and zinc addition in the Ross Sea and Antarctic Circumpolar Current along 170. *Deep Sea Res. II* 50, 635–653. doi: 10.1016/S0967-0645(02)00588-X

Conkright, M. E., Garcia, H. E., O'Brien, T. D., Locarnini, R. A., Boyer, T. P., Stephens, C., et al. (2002). "World Ocean Atlas 2001," in *NOAA Atlas NESDIS 52: Vol. 4, Nutrients*, ed S. Levitus (Washington, DC: US Government Printing Office), 392.

Croot, P. L., Andersson, K., Ozturk, M., and Turner, D. R. (2004). The distribution and speciation of iron along 61E in the Southern Ocean. *Deep Sea Res. II* 51, 2857–2879. doi: 10.1016/j.dsr2.2003.10.012

Del Vecchio, R., Subramaniam, A., Uz, S. S., Ballabrera-Poy, J., Brown, C. W., and Blough, N. V. (2009). Decadal time-series of SeaWiFS retrieved CDOM absorption and estimated CO2 photoproduction on the continental shelf of the eastern United States. *Geophys. Res. Lett.* 36, L02602. doi: 10.1029/2008gl036169

Dickey, T. D., Kattawar, G. W., and Voss, K. J. (2011). Shedding new light on light in the ocean. *Phys. Today* 64, 44–49. doi: 10.1063/1.3580492

Doney, S. C., Lindsay, K., Fung, I., and John, J. (2006). Natural variability in a stable, 1000-Yr global coupled climate–carbon cycle simulation. *J. Clim.* 19, 3033–3054. doi: 10.1175/JCLI3783.1

Dunne, J. P., John, J. G., Shevliakova, E., Stouffer, R. J., Krasting, J. P., Malyshev, S. L., et al. (2013). GFDL's ESM2 Global Coupled Climate–carbon earth system models. Part II: carbon system formulation and baseline simulation characteristics. *J. Clim.* 26, 2247–2267. doi: 10.1175/JCLI-D-12-00150.1

Dutkiewicz, S., Hickman, A. E., Jahn, O., Gregg, W. W., Mouw, C. B., and Follows, M. J. (2015). Capturing optically important constituents and properties in a marine biogeochemical and ecosystem model. *Biogeosciences* 12, 4447–4481. doi: 10.5194/bg-12-4447-2015

Eppley, R. W., Rogers, J. N., and McCarthy, J. J. (1969). Half-saturation constants for uptake of nitrate and ammonium by marine phytoplankton. *Limnol. Oceanogr.*14, 912–920. doi: 10.4319/lo.1969.14.6.0912

Falkowski, P. G., Dubinsky, G. Z., and Wyman, K. (1985). Growth-irradiance relationships in phytoplankton. *Limnol. Oceanogr.* 30, 311–321. doi: 10.4319/lo.1985.30.2.0311

Fung, I. Y., Meyn, S. K., Tegen, I., Doney, S. C., John, J. G., and Bishop, J. K. B. (2000). Iron supply and demand in the upper ocean. *Glob. Biogeochem. Cycles* 14, 281–295. doi: 10.1029/1999GB900059

Furnas, M. J. (1991). Net *in situ* growth rates of phytoplankton in an oligotrophic, tropical shelf ecosystem. *Limnol. Oceanogr.* 36, 13–29. doi: 10.4319/lo.1991.36.1.0013

Gallegos, C. L., Werdell, P. J., and McClain, C. (2011). Long-term changes in light scattering in Chesapeake Bay inferred from Secchi depth, light attenuation, and remote sensing measurements. *J. Geophys. Res.* 116, C00H08. doi: 10.1029/2011JC007160

Garver, S. A., and Siegel, D. A. (1997). Inherent optical property inversion of ocean color spectra and its biogeochemical interpretation: I. Time series from the Sargasso Sea. *J. Geophys. Res.* 102, 18607–18625.

Gavis, J., Guillard, R. R. L., and Woodward, B. L. (1981). Cupric ion activity and the growth of phytoplankton clones isolated from different marine environments. *J. Mar. Res.* 39, 315–333.

Gnanadesikan, A., and Anderson, W. G. (2009). Ocean water clarity and the ocean general circulation in a coupled climate model. *J. Phys. Oceanogr.* 39, 314–332. doi: 10.1175/2008JPO3935.1

Gnanadesikan, A., Dixon, K., Griffies, S. M., Balaji, V., Barreiro, M., Beesley, J. A., et al. (2006). GFDL's CM2 global coupled climate models. Part II: T*he baseline ocean simulation.* J. Clim. 19, 675–697. doi: 10.1175/JCLI3630.1

Goldman, J. C., and Glibert, P. M. (1982). Comparative rapid ammonium uptake by four species of marine phytoplankton. *Limnol. Oceanogr.* 27, 814–827. doi: 10.4319/lo.1982.27.5.0814

Gordon, H. R., Smyth, T. J., Balch, W. M., Boynton, G. C., and Tarran, G. A. (2009). Light scattering by coccoliths detached from *Emiliania huxleyi*. *Appl. Opt.* 48, 6059–6073. doi: 10.1364/AO.48.006059

Gregg, W. W. (2000). "A coupled ocean-atmosphere radiative model for global ocean biogeochemical models," in *NASA Global Modeling and Assimilation Series*, Vol. 22, ed M. Suarez (Greenbelt, MD: NASA Technical Memorandum 2002-104606), 33.

Gregg, W. W. (2002). Tracking the SeaWiFS record with a coupled physical/biogeochemical/radiative model of the global oceans. *Deep Sea Res. II* 49, 81–105. doi: 10.1016/S0967-0645(01)00095-9

Gregg, W. W., and Carder, K. L. (1990). A simple spectral solar irradiance model for cloudless maritime atmospheres. *Limnol. Oceanogr.* 35, 1657–1675. doi: 10.4319/lo.1990.35.8.1657

Gregg, W. W., and Casey, N. W. (2007). Modeling coccolithophores in the global oceans. *Deep Sea Res. II* 54, 447–477. doi: 10.1016/j.dsr2.2006.12.007

Gregg, W. W., and Casey, N. W. (2009). Skill assessment of a spectral ocean-atmosphere radiative model. *J. Mar. Syst.* 76, 49–63. doi: 10.1016/j.jmarsys.2008.05.007

Gregg, W. W., Casey, N. W., and Rousseaux, C. S. (2013). "Global surface ocean carbon estimates in a model forced by MERRA," in *NASA Global Modeling and Assimilation Series,* Vol. 31, ed M. Suarez (Greenbelt, MD: NASA Technical Memorandum 2012-104606), 32.

Gregg, W. W., Ginoux, P., Schopf, P. S., and Casey, N. W. (2003). Phytoplankton and iron: validation of a global three-dimensional ocean biogeochemical model. *Deep Sea Res. II* 50, 3143–3169. doi: 10.1016/j.dsr2.2003.07.013

Griffies, S. M., Harrison, M. J., Pacanowski, R. C., and Rosati, A. (2004). *A Technical Guide to MOM4*. GFDL Ocean Group Technical Report, Princeton.

Henson, S. A., Sarmiento, J. L., Dunne, J. P., Bopp, L., Lima, I., Doney, S. C., et al. (2010). Detection of anthropogenic climate change in satellite records of ocean chlorophyll and productivity. *Biogeosciences* 7, 621–640. doi: 10.5194/bg-7-621-2010

Humphrey, G. F. (1979). Photosynthetic characteristics of algae grown under constant illumination and light-dark regimes. *J. Exp. Mar. Biol. Ecol.* 40, 63–70. doi: 10.1016/0022-0981(79)90034-0

Jiang, M.-S., Chai, F., Dugdale, R. C., Wilkerson, F. P., Peng, T.-H., and Barber, R. T. (2003). A nitrate and silicate budget in the equatorial Pacific Ocean: a coupled physical–biological model study. *Deep Sea Res. II* 50, 2971–2996. doi: 10.1016/j.dsr2.2003.07.006

Karl, D. M., Bidigare, R. R., and Letelier, R. M. (2001). Long-term changes in plankton community structure and productivity in the North Pacific Subtropical Gyre: the domain shift hypothesis. *Deep Sea Res. Part II* 48, 1449–1470. doi: 10.1016/S0967-0645(00)00149-1

Key, R. M., Kozyr, A., Sabine, C. L., Lee, K., Wanninkhof, R., Bullister, J. L., et al. (2004). A global ocean carbon climatology: results from Global Data Analysis Project (GLODAP). *Glob. Biogeochem. Cycles* 18:GB4031. doi: 10.1029/2004GB002247

Kim, G. E., Pradal, M.-A., and Gnanadesikan, A. (2015). Quantifying the biological impact of surface ocean light attenuation by colored detrital matter in an ESM using a new optical parameterization. *Biogeosciences* 12, 5119–5132. doi: 10.5194/bg-12-5119-2015

Kirk, J. T. O. (1992). "The nature and measurement of the light environment in the ocean," in *Primary Productivity and Biogeochemical Cycles in the Sea*, eds P. G. Falkowski and A. D. Woodhead (New York, NY: Springer Science+Business Media), 9–29.

Langdon, C. (1987). On the causes of interspecific differences in the growth–irradiance relationship for phytoplankton. Part I. A comparative study of the growth–irradiance relationship of three *marine phytoplankton species:* Skeletonema costatum, *Olisthodiscus luteus*, and *Gonyaulax tamarensis. J. Plankton Res.* 9, 459–482. doi: 10.1093/plankt/9.3.459

Laufkötter, C., Vogt, M., and Gruber, N. (2013). Long-term trends in ocean plankton production and particle export between 1960–2006. *Biogeosciences* 10, 7373–7393. doi: 10.5194/bg-10-7373-2013

Lee, Z., Du, K., Arnone, R., Liew, S., and Penta, B. (2005). Penetration of solar radiation in the upper ocean: a numerical model for oceanic and coastal waters. *J. Geophys. Res.* 110, C09019. doi: 10.1029/2004JC002780

Lee, Z., Wei, J., Voss, K., Lewis, M., Bricaud, A., and Huot, Y. (2015). Hyperspectral absorption coefficient of "pure" seawater in the range of 350–550 nm inverted from remote sensing reflectance. *Appl. Opt.* 54, 546–558. doi: 10.1364/AO.54.000546

Maier-Reimer, E., Kriest, I., Segschneider, J., and Wetzel, P. (2005). *The HAMburg Ocean Carbon Cycle Model HAMOCC5.1, Berichte zur Erdsystemforschung 14/2005.* Hamburg: Max Planck-Institut für Meteorologie.

Manizza, M., Le Quéré, C., Watson, A. J., and Buitenhuis, E. T. (2005). Bio-optical feedbacks among phytoplankton, upper ocean physics and sea-ice in a global model. *Geophys. Res. Lett.* 32, L05603. doi: 10.1029/2004GL020778

Marinov, I., Doney, S. C., and Lima, I. D. (2010). Response of ocean phytoplankton community structure to climate change over the 21st century: partitioning the effects of nutrients, temperature and light. *Biogeosciences* 7, 3941–3959. doi: 10.5194/bg-7-3941-2010

Maritorena, S., Hembise, O., Fanton d'Andon, A., Mangin, A., and Siegel, D. A. (2010). Merged satellite ocean color data products using a bio-optical model: characteristics, benefits and issues. *Remote Sens. Environ.* 114, 1791–1804. doi: 10.1016/j.rse.2010.04.002

Maritorena, S., and Siegel, D. A. (2005). Consistent merging of satellite ocean color data sets using a bio-optical model. *Remote Sens. Environ.* 94, 429–440. doi: 10.1016/j.rse.2004.08.014

Masotti, I., Moulin, C., Alvain, S., Bopp, L., Tagliabue, A., and Antoine, D. (2011). Large-scale shifts in phytoplankton groups in the Equatorial Pacific during ENSO cycles. *Biogeosciences* 8, 539–550. doi: 10.5194/bg-8-539-2011

Maul, G. A. (1985). *Introduction to Satellite Oceanography*. Boston, MA: Martinus Nijhoff Publishers.

Mobley, C. D., Sundman, L. K., Bissett, W. P., and Cahill, B. (2009). Fast and accurate irradiance calculations for ecosystem models. *Biogeosciences Discuss.* 6, 10625–10662. doi: 10.5194/bgd-6-10625-2009

Moisan, T. A., and Mitchell, B. G. (2001). UV absorption by mycosporine-like amino acids in *Phaeocystis antarctica* Karsten induced by photosynthetically available radiation. *Mar. Biol.* 138, 217–227. doi: 10.1007/s002270000424

Moore, J. K., Doney, S. C., and Lindsay, K. (2004). Upper ocean ecosystem dynamics and iron cycling in a global three-dimensional model. *Glob. Biogeochem. Cycles* 18, 1–21. doi: 10.1029/2004GB002220

Morel, A. (1987). Chlorophyll-specific scattering coefficient of phytoplankton. A simplified theoretical approach. *Deep Sea Res.* 34, 1093–1105. doi: 10.1016/0198-0149(87)90066-5

Morel, A. (1988). Optical modeling of the upper ocean in relation to its biogenous matter content (Case I waters). *J. Geophys. Res.* 93, 10749–10768. doi: 10.1029/JC093iC09p10749

Morel, A., and Bricaud, A. (1981). Theoretical results concerning light absorption in a discrete medium, and application to specific absorption of phytoplankton. *Deep Sea Res.* 28, 1375–1393. doi: 10.1016/0198-0149(81)90039-X

Morel, A., Gentili, B., Claustre, H., Babin, M., Bricaud, A., Ras, J., et al. (2007). Optical properties of the "clearest" natural waters. *Limnol. Oceanogr.* 52, 217–229. doi: 10.4319/lo.2007.52.1.0217

Organelli, E., Bricaud, A., Antoine, D., and Matsuoka, A. (2014). Seasonal dynamics of light absorption by chromophoric dissolved organic matter (CDOM) in the NW Mediterranean Sea (BOUSSOLE Site). *Deep Sea Res. I* 191, 72–85. doi: 10.1016/j.dsr.2014.05.003

Palmer, J. R., and Totterdell, I. J. (2001). Production and export in a global ocean ecosystem model. *Deep Sea Res. I* 48, 1169–1198. doi: 10.1016/S0967-0637(00)00080-7

Peperzak, L., Colijn, F., Koeman, R., Gieskes, W. W. C., and Joordens, J. C. A. (2003). Phytoplankton Sinking Rates in the Rhine Region of Freshwater Influence. *J. Plankton Res.* 25, 365–383. doi: 10.1093/plankt/25.4.365

Perry, M. J., Talbot, M. C., and Alberte, R. S. (1981). Photoadaptation in marine phytoplankton: response of the photosynthetic unit. *Mar. Biol.* 62, 91–101. doi: 10.1007/BF00388170

Pope, R. M., and Fry, E. S. (1997). Absorption spectrum (380–700 nm) of pure water. II. Integrating cavity measurements. *Appl. Opt.* 46, 8710–8723. doi: 10.1364/AO.36.008710

Reader, H. E., and Miller, W. L. (2012). Variability of carbon monoxide and carbon dioxide apparent quantum yield spectra in three coastal estuaries of the South Atlantic Bight. *Biogeosciences* 9, 4279–4294. doi: 10.5194/bg-9-4279-2012

Reader, H. E., and Miller, W. L. (2014). The efficiency and spectral photon dose dependence of photochemically induced changes to the bioavailability of dissolved organic carbon. *Limnol. Oceanogr.* 59, 182–194. doi: 10.4319/lo.2014.59.1.0182

Rienecker, M. M., Suarez, M. J., Gelaro, R., Todling, R., Bacmeister, J., Liu, E., et al. (2011). MERRA - NASA's modern-era retrospective analysis for research and applications. *J. Clim.* 24, 3624–3648. doi: 10.1175/JCLI-D-11-00015.1

Robinson, D. H., Arrigo, K. R., Kolber, Z., Gosselin, M., and Sullivan, C. W. (1998). Photophysiological evidence of nutrient limitation of platelet ice algae in McMurdo Sound, Antarctica. *J. Phycol.* 34, 788–797. doi: 10.1046/j.1529-8817.1998.340788.x

Roesler, C. S., Perry, M. J., and Carder, K. L. (1989). Modeling *in situ* phytoplankton absorption from total absorption spectra in productive inland marine waters. *Limnol. Oceanogr.* 34, 1510–1523. doi: 10.4319/lo.1989.34.8.1510

Romanou, A., Gregg, W. W., Romanski, J., Kelley, M., Bleck, R., Healy, R., et al. (2013). Natural air-sea flux of $CO_2$ in simulations of the NASA-GISS climate model: sensitivity to the physical ocean model formulation. *Ocean Model.* 66, 26–44. doi: 10.1016/j.ocemod.2013.01.008

Romanou, A., Romanski, J., and Gregg, W. W. (2014). Natural ocean carbon cycle sensitivity to parameterizations of the recycling in a climate model. *Biogeosciences* 11, 1137–1154. doi: 10.5194/bg-11-1137-2014

Rousseaux, C. S., and Gregg, W. W. (2012). Climate variability and phytoplankton composition in the Pacific Ocean. *J. Geophys. Res.* 117, C10006. doi: 10.1029/2012JC008083

Rousseaux, C. S., and Gregg, W. W. (2015). Recent decadal trends in global phytoplankton composition. *Glob. Biogeochem. Cycles* 29, 1674–1688. doi: 10.1002/2015GB005139

Sakshaug, E., and Andresen, K. (1986). Effect of light regime upon growth rate and chemical composition of a clone of Skeletonema costatum from the Trondheimsfjord, Norway. *J. Plankton Res.* 8, 619–637.

Sathyendranath, S., Lazzara, L., and Prieur, L. (1987). Variations in the spectral values of specific absorption of phytoplankton. *Limnol. Oceanogr.* 32, 403–415. doi: 10.4319/lo.1987.32.2.0403

Sathyendranath, S., and Platt, T. (1988). The spectral irradiance field at the surface and in the interior of the ocean: a model for applications in oceanography and remote sensing. *J. Geophys. Res.* 93, 9270–9280. doi: 10.1029/JC093iC08p09270

Sathyendranath, S., and Platt, T. (1989). Computation of aquatic primary production: extended formalism to include effect of angular and spectral distribution of light. *Limnol. Oceanogr.* 34, 188–198. doi: 10.4319/lo.1989.34.1.0188

Schoemann, V., Becquevort, S., Stefels, J., Rousseau, V., and Lancelot, C. (2005). Phaeocystis blooms in the global ocean and their controlling mechanisms: a review. *J. Sea Res.* 53, 43–66. doi: 10.1016/j.seares.2004.01.008

Schopf, P. S., and Loughe, A. (1995). A reduced gravity isopycnal ocean model: hindcasts of El Nino. *Monthly Weather Rev.* 123, 2839–2863.

Siegel, D. A., Maritorena, S., Nelson, N. B., Hansell, D. A., and Lorenzi-Kayser, M. (2002). Global distribution and dynamics of colored dissolved and detrital organic materials. *J. Geophys. Res.* 107, 3228. doi: 10.1029/2001JC000965

Smith, R. C., and Baker, K. S. (1981). Optical properties of the clearest natural waters (200–800 nm). *Appl. Opt.* 20, 177–184. doi: 10.1364/AO.20.000177

Stedmon, C. A., Thomas, D. N., Papadimitriou, S., Granskog, M. A., and Dieckmann, G. S. (2011). Using fluorescence to characterize dissolved organic matter in Antarctic sea ice brines. *J. Geophys. Res.* 116:G03027. doi: 10.1029/2011JG001716

Stramski, D., Boss, E., Bogucki, D., and Voss, K. J. (2004). The role of seawater constituents in light backscattering in the ocean. *Prog. Oceanogr.* 61, 27–56. doi: 10.1016/j.pocean.2004.07.001

Stuart, V., Sathyendranath, S., Head, E. J. H., Platt, T., Irwin, B., and Maass, H. (2000). Bio-optical characteristics of diatom and prymnesiophyte populations in the Labrador Sea. *Mar. Ecol. Prog. Ser.* 201, 91–106. doi: 10.4319/lo.1996.41.8.1669

Subba Rao, D. V. (1981). Growth response of marine phytoplankton to selected concentrations of trace metals. *Bot. Mar.* 24, 369–379. doi: 10.1515/botm.1981.24.7.369

Sunda, W. G., and Huntsman, S. A. (1995). Iron uptake and growth limitation in oceanic and coastal Phytoplankton. *Mar. Chem.* 50, 189–206. doi: 10.1016/0304-4203(95)00035-P

Tang, K. W., Smith, W. O. Jr., Shields, A. R., and Elliott, D. T. (2009). Survival and recovery of *Phaeocystis antarctica* (Prymnesiophyceae) from prolonged

darkness and freezing. *Proc. R. Soc. B Biol. Sci.* 276, 81–90. doi: 10.1098/rspb.2008.0598

Tungazara, C., Rousseau, V., Brion, N., Lancelot, C., Gichuki, J., Baeyens, W., et al. (2003). Contrasting nitrogen uptake by diatom and Phaeocystis-dominated phytoplankton assemblages in the North Sea. *J. Exp. Mar. Biol. Ecol.* 292, 19–41. doi: 10.1016/S0022-0981(03)00145-X

Tzortziou, M., Osburn, C. L., and Neale, P. J. (2007). Photobleaching of dissolved organic material from a tidal marsh-estuarine system of the chesapeake bay. *Photochem. Photobiol.* 83, 782–792. doi: 10.1111/j.1751-1097.2007.00142.x

Uitz, J., Claustre, H., Gentili, B., and Stramski, D. (2010). Phytoplankton class-specific primary production in the world's oceans: seasonal and interannual variability from satellite observations. *Glob. Biogeochem. Cycles* 24:GB3016. doi: 10.1029/2009GB003680

Vaillancourt, R. D., Brown, C. W., Guillard, R. R. L., and Balch (2004). Light backscattering properties of marine phytoplankton: relationships to cell size, chemical composition, and taxonomy. *J. Plankton Res.* 26, 191–212. doi: 10.1093/plankt/fbh012

van Hilst, C. M., and Smith, W. O. Jr. (2002). Photosynthesis/irradiance relationships in the Ross Sea, Antarctica, and their control by phytoplankton assemblage composition and environmental factors. *Mar. Ecol. Prog. Ser.* 226, 1–12. doi:10.3354/meps226001

Vogt, M., O'Brien, C., Peloquin, J., Schoemann, V., Breton, E., Estrada, M., et al. (2012). Global marine plankton functional type biomass distributions: *Phaeocystis* spp. *Earth Syst. Sci. Data* 4, 107–120. doi: 10.5194/essd-4-107-2012

Whitmire, A. L., Pegau, W. S., Karp-Boss, L., Boss, E., and Cowles, T. J. (2010). Spectral backscattering properties of marine phytoplankton cultures. *Opt. Expr.* 18, 15073–15093. doi: 10.1364/oe.18.015073

Wozniak, S. B., and Stramski, D. (2004). Modeling the optical properties of mineral particles suspended in seawater and their influence on ocean reflectance and chlorophyll estimation from remote sensing algorithms. *Appl. Opt.* 43, 3489–3503. doi: 10.1364/AO.43.003489

Wyman, M., and Fay, P. (1986). Underwater light climate and the growth and pigmentation of planktonic blue-green algae (Cyanobacteria) I. The influence of light quantity. *Proc. R. Soc. Lond.* 227, 367–380. doi: 10.1098/rspb.1986.0027

Xiu, P., and Chai, F. (2014). Connections between physical, optical and biogeochemical processes in the Pacific Ocean. *Prog. Oceanogr.* 122, 30–53. doi: 10.1016/j.pocean.2013.11.008

Yacobi, Y. Z., Alberts, J. J., Takács, M., and Michelle McElvaine, M. (2003). Absorption spectroscopy of chromophoric dissolved organic carbon in Georgia (USA) rivers: the impact of molecular size distribution. *J. Limnol.* 62, 41–46. doi: 10.4081/jlimnol.2003.41

Zhao, J., Barnes, B., Melo, N., English, D., Lapointe, B., Muller-Karger, F., et al. (2013). Assessment of satellite-derived diffuse attenuation coefficients and euphotic depths in south Florida coastal waters. *Remote Sens. Environ.* 131, 38–50. doi: 10.1016/j.rse.2012.12.009

Zielinski, O., Octavio Llinas, O., Oschlies, A., and Reuter, R. (2002). Underwater light field and its effect on aone-dimensional ecosystem model at station ESTOC, north of the Canary Islands. *Deep Sea Res. II* 49, 3529–3542. doi: 10.1016/S0967-0645(02)00096-6

**Conflict of Interest Statement:** The authors declare that the research was conducted in the absence of any commercial or financial relationships that could be construed as a potential conflict of interest.

The reviewer CM and handling Editor declared their shared affiliation, and the handling Editor states that the process nevertheless met the standards of a fair and objective review.

frontiers in Marine Science

ORIGINAL RESEARCH
published: 15 November 2016
doi: 10.3389/fmars.2016.00225

# Copepod Life Strategy and Population Viability in Response to Prey Timing and Temperature: Testing a New Model across Latitude, Time, and the Size Spectrum

*Neil S. Banas[1]*, Eva F. Møller[2], Torkel G. Nielsen[3] and Lisa B. Eisner[4]*

*[1] Department of Mathematics and Statistics, University of Strathclyde, Glasgow, UK, [2] Department of Bioscience, Arctic Research Center, Aarhus University, Roskilde, Denmark, [3] Section for Ocean Ecology and Climate, National Institute of Aquatic Resources, Technical University of Denmark, Charlottenlund, Denmark, [4] NOAA Fisheries, Alaska Fisheries Science Center, Seattle, WA, USA*

OPEN ACCESS

**Edited by:**
*Dag Lorents Aksnes, University of Bergen, Norway*

**Reviewed by:**
*Øyvind Fiksen, University of Bergen, Norway*
*Nicholas R. Record, Bigelow Laboratory for Ocean Sciences, USA*

***Correspondence:**
*Neil S. Banas*
*neil.banas@strath.ac.uk*

**Specialty section:**
*This article was submitted to Marine Ecosystem Ecology, a section of the journal Frontiers in Marine Science*

**Received:** *03 June 2016*
**Accepted:** *27 October 2016*
**Published:** *15 November 2016*

**Citation:**
*Banas NS, Møller EF, Nielsen TG and Eisner LB (2016) Copepod Life Strategy and Population Viability in Response to Prey Timing and Temperature: Testing a New Model across Latitude, Time, and the Size Spectrum. Front. Mar. Sci. 3:225. doi: 10.3389/fmars.2016.00225*

A new model ("Coltrane": Copepod Life-history Traits and Adaptation to Novel Environments) describes environmental controls on copepod populations via (1) phenology and life history and (2) temperature and energy budgets in a unified framework. The model tracks a cohort of copepods spawned on a given date using a set of coupled equations for structural and reserve biomass, developmental stage, and survivorship, similar to many other individual-based models. It then analyzes a family of cases varying spawning date over the year to produce population-level results, and families of cases varying one or more traits to produce community-level results. In an idealized global-scale testbed, the model correctly predicts life strategies in large *Calanus* spp. ranging from multiple generations per year to multiple years per generation. In a Bering Sea testbed, the model replicates the dramatic variability in the abundance of *Calanus glacialis/marshallae* observed between warm and cold years of the 2000s, and indicates that prey phenology linked to sea ice is a more important driver than temperature *per se*. In a Disko Bay, West Greenland testbed, the model predicts the viability of a spectrum of large-copepod strategies from income breeders with a adult size $\sim$100 $\mu$gC reproducing once per year through capital breeders with an adult size $>$1000 $\mu$gC with a multiple-year life cycle. This spectrum corresponds closely to the observed life histories and physiology of local populations of *Calanus finmarchicus*, *C. glacialis*, and *Calanus hyperboreus*. Together, these complementary initial experiments demonstrate that many patterns in copepod community composition and productivity can be predicted from only a few key constraints on the individual energy budget: the total energy available in a given environment per year; the energy and time required to build an adult body; the metabolic and predation penalties for taking too long to reproduce; and the size and temperature dependence of the vital rates involved.

**Keywords: zooplankton, copepod, life history, diversity, biogeography, modeling, community ecology, Arctic**

## 1. INTRODUCTION

Calanoid copepods occupy a crucial position in marine food webs, the dominant mesozooplankton in many temperate and polar systems, important to packaging of microbial production in a form accessible to higher predators. They also represent the point at which biogeochemical processes, and numerical approaches like NPZ (nutrient–phytoplankton–zooplankton) models, start to be significantly modulated by life-history and behavioral constraints. The population- and community-level response of copepods to environmental change (temperature, prey availability, seasonality) thus forms a crucial filter lying between the biogeochemical impacts of climate change on primary production patterns and the food-web impacts that follow.

Across many scales in many systems, the response of fish, seabirds, and marine mammals to climate change has been observed, or hypothesized, to follow copepod community composition more closely than it follows total copepod or total zooplankton production. Examples include interannual variation in pollock recruitment in the Eastern Bering Sea (Coyle et al., 2011; Eisner et al., 2014), interdecadal fluctuations in salmon marine survival across the Northeast Pacific (Mantua et al., 1997; Hooff and Peterson, 2006; Burke et al., 2013), and long-term trends in forage fish and seabird abundance in the North Sea (Beaugrand and Kirby, 2010; MacDonald et al., 2015). These cases can be all be schematized as following the "junk food" hypothesis (Österblom et al., 2008) in which the crucial axis of variation is not between high and low total prey productivity, but rather between high and low relative abundance of large, lipid-rich prey taxa.

Calanoid copepods range in adult body size by more than two orders of magnitude, from $<10$ to $>1000\,\mu$g C. Lipid content is likewise quite variable (Kattner and Hagen, 2009), even among congeneric species in a single environment (Swalethorp et al., 2011). Many but not all species enter a seasonal period of diapause in deep water, in which they do not feed and basal metabolism is reduced to $\sim$1/4 of what it is during active periods (Maps et al., 2014). Reproductive strategies include both income breeding (egg production fueled by ingestion of fresh prey during phytoplankton blooms) and capital breeding (egg production fueled by stored lipids in winter), as well as hybrids between the two strategies (Hirche and Kattner, 1993; Daase et al., 2013). Generation lengths vary from several weeks to several years.

These life-history traits (generation length, diapause, reproductive strategy, and annual routine more generally) constitute the mechanistic link between environment and the quality of the copepod community as prey (i.e., body size and composition). Lipid storage, coupled to diapause in deep water, is a strategy for surviving the winter in environments where winter foraging is not cost-effective energetically; and just as important, it provides energetic free scope for optimizing reproductive timing relative to prey availability (Falk-Petersen et al., 2009; Varpe et al., 2009). Lipid storage is tied to climate via temperature (which determines the rate at which an animal burns through its reserves during winter and rates of ingestion, growth, and development year-round) and phenology (i.e., timing of the copepods phytoplankton and protist prey: Mackas et al., 2012). This logic provides a route by which the energetics of fish, seabird, and mammal foraging are tied to temperature and phytoplankton phenology via the tradeoffs governing *copepod* life history.

There is likely a gap, then, between the focus of conventional oceanographic plankton models—total productivity by functional group—and the copepod traits of greatest importance to predators. A number of dynamical-modeling studies have attempted to fill this gap by modeling the copepods species by species in relation to climate forcing, often in an individual-based-model (IBM) framework (Miller et al., 2002; Ji et al., 2012; Maar et al., 2013; Wilson et al., 2016). There are two key limitations to the species-by-species approach, however. First, it is difficult to see how it can scale or generalize to the community level, given that our empirical information on the physiology and life history of the copepods is a patchwork, and realistically will always remain so. Second, it does not address the question of adaptation, either on the individual or species level. As individuals make use of their phenotypic plasticity in behavior, physiology, and life cycle, and as natural selection acts on existing species and subpopulations, it is likely that shifts in the biogeography of copepod traits such as size, lipid content, and life history pattern will not move in lockstep with the biogeography of existing species (Barton et al., 2013). Indeed, subpopulations of individual copepod species display so much life-history and physiological diversity (Heath et al., 2004; Daase et al., 2013) that it is not clear what the basic units of a general species-based model would even be. Observations of hybridization among species (Parent et al., 2015) only underscore this problem.

This paper presents a proof-of-concept for a trait-based, as opposed to species-based, copepod IBM, intended for eventual use in problems linking planktivores to climate and environment on global or regional scales. Record et al. (2013) presented a copepod community IBM in which explicit competition via a genetic algorithm was used to pick community assemblages out of a trait-based metacommunity along a latitudinal gradient. That study was concerned mainly with the emergent behavior of a very complex model system (predation-structured competition along with the interacting effects of six variable traits). In contrast, we have included as few explicitly variable traits as possible, guided by a strategic set of heuristic and quantitative comparisons with data (**Figure 1**). The balance point we have sought in this phase of work is the lightest-weight representation of diversity and plasticity that allows the model to (1) generate a realistic landscape of competitors in a single environment, (2) correctly predict fitness fluctuations in one population as a function of habitat, and (3) give sensible results over a wide biogeographic range.

The first of these criteria, captured by a Disko Bay, West Greenland model experiment (**Figure 1**, Section 3.4) is central to the goal of eventually allowing climate-to-copepod model studies to replace hand-picked sets of fixed types with a trait continuum. The second and third criteria (captured by a Bering Sea hindcast experiment and an heuristic, idealized biogeographic experiment: **Figure 1**, Sections 3.2, 3.3) provide complementary constraints on the parameterization of individual energetics, and help

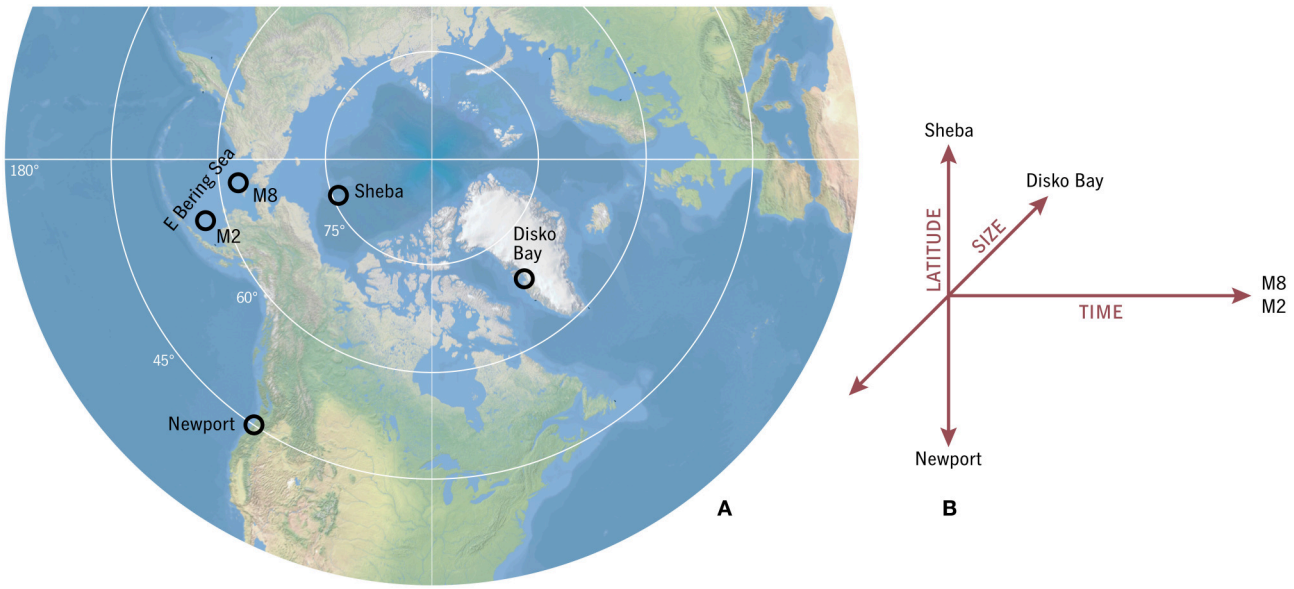


**FIGURE 1 | (A)** Locations of model testbeds. The "global" model experiment spans a gradient from approximately Ice Station Sheba to Newport, Oregon, and beyond. This experiment and the Bering Sea and Disko Bay testbeds constitute **(B)** a complementary set examining variation in space, time, and size diversity.

distinguish the effects of temperature and prey seasonality. As we will show, these initial experiments suggest a general hypothesis: that the viability of the calanoid community, at least near its high-latitude limit, is much more sensitive to prey abundance and phenology than to temperature.

## 2. MODEL DESCRIPTION

### 2.1. General Approach

The model introduced here is "Coltrane" (Copepod Life-history Traits and Adaptation to New Environments) version 1.0. Matlab source code is available at https://github.com/neilbanas/coltrane. An overview of the model structure is shown in **Figure 2**.

Like many individual-based models, Coltrane represents the time-evolution of one cohort of a clonal population, all bearing the same traits and spawned on the same date $t_0$, with a set of ODEs. The state variables describing a cohort are relative developmental stage $D$, where $D = 0$ represents a newly spawned egg and $D = 1$ an adult; survivorship $N$, the fraction of initially spawned individuals that remain after some amount of cumulative predation mortality; structural biomass per individual $S$, and "potential" or "free scope" $\varphi$, which represents all net energy gain not committed to structure, or equivalently, the combination of internal energy reserves and eggs already produced. Combining reserves and eggs into one pool in this way lets us cleanly separate results that depend only on the fundamental energy budget (gain from ingestion, loss to metabolism, and energy required to build somatic structure) from results that depend on particular assumptions about egg production (costs, cues, and strategies). An alternate form of the model explicitly divides $\varphi$ into internal reserves $R$ and egg production rate $E$: the simpler model without this distinction will be called the "potential" or $\varphi$ model and the fuller version the "egg/reserve" or ER model.

The $\varphi$ and ER models take different approaches to generating population-level results from this cohort model, as explained in detail below (Section 2.4). In both cases, the logic changes from the simple forward time-integration at the cohort level: one runs the cohort model for all possible spawning dates $t_0$, retroactively determines which spawning dates would prove optimal or sustainable, and considers the cohort time series from those $t_0$ values, appropriately weighted, to constitute the model solution (Section 2.4). The biological logic here is similar to the backwards-in-time dynamical optimization method frequently used in studies of optimal annual routines (Houston et al., 1993; Varpe et al., 2007), although our solving method is quite different and less exact. This is a compromise with the eventual goal of coupling Coltrane to oceanographic models as a spatially explicit IBM.

Communities are generated in Coltrane 1.0 simply by running families of cases of the population-level model that vary one or more traits. Treating coexisting populations as uncoupled vastly simplifies the interpretation of the *landscape of viable strategies in a given environment*, or the *fundamental niche* of a particular trait combination, our primary modes of analysis. At the same time, it tightly restricts our choices regarding the formulation of predation mortality. In reality, coupling through shared predators can rival bottom-up effects as a determinant of community structure (Holt et al., 1994; Chesson, 2000; Record et al., 2013, 2014), and we expect that many potential applications of this model would require that this be better represented. In the present study, we have taken the minimalist, incrementalist approach of imposing the simplest possible form of predation mortality—a linear function, with scalings that closely mirror the growth and development functions (Section 2.2)—and restricting

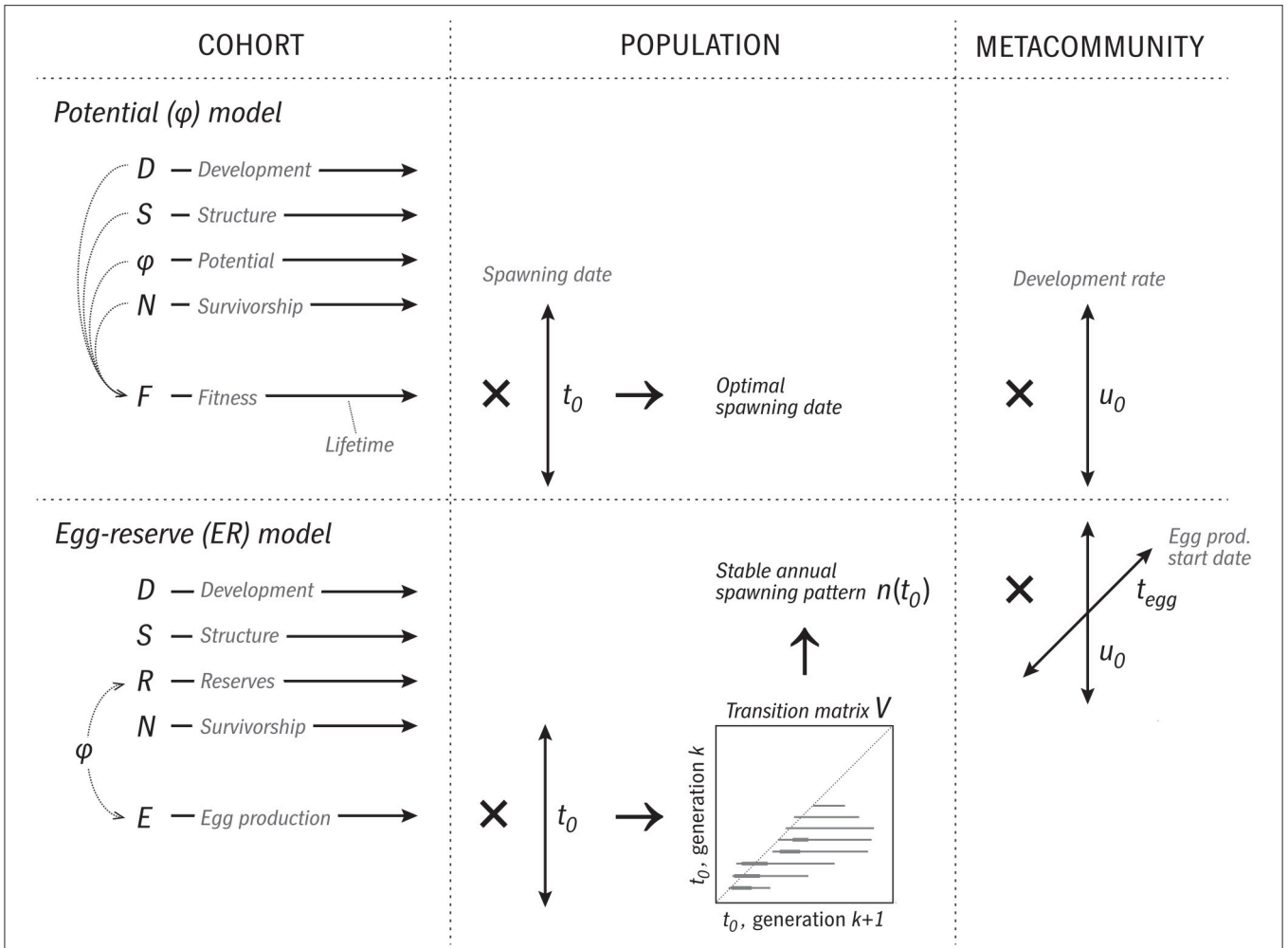


**FIGURE 2 | Overview of the logic and execution of the two versions of the Coltrane 1.0 model.** In the $\varphi$ version, a cohort is represented by four state variables ($D, S, \varphi, N$) integrated forward in time over the cohort's lifespan. These are used to calculate a time series of fitness $F$. Next, this calculation is repeated across a family of spawning dates $t_0$, and optimal and viable $t_0$ cases determined. This constitutes a population-level description, which then can be repeated across a range of trait values ($u_0$, relative development rate) to describe a size-variable metacommunity. In the ER version, at the cohort level, $\varphi$ is replaced by the state variable $R$ and a time series of egg production $E$. Across a family of $t_0$ cases, a transition-matrix method is used to determine a stable annual pattern of relative egg production $n(t_0)$, which is taken as the population-level prediction. A metacommunity is formed by varying two traits, $u_0$ and the date at which egg production begins $t_{egg}$.

the terms of analysis. In particular, we will describe model output in terms of trait correlations, optimality, and viability, but not in terms of absolute copepod biomass or abundance. Likewise, while some plankton models resolve the process of adaptation explicitly (Clark et al., 2013), we address it only in the indirect sense of mapping the viable and optimal regions of the strategy landscape. This approach is less mechanistic but also helpfully agnostic about whether adaptation in the copepods arises through individual plasticity, species composition shifts, or natural selection *per se*.

An environment in Coltrane 1.0 is defined by annual cycles of three variables, total concentration of phytoplankton/microzooplankton prey $P$, surface temperature $T_0$, and deep temperature $T_d$. At present, these annual cycles are assumed to be perfectly repeatable, so that a "viable" strategy can be defined as a set of traits that lead to annual egg production above the replacement rate, given $P$, $T_0$, and $T_d$ as functions of yearday $t$. The level of predation mortality (Section 2.2.4) might also be viewed as an environmental characteristic.

## 2.2. Time Evolution of One Cohort

### 2.2.1. Ontogenetic Development

Calanoid copepods have a determinate developmental sequence, comprising the embryonic period, six naupliiar stages (N1–6), five copepodid stages (C1–5), and adulthood (C6). Similar to Maps et al. (2012), conversions between relative developmental stage $D$ and the actual 13-stage sequence have been done using relative stage durations for *C. finmarchicus* from Campbell et al. (2001), which appear to be appropriate for other *Calanus* spp. with the proviso that C5 duration is particularly variable and strategy-dependent. Development in the model follows

$$\frac{dD}{dt} = u, \;\; D \leq 1 \tag{1}$$

where developmental rate $u$ is

$$u = a\, q_d\, \sigma\, u_0 \tag{2}$$

and

$$q_d \equiv Q_d^{T/10^\circ\mathrm{C}} \tag{3}$$

$$T = a\, T_0 + (1-a)\, T_d \tag{4}$$

$$\sigma \equiv \frac{P}{K_s + P} \tag{5}$$

All variables and parameters are defined in **Table 1**. Activity level $a$ is, in this version of the model, a two-state switch calculated at each time step, 1 during active feeding and 0 during diapause. The temperature-dependent factor $q_d$ describes a power-law response with a $Q_{10}$ of $Q_d$, where temperature is assumed to be $T_0$ during active feeding and $T_d$ during diapause. We use the $Q_{10}$ functional form for convenience: the differences between this and the leading alternatives (Beĕhrádek, Arrhenius: Forster et al., 2011; Record et al., 2012) appear to be small compared with interspecies differences in this study (Banas and Campbell, 2016). Prey saturation $\sigma$ is a simple Michaelis–Menten function with half-saturation $K_s$. The parameter $u_0$, the development rate corrected to 0°C, was found by Banas and Campbell (2016) to be the primary trait responsible for differences in adult body size among *Calanus* spp. and other calanoids >50 $\mu$g C adult size, although not at a broader scale of diversity. It represents the aspect of development-rate variation that we interpret to be a strategy choice as opposed to a physiological or thermodynamic constraint.

### 2.2.2. Energy Gain and Loss

The two energy stores $S$ (structure) and $\varphi$ (reserves/potential) follow

$$\frac{dS}{dt} = f_s G S \tag{6}$$

$$\frac{d\varphi}{dt} = (1-f_s) G S \tag{7}$$

where $G$ is net energy gain (ingestion minus metabolic losses). When net gain is positive, it is allocated between structure and potential according to the factor $f_s$, which commits net gain entirely to structure before a developmental point $D_s$, entirely to potential during adulthood, and to a combination of them in between:

$$f_s = \begin{cases} 1, & D < D_s \\ \frac{1-D}{1-D_s}, & D_s \le D \le 1 \\ 0, & D = 1 \end{cases} \tag{8}$$

When $G \le 0$, the deficit is taken entirely from reserves: $f_s = 0$.

Before the first feeding stage ($D < D_f$) we assume $G = 0$ for simplicity. After feeding begins,

$$G = r_a I - M \tag{9}$$

where ingestion $I$ and metabolic loss $M$ are given by

$$I = a\, \sigma\, q_g\, I_0\, S^{\theta-1} \tag{10}$$

$$M = a^\star\, r_m\, q_g\, I_0\, S^{\theta-1} \tag{11}$$

and $r_a$ is an assimilation efficiency. Ingestion follows a Kleiber's Law-like dependence on structural body mass $S$, with $\theta = 0.7$ (Kleiber, 1932; Saiz and Calbet, 2007). $I_0$ is specific ingestion rate at saturating prey concentration, $T = 0^\circ$C, and $S = 1$ $\mu$g C. This is modulated by the activity switch $a$ and prey saturation $\sigma$ as in Equation (2), and a power-law temperature response for growth

$$q_g \equiv Q_g^{T/10^\circ\mathrm{C}} \tag{12}$$

which is parallel to that for development ($q_d$) but with a different $Q_{10}$. $Q_{10}$ values have been found to vary among copepod species but Banas and Campbell (2016) argue that common values derived from a fit across community-level data are more appropriate for comparing species near their thermal optima. We use $Q_g = 2.5$ and $Q_d = 3.0$, as an approximation to the best-fit complex allometric curves reported by Forster et al. (2011).

Energy loss to metabolism $M$ follows the same temperature and size scalings. The factor $r_m$ is the ratio of metabolism to ingestion when prey is saturating. Unlike development and ingestion, which are assumed zero during diapause, $M$ during diapause is nonzero but reduced to a basal fraction $r_b \approx 1/4$ (Maps et al., 2014):

$$a^\star = r_b + (1 - r_b) a \tag{13}$$

Note that in this formalism, gross growth efficiency $\epsilon$ becomes

$$\epsilon = \frac{G}{I} = r_a - \frac{r_m}{\sigma} \tag{14}$$

when $a = 1$. We have set $r_m = 0.14$ such that $\epsilon = 0$ when $P = 1/4\, K_s$.

### 2.2.3. Starvation

Potential $\varphi$ is allowed to run modestly negative, to represent consumption of body structure during starvation conditions. A cohort is terminated by starvation if

$$\varphi < -r_{starv} S \tag{15}$$

where in this study $r_{starv} = 0.1$. A convenient numerical implementation of this scheme is to integrate $S$ implicitly so that it is guaranteed $> 0$, and to integrate $\varphi$ explicitly so that it is allowed to change sign, with no change of dynamics at $\varphi = 0$.

### 2.2.4. Predation Mortality

Predation mortality is assumed to have the same dependence on temperature and body size as ingestion, metabolism, and net gain (Hirst and Kiørboe, 2002). Survivorship $N$ is set to 1 initially and decreases according to

$$\frac{d(\ln N)}{dt} = -m \tag{16}$$

(it is convenient to calculate the numerical solution using $\ln N$ rather than $N$ as the state variable, since values become extremely small). The mortality rate $m$ is

$$m = a\, q_g\, S^{\theta-1}\, m_0 \tag{17}$$

**TABLE 1 | Parameter values and other symbols used in the manuscript.**

| Symbol | Definition | Value/Units | Source |
|---|---|---|---|
| **ENVIRONMENTAL FORCING** | | | |
| $P$ | Prey concentration | mg chl $m^{-3}$ | |
| $T_0$ | Surface temperature | °C | |
| $T_d$ | Deep temperature | °C | |
| $\delta t$ | Effective duration of prey availability (global testbed) | d | |
| $\delta t'$ | Width of $P$ window (global testbed) | d | |
| **STATE VARIABLES** | | | |
| $D$ | Relative developmental stage | | |
| $N$ | Survivorship | | |
| $R$ | Individual reserve biomass | $\mu$gC | |
| $S$ | Individual structural biomass | $\mu$gC | |
| $\varphi$ | Potential reserves and egg production | $\mu$gC | |
| **TRAITS AND FREE PARAMETERS** | | | |
| $D_{dia}$ | Stage at which diapause becomes possible | 0.49 | Stage C3 |
| $D_f$ | Stage of first feeding | 0.1 | Stage N3: Campbell et al., 2001 |
| $D_s$ | Stage at which lipid storage begins | 0.35 | Stage C1 |
| $I_0$ | Specific ingestion at $\sigma = 1$, $T = 0$°C, $S = 1$ $\mu$gC | 0.4 $d^{-1}$ | Banas and Campbell, 2016 |
| $K_s$ | Half-saturation for ingestion | See **Table 2** | |
| $m_0$ | Specific predation mortality at $T = 0$°C, $S = 1$ $\mu$gC | See **Table 2** | |
| $Q_d$ | $Q_{10}$ for development | 3.0 | Forster et al., 2011 |
| $Q_g$ | $Q_{10}$ for growth | 2.5 | Forster et al., 2011 |
| $r_a$ | Fraction of ingestion assimilated | 0.67 | |
| $r_b$ | Diapause metabolism relative to active metabolism | 0.25 | Maps et al., 2014 |
| $r_{ea}$ | Scaling constant for egg:adult size ratio | 0.013 | Kiørboe and Sabatini, 1995 |
| $r_m$ | Metabolism relative to prey-saturated ingestion | 0.14 | |
| $r_{starv}$ | Fraction of $S$ consumable under starvation conditions | 0.1 | |
| $r_\varphi^{max}$ | Upper limit on $\varphi/S$ used in diapause criterion | 1.5 | *C. hyperboreus*: Swalethorp et al., 2011 |
| $t_{egg}$ | Earliest possible date of egg production | See **Table 2** | |
| $t_0$ | Yearday of spawning | 0–365 | |
| $u_0$ | Development rate corrected to 0°C | See **Table 2** | |
| $\theta$ | Allometric exponent for vital rates | 0.7 | Saiz and Calbet, 2007 |
| $\theta_{ea}$ | Allometric exponent for egg:adult size ratio | 0.62 | Kiørboe and Sabatini, 1995 |
| **OTHER QUANTITIES** | | | |
| $a$ | Activity level | 0, 1 | |
| $a^\star$ | Variation of metabolism with $a$ | $r_b$, 1 | |
| $C_{dia}$ | Coefficient arising in the diapause criterion | | |
| $E$ | Total egg production | $\mu$gC $d^{-1}$ | |
| $E_{cap}$ | Capital egg production | $\mu$gC $d^{-1}$ | |
| $E_{inc}$ | Income egg production | $\mu$gC $d^{-1}$ | |
| $F$ | Egg fitness | | |
| $F_{1/2}, F_1, F_2$ | Maximum egg fitness at 1/2, 1, 2 generations per year | | |
| $f_s$ | Fraction of $G$ allocated to $S$ | | |
| $G$ | Net energy gain | $d^{-1}$ | |
| $I$ | Specific ingestion | $d^{-1}$ | |
| $M$ | Specific metabolism | $d^{-1}$ | |
| $m$ | Specific predation mortality | $d^{-1}$ | |
| $q_d$ | Temperature dependence of development | | |
| $q_g$ | Temperature dependence of growth | | |
| $u$ | Ontogenetic development rate | $d^{-1}$ | |
| $W_a$ | Adult body size | $\mu$gC | |
| $W_e$ | Egg biomass | $\mu$gC | |
| $\lambda$ | Population growth rate | $yr^{-1}$ | |
| $\sigma$ | Prey saturation | | |

such that that predation pressure relative to energy gain is encapsulated in a single parameter $m_0$. In practice $m_0$ is a tuning parameter but we can solve for the value that would lead to an approximate equilibrium between growth and mortality. The condition

$$\frac{1}{NS}\frac{d(NS)}{dt} = 0 \tag{18}$$

is equivalent, by Equations (6) and (16), to

$$m = f_s G \tag{19}$$

and with $a = 1$ this becomes

$$\frac{m_0}{I_0} = (r_a\sigma - r_m)f_s \tag{20}$$

Averaging $f_s$ over the maturation period $0 \leq D \leq 1$ with $D_s = 0.35$, and assuming $\sigma \approx 2/3$ on average for an organism that has aligned its development with the productive season, gives $m_0 \approx 0.2\ I_0$. This is the default level of predation in the model except where otherwise specified.

#### 2.2.5. Activity Level and Diapause

Modulation of activity level $a$ has been treated as simply as possible, using a "myopic" criterion that considers only the instantaneous energy budget, rather than an optimization over the annual routine or lifetime (Sainmont et al., 2015). Furthermore, we treat $a$ as a binary switch—diapause or full foraging activity—although intermediate overwintering states have been sometimes observed, e.g., *C. glacialis/marshallae* on the Eastern Bering Sea shelf in November (Campbell, personal communication). In the present model, we set $a = 0$ if $D > D_{dia}$ (the stage at which diapause first becomes possible) and the environment is such that total population energy gain

$$\frac{d}{dt}(\varphi + S)N = (GS)N \tag{21}$$

would be higher under diapause. We can derive an expression for the threshhold at which this occurs by maximizing population energy gain as a function of $a$. When $d/da$ of $GSN$ is positive, active foraging $a = 1$ is the optimal instantaneous strategy and when it is negative, $a = 0$ is optimal. The threshhold

$$\frac{d}{da}(GSN) = 0 \tag{22}$$

can be rearranged to give a critical prey-saturation level

$$\sigma_{crit} = \frac{r_m(1 - r_b)}{r_a} + \frac{C_{dia}}{r_a}\frac{m_0}{I_0} \tag{23}$$

where $C_{dia} = 1 + \varphi/S$. The first term in Equation (23) can be derived more simply by setting $dG/da = 0$, a criterion based on ingestion and metabolism alone. The second term adjusts this criterion by discouraging foraging at marginal prey concentrations when predation is high. A third, temperature-dependent term has been neglected. The second, mortality-dependent term tends to produce unrealistic, rapid oscillations in which the copepods briefly "top up" on prey and then hide in a brief "diapause" to burn them. It is unclear whether this model behavior is a mathematical artifact—a limitation of combining actual lipid reserves and potential egg production into a single state variable—or whether it suggests that under some conditions the optimal level of foraging is intermediate between full activity and none. Incorporating a more mechanistic treatment of optimal foraging (Visser and Fiksen, 2013) and allowing $a$ to vary continuously would address this. In this study, we have eliminated the phenomenon by approximating $C_{dia}$ as

$$C_{dia} = \max\left[0,\ 1 + \min\left(r_\varphi^{max}, \frac{\varphi}{S}\right)\right] \tag{24}$$

where $r_\varphi^{max} = 1.5$.

### 2.3. Eggs and Potential Eggs

The evolution equations above Equations (1), (6), (7), (16) specify the development of one cohort in the $\varphi$ model. If this model is elaborated with an explicit scheme for calculating total egg production over time $E(t)$, then it is possible to define $R(t)$, individual storage/reserve biomass, and interpret $R$ as a state variable and $\varphi$ as a derived quantity. The relationship between the two is

$$\frac{dR}{dt} = (1 - f_s)GS - E \tag{25}$$

$$\varphi(t) = R(t) + \int_{t_0}^{t} E(t')\ dt' \tag{26}$$

Thus, $\varphi$ tracks the reserves that an animal would have remaining if it had not previously started egg production. This is a useful metric for optimizing reproductive timing, as we will show (Section 2.4).

Any explicit expression for $E(t)$ allows Equation (25) to replace Equation (7). In one model experiment below (Section 3.4), we use the following scheme: $E(t)$ is the sum of income egg production $E_{inc}$ and capital egg production $E_{cap}$, which are 0 until maturity is reached ($D = 1$) and an additional timing threshhold has been passed ($t > t_{egg}$). Past those threshholds, they are calculated as

$$\begin{aligned} E_{inc} &= G, & G > 0 \\ E_{cap} &= E_{max} - E_{inc}, & D > 0 \end{aligned} \tag{27}$$

where $E_{max}$ is a maximum egg production rate which we assume to be equal to food-saturated assimilation:

$$E_{max} = r_a\ q_g\ I_0\ S^\theta \tag{28}$$

Thus, the trait $t_{egg}$ determines whether egg production begins immediately upon maturation (if $t_{egg}$ is prior to the date on which $D$ reaches 1) or after some additional delay. Instead of $t_{egg}$, expressed in terms of calendar day, one could introduce the same

timing freedom through a trait linked to light, an ontogenetic clock that continues past $D = 1$, or a more subtle physiological scheme. However, since we run a complete spectrum of trait values in each environmental case, it is not important to the results how the delay is formulated, provided we only compare model output, rather than actual trait values, across cases.

## 2.4. Population-Level Response

A population-level simulation (**Figure 2**) consists of integrating either the $\varphi$ model (Equations 1, 6, 7, 16) or ER model (Equations 1, 6, 16, 25) for a full annual cycle of spawning dates $t_0$, and then identifying optimal and viable values of $t_0$ in terms of the egg fitness $F$, future egg production per egg (Varpe et al., 2007). Calculating a time series of $F$ in the $\varphi$ model requires an estimate of individual egg biomass $W_e$ in order to convert $\varphi(t)$ from carbon units into a number of eggs, and a similar issue arises in the ER population model. Thus, a digression on the determination of $W_e$ is required.

### 2.4.1. Egg and Adult Size

The problem of estimating $W_e$ can be replaced by the problem of estimating adult size $W_a$ using the empirical relationship for broadcast spawners determined by Kiørboe and Sabatini (1995):

$$\ln W_e \approx \ln r_{ea} + \theta_{ea} \ln W_a \tag{29}$$

where $r_{ea} = 0.013$, $\theta_{ea} = 0.62$ (In the ER model, $W_a \equiv S + R$ at $D = 1$, but in the $\varphi$ model we approximate it as $S$ alone for simplicity). Adult size itself is an important trait for the model to predict, but the controls on it are rather buried in the model formulation above. Banas and Campbell (2016) describe a theory relating body size to the ratio of development rate to growth rate based on a review of laboratory data for copepods with adult body sizes 0.3–2000 $\mu$gC. In our notation, their model can be derived as follows: if we approximate Equations (6), (7) in terms of a single biomass variable as

$$\frac{dW}{dt} = \epsilon' \, q_g \, I_0 \, W^\theta, \;\; D \geq D_f \tag{30}$$

then integrating from spawning to maturation gives

$$\frac{1}{1-\theta} W^{1-\theta} \Big|_{D=0}^{D=1} = (1 - D_f) \, \epsilon' \, q_g \, I_0 \, \frac{1}{u} \tag{31}$$

since $u$ is the reciprocal of the total development time. Growth rate has been written in terms of $I_0$ and an effective growth efficiency over the development period $\epsilon'$. If we assume that egg biomass $W_e = W|_{D=0}$ is much smaller than $W_a = W|_{D=1}$, then combining Equation (31) with Equation (2) gives

$$W_a \approx \left[ (1-\theta)\,(1-D_f)\;\epsilon' \left(\frac{Q_g}{Q_d}\right)^{T/10^\circ\mathrm{C}} \frac{I_0}{u_0} \right]^{\frac{1}{1-\theta}} \tag{32}$$

Properly speaking, both $\epsilon'$ and $T$ in Equation (32) are functions of $t_0$ since they depend on the alignment of the development period with the annual cycle. Since we are trying to use Equations (29), (32) to optimize $t_0$, we have a circular problem. Record et al. (2013) derive an expression similar to Equation (32) and apply it iteratively because of this circularity. Some applications of Coltrane might require the same level of accuracy, but in the present study we take the expedient approach of simply assuming that $T$ is the annual mean of $T_0$ and that $\epsilon' \approx 1/3$: i.e., that after $t_0$ is optimized, some diapause/spawning strategy will emerge that aligns the maturation period moderately well with a period of high prey availability. This assumption eliminates the need to run the model before estimating $W_e$ via Equations (29), (32).

### 2.4.2. Optimal Timing in the $\varphi$ Model

With a method for approximating $W_e$ in hand, we can define egg fitness $F$ as a function of $\varphi$. If a cohort spawned on $t_0$ were to convert all of its accumulated free scope $\varphi$—all net energy gain beyond that required to build an adult body structure—into eggs on a single day $t_1$, the eggs produced per starting egg would be

$$F(t_0 \rightarrow t_1) = \frac{\varphi(t_1)}{W_e} N(t_1) \tag{33}$$

This expression condenses one copepod generation into a *mapping* $F$ similar to the "circle map" of Gurney et al. (1992). Once the ODE model has been run for a family of $t_0$ cases, this mapping can be used to quickly identify optimal life cycles of any length. The optimal one-generation-per-year strategy is the $t_0$ that maximizes $F_1 = F(t_0 \rightarrow t_0 + 365)$. The optimal one-generation-per-two-years strategy has $t_0$ that maximizes $F_{1/2} = F(t_0 \rightarrow t_0 + 2{\cdot}365)$. The optimal two-generation-per-year strategy has spawning dates $t_0$, $t_1$ that maximize the product $F_2 = F(t_0 \rightarrow t_1) \cdot F(t_1 \rightarrow t_0 + 365)$; and so on. A viable strategy is a combination of spawning dates and model parameters that give $F \geq 1$.

### 2.4.3. Optimal Timing in the ER Model

In reality, of course, copepods are not free to physically store indefinite amounts of reserves within their bodies and then instantaneously convert them into eggs when the timing is optimal. If a scheme for calculating egg production over time $E(t)$ is added to the model as in Section 2.3, then the per-generation mapping represented by $F$ takes a different form. First, for each cohort, we use the assumption that the environmental annual cycle repeats indefinitely to convert the time series of $EN$—egg production discounted by survivorship—to a function of yearday, by adding the value on days $365{+}i$, $2{\cdot}365{+}i$, ... to the value on day $i$ (in practice we discretize the year into 5 d segments rather than yeardays *per se*). Next, we construct a matrix $V$ whose rows are the year-long time series of $EN/W_e$ for each spawning date $t_0$. $V$ is thus a *transition matrix* with spawning date in generation $k$ running down rows and spawning date in generation $k{+}1$ running across columns. Given a discrete annual cycle $n_k$ of eggs spawned in generation $k$, one can calculate the expected annual cycle of egg production in the next generation as $n_{k+1} = V \cdot n_k$, where $n$ is given as a column vector.

The first eigenvector of $V$ gives a seasonal pattern of egg production that is stable in shape, with the corresponding

eigenvalue λ giving one plus the population growth rate per generation:

$$n_{k+1}(t) = V \cdot n_k(t) = \lambda n_k(t) \tag{34}$$

$$\frac{n_{k+1}(t) - n_k(t)}{1 \text{ generation}} \approx \lambda - 1 \tag{35}$$

A strict criterion for strategy viability would then be $\lambda \geq 1$, although this criterion is unhelpfully sensitive to predation mortality. A more robust criterion (which we use in Section 3.4 below) is to consider a strategy viable if it yields lifetime egg production above the replacement rate: if $E(t_0; t)$ and $N(t_0; t)$ are the time series of egg production and survivorship for a cohort spawned on $t_0$, and $n(t_0)$ is a normalized annual cycle of egg production,

$$\int_0^{365} \int_0^{\infty} n(t_0) \frac{E(t_0; t) N(t_0; t)}{W_e} \, dt \, dt_0 \geq 1 \tag{36}$$

Thus, in the ER version of the model, as in the $\varphi$ version, we have an efficient method that describes the long-term viability of a trait combination under a stable annual cycle, along with the optimal spawning timing associated with those traits in that environment; and these methods only require us to explicitly simulate one generation.

## 2.5. Assembling Communities

Community-level predictions in Coltrane take the form of bounds on combinations of traits that lead to viable populations in a given environment (**Figure 2**). There are many copepod traits represented in the model that one might consider to be axes of diversity or degrees of freedom in life strategy: $u_0$, $I_0$, $\theta$, $D_s$, $K_s$, $W_e/W_a$, and even $m_0$ to the extent that predation pressure is a function of behavior (Visser et al., 2008). Record et al. (2013) allowed five traits to vary among competitors in their copepod community model. We have taken a minimalist approach, where in the $\varphi$ model we allow only one degree of freedom: variation in $u_0$ from 0.005 to 0.01 $d^{-1}$. Banas and Campbell (2016) showed from a review of lab studies that $u_0$ variations appear to be the primary mode of variation in adult size among large calanoids ($W_a > 50$ $\mu$gC) including *Calanus* and *Neocalanus* spp., with slower development leading to larger adult sizes. That study also suggests that variation in $I_0$ is responsible for copepod size diversity on a broader size or taxonomic scale (e.g., between *Calanus* and small cyclopoids like *Oithona*). However, variation in $I_0$ (energy gain from foraging) probably only makes sense as part of a tradeoff with predation risk or egg survivorship (Kiørboe and Sabatini, 1995) and we have left the formulation of that tradeoff for future work. We therefore expect Coltrane 1.0 to generate analogs for large and small *Calanus* spp. (~100–1000 $\mu$gC adult size) but not analogs for *Oithona* spp. or even small calanoids like *Pseudocalanus* or *Acartia*.

Choices regarding reproductive strategy require another degree of freedom. In the $\varphi$ model, this does not require additional parameters, because the difference between, e.g., capital spawning in winter and income spawning in spring is simply a matter of the time $t$ at which $F$ is evaluated in postprocessing: each model run effectively includes all timing possibilities (Equation 33). In the ER model, however, diversity in reproductive timing must be made explicit. Under the simple scheme for egg production specified above (Section 2.3), this takes the form of running a family of cases varying $t_{egg}$ for each $t_0$ and $u_0$.

## 2.6. Model Experiments

This study comprises three complementary experiments (**Table 2**). The first of these is an idealized global testbed which addresses broad *biogeographic* patterns. The second is a testbed representing the Eastern Bering Sea shelf, which addresses *time-variability* in one population in one environment. The last is a testbed representing Disko Bay, West Greenland, which addresses *trait relationships along the size spectrum* in detail. The first two are evaluated entirely in terms of the $\varphi$ model, while in the Disko Bay case we use the ER model to allow more specific comparisons with observations.

The global testbed consists of a family of idealized environments in which surface temperature $T_0$ is held constant, and prey availability is a Gaussian window of width $\delta t'$ centered on yearday 365/2:

$$P(t) = (10 \text{ mg chl m}^{-3}) \exp\left[ - \left( \frac{t - \frac{365}{2}}{\delta t'} \right)^2 \right] \tag{37}$$

We compare environmental cases in terms of $T_0$ and an effective season length

$$\delta t = \int_0^{365 \text{ d}} \sigma \, dt \tag{38}$$

which rescales the $\delta t'$ cases in terms of the equivalent number of days of saturating prey per year. We assume that deep, overwintering temperature $T_d = 0.4 \, T_0$. The ratio 0.4 matches results of a regression between mean temperature at 0 and 1000 m in the Atlantic between 20 and 90°N, or 0 and 500 m in the Northeast Pacific over the same latitudes (World Ocean Atlas 2013: http://www.nodc.noaa.gov/OC5/woa13/). Over the same data compilation, the mean seasonal range in temperature is approximately 5°C at the surface (and approximately zero at 500–1000 m); an alternate formulation of the testbed that models $T_0$ as an annual sinusoid with this range gives results that are somewhat noisier but heuristically very similar to those shown in Section 3.2 below.

The Bering Sea testbed considers interannual variation in temperature, ice cover, and the effect of ice cover on in-ice and pelagic phytoplankton production (Stabeno et al., 2012b; Sigler et al., 2014; Banas et al., 2016). Variation between warm, low-ice years and cold, high-ice years has previously been linked to the relative abundance of large zooplankton including *C. glacialis/marshallae* (Eisner et al., 2014), and we test Coltrane predictions against 8 years of *C. glacialis/marshallae* observations from the BASIS program. Seasonal cycles of $T_0$, $T_d$, and $P$ are parameterized using empirical relationships between ice and phytoplankton from Sigler et al. (2014) and a 42-year physical

**TABLE 2 | Setup of model experiments.**

| Experiment | Environmental forcing | Variable traits | $K_s$ | $m_0$ | Model |
|---|---|---|---|---|---|
| Global | Surface, deep temperatures constant; Gaussian window of prey availability | $u_0 = 0.005 - 0.01$ d$^{-1}$ | 1 mg chl m$^{-3}$ | 0.08 d$^{-1}$ | $\varphi$ |
| Bering | Family of seasonal cycles on the middle shelf: see Appendix in Supplementary Material | $u_0 = 0.007$ d$^{-1}$ | 3 | 0.08 | $\varphi$ |
| Disko | One seasonal cycle (1996–97): see Appendix in Supplementary Material | $u_0 = 0.005 - 0.01$ d$^{-1}$, $t_{egg} = 0 - 1095$ | 1 | 0.06 | ER |

*All other parameters are as in* ***Table 1****.*

hindcast using BESTMAS (Bering Ecosystem Study Ice-ocean Modeling and Assimilation System: Zhang et al., 2010; Banas et al., 2016). Details are given in the Appendix in Supplementary Material .

The Disko Bay testbed represents one seasonal cycle of temperature and phytoplankton and microzooplankton prey, based on the 1996–1997 time series described by Madsen et al. (2001). We use this particular dataset not primarily as a guide to the current or future state of Disko Bay but rather as a specific circumstance in which the life-history patterns of three coexisting *Calanus* spp. (*C. finmarchicus*, *C. glacialis*, *C. hyperboreus*) were documented (Madsen et al., 2001). Details are given in Section 3.4 and the Appendix in Supplementary Material.

# 3. RESULTS

## 3.1. An Example Population

One case from the global experiment with $u_0 = 0.007$ d$^{-1}$, $T_0 = 1$°C, and $\delta t = 135$ is shown in detail in **Figure 3** to illustrate the analysis method described in Section 2.4.2. In this case, out of cohorts spawned over the full first year, only those spawned in spring reached adulthood without starving (**Figure 3B**, blue–green lines; non-viable cohorts not shown). The fitness function $F$ (Equation 33) declines during winter diapause and rises during the following summer when prey are available. There is no equivalent peak during the third summer, indicating that by this time cumulative predation mortality is so high that there is no net advantage to continuing to forage before spawning.

The maximum value of $F$ for most cohorts (*, **Figure 3C**) comes at ∼1.5 year into the simulation, at the peak in prey availability following maturation. This point in the annual cycle, however, does not fall within the window of spawning dates at which maturation is possible (compare year 2 in **Figure 3C** with year 1 in **Figure 3B**), and thus is an example of "internal life history mismatch" (Varpe et al., 2007), the common situation in which the spawning timing that maximizes egg production by the parent is not optimal for the offspring. The long-term egg fitness corresponding to stable 1-year and 2-year cycles is marked for each cohort (**Figure 3C**, red, orange circles). Some but not all of the cohorts that reach maturity are able to achieve $F >$ 1, egg production above the replacement rate, in these cyclical solutions (solid circles). The best 1-year and 2-year strategies achieve similar maximum fitness values (red vs. orange solid dots), although they require slightly different seasonal timing.

Note that although $F$ can be described as the egg-fitness function, the lines in **Figure 3C**—time series of $F$ for particular spawning dates $t_0$—are not the same as the seasonal curve of egg fitness that results from a backwards-in-time dynamic optimization (e.g., Figure 6F in Varpe et al., 2007). Rather, each curve of $F(t_0; t)$ in our approach gives a series of possible values for egg fitness at $t_0$ depending on what future strategy is taken. The forwards and backwards calculations converge (at least qualitatively) once the internal life-history mismatch is resolved and a stable long-term cycle is found (red and orange circles, **Figure 3C**). As expected (Varpe et al., 2007), these stable values of egg fitness peak, for each generation length, somewhat prior to the bloom maximum (**Figure 3C**).

## 3.2. Global Behavior

In the global experiment, populations like that shown in **Figure 3** were run for a spectrum of $u_0$ values, across combinations of $T_0$ and $\delta t$ from −2 to 16°C and 0 to 310 d (the latter corresponding to $\delta t'$ from 0 to 150 d). Across these cases, at a given $u_0$, the model predicts a log-linear relationship between adult size and temperature, which is not much perturbed by variation in prey availability (**Figure 4**). The slope of this relationship is equivalent to a $Q_{10}$ of 1.8–2.0, consistent with that predicted by Equation (32):

$$\left(\frac{Q_d}{Q_g}\right)^{\frac{1}{1-\vartheta}} \approx 1.84 \tag{39}$$

Field observations of size in relation to temperature in *C. finmarchicus* and *C. helgolandicus* across the North Atlantic show a similar relationship ($Q_{10} = 1.65$, Wilson et al., 2015, with prosome length converted to carbon weight based on Runge et al., 2006). Somewhat surprisingly, even wide variation in prey conditions (clusters of gray dots, **Figure 4**) has only minor effects on this slope.

The intercept of the size-temperature relationship depends on $u_0$ (**Figure 4**), with $u_0 = 0.005$–$0.01$ d$^{-1}$ corresponding to the

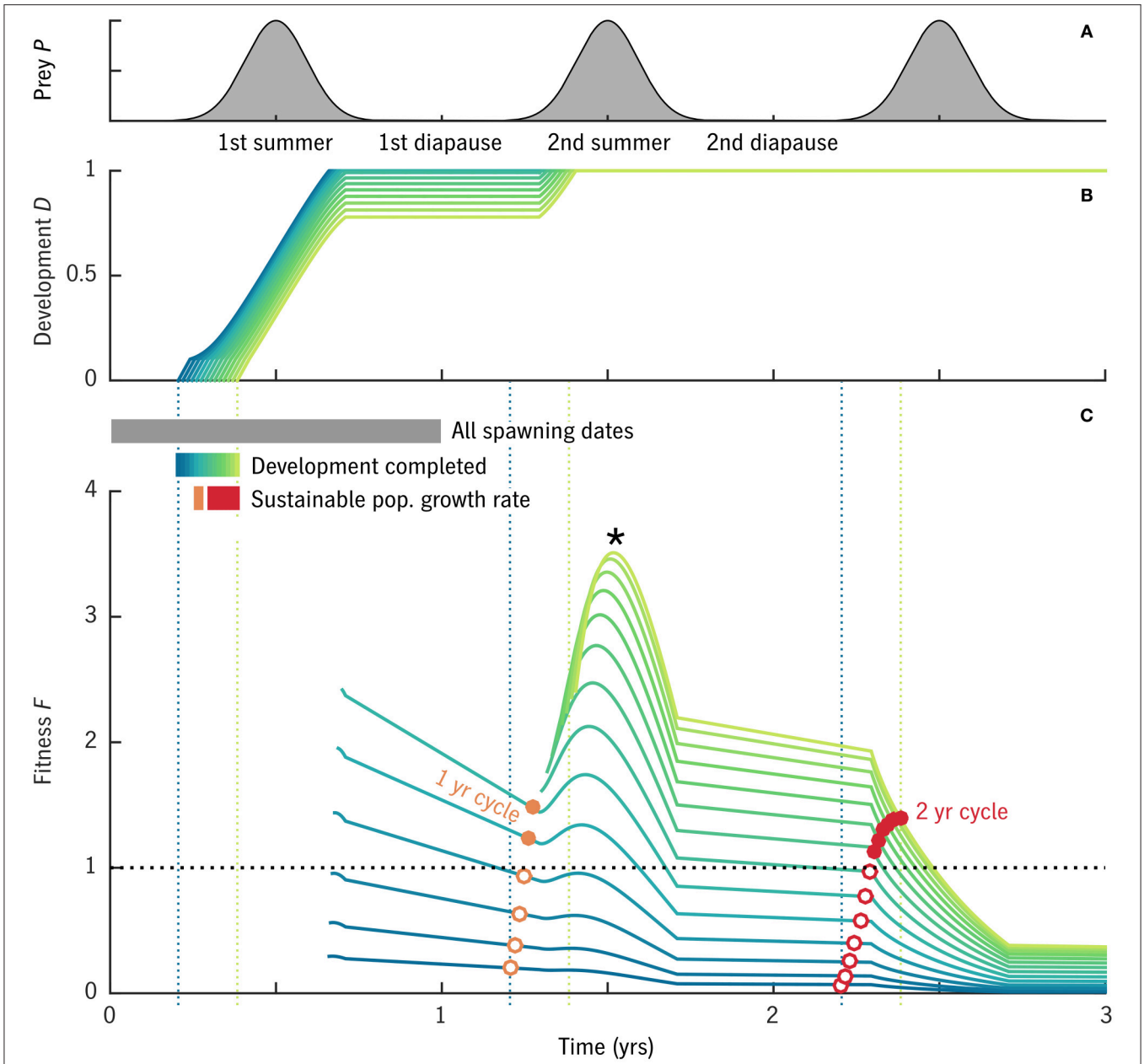


**FIGURE 3 | Results of an example model case with $u_0 = 0.007$ d$^{-1}$, $T_0 = 1$°C, and $\delta t = 135$.** Cohorts were simulated beginning from all spawning dates in year 1. **(A)** Prey availability over time. **(B)** Developmental stage $D$ for cohorts that reach maturity ($D = 1$) without starving: the blue–yellow color scale corresponds to spawning dates $t_0$ over the viable period from pre-bloom to bloom maximum. **(C)** Fitness $F$ over time for the cohorts shown in **(B)**, i.e., the expected value (eggs egg$^{-1}$) of converting all free scope $\varphi$ to eggs on a given date. Curves of $F$ begin when maturity is reached ($D = 1$) and egg production becomes possible. Open and solid circles mark the value of $F$ on the 1-year (orange) and 2-year (red) anniversaries of the original spawning date. Solid circles mark cohorts that achieve a fitness above the replacement rate.

range of adult size from *C. finmarchicus* to *C. hyperboreus* at the cold end of the temperature spectrum (Disko Bay, ~ 0°C: Swalethorp et al., 2011). It is not always fair, however, to associate a particular $u_0$ value with a particular species over the full range of temperatures included. As Banas and Campbell (2016) discuss further, the temperature response of an individual species is often dome-shaped, a window of habitat tolerance (Møller et al., 2012; Alcaraz et al., 2014), whereas Coltrane 1.0 uses the monotonic, power-law response observable at the community level (Forster et al., 2011). *C. finmarchicus*, for example, is fit well by $u_0 = 0.007$ d$^{-1}$ at higher temperatures (4–12°C), whereas near 0°C in Disko Bay, it has been observed to be considerably smaller than extrapolation along the $u_0 = 0.007$ d$^{-1}$ power law would predict. Past studies have also found *C. finmarchicus* growth and ingestion

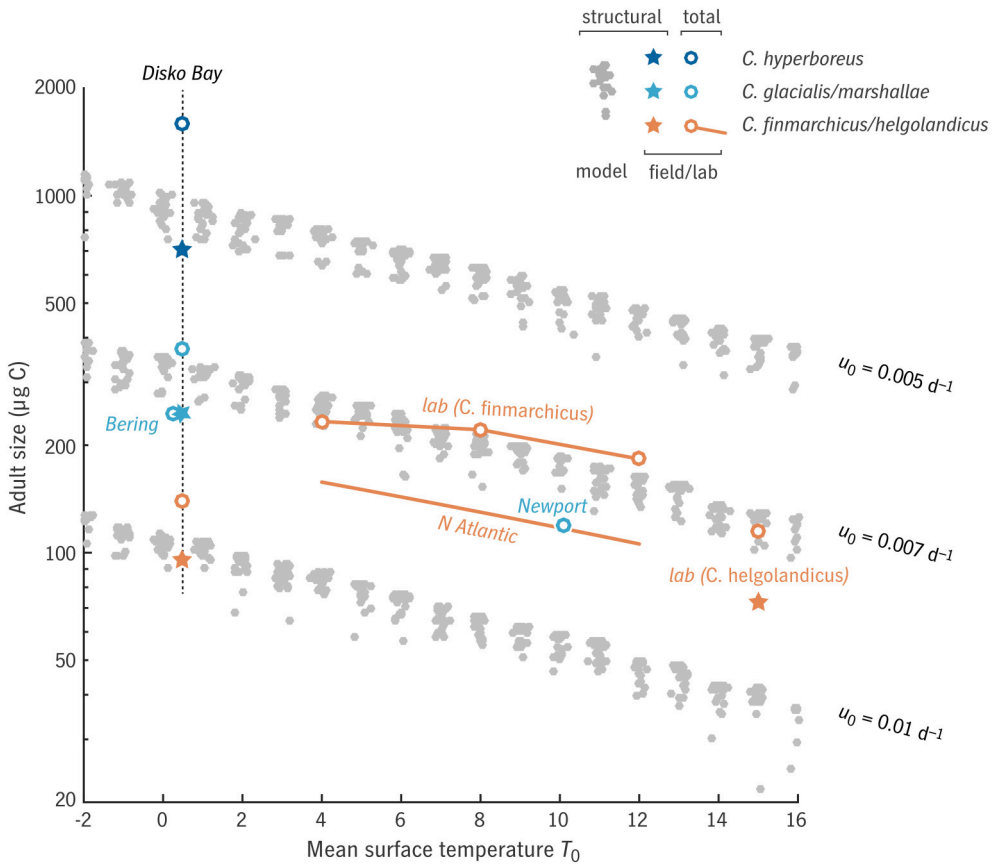


**FIGURE 4 | Relationship between adult size $W_a$ and mean surface temperature $T_0$ in the "global" model experiment, for three values of relative development rate $u_0$, in comparison with observations (Peterson, 1986; Swalethorp et al., 2011; Wilson et al., 2015; Campbell et al., in press) and laboratory results (Campbell et al., 2001; Rey-Rassat et al., 2002).** Model results (gray dots) represent structural biomass $S$, as do observations marked with a ⋆; observations marked with a ○ represent total biomass $R + S$. Clusters of gray dots indicate families of model cases varying productive season length (horizontal axis in **Figure 5**).

to be suppressed at low temperatures, i.e., to show a very high $Q_{10}$ compared with the community-level value (Campbell et al., 2001; Møller et al., 2012).

With this caveat on the interpretation of $u_0$, we can observe a sensible gradation in life strategy along the $u_0$ axis (**Figure 5**). From $u_0 = 0.01$ d$^{-1}$ (*C. finmarchicus*-like at 0°C) to $u_0 = 0.005$ d$^{-1}$ (*C. hyperboreus*-like), the environmental window in which multi-year life cycles are viable ($F_{1/2} \geq 1$) expands dramatically. This window overlaps significantly with the window of viability for 1-year life cycles ($F_1 \geq 1$; **Figure 5**, black vs. gray contours). In all $u_0$ cases, there is a non-monotonic pattern in maximum fitness as a function of either temperature or prey (**Figure 5**, color contours), as environments align and misalign with integer numbers of generations per year or years per generation.

The overall gradient from high to moderate $F$ with increasing temperature (**Figure 5**) is largely an artifact of displaying $F$ normalized to generation as opposed to per calendar year. In general, these results should not be taken as a quantitative prediction of annual production rates: the linear mortality closure that simplifies the analysis also omits the role of density dependence in stabilizing growth rates. Accordingly, in what follows, we consider only whether $F$ in a given circumstance exceeds replacement rate, not whether it exceeds it modestly or dramatically.

The number of generations per year in the timing strategy that optimizes $F$ for each $(T_0, \delta t)$ habitat combination is shown in **Figure 6** for $u_0 = 0.007$ d$^{-1}$. This $u_0$ value corresponds in adult size to Arctic *C. glacialis* and temperate *C. marshallae* populations in the Pacific (**Figure 4**), species which coexist and are nearly indistinguishable in the Bering Sea. In the lowest-prey conditions, no timing strategy is found to be viable. As prey and temperature increase, the model predicts bands proceeding monotonically from multiple years per generation to multiple generations per year. Validating these model predictions requires parameterizing places (in terms of $T_0$ and $\delta t$) in addition to parameterizing their inhabitants, and thus the meaning of either success of failure is ambiguous. Still, we can observe the following. Ice Station Sheba in the high Pacific Arctic (**Figure 1**) falls in the non-viable regime (**Figure 6**), consistent with the conclusion of

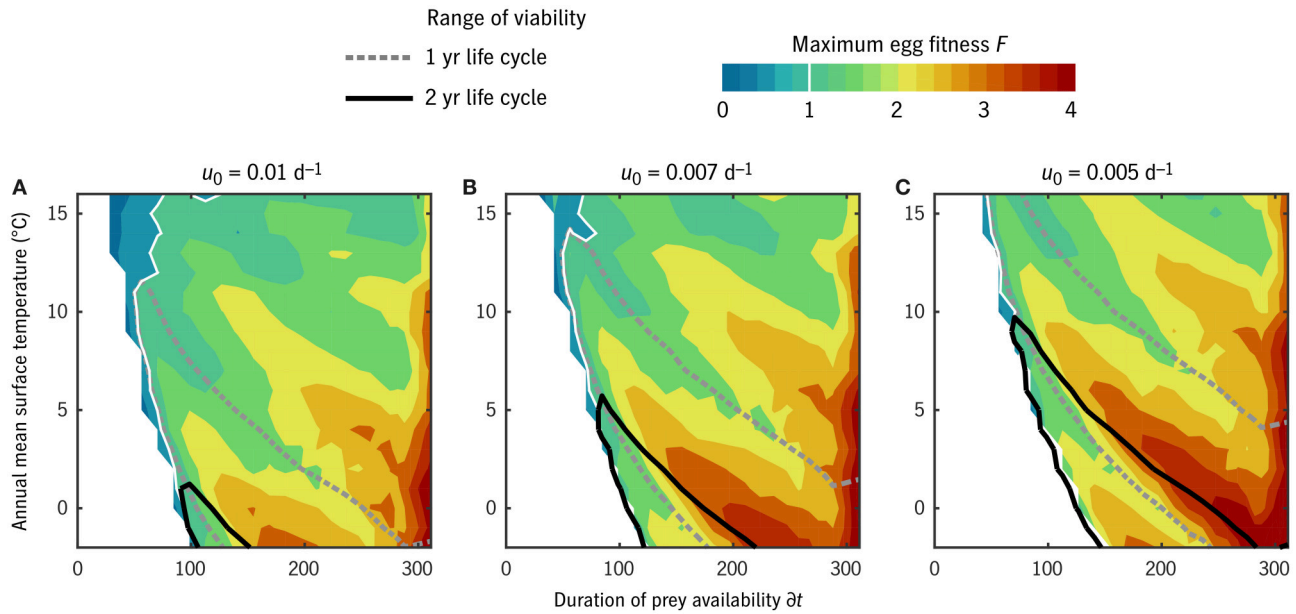


**FIGURE 5 | Maximum egg fitness (eggs per starting egg per generation) across all combinations of temperature and duration of prey availability in the "global" experiment.** Unfilled contour lines give the environmental range over which 1-year (gray, dotted) and 2-year (black, solid) life cycles are viable. The white regions at low prey availability indicate environments in which no timing strategy exists that allows successful maturation. **(A–C)** Give results for three values of $u_0$ corresponding to the families of cases shown in **Figure 4**.

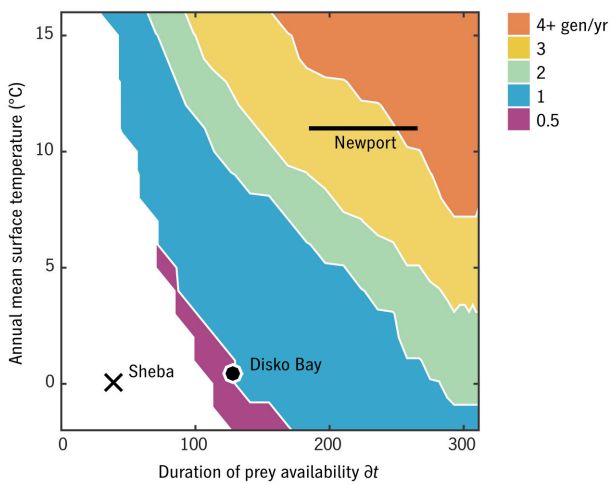


**FIGURE 6 | Generations per year of the optimal strategy in each environmental combination for relative development rate $u_0$ = 0.007 d$^{-1}$ (*C. glacialis/marshallae* analogs).** Ice Station Sheba, Disko Bay, and Newport (**Figure 1**) have been placed approximately for comparison.

Ashjian et al. (2003) that *Calanus* spp. are unable to complete their life cycle there. Disko Bay falls on the boundary of 1- and 2-year generation lengths, consistent with observations of *C. glacialis* there (Madsen et al., 2001). At Newport, Oregon, near the southern end of the range of *C. marshallae*, the model predicts multiple generations per year, consistent with observations by Peterson (1979).

## 3.3. A High-Latitude Habitat Limit in Detail: The Eastern Bering Sea

These idealized experiments (**Figures 5**, **6**) suggest that very short productive seasons place a hard limit on the viability of *Calanus* spp., regardless of size, temperature, generation length, or match/mismatch considerations (although these factors affect where exactly the limit falls). A decade of observations in the Eastern Bering Sea provide a unique opportunity to resolve this viability limit with greater precision. This analysis takes advantage of the natural variability on the Southeastern Bering Sea shelf described by the "oscillating control hypothesis" of Hunt et al. (2002, 2011): in warm, low-ice years, the spring bloom in this region is late (∼ yearday 150; Sigler et al., 2014) and the abundance of large crustacean zooplankton including *C. glacialis/marshallae* is very low, while in colder years with greater ice cover, the pelagic spring bloom is earlier, ice algae are present in late winter, and large crustacean zooplankton are much more abundant. The task of replicating these observations serves to test the Coltrane parameterization, and situating them within a complete spectrum of temperature/ice cover cases also allows the model to provide some insight into mechanisms.

Mean surface temperature $\overline{T_0}$ was used to index annual cycles of surface and bottom temperature on the Eastern Bering Sea middle shelf (Appendix in Supplementary Material; insets in **Figure 7**). Date of ice retreat $t_{ice}$ was likewise used to index phytoplankton availability over each calendar year (Appendix in Supplementary Material; insets in **Figure 7**). Coltrane was run for each ($\overline{T_0}$, $t_{ice}$) combination with $u_0$ = 0.007 d$^{-1}$, thus consistent with **Figure 6** except for the more refined treatment of

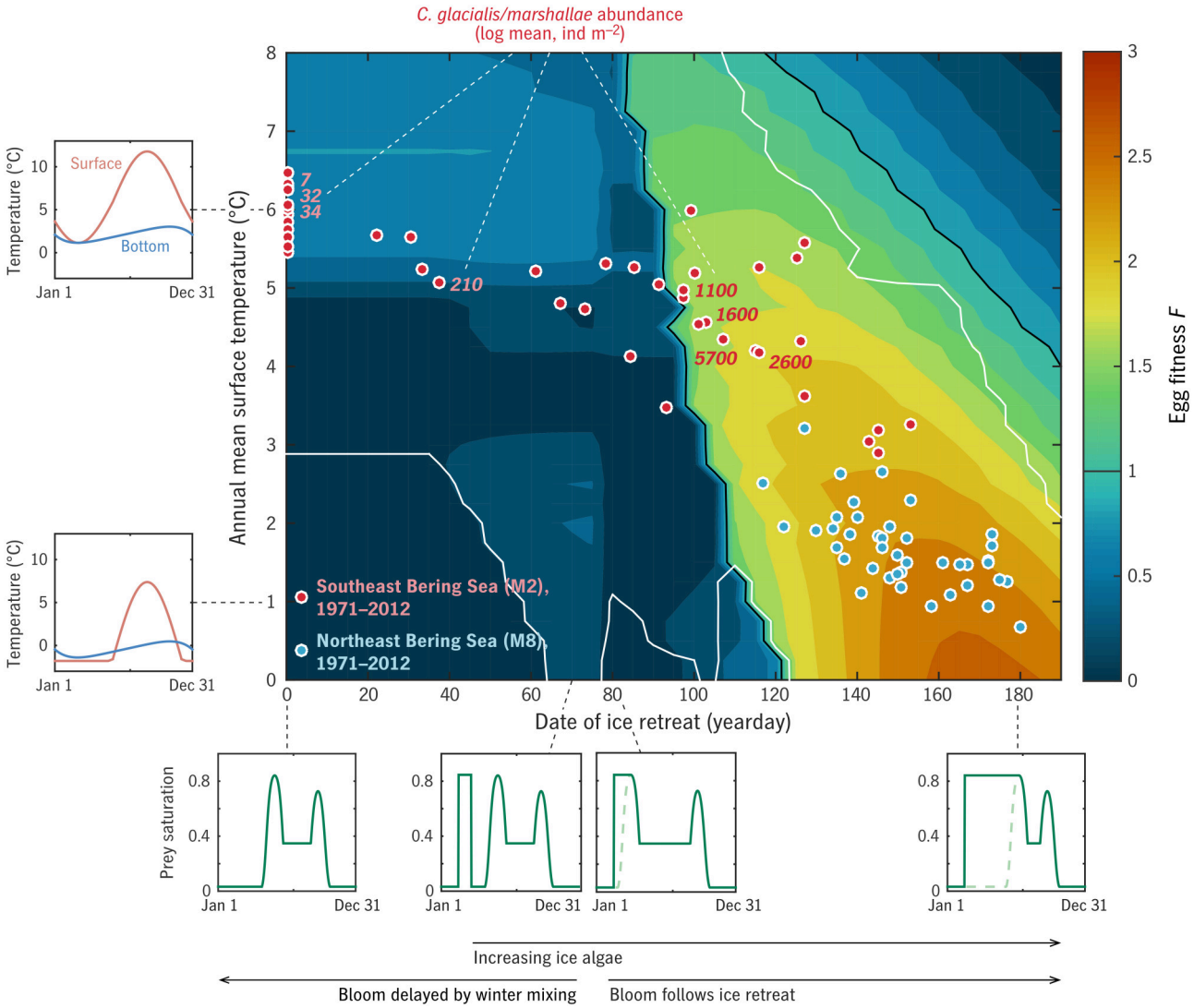


**FIGURE 7 | Results of the "Bering" experiment.** Color contours give the predicted egg fitness of a *C. glacialis/marshallae* analog under combinations of ice retreat timing (assumed to control spring bloom timing: Appendix in Supplementary Material) and temperature. Examples of the annual cycles of prey availability *P* and surface and bottom temperature $T_0$, $T_d$ are given at left and bottom. Dots locate years 1971–2012 in this timing/temperature parameter space, for the northern (blue) and southern (red) middle shelf. Numbers beside red dots give the measured summer abundance of *C. glacialis/marshallae* on the southern shelf across years. White contours give the bounds of the central region within which Coltrane predicts one generation per year to be the optimal generation length.

environmental forcing, and an adjustment to $K_s$ to match results of Bering Sea feeding experiments (Campbell et al., in press). The maximum egg fitness *F* for a one-generation-per-year strategy is shown as a function of $\overline{T_0}$ and $t_{ice}$ in the main panel of **Figure 7**. Coltrane predicts that one generation per year is the optimal life cycle length everywhere in this parameter space except for the cold/ice-free and warm/high-ice-cover extremes (white contours), combinations which do not occur anywhere in a model hindcast of middle-shelf conditions back to 1971 (**Figure 7**, red and blue dots).

Late summer measurements of *C. glacialis/marshallae* abundance (individuals $m^{-2}$), averaged over the middle/outer shelf south of 60°N, are shown in **Figure 7** for 2003–2010 ($n$ = 364 over the 8 years; Eisner et al., 2014, 2015). Both these observations and the predicted maximum *F* from Coltrane show a dramatic contrast between the warm years of 2003–05 ($t_{ice}$ = 0) and the cold years of 2007–2010 ($t_{ice}$ = 100–130), with the transitional year 2006 harder to interpret. Eisner et al. (2014) found that there was less contrast between cold year/warm year abundance patterns on the northern middle/outer shelf, consistent with the model prediction that all hindcast years on the northern shelf fall within the "viable" habitat range for *C. glacialis/marshallae* (**Figure 7**, blue dots).

The viability threshhold that the Southeastern Bering Sea appears to straddle is qualitatively similar to that in the more idealized global experiment (**Figures 5**, **6**), primarily aligned with the phenological index (horizontal axis) rather than the temperature index (vertical axis). The threshhold in

the Bering Sea experiment ($t_{ice} \approx 90$–$100$) falls somewhat beyond the dividing line imposed in the experiment setup between early, ice-retreat-associated blooms and late, open-water blooms ($t_{ice} = 75$: see Appendix in Supplementary Material, Sigler et al., 2014). This gap (whose width depends on the mortality level $m_0$: not shown) indicates that some period of ice algae availability is required by *C. glacialis/marshallae* in this system, in addition to a favorable pelagic bloom timing.

## 3.4. Coexisting Life Strategies in Detail: Disko Bay

The experiments above test the ability of Coltrane 1.0 to reproduce first-order patterns in latitude and time but do not provide sensitive tests of the model biology. A model case study in Disko Bay, where populations of three *Calanus* spp. coexist and have been described in detail (Madsen et al., 2001; Swalethorp et al., 2011), allows a closer examination of the relationships among traits within the family of viable life strategies predicted by Coltrane.

The model forcing (**Figure 8**) describes a single annual cycle, starting with the 1996 spring bloom. This represents a cold, high-ice state of the system, compared with more recent years in which the spring bloom is earlier (e.g., 2008, **Figure 8**, Swalethorp et al., 2011) and the deep layer is warmed by Atlantic water intrusions (Hansen et al., 2012). This particular year was chosen because measurements of prey availability and *Calanus* response by Madsen et al. (2001) were particularly complete and coordinated. A simple attempt to correct the prey field for quality and *Calanus* preference was made by keeping only the >11 $\mu$m size fraction of phytoplankton and adding total microzooplankton, in $\mu$g C. The measured phytoplankton C:chl ratio was used to convert the sum to an equivalent chlorophyll concentration, and this time series was then slightly idealized for clarity (**Figure 8**, Appendix in Supplementary Material).

Sensible results were only possible after tuning the predation mortality scale coefficient $m_0$. It is likely that our simple mortality scheme introduces some form of bias, compared with the reality in this system of predation by successive waves of visual and non-visual predators, which will be considered in a separate study. Still, a sensitivity experiment using the $\varphi$ model shows that varying $m_0$ has, as intended, a simple, uniform effect on fitness/population growth (**Figure 9**) that leaves other trait relationships along the size spectrum unaffected. The $\varphi$ model predicts that copepods similar to *C. finmarchicus* in size have much greater fitness at a generation length of 1 year than at 2 years or more; that *C. hyperboreus* would be unable to complete its life cycle in 1 year, but is well-suited to a 2-year cycle; and that *C. glacialis* falls in the size range where 1- and 2-year life cycles have comparable fitness value. These results are consistent with observations (Madsen et al., 2001) and more general surveys of life strategies in the three species (Falk-Petersen et al., 2009; Daase et al., 2013).

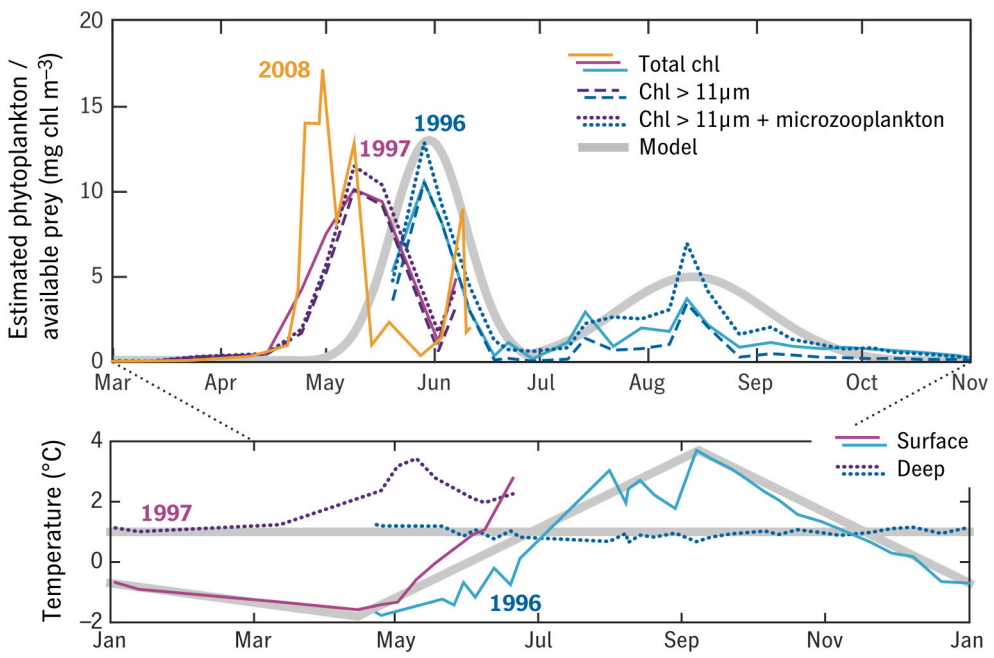


**FIGURE 8 | Observations of temperature and prey in Disko Bay 1996–1997 from Madsen et al. (2001) (blue and purple thin lines) used to construct semi-idealized forcing time series for the model (thick gray lines).** Three observation-based estimates of the prey field are shown, in each case averaged between the surface and subsurface fluorescence maximum: total chlorophyll (solid), chlorophyll in the >11 $\mu$m size fraction (dashed), and >11 $\mu$m chlorophyll plus a correction for microzooplankton (dotted). A 2008 time series of total chlorophyll is shown for comparison (orange). Temperature in the upper 50 m ("surface") and water-column minimum temperature ("deep") are also shown.

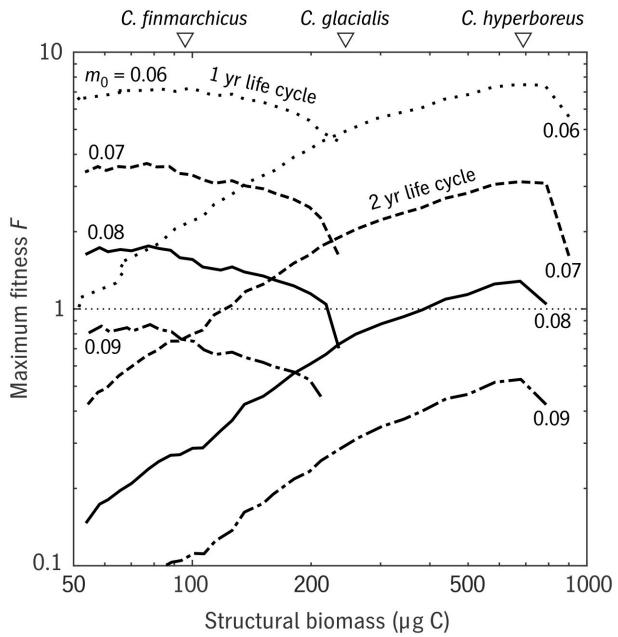


**FIGURE 9 | Results of the $\varphi$ model for a range of $u_0$ (relative development rate) values in the Disko Bay testbed (Figure 8).** Maximum egg fitness $F$ is plotted for 1-year and 2-year strategies, for each of four values of the mortality scaling parameter $m_0$ (0.06–0.09 $d^{-1}$), as a function of adult size $S$. The mean structural weights of the three *Calanus* spp. that coexist in Disko Bay are also shown (white triangles, top). Curves of $F$ are shown over ranges where survival to adulthood without starvation is possible.

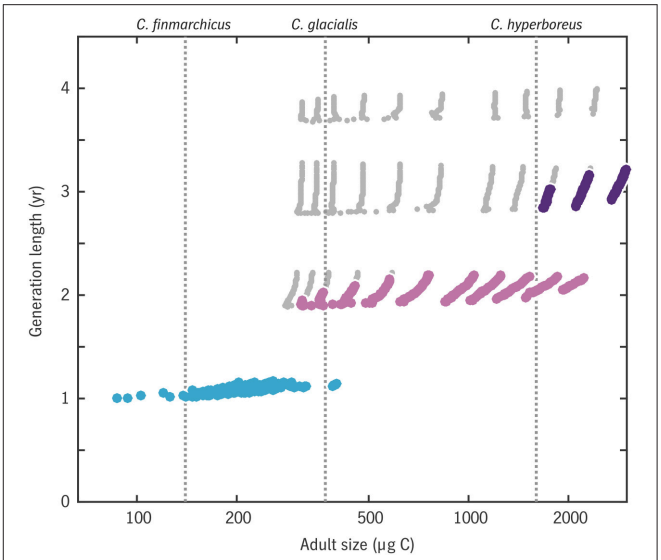


**FIGURE 10 | Emergent relationship between generation length and adult size in the Disko Bay model experiment.** Large colored dots indicate results for trait combinations that achieve a viable rate of egg production per generation (color coding matches that in **Figure 12**: blue, generation length of 1 year; light purple, 2 years; dark purple, 3 years) while small gray dots indicate trait combinations that reach maturity without starvation but have egg production rates below replacement level.

These results naturally raise the question of whether even lower values of $u_0$—further reductions in development rate—would produce even larger copepods with even longer life cycles in this environment. *C. hyperboreus* has been reported to have a life cycle of up to 5 years in other systems (Falk-Petersen et al., 2009) and so the question is more than theoretical. In this version of Coltrane, the lower limit on development rate (and thus the upper limit on adult size) are set by the assumption that modulation of this rate is spread uniformly across the developmental period, rather than concentrated in late copepodid stages, as might be more realistic (Campbell et al., 2001). The largest viable adults in the Disko experiment are those that barely reach $D = D_s$, the start of reserve accumulation, before a first diapause is required.

For greater specificity, we switched from the $\varphi$ to the ER model version, running a spectrum of $t_{egg}$ cases (earliest possible egg-production date: see Section 2.5) along with a spectrum of $u_0$ (development rate) cases. The predicted "community," then is the set of all combinations of $u_0$ and $t_{egg}$ that lead to a viable level of lifetime egg production. An analog for each of the three *Calanus* spp. is constructed by averaging model results over the set of viable ($u_0$, $t_{egg}$) cases that predict an adult size within 30% of the average measured adult size for that species. The ER model imposes additional constraints on the model organisms—e.g., they are no longer allowed an infinite egg production rate—and to compensate we reduced $m_0$ from 0.08 $d^{-1}$ to 0.06 $d^{-1}$.

The relationship between generation length and adult size across all ($u_0$, $t_{egg}$) combinations is shown in **Figure 10**. Results are consistent with the $\varphi$ model (**Figure 9**) only a 1-year life cycle is viable for *C. finmarchicus* in this environment, only a 2-year or longer cycle is viable for *C. hyperboreus*, and *C. glacialis* again lies near the boundary where the two strategies are comparable. Note that the model allows for a continuum of intermediate cases in the *C. finmarchicus*–*C. glacialis* size range, consistent with the observation of hybridization between these species (Parent et al., 2015).

The ER model also predicts a time series of egg production associated with each trait combination, which we can compare with observations for each species. The model predicts that *C. finmarchicus* analogs spawn in close association with the spring bloom, that *C. hyperboreus* spawns well before the spring bloom, and that *C. glacialis* is intermediate (**Figures 11**, **12A**). These patterns are all in accordance with Disko Bay observations (Madsen et al., 2001; Swalethorp et al., 2011), although the absolute range is muted: Madsen et al. (2001) report *C. hyperboreus* spawning as early as February. As one would expect from these timing patterns, the model predicts a significant trend between size and the capital fraction of total egg production $E_{cap}/(E_{inc} + E_{cap})$ (**Figure 12C**). Again, the pattern is qualitatively correct but muted: Coltrane predicts 80% income breeding at the size of *C. finmarchicus* (a pure income breeder in reality) and 80% capital breeding at the size of *C. hyperboreus* (a pure capital breeder in reality). More notable than the error is how much of the income/capital spectrum can apparently be reproduced as a consequence of optimizing reproductive timing alone Varpe et al.

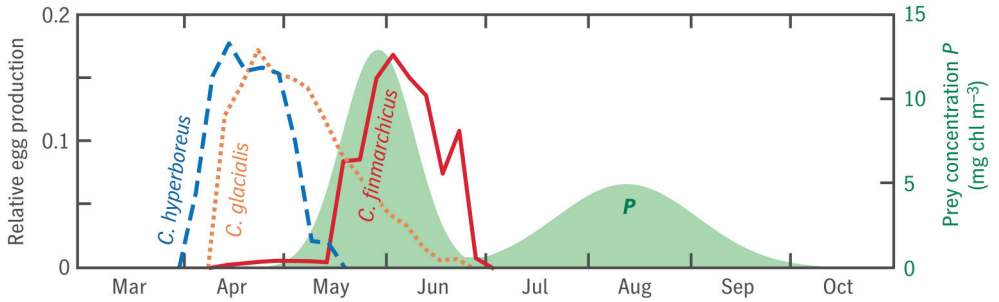


**FIGURE 11 | Seasonal progression of egg production in model analogs for three *Calanus* spp. in Disko Bay (lines), in relation to prey concentration *P* (shaded).** Egg production time series consist of $n(t_0)$, the first eigenvector of the transition matrix $V$ discussed in Section 2.4.3, normalized to integrate to 1.

(2009), without imposing the physiological difference between the two strategies as an independent trait (Ejsmond et al., 2015).

The model predicts (**Figure 12B**) that the largest model organisms, with the longest generation lengths, enter their first diapause near the boundary between copepodite stages C4 and C5 ($D \approx 0.75$), whereas smaller organisms enter first diapause well into stage C5. Madsen et al. (2001) found that both *C. glacialis* and *C. hyperboreus* diapause as C4, C5, and adults in Disko Bay, suggesting that the model is biased toward fast maturation. The discrepancy could also be related to intraspecific variation in the real populations or non-equiproportional development in the late stages, i.e., a variable conversion scale between actual developmental stage and $D$.

Finally, the ER version of Coltrane allows an estimate of the fraction of individual carbon in the form of storage lipids $R/(R + S)$ (**Figure 12D**). Averaging each model population from the first diapause-capable stage $D = D_{dia}$ through adulthood, weighted by survivorship $N$, yields an overall range that compares well with the species-mean wax ester fractions measured by Swalethorp et al. (2011): ∼30% for *C. finmarchicus* to ∼60% for *C. hyperboreus*. In the middle of the size spectrum, reserve fraction is highly variable across viable 2-year strategies, a warning that the success of this final model prediction may be partly fortuitous. Still, taken as a whole, this experiment has yielded a striking result: that a small set of energetic and timing contraints is able to correctly predict, a priori, that Disko Bay should be able to support a spectrum of calanoid copepods from income breeders with an adult size ∼100 $\mu$g C, a 1-year life cycle, and a wax ester fraction ∼30% to capital breeders with an adult size ∼1000 $\mu$g C, a two-or-more-year life cycle, and a wax ester fraction ∼60%.

# 4. DISCUSSION

## 4.1. Temperature and Timing

In the results above, whether prey availability is treated simply (**Figures 5**, **6**) or with site-specific detail (**Figure 7**), it appears that the viability of the calanoid community near its high-latitude limit is more sensitive to prey abundance and phenology than to temperature. This result is heuristically similar to the conclusions of Ji et al. (2012) and Feng et al. (2016), although the exact physiological mechanisms differ. Alcaraz et al. (2014) suggested based on lab experiments that *C. glacialis* reaches an bioenergetic limit near 6°C, and Holding et al. (2013) and others have hypothesized that thermal limits will produce ecosystem-level tipping points in the warming Arctic. Our results, in contrast, suggest that thermal tipping points, even if present at the population level, do not generalize to the community level in copepods. Rather, the model predicts complete continuity between the life strategy of Arctic *C. glacialis* and temperate congeners like *C. marshallae* (**Figure 6**). It also suggests that even on the population level in the Bering Sea, warm/cold-year variation in prey availability is a sufficient explanation of variability in the abundance of *C. glacialis/marshallae* (**Figure 7**), without the invocation of a thermal threshhold.

Both the global and Bering experiments suggest, furthermore, that increasing water temperature *per se* is not necessarily a stressor on copepod communities, even high-latitude communities. In both cases, the low-prey viability threshhold actually relaxes (i.e., is tilted toward lower prey values) as temperature increases, indicating that in these testbeds, the positive effect of temperature on growth and maturation rate actually outweighs the effect of temperature on metabolic losses and overwinter survival (This result may be reliant on the model assumption that the stage of first diapause is highly plastic). In cases where deep, overwintering temperatures increase faster than surface temperatures (Hansen et al., 2012) this balance may not hold, and in the real ocean changes in temperature are highly confounded with changes in phytoplankton production and phenology. Still, it is notable that the model predicts that warming temperatures will have a non-monotonic effect on copepod populations ($\partial F/\partial T_0 \gtrless 0$, **Figures 5**, **6**) even when metabolic thermal threshholds *sensu* Alcaraz et al. (2014) and changes in prey availability are not considered. These results are a caution against overly simple climate-impacts projections based on temperature alone.

## 4.2. Uncertainties and Unresolved Processes

The biology in Coltrane could be refined in many ways, but two issues stand out as being both mechanistically uncertain

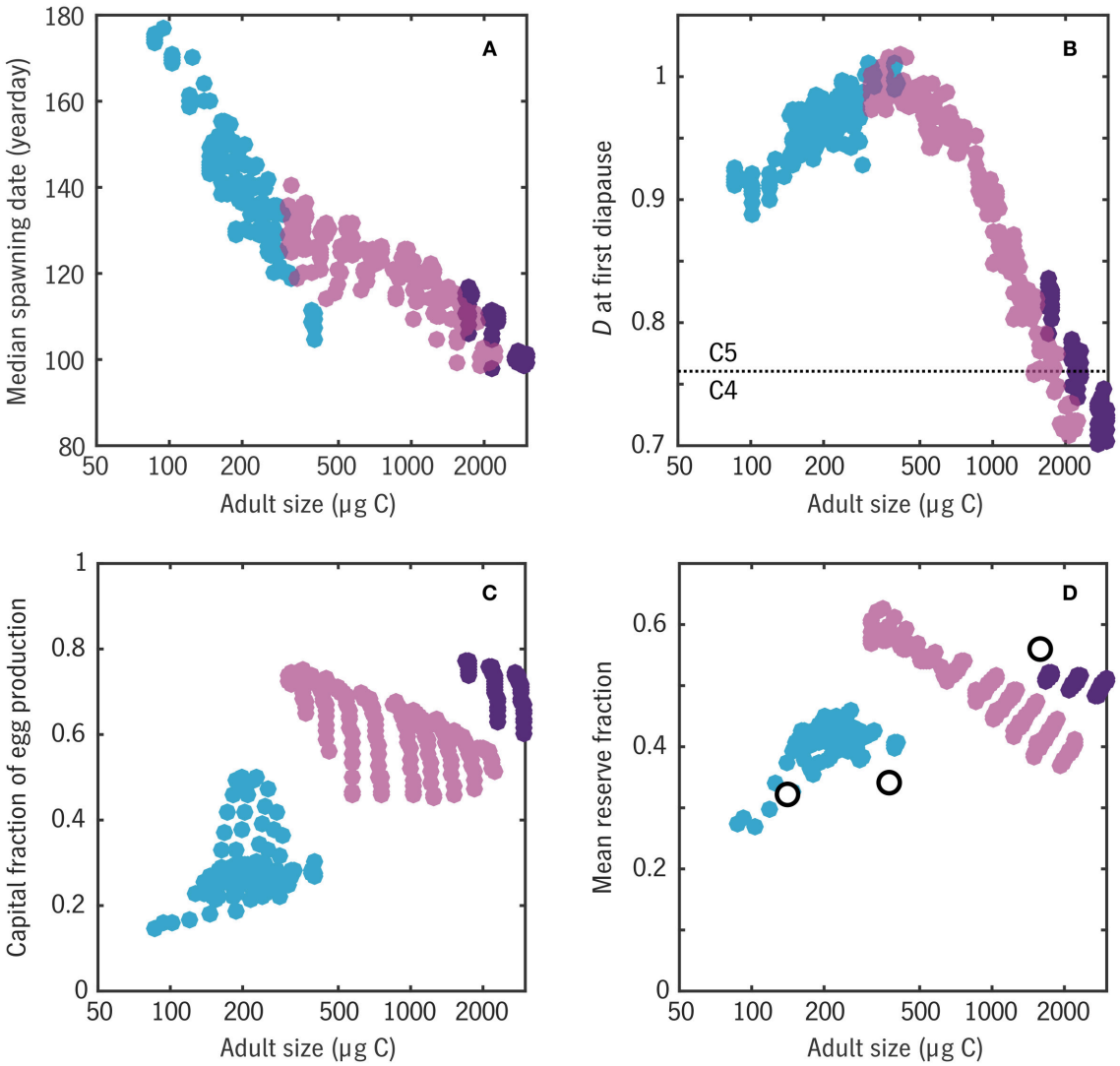


**FIGURE 12 | Relationships between a number of emergent traits with adult body size in the Disko Bay experiment.** Color coding matches **Figure 10**, distinguishing 1-year (blue), 2-year (light purple), and 3-year (dark purple) life cycles. **(A)** Median spawning date: cf. peaks of egg production curves in **Figure 11**. **(B)** Earliest developmental stage $D$ at which diapause ($a = 0$) occurs: values have been jittered slightly in the vertical for clarity. **(C)** Capital fraction of egg production $E_{cap}/(E_{inc} + Ecap)$. **(D)** Mean reserve fraction of individual biomass $R/(R + S)$, compared with wax esters as a fration of total body carbon for three *Calanus* spp. from Swalethorp et al. (2011) (open circles).

and sensitive controls on model behavior. These correspond to the two parameters that it was necessary to tune among model experiments (**Table 2**) the obstacles to formulation of a fully portable scheme that could produce accurate results across the full range of environments considered here with a single parameterization.

The first of these is the perennial problem of the mortality closure. We modeled predation mortality as size-dependent according to the same power law used for ingestion and metabolism, a choice which is mathematically convenient and makes the effect of top-down controls, if not minor, then at least simple and easy to detect (**Figure 9**). This size scaling is consistent with the review by Hirst and Kiørboe (2002) but that study also shows that the variation in copepod mortality not explained by allometry spans orders of magnitude (cf. Ohman et al., 2004). Indeed, in some cases one might posit exactly the opposite pattern, in which mortality due to visual predators like larval fish increases with prey body size (Fiksen et al., 1998; Varpe et al., 2015). This latter pattern is one hypothesis for why in reality *C. hyperboreus* is confined to high latitudes, whereas the model predicts no southern (warm, high-prey) habitat limit to *C. hyperboreus* analogs based on bottom-up considerations (**Figure 5**). Merging Coltrane 1.0 with a light- and size-based predation scheme similar to Varpe et al. (2015) or Ohman and Romagnan (2015) would allow one to better test the balance of bottom-up and top-down controls on calanoid biogeography.

Second, our experience constructing the Bering Sea and Disko Bay cases suggests that the greatest uncertainty in the model bioenergetics is actually not the physiology itself—empirical reviews like Saiz and Calbet (2007), Maps et al. (2014),

Kiørboe and Hirst (2014), and Banas and Campbell (2016) have constrained the key rates moderately well—but rather the problem of translating a prey field into a rate of ingestion. Within each of our model testbeds, the prey time series $P$ remains subject to uncertainty in relative grazing rates on ice algae, large and small pelagic phytoplankton, and microzooplankton, despite a wealth of local observations and a history of work on this problem in *Calanus* specifically (Olson et al., 2006; Campbell et al., 2009, in press). The precision of each testbed, and even moreso the ambition of generalizing across them, is also limited by uncertainty in the shape of the functional response (Frost, 1980; Gentleman et al., 2003), here represented by a half-saturation coefficient, which has not been found to be consistent across site-specific studies (Campbell et al., in press; Møller et al., 2016) or well-constrained by general reviews (Hansen et al., 1997). This ambiguity is perhaps not surprising when one considers that ingestion as a function of chlorophyll or prey carbon is not a simple biomechanical property, but in fact a plastic behavioral choice. Accordingly, it might well be responsive not only to mean or maximum prey concentration but also to the prey distribution over the water column, the tradeoff between energy gain and predation risk (Visser and Fiksen, 2013), prey composition and nutritional value, and the context of the annual routine. These issues are fundamental to concretely modeling the effect of microplankton dynamics on mesozooplankton grazers. Addressing them systematically in models will require novel integration between what could be called oceanographic and marine-biological perspectives on large zooplankton.

## 5. CONCLUSION

Coltrane 1.0, introduced here, is a minimalist model of copepod life history and population dynamics, a metacommunity-level framework on which additional species- or population-level constraints can be layered. Many present and future patterns in large copepods might well prove to be sensitive to species-specific constraints that Coltrane 1.0 does not resolve, such as thermal adaptation, physiological requirements for egg production, or cues for diapause entry and exit. Nevertheless, the model experiments above demonstrate that many patterns in latitude, time, and trait space can be replicated numerically even when we only consider a few key constraints on the individual energy budget: the total energy available in a given environment per year; the energy and time required to build an adult body; the metabolic and predation penalties for taking too long to reproduce; and the size and temperature dependence of the vital rates involved.

Results of the global and Bering experiments (**Figures 5**–**7**) suggest that timing and seasonality are crucial to large copepods, but not because of match/mismatch (Edwards and Richardson, 2004) the model organisms are free to resolve timing mismatches with complete plasticity. Rather, these results highlight the role of seasonality in the sense of total energy available for growth and development per year, or the number of weeks per year of net energy gain relative to the number of weeks of net deficit. The simplicity of this view means that the model scheme and results may generalize far beyond copepods with only minor modification.

The exercise of parameterizing the Bering Sea and Disko Bay cases, and of attempting to map real environments onto an idealized parameter space in the global experiment (**Figure 6**), highlighted that the real limit on our ability to predict the fate of copepods in changing oceans may not be our incomplete knowledge of their physiology, but rather our incomplete knowledge of how their environments appear from their point of view. How do standard oceanographic measures of chlorophyll and particulate chemistry relate to prey quality, and how much risk a copepod should take on in order to forage in the euphotic zone? How do bathymetry, the light field, and other metrics relate to the predator regime? Further experiments in a simple, fast, mechanistically transparent model like Coltrane may suggest new priorities for field observations, in addition to new approaches to regional and global modeling.

## AUTHOR CONTRIBUTIONS

NB designed the model, performed the analysis, and led the writing of the manuscript. EM and TN helped formulate and interpret the Disko Bay case study, and LE the Bering Sea case study. All authors contributed to revision of the manuscript.

## FUNDING

This work was supported by grants PLR-1417365 and PLR-1417224 from the National Science Foundation.

## ACKNOWLEDGMENTS

Many thanks to Bob Campbell, Thomas Kiørboe, Øystein Varpe, Dougie Speirs, and Aidan Hunter for discussions that helped shape both the model and the questions we asked of it. Thanks as well to Nick Record, Carin Ashjian, and ØF, whose comments much improved the manuscript.

## SUPPLEMENTARY MATERIAL

The Supplementary Material for this article can be found online at: http://journal.frontiersin.org/article/10.3389/fmars.2016.00225/full#supplementary-material

## REFERENCES

Alcaraz, M., Felipe, J., Grote, U., Arashkevich, E., and Nikishina, A. (2014). Life in a warming ocean: thermal thresholds and metabolic balance of arctic zooplankton. *J. Plankton Res.* 36, 3–10. doi: 10.1093/plankt/fbt111

Ashjian, C. J., Campbell, R. G., Welch, H. E., Butler, M., and Van Keuren, D. (2003). Annual cycle in abundance, distribution, and size in relation to hydrography of important copepod species in the western Arctic Ocean. *Deep Sea Res. Part I* 50, 1235–1261. doi: 10.1016/S0967-0637(03)00129-8

Banas, N. S. and Campbell, R. G. (2016). Traits controlling body size in copepods: separating general constraints from species-specific strategies. *Mar. Ecol. Prog. Ser.* 558, 21–33. doi: 10.3354/meps11873

Banas, N. S., Zhang, J., Campbell, R. G., Sambrotto, R. N., Lomas, M. W., Sherr, E., et al. (2016). Spring plankton dynamics in the Eastern Bering Sea, 1971-2050: mechanisms of interannual variability diagnosed with a numerical model. *J. Geophys. Res.* 121, 1476–1501. doi: 10.1002/2015jc011449

Barton, A. D., Pershing, A. J., Litchman, E., Record, N. R., Edwards, K. F., Finkel, Z. V., et al. (2013). The biogeography of marine plankton traits. *Ecol. Lett.* 16, 522–534. doi: 10.1111/ele.12063

Beaugrand, G. and Kirby, R. R. (2010). Climate, plankton and cod. *Glob. Change Biol.* 16, 1268–1280. doi: 10.1111/j.1365-2486.2009.02063.x

Burke, B. J., Peterson, W. T., Beckman, B. R., Morgan, C., Daly, E. A., and Litz, M. (2013). Multivariate models of adult pacific salmon returns. *PLoS ONE* 8:e54134. doi: 10.1371/journal.pone.0054134

Campbell, R. G., Ashjian, C. J., Sherr, E. B., Sherr, B. F., Lomas, M. W., Ross, C., et al. (in press). Mesozooplankton grazing during spring sea-ice conditions in the eastern Bering Sea. *Deep Sea Res. Part II*. doi: 10.1016/j.dsr2.2015.11.003

Campbell, R. G., Sherr, E. B., Ashjian, C. J., Plourde, S., Sherr, B. F., Hill, V., et al. (2009). Mesozooplankton prey preference and grazing impact in the western Arctic Ocean. *Deep Sea Res. Part II* 56, 1274–1289. doi: 10.1016/j.dsr2.2008.10.027

Campbell, R. G., Wagner, M. M., Teegarden, G. J., Boudreau, C. A., and Durbin, E. G. (2001). Growth and development rates of the copepod *Calanus finmarchicus* reared in the laboratory. *Mar. Ecol. Prog. Ser.* 221, 161–183. doi: 10.3354/meps221161

Chesson, P. (2000). Mechanisms of maintenance of species diversity. *Annu. Rev. Ecol. Syst.* 31, 343–366. doi: 10.1146/annurev.ecolsys.31.1.343

Clark, J. R., Lenton, T. M., Williams, H. T. P., and Daines, S. J. (2013). Environmental selection and resource allocation determine spatial patterns in picophytoplankton cell size. *Limnol. Oceanogr.* 58, 1008–1022. doi: 10.4319/lo.2013.58.3.1008

Cooper, L. W., Sexson, M. G., Grebmeier, J. M., Gradinger, R., Mordy, C. W., and Lovvorn, J. R. (2013). Linkages between sea-ice coverage, pelagic-benthic coupling, and the distribution of spectacled eiders: observations in March 2008, 2009 and 2010, northern Bering Sea. *Deep Sea Res.* 94, 31–43. doi: 10.1016/j.dsr2.2013.03.009

Coyle, K. O., Eisner, L. B., Mueter, F. J., Pinchuk, A. I., Janout, M. A., Cieciel, K. D., et al. (2011). Climate change in the southeastern Bering Sea: impacts on pollock stocks and implications for the oscillating control hypothesis. *Fish. Oceanogr.* 20, 139–156. doi: 10.1111/j.1365-2419.2011.00574.x

Daase, M., Falk-Petersen, S., Varpe, Ø., Darnis, G., Søreide, J. E., Wold, A., et al. (2013). Timing of reproductive events in the marine copepod *Calanus glacialis*: a pan-Arctic perspective. *Can. J. Fish. Aquat. Sci.* 70, 871–884. doi: 10.1139/cjfas-2012-0401

Durbin, E. G. and Casas, M. C. (2014). Early reproduction by *Calanus glacialis* in the Northern Bering Sea: the role of ice algae as revealed by molecular analysis. *J. Plankton Res.* 36, 523–541. doi: 10.1093/plankt/fbt121

Edwards, M. and Richardson, A. J. (2004). Impact of climate change on marine pelagic phenology and trophic mismatch. *Nature* 430, 881–884. doi: 10.1038/nature02808

Eisner, L. B., Napp, J. M., Mier, K. L., Pinchuk, A. I., and Andrews, A. G. (2014). Climate-mediated changes in zooplankton community structure for the eastern Bering Sea. *Deep Sea Res. Part II* 109, 157–171. doi: 10.1016/j.dsr2.2014.03.004

Eisner, L. B., Siddon, E. C., and Strasburger, W. W. (2015). Spatial and temporal changes in assemblage structure of zooplankton and pelagic fish in the eastern Bering Sea across varying climate conditions. *Izvestia TINRO* 181, 141–160. Available online at: http://cyberleninka.ru/article/n/spatial-and-temporal-changes-in-assemblage-structure-of-zooplankton-and-pelagic-fish-in-the-eastern-bering-sea-across-varying-climate

Ejsmond, M. J., Varpe, Ø., Czarnoleski, M., and Kozłowski, J. (2015). Seasonality in offspring value and trade-offs with growth explain capital breeding. *Am. Nat.* 186, E111–E125. doi: 10.1086/683119

Falk-Petersen, S., Mayzaud, P., Kattner, G., and Sargent, J. R. (2009). Lipids and life strategy of Arctic Calanus. *Mar. Biol. Res.* 5, 18–39. doi: 10.1080/17451000802512267

Feng, Z., Ji, R., Campbell, R. G., Ashjian, C. J., and Zhang, J. (2016). Early ice retreat and ocean warming may induce copepod biogeographic boundary shifts in the Arctic Ocean. *J. Geophys. Res.* 121, 6137–6158. doi: 10.1002/2016JC011784

Fiksen, Ø., Utne, A. C. W., Aksnes, D. L., Eiane, K., Helvik, J. V., and Sundby, S. (1998). Modeling the influence of light, turbulence and ontogeny on ingestion rates in larval cod and herring. *Fish. Oceanogr.* 7, 355–363. doi: 10.1046/j.1365-2419.1998.00068.x

Forster, J., Hirst, A. G., and Woodward, G. (2011). Growth and development rates have different thermal responses. *Am. Nat.* 178, 668–678. doi: 10.1086/662174

Frost, B. W. (1980). "The inadequacy of body size as an indicator of niches in the zooplankton," in *Evolution and Ecology of Zooplankton Communities,* ed W. C. Kerfoot (Hanover, NH: University Press), 742–753.

Gentleman, W., Leising, A. W., Frost, B. W., Strom, S. L., and Murray, J. (2003). Functional responses for zooplankton feeding on multiple resources: a review of assumptions and biological dynamics. *Deep Sea Res. Part II* 50, 2847–2875. doi: 10.1016/j.dsr2.2003.07.001

Gurney, W. S. C., Crowley, P. H., and Nisbet, R. M. (1992). Locking life-cycles onto seasons: circle-map models of population dynamics and local adaptation. *J. Math. Biol.* 30, 251–279. doi: 10.1007/BF00176151

Hansen, J., Bjornsen, P. K., and Hansen, B. W. (1997). Zooplankton grazing and growth: scaling within the 2-2,000 $\mu$m body size range. *Limnol. Oceanogr.* 42, 687–704. doi: 10.4319/lo.1997.42.4.0687

Hansen, M. O., Nielsen, T. G., Stedmon, C. A., and Munk, P. (2012). Oceanographic regime shift during 1997 in Disko Bay, Western Greenland. *Limnol. Oceanogr.* 57, 634–644. doi: 10.4319/lo.2012.57.2.0634

Heath, M., Boyle, P., Gislason, A., Gurney, W., Hay, S. J., Head, E. J. H., et al. (2004). Comparative ecology of over-wintering *Calanus finmarchicus* in the northern North Atlantic, and implications for life-cycle patterns. *ICES J. Mar. Sci.* 61, 698–708. doi: 10.1016/j.icesjms.2004.03.013

Hirche, H.-J. and Kattner, G. (1993). Egg production and lipid content of Calanus glacialis in spring: indication of a food-dependent and food-independent reproductive mode. *Mar. Biol.* 117, 615–622. doi: 10.1007/BF00349773

Hirst, A. G. and Kiørboe, T. (2002). Mortality of marine planktonic copepods: global rates and patterns. *Mar. Ecol. Prog. Ser.* 230, 195–209. doi: 10.3354/meps230195

Holding, J. M., Duarte, C. M., and Arrieta, J. M. (2013). Experimentally determined temperature thresholds for Arctic plankton community metabolism. *Biogeosciences* 10, 357–370. doi: 10.5194/bg-10-357-2013

Holt, R. D., Grover, J., and Tilman, D. (1994). Simple rules for interspecific dominance in systems with exploitative and apparent competition. *Am. Nat.* 144, 741–771. doi: 10.1086/285705

Hooff, R. C. and Peterson, W. (2006). Copepod biodiversity as an indicator of changes in ocean and climate conditions of the northern California current ecosystem. *Limnol. Oceanogr.* 51, 2607–2620. doi: 10.4319/lo.2006.51.6.2607

Houston, A. I., McNamara, J. M., and Hutchinson, J. M. C. (1993). General results concerning the trade-off between gaining energy and avoiding predation. *Philos. Trans. Roy. Soc. Lond. B* 341, 375–397. doi: 10.1098/rstb.1993.0123

Hunt, G. L., Coyle, K. O., Eisner, L. B., Farley, E. V., Heintz, R. A., Mueter, F. J., et al. (2011). Climate impacts on eastern Bering Sea foodwebs: a synthesis of new data and an assessment of the Oscillating Control Hypothesis. *ICES J. Mar. Sci.* 68, 1230–1243. doi: 10.1093/icesjms/fsr036

Hunt, G. L., Stabeno, P. J., Walters, G., Sinclair, E., Brodeur, R. D., Napp, J. M., et al. (2002). Climate change and control of the southeastern Bering Sea pelagic ecosystem. *Deep Sea Res.* 49, 5821–5853. doi: 10.1016/s0967-0645(02)00321-1

Ji, R., Ashjian, C. J., Campbell, R. G., Chen, C., Gao, G., Davis, C., et al. (2012). Life history and biogeography of *Calanus copepods* in the Arctic Ocean: an individual-based modeling study. *Prog. Oceanogr.* 96, 40–56. doi: 10.1016/j.pocean.2011.10.001

Kattner, G. and Hagen, W. (2009). "Lipids in marine copepods: latitudinal characteristics and perspective to global warming," in *Lipids in Aquatic Ecosystems*, ed M. T. Arts (New York, NY: Springer), 257–280.

Kiørboe, T. and Hirst, A. G. (2014). Shifts in mass scaling of respiration, feeding, and growth rates across life-form transitions in marine pelagic organisms. *Am. Nat.* 183, E118–E130. doi: 10.1086/675241

Kiørboe, T. and Sabatini, M. (1995). Scaling of fecundity, growth and development in marine planktonic copepods. *Mar. Ecol. Prog. Ser.* 120, 285–298. doi: 10.3354/meps120285

Kleiber, M. (1932). Body size and metabolism. *Hilgardia* 6, 315–353. doi: 10.3733/hilg.v06n11p315

Maar, M., Møller, E. F., Gürkan, Z., Jónasdóttir, S. H., and Nielsen, T. G. (2013). Sensitivity of *Calanus* spp. copepods to environmental changes in the North Sea using life-stage structured models. *Prog. Oceanogr.* 111, 24–37. doi: 10.1016/j.pocean.2012.10.004

MacDonald, A., Heath, M., Edwards, M., Furness, R., Pinnegar, J., Wanless, S., et al. (2015). "Climate-driven trophic cascades affecting seabirds around the British Isles," in *Oceanography and Marine Biology,* eds R. N. Hughes, D. J. Hughes, I. P. Smith, and A. C. Dale (Oxford: CRC Press), 55–80.

Mackas, D. L., Greve, W., Edwards, M., Chiba, S., Tadokoro, K., Eloire, D., et al. (2012). Changing zooplankton seasonality in a changing ocean: comparing time series of zooplankton phenology. *Prog. Oceanogr.* 97–100, 31–62. doi: 10.1016/j.pocean.2011.11.005

Madsen, S. D., Hansen, B. W., and Nielsen, T. G. (2001). Annual population development and production by *Calanus finmarchicus*, *C. glacialis* and *C. hyperboreus* in Disko Bay, western Greenland. *Mar. Biol.* 139, 75–83. doi: 10.1007/s002270100552

Mantua, N. J., Hare, S. R., Zhang, Y., Wallace, J. M., and Francis, R. C. (1997). A Pacific interdecadal climate oscillation with impacts on salmon production. *Bull. Am. Meteorol. Soc.* 78, 1069–1079. doi: 10.1175/1520-0477(1997)078<1069:APICOW>2.0.CO;2

Maps, F., Pershing, A. J., and Record, N. R. (2012). A generalized approach for simulating growth and development in diverse marine copepod species. *ICES J. Mar. Sci.* 69, 370–379. doi: 10.1093/icesjms/fsr182

Maps, F., Record, N. R., and Pershing, A. J. (2014). A metabolic approach to dormancy in pelagic copepods helps explaining inter- and intra-specific variability in life-history strategies. *J. Plankton Res.* 36, 18–30. doi: 10.1093/plankt/fbt100

Miller, C. B., Lynch, D. R., Carlotti, F., Gentleman, W., and Lewis, C. V. W. (2002). Coupling of an individual-based population dynamic model of *Calanus finmarchicus* to a circulation model for the Georges Bank region. *Fish. Oceanogr.* 7, 219–234. doi: 10.1046/j.1365-2419.1998.00072.x

Møller, E. F., Bohr, M., Kjellerup, S., Maar, M., Mohl, M., Swalethorp, R., et al. (2016). *Calanus finmarchicus* egg production at its northern border. *J. Plankton Res.* 38, 1206–1214. doi: 10.1093/plankt/fbw048

Møller, E. F., Maar, M., Jónasdóttir, S. H., Gissel Nielsen, T., and Tönnesson, K. (2012). The effect of changes in temperature and food on the development of *Calanus finmarchicus* and *Calanus helgolandicus* populations. *Limnol. Oceanogr.* 57, 211–220. doi: 10.4319/lo.2012.57.1.0211

Ohman, M. D., Eiane, K., Durbin, E., Runge, J., and Hirche, H.-J. (2004). A comparative study of *Calanus finmarchicus* mortality patterns at five localities in the North Atlantic. *ICES J. Mar. Sci.* 61, 687–697. doi: 10.1016/j.icesjms.2004.03.016

Ohman, M. D. and Romagnan, J.-B. (2015). Nonlinear effects of body size and optical attenuation on Diel vertical migration by zooplankton. *Limnol. Oceanogr.* 61, 765–770. doi: 10.1002/lno.10251

Olson, M. B., Lessard, E. J., and Wong, C. (2006). Copepod feeding selectivity on microplankton, including the toxigenic diatoms *Pseudo-nitzschia* spp., in the coastal Pacific Northwest. *Mar. Ecol. Prog. Ser.* 326, 207–220. doi: 10.3354/meps326207

Österblom, H., Olsson, O., Blenckner, T., and Furness, R. W. (2008). Junk-food in marine ecosystems. *Oikos* 117, 967–977. doi: 10.1111/j.0030-1299.2008.16501.x

Parent, G. J., Plourde, S., Joly, P., and Turgeon, J. (2015). Phenology and fitness of *Calanus glacialis*, *C. finmarchicus* (Copepoda), and their hybrids in the St. Lawrence Estuary. *Mar. Ecol. Prog. Ser.* 524, 1–9. doi: 10.3354/meps11240

Peterson, W. T. (1979). *Life History and Ecology of Calanus marshallae Frost in the Oregon Upwelling Zone*. Ph.D. thesis, Oregon State University.

Peterson, W. T. (1986). Development, growth, and survivorship of the copepod *Calanus marshallae* in the laboratory. *Mar. Ecol. Prog. Ser.* 29, 61–72. doi: 10.3354/meps029061

Record, N. R., Pershing, A. J., and Maps, F. (2012). First principles of copepod development help explain global marine diversity patterns. *Oecologia* 170, 289–295. doi: 10.1007/s00442-012-2313-0

Record, N. R., Pershing, A. J., and Maps, F. (2013). Emergent copepod communities in an adaptive trait-structured model. *Ecol. Model.* 260, 11–24. doi: 10.1016/j.ecolmodel.2013.03.018

Record, N. R., Pershing, A. J., and Maps, F. (2014). The paradox of the "paradox of the plankton." *ICES J. Mar. Sci.* 71, 236–240. doi: 10.1093/icesjms/fst049

Rey-Rassat, C., Irigoien, X., Harris, R., Head, R., and Carlotti, F. (2002). Growth and development of *Calanus helgolandicus* reared in the laboratory. *Mar. Ecol. Prog. Ser.* 238, 125–138. doi: 10.3354/meps238125

Runge, J. A., Plourde, S., Joly, P., Niehoff, B., and Durbin, E. (2006). Characteristics of egg production of the planktonic copepod, *Calanus finmarchicus*, on Georges Bank: 1994–1999. *Deep Sea Res. Part II* 53, 2618–2631. doi: 10.1016/j.dsr2.2006.08.010

Sainmont, J., Andersen, K. H., Thygesen, U. H., Fiksen, Ø., and Visser, A. W. (2015). An effective algorithm for approximating adaptive behavior in seasonal environments. *Ecol. Model.* 311, 20–30. doi: 10.1016/j.ecolmodel.2015.04.016

Saiz, E. and Calbet, A. (2007). Scaling of feeding in marine calanoid copepods. *Limnol. Oceanogr.* 52, 668–675. doi: 10.4319/lo.2007.52.2.0668

Sigler, M. F., Stabeno, P. J., Eisner, L. B., Napp, J. M., and Mueter, F. J. (2014). Spring and fall phytoplankton blooms in a productive subarctic ecosystem, the eastern Bering Sea, during 1995–2011. *Deep Sea Res. Part II* 109, 71–83. doi: 10.1016/j.dsr2.2013.12.007

Stabeno, P. J., Farley, E. V. Jr., Kachel, N. B., Moore, S., Mordy, C. W., Napp, J. M., et al. (2012a). A comparison of the physics of the northern and southern shelves of the eastern Bering Sea and some implications for the ecosystem. *Deep Sea Res. Part II* 65–70, 14–30. doi: 10.1016/j.dsr2.2012.02.019

Stabeno, P. J., Kachel, N. B., Moore, S., Napp, J. M., Sigler, M. F., Yamaguchi, A., et al. (2012b). Comparison of warm and cold years on the southeastern Bering Sea shelf and some implications for the ecosystem. *Deep Sea Res. Part II* 65–70, 31–45. doi: 10.1016/j.dsr2.2012.02.020

Swalethorp, R., Kjellerup, S., Dünweber, M., Nielsen, T. G., Møller, E. F., Rysgaard, S., et al. (2011). Grazing, egg production, and biochemical evidence of differences in the life strategies of *Calanus finmarchicus*, *C. glacialis* and *C. hyperboreus* in Disko Bay, western Greenland. *Mar. Ecol. Prog. Ser.* 429, 125–144. doi: 10.3354/meps09065

Varpe, Ø., Daase, M., and Kristiansen, T. (2015). A fish-eye view on the new Arctic lightscape. *ICES J. Mar. Sci.* 72, 2532–2538. doi: 10.1093/icesjms/fsv129

Varpe, Ø., Jørgensen, C., Tarling, G. A., and Fiksen, Ø. (2007). Early is better: seasonal egg fitness and timing of reproduction in a zooplankton life-history model. *Oikos* 116, 1331–1342. doi: 10.1111/j.0030-1299.2007.15893.x

Varpe, Ø., Jørgensen, C., Tarling, G. A., and Fiksen, Ø. (2009). The adaptive value of energy storage and capital breeding in seasonal environments. *Oikos* 118, 363–370. doi: 10.1111/j.1600-0706.2008.17036.x

Visser, A. W. and Fiksen, Ø. (2013). Optimal foraging in marine ecosystem models: selectivity, profitability and switching. *Mar. Ecol. Prog. Ser.* 473, 91–101. doi: 10.3354/meps10079

Visser, A. W., Mariani, P., and Pigolotti, S. (2008). Swimming in turbulence: zooplankton fitness in terms of foraging efficiency and predation risk. *J. Plankton Res.* 31, 121–133. doi: 10.1093/plankt/fbn109

Wilson, R. J., Heath, M. R., and Speirs, D. C. (2016). Spatial modeling of *Calanus finmarchicus* and *Calanus helgolandicus*: parameter differences explain differences in biogeography. *Front. Mar. Sci.* 3:157. doi: 10.3389/fmars.2016.00157

Wilson, R. J., Speirs, D. C., and Heath, M. R. (2015). On the surprising lack of differences between two congeneric calanoid copepod species, *Calanus finmarchicus* and *C. helgolandicus*. *Prog. Oceanogr.* 134, 413–431. doi: 10.1016/j.pocean.2014.12.008

Zhang, J., Woodgate, R., and Mangiameli, S. (2012). Towards seasonal prediction of the distribution and extent of cold bottom waters on the Bering Sea shelf. *Deep Sea Res. Part II* 65, 58–71. doi: 10.1016/j.dsr2.2012.02.023

Zhang, J., Woodgate, R., and Moritz, R. (2010). Sea ice response to atmospheric and oceanic forcing in the Bering Sea. *J. Phys. Oceanogr.* 40, 1729–1747. doi: 10.1175/2010JPO4323.1

**Conflict of Interest Statement:** The authors declare that the research was conducted in the absence of any commercial or financial relationships that could be construed as a potential conflict of interest.

The reviewer ØF and handling Editor declared their shared affiliation, and the handling Editor states that the process nevertheless met the standards of a fair and objective review.

frontiers in Marine Science

ORIGINAL RESEARCH
published: 09 September 2016
doi: 10.3389/fmars.2016.00157

# Spatial Modeling of *Calanus finmarchicus* and *Calanus helgolandicus*: Parameter Differences Explain Differences in Biogeography

*Robert J. Wilson *, Michael R. Heath and Douglas C. Speirs*

*Department of Mathematics and Statistics, University of Strathclyde, Glasgow, Scotland*

The North Atlantic copepods *Calanus finmarchicus* and *C. helgolandicus* are moving north in response to rising temperatures. Understanding the drivers of their relative geographic distributions is required in order to anticipate future changes. To explore this, we created a new spatially explicit stage-structured model of their populations throughout the North Atlantic. Recent advances in understanding *Calanus* biology, including U-shaped relationships between growth and fecundity and temperature, and a new model of diapause duration are incorporated in the model. Equations were identical for both species, but some parameters were species-specific. The model was parameterized using Continuous Plankton Recorder Survey data and tested using time series of abundance and fecundity. The geographic distributions of both species were reproduced by assuming that only known interspecific differences and a difference in the temperature influence on mortality exist. We show that differences in diapause capability are not necessary to explain why *C. helgolandicus* is restricted to the continental shelf. Smaller body size and higher overwinter temperatures likely make true diapause implausible for *C. helgolandicus*. Known differences were incapable of explaining why only *C. helgolandicus* exists southwest of the British Isles. Further, the fecundity of *C. helgolandicus* in the English Channel is much lower than we predict. We hypothesize that food quality is a key influence on the population dynamics of these species. The modeling framework presented can potentially be extended to further *Calanus* species.

**Keywords: copepods, zooplankton, modeling, biogeography, diapause**



***Edited by:***
*Dag Lorents Aksnes, University of Bergen, Norway*

***Reviewed by:***
*Jan Marcin Weslawski, Institute of Oceanology of the Polish Academy of Sciences, Poland*
*Nicholas R. Record, Bigelow Laboratory for Ocean Sciences, USA*

****Correspondence:***
*Robert J. Wilson*
*robert.wilson@strath.ac.uk*

***Specialty section:***
*This article was submitted to Marine Ecosystem Ecology, a section of the journal Frontiers in Marine Science*

***Received:*** *22 June 2016*
***Accepted:*** *19 August 2016*
***Published:*** *09 September 2016*

***Citation:***
*Wilson RJ, Heath MR and Speirs DC (2016) Spatial Modeling of Calanus finmarchicus and Calanus helgolandicus: Parameter Differences Explain Differences in Biogeography. Front. Mar. Sci. 3:157. doi: 10.3389/fmars.2016.00157*

## 1. INTRODUCTION

Zooplankton communities are now reorganizing throughout the North Atlantic (Beaugrand et al., 2009; Chust et al., 2013). Rising temperatures are causing species to expand at the northern edge of their distribution, while they are retreating at the southern edge (Beaugrand, 2012). As a consequence, communities are changing and many species are being replaced by their southern congenerics (Beaugrand et al., 2002).

Changes in communities dominated by the calanoid copepods *Calanus finmarchicus* and *C. helgolandicus* are among the most well-studied (Wilson et al., 2015). *C. finmarchicus* is an oceanic

species that is found from the Gulf of Maine to the North Sea (Melle et al., 2014). In contrast, *C. helgolandicus* is a shelf species that lives from the North Sea to the Mediterranean Sea (Bonnet et al., 2005). Both species are now moving north, which has caused *C. helgolandicus* to replace *C. finmarchicus* as the dominant calanoid copepod in the North Sea (Reid et al., 2003). Future temperature rises will likely cause this to be repeated further north (Villarino et al., 2015). We must therefore understand differences in the impacts of climate change on congeneric zooplankton species, so that we can anticipate changes in communities and their consequences.

A key test of our understanding of the interspecific differences in demography of these species is whether we can simulate their population dynamics in such a way that the relative geographic distributions of both species are a result of the differences in biology. An inability to do this can highlight important knowledge gaps that must be filled to make projections of the impact of climate change on *Calanus* communities more biologically credible.

In this spirit, we tested the ability of known interspecific differences to explain the geographic distributions of both species by creating a new unified model. We created a stage-structured model which represents each life stage of *C. finmarchicus* and *C. helgolandicus*, and that represents body size by dividing each stage into a set of size classes. This work is based on the previous model of *C. finmarchicus* in the North Atlantic of Speirs et al. (2005, 2006). Continuous Plankton Recorder survey data was used to parameterize the model and simulated annual cycles of abundance and fecundity were compared with empirical time series in a number of North Atlantic locations.

Recently, an increasing number of researchers have taken a trait-based approach to understanding zooplankton communities (Barton et al., 2013; Litchman et al., 2013). Key traits such as body size, development rate and fecundity are identified, and the functional role of species in ecosystems is thus thought to be a function of their positions within trait-space. A trait-based approach has previously been used to model copepod communities in Cape Cod Bay, Massachusetts (Record et al., 2010). We used this approach to understand the biogeography of two species, under the assumption that where species lie in trait-space is the fundamental determinant of relative biogeography.

Our underlying philosophy is that the equations describing the population dynamics of both species should be identical, but with potential differences in parameters. This constraint will arguably result in suboptimal models for each species when viewed separately. However, it enables us to more clearly understand the biological differences that drive the large-scale differences in distribution. Fundamentally, this work is based on the assumption that if knowledge of key interspecific differences is sufficient, then known interspecific differences are all that is needed for a model to reproduce the geographic distributions of both species. The only known difference between the species that could influence population dynamics is the response of ingestion rate, and thus growth, development and fecundity, to temperature (Wilson et al., 2015). We therefore begin with the hypothesis that this difference alone can explain most of the differences in geographic distribution.

# 2. MODEL

## 2.1. Model Background and Framework

We present an extension of the previous work by Speirs et al. (2005, 2006), who modeled the population dynamics of *C. finmarchicus* over the entire North Atlantic. This extension took two key forms. First, we incorporated recent developments in our understanding of *Calanus* biology. Second, we modified the model of Speirs et al. (2006) so that it could represent the population dynamics of both *C. finmarchicus* and *C. helgolandicus*. Full mathematical details of the model, along with relevant parameters, are given in Appendix 1 (Supplementary Material). Here we will summarize the modeling framework of Speirs et al. and then the extensions to it.

The model of Speirs et al. was discrete in time and space. It covered the entire North Atlantic, ranging from 30 to 80°N and 80°W to 90°E. The population of *C. finmarchicus* was distributed over a regular grid of cells of size 0.5°longitude by 0.25°latitude. They had two update processes. First, the population of each cell was updated to account for development, reproduction and mortality. After these updates, the population is redistributed between cells to account for physical population transport. A separate physical model was used to create the flow-field and temperature drivers for the relevant biological and physical update. The annual cycle of food in each cell was estimated by deriving phytoplankton carbon fields from satellite sea-color observations. 1997 was used as the target year for simulations because this was the year when the Trans-Atlantic Study of *Calanus* (TASC) collected a large number of time series of *C. finmarchicus* abundance in the North Atlantic. The framework of Speirs et al. was as follows. Surface developers are made up of eggs (E), naupliar stages (N1 to N6), and copepodite stages (C1 to C5). Finally, there are diapausers (C5d) and adults (C6).

*Calanus* development follows the equiproportional rule, that is relative stage duration is independent of temperature (Campbell et al., 2001). Development from egg to adult can therefore be divided into a fixed number of steps, with each having identical time duration under identical environmental conditions (Gurney et al., 2001). In total, there were 57 development steps, which cover the 13 stages of *Calanus* development.

This framework allows the entire population to be updated simultaneously, and for the entire population to be simulated with high computational efficiency (Speirs et al., 2006). However, modeling the populations of *C. finmarchicus* and *C. helgolandicus* required one modification.

We began with the hypothesis that differences in the response of growth and development to temperature are sufficient to explain the geographic distributions of both species. In other words, all equations and parameters would be the same, except for those related to growth and development. This could not be satisfactorily achieved in the original framework. Large-scale patterns of fecundity are not only the result of the effects of environmental conditions, but also of body size. Further, the ability of animals to diapause is strongly influenced by size (Wilson et al., 2016). We therefore incorporated body size into the framework. Large-scale patterns of fecundity and diapause duration could therefore be represented as the combined effects

of body size and the environment, and did not require the introduction of interspecific differences. The geographic domain used by Speirs et al. covers all regions of high *C. helgolandicus* abundance (Bonnet et al., 2005), and was therefore maintained.

## 2.2. Biological Processes: A New View of *Calanus* Biology

The following biological processes are represented in our model: development, egg production, diapause and mortality. In each case, we modified the model of Speirs et al. to account for recent developments in the understanding of *Calanus* biology.

A recent review of the differences between the two species found that the only known relevant difference was the influence of temperature on ingestion, and thus growth, development and fecundity (Wilson et al., 2015). We therefore constrained the model by making a number of assumptions about the differences between the species based on this review. These assumptions were as follows:

- There is a dome-shaped response of ingestion rate to temperature for both species, with ingestion rate higher for *C. finmarchicus* than *C. helgolandicus* below a temperature of 13°C.
- An emergent property of this is that there are dome-shaped relationships between growth and egg production rate and temperature, and a U-shaped relationship between development time and temperature for both species.
- Under identical conditions, both species will grow to the same size.
- There are no differences in the ability to accumulate lipids or diapause.

Further, we take the following assumptions and simplifications about the biology and ecology of both species.

- There are no interactions between the two species.
- The species do not hybridize. However, hybridization has been observed among other *Calanus* species (Parent et al., 2011, 2012; Gabrielsen et al., 2012).
- The relationships between traits and the environment do not vary in time or space.

The key modeled relationships between body size, development time, egg production rate and diapause duration with temperature are shown in **Figure 1**.

There are no apparent interspecific differences in body size, and large-scale geographic patterns of body size are largely driven by temperature (Wilson et al., 2015). We therefore modeled body size under the simplified assumption that it is determined by temperature experienced at birth for all development classes (**Figure 1A**). This assumption is derived from the fact that egg size is determined by temperature (Campbell et al., 2001) and that the existence of an exo-skeleton likely greatly constrains size over all development classes. The temperature-prosome length relationship of Campbell et al. (2001) was used with a multiplier, which was fitted based on the relationship between predicted and observed female prosome length. Prosome length reduces linearly with increasing temperature. This approach contrasts with Speirs et al., which did not represent size.

Egg-adult development time was assumed to be influenced purely by temperature and food concentration. The relationship between egg-adult development time and temperature under food-saturated conditions is assumed to follow that derived by the model of Wilson et al. (2015). Development time saturates at high food levels, and we use the relationship between food concentration and development time of Campbell et al. (2001). There is a U-shaped response of development time to temperature (**Figure 1B**), which contrasts with the monotonically decreasing form used by Speirs et al. The computational approach is that of Gurney et al. (2001) and uses dynamic time-step constraints. This is the same approach as in Speirs et al. (2005, 2006) and it is effective in minimizing numerical diffusion (Gurney et al., 2001; Record and Pershing, 2008).

Fecundity was related to temperature, food concentration and body size. We assumed that egg production and growth are equivalent (McLaren and Leonard, 1995). Egg laying females have stopped growing and we therefore assume that carbon previously directed to growth will be used to make eggs. The growth rate equation of Wilson et al. (2015) forms the basis of our egg production rate (EPR) model for both species, with the food saturation component taken from Hirche et al. (1997). EPR therefore has a dome-shaped response to temperature (**Figure 1C**). Further, EPR has a saturating response to food concentration and we use a conventional allometric relationship between EPR and carbon weight, i.e., EPR $\sim$ carbon weight$^{0.75}$. This contrasts with Speirs et al., who represented EPR as a monotonically increasing function of temperature, but using the same food response as we have assumed. We assume that 50% of adults are female.

A recent modeling study, which synthesized empirical findings, showed that maximum potential diapause duration is largely determined by prosome length and overwintering temperature (Wilson et al., 2016). We therefore modeled diapause duration using the maximum potential diapause duration equation from that study (**Figure 1D**). Diapause duration declines at higher temperature because of increased metabolic rates, and is shorter at smaller prosome lengths because of lower relative lipid levels and higher relative metabolic costs. We assumed that a fraction of the C5 population enters diapause at the end of the C5 stage. This fraction is dependent on growth rate, with it increasing at lower growth rates, so that more animals diapause when development conditions are poor. In the model, animals exit diapause at the end of their potential diapause duration. This differs from Speirs et al., who assumed that diapause exit was triggered by a photoperiod cue.

Mortality is modeled using a stage-dependent background rate, alongside a starvation and density dependent term. Field studies indicate that mortality in both species is stage-dependent (Eiane et al., 2002; Ohman et al., 2004; Hirst et al., 2007). These estimates of stage-dependent mortality include all sources of mortality. However, we need to distinguish between different sources of mortality to properly represent population dynamics. We therefore used a fraction of the stage-specific mortality rates calculated by Eiane et al. (2002) as the background mortality rate, with additional temperature, starvation and density dependent terms. Starvation dependent mortality was modeled in the same

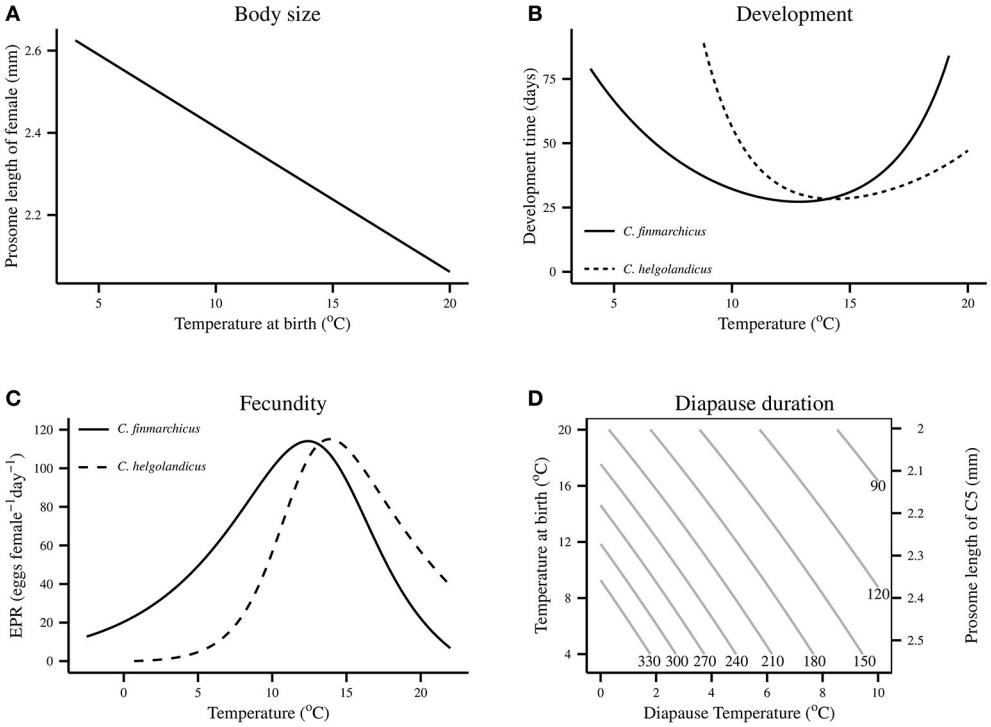


**FIGURE 1 | Influence of temperature on Calanus's body size, development and growth in the model.** Body size and diapause duration are assumed to be the same in both species. Development time is based on the model of Wilson et al. (2015), and the EPR model is derived from that model's growth equation assuming that female's use carbon for egg production instead of growth. Egg-adult development times assume an animal is of size 280 $\mu$g C. **(A)** Modeled relationship between female body size and temperature at birth for both species. **(B)** Modeled relationship between egg-adult development time under food-saturated conditions for both species. **(C)** Modeled relationship between fecundity and temperature for both species. Fecundity relationships assume an animal is of size 280 $\mu$g C. **(D)** Modeled relationship between diapause temperature and prosome length of C5 and diapause temperature for both species. Body size is assumed to be determined by temperature at birth.

way for both species by assuming that it relates to growth rate; with starvation mortality only occurring below a threshold growth rate and increasing as growth rate decreases. Background mortality is temperature dependent, with mortality increasing with temperature and the relationship taking the form mortality $\sim (T/8)^z$. Density dependent mortality is assumed to be proportional to total biomass. Mortality was represented the same way as in Speirs et al., with the exception of starvation-dependence. Speirs et al. represented this purely as a function of food concentration. However, the differences in ingestion rate between the two species (Møller et al., 2012) show that *C. helgolandicus* is likely to face much greater starvation levels at temperatures below approximately 11°C. We therefore viewed growth rate as a better indicator of starvation than food concentration.

## 2.3. Environmental Drivers

Seasonal cycles in food concentration, temperature and oceanic circulation drive the model. The only data with sufficient spatial and temporal coverage of food concentration are satellite estimates of sea surface color. SeaWIFS satellite estimates of chlorophyll were therefore used to derive food fields.

Insufficient observations are available for 1997. We therefore used a climatological 8 day mean of chlorophyll concentration from 1998 to 2000. There is a poor relationship between time series derived from SeaWIFS and field estimates of chlorophyll (Speirs et al., 2005; Clarke et al., 2006). We used the estimates of Clarke et al. (2006), who developed a statistical methodology, where thin plate regression splines modeled local estimates of chlorophyll concentration in relation to SeaWIFS estimates, bathymetry and time of year. Field estimates of chlorophyll concentration in the top 5 m were used, assuming they reflect chlorophyll concentration throughout the vertical distribution of *Calanus*. However, it is possible that this does not fully capture deep-water chlorophyll concentrations. Phytoplankton abundance was calculated assuming that 1 mg $m^{-3}$ of Chl *a* is equivalent to 40 mg $Cm^{-3}$ (the approximate median of the values reported by Parsons et al. (1984). Estimates of food extend to regions covered by sea ice, where we masked food levels to zero. This mask was derived from 1997 satellite percentage ice cover from the Defense Meteorological Satellite Program's (DMSP) spatial sensor microwave/imager (SSM/I) (Comiso, 1997). The approach taken to food was the same as in Speirs et al.

Temperature and velocity fields come from the Nucleus for European Modeling of the Ocean (NEMO) Ocean General Circulation Model (OCGM) (version 3.2) (Madec, 2012). The forcings and model implementation are described in Yool et al. (2011). NEMO is resolved at 64 vertical levels, and it resolves the

primitive equations on a C-type Arawkawa grid. Ocean surface forcing comes from the DFS4.1 fields produced by the European DRAKKAR collaboration. This differs from Speirs et al., who used the OCCAM model to derive temperatures and flow fields. Computation of the NEMO model was performed using the free Java tool Ichthyop version 3.2 (Lett et al., 2008).

We assumed that surface developers experience the temperatures and velocities which occur at a depth of 20 m. Diapause depth varies in space. We therefore derived a map of diapause from the data reported by Heath et al. (2004). A loess smooth was used to estimate the median diapause depth in regions close to where Heath et al. (2004) reported data.

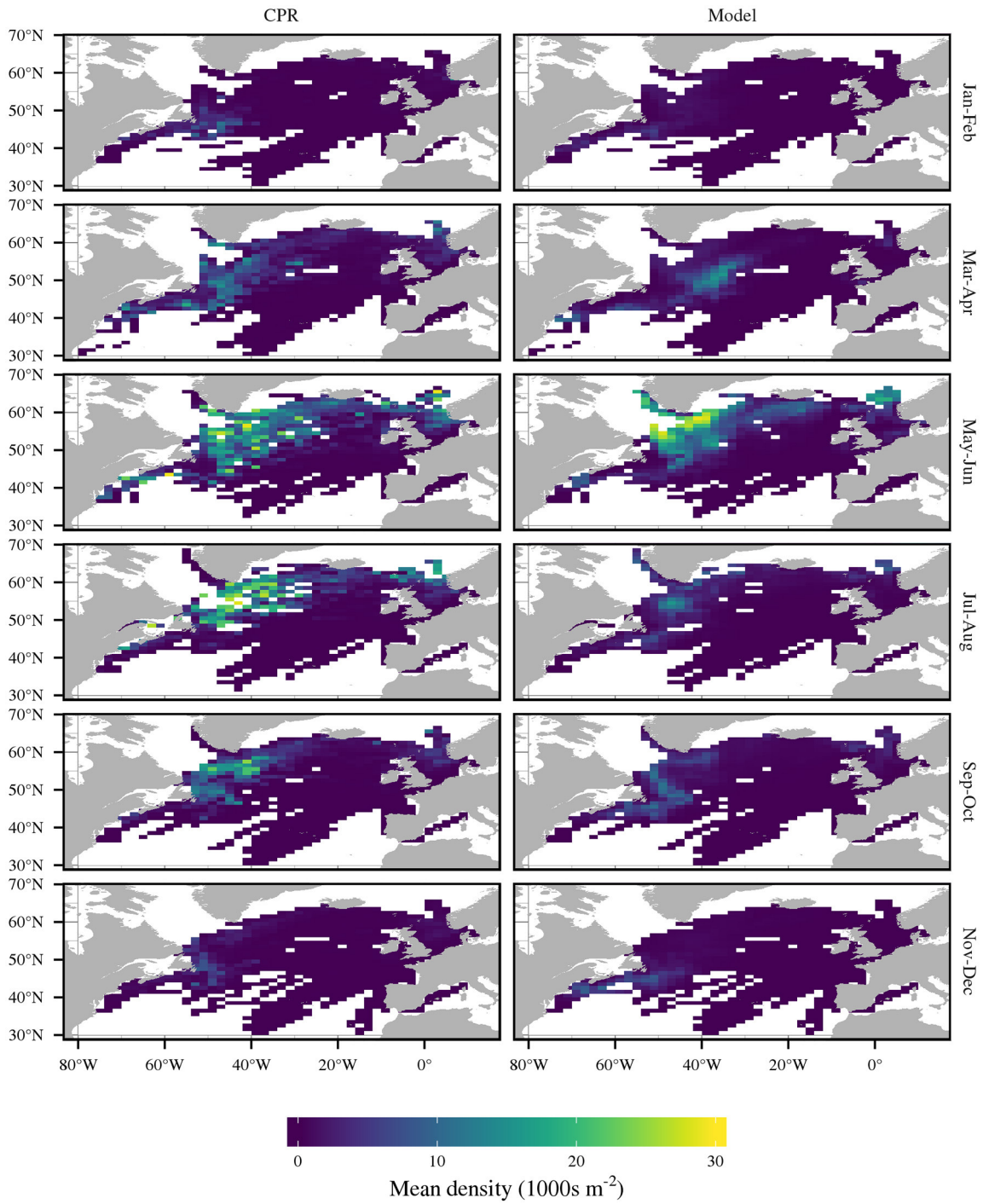


**FIGURE 2 | Comparison of bimonthly *C. finmarchicus* abundance as recorded by CPR and by the model.** Density is mean C5 and adult abundance.

Where the smoothed estimate exceeded bathymetry, we used a depth 10 m shallower than the bathymetry at a location. In other regions we assumed that if bathymetry was greater than 800 m that diapause depth was 800 m. For locations where bathymetry was shallower than 800 m we used the predictions of a general additive model which related median diapause depth with bathymetry using the data of Heath et al. (2004). Transport updates occurred every 7 days. At the start of each time step, 100 seeds were placed at the center of each model cell. Particle trajectories over a 7-day period were then calculated, and transition matrices were calculated to show the proportion of particles which move to each nearby

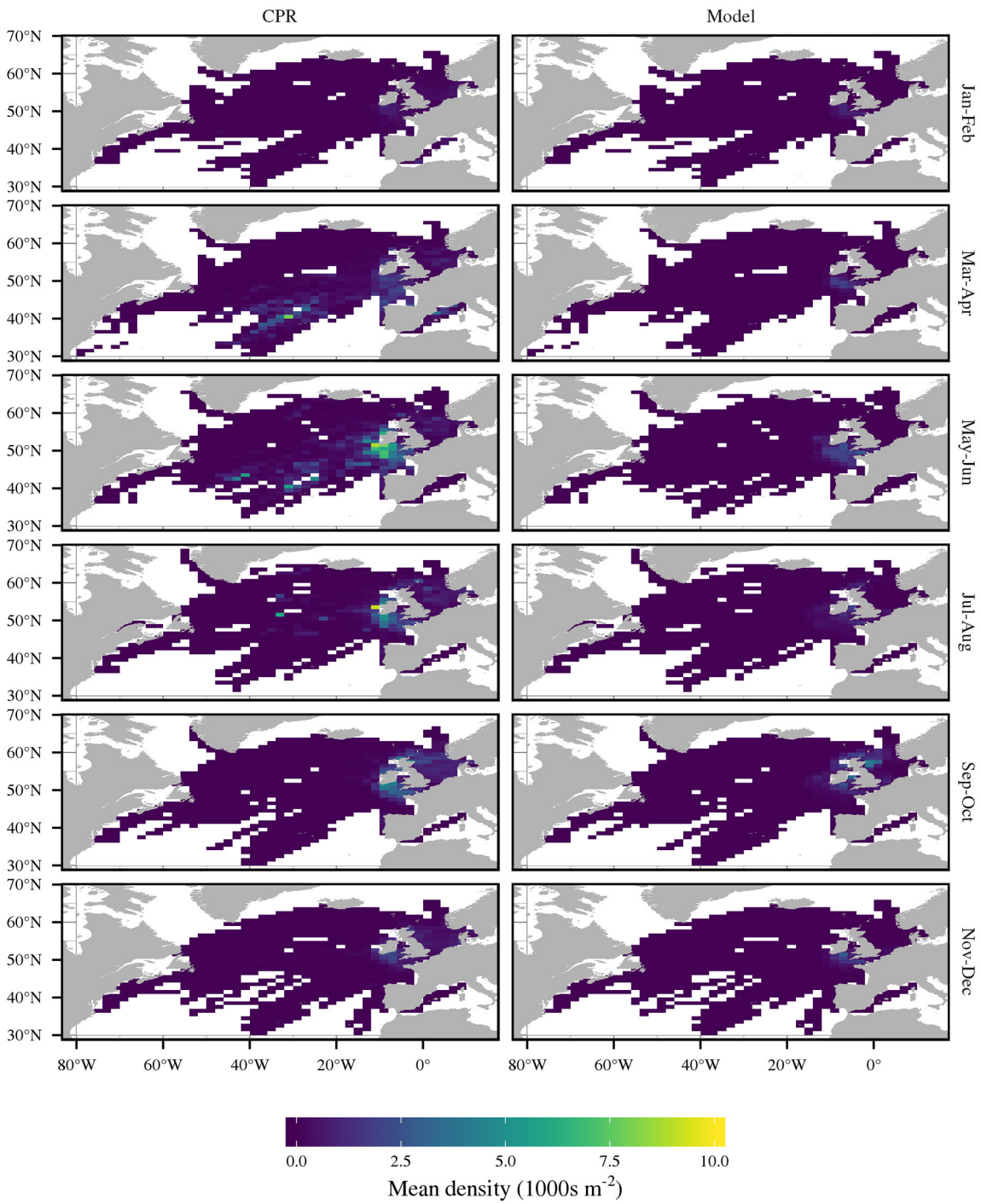


**FIGURE 3 | Comparison of bimonthly *C. helgolandicus* abundance as recorded by CPR and by the model.** Density is mean C5 and adult abundance.

cell. The approach outlined above was in agreement with Speirs et al.

## 2.4. Data Sources

### 2.4.1. The Continuous Plankton Recorder Survey

The Continuous Plankton Recorder Survey (CPR) is made up of data collected by devices attached to ships which traverse commercial shipping lanes. It is designed for towing depths of 10 m at the operating speeds of vessels (Batten et al., 2003). Water enters the CPR through a 1.27 $cm^2$ opening and is filtered by a 270 $\mu$m silk mesh. Abundance estimates are semi-quantitative, with each observation being placed in one of 12 distinct abundance categories (Rae, 1952). CPR provides reliable temporal and spatial measures (Batten et al., 2003; Hélaouët et al., 2016) of abundance. We used CPR data from 1958 to 2002.

### 2.4.2. Time Series

The EU TASC project collected time series of *C. finmarchicus* copepodite abundance in 1997 at three locations (Planque and Batten, 2000). Data was collected at Ocean Weather Ship Mike (OWS M) (66°N, 2°E) from 24 February to 17 December 1997 (Heath et al., 2000; Hirche et al., 2001) using a 180 $\mu$m mesh opening and closing multinet. Concentrations of copepodite stages ($m^{-3}$) were converted to stage abundances ($m^{-2}$) at 0–100 and 100–1600 m. During autumn and winter the population largely resided in the deep layer. We assume that deep animals were diapausing at that time. Per-capita egg production rates were also recorded at this station (Niehoff et al., 1999).

Data was collected at 2 locations near the Westmann Islands (63°27.25′N, 20°00.00′W, depth 100 m, and 63°22.20′N, 19°54.85′W, depth 200 m) (Gislason and Astthorsson, 2000). This site was visited 29 times, with *C. finmarchicus* being collected by vertically integrating hauls from 5 m above the seabed to the surface with a 200 $\mu$m mesh, 56 cm Bongo net. In addition, data was collected from Murchison (61°30.00′ N, 01°40.00′ E, depth 160 m) on 29 occasions, using a 200 $\mu$m mesh with a 30 cm Bongo net from a depth of 150 m to the surface.

We include data from Ocean Weather Ship India (OWS I) (59°N, 19°E), which was collected between 1971 and 1975 (Irigoien, 1999). This time series is used because we lack data for a truly oceanic location in 1997. Sampling occurred at approximately weekly intervals from 1971 to 1975 using oblique hauls of a Longhurst-Hardy plankton recorder (280 $\mu$m mesh). Stage-resolved copepod samples were then collected from a depth of 500 m to the surface, with a resolution of 10 m. We used data from the top 100 m.

The US GLOBEC program started in 1995 (Durbin et al., 2000), and includes extensive zooplankton sampling in the Gulf of Maine and Georges Bank. *C. finmarchicus* densities ($m^{-3}$) were estimated during the first half of the year at varying depths using a 1 $m^2$ MOCNESS fitted with 0.15 mm mesh nets. Estimates of density ($m^{-2}$) were calculated for the top 100 m and from 100 m to the sea floor by considering regions where bathymetry exceeded 200 m.

*C. helgolandicus* abundance data has been collected of Stonehaven, Scotland (56°57.8′ N, 2°6.2′W) since 1997. Sampling uses fine mesh nets, which collect an integrated sample of zooplankton throughout the water column (Bresnan et al., 2015). Integrated abundance data is provided for C5, female and male stages.

Station L4 in the English Channel (50°15′N, 4°13′W) is one of the longest standing zooplankton time series in European waters (Harris, 2010), with monitoring beginning in 1988. Seabed depth is 51 m, while observations typically range between 40 and 45 times each year (Harris, 2010). This time series contains information on the abundance of male, female and total copepodites, and egg production rate (Irigoien et al., 2000).

## 2.5. Parameter Derivation and Sensitivity Experiments

Our underlying goal was to reproduce the biogeography of both species displayed by the CPR. We therefore carried out an extensive set of simulations to assess how well different parameter sets could reproduce the geographic distributions of both species.

As discussed in Section 2.2, laboratory and field data were used to derive the following traits: development time, growth, fecundity, diapause duration, background mortality and body size. The remaining free, i.e., unknown, parameters related to the equations for diapause entry and starvation and biomass dependent mortality. We initially sought a single parameter set for mortality and diapause entry that would result in credible predictions of geographic distributions for both species. However, a large number of exploratory runs showed that this was not possible. We therefore sought parameter sets that reproduce the geographic distributions of both species while minimizing the differences between the model parameters of both species. A suite of runs showed that this was only achievable by assuming that mortality responded differently to temperature in both species.

Model parameters were derived by simultaneously altering the terms for mortality and diapause entry for both species and recording each parameterization's fit to CPR abundance data. First, CPR data was split into cells of dimension 2°E and 1°N, and we then removed cells without a CPR abundance record for each month of the year. Annual mean abundance was then calculated by averaging the mean abundance of the mean monthly abundance for C5 and adults in each cell.

This resulted in 333 cells for model comparisons. Each CPR abundance record represents approximately 3 $m^3$ of filtered seawater (Richardson et al., 2006). Therefore, CPR data must be divided by 3 to get estimates of abundance per $m^3$. This must then be multiplied by a further conversion factor of 20 (Speirs et al., 2006) to provide estimates of abundance ($m^{-2}$) over the top 100 m of the water column.

Simulations began by seeding a large number of eggs over the entire North Atlantic and in the eastern North Atlantic for *C. finmarchicus* and *C. helgolandicus*, respectively. The model was then run to a quasi-stable state and we then calculated the correlation coefficient ($r$) between predicted annual surface abundance ($m^{-2}$) and CPR abundance ($m^{-2}$).

We report two sensitivity experiments. First, we show the geographic distributions of both species when there are no interspecific differences in free parameters, i.e., only differences in growth, development and fecundity are assumed. In this case we are using the diapause entry and starvation and temperature

dependent mortality parameters for *C. helgolandicus* for both species.

Our initial model of diapause duration used a model of maximum potential diapause duration (Wilson et al., 2016), which possibly results in diapause durations which are unrealistically long. We therefore carried out a sensitivity analysis which relates the ability to reproduce the geographic distributions of both species to the assumptions for diapause duration and temperature dependent mortality. Temperature dependent mortality is proportional to $(T/8)^z$ for temperature T (°C). The parameterization assumed different values of $z$ for each species.

## 3. RESULTS

### 3.1. Model Results

**Figures 2**, **3** compare the model predictions and CPR estimates of bimonthly abundance for *C. finmarchicus* and *C. helgolandicus* respectively. **Table 1** shows the correlation coefficients between monthly modeled and CPR abundance for both species. The large-scale geographic pattern of *C. finmarchicus* abundance was successfully reproduced in comparison with CPR. The correlation coefficient between simulated mean annual abundance and CPR abundance over the 2°E by 1°N cells is 0.75. Bimonthly comparisons between *C. finmarchicus* predictions and the CPR abundance are shown in **Figure 2**. Importantly, we reproduced the relatively high abundance of *C. finmarchicus* in the West Atlantic in autumn. In addition, the model predicts a year round surface population in coastal waters in the West Atlantic, in accordance with CPR. However, it perhaps over-predicted abundance in November and December.

A comparison of bimonthly predictions of *C. helgolandicus* abundance with the CPR abundance is shown in **Figure 3**. The correlation coefficient between predicted mean annual abundance and CPR abundance over the 2°E by 1°N cells was 0.76. Importantly, *C. helgolandicus* was restricted to the continental shelf. The autumn bloom of *C. helgolandicus* in the North Sea was also reproduced. However, predicted abundance

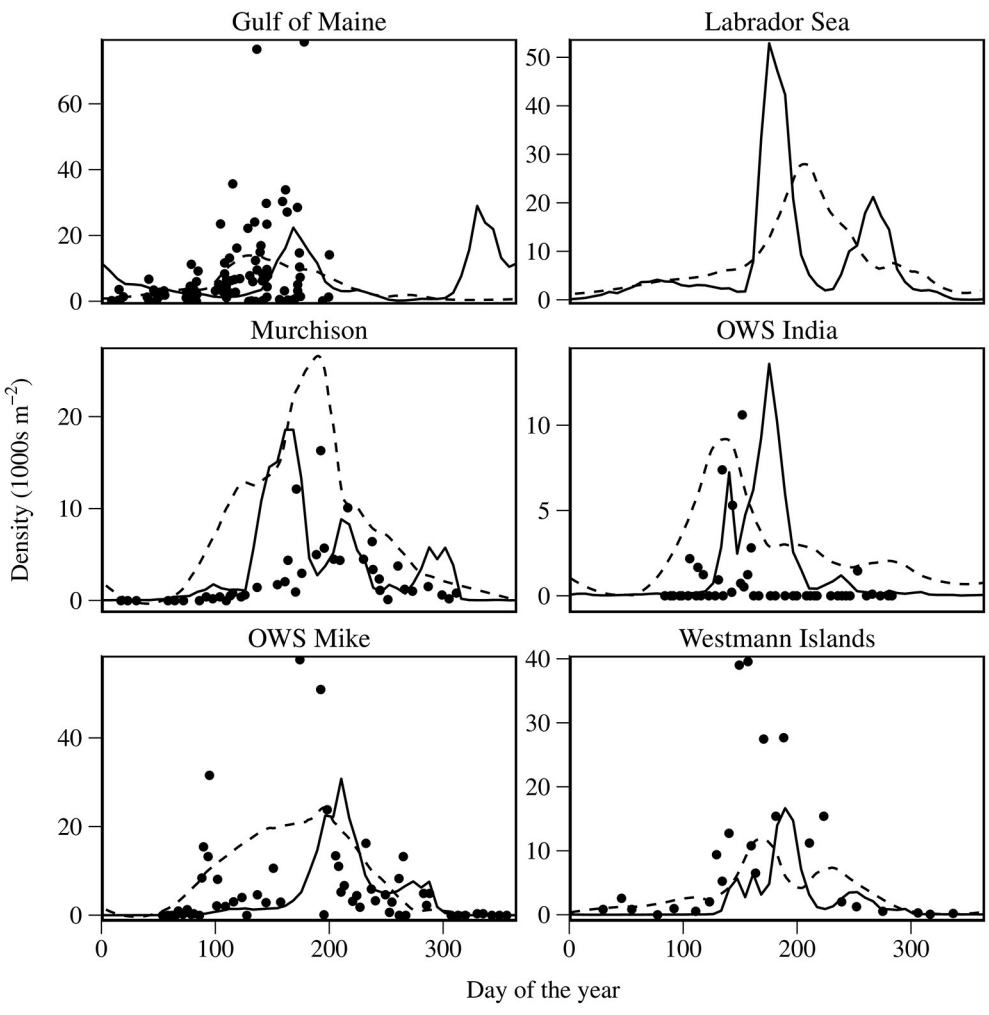


**FIGURE 4 | Comparison of modeled *C. finmarchicus* abundance for combined states C5 and adult with time series data.** Solid lines represent model output; dashed lines represent smooths of CPR abundance; points represent time series data. Abundance is depth integrated over the top 100 m of the water column.

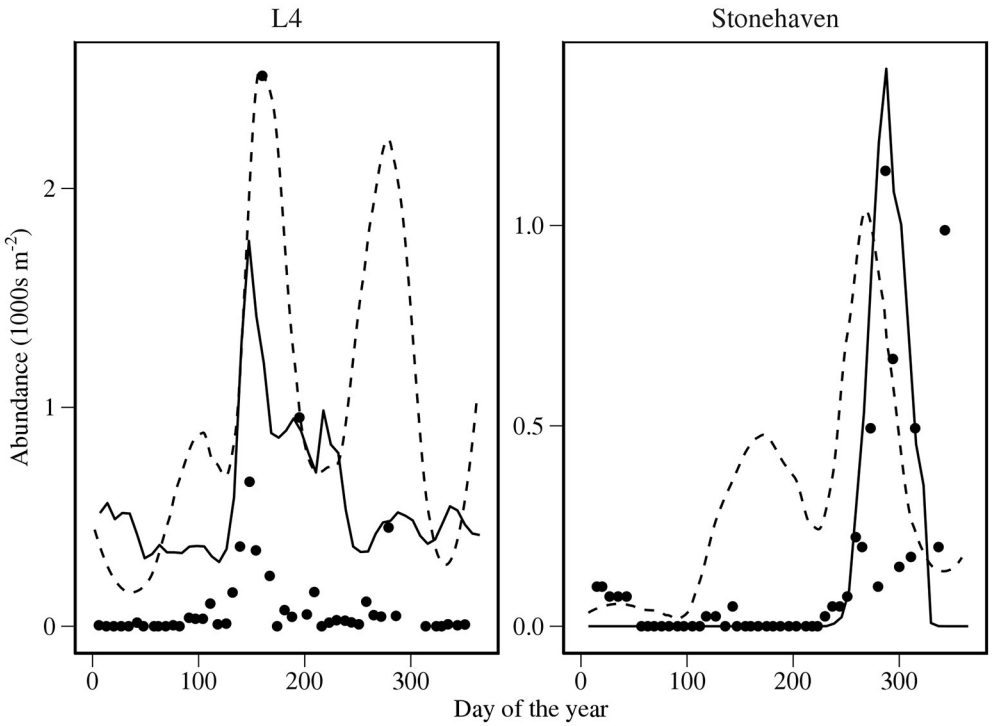


**FIGURE 5 | Comparison of modeled abundance of *C. helgolandicus* for combined states C5 and adult with time series data.** Solid lines represent model output; dashed lines represent smooths of CPR abundance; points represent time series data. Abundance is depth integrated over the top 100 m of the water column.

**TABLE 1 | The correlation coefficient (*r*) between modeled monthly abundance and the mean CPR abundance in each cell.**

| Month | *C. finmarchicus* | *C. helgolandicus* |
|---|---|---|
| January | 0.52 | 0.56 |
| February | 0.31 | 0.61 |
| March | 0.54 | 0.32 |
| April | 0.50 | 0.55 |
| May | 0.32 | 0.70 |
| June | 0.64 | 0.65 |
| July | 0.67 | 0.67 |
| August | 0.61 | 0.49 |
| September | 0.60 | 0.55 |
| October | 0.47 | 0.57 |
| November | 0.27 | 0.65 |
| December | 0.22 | 0.69 |

in November and December in the region to the south west of the British Isles appears too high.

**Figure 4** shows simulated combined abundance for stage C5 and adult *C. finmarchicus* compared with those from the time series. Predicted peak abundances are within a factor of 2 of those recorded in the time series, with the exception of the Westmann Islands. OWS I is notable for getting the scale of the first generation very accurate, but we predicted a much larger second generation than is apparent in the time series. We failed to show the apparent sharp increase in C5 and adult at OWS M before day 100. Additionally, the second peak in C5 and adult abundance at OWS M appears to be time shifted by approximately 50 d.

We compare predictions for *C. helgolandicus* with field time series and time series derived from CPR in **Figure 5**. The timing of the autumn peak of *C. helgolandicus* abundance at Stonehaven was successfully reproduced. However, we failed to reproduce the small spring bloom. Predicted time and the magnitude of peak abundance was close to that in the L4 time series. However, abundance appeared to be over-predicted during winter.

Predicted EPR is compared with field time series at OWS M and L4 for *C. finmarchicus* and *C. helgolandicus* respectively in **Figure 6**. Predicted *C. helgolandicus* EPR is lower in the first half of the year of the time series, and is slightly time shifted compared with the time series. Predictions depart significantly from the times series in the second half of the year, with EPR being significantly higher than in the time series. The *C. finmarchicus* EPR time series at OWS M is of short duration. We can therefore only make a limited comparison. However, the predicted EPR is approximately the same as the median EPR in the time series.

## 3.2. Sensitivity Experiments

In the results shown in Section 3.1, the only differences between the species are the relationship between growth, development and fecundity and temperature, and a parameterized difference in the response of mortality to temperature. **Figure 7** shows the predicted geographic distribution of *C. finmarchicus* when the

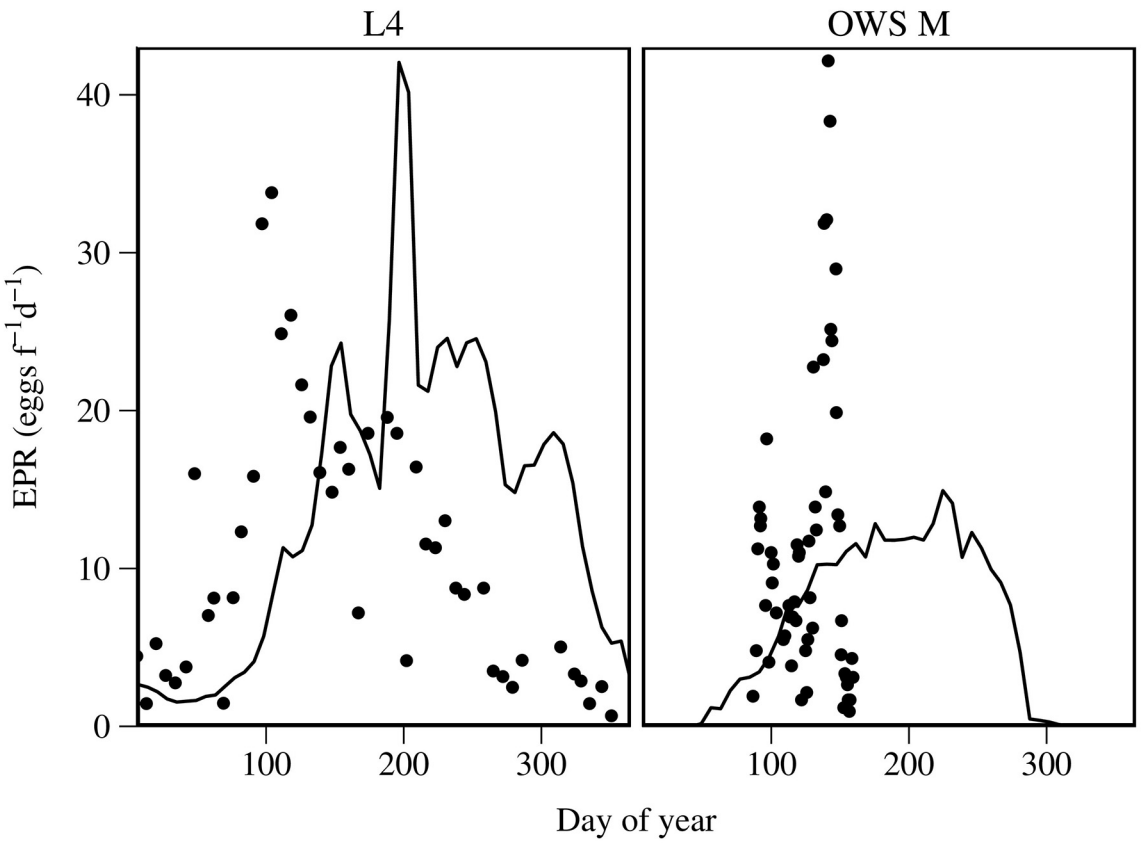


**FIGURE 6 | Predicted EPR for *C. helgolandicus* at L4, English Channel and for *C. finmarchicus* at OWS M compared with field estimates.** Solid lines are modeled EPR; points are field estimates.

temperature-dependent mortality parameter for *C. helgolandicus* was used. The geographic distribution in the west Atlantic is successfully reproduced. However, the geographic distribution in the east Atlantic is too southerly, with a large population predicted to exist in the Celtic Sea.

Exploratory simulations showed that the *C. helgolandicus* predictions were sensitive to diapause assumptions. First, the model performed well if *C. helgolandicus* was assumed to remain at the surface year round and to never diapause. In fact, this simplified model arguably performed better than the original. The key features of the distribution of *C. helgolandicus* were largely reproduced, with the correlation coefficient (0.78) of model performance compared with CPR actually improving in comparison with our original model.

Further exploratory simulations showed that the state of populations of *C. helgolandicus* is sensitive to diapause duration. A sensitivity analysis showed that small changes to diapause or mortality assumptions can result in *C. helgolandicus* becoming an oceanic species. **Figure 8** shows the correlation coefficient between predictions and CPR abundance of *C. helgolandicus* under varying assumptions for diapause duration and the scaling of mortality with temperature. A small reduction in how steeply mortality scales with temperature results in a reduction in model performance, with *C. helgolandicus* becoming an oceanic species. Likewise, an increase in diapause duration can result in *C. helgolandicus* becoming an oceanic species. Notably, the high sensitivity to changes in temperature dependent mortality was not evident diapause duration is reduced by 60%, which is potentially a more biologically realistic assumption for diapause duration.

## 4. DISCUSSION

This study can be framed by a single question. What differences between *C. finmarchicus* and *C. helgolandicus* explain the relative geographic distributions of these two species? Alternatively, we can ask how much we need to change *C. finmarchicus*'s traits before it effectively becomes *C. helgolandicus*.

In this setting, the model equations can be viewed as describing a generic *Calanus* species, while the parameters determine where a species lies in trait space. We showed that the geographic distributions of both species can be reproduced by assuming only two interspecific differences. These were the temperature response of mortality and the temperature influence on ingestion rate, which in turn influences growth, development and fecundity. In other words, we can effectively turn *C. finmarchicus* into *C. helgolandicus* by modifying those two traits. This framework has the potential to be applied to a number of

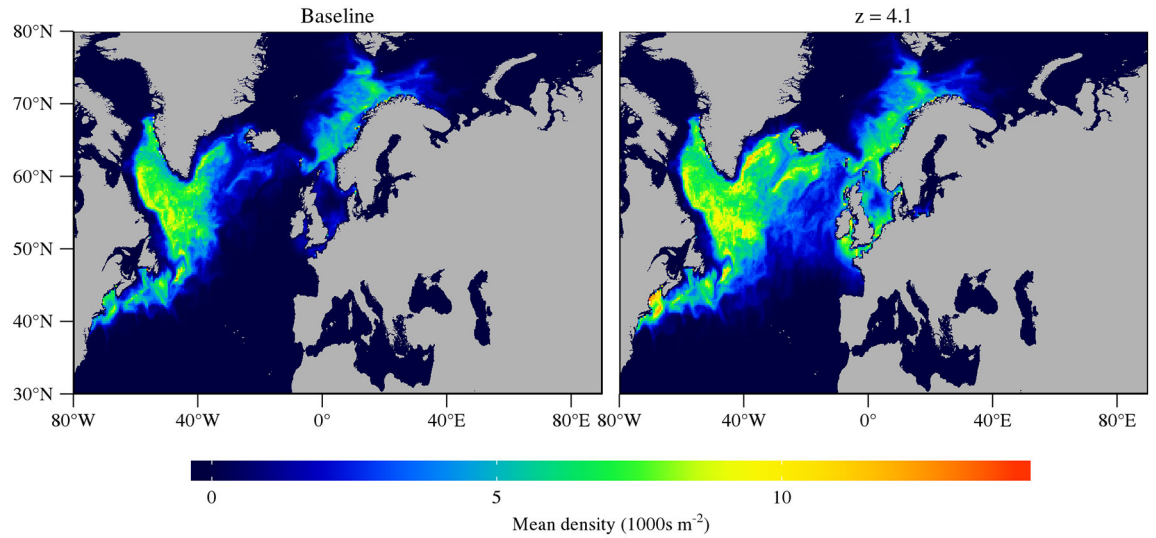


**FIGURE 7 | Mean annual abundance of C5 and adult *C. finmarchicus* under the assumption that temperature scaling of mortality, $z = 7$ and $z = 4.1$.** A higher value of $z$ means that mortality scales much more steeply with temperature.

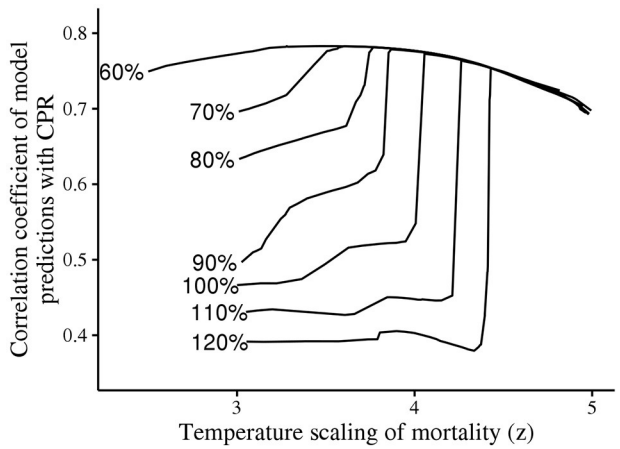


**FIGURE 8 | Sensitivity of *C. helgolandicus* model to diapause duration.** Diapause duration was altered by a fixed percentage throughout the model domain, and the temperature scaling of mortality was varied. Abrupt changes in model fit close to the optimum indicates that *C. helgolandicus* switches from being a shelf to an oceanic species.

*Calanus* species, and represents a complimentary approach to that taken by others (e.g., Record et al., 2010, 2013; Maps et al., 2012).

A key assumption underlying almost all population models of *Calanus* is that growth and egg production rate increase monotonically with temperature. This is the second study after Maar et al. (2013) to assume they do not. Instead, we use a dome-shaped relationship between growth and fecundity and temperature. Similar responses have now been established for a number of zooplankton species (White and Roman, 1992; Koski and Kuosa, 1999; Halsband-Lenk et al., 2002; Holste and Peck, 2006; Holste et al., 2009; Rhyne et al., 2009; Pasternak et al., 2013).

The relationships between fecundity and development time and temperature were derived from the experimental ingestion rate data of Møller et al. (2012). A review of the literature shows that we have little knowledge of the key traits of *C. finmarchicus* such as development, growth and fecundity above 12°C (**Table 2**). Further, we are not aware of published evidence of the influence of temperature on *C. helgolandicus*'s fecundity. Clarifications of the relationship between growth and temperature are therefore a priority of *Calanus* research. Importantly, conventional models of development are problematic in the context of climate change, where they may falsely predict ever increasing growth rates as temperatures rise. This is highlighted in the Gulf of Maine, where despite summer surface temperatures now often exceeding 20°C (Mills et al., 2013) there have recently been record high levels of *C. finmarchicus* abundance (Runge et al., 2014).

Understanding the relative geographic distributions of both species can arguably be answered by asking why only *C. helgolandicus* exists in the region south west of the British Isles. On the basis of our models of growth and fecundity, this region is not noticeably favorable to *C. helgolandicus*. However, the population model's performance is instructive. Simulated abundance of *C. helgolandicus* is much higher in winter at L4 than in reality, and we significantly over-predicted EPR in the second half of the year compared with the long-term seasonal pattern (Maud et al., 2015). This is potentially related to food quality. Resolving the apparent contradictions in understanding of the influence of food quality on fecundity (Niehoff et al., 1999; Jønasdøttir et al., 2002; Maud et al., 2015) and development time (Diel and Klein Breteler, 1986) may therefore be the key to fully explaining the relative biogeographies of both species.

Measuring mortality in copepods is commonly viewed as an intractable problem (Ohman, 2012), and therefore models of mortality are inherently uncertain and difficult to validate. This problem is highlighted by our formulation of starvation

**TABLE 2 | Temperature ranges for measurement of key *C. finmarchicus* traits.**

| Trait | Maximum temperature (°C) | References |
|---|---|---|
| Growth | 12 | 3, 4, 5, 9,19, 23 |
| Development | 12 | 4, 18, 19, 21, 23 |
| Fecundity | 13.5 | 2, 3, 7*, 8, 12, 16 |
| Egg hatching success | 22 | 15 |
| Ingestion rate | 21 | 3, 11, 14* |
| Respiration rates | 17.9 | 1, 6, 10, 13*, 20 |
| Costs of gonad formation | 8 | 17 |

**indicates the reference with the highest reported temperature. References: 1. Ingvarsdøttir et al., 1999; 2. Rey et al., 1999; 3. Harris, 2000; 4. Campbell et al., 2001 5. Hygum et al., 2000b; 6. Saumweber and Durbin, 2006; 7. Runge and Plourde, 1996; 10. Hirche, 1983; 11. Meyer et al., 2002; 12. Hirche et al., 1997; 13. Hirche, 1987; 14. Møller et al., 2012; 15. Preziosi and Runge, 2014; 16. Kjellerup et al., 2012; 17. Rey-Rassat et al., 2002; 18. Cook et al., 2007; 19. Hygum et al., 2000a; 20. Ikeda et al., 2001; 21. Corkett et al., 1986; 22. Tande, 1988; 23. Diel and Klein Breteler, 1986.*

mortality, where it was related to growth rate. The formulation was similar to that used by other modelers (e.g., Tittensor et al., 2003), however it was *ad-hoc* and impossible to validate. Importantly, the modeled biogeography of *C. helgolandicus* was dependent on starvation mortality, where it plays a key role in reducing post-diapause populations in oceanic regions to a low enough level to eliminate long-term persistence. However, alternative formulations of mortality could potentially achieve this. Some zooplankton modelers have used U-shaped relationships between mortality and temperature (Rajakaruna et al., 2012), which could act as a limit on the north-western distribution of *C. helgolandicus*. Further, allee effects (Kiørboe, 2006) and the impact of starvation on long-term fecundity (Niehoff, 2004) could significantly deplete the populations of low-abundance post-diapause *C. helgolandicus* populations. Including these mortality effects in our model would result in a more complete representation of copepod ecology. However, there is little evidence to quantify the relative magnitude of these sources of mortality. Further advances in understanding copepod mortality (Gentleman et al., 2012; Ohman, 2012) are therefore likely necessary to justify increasingly complex mortality models. However, the influence of mortality should be considered if the model is to be applied, particularly in climate change contexts where changes might be dependent on the specific mortality formulation.

There is a spring bloom of *C. helgolandicus* in the North Sea (Bresnan et al., 2015), which we did not predict. However, the apparent phenology of *C. helgolandicus* in the North Sea is difficult to reconcile with the known influence of temperature on its development time (Cook et al., 2007; Bonnet et al., 2009). The first Stonehaven bloom typically occurs before day 130, and temperatures are below 9 °C before then. Evidence indicates that *C. helgolandicus* either cannot develop from egg to adult (Bonnet et al., 2009) or has a development time greater than 120 d at these temperatures (Møller et al., 2012). Research is therefore needed to reconcile development time studies of *C. helgolandicus* and phenology in the North Sea. Further, additional model runs (not shown) indicated that most of the modeled autumn bloom in the northern North Sea resulted from animals that are advected into the North Sea from the North. The importance of advection for North Sea *C. finmarchicus* populations has been previously been studied (Heath et al., 1999), however the role of advection in influencing year to year North Sea *C. helgolandicus* abundance has not. It may be possible that *C. helgolandicus* phenology in the North Sea can be explained by the existence of hybrids of *C. helgolandicus* and *C. finmarchicus*. This is a speculative hypothesis. However, at the fringes of its northern distribution, *C. finmarchicus* hybridizes with *C. glacialis* (Parent et al., 2011; Gabrielsen et al., 2012; Berchenko and Stupnikova, 2014), and we cannot rule out a similar phenomenon for *C. finmarchicus* and *C. helgolandicus*.

Finally, our model highlights the importance of lipid dynamics and deep-water temperatures as influences on the distribution of *Calanus*. Existing statistical models of *Calanus* biogeography (Helaouët and Beaugrand, 2007; Chust et al., 2013; Hinder et al., 2013) and projections of future distributions (Reygondeau and Beaugrand, 2011; Villarino et al., 2015) have only considered surface conditions. However, the distribution of *C. helgolandicus* appears to be strongly influenced by deep-water temperatures. Conditions in large parts of the North Atlantic are sufficient to support at least one generation of *C. helgolandicus*, but high overwintering temperatures result in the inability of a sufficiently large overwintering population to maintain a persistent population. Recent work showed that projected potential diapause duration of *C. finmarchicus* in the Norwegian Sea under a high emissions scenario was largely unchanged this century, whereas surface temperature increases significantly (Wilson et al., 2016). Development conditions will therefore improve significantly for *C. helgolandicus* in the Norwegian Sea, whereas diapause conditions would remain largely unchanged. There is therefore potential for *C. helgolandicus* to become an oceanic species as a result of deep-water warming lagging that at the surface. Similarly, these marginal changes in potential diapause duration may act as a brake on the northward retreat of *C. finmarchicus*. However, the expected temperature increases across the North Atlantic will reduce lipid levels of animals (Wilson et al., 2016) and the consequences are poorly understood. The future evolution of lipid dynamics may therefore be pivotal in determining the fate of *Calanus* communities and will have important consequences for the fish, seabirds and marine mammals that depend on the lipids provided by copepods (Beaugrand and Kirby, 2010; Frederiksen et al., 2013).

## AUTHOR CONTRIBUTIONS

RW, MH, and DS contributed to the design of the model. RW implemented and analyzed the model and led the writing of the paper. All authors contributed to the editing and refining of the paper.

## FUNDING

This work received funding from the MASTS pooling initiative (The Marine Alliance for Science and Technology for Scotland) and their support is gratefully acknowledged. MASTS is funded

by the Scottish Funding Council (grant reference HR09011) and contributing institutions.

## ACKNOWLEDGMENTS

We thank the Continuous Plankton Recorder Survey for providing access to data, and Neil Banas for fruitful discussions that helped shape the diapause model in the paper. Andrew Yool provided output from the NEMO model. Nicholas Record and a second reviewer provided helpful critical comments which improved the manuscript. Finally, we thank Ian Thurlbeck for invaluable IT support.

## SUPPLEMENTARY MATERIAL

The Supplementary Material for this article can be found online at: http://journal.frontiersin.org/article/10.3389/fmars.2016.00157

## REFERENCES

Barton, A. D., Pershing, A. J., Litchman, E., Record, N. R., Edwards, K. F., Finkel, Z. V., et al. (2013). The biogeography of marine plankton traits. *Ecol. Lett.* 16, 522–534. doi: 10.1111/ele.12063

Batten, S. D., Clark, R., Flinkman, J., Hays, G., John, E., John, A. W. G., et al. (2003). CPR sampling: the technical background, materials and methods, consistency and comparability. *Prog. Oceanogr.* 58, 193–215. doi: 10.1016/j.pocean.2003.08.004

Beaugrand, G. (2012). Unanticipated biological changes and global warming. *Mar. Ecol. Prog. Ser.* 445, 293–301. doi: 10.3354/meps09493

Beaugrand, G., and Kirby, R. R. (2010). Climate, plankton and cod. *Global Change Biol.* 16, 1268–1280. doi: 10.1111/j.1365-2486.2009.02063.x

Beaugrand, G., Luczak, C., and Edwards, M. (2009). Rapid biogeographical plankton shifts in the North Atlantic Ocean. *Global Change Biol.* 15, 1790–1803. doi: 10.1111/j.1365-2486.2009.01848.x

Beaugrand, G., Reid, P. C., Ibañez, F., Lindley, J. A., and Edwards, M. (2002). Reorganization of North Atlantic marine copepod biodiversity and climate. *Science* 296, 1692–1694. doi: 10.1126/science.1071329

Berchenko, I. V., and Stupnikova, A. N. (2014). Morphological peculiarities of *Calanus finmarchicus* and *Calanus glacialis* in the areas of the co-existence of their populations. *Oceanology* 54, 450–457. doi: 10.1134/S0001437014040031

Bonnet, D., Harris, R. P., Yebra, L., Guilhaumon, F., Conway, D. V. P., and Hirst, A. G. (2009). Temperature effects on *Calanus helgolandicus* (Copepoda: Calanoida) development time and egg production. *J. Plankton Res.* 31, 31–44. doi: 10.1093/plankt/fbn099

Bonnet, D., Richardson, A., Harris, R., Hirst, A., Beaugrand, G., Edwards, M., et al. (2005). An overview of *Calanus helgolandicus* ecology in European waters. *Prog. Oceanogr.* 65, 1–53. doi: 10.1016/j.pocean.2005.02.002

Bresnan, E., Cook, K. B., Hughes, S. L., Hay, S. J., Smith, K., Walsham, P., et al. (2015). Seasonality of the plankton community at an east and west coast monitoring site in Scottish waters. *J. Sea Res.* 105, 16–29. doi: 10.1016/j.seares.2015.06.009

Campbell, R. G., Wagner, M. M., Teegarden, G. J., Boudreau, C. A., and Durbin, E. G. (2001). Growth and development rates of *Calanus finmarchicus* the copepod reared in the laboratory. *Mar. Ecol. Prog. Ser.* 221, 161–183. doi: 10.3354/meps221161

Chust, G., Castellani, C., Licandro, P., Ibaibarriaga, L., Sagarminaga, Y., and Irigoien, X. (2013). Are *Calanus* spp. shifting poleward in the North Atlantic? A habitat modelling approach. *ICES J. Mar. Sci.* 71, 241–253. doi: 10.1093/icesjms/fst147

Clarke, E. D., Speirs, D. C., Heath, M., Wood, S. N., Gurney, W. S. C., and Holmes, S. J. (2006). Calibrating remotely sensed chlorophyll-a data by using penalized regression splines. *J. R. Stat. Soc. Ser. C* 55, 331–353. doi: 10.1111/j.1467-9876.2006.00540.x

Comiso, J. (1997). *Bootstrap Sea Ice Concentrations from Nimbus-7 SMMR and DMSP SSM/I-SSMIS*. Boulder, CO: Natinoal Snow and Ice Data Center.

Cook, K. B., Bunker, A., Hay, S., Hirst, A. G., and Speirs, D. C. (2007). Naupliar development times and survival of the copepods *Calanus helgolandicus* and *Calanus finmarchicus* in relation to food and temperature. *J. Plankton Res.* 29, 757–767. doi: 10.1093/plankt/fbm056

Corkett, C. J., McLaren, I. A., and Sevigny, J.-M. (1986). The rearing of the marine calanoid copepods *Calanus finmarchicus* (Gunnerus), *C. glacialis* Jaschnov and *C. hyperboreus* Krøyer with comment on the equiproportional rule. *Syllogeus* 58, 539–546.

Diel, S., and Klein Breteler, W. C. M. (1986). Growth and development of *Calanus* spp. (Copepoda) during spring phytoplankton succession in the North Sea. *Mar. Biol.* 92, 85–92. doi: 10.1007/BF00397574

Durbin, E. G., Garrahan, P. R., and Casas, M. C. (2000). Abundance and distribution of *Calanus finmarchicus* on the Georges Bank during 1995 and 1996. *ICES J. Mar. Sci.* 57, 1664–1685. doi: 10.1006/jmsc.2000.0974

Eiane, K., Aksnes, D. L., Ohman, M. D., Wood, S., and Martinussen, M. B. (2002). Stage-specific mortality of *Calanus* spp. under different predation regimes. *Sarsia* 47, 636–645. doi: 10.4319/lo.2002.47.3.0636

Frederiksen, M., Anker-Nilssen, T., Beaugrand, G., and Wanless, S. (2013). Climate, copepods and seabirds in the boreal Northeast Atlantic - current state and future outlook. *Global Change Biol.* 19, 364–372. doi: 10.1111/gcb.12072

Gabrielsen, T. M., Merkel, B., Sreide, J. E., Johansson-Karlsson, E., Bailey, A., Vogedes, D., et al. (2012). Potential misidentifications of two climate indicator species of the marine arctic ecosystem: *Calanus glacialis* and *C. finmarchicus*. *Polar Biol.* 35, 1621–1628. doi: 10.1007/s00300-012-1202-7

Gentleman, W. C., Pepin, P., and Doucette, S. (2012). Estimating mortality: clarifying assumptions and sources of uncertainty in vertical methods. *J. Mar. Syst.* 105–108, 1–19. doi: 10.1016/j.jmarsys.2012.05.006

Gislason, A., and Astthorsson, O. S. (2000). Winter distribution, ontogenetic migration, and rates of egg production of *Calanus finmarchicus* southwest of Iceland. *ICES J. Mar. Sci.* 57, 1727–1739. doi: 10.1006/jmsc.2000.0951

Gurney, W. S. C., Speirs, D. C., Wood, S. N., Clarke, E. D., and Heath, M. R. (2001). Simulating spatially and physiologically structured populations. *J. Anim. Ecol.* 70, 881–894. doi: 10.1046/j.0021-8790.2001.00549.x

Halsband-Lenk, C., Hirche, H.-J., and Carlotti, F. (2002). Temperature impact on reproduction and development of congener copepod populations. *J. Exp. Mar. Biol. Ecol.* 271, 121–153. doi: 10.1016/S0022-0981(02)00025-4

Harris, R. (2000). Feeding, growth, and reproduction in the genus *Calanus*. *ICES J. Mar. Sci.* 57, 1708–1726. doi: 10.1006/jmsc.2000.0959

Harris, R. (2010). The L4 time-series: the first 20 years. *J. Plankton Res.* 32, 577–583. doi: 10.1093/plankt/fbq021

Heath, M. R., Astthorsson, O. S., Dunn, J., Ellertsen, B., Gaard, E., Gislason, A., et al. (2000). Comparative analysis of *Calanus finmarchicus* demography at locations around the Northeast Atlantic. *ICES J. Mar. Sci.* 57, 1562–1580. doi: 10.1006/jmsc.2000.0950

Heath, M. R., Backhaus, J. O., Richardson, K., McKenzie, E., Slagstad, D., Beare, D., et al. (1999). Climate fluctuations and the spring invasion of the North Sea by *Calanus finmarchicus*. *Fish. Oceanogr.* 8, 163–176. doi: 10.1046/j.1365-2419.1999.00008.x

Heath, M. R., Boyle, P., Gislason, A., Gurney, W. S. C., Hay, S. J., Head, E. J. H., et al. (2004). Comparative ecology of over-wintering *Calanus finmarchicus* in the northern North Atlantic, and implications for life-cycle patterns. *ICES J. Mar. Sci.* 61, 698–708. doi: 10.1016/j.icesjms.2004.03.013

Helaouët, P., and Beaugrand, G. (2007). Macroecology of *Calanus finmarchicus* and *C. helgolandicus* in the North Atlantic Ocean and adjacent seas. *Mar. Ecol. Prog. Ser.* 345, 147–165. doi: 10.3354/meps06775

Hélaouët, P., Beaugrand, G., and Reygondeau, G. (2016). Reliability of spatial and temporal patterns of *C. finmarchicus* inferred from the CPR survey. *J. Mar. Syst.* 153, 18–24. doi: 10.1016/j.jmarsys.2015.09.001

Hinder, S. L., Gravenor, M. B., Edwards, M., Ostle, C., Bodger, O. G., Lee, P. L. M., et al. (2013). Multi-decadal range changes vs. thermal adaptation for north east

Atlantic oceanic copepods in the face of climate change. *Global Change Biol.* 20, 140–146. doi: 10.1111/gcb.12387

Hirche, H.-J. (1983). Overwintering of *Calanus finmarchicus* and *Calanus helgolandicus*. *Mar. Ecol. Prog. Ser.* 11, 281–290. doi: 10.3354/meps011281

Hirche, H.-J. (1987). Temperature and plankton II. Effect on respiration and swimming activity in copepods from the Greenland Sea. *Mar. Biol.* 95, 347–356. doi: 10.1007/BF00428240

Hirche, H.-J., Brey, T., and Niehoff, B. (2001). A high-frequency time series at Ocean Weather Ship Station M (Norwegian Sea): population dynamics of *Calanus finmarchicus*. *Mar. Ecol. Prog. Ser.* 219, 205–219. doi: 10.3354/meps219205

Hirche, H.-J., Meyer, U., and Niehoff, B. (1997). Egg production of *Calanus finmarchicus*: effect of temperature, food and season. *Mar. Biol.* 127, 609–620. doi: 10.1007/s002270050051

Hirst, A. G., Bonnet, D., and Harris, R. P. (2007). Seasonal dynamics and mortality rates of *Calanus helgolandicus* over two years at a station in the English Channel. *Mar. Ecol. Prog. Ser.* 340, 189–205. doi: 10.3354/meps340189

Holste, L., and Peck, M. A. (2006). The effects of temperature and salinity on egg production and hatching success of Baltic *Acartia tonsa* (Copepoda: Calanoida): a laboratory investigation. *Mar. Biol.* 148, 1061–1070. doi: 10.1007/s00227-005-0132-0

Holste, L., St. John, M. A., and Peck, M. A. (2009). The effects of temperature and salinity on reproductive success of *Temora longicornis* in the Baltic Sea: a copepod coping with a tough situation. *Mar. Biol.* 156, 527–540. doi: 10.1007/s00227-008-1101-1

Hygum, B. H., Rey, C., and Hansen, B. W. (2000a). Growth and development rates of *Calanus finmarchicus* nauplii during a diatom spring bloom. *Mar. Biol.* 136, 1075–1085. doi: 10.1007/s002270000313

Hygum, B. H., Rey, C., Hansen, B. W., and Tande, K. (2000b). Importance of food quantity to structural growth rate and neutral lipid reserves accumulated in *Calanus finmarchicus*. *Mar. Biol.* 136, 1057–1073. doi: 10.1007/s002270000292

Ikeda, T., Kanno, Y., Ozaki, K., and Shinada, A. (2001). Metabolic rates of epipelagic marine copepods as a function of body mass and temperature. *Mar. Biol.* 139, 587–596. doi: 10.1007/s002270100608

Ingvarsdøttir, A., Houlihan, D. F., Heath, M. R., and Hay, S. J. (1999). Seasonal changes in respiration rates of copepodite stage V *Calanus finmarchicus* (Gunnerus). *Fish. Oceanogr.* 8, 73–83. doi: 10.1046/j.1365-2419.1999.00002.x

Irigoien, X. (1999). Vertical distribution and population structure of *Calanus* fimarchicus at station India (59 °N, 19 °W) during the passage of the great salinity anomaly , 1971-1975. *Deep Sea Res. I* 47, 1–26. doi: 10.1016/S0967-0637(99)00045-X

Irigoien, X., Head, R. N., Harris, R. P., Cummings, D., and Harbour, D. (2000). Feeding selectivity and egg production of *Calanus helgolandicus* in the English Channel. *Limnol. Oceanogr.* 45, 44–54. doi: 10.4319/lo.2000.45.1.0044

Jønasdøttir, S. H., Gudfinnsson, H. G., Gislason, A., and Astthorsson, O. S. (2002). Diet composition and quality for *Calanus finmarchicus* egg production and hatching success off south-west Iceland. *Mar. Biol.* 140, 1195–1206. doi: 10.1007/s00227-002-0782-0

Kiørboe, T. (2006). Sex, sex-ratios, and the dynamics of pelagic copepod populations. *Oecologia* 148, 40–50. doi: 10.1007/s00442-005-0346-3

Kjellerup, S., Dünweber, M., Swalethorp, R., Nielsen, T. G., Møller, E. F., Markager, S., et al. (2012). Effects of a future warmer ocean on the coexisting copepods *Calanus finmarchicus* and *C. glacialis* in Disko Bay, western Greenland. *Mar. Ecol. Prog. Ser.* 447, 87–108. doi: 10.3354/meps09551

Koski, M., and Kuosa, H. (1999). The effect of temperature, food concentration and female size on the egg production of the planktonic copepod *Acartia bifilosa*. *J. Plankton Res.* 21, 1779–1789. doi: 10.1093/plankt/21.9.1779

Lett, C., Verley, P., Mullon, C., Parada, C., Brochier, T., Penven, P., et al. (2008). A Lagrangian tool for modelling ichthyoplankton dynamics. *Environ. Model. Softw.* 23, 1210–1214. doi: 10.1016/j.envsoft.2008.02.005

Litchman, E., Ohman, M. D., and Kiørboe, T. (2013). Trait-based approaches to zooplankton communities. *J. Plankton Res.* 35, 473–484. doi: 10.1093/plankt/fbt019

Maar, M., Møller, E. F., Gürkan, Z., Jønasdøttir, S. H., and Nielsen, T. G. (2013). Sensitivity of *Calanus* spp. copepods to environmental changes in the North Sea using life-stage structured models. *Prog. Oceanogr.* 111, 24–37. doi: 10.1016/j.pocean.2012.10.004

Madec, G. (2012). "NEMO ocean engine," in *Note du Pole de modélisation, Institut Pierre-Simon Laplace (IPSL)* (Paris).

Maps, F., Pershing, A. J., and Record, N. R. (2012). A generalized approach for simulating growth and development in diverse marine copepod species. *ICES J. Mar. Sci.* 69, 370–379. doi: 10.1093/icesjms/fsr182

Maud, J. L., Atkinson, A., Hirst, A. G., Lindeque, P. K., Widdicombe, C. E., Harmer, R. A., et al. (2015). How does *Calanus helgolandicus* maintain its population in a variable environment? Analysis of a 25-year time series from the English Channel. *Prog. Oceanogr.* 137, 513–523. doi: 10.1016/j.pocean.2015.04.028

McLaren, I. A., and Leonard, A. (1995). Assessing the equivalence of growth and egg production of copepods. *ICES J. Mar. Sci.* 52, 397–408. doi: 10.1016/1054-3139(95)80055-7

Melle, W., Runge, J., Head, E., Plourde, S., Castellani, C., Licandro, P., et al. (2014). The North Atlantic Ocean as habitat for *Calanus finmarchicus*: environmental factors and life history traits. *Prog. Oceanogr.* 129, 244–284. doi: 10.1016/j.pocean.2014.04.026

Meyer, B., Irigoien, X., Graeve, M., Head, R. N., and Harris, R. P. (2002). Feeding rates and selectivity among nauplii, copepodites and adult females of *Calanus finmarchicus* and *Calanus helgolandicus*. *Helgoland Mar. Res.* 56, 169–176. doi: 10.1007/s10152-002-0105-3

Mills, K., Pershing, A., and Brown, C. (2013). Fisheries management in a changing climate: lessons from the 2012 ocean heat wave in the northwest Atlantic. *Oceanography* 26, 191–195. doi: 10.5670/oceanog.2013.27

Møller, E. F., Maar, M., Jónasdóttir, S. H., Gissel Nielsen, T., and Tönnesson, K. (2012). The effect of changes in temperature and food on the development of *Calanus finmarchicus* and *Calanus helgolandicus* populations. *Limnol. Oceanogr.* 57, 211–220. doi: 10.4319/lo.2012.57.1.0211

Niehoff, B. (2004). The effect of food limitation on gonad development and egg production of the planktonic copepod *Calanus finmarchicus*. *J. Exp. Mar. Biol. Ecol.* 307, 237–259. doi: 10.1016/j.jembe.2004.02.006

Niehoff, B., Klenke, U., Hirche, H. J., Irigoien, X., Head, R., and Harris, R. (1999). A high frequency time series at Weathership M, Norwegian Sea, during the 1997 spring bloom: the reproductive biology of *Calanus finmarchicus*. *Mar. Ecol. Prog. Ser.* 176, 81–92. doi: 10.3354/meps176081

Ohman, M. D. (2012). Estimation of mortality for stage-structured zooplankton populations: what is to be done? *J. Mar. Syst.* 93, 4–10. doi: 10.1016/j.jmarsys.2011.05.008

Ohman, M. D., Eiane, K., Durbin, E. G., Runge, J. A., and Hirche, H. J. (2004). A comparative study of *Calanus finmarchicus* mortality patterns at five localities in the North Atlantic. *ICES J. Mar. Sci.* 61, 687–697. doi: 10.1016/j.icesjms.2004.03.016

Parent, G. J., Plourde, S., and Turgeon, J. (2011). Overlapping size ranges of *Calanus* spp. off the Canadian Arctic and Atlantic Coasts: impact on species' abundances. *J. Plankt. Res.* 33, 1654–1665. doi: 10.1093/plankt/fbr072

Parent, G. J., Plourde, S., and Turgeon, J. (2012). Natural hybridization between *Calanus finmarchicus* and *C. glacialis* (Copepoda) in the Arctic and Northwest Atlantic. *Limnol. Oceanogr.* 57, 1057–1066. doi: 10.4319/lo.2012.57.4.1057

Parsons, T. R., Takahashi, M., and Hargrave, B. (1984). *Biological Oceanographic Processes*. Oxford: Pergamon Press.

Pasternak, A. F., Arashkevich, E. G., Grothe, U., Nikishina, A. B., and Solovyev, K. A. (2013). Different effects of increased water temperature on egg production of *Calanus finmarchicus* and *C. glacialis*. *Mar. Biol.* 53, 547–553. doi: 10.1134/s0001437013040085

Planque, B., and Batten, S. D. (2000). *Calanus finmarchicus* in the North Atlantic: the year of *Calanus* in the context of interdecadal change. *ICES J. Mar. Sci.* 57, 1528–1535. doi: 10.1006/jmsc.2000.0970

Preziosi, B. M., and Runge, J. A. (2014). The effect of warm temperatures on hatching success of the marine planktonic copepod, *Calanus finmarchicus*. *J. Plankton Res.* 36, 1381–1384. doi: 10.1093/plankt/fbu056

Rae, K. S. M. (1952). Continuous plankton records: explanation and methods, 1946-1949. *Bull. Mar. Ecol.* 3, 135–155.

Rajakaruna, H., Strasser, C., and Lewis, M. (2012). Identifying non-invasible habitats for marine copepods using temperature-dependent R 0. *Biol. Invas.* 14, 633–647. doi: 10.1007/s10530-011-0104-x

Record, N. R., and Pershing, A. J. (2008). Modeling zooplankton development using the monotonic upstream scheme for conservation laws. *Limnol. Oceanogr. Methods* 6, 364–373. doi: 10.4319/lom.2008.6.364

Record, N. R., Pershing, A. J., and Maps, F. (2013). Emergent copepod communities in an adaptive trait-structured model. *Ecol. Model.* 260, 11–24. doi: 10.1016/j.ecolmodel.2013.03.018

Record, N. R., Pershing, A. J., Runge, J. A., Mayo, C. A., Monger, B. C., and Chen, C. (2010). Improving ecological forecasts of copepod community dynamics using genetic algorithms. *J. Mar. Syst.* 82, 96–110. doi: 10.1016/j.jmarsys.2010.04.001

Reid, P. C., Edwards, M., Beaugrand, G., Skogen, M., and Stevens, D. (2003). Periodic changes in the zooplankton of the North Sea during the twentieth century linked to oceanic inflow. *Fish. Oceanogr.* 12, 260–269. doi: 10.1046/j.1365-2419.2003.00252.x

Rey, C., Carlotti, F., Tande, K., and Hansen, B. H. (1999). Egg and faecal pellet production of *Calanus finmarchicus* females from controlled mesocosms and *in situ* populations: influence of age and feeding history. *Mar. Ecol. Prog. Ser.* 188, 133–148. doi: 10.3354/meps188133

Rey-Rassat, C., Irigoien, X., Harris, R., and Carlotti, F. (2002). Energetic cost of gonad development in *Calanus finmarchicus* and *C. helgolandicus*. *Mar. Ecol. Prog. Ser.* 238, 301–306. doi: 10.3354/meps238301

Reygondeau, G., and Beaugrand, G. (2011). Future climate-driven shifts in distribution of *Calanus finmarchicus*. *Global Change Biol.* 17, 756–766. doi: 10.1111/j.1365-2486.2010.02310.x

Rhyne, A. L., Ohs, C. L., and Stenn, E. (2009). Effects of temperature on reproduction and survival of the calanoid copepod *Pseudodiaptomus pelagicus*. *Aquaculture* 292, 53–59. doi: 10.1016/j.aquaculture.2009.03.041

Richardson, A. J., Walne, A. W., John, A. W. G., Jonas, T. D., Lindley, J. A., Sims, D. W., et al. (2006). Using Continuous Plankton Recorder data. *Prog. Oceanogr.* 68, 27–74. doi: 10.1016/j.pocean.2005.09.011

Runge, J. A., Ji, R., Thompson, C. R. S., Record, N. R., Chen, C., Vandemark, D. C., et al. (2014). Persistence of *Calanus finmarchicus* in the western Gulf of Maine during recent extreme warming. *J. Plank. Res.* 37, 221–232. doi: 10.1093/plankt/fbu098

Runge, J. A., and Plourde, S. (1996). Fecundity characteristics of *Calanus finmarchicus* in coastal waters of eastern Canada. *Ophelia* 44, 171–187. doi: 10.1080/00785326.1995.10429846

Saumweber, W. J., and Durbin, E. G. (2006). Estimating potential diapause duration in *Calanus finmarchicus*. *Deep Sea Res. II* 53, 2597–2617. doi: 10.1016/j.dsr2.2006.08.003

Speirs, D. C., Gurney, W. S. C., Heath, M. R., Horbelt, W., Wood, S. N., and de Cuevas, B. A. (2006). Ocean-scale modelling of the distribution, abundance, and seasonal dynamics of the copepod *Calanus finmarchicus*. *Mar. Ecol. Prog. Ser.* 313, 173–192. doi: 10.3354/meps313173

Speirs, D. C., Gurney, W. S. C., Heath, M. R., and Wood, S. N. (2005). Modelling the basin-scale demography of *Calanus finmarchicus* in the north-east Atlantic. *Fish. Oceanogr.* 14, 333–358. doi: 10.1111/j.1365-2419.2005.00339.x

Tande, K. S. (1988). Aspects of developmental and mortality rates in *Calanus finmarchicus* related to equiproportional development. *Mar. Ecol. Prog. Ser.* 44, 51–58. doi: 10.3354/meps044051

Tittensor, D. P., Deyoung, B., and Tang, C. L. (2003). Modelling the distribution, sustainability and diapause emergence timing of the copepod *Calanus finmarchicus* in the Labrador Sea. *Fish. Oceanogr.* 12, 299–316. doi: 10.1046/j.1365-2419.2003.00266.x

Villarino, E., Chust, G., Licandro, P., Butenschön, M., Ibaibarriaga, L., Larrañaga, A., et al. (2015). Modelling the future biogeography of North Atlantic zooplankton communities in response to climate change. *Mar. Ecol. Prog. Ser.* 531, 121–142. doi: 10.3354/meps11299

White, J. R., and Roman, M. R. (1992). Egg production by the calanoid copepod *Acartia tonsa* in the mesohaline Chesapeake Bay: the importance of food resources and temperature. *Mar. Ecol. Prog. Ser.* 86, 239–249. doi: 10.3354/meps086239

Wilson, R. J., Banas, N. S., Heath, M. R., and Speirs, D. C. (2016). Projected impacts of 21st century climate change on diapause in *Calanus finmarchicus*. *Glob. Chang. Biol.* 22, 3332–3340. doi: 10.1111/gcb.13282

Wilson, R. J., Speirs, D. C., and Heath, M. R. (2015). On the surprising lack of differences between two congeneric calanoid copepod species, *Calanus finmarchicus* and *C. helgolandicus*. *Prog. Oceanogr.* 134, 413–431. doi: 10.1016/j.pocean.2014.12.008

Yool, A., Popova, E. E., and Anderson, T. R. (2011). Medusa-1.0: a new intermediate complexity plankton ecosystem model for the global domain. *Geosci. Model Dev.* 4, 381–417. doi: 10.5194/gmd-4-381-2011

**Conflict of Interest Statement:** The authors declare that the research was conducted in the absence of any commercial or financial relationships that could be construed as a potential conflict of interest.

frontiers in Marine Science

HYPOTHESIS AND THEORY
published: 04 April 2017
doi: 10.3389/fmars.2017.00052

# Resource Competition Affects Plankton Community Structure; Evidence from Trait-Based Modeling

*Marc Sourisseau[1]*, Valerie Le Guennec[2,3], Guillaume Le Gland[4], Martin Plus[1] and Annie Chapelle[1]*

*[1] Unité Dynamiques des Écosystèmes Côtiers, Laboratoire D'écologie Pélagique, Département Océanographie et Dynamique des Ecosystèmes, Institut Français de Recherche pour l'Exploitation de la Mer, Plouzané, France, [2] National Oceanography Center, Liverpool, UK, [3] Department of Earth, Ocean and Ecological Sciences, School of Environmental Sciences, University of Liverpool, Liverpool, UK, [4] Laboratoire des Sciences de l'environnement Marin (UMR6539), Institut Universitaire Européen de la Mer, Université de Bretagne Occidentale, Plouzané, France*

Understanding the phenology of phytoplankton species is a challenge and despite a lot of theoretical work on competition for resources, this process is under-represented in deterministic models. To study the main driver of the species selection, we used a trait-based model that keeps phenotypic variability through physiological trait parameterization. Next, we validated the results by using the toxic dinoflagellate *Alexandrium minutum* which is a toxic species. Due to their monitoring, we show that harmful algae are ideal models for studying ecological niches and for contributing to this more global challenge. As a first step, a dimensionless model of an estuary (France) was built with water temperature and water exchanges deduced from a hydro-dynamic model. The biological parametrization takes into account the size (from pico- to microphytoplankton) and the type of assimilation. The results show that temperature, competition for nutrients and dilution are important factors regulating the community structure and *Alexandrium minutum* dynamics (more especially the bloom initiation and magnitude). These drivers contribute to the determination of the ecological niche of *A. minutum*, influence the shape of its blooms and provide potential explanations of its interannual variability. This approach makes the community structure more flexible in order to study how environmental forcings could drive its evolution.

**Keywords: Droop, competition, inter-specific, estuary, Bay of Brest, *Alexandrium minutum*, phenology, niches**

OPEN ACCESS

***Edited by:***
*Kevin John Flynn, Swansea University, UK*

***Reviewed by:***
*Akkur Vasudevan Raman, Andhra University, India*
*David Suggett, University of Technology Sydney, Australia*

****Correspondence:***
*Marc Sourisseau*
*marc.sourisseau@ifremer.fr*

***Specialty section:***
*This article was submitted to Marine Ecosystem Ecology, a section of the journal Frontiers in Marine Science*

***Received:*** *26 May 2016*
***Accepted:*** *14 February 2017*
***Published:*** *04 April 2017*

***Citation:***
*Sourisseau M, Le Guennec V, Le Gland G, Plus M and Chapelle A (2017) Resource Competition Affects Plankton Community Structure; Evidence from Trait-Based Modeling. Front. Mar. Sci. 4:52. doi: 10.3389/fmars.2017.00052*

## 1. INTRODUCTION

Over the past few decades, the frequency and intensity of observed events termed Harmful Algal Blooms (HABs), and commonly called red tides, have rapidly increased in global coastal waters (Hallegraeff, 1993, 2010). These phenomena are characterized by the fast growth or accumulation of one phytoplankton species (which can grow up to several million cells.$L^{-1}$) which can color the surface water. Being photosynthetic, their occurrence is mainly dependent on light, nutrient availability and temperature. However, although phytoplankton enhances biological productivity and plays an outstanding role in the regulation of atmospheric carbon by scavenging it into deep water (Falkowski and Oliver, 2007), these algal blooms can be harmful by causing hypoxia or anoxia

during bloom degradation or by spreading toxicity through the food chain for species producing toxin. They have a dramatic impact on aquaculture, fisheries, tourism and public health and often lead to severe economic losses. Among the dinoflagellates which are only a part of the marine phytoplankton, it is estimated that at least 60 species produce endogenous toxins (Burkholder, 1998) that can accumulate in shellfish (clams, mussels, oysters, scallops), fish, and even in birds and mammals to levels that can be lethal for humans.

Monitoring programs dedicated to these algae have provided a large (twice a month to weekly measurements on several years) data sets at the species level to test assumptions on ecological process such as the ecological niche definition. The description of species niches (specially for toxic species) and their evolution through abiotic and sometimes biotic factors is an important and useful goal to forecast the evolution of communities (Wiens et al., 2009; Elith et al., 2010; Kearney et al., 2010) but it requires a detailed understanding of the mechanisms driving their fitness. Our capacity of realistic predictions of species niches with mechanistic model remains however weak and mainly because mechanistic models still include a great deal of empirical fitting that decreases their generic aspect. Although our understanding of HABs events has increased, it remains complex and difficult to assess all the pathways that generate a succession of monospecific blooms (resources, predation, life cycle, etc...). Among all ecological processes and despite its use in conceptual models (Margalef, 1978; Reynolds, 2003), competition has been only poorly or partially used by mechanistic models for understanding and/or predicting future outcomes. However, during a bloom; when the resources required for phytoplankton growth become limited, strong interspecific competition should occur in most cases. The familiar assumption in aquatic microbiology (Bass Becking, 1934) that all the species are in the environment (Everything Is Everywhere) but environmental selection leads to species succession, also identifies interspecific competition as one of the key processes in coastal environment management. However, HABs species are mainly simulated in the environment alone (MacIntyre et al., 2004; Fauchot et al., 2008; He et al., 2008; Jeong et al., 2015 for three of the four groups proposed) or with a physiological description that differs between the other phytoplankton functional types (Lacroix et al., 2007). The relevance of the competition for resources is thus difficult to estimate because a great part of the community adaptation is removed by this reduction. A trait-based approach (Litchman et al., 2012) associated with the EIE assumption provides an interesting methodology that allows us to go further in understanding bloom events.

Thus, we present the first trait-based model that simulates the competition for resources between several phytoplankton species (including the toxic species *A. minutum*) with a consistent physiological resolution and in realistic conditions. Obtained from trade-offs, this consistency enables species fitness to be analyzed in a more reliable way. With this general model framework, the challenge was to reproduce phytoplankton phenology and *A. minutum* bloom dynamics. The approach was based on trait-based models that already exist on a global scale (Dutkiewicz et al., 2009; Barton et al., 2010) and one of the difficulties initially considered was the selection of traits and their parametrization for coastal waters. The parametrization of traits was achieved with a random process using a range of realistic values. In doing so, defining the trade-offs (evolutionary compromise for the resource allocation between different functional traits) was also an important step. By using this general approach, we also propose a way of studying phytoplanktonic bloom by understanding which relevant factors may favor *A. minutum* blooms and how the diversity of trait values can control species invasion and succession. The study was applied in the Bay of Brest due to the fact that since summer 2012, the bay has been affected by one of the most problematic organisms, i.e., the dinoflagellate *Alexandrium minutum* (Erard-Le Denn, 1997), which gives rise to toxic events. The selection of this species was driven by the large set of physiological parameters provided by the literature and previous studies with local strains (Labry et al., 2008). We focused on the simulated timing of *A. minutum* and its maximal intensity values for comparison with *in-situ* observations. This capacity to predict *A. minutum* blooms could be a good step toward improving coastal management measures.

# 2. MATERIALS AND METHODS

## 2.1. Study Site

The Mignonne estuary, located within the Bay of Brest (**Figure 1**), was chosen as a good example of a so-called "invasion" by a toxic pelagic species. The *Alexandrium minutum* blooms started in 2012 despite a few earlier observations of low densities in the water (close to the detection threshold of the methodology used by the monitoring program: 10,000 cells.$L^{-1}$ ). This site is a typical shallow estuary of Brittany with a mean depth of 3.75 m subjected to tidal effects. The Mignonne is a small coastal river with a mean discharge of 1.47 $m^3.s^{-1}$. The Mignonne river inputs exhibit very high concentrations of nutrients such as nitrate, silicate and phosphate with concentrations reaching 2,000 $\mu$mol.$L^{-1}$, 2,000 $\mu$mol.$L^{-1}$ and 20 $\mu$mol.$L^{-1}$ respectively.

## 2.2. Area Definition and Forcings

To simulate inter-specific competition in a simple way, we chose to remove the spatial dimension by using a model similar to a chemostat with a Droop model (Droop, 1968, 1974) which is more reliable to physiological traits (Flynn, 2005) and accurate in many comparative studies (Grover, 1991, 1992). With this simplification, only the temporal variability of the niches in this small environment was analyzed and the spatial definition of this environment was fixed according to the recurrent observed distribution of *Alexandrium minutum* blooms during the 3 years considered: the Mignonne estuary (**Figure 1**). This approximation was possible because the strong tidal mixing and shallow depths in this area prevent front and stratification formation.

The considered area which sometimes provides favorable conditions for *A. minutum* growth; undergoes water exchanges associated with tide and river inputs. All these physical values (water residence time, water depth, nutrient exchanges and water temperature) were estimated using the hydrodynamic model MARS3D (Lazure and Dumas, 2008) configured for

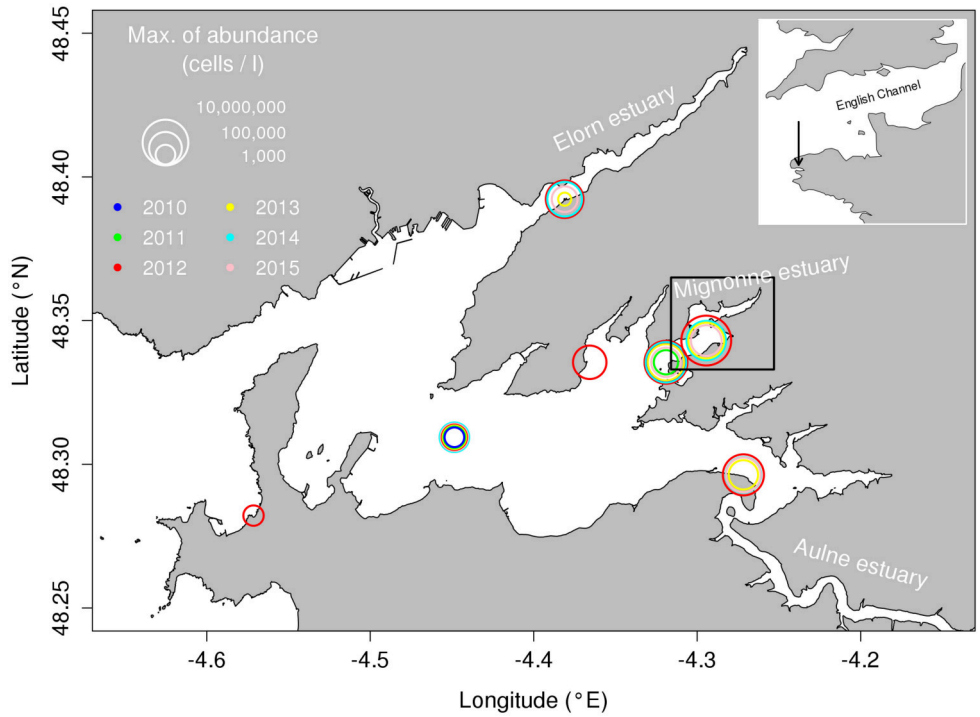


**FIGURE 1 | Bay of Brest with the *A. minutum* maximum abundance during the last 6 years and at the different monitoring stations.** Black box shows the spatial coverage of the Mignonne estuary used by the hydrodynamic model to estimate water exchanges.

the Bay of Brest and forced by realistic weather conditions (wind, air temperature, relative humidity and atmospheric pressure from Météo-France AROME model, Seity et al., 2011) as well as by the measured daily Mignonne flow (HYDRO database, Governmental Environmental Agency, monitoring station Irvillac, see **Figure 1** for river location). These forcing fields constitute the best set available for this area and the water residence time remains rather insensitive to the weather conditions. The model bathymetry was provided by the SHOM (French Naval Hydrographic and Oceanographic Service). Three years of interest (2012, 2013, and 2014) were simulated. The dilution rates ($D$) were computed by a classic methodology of tracer dilution over a time period close to 25 h (the period between two high tides): a passive tracer was initialized in the whole area at high tide and the decreasing concentration due to dilution was simulated by the three-dimensional (3D) model during 25 h until the next high tide. The dilution rate was computed as the difference between the two concentrations divided by the exact time lag between the two high tides, and the tracer was re-initialized for the next 25 h. Concomitantly, the simulated water temperature was recorded to calculate the mean temperature. Then, both dilution rates and temperatures were interpolated to provide values for a 24-h period. The mean water volume of the Mignonne estuary ($V$) was estimated at mean sea level height using the model bathymetry.

Commonly used to simulate phytoplankton dynamics in experiments or coastal waters (Flynn, 2005), the selected resources for phytoplankton competition were light and three macronutrients: nitrogen (as ammonium and nitrate), phosphorus (as phosphate) and silicium (as silicate). Light intensity was estimated from Sea Surface Irradiance (SSI) of daily satellite data (provided by METEOSAT Second generation satellites, full description available on the OSI-SAF web server www.osi-saf.org/index.php, validation by Le Borgne et al., 2006). The SSI is the mean daily solar irradiance reaching the earth's surface in the 0.3–4 m band expressed in $W.m^{-2}$. It was multiplied by 0.95 to remove sea surface albedo and then by 0.425 (fraction of the total spectra wavelengths that is used by photosynthetic pigments) in order to estimate the mean daily Photosynthetically Active Radiation (PAR, $I_0$). Then, instantaneous PAR was calculated as a sinusoidal function of the mean daily PAR and the Julian day length was calculated following the method described in Forsythe et al. (1995). The light extinction coefficient due to the water column ($K_{par}$) was calculated following Gohin et al. (2005) using OSI-SAF satellite data for suspended matter ($SM$ in $mg.L^{-1}$) and chlorophyll a (in $mg.L^{-1}$).

Nutrient concentrations in Mignonne waters were calculated by taking into account (i) the nutrients brought by the Mignonne River (interpolated from monthly data measured by Brest Metropole Oceane) and (ii) the nutrient concentrations prevailing in the rest of the Bay of Brest (interpolated from weekly data provided by the SOMLIT "Service d'Observation en Milieu Littoral," INSU-CNRS, at the Porzic station).

## 2.3. Traits Description of Phytoplankton Model

A large diversity of traits and trade-offs associated can structure phytoplankton communities (Litchman et al., 2007; Litchman and Klausmeier, 2008). From these, we pragmatically selected only the traits (cell size, optimal temperature and silicate dependence, see **Figure 2**) relevant for the considered area and well defined for phytoplankton groups and species.

### 2.3.1. Cell Size and Cell Quotas

Cell size is a key trait that impacts growth, metabolism and access to resources (Litchman and Klausmeier, 2008). Major parameters of nutrient uptake and growth scale with cell size and the size is here considered as a fixed trait for each phenotype. The size range covers the whole size spectrum usually used to characterize the phytoplankton community from 1 to 120 μm (**Figure 2**). Size corresponds to the equivalent spherical diameter (Equivalent Spherical Diameter - *ESD*) and allows calculating cell volume which is next used to simulate trade-offs with nutrient uptake and growth. The Capacity of the phytoplankton cells to modify their size (Smith and Zhao, 2001; Arino et al., 2002; Flynn, 2005) was not considered here as we decided to simulate nutrients storage capacity (quota). In fact, the quota-based approach was used (Droop, 1968, 1974) because it is more reliable for physiological traits (Flynn, 2005) and simulations. All previous comparative studies concluded that growth is better described as a function of internal rather than environmental nutrient concentration (Grover, 1991, 1992). This approach and its application to species competition has been widely investigated in the literature (Pascual, 1994; Legovic and Cruzado, 1997; Smith, 1997; Smith and Zhao, 2001; Sunda et al., 2009) and the theoretical results are also fully applicable in our study. As the conditions are not stationary and perturbations occur at several frequencies from the seasonal cycle to tidal oscillations, the exclusive competition in our simulations was better reproduced by a Droop model. In this way, our approach is close to Sommer (1991) work and novative compared to Darwin model (Follows and Dutkiewicz, 2011). Intracellular cell quotas of phosphate and nitrogen were also considered.

### 2.3.2. Optimal Temperature

Temperature is a major environmental parameter that governs physiological functions like photosynthesis, respiration, growth, resource acquisition, motility and sinking (Eppley, 1972; Litchman and Klausmeier, 2008). This dependence may be characterized by the optimal temperature. It has been used here to model phytoplankton maximal growth rate with all other factors (nutrient, light) being optimal.

### 2.3.3. Silicate Dependence

Diatoms are one of the major microphytoplankton group observed in the Bay of Brest. All species in this taxonomic group are silicified species and this major trait induces a silicate assimilation. Without considering any relation between this trait and physiological rate (uptake, growth...) in our simulation, we wanted to determine how the relevance of the potential specific limitation of this large cell size could occur to permit a higher growth of non-silicate large size species (including *Alexandrium minutum*).

Other traits proposed by Litchman and Klausmeier (2008) such as toxin production, light adaptation and swimming capacities were considered but rejected. Chemical cues are relevant processes for species interactions (Ianora et al., 2011). Several metabolites have allelopathic effects and toxins of toxic algae are obviously widely studied in this way (Hulot and Huisman, 2004; Graneli et al., 2008). *A. minutum* thus produce allelopathic substances that would shift the grazing pressure to non-toxic species (Guisande et al., 2002) or decrease the growth rate of other phytoplankton species (Arzul et al., 1999). However, the "toxin" property is linked to a negative effects on humans (from a food safety aspect) and/or macro-organisms (fish or shellfish). This characteristic is not linked to the competition for resources or interactions with specific grazers. Even the toxic blooms can be grazed extensively (Jeong et al., 2015). We can thus assume that many other cellular metabolites can have allelopathic effects without affecting animal physiology and conversely, are not measured. The action of toxins in the environment is still being debated in the scientific community (Hulot and Huisman, 2004; Jonsson et al., 2009), we therefore chose to neglect this trait despite its potential implication in the results of competition (Roy and Chattopadhyay, 2007; Grover and Wang, 2014). The optimal irradiance for a cell is also a key parameter and is modulated by the quantity and quality of its pigment content. Although, the tidal mixing in the considered area removed the possibility of a vertical discretization of the phenotypes (Hickman et al., 2010), the bloom timing of each one could be modified according to their optimal irradiance. MacIntyre et al. (2004) used a remarkable adaptation to low light levels of one phytoplankton species to simulated its bloom initiation. However, despite the interest of such trait integration, we first used a constant optimal irradiance for all phenotypes by considering that, at the first order, the relevance should remain low because the light resource is rarely limiting during the blooming period of *Alexandrium minitum* (mid-May to August). One of the last critical traits considered is the organism's behavior and mobility. Dinoflagellates have especially significant swimming capacities (Kamykowski, 1995) that can lead: to heterogeneous vertical distributions (Kamykowski et al., 1992) and accumulation processes (Anderson and Stolznbach, 1985; Janowitz and Kamykowski, 2006) and to higher nutrients uptakes in oligotrophic conditions due to the depletion around the cell (Falkowski and Oliver, 2007). However, according to the hydrodynamic of the considered estuary (Raine, 2014), stratification (haline or thermal) never occurs over the year in the estuary because the mixing intensity is mainly driven by the interaction of the tide and the bathymetry. We therefore assume that this physical-biological interaction remains stable over the year and is included in the parametrization of the uptake rates.

### 2.3.4. Modeling the Phytoplankton Diversity

The large variability was implemented by using 50 species (or phenotypes for the selected traits) (*Ns*) with random trait values. Each species is defined by its cell size, its capacity or not to

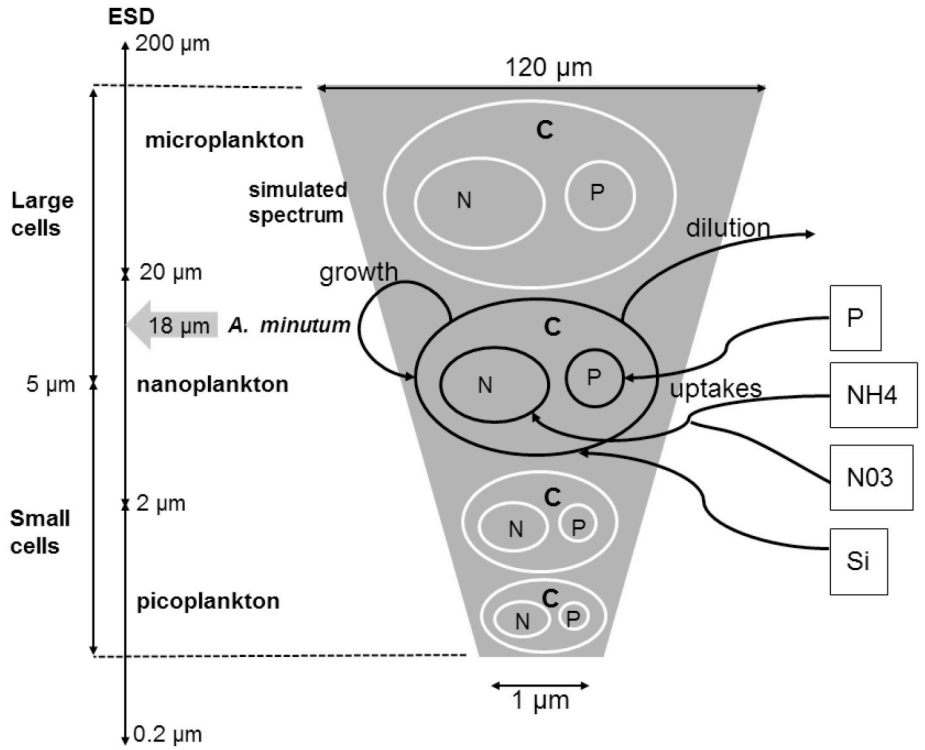


**FIGURE 2 | Conceptual model of the size class spectrum used.** For each cell size, a quota of nitrogen and phosphate controls the growth rate ($\mu$). The quota and the cellular volume (Vol.$C^{-1}$) are based on allometric laws. For the diatoms, the silicates are not stored in the cells but directly used with a potential limitation directly on the growth rate. The size was randomly selected between 1 and 120 µm of ESD.

assimilate silicate and its optimal temperature. As it isnt linked to precise species, it can also be considered as phenotype. Only one species was fixed and defined for *A. minutum*. 51 phenotypes were thus in competition for a limited number of resources in each simulation. To analyze the outputs of the simulated phytoplanktonic community, 2 or 4 cell groups were created according to their size (or volume, see **Figure 2**). The small cells include the picoplankton (0.5–5 $\mu m^3$) and a fraction of the small nanoplankton (ESD < 5 µm) while the large cells include the largest cells of the nanoplankton (ESD < 5 µm) and the microplankton (4,000–$10^6$ $\mu m^3$). This size range covers the whole size spectrum (pico-, nano-, and micro-phytoplankton) usually used to characterize the phytoplankton community. The size division in nanoplankton is related to the identification limit by optic microscopy (ESD > 5 µm). Alexandrium minutum belongs to the microplankton group with a volume close to the value of 5,832 $\mu m^3$ (18 µm of ESD, Maranon et al., 2013).

## 2.4. Mathematical Model Description

The differential equations governing the dynamics of the system are usual. The abundance of each species ($N_i$), nutrient concentrations ($[PO_4]$, $[NH_4]$, $[NO_3]$, and $[Si]$) and intracellular cell quotas of phosphate and nitrogen ($Q_{P,i}$ and $Q_{N,i}$) are state variables whose evolution over time can be expressed as follows (for symbols and parameter values, see **Tables 1**, **2**, respectively):

$$
\begin{aligned}
\frac{dN_i}{dt} &= \mu_i N_i - D N_i \\
\frac{d[PO_4]}{dt} &= -\sum_{i=1}^{Ns} V_{P,i} N_i - D[PO_4] \\
&\quad + [PO_4]_{riv}\frac{F}{V} + [PO_4]_{bay}(D - \frac{F}{V}) \\
\frac{d[NH_4]}{dt} &= -k_{NH_4,i}[NH_4] - \sum_{i=1}^{Ns} V_{NH_4,i} N_i - D[NH_4] \\
&\quad + [NH_4]_{riv}\frac{F}{V} + [NH_4]_{bay}(D - \frac{F}{V}) \\
\frac{d[NO_3]}{dt} &= k_{NH_4,i}[NH_4] - \sum_{i=1}^{Ns} V_{NO_3,i} N_i - D[NO_3] \\
&\quad + [NO_3]_{riv}\frac{F}{V} + [NO_3]_{bay}(D - \frac{F}{V}) \\
\frac{d[Si]}{dt} &= -\sum_{i=1}^{Ns} Q_{Si,i}\mu_i N_i - D[Si] \\
&\quad + [Si]_{riv}\frac{F}{V} + [Si]_{bay}(D - \frac{F}{V})
\end{aligned}
\tag{1}
$$

$$
\begin{aligned}
\frac{dQ_{P,i}}{dt} &= V_{P,i} - \mu_i Q_{P,i} \\
\frac{dQ_{N,i}}{dt} &= V_{N,i} - \mu_i Q_{N,i}
\end{aligned}
\tag{2}
$$

**TABLE 1 | Table of symbols.**

| Symbol | Description | Unit |
|---|---|---|
| $N_s$ | Total number of phenotypes | – |
| $N_i$ | Abundance of phenotype *i* | cells.L$^{-1}$ |
| $N_{min,i}$ | Minimum abundance of phenotype *i* | cells.L$^{-1}$ |
| $Q_{j,i}$ | Variable cell quota for N and P for phenotype *j* | µmol cell$^{-1}$ |
| $Q_{Si,i}$ | Fixed cell quota for silicate | µmol cell$^{-1}$ |
| $[NO_3]$ | Nitrogen concentration | µmol L$^{-1}$ |
| $[NH_4]$ | Ammonium concentration | µmol L$^{-1}$ |
| $[Si]$ | Silicium concentration | µmol L$^{-1}$ |
| $k_{NH_4}$ | Nitrification rate | d$^{-1}$ |
| $\mu_i$ | Growth rate of the phenotype *i* | d$^{-1}$ |
| $\mu_{max,i}$ | Maximal growth rate of phenotype *i* | d$^{-1}$ |
| $V_{NH_4,i}$ | Ammonium uptake rate | µmol cell$^{-1}$d$^{-1}$ |
| $V_{NO_3,i}$ | Nitrogen uptake rate | µmol cell$^{-1}$d$^{-1}$ |
| $V_{N,i}$ | Ammonium+Nitrogen uptake rate | µmol cell$^{-1}$d$^{-1}$ |
| $V_{P,i}$ | Phosphate uptake rate | µmol cell$^{-1}$d$^{-1}$ |
| $f_{T,i}$ | Temperature limitation ∈ [0, 1] | – |
| $f_{L,i}$ | Light limitation ∈ [0, 1] | – |
| $f_{N,i}$ | Nitrogen quota limitation ∈ [0, 1] | – |
| $f_{P,i}$ | Phosphate quota limitation ∈ [0, 1] | – |
| $f_{Si,i}$ | Silicate quota limitation ∈ [0, 1] | – |
| $Q_{j,i}^{min}$ | Min Cell quota of the element j | µmol cell$^{-1}$ |
| $Q_{j,i}^{max}$ | Max Cell quota of the element j | µmol cell$^{-1}$ |
| $V_{j,i}^{max}$ | Max uptake rate of the element j | µmol cell$^{-1}$ d$^{-1}$ |
| $K_{j,i}$ | Half saturation for the element j | µmol L$^{-1}$ |
| $D$ | Dilution rate | d$^{-1}$ |
| $V$ | Volume of sea water | m$^3$ |
| $F$ | River flow | m$^3$ d$^{-1}$ |
| $T$ | Temperature | °C |
| $I_0$ | PAR at the sea surface | W.m$^{-2}$ |
| $I$ | PAR at the depth Z | W.m$^{-2}$ |
| $K_{par}$ | Light attenuation coefficient | – |

**TABLE 2 | Global parameters and allometric coefficients.**

| Parameter | Process | Value | Unit | References |
|---|---|---|---|---|
| $\alpha_1$ | $Q_N^{min}$, $Q_P^{min}$, $Q_{Si}$ | 0.84 | w.d. | Maranon et al., 2013 |
| $\beta_{Q_N^{min}}$ | | 2.3 10$^{-9}$ | µmol cell$^{-1}$ | / |
| $\beta_{Q_P^{min}}$ | | 1.1 10$^{-10}$ | – | / |
| $\beta_{Q_{Si}}$ | | 2.3 10$^{-9}$ | – | / |
| $\alpha_2$ | $Q_N^{max}$, $Q_P^{max}$ | 0.92 | w.d. | Maranon et al., 2013 |
| $\beta_{Q_N^{max}}$ | | 6.9 10$^{-9}$ | µmol cell$^{-1}$ | / |
| $\beta_{Q_P^{max}}$ | | 3.3 10$^{-10}$ | – | / |
| $\alpha_3$ | $V_{NH_4}^{max}$, $V_{NO_3}^{max}$,$V_{P0_4}^{max}$ | 0.97 | w.d. | Maranon et al., 2013 |
| $\beta_{V_{NH_4}^{max}}$ | | 8.74 10$^{-10}$ | µmol d$^{-1}$ cell$^{-1}$ | / |
| $\beta_{V_{NO_3}^{max}}$ | | 4.37 10$^{-10}$ | – | / |
| $\beta_{V_{PO_4}^{max}}$ | | 4.18 10$^{-11}$ | – | / |
| $\alpha_4$ | $K_N$, $K_P$, $K_Si$ | 0.33 | w.d. | Edwards et al., 2012 |
| $\beta_{K_N}$ | | 0.2 | µmol l$^{-1}$ | Cugier et al., 2005 |
| $\beta_{K_P}$ | | 0.01 | – | – |
| $\beta_{K_Si}$ | | 0.1 | – | – |
| $I_{opt}$ | | 20 | W.m$^{-2}$ | Erard-Le Denn, 1997 |
| $k_T$ | | 0.063 | °C$^{-1}$ | Eppley, 1972 |
| $K_{nitrif}$ | | 0.2 | j$^{-1}$ | Cugier et al., 2005 |

The net growth rate ($\mu_i^{net}$) of change in the abundance ($N_i$) is the gain from the growth rate ($\mu_i$) minus the dilution ($D$). There is no specific term for a mortality process because it was overlooked compared to the dilution values. To prevent the extinction of a species due to dilution and to simulate a possible migration after unfavorable conditions, a minimal concentration ($N_{min,i}$) is considered for each species. Due to the exponential distribution of the cell abundance according to their sizes, it is calculated in such a way that the total cell volume of each species is equal to $10^6 \mu m^3$ L$^{-1}$. This approach gives lower abundances for big cells (at least 1 cells.L$^{-1}$) compared to small cells (at least $10^6$ cells.L$^{-1}$). Concerning *A.minutum*, the threshold is thus 171 cells.L$^{-1}$ and similar to the detection threshold by using the protocol of the monitoring program (100 cells.L$^{-1}$).

## 2.5. Parameter Values

The growth rate of each species is modulated by their maximal growth rate $\mu_{max,i}$ ($d^{-1}$), the temperature $f_{T,i}$, and four limitation factors $f_{L,i}$, $f_{N,i}$, $f_{P,i}$, $f_{Si,i}$ (dimensionless ranging from 0 to 1) where only the most constraining is retained (Liebig's minimum law):

$$\mu_i = \mu_{max,i} f_{T,i} min(f_{L,i}, f_{N,i}, f_{P,i}, f_{Si,i}) \quad (3)$$

Temperature limitation ($f_{T,i}$) is simulated in the same way for all species with a function developed for *A. minutum* in the Bay of Cork (Nì Rathaille, 2007):

$$f_{T,i} = \begin{cases} 0 \; if \; T < T_{opt,i} - 10 \\ 0.1(T - T_{opt,i} - 10) \; if \; T_{opt,i} - 10 < T < T_{opt,i} \\ 1 \; if \; T > T_{opt,i} \end{cases} \quad (4)$$

where $T_{opt,i}$ is the optimal temperature of growth for each species and $T$ is the simulated temperature. The light limitation ($f_{L,i}$) on phytoplankton growth rate is expressed by a hyperbolic tangent (Jassby and Platt, 1976):

$$f_{L,i} = tanh(\frac{I}{I_{opt}}) \quad (5)$$

where $I$ corresponds to the Photosynthetically Available Radiation (PAR) and $I_{opt}$ to the optimal light intensity. This value is assumed to be constant for all the phenotypes. Variations of the water depth associated with the tide are taken into account by calculating I for each given depth ($z$) with the Beer-Lambert law:

$$I = I_0 e^{(-K_{par} \cdot Z)} \quad (6)$$

where $K_{par}$ is the light attenuation coefficient. The growth rate is calculated for each depth and the mean of these growth rates was used in the model.

Nitrogen ($f_{N,i}$) and phosphorus ($f_{P,i}$) limitations follow a normalized Droop function (Droop, 1974), which is a hyperbole depending on the minimum ($Q_{j,i}^{min}$) and maximum ($Q_{j,i}^{max}$) cell quotas for the element $j$:

$$f_{j,i} = \frac{Q_{j,i}^{max}}{Q_{j,i}^{max} - Q_{j,i}^{min}}\left(1 - \frac{Q_{j,i}^{min}}{Q_{j,i}}\right) \tag{7}$$

According to Flynn (2008), silicate is not stored by siliceous cells and is only used for the fabrication of the frustule which occurs during cell division. The limitation in silicate is therefore expressed through a simple Michaelis-Menten formulation :

$$f_{Si,i} = \frac{[Si]}{K_{si,i} + [Si]} \tag{8}$$

where $K_{Si}$ is the half-saturation constant for siliceous species.

The nutrient uptake rates ($V_{NO_3,i}^{max}$, $V_{NH_4,i}^{max}$, and $V_{P,i}^{max}$) follow Michaelis-Menten kinetics and decrease linearly when cell quotas increase:

$$\begin{aligned} V_{NH_4,i} &= V_{NH_4,i}^{max} * \frac{[NH_4]}{k_{N,i} + [NH_4]} \frac{(Q_{N,i}^{max} - Q_{N,i}) \cdot N_i}{Q_{N,i}^{max} - Q_{N,i}^{min}} \\ V_{NO_3,i} &= V_{NO_3,i}^{max} * \frac{[NO_3]}{k_{N,i} + [NO_3]} \left(1 - \frac{[NH_4]}{k_{N,i} + [NH_4]}\right) \\ &\quad \frac{(Q_{N,i}^{max} - Q_{N,i}) \cdot N_i}{Q_{N,i}^{max} - Q_{N,i}^{min}} \\ V_{P,i} &= V_{P,i}^{max} * \frac{[PO_4]}{k_{P,i} + [PO_4]} \frac{(Q_{P,i}^{max} - Q_{P,i}) \cdot P_i}{Q_{P,i}^{max} - Q_{P,i}^{min}} \end{aligned} \tag{9}$$

The absorption of nitrogen as nitrate is inhibited by ammonium absorption (Parker, 1993) because the necessary reduction of nitrate ions to ammonium ions requires a great deal of energy.

## 2.6. Key Physiological Trade-Offs

Some trade-offs are used in order to define competition between all the species within the model ecosystem. Functional traits used to simulate phytoplanktonic diversity thus follow different types of distribution (see **Table 3**). Although, a large proportion of the traits is related to the cell volume, phytoplankton maximal growth rate is simulated by the temperature according to a global exponential law (Eppley, 1972). There is a relationship with $T_{opt}$ but not with cell size:

$$\mu_{max,i} = \mu_{max,ref} \cdot e^{(k_T \cdot T_{opt,i})} \tag{10}$$

$k_T$ is the temperature coefficient for the growth rate and $\mu_{max,ref}$ is the growth rate at 0° without other limitations. The following traits $Q_{N,i}^{min}$, $Q_{N,i}^{max}$, $V_{NH_4,i}^{max}$, $V_{NO_3,i}^{max}$, $Q_{P,i}^{min}$, $Q_{P,i}^{max}$, $V_{P,i}^{max}$, $Q_{Si,i}$, $K_{N,i}$, $K_{P,i}$ and $K_{Si,i}$ are dependent on the cell volume through an allometric relationship in the form of a power function $\beta \cdot V^{\alpha}$(see **Table 3** for the allometric coefficient values). Hence, some size-related differences are introduced in the storage capacity and maximal nutrients uptake rate. Indeed, large cells possess a bigger storage capacity than small ones. The maximal uptake rate of small cells is lower than that of large cells but the reverse is true for nutrient affinity ($1/K_{N,i}$, $1/K_{P,i}$). Consequently, small cells will outcompete large ones in oligotrophic conditions.

**TABLE 3 | Distribution of the functional trait.**

| Trait | Type of distribution | References |
|---|---|---|
| Siliceous or not | Random law (Boolean) | / |
| Volume ($V$) | Random and uniform law $\in [1, 10^6]\mu m^3$ | / |
| Optimal temperature ($T_{opt}$) | Random and uniform law $\in [10, 20]°C$ | / |
| Maximum growth rate ($\mu_{max}$) | Eppley function | Eppley, 1972 |
| Minimum cell quota ($Q_N^{min}, Q_P^{min}$) | Allometric law | Maranon et al., 2013 |
| Maximum cell quota ($Q_N^{max}, Q_P^{max}$) | Allometric law | Maranon et al., 2013 |
| Half saturation constant ($K_N, K_P, K_{Si}$) | Allometric law | Edwards et al., 2012 |

*The optimum irradiance is fixed for all the species (20 $Wm^2$).*

*Alexandrium minutum* traits were obtained from the literature (see **Table 4** for references). Its maximal growth rate is identical to species with the same volume but its distinction lies in its maximum phosphate uptake rate and its maximum cell quota which are both higher than in other cells (Chapelle et al., 2010).

## 2.7. Phenological Characterization of *A. minutum* Bloom

Phenology refers to changes in the timing of seasonally re-occurring biological events due to environmental changes. Due to the random selection, 200 simulations were carried out with different random draws and their mean values were analyzed. To compare the simulated dynamics of *A. minutum* with the *in situ* observations, the method developed by Rolinski et al. (2007) was used instead of a simple correlation with the data. Some particular points of *A. minutum* phenology such as the maximum abundance, the date of this maximum, the beginning, end and duration of the bloom were thus obtained. To determine these shape parameters, a Weibull function is proposed by Rolinski et al. (2007):

$$w(x) = \left(d + e^{\left(-(x/e)^f\right)}\right) . (1 - a \cdot exp(-(\frac{x}{b})^c)) \tag{11}$$

After a log-transformation of the data, the values of the parameters ($a$, $b$, $c$, $d$, $e$, and $f$) that provide the best fit are chosen. The maximum abundance and its date are directly provided by the Weibull function. From these values, the area under the curve is calculated. The start date of the bloom corresponds therefore to the 2% quantile of the area under the curve before the date of the maximum. By contrast, the 98% quantile of the area under the curve after the date of the maximum, corresponds to the date of the end of the bloom. The duration of the bloom is the difference between the beginning and end of the bloom. This part aims to

**TABLE 4 | Specific parameters used for *A. minutum*.**

| Parameter | Value | References |
|---|---|---|
| $V$ | 5 800 $\mu m^3$ | / |
| $T_{opt}$ | 18°C | / |
| $\mu max$ | 0.9 $d^{-1}$ | / |
| $Q_N^{min}, Q_N^{max}$ | 4.08 $10^{-5}$, 27 $10^{-5}$ $\mu$mol cell$^{-1}$ | Davidson and Gurney, 1999 |
| $Q_P^{min}, Q_P^{max}$ | 0.1951 $10^{-5}$, 1.55 $10^{-5}$ $\mu$mol cell$^{-1}$ | Labry et al., 2008; Chapelle et al., 2010 |
| $V_{NO_3}^{max}$, $V_{NH_4}^{max}$ | 7.35 $10^{-6}$, 14.7 $10^{-5}$ $\mu$mol cell$^{-1}$ day$^{-1}$ | Davidson and Gurney, 1999 |
| $V_P^{max}$ | 1.53 $10^{-5}$ $\mu$mol cell$^{-1}$ day$^{-1}$ | Labry et al., 2008; Chapelle et al., 2010 |
| $K_N$ | 3.93 $\mu$mol l$^{-1}$ | Davidson and Gurney, 1999 |
| $K_P$ | 0.28 $\mu$mol l$^{-1}$ | Labry et al., 2008 |

discover if the modeled phenology reveals strong variations over the years as observed in the field.

Several ensembles of simulations were then carried out through a selected range of phenotype numbers ($Ns = 20$, $Ns = 100$, $Ns = 150$, and $Ns = 200$). Next, the cardinal dates (beginning, maximum, and termination), timing and maximum abundances of the *A. minutum* bloom were recalculated with the same process (**Table 5**).

# 3. RESULTS

## 3.1. *A. minutum* Appearance and Bloom Characteristics

Whatever the year and the simulation, the presence of *A. minutum* is simulated from the beginning of May until the beginning of September (**Figure 3**). Despite a simulated interannual variability for the *A. minutum* bloom, the duration of the bloom is quite constant (≈ four and a half months). The random number of species is also sufficient to limit the variability of each ensemble with some reduced differences between the 25TH and 75TH percentiles. This observation enables some comparisons to be made between each year.

The model simulates the highest abundances of *A. minutum* in 2012 with a mean value of 1 million cells.$L^{-1}$ on 5TH July. In 2014, the maximum abundance remains large (around $3.10^5$ cells.$L^{-1}$) but three times lower than in 2012. The lowest values are observed in 2013 with 85,000 cells.$L^{-1}$. Besides these maximal values and close bloom duration, some differences in the timing of the maximal abundances are also simulated in a significant way. In 2014, the maximum is reached on 5TH July which is a little bit sooner than in 2013 (8TH July) and 2012 (14TH July). Again, the percentiles indicate a low variability in these values related to the random process. They are driven by the phenotype succession and the environmental forcing. Regarding 2013, the lowest maximum abundance is simulated but with a long duration around this value (≈ one month). The earliest bloom initiation is simulated in 2014 (4TH May) and the latest in 2012 (25TH May). Concerning the termination, the bloom in 2014 ended earlier (end of August) whereas the one in 2012 ended the latest (end of September). The small oscillations during the bloom dynamics (notably in 2012) are associated with the spring/neap tidal cycle which affects the dilution rate.

**TABLE 5 | Parameters obtained with the Weibull function fitted on *A. minutum* blooms for the three years.**

| Year | Dates of Max. for Ns = [20;50;100;150;200] | bloom initiation | bloom termination | maximal value |
|---|---|---|---|---|
| 2012 | [1;4;4;4;4] July | 22 May | 3 Oct. | 959,000 |
| 2013 | [13;18;14;10;19] July | 5 May | 19 Sept. | 84,400 |
| 2014 | [26;28;26;25;24] June | 17 April | 29 Oct. | 253,000 |

*Date of maximum was estimated for different number of phenotypes, and bloom initiation, termination and maximal values (cells $L^{-1}$) were estimated with only 50 phenotypes ($N_s = 50$).*

## 3.2. Factors Controlling *A. minutum* Blooms

The difference between sink and source terms (the net growth) controls the simulated bloom timing and intensity, and thus the potential *A. minutum* appearance period during 2012 is four months from mid-May to the end of September (**Figure 4**). The growth rate depends on the following factors: temperature, nutrients (nitrogen and phosphate) and light. At the end of the winter of 2012, despite nitrogen and phosphate cell quota values close to their maximums, *A. minutum* growth is limited at low water temperatures (below 10°C). During the spring, the main limitation remains the temperature until the beginning of May after which the growth period occurs (**Figure 5**). Until mid-June, the nitrogen limitation is the most important, followed by a phosphate limitation that limits *A. minutum* growth in summer (after mid-June) until October 2012. In autumn, despite some new nutrient inputs from the river, the second growth period remains limited to 1 month and the simulated abundances remain very low due to light and temperature limitations.

The same patterns are observed for subsequent years. There is therefore a marked temperature control for bloom initiation (**Tables 5**, **6**). The shift of the onset toward an earlier period in 2014 is explained by a warmer temperature in mid April (12.8°C) compared to 2012 and 2013 (11.8 and 11.9°C, respectively). The simulated variability of the *A. minutum* bloom intensity is next explained by nutrient concentrations. Phosphate limitation is less important in 2012 due to higher flow rates from the Mignonne river (respectively 1.5, 0.47, 0.66, $0.55{\cdot}10^5 m^3 s^{-1}$ mean flow from May to August in 2012, 2013, 2014, and 2015) which allow higher maximum abundances. The relationship between river flow and nutrient concentrations is illustrated by the mean *in situ* PO4 concentrations that have been weekly measured in 2013, 2014, and 2015 with respective values of 0.12, 0.26, and 0.17 $\mu$mol.$l^{-1}$. These measurements follow *A. minutum* maximum abundances, 2012 being higher than 2013.

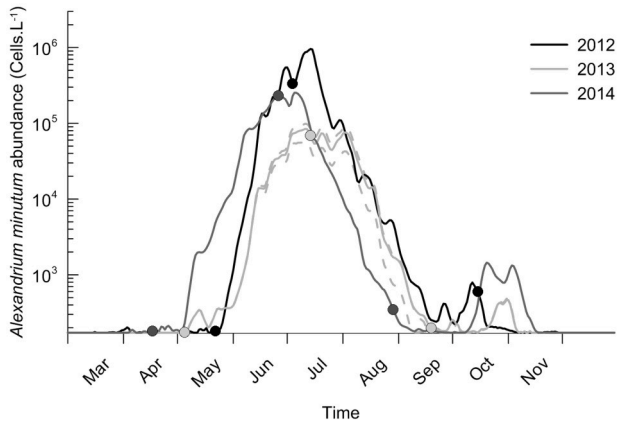


**FIGURE 3 | Interannual variability of *A. minutum* abundance for the years 2012, 2013, and 2014.** Abundances are the mean of the simulation ensemble and 25th and 75th percentiles are plotted only for 2013 (dashed lines). Positions of the three estimated Weibull parameters are added (date of initiation, maximum and termination of the bloom).

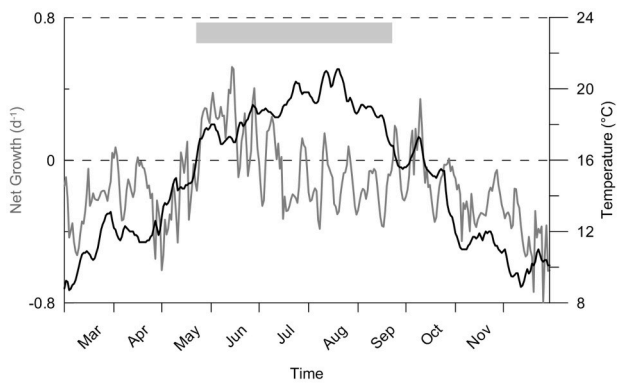


**FIGURE 4 | Net growth ($\mu - D$) of *A. minutum* during the year 2012 and temperature variability in the considered area.** The period of potential *A. minutum* occurence is indicated in gray.

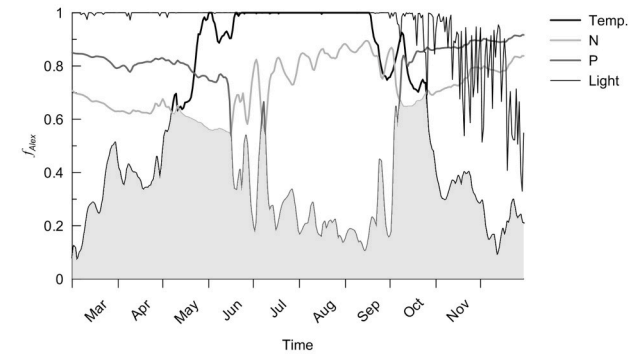


**FIGURE 5 | Temperature, nitrogen (N), phosphate (P) and light limitations for *A. minutum* during 2012.** The gray area indicates the maximal limitation (Liebig's Law).

## 3.3. Phenology of *A. minutum* and Phytoplankton Successions

The outputs show a variation in the community structure that is repeated for each year. In fact, large cells (ESD $>$ 5 μm) are the first to grow (**Figure 6**) and can be considered opportunist phenotypes (higher growth rates when nutrients are high). They are then replaced by smaller cells as the phosphate concentration decreases with a low evolution from opportunists to gleaners (more competitive cells when nutrients are low) from mid-May to September. Small cell abundances increase at the beginning of June and due to their higher affinity for phosphate than large cells, they generate a sharp decrease in phosphate concentration after 15th June (with a minimum of 0.01 $\mu mol.L^{-1}$). Until October, phosphate concentration is the most limiting factor, which only rises in October because nutrient inputs from the river increase. The model thus simulates a second peak of *A. minutum* and large cell abundances well marked in October 2014 (with 2,000 $cells.L^{-1}$). This is due to a lower dilution rate (0.2 $d^{-1}$ in 2013 and 2012 against 0.1 $d^{-1}$ in 2014). However, the growth period remains too short to create a significant peak. At the end of November in the 3 years simulated, *A. minutum* and large cell abundances return to their initial and minimal values. It is through an exclusive competition via phosphate limitation, that the termination of the *A. minutum* bloom is simulated.

To sum up, simulated *A. minutum* bloom initiation is controlled by temperature while the bloom duration and termination are controlled by interspecific competition for the nutrient resources (nitrogen and phosphate). The simulated difference in the *A. minutum* bloom intensity for the three years is due to the nutrient concentrations inside the area and the simulated limitation in phosphate is less in 2012 thus leading to higher values of maximum abundances.

## 3.4. Sensitivity Analysis and Comparison with the Data Set

Due to the small variability within the ensemble (see the percentiles in **Figure 3**), we assume the ensemble size sufficient to permit comparison between average results. The sensitivity tests were thus conducted on the number of selected phenotypes (*Ns*). Four quantities of phenotypes in competition with *A. minutum* inside the ecosystem were used ($Ns = [20; 50; 100; 150]$). By doubling the number of species, ($Ns = 50–100\}$ and $Ns = 100–200\}$), the maximum abundance is divided by 2 for the 3 years (**Figure 7**). The total cells per size class remain however constant and show the redundancy between phenotypes. Except for the lowest number ($Ns = 20$), the timing of the highest concentration remains independent of the number of selected species (**Table 5**). The small differences (±3 days) in 2013 are created by the fitting of the Weibull function and the relatively large bloom duration around the highest concentration.

Although the more realistic maximum values are obtained with $Ns = 20$ for all 3 years, the beginning and end of the associated bloom do not fit with these observations. By comparison with the *in situ* observations, the simulation with

**TABLE 6 | Observed interannual variability of *A. minutum* blooms.**

| Year | 2012 | 2013 | 2014 |
|---|---|---|---|
| Temperature °C (15th April) | 11.8 | 11.9 | 12.8 |
| Temperature °C (1st May) | 18 | 15 | 18 |
| Maximal abundance cells $L^{-1}$ | 42,000,000 | 360,000 | 1,500,000 |
| Temporal feature of the bloom | Restricted | Spread | Early and long |

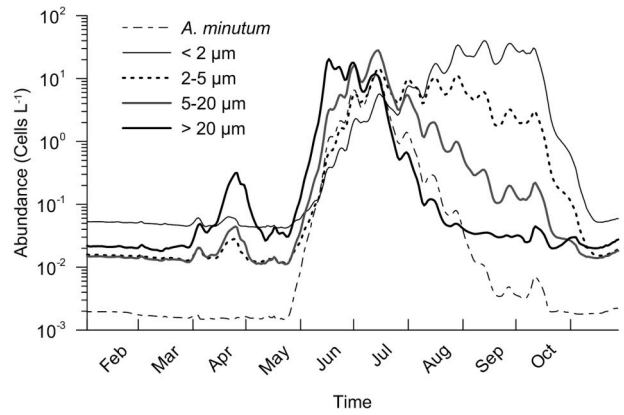


**FIGURE 6 | Seasonal evolution of the phytoplankton community in 2012.** Four size classes were used.

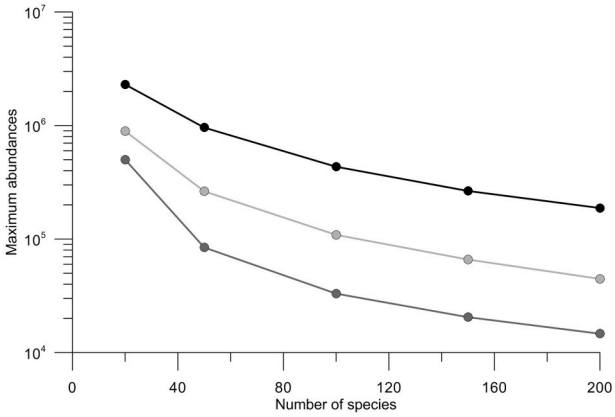


**FIGURE 7 | Variation in maximum abundance of *A. minutum* related to the number of species for the years 2012, 2013, and 2014 in black, light gray and gray, respectively.**

50 phenotypes is more realistic and this was the main reason for choosing this value for the model validation.

For the 3 years and as explained above, the simulated intensity of the *A. minutum* bloom is slightly underestimated and reaches the values of $10^6$, $4{\cdot}10^5$, and $7.8{\cdot}10^5$ cells.$L^{-1}$ against $4.2{\cdot}10^6$, $8.4{\cdot}10^5$, and $1.5{\cdot}10^6$ respectively (**Figure 8**). Otherwise, for the years 2012 and 2013, the model reproduces very well the seasonal dynamics of *A. minutum* with a growth starting at the end of May, a maximum at the end of June and a rapid decrease in July. Concerning the year 2014, the growth of *A. minutum* occurs earlier and is well reproduced by the model. However, it does not fit with the decrease phase which is simulated on 29TH August instead of the 16TH September.

The total microphytoplankton flora was compared to the simulated dynamics of the large cells (large nanoflagellates + microphytoplankton, *A.minutum* included). Their spring bloom initiation is clearly not well simulated by the model (**Figure 8**). In fact, this delay in the bloom timing is related to an underestimation of the net growth rate and/or immigration. In 2012, the model simulates a maximum of $5.7{\cdot}10^6$ against $7.4{\cdot}10^6$ for the observations on approximately the same date. In 2013, the maximum abundance simulated reached $2.8{\cdot}10^6$ against $5.5{\cdot}10^5$ for the observations.

Conversely, for all 3 years, the dynamics after the bloom maximum fit well with the observations although small differences do appear in 2014. These simulated values are higher than the observations that were made that year ($4.5{\cdot}10^6$ against $2.4{\cdot}10^6$). The decrease is also simulated earlier than observed (one month of delay) and overestimated by the model. A second increase in the abundance is simulated during October with values again higher than the observations.

# 4. DISCUSSION

## 4.1. Dynamic of the Community Structure

Despite all the assumptions inherent to a model conception, the simulations are in good agreement with the observations. The community starts from opportunist phenotypes and during 2 months, progress to gleaners due to an increase of the resources competition. The strong initial assumption that the predation was negligible compared to dilution and constant over the years appears consistent for the selected area and period. However, for an application of the model in another area or over an extended period, this assumption could be challenged. An integration of a predation more or less specific could be required with a large set of formulation available in the literature going from a generalist grazer by keeping the same differences between phenotypes fitness (its capacity to invade the environment considered) only driven by their growth rates to the use of a "Kill The Winner" (KTW) strategy (Prowe et al., 2012; Vallina et al., 2014) which modifies the inter-specific competition by bringing the fitness of phenotypes very close.

The main error of the model is the delay of the bloom timing for diatoms and large flagellates. We link this bias to the lack of spatial dimension and the migration processes through open boundaries. The bloom timing of large cells is dependent on the available light and temperature but is mainly driven by the dilution rate. By considering another area or by increasing the considered area, the dilution rate will be strongly modified. All the connected areas, such as the up- and down-stream parts of the estuary, are associated with different dilution rates and later or earlier blooms can be expected with phenotypes having different optimal temperatures. The results of the simulation can thus be analyzed by assuming that an earlier bloom should take place in the bay of Brest from March to April before an advection

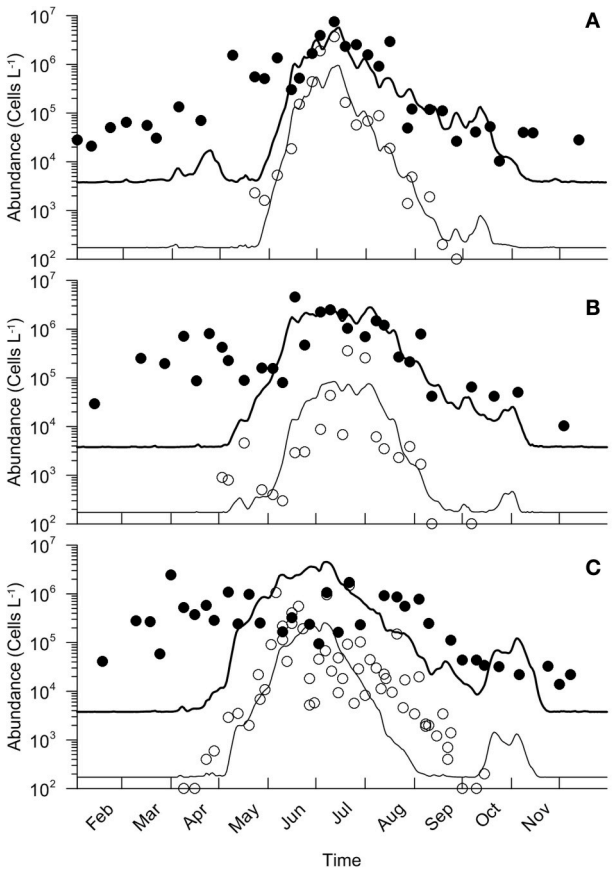


**FIGURE 8 | Comparison between simulations of *A. minutum* (thin line) and total cells (bold line) with density estimates for *A. minutum* and large phytoplankton (> 5 μm of ESD) in circles and black dots respectively.** Comparison are made for 2012, 2013, and 2014 in **(A–C)** respectively.

in the estuary but that these phenotypes are not adapted to the Mignonne estuary conditions.

## 4.2. Dynamic of *A. minutum*

The initial objective, to simulate one species of interest with similar organisms inside a common framework based on trait, was successful. Without any particular fitting of the physiological parameters (all the parameters used are based on the literature at the community and species levels) and the same resolution of the biological processes for all the organisms, the model shows very interesting capacities to simulate the right timing and variability of the bloom intensity over the 3 years. Only one condition was required for *A. minutum* parameter set: for at least one trait, this species must have an equivalent or a better fitness than other theoretical species with the same size and optimal temperature. Without respecting this condition, *A. minutum* would not be able to invade.

The model also shows that the local growth is sufficient to support the observed densities and that the timing and intensities were driven only by local conditions and resources competition. This simulated growth and presence period must however be analyzed as the potential ecological niche defined by abiotic factors and inter-specific competition for resources with all external forcings being constant over time. Similar to the community structure, a modification of the phenotype fitness due to a variation of the selective grazing pressure will introduce a bias between the simulated and the observed inter-annual variability. Such variations over time in the grazers community were already observed in similar estuaries in recent studies. The grazer community observed was dinoflagellate parasites (Erard-Le Denn et al., 2000; Guillou et al., 2008) that can be both highly specific of their prey (Coats and Park, 2002; Chambouvet et al., 2008) or not (Figueroa et al., 2008) and can change over time.

The main difference between our work and previous theoretical studies focused at the community level (Grover, 1991, 1992; Pascual, 1994; Legovic and Cruzado, 1997; Smith, 1997; Smith and Zhao, 2001; Sunda et al., 2009) is the introduction of temperature preferences. This additional trait is independent of all the others with an optimal temperature that was randomly selected in the temperature range measured in the area [10–20]°C. The use of these two independent traits (size and optimal temperature) explains the minimum number of phenotypes required to obtain a good estimation of the bloom duration. Fifty is the minimal value required to sample correctly the traits-space. It must also be notice that the maximal densities of *A. minutum* bloom are always strongly correlated with this number of phenotypes (**Figure 7**). With a random process to select size and temperature instead of a regular distribution along the trait ranges, we accept the possibility of a full redundancy between a few phenotypes if the total number is large enough to sample correctly all the traits-space. The biomasses of these redundant phenotypes are obviously close but the temporal niche remains stable and particularly the bloom initiation timing. The relevance of the forcing on the timing is thus highlighted by the model: temperature and dilution appear as the main drivers of the bloom timing for *A. minutum* in the Mignonne estuary; the nutrient inflows mainly drive the maximal abundance values reached by the bloom while the inter-specific competition can also drive the bloom magnitude and termination.

The high capacity of the model to simulate correctly the right timing of the bloom initiation with only one average phenotype for one species raises the question of the phenotypic variability. The parameters used here are provided by only a few strains whereas intra-specific variability studies have highlighted a high heterogeneity of physiological parameters (Aguilera-Belmonte et al., 2011; Kremp et al., 2012; Hadjadji et al., 2012). The "surprising" good fit between the observations and simulations using this average phenotype could result from an average of many local dynamics mixed by the tide and the average of the ensemble simulation. Nevertheless, the effect of this intra-specific variability on the species dynamics remains another process to understand and a great challenge to the ecology of communities.

## 5. CONCLUSION AND PERSPECTIVES

The main interest of the model was to understand, due to the mechanistic aspect, the processes driving the seasonal and inter-annual variability of the niche successions in the community. In this respect, this work was successful and was validated by considering one particular species in this area. Temperature and dilution appear to be the main factors enabling bloom events but competition process is also an important factor despite the high nutrient inputs. The trait based approach that integrates some variability in the organisms fitness instead of an empiric selection and limitation of the ecosystem complexity keeps more flexibilities for the adaptation of the community to environment pressure. We expect that by using and developing (increase of the traits complexity) this approach for ecosystem management, there will be larger spectrum of potential replies by the phytoplankton community to environment modifications. Despite that the forecasting potential of the model was not the initial objective, the model thus shows some very good capacities to simulate the ecological niche of *A. minutum* as well as the potential link with warning period. Finally, in the context of global change, these models could be used to study the relevance of abiotic factors on the species niches as well as their interaction through the competition process which could lead to more efficient management efforts.

## AUTHOR CONTRIBUTIONS

MS, MP, and AC had substantial contributions to the conception and design of the work. VL and GL contributed mainly to the acquisition but all the authors participated to analysis of data for the work. MS and VL participated mainly to the draft the work but all the authors revised it critically. All the authors approved the submitted version and agreed to be accountable for all aspects.

## FUNDING

The project was supported by the Agence de l'Eau Loire Bretagne and the Region Bretagne (Daoulex project).

## ACKNOWLEDGMENTS

We thank Meteo-France, the REPHY monitoring program and the VELYGER program for providing the data set (Pouvreau et al., 2016). Data were successively collected in the framework of the Daoulex project. We thank S. Petton for the setting of the hydrodynamic configuration.

## REFERENCES

Aguilera-Belmonte, A., Inostroza, I., Franco, J. M., Riobo, P., and Gomez, P. I. (2011). The growth, toxicity and genetic characterization of seven strains of Alexandrium catenella (Whedon and Kofoid) Balech 1985 (Dinophyceae) isolated during the 2009 summer outbreak in southern Chile. *Harmful Algae* 12, 105–112. doi: 10.1016/j.hal.2011.09.006

Anderson, D. M., and Stolznbach, K. (1985). Selective retention of 2 dinoflagellates in a well-mixed estuarine embayment - the importance of diel vertical migration and surface avoidance. *Marine Ecol. Progr. Ser.* 25, 39–50. doi: 10.3354/meps025039

Arino, J., Gouze, J. L., and Sciandra, A. (2002). A discrete, size-structured model of phytoplankton growth in the chemostat - introduction of inhomogeneous cell division size. *J. Math. Biol.* 45, 313–336. doi: 10.1007/s002850200160

Arzul, G., Seguel, M., Guzman, L., and Erard-Le Denn, E. (1999). Comparison of allelopathic properties in three toxic Alexandrium species. *J. Exp. Marine Biol. Ecol.* 232, 285–295. doi: 10.1016/S0022-0981(98)00120-8

Barton, A. D., Dutkiewicz, S., Flierl, G., Bragg, J., and Follows, M. J. (2010). Patterns of diversity in marine phytoplankton. *Science* 327, 1509–1511. doi: 10.1126/science.1184961

Bass Becking, L. (1934). *Geobiologie of Inleiding Tot de Milieukunde.* The Hague: W. P. Van Stockum & Zoon.

Burkholder, J. M. (1998). Implications of harmful microalgae and heterotrophic dinoflagellates in management of sustainable marine fisheries. *Ecol. Appl.* 8, S37–S62.

Chambouvet, A., Morin, P., Marie, D., and Guillou, L. (2008). Control of Toxic Marine Dinoflagellate Blooms by Serial Parasitic Killers. *Science* 322, 1254–1257. doi: 10.1126/science.1164387

Chapelle, A., Labry, C., Sourisseau, M., Lebreton, C., Youenou, A., and Crassous, M. (2010). *Alexandrium minutum* growth controlled by phosphorus: an applied model. *GEOHAB Model.* 83, 181–191. doi: 10.1016/j.jmarsys.2010.05.012

Coats, D. W., and Park, M. G. (2002). Parasitism of photosynthetic dinoflagellates by three strains of Amoebophrya (Dinophyta): parasite survival, infectivity, generation time, and host specificity. *J. Phycol.* 38, 520–528. doi: 10.1046/j.1529-8817.2002.01200.x

Cugier, P., Billen, G., Guillaud, J. F., Garnier, J., and Menesguen, A. (2005). Modelling the eutrophication of the Seine Bight (France) under historical, present and future riverine nutrient loading. *J. Hydrol.* 304, 381–396. doi: 10.1016/j.jhydrol.2004.07.049

Davidson, K., and Gurney, W. S. C. (1999). An investigation of non-steady-state algal growth. II. Mathematical modelling of co-nutrient-limited algal growth. *J. Plankton Res.* 21, 839–858. doi: 10.1093/plankt/21.5.839

Droop, M. R. (1968). Vitamin B12 and Marine Ecology. IV. The Kinetics of Uptake, Growth and Inhibition in Monochrysis Lutheri. *J. Marine Biol. Assoc. U.K.* 48, 689–733.

Droop, M. R. (1974). Some thoughts on nutrient limitation in algae. *Coll. Reprints Scott. Marine Biol. Assoc.* 9:263. doi: 10.1017/S0025315400019238

Dutkiewicz, S., Follows, M. J., and Bragg, J. G. (2009). Modeling the coupling of ocean ecology and biogeochemistry. *Global Biogeoch. Cycles* 23, GB4017. doi: 10.1029/2008GB003405

Edwards, K. F., Thomas, M. K., Klausmeier, C. A., and Litchman, E. (2012). Allometric scaling and taxonomic variation in nutrient utilization traits and maximum growth rate of phytoplankton. *Limnol. Oceanogr.* 57, 554–566. doi: 10.4319/lo.2012.57.2.0554

Elith, J., Kearney, M., and Phillips, S. (2010). The art of modelling range-shifting species. *Methods Ecol. Evol.* 1, 330–342. doi: 10.1111/j.2041-210X.2010.00036.x

Eppley, R. W. (1972). Temperature and phytoplankton growth in the sea. *Fish. Bull.* 70, 1063–1085.

Erard-Le Denn, E. (1997). "Alexandrium minutum," in *Efflorescences Toxiques Des Eaux Cotieres Francaises. Ecologie, Ecophysiologie, Toxicologie, Ifremer Edn.,* eds B. Berland and P. Passus (Plouzané: Reperes Ocean), 53–65.

Erard-Le Denn, E., Chretiennot-Dinet, M. J., and Probert, I. (2000). First report of parasitism on the toxic dinoflagellate *Alexandrium minutum* Halim. *Estuar. Coast. Shelf Sci.* 50, 109–113. doi: 10.1006/ecss.1999.0537

Falkowski, P. G., and Oliver, M. J. (2007). Mix and match: how climate selects phytoplankton. *Nat. Rev. Microbiol.* 5, 813–819. doi: 10.1038/nrmicro1751

Fauchot, J., Saucier, F. J., Levasseur, M., Roy, S., and Zakardjian, B. (2008). Wind-driven river plume dynamics and toxic *Alexandrium tamarense* blooms in the St. Lawrence estuary (Canada): a modeling study. *Harmful Algae* 7, 214–227. doi: 10.1016/j.hal.2007.08.002

Figueroa, R. I., Garces, E., Massana, R., and Camp, J. (2008). Description, host-specificity, and strain selectivity of the dinoflagellate parasite *Parvilucifera sinerae* sp. nov. (Perkinsozoa). *Protist* 159, 563–578. doi: 10.1016/j.protis.2008.05.003

Flynn, K. J. (2005). Modelling marine phytoplankton growth under eutrophic conditions. *J. Sea Res.* 54, 92–103. doi: 10.1016/j.seares.2005.02.005

Flynn, K. J. (2008). "Use, abuse, misconceptions and insights from quota models - the droop cell quota model 40 years on," in *Oceanography and Marine Biology: An Annual Review*, Vol. 46, eds R. N. Gibson, R. J. A. Atkinson, and J. D. M. Gordon (Boca Raton, FL: CRC Press), 1–23.

Follows, M. J., and Dutkiewicz, S. (2011). Modeling diverse communities of marine microbes. *Annu. Rev. Mar. Sci.* 3, 427–451. doi: 10.1146/annurev-marine-120709-142848

Forsythe, W., Rykiel, E., Stahl, R., Wu, H., and Schoolfiled, R. (1995). A model comparison for daylength as a function of latitude and day of year. *Ecol. Model.* 80, 87–95. doi: 10.1016/0304-3800(94)00034-F

Gohin, F., Loyer, S., Lunven, M., Labry, C., Froidefond, J.-M., Delmas, D., et al. (2005). Satellite-derived parameters for biological modelling in coastal waters: illustration over the eastern continental shelf of the Bay of Biscay. *Remote Sens. Environ.* 95, 29–46. doi: 10.1016/j.rse.2004.11.007

Graneli, E., Salomon, P. S., and Fistarol, G. O. (2008). "The role of allelopathy for harmful algae bloom formation," in *Algal Toxins: Nature, Occurrence, Effect and Detection, NATO Science for Peace and Security Series A: Chemistry and Biology*, eds V. Evangelista, L. Barsanti, A.M. Frassanito, V. Passarelli, and P. Gualtieri (Dordrecht: Springer), 159–178.

Grover, J. (1991). Resource competition in a variable environment - phytoplankton growing according to the variable-internal-stores model. *Am. Nat.* 138, 811–835.

Grover, J. (1992). Constant-yield and variable-yield models of population-growth - responses to environmental variability and implications for competition. *J. Theor. Biol.* 158, 409–428.

Grover, J. P., and Wang, F.-B. (2014). Competition and allelopathy with resource storage: two resources. *J. Theo. Biol.* 351, 9–24. doi: 10.1016/j.jtbi.2014.02.013

Guillou, L., Viprey, M., Chambouvet, A., Welsh, R. M., Kirkham, A. R., Massana, R., et al. (2008). Widespread occurrence and genetic diversity of marine parasitoids belonging to Syndiniales (Alveolata). *Environ. Microbiol.* 10, 3349–3365. doi: 10.1111/j.1462-2920.2008.01731.x

Guisande, C., Frangopulos, M., Maneiro, I., Vergara, A. R., and Riveiro, I. (2002). Ecological advantages of toxin production by the dinoflagellate *Alexandrium minutum* under phosphorus limitation. *Marine Ecol. Prog. Ser.* 225, 169–176. doi: 10.3354/meps225169

Hadjadji, I., Masseret, E., Plisson, B., Laabir, M., Cecchi, P., and Collos, Y. (2012). Clonal variation in physiological parameters of *Alexandrium tamarense:* implications for biological invasions and maintenance. *Cahiers De Biologie Marine* 53, 357–363.

Hallegraeff, G. M. (1993). A review of harmful algal blooms and their apparent global increase. *Phycologia* 32, 79–99. doi: 10.2216/i0031-8884-32-2-79.1

Hallegraeff, G. M. (2010). Ocean climate phytoplankton community responses, and harmful algal blooms: a formidable predictive challenge. *J. Phycol.* 46, 220–235. doi: 10.1111/j.1529-8817.2010.00815.x

He, R., McGillicuddy, D. J., Keafer, B. A., and Anderson, D. M. (2008). Historic 2005 toxic bloom of *Alexandrium fundyense* in the western Gulf of Maine: 2. Coupled biophysical numerical modeling. *J. Geophys. Res. Oceans* 113, C07040. doi: 10.1029/2007JC004602

Hickman, A. E., Dutkiewicz, S., Williams, R. G., and Follows, M. J. (2010). Modelling the effects of chromatic adaptation on phytoplankton community structure in the oligotrophic ocean. *Marine Ecol. Prog. Ser.* 406, 1–17. doi: 10.3354/meps08588

Hulot, F. D., and Huisman, J. (2004). Allelopathic interactions between phytoplankton species: the roles of heterotrophic bacteria and mixing intensity. *Limnol. Oceanogr.* 49, 1424–1434. doi: 10.4319/lo.2004.49.4_part_2.1424

Ianora, A., Bentley, M. G., Caldwell, G. S., Casotti, R., Cembella, A. D., Engstrom-Ost, J., et al. (2011). The relevance of marine chemical ecology to Plankton and Ecosystem Function: an emerging field. *Marine Drugs* 9, 1625–1648. doi: 10.3390/md9091625

Janowitz, G. S., and Kamykowski, D. (2006). Modeled Karenia brevis accumulation in the vicinity of a coastal nutrient front. *Marine Ecol. Prog. Ser.* 314, 49–59. doi: 10.3354/meps314049

Jassby, A., and Platt, T. (1976). mathematical formulation of relationship between photosynthesis and light for phytoplankton. *Limnol. Oceanogr.* 21, 540–547. doi: 10.4319/lo.1976.21.4.0540

Jeong, H. J., Lim, A. S., Franks, P. J. S., Lee, K. H., Kim, J. H., Kang, N. S., et al. (2015). A hierarchy of conceptual models of red-tide generation: Nutrition, behavior, and biological interactions. *Harmful Algae* 47, 97–115. doi: 10.1016/j.hal.2015.06.004

Jonsson, P. R., Pavia, H., and Toth, G. (2009). Formation of harmful algal blooms cannot be explained by allelopathic interactions. *Proc. Natl. Acad. Sci. U.S.A.* 106, 11177–11182. doi: 10.1073/pnas.0900964106

Kamykowski, D. (1995). Trajectories of autotrophic marine dinoflagellates. *J. Phycol.* 31, 200–208.

Kamykowski, D., Reed, R. E., and Kirkpatrick, G. J. (1992). Comparison of sinking velocity, swimming velocity, rotation and path characteristics among six marine dinoflagellate species. *Marine Biol.* 113, 319–328.

Kearney, M., Simpson, S. J., Raubenheimer, D., and Helmuth, B. (2010). Modelling the ecological niche from functional traits. *Philos. Trans. R. Soc. B Biol. Sci.* 365, 3469–3483. doi: 10.1098/rstb.2010.0034

Kremp, A., Godhe, A., Egardt, J., Dupont, S., Suikkanen, S., Casabianca, S., et al. (2012). Intraspecific variability in the response of bloom-forming marine microalgae to changed climate conditions. *Ecol. Evol.* 2, 1195–1207. doi: 10.1002/ece3.245

Labry, C., Denn, E. E.-L., Chapelle, A., Fauchot, J., Youenou, A., Crassous, M. P., et al. (2008). Competition for phosphorus between two dinoflagellates: a toxic *Alexandrium minutum* and a non-toxic Heterocapsa triquetra. *J. Exp. Marine Biol. Ecol.* 358, 124–135. doi: 10.1016/j.jembe.2008.01.025

Lacroix, G., Ruddick, K., Park, Y., Gypens, N., and Lancelot, C. (2007). Validation of the 3D biogeochemical model MIRO&CO with field nutrient and phytoplankton data and MERIS-derived surface chlorophyll *a* images. *J. Marine Sys.* 64, 66–88. doi: 10.1016/j.jmarsys.2006.01.010

Lazure, P., and Dumas, F. (2008). An external-internal mode coupling for a 3D hydrodynamical model for applications at regional scale (MARS). *Adv. Water Res.* 31, 233–250. doi: 10.1016/j.advwatres.2007.06.010

Le Borgne, P., Legendre, G., and Marsouin, A. (2006). "Validation of the OSI SAF radiative fluxes," in *Proceedings of the 2006 EUMETSAT Meteorological Satellite Conference* (Helsinki).

Legovic, T., and Cruzado, A. (1997). A model of phytoplankton growth on multiple nutrients based on the Michaelis-Menten-Monod uptake, Droop's growth and Liebig's law. *Ecol. Model.* 99, 19–31. doi: 10.1016/S0304-3800(96)01919-9

Litchman, E., Edwards, K. F., Klausmeier, C. A., and Thomas, M. K. (2012). Phytoplankton niches, traits and eco-evolutionary responses to global environmental change. *Marine Ecol. Prog. Ser.* 470, 235–248. doi: 10.3354/meps09912

Litchman, E., and Klausmeier, C. A. (2008). Trait-based community ecology of Phytoplankton. *Ann. Rev. Ecol. Evol. Syst.* 39, 615–639. doi: 10.1146/annurev.ecolsys.39.110707.173549

Litchman, E., Klausmeier, C. A., Schofield, O. M., and Falkowski, P. G. (2007). The role of functional traits and trade-offs in structuring phytoplankton communities: scaling from cellular to ecosystem level. *Ecol. Lett.* 10, 1170–1181. doi: 10.1111/j.1461-0248.2007.01117.x

MacIntyre, H. L., Lomas, M. W., Cornwell, J., Suggett, D. J., Gobler, C. J., Koch, E. W., et al. (2004). Mediation of benthic–pelagic coupling by microphytobenthos: an energy- and material-based model for initiation of blooms of *Aureococcus anophagefferens*. *Harmful Algae* 3, 403–437. doi: 10.1016/j.hal.2004.05.005

Maranon, E., Cermeno, P., Lopez-Sandoval, D. C., Rodriguez-Ramos, T., Sobrino, C., Huete-Ortega, M., et al. (2013). Unimodal size scaling of phytoplankton growth and the size dependence of nutrient uptake and use. *Ecol. Lett.* 16, 371–379. doi: 10.1111/ele.12052

Margalef, R. (1978). Life-forms of phytoplankton as survival alternatives in an unstable environment. *Oceanol. Acta* 1, 493–509.

Nì Rathaille, A. (2007). *Modelling Alexandrium Bloom Dynamics in Cork Harbour*. Ph.D. thesis, National University of Ireland, Galway.

Parker, R. A. (1993). Dynamic models for ammonium inhibition of nitrate uptake by phytoplankton. *Ecol. Modell.* 66, 113–120. doi: 10.1016/0304-3800(93)90042-Q

Pascual, M. (1994). Periodic-response to periodic forcing of the droop equations for phytoplankton growth. *J. Math. Biol.* 32, 743–759. doi: 10.1007/BF00168795

Prowe, A. E. F., Pahlow, M., Dutkiewicz, S., Follows, M., and Oschlies, A. (2012). Top-down control of marine phytoplankton diversity in a global ecosystem model. *Prog. Oceanogr.* 101, 1–13. doi: 10.1016/j.pocean.2011.11.016

Raine, R. (2014). A review of the biophysical interactions relevant to the promotion of HABs in stratified systems: the case study of Ireland. *Deep Sea Res. II Topic. Stud. Oceanogr.* 101, 21–31. doi: 10.1016/j.dsr2.2013.06.021

Reynolds, C. S. (2003). Pelagic community assemblage and the habitat template. *Bocconea* 16, 323–339.

Rolinski, S., Horn, H., Petzoldt, T., and Paul, L. (2007). Identifying cardinal dates in phytoplankton time series to enable the analysis of long-term trends. *Oecologia* 153, 997–1008. doi: 10.1007/s00442-007-0783-2

Roy, S., and Chattopadhyay, J. (2007). Toxin-allelopathy among phytoplankton species prevents competitive exclusion. *J. Biol. Sys.* 15, 73–93. doi: 10.1142/S021833900700209X

Seity, Y., Brousseau, P., Malardel, S., Hello, G., Benard, P., Bouttier, F., et al. (2011). The AROME-France convective-scale operational model. *Mon. Weather Rev.* 139, 976–991. doi: 10.1175/2010MWR3425.1

Smith, H. L. (1997). The periodically forced Droop model for phytoplankton growth in a chemostat. *J. Math. Biol.* 35, 545–556. doi: 10.1007/s002850050065

Smith, H. L., and Zhao, X. Q. (2001). Competitive exclusion in a discrete-time, size-structured chemostat model. *Discrete Continuous Dyn. Sys. Ser. B* 1, 183–191. doi: 10.3934/dcdsb.2001.1.183

Sommer, U. (1991). A comparison of the droop and the monod models of nutrient limited growth applied to natural-populations of phytoplankton. *Funct. Ecol.* 5, 535–544. doi: 10.2307/2389636

Pouvreau, S., Daniele, M., Auby, I., Lagarde, F., Le Gall, P., Cochet, H., et al. (2016). *VELYGER Database: The Oyster Larvae Monitoring French Project*. SEANOE. doi: 10.17882/41888

Sunda, W. G., Shertzer, K. W., and Hardison, D. R. (2009). Ammonium uptake and growth models in marine diatoms: Monod and Droop revisited. *Marine Ecol. Prog. Ser.* 386, 29–41. doi: 10.3354/meps08077

Vallina, S. M., Ward, B. A., Dutkiewicz, S., and Follows, M. J. (2014). Maximal feeding with active prey-switching: a kill-the-winner functional response and its effect on global diversity and biogeography. *Prog. Oceanogr.* 120, 93–109. doi: 10.1016/j.pocean.2013.08.001

Wiens, J. A., Stralberg, D., Jongsomjit, D., Howell, C. A., and Snyder, M. A. (2009). Niches, models, and climate change: assessing the assumptions and uncertainties. *Proc. Natl. Acad. Sci. U.S.A.* 106, 19729–19736. doi: 10.1073/pnas.0901639106

**Conflict of Interest Statement:** The authors declare that the research was conducted in the absence of any commercial or financial relationships that could be construed as a potential conflict of interest.

frontiers in Marine Science

REVIEW
published: 22 March 2017
doi: 10.3389/fmars.2017.00077

# Modeling What We Sample and Sampling What We Model: Challenges for Zooplankton Model Assessment

*Jason D. Everett[1,2]*, Mark E. Baird[3], Pearse Buchanan[4], Cathy Bulman[3], Claire Davies[3], Ryan Downie[3], Chris Griffiths[4,5], Ryan Heneghan[6], Rudy J. Kloser[3], Leonardo Laiolo[3,7], Ana Lara-Lopez[8], Hector Lozano-Montes[9], Richard J. Matear[3], Felicity McEnnulty[3], Barbara Robson[10], Wayne Rochester[11], Jenny Skerratt[3], James A. Smith[1,2], Joanna Strzelecki[9], Iain M. Suthers[1,2], Kerrie M. Swadling[4,12], Paul van Ruth[13] and Anthony J. Richardson[6,11]*

[1] Evolution and Ecology Research Centre, University of New South Wales, Sydney, NSW, Australia, [2] Sydney Institute of Marine Science, Sidney, NSW, Australia, [3] CSIRO Oceans and Atmosphere, Hobart, TAS, Australia, [4] Institute for Marine and Antarctic Studies, University of Tasmania, Hobart, TAS, Australia, [5] School of Mathematics and Statistics, University of Sheffield, Sheffield, UK, [6] Centre for Applications in Natural Resource Mathematics, School of Mathematics and Physics, University of Queensland, St. Lucia, QLD, Australia, [7] Plant Functional Biology and Climate Change Cluster, Faculty of Science, University of Technology Sydney, NSW, Australia, [8] Integrated Marine Observing System, University of Tasmania, Hobart, TAS, Australia, [9] CSIRO Oceans and Atmosphere, Floreat, WA, Australia, [10] CSIRO Land and Water, Canberra, ACT, Australia, [11] CSIRO Oceans and Atmosphere, Dutton Park, QLD, Australia, [12] Antarctic Climate & Ecosystems CRC, Hobart, TAS, Australia, [13] South Australian Research and Development Institute - Aquatic Sciences, West Beach, SA, Australia

OPEN ACCESS

**Edited by:**
*Dag Lorents Aksnes, University of Bergen, Norway*

**Reviewed by:**
*Frederic Maps, Université Laval, Canada*
*Webjørn Melle, Institute of Marine Research, Norway*

***Correspondence:**
*Jason D. Everett*
*Jason.Everett@unsw.edu.au*

**Specialty section:**
*This article was submitted to Marine Ecosystem Ecology, a section of the journal Frontiers in Marine Science*

**Received:** *03 August 2016*
**Accepted:** *07 March 2017*
**Published:** *22 March 2017*

**Citation:**
*Everett JD, Baird ME, Buchanan P, Bulman C, Davies C, Downie R, Griffiths C, Heneghan R, Kloser RJ, Laiolo L, Lara-Lopez A, Lozano-Montes H, Matear RJ, McEnnulty F, Robson B, Rochester W, Skerratt J, Smith JA, Strzelecki J, Suthers IM, Swadling KM, van Ruth P and Richardson AJ (2017) Modeling What We Sample and Sampling What We Model: Challenges for Zooplankton Model Assessment. Front. Mar. Sci. 4:77. doi: 10.3389/fmars.2017.00077*

Zooplankton are the intermediate trophic level between phytoplankton and fish, and are an important component of carbon and nutrient cycles, accounting for a large proportion of the energy transfer to pelagic fishes and the deep ocean. Given zooplankton's importance, models need to adequately represent zooplankton dynamics. A major obstacle, though, is the lack of model assessment. Here we try and stimulate the assessment of zooplankton in models by filling three gaps. The first is that many zooplankton observationalists are unfamiliar with the biogeochemical, ecosystem, size-based and individual-based models that have zooplankton functional groups, so we describe their primary uses and how each typically represents zooplankton. The second gap is that many modelers are unaware of the zooplankton data that are available, and are unaccustomed to the different zooplankton sampling systems, so we describe the main sampling platforms and discuss their strengths and weaknesses for model assessment. Filling these gaps in our understanding of models and observations provides the necessary context to address the last gap—a blueprint for model assessment of zooplankton. We detail two ways that zooplankton biomass/abundance observations can be used to assess models: data wrangling that transforms observations to be more similar to model output; and observation models that transform model outputs to be more like observations. We hope that this review will encourage greater assessment of zooplankton in models and ultimately improve the representation of their dynamics.

**Keywords: plankton net, bioacoustics, optical plankton counter, Continuous Plankton Recorder, size-spectra, ecosystem model, observation model, model assessment**

## THE IMPORTANCE OF ZOOPLANKTON

All marine phyla are part of the zooplankton—either permanently as holoplankton (e.g., copepods or arrow worms) or temporarily as meroplankton (e.g., crab or fish larvae). In this review we define zooplankton as all organisms drifting in the water whose locomotive abilities are insufficient to progress against ocean currents (Lenz, 2000). Their sizes range from flagellates (about 20 μm) to siphonophores up to 30 m long. Zooplankton are the intermediate trophic level between phytoplankton and fish and are an important component of carbon and nutrient cycles in the ocean. They account for a large proportion of the energy transfer to fish on continental shelves (Marquis et al., 2011), temperate reefs (Kingsford and MacDiarmid, 1988; Champion et al., 2015), seagrass meadows (Edgar and Shaw, 1995), and coral reefs (Hamner et al., 1988; Frisch et al., 2014). Zooplankton are also key in the transfer of energy between benthic and pelagic domains (Lassalle et al., 2013). Zooplankton are responsible for transferring energy to deep water through the sinking of fecal pellets and moribund carcases (Stemmann et al., 2000; Henschke et al., 2013, 2016) or through diel vertical migration (Ariza et al., 2015) and can play an important role in deoxygenating the upper ocean (Bianchi et al., 2013). In a review of 41 Ecopath models, (Libralato et al., 2006) found that zooplankton (including Euphausiids) had high "keystoneness" (i.e., the largest structuring role in food webs relative to its biomass) in 68% of the ecosystems studied (from tropical to polar regions, and reefs to gyres), including 100% of the eight upwelling systems. Accounting for variations in the dynamics of zooplankton is thus essential to understanding energy flow in marine systems (Mitra et al., 2014), particularly to fisheries (Friedland et al., 2012).

Given the critical role zooplankton plays in the marine environment, models need to capture adequately the dynamics of zooplankton. Models are extremely sensitive to zooplankton parameterization (Edwards and Yool, 2000; Mitra, 2009) and undoubtedly poor parameterization has hindered model performance (Carlotti and Poggiale, 2010). However, significant progress in modeling zooplankton has been made in recent research and reviews focused on improving zooplankton parameterization (Tian, 2006; Mitra et al., 2014) and in better representing zooplankton functional groups (Le Quere et al., 2015). What remains a major obstacle is the lack of model assessment. Based on an examination of 153 published biogeochemical models, Arhonditsis and Brett (2004) found that 95% of them compared output with phytoplankton data, but <20% compared model output with zooplankton data. And in the relatively rare instances where zooplankton were assessed in biogeochemical models, they were more poorly simulated than almost any other state variable (Arhonditsis and Brett, 2004).

In this manuscript, we focus on how we can best use observations of zooplankton biomass and abundance for assessment of zooplankton in models. We define model assessment as the process whereby model output is compared with observed data in time and space to evaluate model performance. We identify and fill three key gaps we perceive as hampering assessment of zooplankton in models. First, many zooplankton observationalists are unfamiliar with the models that typically have zooplankton functional groups, so we describe the primary research questions addressed by biogeochemical, ecosystem, size-based and individual-based models, and how each typically represents zooplankton (**Table 1**). Second, many modelers are unaware of the available data on zooplankton biomass and abundance (**Table 2**) and are unaccustomed to the different types of zooplankton sampling systems and observations they produce (**Table 3**). We thus describe the traditional sampling platforms [e.g., nets (Wiebe and Benfield, 2003) and Continuous Plankton Recorders (CPRs; Richardson et al., 2006)] used for assessing zooplankton in models and more modern techniques [e.g., Laser Optical Plankton Counters (Herman, 2004) and bioacoustics (Greene and Wiebe, 1990)] that present new opportunities for incorporating high-resolution observations into models. Filling these gaps in our understanding of models and observations provides the necessary context to address the last gap—a blueprint for model assessment of zooplankton. Our last section thus provides a detailed discussion and case studies of the two most common ways that zooplankton observations can be used for model assessment: data wrangling that transforms observations to be more similar to model output (Kandel et al., 2011); and observation models that transform model outputs to be more like observations (Dee et al., 2011; Handegard et al., 2012; Baird et al., 2016).

Our focus in this review is on assessment of zooplankton state variables (i.e., abundance and biomass pools) and we do not address better model parameterization (Mitra et al., 2014) or better representation of zooplankton functional groups (Le Quere et al., 2005) which have previously been well-reviewed. Additionally, we do not consider model initialization, although the approaches we suggest for model assessment are equally applicable. We also do not consider data assimilation, although we would highlight that the more modern observation approaches (e.g., laser optical plankton counters and bioacoustics) have considerable potential in this regard. This review will be useful for both zooplankton observationalists who want to produce useful data products for modelers, and modelers interested in new and robust ways of assessment of zooplankton biomass and abundance in their models.

## CURRENT ZOOPLANKTON REPRESENTATION IN MODELS

### Biogeochemical Models

The classic structure of a marine biogeochemical model includes Nutrients, Phytoplankton, Zooplankton, Detritus (NPZD; **Figure 1A**). In the simplest NPZD structure, a single zooplankton compartment represents a broad spectrum of zooplankton and denotes the highest trophic level, which grazes on the single phytoplankton class (Wroblewski et al., 1988; Oke et al., 2013; Robson, 2014). In many biogeochemical models, if zooplankton are included, it is often as the top closure term (Steele and Henderson, 1992; Edwards and Yool, 2000), meaning that the mortality rate in the zooplankton compartment is treated as both a natural and predatory mortality rate. This releases

**TABLE 1 | A list of common biogeochemical, ecosystem and size-based models and how they represent zooplankton groups.**

| | Typical uses of the models | Typical number of groups and role of zooplankton | References |
|---|---|---|---|
| **BIOGEOCHEMICAL MODELS** | | | |
| TOPAZ2 | Global carbon cycle processes and feedbacks with climate | No zooplankton groups. Specific grazing rate for each phytoplankton functional type | Dunne et al., 2013 |
| Diat-HadOCC | Climate predictions, and investigating the strengths of biogeochemical feedbacks | 1 zooplankton group which mediates transfer of energy between phytoplankton, detritus and nutrients | Palmer and Totterdell, 2001; Collins et al., 2011 |
| PISCES | Air-sea fluxes of carbon, global carbon cycle processes and feedbacks with climate | 2 zooplankton groups (Micro- and Meso-) which contribute to elemental cycling through explicitly defined mortality rates, aggregation, fecal pellet production and grazing | Dufresne et al., 2013 |
| NPZD | Global carbon cycle processes and feedbacks with climate | 1 zooplankton group which mediates transfer of energy via grazing and mortality rates | Oschlies, 2001; Watanabe et al., 2011 |
| HAMOCC | Air-sea fluxes of carbon, global carbon cycle processes and feedbacks with climate | 1 zooplankton group which mediates transfer of energy via grazing and mortality rates. Fecal pellet production is implicitly calculated as a fraction of grazing | Maier Reimer et al., 2005 |
| **ECOSYSTEM MODELS** | | | |
| ATLANTIS | Ecosystem impacts due to fishing, management of ecosystems and human behavior in fisheries systems | Typically, 3-4 zooplankton groups classified as small, omnivorous, carnivorous or gelatinous. | Fulton et al., 2005, 2011; Smith et al., 2011 |
| ERSEM (The Regional Seas Ecosystem Model) | Impacts of ecosystem processes (e.g., ocean acidification) on lower TLs | 3 zooplankton groups - microzooplankton, mesozooplankton and nanoflagellates | Baretta et al., 1995; Blackford and Gilbert, 2007 |
| Ecopath with Ecosim (EwE) | Effects of climate and fishing; | Typically, 2-4 zooplankton groups classified as small, large and predatory or jellyfish. | Christensen and Pauly, 1992; Christensen and Walters, 2004; Christensen et al., 2015 |
| NEMURO-FISH, North Pacific | Biogeochemical model coupled with higher TLs such as saury and herring | 3 zooplankton groups: small, large and predatory zooplankton | Megrey et al., 2007 |
| SEAPODYM (Spatial Ecosystem And Populations Dynamics Model) | Impacts of fishing on Pacific tuna species | 2 zooplankton groups: small and large zooplankton | Lehodey et al., 2008, 2014 |
| **SIZE-SPECTRUM MODELS** | | | |
| APECOSM | Impacts of fishing and climate change on tuna species and open ocean ecosystems | 2 groups in an external NPZ model (PISCES). Food source for higher trophic levels | Maury, 2010; Dueri et al., 2014; Lefort et al., 2015; Le Mezo et al., 2016 |
| OSMOSE | Impacts of fishing and climate change on higher trophic levels in marine ecosystems | 2 groups (small, large). Predators of phytoplankton and food for higher trophic levels | Shin and Cury, 2004; Travers-Trolet et al., 2014; Grüss et al., 2016 |
| Discrete size class | Impacts of fishing on marine ecosystems, and the effect of parameter uncertainty | Background food source for fish species, but not explicitly resolved | Hall et al., 2006; Pope et al., 2006; Thorpe et al., 2015 |
| Static size continuum | Establishing baseline, unperturbed abundance of marine ecosystems | No zooplankton groups | Jennings et al., 2008b; Jennings and Collingridge, 2015 |
| Trait-based multi-species | Impacts of fishing and climate change on fish in marine ecosystems | Smaller zooplankton grouped with phytoplankton into background resource spectrum for larger size classes, modeled as a semi-chemostat system. Larger zooplankton represented as small fish | Blanchard et al., 2014; Scott et al., 2014 |

*The key references for each model is provided. The list is not intended to be an exhaustive list, but rather provide a starting point for those researchers interested in a particular modeling approach. For a more detailed list of models we point the reader to Bopp et al. (2013) and Arora et al. (2013).*

nutrients held within the zooplankton back into the environment over time. Given this simple structure, it is arguable whether "zooplankton" included in some biogeochemical (lower trophic level) models can be considered to equate even conceptually with zooplankton in real systems. The "zooplankton" pool in these models must account for storage of all carbon and nutrients that has been taken up from phytoplankton and detritus by grazing but not yet returned to the pool of detritus and available nutrients through respiration and mortality, i.e., the biomass of all animals in the system.

In addition, many of the global biogeochemical models do not include a zooplankton compartment. Instead, the role of

**TABLE 2 | A list of some zooplankton data repositories whose data can be used for model assessment.**

| Program | Region | Availability |
|---|---|---|
| **CPR** | | |
| SAHFOS | North Atlantic | Available on request: http://www.sahfos.ac.uk |
| Scientific Committee on Antarctic Research (SCAR) | Southern Ocean | Available on request: https://data.aad.gov.au |
| Integrated Marine Observing System (IMOS) | Australia | Download from: https://portal.aodn.org.au |
| **NETS** | | |
| Bermuda-Atlantic Time-Series (BATS) | Sargasso Sea | Download from: http://bats.bios.edu |
| California Cooperative Oceanic Fisheries Investigations (CalCOFI) | California, U.S.A | Download from: http://calcofi.org/data.html |
| Census of Marine Zooplankton (CMarZ) | Global repository | Download from: http://www.cmarz.org/ |
| Coastal and Oceanic Plankton Ecology, Production, and Observation Database (COPEPOD) | Global repository | Download from: http://www.st.nmfs.noaa.gov/copepod/ (Tools for data-analysis also available) |
| Hawaii Ocean Time-Series (HOTS) | Oahu, Hawaii, U.S.A | Download from: http://hahana.soest.hawaii.edu/hot/ |
| Integrated Marine Observing System (IMOS) | Australia | Download from: https://portal.aodn.org.au |
| Ocean Biogeographic Information System (OBIS) | Global Repository | Download from: http://beta.iobis.org |
| Scientific Committee on Antarctic Research (SCAR) | Southern Ocean | Download from: https://data.aad.gov.au |
| Western Channel Observatory (L4) | W. English Channel | Download from: http://www.bodc.ac.uk/ |
| MARine Ecosystem DATa (MAREDAT) | Global Repository | Download from: http://www.pangaea.de/search?&q=maredat |
| **BIOACOUSTICS** | | |
| IMOS | Australia | Download from: https://portal.aodn.org.au |
| National Centers for Environmental Information (NCEI) | Global | Download from: https://www.ngdc.noaa.gov |
| Southern Ocean Network of Acoustics (SONA) | Southern Ocean | Download from: https://sona.aq |

*Please note there will be overlap in the data contained within some of these repositories.*

**TABLE 3 | An overview of the resolution, data type and strengths and weaknesses of the four main observation platforms described in this manuscript.**

| | Net sampling | Continuous Plankton Recorder | Optical plankton counters | Bioacoustics |
|---|---|---|---|---|
| Type of plankton data | Taxonomic, abundance, biomass, size | Taxonomic, abundance | Abundance, size | Biomass, functional size |
| Nature of data | Quantitative | Semi-quantitative | Quantitative | Quantitative |
| Spatial scale* | 10s meters to 100s kilometers | 10s to 1,000s kilometers | 10s meters to 100s kilometers | Meters to 1,000s kilometers |
| Temporal scale* | Hours to years | Days to years | Minutes to years | Minutes to years |
| Vertical resolution | Depth resolved | Near-surface | Depth resolved | Depth resolved |
| Vessels | Research | SOOP/research | Research | SOOP/research |
| Cost of collecting | Expensive (research vessel) | Cheap (unaccompanied on SOOP) | Expensive (research vessel) | Expensive (research vessel or SOOP) |
| Cost of processing | Expensive | Expensive | Cheap | Cheap |
| Cost of installation | Cheap to Expensive | Cheap | Expensive | Expensive |
| Sample collected and archived | Yes | Yes | No | No |
| Main strengths | Quantitative local measure of zooplankton | Community composition over large time and space scales | Rapid measurement of particle size | Automatic identification of taxa High spatial resolution |
| Some limitations | Small zooplankton extruded | Zooplankton damaged Abundance underestimated | No identification. Particles could be detritus or inorganic | Not identified to species Under samples some groups |
| Application in model assessment | Assessment of zooplankton biomass in BGC and ecosystem models. Good information on functional groups | Assessment of zooplankton biomass in BGC & ecosystem models, but only after standardization. Good information on functional groups | Assessment of zooplankton size structure in size-based models. Currently limited information on functional groups | Assessment of zooplankton biomass in BGC and ecosystem models. Currently limited information on functional groups |

**Typical scales over which observations are made and analyzed. Not the resolution of the instrument.*

zooplankton is represented as an all-encompassing mortality rate for phytoplankton (Christian et al., 2010; Dunne et al., 2013; Holzer and Primeau, 2013; Matear and Lenton, 2014). Instead of explicitly modeling the interaction between primary and secondary consumers, these models include a parameter that captures the consumption of phytoplankton. These kinds of scaling parameters are rarely determined experimentally but rather they are tuned during model development and assessment to produce realistic model outputs for the region and parameter set (e.g., Holzer and Primeau, 2013).

Biological complexity can be increased within this simple NPZD structure to represent the lower trophic levels of marine ecosystems with various elemental cycles or to include multi-zooplankton compartments separated into different functional and/or size groups (Fennel and Neumann, 2004). The use of multiple phytoplankton functional groups based on physiology (Follows et al., 2007), taxonomy (Chan et al., 2002), or morphology (Kruk et al., 2010) is common, but the use of zooplankton functional groups is relatively less common. There are however some examples that distinguish zooplankton functional groups on the basis of grazing strategies and basal metabolism (Zhao et al., 2008) or feeding strategies, size and palatability to higher trophic levels (Sun et al., 2010). If we are to increase the complexity of zooplankton in a biogeochemical model, we not only need improved parameterization (Mitra, 2009), but also quantitative observations with which to help assess an expanded model that includes multiple zooplankton functional groups.

## Ecosystem Models

Ecosystem models attempt to describe the whole ecological system, from primary producers to higher trophic levels, often including human components (**Figure 1B**). Generally, these models have complex predator-prey interactions, including dozens to hundreds of species. Zooplankton however, are generally only represented by a few classes (e.g., Yool et al., 2011; Piroddi et al., 2015; **Table 2**), defined by diet (Pinnegar et al., 2005), functional type (Le Quere et al., 2005), or size (Griffiths et al., 2010; Ward et al., 2012; Savina et al., 2013; Watson et al., 2013; Pedersen et al., 2016), or a combination of these. Of course, some ecosystem models have many more zooplankton classes (e.g., Pavés et al., 2013). Despite these exceptions, research using common ecosystem modeling approaches—ECOPATH with ECOSIM (Christensen and Walters, 2004), ATLANTIS (Fulton et al., 2005), ERSEM (Baretta et al., 1995), and SEAPODYM (Lehodey et al., 2008)—tend to focus on fish and fisheries (Griffiths et al., 2010) and are hindered by uncertainties in the prey and predator relationships of zooplankton (Mitra and Flynn, 2006). Of course, models (of any kind) do not need to represent every detail of the environment to be useful or address a specific question (Fulton et al., 2003), however we do know that zooplankton is essential to understanding the transfer of energy to fish and fisheries (Friedland et al., 2012; Lassalle et al., 2013), and therefore care needs to be taken in the representation of this link between the lower and upper tropic levels (Rose et al., 2010; Shin et al., 2010).

The simplification of zooplankton groups in ecosystem models, while not always ideal, enables operationalization of the model, however understanding the effects of climate variability and change on the target species or fisheries (for example), can only be understood if the trophic pathways leading to them are well-defined. A common problem with how zooplankton are represented in both ecosystem and biogeochemical models is the false assumption that the same zooplankton assemblage is present throughout the whole domain, both horizontally and vertically, and the structure of this assembly does not change over time (Ward et al., 2014). These models lump multiple zooplankton functional groups together and use an "average" set of parameter estimates. Zooplankton assemblages change markedly in character from eutrophic systems, dominated by the classic short food chains and larger species, to oligotrophic systems, dominated by longer food chains and smaller species. They differ vertically, with predatory and larger species below the euphotic zone and are further complicated due to the complexity of zooplankton behavior and life-cycle strategies such as molting and diapause. These changes, which fundamentally affect nutrient cycles and fisheries production, are often poorly represented in models.

## Size-Based Models

The size-based approach to marine ecosystem modeling (**Figure 1C**) has developed as an alternative to more traditional taxonomy-based frameworks by simplifying the community structure through classifying individuals based on size as opposed to species identity (**Figure 1C**; Sheldon and Parsons, 1967; Sheldon et al., 1972; Andersen and Beyer, 2015; Andersen et al., 2016). Developed over the past 50 years, this approach is based on empirical observations that individual and community processes such as growth, respiration, and predator-prey relationships and trophic position all scale with body size (Peters, 1983; Jennings et al., 2001; Brown et al., 2004; Andersen et al., 2016). Size-based modeling has two main approaches: (1) static size spectra models (Trebilco et al., 2013) and (2) dynamic size spectra models (Blanchard et al., 2017). Similar to the trophic food web structuring of Lindeman (1942), discrete size spectrum models (or macroecological models) aggregate individual organisms into discrete trophic levels based on size (Jennings and Mackinson, 2003; Jennings et al., 2008a). In comparison, dynamic size spectrum models add the element of time, and scale individual size-based growth and mortality rates to the population and community level (Benoit and Rochet, 2004; Blanchard et al., 2009; Hartvig et al., 2011; Jacobsen et al., 2013; Maury and Poggiale, 2013; Dueri et al., 2014; Guiet et al., 2016).

How zooplankton are treated in size-based models depends on the primary focus. Most of these models focus on higher trophic levels and simply lump microzooplankton together with phytoplankton into a background food source for fish and macrozooplankton as "small fish"—i.e., using equations and parameters for metabolism and feeding for fish that are the size of zooplankton (Heneghan et al., 2016). This simplification eases computational costs, but has recently been called into question because lower trophic levels are critical to improving predictions

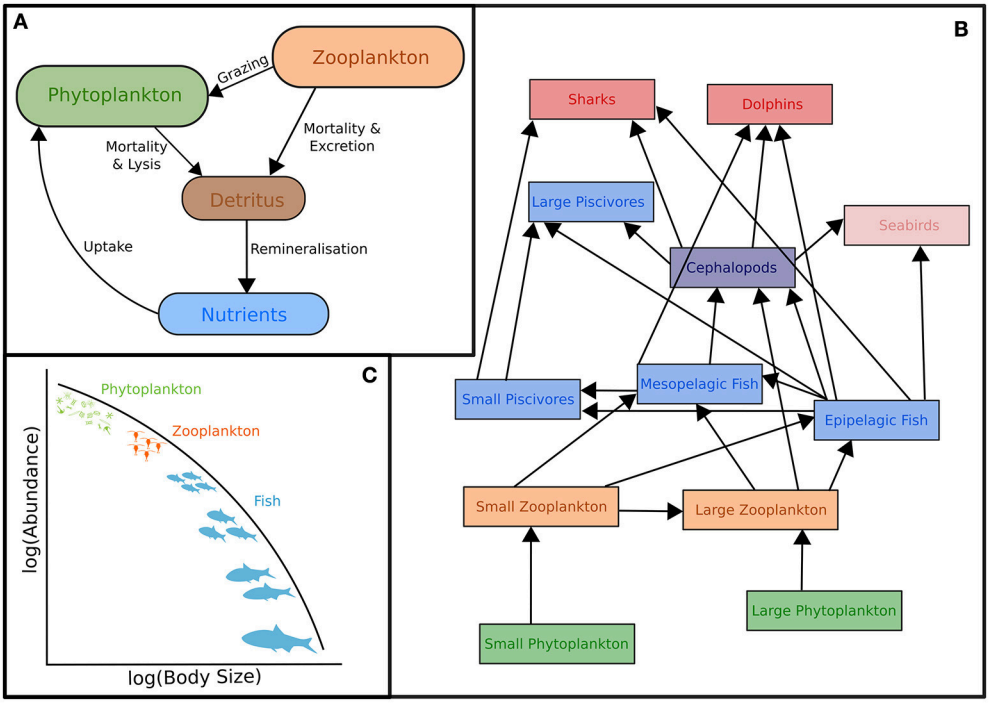


**FIGURE 1 | Representation of typical models featuring zooplankton: (A)** Biogeochemical (NPZD or LTL) models, **(B)** Ecosystem models (HTL) and **(C)** Size-spectra models. Although not shown, all these models have temporal and spatial components. Individual-Based Models are not included in this schematic because they have many different forms which cover **(A–C)**. For more information on IBMs see Section Individual Based Models and references therein.

of biomass and production at higher tropic levels in these models (Jennings and Collingridge, 2015).

Those models that have focused on zooplankton dynamics and food web structure explicitly resolve size-based zooplankton dynamics (Zhou and Huntley, 1997; Zhou, 2006; Baird and Suthers, 2007, 2010; Zhou et al., 2010), but do not explicitly include fish. To date, there have been few attempts to link these size-based zooplankton models to dynamic size spectrum models that have focused on higher trophic levels (but see OSMOSE; Shin and Cury, 2004). With increasing emphasis on understanding ecosystem impacts of climate variability and change, comes the need to better model bottom-up processes and thus the representation of zooplankton.

## Individual Based Models

Individual based models (IBM) simulate individual animals, or groups of individuals as "superorganisms" that are treated as individuals. This allows a sophisticated representation of the behavior and/or physiology of each animal. For instance, IBMs can be structured so that they simulate the movements of animals in response to local light conditions (Batchelder et al., 2002), predator/prey encounters (Gerritsen and Strickler, 1977), or other environmental cues (Batchelder et al., 2002). In the planktonic environment, the main advantage of using an IBM is to account for rare individuals, circumstances or behaviors that contribute strongly to determining the overall population structure or variability; these are difficult to include in a state-variable approach (Werner et al., 2001). Rice et al. (1993), for example, show how variability in larval growth and survival rates can mean that the characteristics of a population of zooplankton can be quite different from the mean characteristics of the individuals within that population.

By simulating individual organisms, IBMs replicate the stochastic variability in the nutritional status, life-cycle stage, or behavior that exists within a population and that may have emergent implications for the overall properties of that population. These include modeling the variability in the survival of larval fish (Letcher et al., 1996), investigating implications of nutrition and reproductive status for food web dynamics of *Daphnia* (Perhar et al., 2016), the role of individual variability in physiological traits in sustaining zooplankton populations (Bi and Liu, 2017), and examining the effect of early/late diapause termination, food availability and initial stock size of the copepod *Calanus finmarchicus* in the Norwegian Sea (Hjøllo et al., 2012). This may come at a cost of increased model complexity and computational costs. In addition, IBMs require significantly more information on the modeled species if the model is to be rigorously parameterised and evaluated. As a result, IBMs are often applied to well-studied species such as the krill *Euphausia pacifica* (Dorman et al., 2015a,b) and the copepod *C. finmarchicus* (Skaret et al., 2014; Opdal and Vikebø, 2016). IBMs are also coupled to hydrodynamic, ecosystem or biogeochemical models (Skaret et al., 2014; Dorman et al., 2015a; Opdal and Vikebø, 2016; Parada et al., 2016), thus allowing two-way nesting within larger-scale modeling environments. Werner et al. (2001) reviewed the use of IBMs in marine modeling, while

Breckling et al. (2006) provide a more general discussion of the use of IBMs in ecological theory.

## ZOOPLANKTON SAMPLING SYSTEMS FOR MODEL ASSESSMENT

Before we discuss approaches to integrate zooplankton observations and models, we will briefly describe the major zooplankton sampling systems used for collecting zooplankton observations (**Table 3**), the different types of data each produces, and the characteristic temporal and spatial sampling scale, which includes the sampling extent, interval, and grain size (resolution).

There is no single best way to sample zooplankton. In the treatise by Wiebe and Benfield (2003), essential reading for observationalists and modelers, they describe 164 different zooplankton sampling systems, ranging from nets to optical sensors. This staggering variety of systems, each with distinct sampling characteristics, has evolved to answer specific zooplankton research questions, not for ease of uptake into models. Here we discuss four major types of zooplankton sampling systems that have been used in model assessment: nets; the CPR; size-based systems (e.g., OPC/LOPC and ZooScan); and bioacoustics (see **Table 3**).

### Net Sampling

The use of nets is the oldest and most common method of sampling zooplankton. The recent history of zooplankton net sampling dates back to Thompson in 1828 (Wiebe and Benfield, 2003), but there are recorded observations prior to this (e.g., Sir Joseph Banks on the Endeavor in 1770; Baird et al., 2011). There are many different net configurations in use, but the key attributes that influence model assessment are the monitoring design, sampling characteristics, and the information derived from samples.

#### Sampling Characteristics

The large spatial and temporal extents of net sampling programs make their data well-suited for model assessment. Nets are used to collect zooplankton over a broad range of temporal extents—from hours to decades—and horizontal and vertical sampling grain sizes—from 10s of meters to 100s of kilometers (**Table 3**). The scale of a particular data set is usually dependent upon the aim of the survey. Process cruises tend to be one-off and are usually less useful for model assessment, unless the research cruise was specifically designed to answer a question that the model is addressing. Typically, data collected from long-term monitoring programs are more useful. Most monitoring programs involve point sampling, sampling weekly or monthly over many years. There are also many larger-scale surveys, often linked with fisheries assessments, that are collected seasonally or annually (e.g., CalCOFI: Edwards et al., 2010; or SARDI: Ward and Staunton-Smith, 2002).

There are four main characteristics to consider when using zooplankton data for model evaluation: type of tow, depth (and vertical resolution) of sampling, time of day, and mesh size. In terms of type of tow, nets can be dragged vertically, obliquely or more or less horizontally at specific depths (depth-stratified by an opening-closing net). All three types of net tows are good for sampling mesozooplankton (0.2–20 mm), although oblique and depth-stratified tows are better for capturing macrozooplankton (2–20 cm), as the net often has a larger mouth area and is towed faster, providing less opportunity for zooplankton to escape. Conversely, faster tow-speeds can result in increased extrusion of smaller individuals. Net avoidance of macrozooplankton such as Antarctic Krill can be minimized with the use of strobe-lights (Wiebe et al., 2004) which are thought to either "dazzle" the plankton, or attract them. Nets are typically towed in the mixed layer (top 50–100 m) or from near the seafloor to the surface. Nets that sample in the mixed layer during the day typically underestimate zooplankton abundance and biomass because larger zooplankton often vertically migrate out of the mixed layer during the day; thus, higher biomass is typically found during the night.

Mesh size is probably the most important net characteristic and varies depending on the size of the target group of zooplankton and the ecosystem of interest. Macrozooplankton are usually sampled with a larger mesh size—500 μm, for example, is commonly used for fish larvae. Historically, many researchers have used 330 μm mesh for mesozooplankton (Moriarty and O'Brien, 2013), but a finer mesh of 200 μm is now almost universally used in temperate and polar systems to better sample smaller zooplankton (Sameoto et al., 2000). However, fine mesh nets (100 μm) more quantitatively capture the smaller part of the mesozooplankton and some of the larger microzooplankton (e.g., juvenile stages of small copepods). Fine mesh nets are most commonly used in tropical areas where the zooplankton are generally smaller. Although coarse mesh nets extrude smaller zooplankton and thus underestimate abundance and biomass (**Box 1**), they still capture large organisms reasonably well (Sameoto et al., 2000).

#### Information Derived from Net Samples

For model assessment, probably the simplest and most useful information derived from net samples is zooplankton biomass. Biomass is measured in several different ways: settled volume, displacement volume, wet weight, dry weight, or occasionally carbon (Postel et al., 2000). Each is measured on different scales, and can be converted from one to another using standard conversions (**Box 1**). Occasionally, samples are poured through meshes of several different sizes and then weighed, providing biomass in different size categories (Huo et al., 2012; Banaru et al., 2014). Other information available from net samples is typically some idea of the zooplankton community present. This can vary from a coarse identification of the community (e.g., copepods, chaetognaths, jellyfish) to species-level identification. Taxonomic identification allows for use in IBM, or the subsequent aggregation of data into functional groups that might be represented in ecosystem models (e.g., mesozooplankton, herbivores, calcifiers).

### The Continuous Plankton Recorder

The CPR has been used for the past 85 years to sample over large regions of the North Atlantic Ocean, and has spawned surveys in the North Pacific Ocean, Southern Ocean, around Australia,

**BOX 1 | DATA WRANGLING: CONVERTING ZOOPLANKTON BIOMASS BETWEEN DIFFERENT UNITS.**

Model assessment using zooplankton biomass is not as straightforward as it might seem because observationalists use a range of different measures, from volumetric to elemental measures, of zooplankton biomass. **Table B1** briefly outlines the different units used to measure zooplankton biomass; for detailed information on the various methods see Postel et al. (2000). These different measures of zooplankton biomass all have their different strengths and weaknesses. We have ordered the rows of **Table B1** by the robustness of the different methods and the ease in which they can be used in modeling, ranging from the most imprecise (Settled Volume) to the most robust (Carbon Mass).

Most models usually use a currency of Nitrogen (or sometimes Carbon) biomass, which is rarely measured. **Table B2** provides a series of equations to convert different biomass to Carbon Mass. Once estimates are in Carbon Mass, they can be converted to Nitrogen Mass by using the C:N ratio of zooplankton, which typically varies from 4:1 to 6:1, but is commonly 5:1 (Postel et al., 2000).

**TABLE B1 | Glossary of zooplankton biomass terms, and their strengths/weaknesses.**

| Methods | Description | Strengths/Weaknesses |
|---|---|---|
| Settled Volume (SV) | Sample poured into graduated cylinder, carefully mixed, and left to settle for 24 h. Volume of zooplankton then read | Imprecise method because of interstitial space between zooplankton of different shapes |
| Displacement Volume (DV) | Samples poured into graduated cylinder with known water volume. Increase in volume indicates zooplankton volume | Overcomes problem of interstitial gaps with SV |
| Wet Mass (WM; also Fresh or Live Mass) | Mass of zooplankton after elimination of excess and interstitial water | Excess water difficult to remove |
| Dry Mass, Dry Weight (DM) | Mass of zooplankton after drying in an oven | Most common method. Provides good information on zooplankton biomass. Problematic in areas with high sediment and includes detritus |
| Ash-Free Dry Mass (AFDM) | DM minus mass of all inorganic material (ash) within sample after drying at a high temperature (to remove organics) | More robust than DM as sediment is removed. Includes detritus |
| Carbon Mass (CM) | Mass of C within zooplankton. C is preferred, as N mainly restricted to protein and P to lipids. Based on measuring liberated product such as $CO_2$ | Good index of zooplankton biomass but includes detritus |

**TABLE B2 | Equations to convert different biomass methods to carbon mass, Rearranged from Postel et al. (2000).**

| Conversion | Equation | References |
|---|---|---|
| SV to DM | $\log_{10}(DM) = 1.15 * \log_{10}(SV) - 2.292$ | Postel, 1990 |
| DV to CM | $\log_{10}(CM) = (\log_{10}(DV) + 1.434)/0.820$ | Wiebe, 1988 |
| WM to CM | $\log_{10}(CM) = (\log_{10}(WM) + 1.537)/0.852$ | Wiebe, 1988 |
| DM to CM | $\log_{10}(CM) = (\log_{10}(DM) + 0.499)/0.991$ | Wiebe, 1988 |
| AFDM to CM | $\log_{10}(CM) = (\log_{10}(AFDM) - 0.410)/0.963$ | Bode et al., 1998 |

and in southern Africa. Unlike nets, there is only one main CPR design that has remained relatively unchanged over the years (Reid et al., 2003). Key attributes of the CPR that influence model assessment are monitoring design, its sampling characteristics, and the information derived from the samples (Richardson et al., 2006).

## Sampling Characteristics

The large spatial and temporal extents characteristic of CPR surveys make the data well-suited for model assessment. The CPR collects zooplankton over greater time and space scales than net sampling—from days to decades and from 10s of kilometers to 1,000s of kilometers (**Table 3**). The temporal grain size (duration of a transect segment) is 15–30 min and the sampling interval between transects is typically a month or longer. The horizontal resolution (length of a transect segment) is 10–20 km. The CPR is not used for short-term process studies, but is deployed routinely by commercial vessels plying common shipping routes, making it ideal for studying trends over time (Richardson et al., 2006).

The CPR is towed near-surface (~7 m), but the draft of the large towing vessels probably mixes water down to 15 m. The aperture of the CPR is small (1.27 × 1.27 cm) and prevents large macrozooplankton such as jellyfish (scyphomedusae) from entering, although small and juvenile euphausiids are sampled (Hunt and Hosie, 2003). Fragile organisms, such as gelatinous plankton, are poorly sampled by the CPR because they are damaged when they come in contact with the silk mesh. For more detailed information about CPR sampling characteristics, see Richardson et al. (2006).

It is well-known that the CPR provides semi-quantitative rather than truly quantitative estimates of zooplankton abundance (Clark et al., 2001; John et al., 2001; Batten et al., 2003; Richardson et al., 2004, 2006), underestimating absolute numbers of zooplankton, but relative changes through time and

over space are robust (see Section Simple Observation Models: Simulated Sampling from a Model). Small zooplankton are likely to be under-sampled because of extrusion through the relatively large mesh size of silk used in the CPR (270 μm) compared with standard nets (Sameoto et al., 2000). Large zooplankton are likely to be under-sampled by the CPR because of active avoidance (Clark et al., 2001; Hunt and Hosie, 2003; Richardson et al., 2004).

Notwithstanding the semi-quantitative nature of CPR sampling, it captures a roughly consistent fraction of the *in situ* abundance of each taxon and thus reflects the major patterns observed in the plankton (Batten et al., 2003). Seasonal cycles estimated from CPR data for relatively abundant taxa are repeatable each year (Edwards and Richardson, 2004) and show good agreement with other samplers such as WP-2 nets (Clark et al., 2001; John et al., 2001) and the Longhurst Hardy Plankton Recorder (Richardson et al., 2004). Inter-annual changes in plankton abundance are also captured relatively well by the CPR (Clark et al., 2001; John et al., 2001; Melle et al., 2014) because the time-series has remained internally consistent, with few changes in the design of the CPR or in counting procedures.

### Information Derived from CPR Samples

Data from the CPR are zooplankton abundance, with no direct estimate of biomass. Data are normally expressed in numbers per sample. Although each sample represents ∼3 $m^3$ of filtered seawater, abundance estimates are seldom converted to per $m^3$ estimates in practice because of their semi-quantitative nature.

As with net samples, a strength of CPR data is that taxonomic information is available. Typically, the copepods are well-resolved to species and the other groups to higher taxonomic levels (see Table 5 in (Richardson et al., 2006) for the taxa counted). This means that the data may be aggregated into functional groups that equate to those in models (e.g., Lewis et al., 2006). The CPR also retains phytoplankton (although not quantitatively) because of the leno silk weave of the mesh (see Richardson et al., 2006 for details). Phytoplankton are counted to the lowest possible level using light microscopy and these data can be aggregated into phytoplankton functional groups that equate to those in models, such as diatoms and dinoflagellates, and used for model assessment alongside zooplankton data (e.g., Lewis et al., 2006).

## Optical Plankton Counters

The most common instruments for measuring *in-situ* size spectra are the Optical Plankton Counter (Herman, 1988) and Laser Optical Plankton Counter (Herman, 2004). These instruments use either light emitting diodes-LEDs (LED-OPC) or lasers (LOPC) to measure the optical density and cross-sectional area of each particle as it passes through the sampling tunnel, and thereby estimate surface area (Sprules and Munawar, 1986; Suthers et al., 2006; Basedow et al., 2010). Hereafter we generalize, and refer collectively to both instruments as an OPC.

### Sampling Characteristics

The large temporal and/or spatial extents and high temporal and spatial resolutions characteristic of OPC deployments make the data well-suited for model assessment. The OPC collects information of the size-spectra of zooplankton over a broad range of temporal and spatial extents—from minutes to years and from 10s of meters to 100s of kilometers (**Table 3**). Due to the continuous electronic data collection of OPCs, there is no typical grain size (length of sample segment), and it depends largely on the purpose of the study and deployment method. OPCs can be deployed vertically (Vandromme et al., 2014; Marcolin et al., 2015; Wallis et al., 2016), mounted on a towed undulating vehicle to obtain high-resolution estimates of size spectra through space and time (Zhou et al., 2009; Everett et al., 2011; Basedow et al., 2014), mounted on a net frame (Herman and Harvey, 2006; Checkley et al., 2008; Marcolin et al., 2013), integrated with autonomous floats (Checkley et al., 2008), or mounted in the laboratory for the processing of net-samples (Moore and Suthers, 2006). OPCs are capable of sampling through the water column (up to 660 m deep) and if mounted on a towed body, over regional scales (100s km). OPCs are only deployable on research vessels for a range of reasons including: they need a trained technician to monitor them, require power via the tow-cable (or regular changing of data-logger batteries) and cannot be towed at the full speed of most commercial vessels. Therefore, unlike the CPR, they are not suited to ships of opportunity.

Taxonomic information is not directly available from OPCs, but they are often partnered with net samples, either by mounting within the net mouth (Herman, 2004) or as part of a broader sampling program whereby net and OPC samples are taken in close proximity to provide species-specific information, particularly for mono-cultures (e.g., overwintering *C. finmarchicus*; Gaardsted et al., 2011 or swarms of *Thalia democratica*; Everett et al., 2011). As for all sampling techniques, gear avoidance and sampling volume can be a problem when zooplankton abundance is low (Basedow et al., 2013), due to the small aperture of the OPC (20–49 $cm^2$) however these can be partially resolved by towing at a higher speed or for longer periods. Size-based data are also available from other instruments such as the *in-situ* Video Plankton Recorder (Davis et al., 2004) or the lab-based ZooScan (Vandromme et al., 2014 requires net samples). Inter-comparisons of size spectra between LOPC and ZooScan (Schultes and Lopes, 2009; Vandromme et al., 2014; Marcolin et al., 2015) or LOPC and VPR (Basedow et al., 2013) have shown mixed results. The biggest differences between ZooScan and the LOPC are thought to be due to the sampling of sediment in the small size-classes by the LOPC in coastal areas (Schultes and Lopes, 2009), although techniques have been developed to account for this (Jackson and Checkley, 2011) and can result in improved correlations between LOPC and ZooScan (Marcolin et al., 2015).

### Information Derived from OPC

The key strength of OPCs is their ability to quantify abundance, size and biovolume of plankton simultaneously over a large size range (0.1–35 mm for LOPC; Herman, 2004). In particular, OPCs are ideal for comparison with size-based models as they share the common currency of size and abundance. One common way to represent the size-distribution of plankton in the ocean is the normalized biomass size spectrum (NBSS; Silvert and Platt,

1978). The NBSS is a histogram-style size-distribution, in which the biovolume (or biomass) in a size class is normalized by the width of the size-class, such that the normalized distribution is independent of the width of size-classes (Platt and Denman, 1977). Using size-spectra theory, it is possible to extract trophic level and growth and mortality rates from *in-situ* OPC data (Edvardsen et al., 2002; Zhou, 2006; Basedow et al., 2014).

### Other Optical Instruments

While OPCs are the most common *in-situ* optical instruments, the field is developing rapidly and there are a range of other systems which deserve to be mentioned. In particular, camera and imaging systems such as ZooScan (Laboratory only; Grosjean et al., 2004), FlowCam (Laboratory only; Sieracki et al., 1998), Zooplankton Visualization system (ZOOVIS; Trevorrow et al., 2005), Video Plankton Recorder (VPR; Davis et al., 2005), Lightframe On-sight Keyspecies Investigation (LOKI; Schmid et al., 2016), and the *In Situ* Ichthyoplankton Imaging System (ISIIS; Cowen and Guigand, 2008) have become more widespread. Additionally, increased effort has been invested in the identification of zooplankton from images (Zooniverse, www.planktonportal.org). The highly depth-resolved individual images from these systems provide detailed information on both taxonomy and individual features (e.g., proportion of females carrying egg sacs) which will be beneficial to model assessment of IBM's. Moreover, developing artificial intelligence techniques (Layered neural networks, random forest algorithm and evolutionary algorithms) have permitted impressive advances in the automated detection of such features (Bi et al., 2015) and will add significant value to these optical systems.

## Bioacoustics

### Sampling Characteristics

Bioacoustic data can provide estimates of zooplankton and fish distribution, behavior and abundance using soundwaves and knowledge of the target strength of individual taxa (Foote and Stanton, 2000; Simmonds and MacLennan, 2005). Bioacoustic systems operate over fine to large scales, and are able to measure horizontal and vertical scales simultaneously (**Table 3**). Bioacoustic data for zooplankton can be obtained from single, multiple and broad band frequencies using ship-based systems or fixed platforms such as moorings (Godø et al., 2014). For mesozooplankton (∼0.2–20 mm) high frequencies are used from 100 KHz to 10 MHz in moored or profiling devices to resolve the size classes and types of organisms (Holliday et al., 2009). Acoustical backscatter from zooplankton are collected by the acoustic receiver and analyzed to estimate biomass or relative change in biomass of dominant scattering groups (Holliday and Pieper, 1995; Lavery et al., 2007; Kloser et al., 2009; Godø et al., 2014; Irigoien et al., 2014; Lehodey et al., 2014). The spatial resolution can be increased by moving the acoustic sensor, by using multiple spatially distributed sensors, or by tracking organisms within the acoustic beam (Godø et al., 2014). The temporal resolution of the backscatter can be improved by increasing the ping rates to resolve an individual's distribution and behavior patterns (Holliday et al., 2009; Godø et al., 2014).

Bioacoustic techniques offer a number of advantages over traditional net or CPR sampling because they provide high-resolution data at both spatial (horizontal and vertical) and temporal scales depending on the deployment platform. High-frequency, broadband systems enhance the sampling resolution to millimeter scale so that smaller targets, such as copepods, can be quantified (Holliday et al., 2009; Godø et al., 2014). Where patches of plankton and fish are small (Benoit-Bird et al., 2013), plankton nets and the CPR do not provide an accurate picture of the spatial distribution of the organisms that they capture as the sampling volumes are far larger than the patches (Godø et al., 2014). In addition, bioacoustics can provide better biomass estimates when combined with other methods such as nets (Kaartvedt et al., 2012) as there are minimal gear avoidance problems.

### Information Derived from Bioacoustics

Raw data from bioacoustics platforms is backscatter intensity over a single multiple or broad band of frequencies. A skilled analyst, using in isolation or a combination of scattering models, nets or optical sampling, is able to convert backscatter intensity to estimates of either biomass, abundance or (with more difficulty) broad taxa or potentially size groups (Holliday et al., 2009) depending on the region being considered. The high spatial and temporal resolution of these data are ideal for integration with modeling techniques. In the case of zooplankton, a major complicating factor in the use of multi-frequency bio-acoustic techniques is the diversity of this community, where a wide range of organisms of different sizes, shapes, orientations, and material properties occur together in the water column (Holliday and Pieper, 1995; Lavery et al., 2007). All these characteristics, along with their behavior, influence the way in which they scatter sound. To estimate their individual acoustic reflectance or target strength (TS), a series of zooplankton sound scattering models have been developed (Table 1 from Lavery et al., 2007) to account for that diversity.

# ZOOPLANKTON DATA IN MODEL ASSESSMENT

The performance of the zooplankton component of numerical models is rarely assessed against field observations because, unlike other parameters such as temperature or chlorophyll *a* biomass, observations of zooplankton do not generally resemble the resolution of the modeled zooplankton variables (temporally or spatially), are in a very different format (species abundance rather than mass of nitrogen), or are inaccessible (e.g., hidden in gray literature/personal collections). Because zooplankton observations are collected using a range of platforms that measure different parameters such as abundance (e.g., CPR, nets, bioacoustics), size (e.g., LOPC) or biomass (e.g., nets), model assessment requires uncertain and generally species- and location-dependent conversion factors (Arhonditsis and Brett, 2004) to approximate the zooplankton biomass in models (Postel et al., 2000). This makes it difficult to compare modeled zooplankton information with observed data. To address this

challenge, we turn our focus to a discussion of the two primary ways to link zooplankton in models with zooplankton observations: (1) data wrangling that transforms observational data to be directly comparable with model outputs; and (2) observation models that transform model output to be more comparable with observational data.

## Data Wrangling: Transforming Observational Data to Be More Like Model Outputs

Data wrangling is the process of iterative data exploration and transformation from one format to another to make them more useful (Kandel et al., 2011). We use the term here to describe the series of steps that transforms observational data into a form that is more comparable with model output. Data wrangling transforms observed data into model-ready datasets. Data wrangling takes many forms, but two of the most important are conversion of observed biomass into appropriate values to compare with model estimates (see **Box 1** for details), and collating biomass estimates collected using nets with different mesh sizes or different sampling devices (see **Box 2** for details).

One example of data wrangling is finding the optimal way to interpolate scattered observations onto a regular model grid at a fixed point in time (Buitenhuis et al., 2013; Moriarty and O'Brien, 2013). A more complex example is the conversion of observed zooplankton abundance (or biovolume) to nitrogen (or carbon) biomass, which is how many models represent zooplankton biomass (**Box 1**). This approach requires assumptions about the size distribution and stoichiometry of zooplankton in the sample. Given these assumptions, modelers are able to use these data, but need to understand the basis of the assumptions that are made, and the magnitude of the error inherent in the conversion.

Often gridded data products—think of the global chlorophyll *a* products—are the most readily used for model assessment of phytoplankton. Similarly, the wrangling of 153,163 zooplankton biomass values, from a variety of locations, formats and collection methods, into a freely-available gridded global database of consistent biomass units was an amazing effort (COPEPOD; http://www.st.nmfs.noaa.gov/copepod/; Moriarty and O'Brien, 2013). Unlike chlorophyll *a* however whose global satellite maps are updated daily, the time-consuming nature of zooplankton collection means there isn't a truly global database (see gaps in **Figure 2**) which is updated on time-scales relevant to many modeling studies. These data are extremely useful however, to constrain model estimates by providing biomass limits against which to assess our models. There are many statistical tools available to assist with the practical side of data-wrangling (e.g., "tidyr" or "dplyr" in R), but the most important aspect is dialogue between modelers and observationalists.

## Observation Models: Transforming Model Output So It Is More Like Observational Data

Where zooplankton observations are incorporated into models, there is often a mismatch between the observations (often infrequent point measurements) and the high spatial and temporal resolution of models. Observation models are one technique that can help address these mismatches, allowing model assessment at a range of scales. We define an observation model as a model that takes the output of a simulation and transforms it to a form that closely resembles the observations with which it is being compared. This approach of generating observations from models is used in numerical weather prediction (Dee et al., 2011), acoustic observations of mid-trophic levels (Handegard et al., 2012), and remotely-sensed ocean color observations (Baird et al., 2016).

The observation model needs to be based on sufficient process understanding, so that it applies well over a broad range of environments and the error in the output of the observation model is due primarily to the simulation model estimate (i.e., zooplankton biomass) and not the accuracy of the parameters or equations within the observation model itself. Essentially, the rationale of an observation model is to allow comparison of observed and modeled data, by removing inconsistencies in the structure or scale of these data. Here we review some of the steps and challenges to developing zooplankton observation models, for improved interpretation of the observations and assessment of numerical models. Below we discuss the range of observation models, from simple to more complex.

### Simple Observation Models: Simulated Sampling from a Model

The simplest approach to developing an observation model is to undertake simulated sampling within a model, and compare these sampled data to zooplankton observations. For example, zooplankton biomass estimates can be extracted from a simulation corresponding to the time, location, and depth of the samples collected by nets, CPR, OPC, or bioacoustics. While not directly comparing their model to observations, Wiebe and Holland (1968) were likely the first to simulate net tows within a computer simulation when they determined the effect of net size and patchiness on sampling error.

An example using the CPR highlights the approach of simulated sampling from a model. Lewis et al. (2006) compared the abundance of zooplankton as measured by the CPR with plankton output from an ecosystem model of the Northeast Atlantic Ocean. Simulated "tows" were performed by extracting biomass data of omnivorous mesozooplankton from the model at the time (day and nearest hour), location (longitude and latitude), and depth (7 m) of corresponding samples collected by the CPR (**Figure 3**). Because the CPR provides semi-quantitative abundance estimates, and not biomass (Richardson et al., 2006), both the samples and corresponding model output were standardized to a mean of zero and a unit standard deviation to produce a dimensionless z-score (Cheadle et al., 2003). This allowed a direct semi-quantitative evaluation of spatio-temporal model performance of omnivorous mesozooplankton. This evaluation highlighted that the model had the ability to reproduce the main seasonal features such as the spring and autumn blooms, and plankton succession observed in the CPR data and showed good correlation between magnitudes of these features with respect to standard deviations from a long-term mean. The model assessment also highlighted differences in the timing of

**BOX 2 | DATA WRANGLING: CONVERTING ZOOPLANKTON BIOMASS BETWEEN DIFFERENT MESH SIZES AND USING PROXY ESTIMATES**

**Different mesh sizes:** Different mesh sizes of nets provide very different biomass values, with higher zooplankton biomass estimates from finer mesh nets. To convert biomass data collected with different mesh sizes to an equivalent mesh size, common conversions can be applied (**Table B3**; Moriarty and O'Brien, 2013), although it must be acknowledged that the best conversion is dependent upon the zooplankton assemblage present. Fortunately, different net systems produce similar estimates of zooplankton when operated with similar mesh sizes (Skjoldal et al., 2013).

**TABLE B3 | Equivalent mesh size conversions (modified from Moriarty and O'Brien, 2013).**

| Conversion | Equation | References |
|---|---|---|
| 333 μm to 200 μm mesh | $\log_{10}(CM_{200}) = 1.4461 * \log_{10}(CM_{333})$ | O'Brien, 2005 |
| 505 μm to 330 μm mesh | $\log_{10}(CM_{333}) = 1.2107 * \log_{10}(CM_{505})$ | O'Brien, 2005 |

**Proxy estimates—Abundance:** Sometimes zooplankton abundance and not biomass is measured. It is difficult to convert abundance to biomass because you do not know the size of individuals and thus their mass. In this situation, we recommend using abundance data for relative patterns—for example seasonal cycles, spatial variation, or inter-annual variation. Lewis et al. (2006) assessed their ecosystem model by normalizing both the model biomass and the observed abundance data and comparing the normalized patterns spatially and temporally.

**Proxy estimates—Biovolume:** Size-based methods of measuring zooplankton (LOPC/OPC/VPR/ZooScan) can provide estimates of zooplankton biomass. These instruments measure organism size (2-D area) and this can be converted to organism volume. Biovolume can then be converted to biomass by summing organism volume across all individuals and assuming zooplankton has the same density of seawater. Zooplankton biomass from the VPR and ZooScan has the advantage that detritus and sediment can be removed. An advantage of these size-based methods are that they can be used to estimate biomass in size classes. They could also be used to partition observed zooplankton total biomass into size classes (i.e., using the size spectra to estimate the % of biomass in different size classes and applying this to measured biomass).

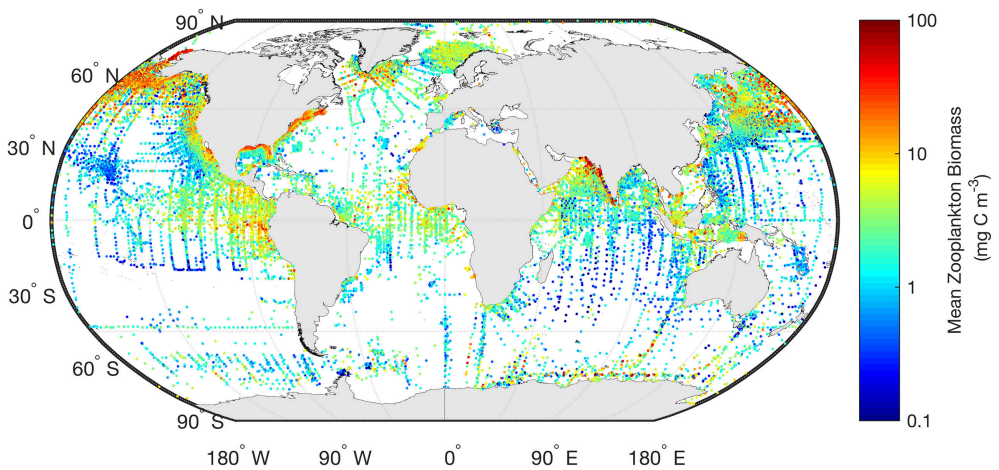


**FIGURE 2 | The mean marine zooplankton biomass (mg C $m^{-3}$) for mesozooplankton (0–200 m depth) is shown illustrating the distribution of records from the most comprehensive database available.** The data shown here are freely available from "COPEPOD: The Global Plankton Database" (http://www.st.nmfs.noaa.gov/copepod/).

patterns in phytoplankton seasonality (e.g., spring diatom bloom in the model is too early), allowing the reparametrizing of the model (Lewis et al., 2006).

## More Complex Observation Models: Add-On Models That Convert Output to Observations

With improving technologies and computing power comes the opportunity to embrace increasingly complex observation models. Here we borrow many examples from state-of-the-art applications in other fields of model assessment that have not yet been fully applied to zooplankton. These are ideally suited for the assessment of zooplankton models due to the inherent disconnect between the spatial and temporal resolution and model currency of observations and models.

Historically, in phytoplankton model assessment, satellite-derived chlorophyll *a* is compared with modeled phytoplankton (Oschlies and Schartau, 2005; Lacroix et al., 2007; Gregg, 2008; Brewin et al., 2010; Kidston et al., 2011, 2013), but inaccuracies in both the satellite observation (e.g., measurement error due to CDOM in the water) and conversion of model units (e.g., conversion of nitrogen biomass to chlorophyll *a*) introduce errors into the model assessment. To limit these inaccuracies, Baird et al. (2016) used an optical observation model, nested within a biogeochemical model, to assess water-leaving irradiance from

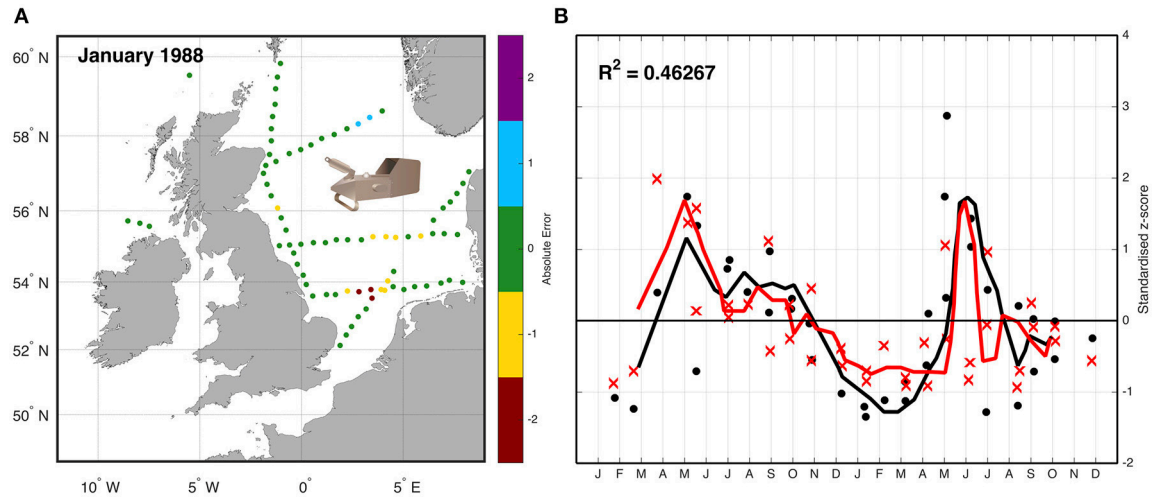


**FIGURE 3 | Sampling the model—(A)** Simulated "tows" within the model were performed by extracting biomass data of omnivorous mesozooplankton from the exact time (day and nearest hour), location (longitude and latitude), and depth (7 m) of corresponding samples collected by the CPR. **(B)** The data are then standardized due to the different units, and the difference between normalized z -scores for both simulation and observation between January 1988 and December 1989 with a 3-day running mean (solid line) is shown. Black is model data, red is CPR data; dots are individual model tow points, crosses are individual CPR tow points (redrawn from Lewis et al., 2006).

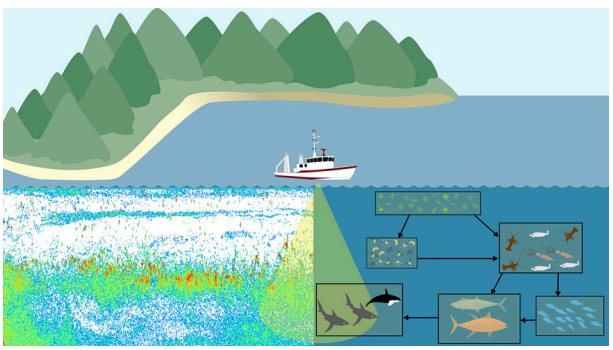

**FIGURE 4 | A bioacoustic observation model would apply the same scattering models to both the backscatter measurements from the ocean and the ecosystem model.** Regardless of environment (ocean or model), we can use the same principle of the scattering models to produce echograms which can be directly compared.

the model, against satellite-derived water-leaving irradiance. The water-leaving irradiances, from the observation model and the satellite, can be directly compared against each other to assess the model. Alternatively, the water-leaving irradiance measures from both the observation model and the satellite, can be converted to chlorophyll *a* using one of the satellite algorithms in order to allow a comparison which may be more informative for those used to thinking about chlorophyll *a*. In either case, both the units of assessment, and the method used to derive them, are the same. Thus, the mismatch between simulated and observed remote-sensing reflectance provides an excellent metric for model assessment of the coupled biogeochemical model (Baird et al., 2016; Jones et al., 2016).

This approach—of building an observation model that enables the model to produce information more comparable to observations—has not yet been applied to zooplankton but would be a valuable way forward. For zooplankton model assessment, building observation models for size-spectra models would be fairly straightforward given that observational techniques (OPC, ZooScan and VPR) measure the size and abundance of the zooplankton community—metrics easily extracted from size-spectra models. It is also made easier because size spectra are typically represented as Normalized Biomass Size Spectra (NBSS; Section Optical Plankton Counters), where size classes are normalized by the width of the size-class, making the shape of the spectrum independent of the size-classes chosen (Platt and Denman, 1977). The NBSS can thus be generated from both the observations and models, even if they each have different size-resolutions. In addition to comparing state-variables, the size-based approach developed by Zhou (2006), Zhou et al. (2010) provides an intuitive framework for estimating time-averaged rates (e.g., growth, mortality) for zooplankton from observed NBSS, which could then be tested within dynamic size spectrum models that include zooplankton (Heneghan et al., 2016) or compared to observed rates in the field (Zhou et al., 2010).

Another potential area for development of an observation model is in bioacoustics. Traditional outputs from zooplankton bioacoustic observations are the distribution, behavior, biomass and abundance of trophic levels, size categories, or species of interest derived from scattering models (Lavery et al., 2007; Holliday et al., 2009; Kloser et al., 2009; Godø et al., 2014). These scattering model measures can then be used to assess ecosystem models (Luo and Brandt, 1993; Holliday et al., 2009; Kloser et al., 2009). This requires the aggregation of focal taxa from the ecosystem model output and conversion to a common currency. This need to transform both observation

and model outputs to a common format introduces error and inconsistencies into each. An alternative approach is to create a bioacoustic observation model which uses scattering models to estimate the backscatter intensity of zooplankton within the ecosystem model and compare this to bioacoustic observations in the ocean (**Figure 4**; Handegard et al., 2012). The main challenge for the observation model is to simulate the observed backscatter at a particular frequency and depth within the model. In this case, we are not directly modeling sound within the ecosystem model, so this observation model does not provide feedback (external forcings or changes in state variables) to the ecosystem model. It is simply about avoiding inconsistencies in the comparison of modeled and observed data, and enabling the comparison of "like with like." Building such an acoustic observation model would simulate acoustic observations, producing an echogram (**Figure 4**). Thus, for all model points in time and space, the observation model could produce an echogram based on the zooplankton functional groups predicted by the ecosystem model. As with all model-observation comparisons, care must be taken to consider the temporal and spatial resolution measured or modeled. In the case of bioacoustics, the measurements will often be at a higher spatial resolution (meters; **Table 3**), but lower temporal resolution (minutes; **Table 3**) than the model. High-resolution bioacoustic measurements of abundance and biomass can be downscaled to match the resolution of ecosystem models. Clean acoustic observations will need to be readily available for comparison with the simulated outputs of the observation model, which could be achieved with the use of a multi-frequency acoustic mooring, which delivers acoustic data resolved vertically and temporally at a single site (Urmy et al., 2012).

## CONCLUDING REMARKS

In this review, we summarize many of the fundamentals of zooplankton modeling for observationalists and zooplankton observations for modelers. As highlighted by Flynn (2005), we believe that there needs to be greater discussion and collaboration between modelers and observationalists. Only through dialogue will we be able to perform the data wrangling and develop the observation models that are needed so our observations and model outputs align. In particular, observation models have not been applied in the assessment of zooplankton in models and are likely to be a powerful approach, as they have been in other disciplines. These observation models range from the simple (sampling the model) to the more complex (bioacoustics) and can even result in the underlying model being changed to output data that is directly comparable to the observations (e.g., water leaving irradiance and chlorophyll *a*). The development and use of complex observing models can be time consuming, but many of the techniques described above are already being implemented (Handegard et al., 2012; Baird et al., 2016). The adoption of these ideas for use in zooplankton research would be a major step forward, allowing zooplankton observations to be more readily used in model assessment as real-time data becomes a possibility with optical and acoustic systems. Here we have provided a few ideas. We hope that this review will increase the dialogue between modelers and observationalists, and provide the impetus for greater model assessment of zooplankton output through data wrangling and state-of-the-art observation models.

## AUTHOR CONTRIBUTIONS

JE, AR, and MB conceived the original idea for this workshop and manuscript. All authors contributed to the writing of the manuscript. JE and AR wrote the final draft.

## ACKNOWLEDGMENTS

This manuscript was written as part of the Integrated Marine Observing System (IMOS) "Zooplankton Ocean Observing and Modelling" workshop held in Hobart 15–16 February 2016. The workshop was funded by IMOS. JE was funded by an Australian Research Council Discovery Grant (DP150102656). The CPR and fauna images in Figures 1, 4, and 5 were provided by the Integration and Application Network, University of Maryland Center for Environmental Science (ian.umces.edu/imagelibrary/).

## REFERENCES

Andersen, K. H., and Beyer, J. E. (2015). Size structure, not metabolic scaling rules, determines fisheries reference points. *Fish Fish.* 16, 1–22. doi: 10.1111/faf.12042

Andersen, K. H., Berge, T., Gonçalves, R. J., Hartvig, M., Heuschele, J., Hylander, S., et al. (2016). Characteristic sizes of life in the oceans, from bacteria to whales. *Annu. Rev. Mar. Sci.* 8, 217–241. doi: 10.1146/annurev-marine-122414-034144

Arhonditsis, G. B., and Brett, M. T. (2004). Evaluation of the current state of mechanistic aquatic biogeochemical modeling. *Mar. Ecol. Prog. Ser.* 271, 13–26. doi: 10.3354/meps271013

Ariza, A., Garijo, J. C., Landeira, J. M., Bordes, F., and Hernandez-Leon, S. (2015). Migrant biomass and respiratory carbon flux by zooplankton and micronekton in the subtropical northeast Atlantic Ocean (Canary Islands). *Prog. Oceanogr.* 134, 330–342. doi: 10.1016/j.pocean.2015.03.003

Arora, V. K., Boer, G. J., Friedlingstein, P., Eby, M., Jones, C. D., Christian, J. R., et al. (2013). Carbon–concentration and carbon–climate feedbacks in CMIP5 earth system models. *J. Clim.* 26, 5289–5314. doi: 10.1175/JCLI-D-12-00494.1

Baird, M. E., and Suthers, I. M. (2007). A size-resolved pelagic ecosystem model. *Ecol. Modell.* 203, 185–203. doi: 10.1016/j.ecolmodel.2006.11.025

Baird, M. E., and Suthers, I. M. (2010). Increasing model structural complexity inhibits the growth of initial condition errors. *Ecol. Complexity* 7, 478–486. doi: 10.1016/j.ecocom.2009.12.001

Baird, M. E., Cherukuru, N., Jones, E., Margvelashvili, N., Mongin, M., Oubelkheir, K., et al. (2016). Remote-sensing reflectance and true colour produced by a coupled hydrodynamic, optical, sediment, biogeochemical model of the Great Barrier Reef, Australia: comparison with satellite data. *Environ. Modell. Softw.* 78, 79–96. doi: 10.1016/j.envsoft.2015.11.025

Baird, M. E., Everett, J. D., and Suthers, I. M. (2011). Analysis of southeast Australian zooplankton observations of 1938–42 using synoptic oceanographic conditions. *Deep Sea Res. Part II Top. Stud. Oceanogr.* 58, 699–711. doi: 10.1016/j.dsr2.2010.06.002

Banaru, D., Carlotti, F., Barani, A., Gregori, G., Neffati, N., and Harmelin-Vivien, M. (2014). Seasonal variation of stable isotope ratios of size-fractionated zooplankton in the Bay of Marseille (NW Mediterranean Sea). *J. Plankton Res.* 36, 145–156. doi: 10.1093/plankt/fbt083

Baretta, J. W., Ebenhoh, W., and Ruardij, P. (1995). The european-regional-seas-ecosystem-model, a complex marine ecosystem model. *Neth. J. Sea Res.* 33, 233–246. doi: 10.1016/0077-7579(95)90047-0

Basedow, S. L., Tande, K. S., and Zhou, M. (2010). Biovolume spectrum theories applied: spatial patterns of trophic levels within a mesozooplankton community at the polar front. *J. Plankton Res.* 32, 1105–1119. doi: 10.1093/plankt/fbp110

Basedow, S. L., Tande, K. S., Norrbin, M. F., and Kristiansen, S. A. (2013). Capturing quantitative zooplankton information in the sea: performance test of laser optical plankton counter and video plankton recorder in a *Calanus finmarchicus* dominated summer situation. *Prog. Oceanogr.* 108, 72–80. doi: 10.1016/j.pocean.2012.10.005

Basedow, S. L., Zhou, M., and Tande, K. S. (2014). Secondary production at the polar front, barents sea, August 2007. *J. Mar. Syst.* 130, 147–159. doi: 10.1016/j.jmarsys.2013.07.015

Batchelder, H. P., Edwards, C. A., and Powell, T. M. (2002). Individual-based models of copepod populations in coastal upwelling regions: implications of physiologically and environmentally influenced diel vertical migration on demographic success and nearshore retention. *Prog. Oceanogr.* 53, 307–333. doi: 10.1016/S0079-6611(02)00035-6

Batten, S. D., Clark, R., Flinkman, J., Hays, G., John, E., John, A. W. G., et al. (2003). CPR sampling: the technical background, materials and methods, consistency and comparability. *Prog. Oceanogr.* 58, 193–215. doi: 10.1016/j.pocean.2003.08.004

Benoit, E., and Rochet, M. J. (2004). A continuous model of biomass size spectra governed by predation and the effects of fishing on them. *J. Theor. Biol.* 226, 9–21. doi: 10.1016/S0022-5193(03)00290-X

Benoit-Bird, K. J., Shroyer, E. L., and McManus, M. A. (2013). A critical scale in plankton aggregations across coastal ecosystems. *Geophys. Res. Lett.* 40, 1–7. doi: 10.1002/grl.50747

Bi, H., Guo, Z., Benfield, M. C., Fan, C., Ford, M., Shahrestani, S., et al. (2015). A Semi-automated image analysis procedure for *in situ* plankton imaging systems. *PLoS ONE* 10:e0127121. doi: 10.1371/journal.pone.0127121

Bi, R., and Liu, H. (2017). Effects of variability among individuals on zooplankton population dynamics under environmental conditions. *Mar. Ecol. Prog. Ser.* 564, 9–28. doi: 10.3354/meps11967

Bianchi, D., Galbraith, E. D., Carozza, D. A., Mislan, K. A. S., and Stock, C. A. (2013). Intensification of open-ocean oxygen depletion by vertically migrating animals. *Nat. Geosci.* 6, 545–548. doi: 10.1038/ngeo1837

Blackford, J. C., and Gilbert, F. J. (2007). pH variability and CO2 induced acidification in the North Sea. *J. Mar. Syst.* 64, 229–241. doi: 10.1016/j.jmarsys.2006.03.016

Blanchard, J. L., Andersen, K. H., Scott, F., Hintzen, N. T., Piet, G., and Jennings, S. (2014). Evaluating targets and trade-offs among fisheries and conservation objectives using a multispecies size spectrum model. *J. Appl. Ecol.* 51, 612–622. doi: 10.1111/1365-2664.12238

Blanchard, J. L., Heneghan, R. F., Everett, J. D., Trebilco, R., and Richardson, A. J. (2017). From bacteria to whales: using functional size spectra to model marine ecosystems. *Trends Ecol. Evol.* 32, 174–186. doi: 10.1016/j.tree.2016.12.003

Blanchard, J. L., Jennings, S., Law, R., Castle, M. D., McCloghrie, P., Rochet, M.-J., et al. (2009). How does abundance scale with body size in coupled size-structured food webs? *J. Anim. Ecol.* 78, 270–280. doi: 10.1111/j.1365-2656.2008.01466.x

Bode, A., Álvarez-Ossorio, M. T., and González, N. (1998). Estimations of mesozooplankton biomass in a coastal upwelling area off NW Spain. *J. Plankton Res.* 20, 1005–1014. doi: 10.1093/plankt/20.5.1005

Bopp, L., Resplandy, L., Orr, J. C., Doney, S. C., Dunne, J. P., Gehlen, M., et al. (2013). Multiple stressors of ocean ecosystems in the 21st century: projections with CMIP5 models. *Biogeosciences* 10, 6225–6245. doi: 10.5194/bg-10-6225-2013

Breckling, B., Middelhoff, U., and Reuter, H. (2006). Individual-based models as tools for ecological theory and application: understanding the emergence of organisational properties in ecological systems. *Ecol. Modell.* 194, 102–113. doi: 10.1016/j.ecolmodel.2005.10.005

Brewin, R. J. W., Sathyendranath, S., Hirata, T., Lavender, S. J., Barciela, R. M., and Hardman-Mountford, N. J. (2010). A three-component model of phytoplankton size class for the Atlantic Ocean. *Ecol. Modell.* 221, 1472–1483. doi: 10.1016/j.ecolmodel.2010.02.014

Brown, J. H., Gillooly, J. F., Allen, A. P., Savage, V. M., and West, G. B. (2004). Toward a metabolic theory of ecology. *Ecology* 85, 1771–1789. doi: 10.1890/03-9000

Buitenhuis, E., Vogt, M., Moriarty, R., Bednaršek, N., Doney, S. C., Leblanc, K., et al. (2013). MAREDAT: towards a world atlas of MARine Ecosystem DATa. *Earth Syst. Sci. Data* 5, 227–239. doi: 10.5194/essd-5-227-2013

Carlotti, F., and Poggiale, J. C. (2010). Towards methodological approaches to implement the zooplankton component in "end to end" food-web models. *Prog. Oceanogr.* 84, 20–38. doi: 10.1016/j.pocean.2009.09.003

Champion, C., Suthers, I. M., and Smith, J. A. (2015). Zooplanktivory is a key process for fish production on a coastal artificial reef. *Mar. Ecol. Prog. Ser.* 541, 1–14. doi: 10.3354/meps11529

Chan, T. U., Hamilton, D. P., Robson, B. J., Hodges, B. R., and Dallimore, C. (2002). Impacts of hydrological changes on phytoplankton succession in the Swan River, Western Australia. *Estuaries* 25, 1406–1415. doi: 10.1007/BF02692234

Cheadle, C., Vawter, M. P., Freed, W. J., and Becker, K. G. (2003). Analysis of microarray data using Z score transformation. *J. Mol. Diagn.* 5, 73–81. doi: 10.1016/S1525-1578(10)60455-2

Checkley, D. M. Jr., Davis, R. E., Herman, A. W., Jackson, G. A., Beanlands, B., and Regier, L. A. (2008). Assessing plankton and other particles *in situ* with the SOLOPC. *Limnol. Oceanogr.* 53, 2123–2136. doi: 10.4319/lo.2008.53.5_part_2.2123

Christensen, V., and Pauly, D. (1992). Ecopath-II - a software for balancing steady-state ecosystem models and calculating network characteristics. *Ecol. Modell.* 61, 169–185. doi: 10.1016/0304-3800(92)90016-8

Christensen, V., and Walters, C. J. (2004). Ecopath with Ecosim: methods, capabilities and limitations. *Ecol. Modell.* 172, 109–139. doi: 10.1016/j.ecolmodel.2003.09.003

Christensen, V., Coll, M., Buszowski, J., Cheung, W. W. L., Frölicher, T., Steenbeek, J., et al. (2015). The global ocean is an ecosystem: simulating marine life and fisheries. *Glob. Ecol. Biogeogr.* 24, 507–517. doi: 10.1111/geb.12281

Christian, J. R., Arora, V. K., Boer, G. J., Curry, C. L., Zahariev, K., Denman, K. L., et al. (2010). The global carbon cycle in the Canadian Earth system model (CanESM1): preindustrial control simulation. *J. Geophys. Res.* 115, G03014–G03020. doi: 10.1029/2008JG000920

Clark, R. A., Frid, C. L. J., and Batten, S. (2001). A critical comparison of two long-term zooplankton time series from the Central-west North Sea. *J. Plankton Res.* 23, 27–39. doi: 10.1093/plankt/23.1.27

Collins, W. J., Bellouin, N., Doutriaux-Boucher, M., Gedney, N., Halloran, P., Hinton, T., et al. (2011). Development and evaluation of an Earth-System model – HadGEM2. *Geosci. Model Dev.* 4, 1051–1075. doi: 10.5194/gmd-4-1051-2011

Cowen, R. K., and Guigand, C. M. (2008). *In situ* ichthyoplankton imaging system (ISIIS): system design and preliminary results. *Limnol. Oceanogr. Methods* 6, 126–132. doi: 10.4319/lom.2008.6.126

Davis, C. S., Hu, Q., Gallager, S. M., Tang, X., and Ashjian, C. J. (2004). Real-time observation of taxa-specific plankton distributions: an optical sampling method. *Mar. Ecol. Prog. Ser.* 284, 77–96. doi: 10.3354/meps284077

Davis, C. S., Thwaites, F. T., Gallager, S. M., and Hu, Q. (2005). A three-axis fast-tow digital Video Plankton Recorder for rapid surveys of plankton taxa and hydrography. *Limnol. Oceanogr. Methods* 3, 59–74. doi: 10.4319/lom.2005.3.59

Dee, D. P., Uppala, S. M., Simmons, A. J., Berrisford, P., Poli, P., Kobayashi, S., et al. (2011). The ERA-Interim reanalysis: configuration and performance of the data assimilation system. *Q. J. R. Meteorol. Soc.* 137, 553–597. doi: 10.1002/qj.828

Dorman, J. G., Sydeman, W. J., Bograd, S. J., and Powell, T. M. (2015a). An individual-based model of the krill *Euphausia pacifica* in the California Current. *Prog. Oceanogr.* 138, 504–520. doi: 10.1016/j.pocean.2015.02.006

Dorman, J. G., Sydeman, W. J., García-Reyes, M., Zeno, R. A., and Santora, J. A. (2015b). Modeling krill aggregations in the central-northern California Current. *Mar. Ecol. Prog. Ser.* 528, 87–99. doi: 10.3354/meps11253

Dueri, S., Bopp, L., and Maury, O. (2014). Projecting the impacts of climate change on skipjack tuna abundance and spatial distribution. *Glob. Chang. Biol.* 20, 742–753. doi: 10.1111/gcb.12460

Dufresne, J. L., Foujols, M. A., Denvil, S., Caubel, A., Marti, O., Aumont, O., et al. (2013). Climate change projections using the IPSL-CM5 Earth System Model: from CMIP3 to CMIP5. *Clim. Dyn.* 40, 2123–2165. doi: 10.1007/s00382-012-1636-1

Dunne, J. P., John, J. G., Shevliakova, E., Stouffer, R. J., Krasting, J. P., Malyshev, S. L., et al. (2013). GFDL's ESM2 Global Coupled Climate–Carbon Earth System Models. Part II: carbon system formulation and baseline simulation characteristics*. *J. Clim.* 26, 2247–2267. doi: 10.1175/JCLI-D-12-00150.1

Edgar, G. J., and Shaw, C. (1995). The production and trophic ecology of shallow-water fish assemblages in southern Australia. 2. Diets of fishes and trophic relationships between fishes and benthos at Western Port, Victoria. *J. Exp. Mar. Biol. Ecol.* 194, 83–106. doi: 10.1016/0022-0981(95)00084-4

Edvardsen, A., Zhou, M., Tande, K. S., and Zhu, Y. W. (2002). Zooplankton population dynamics: measuring *in situ* growth and mortality rates using an Optical Plankton Counter. *Mar. Ecol. Prog. Ser.* 227, 205–219. doi: 10.3354/meps227205

Edwards, A. M., and Yool, A. (2000). The role of higher predation in plankton population models. *J. Plankton Res.* 22, 1085–1112. doi: 10.1093/plankt/22.6.1085

Edwards, M., and Richardson, A. J. (2004). Impact of climate change on marine pelagic phenology and trophic mismatch. *Nature* 430, 881–884. doi: 10.1038/nature02808

Edwards, M., Beaugrand, G., Hays, G. C., Koslow, J. A., and Richardson, A. J. (2010). Multi-decadal oceanic ecological datasets and their application in marine policy and management. *Trends Ecol. Evol.* 25, 602–610. doi: 10.1016/j.tree.2010.07.007

Everett, J. D., Baird, M. E., and Suthers, I. M. (2011). Three-dimensional structure of a swarm of the salp *Thalia democratica* within a cold-core eddy off southeast Australia. *J. Geophys. Res. Oceans* 116:C12046. doi: 10.1029/2011JC007310

Fennel, W., and Neumann, T. (2004). *Introduction to the Modelling of Marine Ecosystems*. Amsterdam: Elsevier Science.

Flynn, K. J. (2005). Castles built on sand: dysfunctionality in plankton models and the inadequacy of dialogue between biologists and modellers. *J. Plankton Res.* 27, 1205–1210. doi: 10.1093/plankt/fbi099

Follows, M. J., Dutkiewicz, S., Grant, S., and Chisholm, S. W. (2007). Emergent biogeography of microbial communities in a model ocean. *Science* 315, 1843–1846. doi: 10.1126/science.1138544

Foote, K. G., and Stanton, T. K. (2000). "Chapter 6: acoustical methods," in *Zooplankton Methodology Manual*, eds R. P. Harris, P. H. Wiebe, J. Lenz, H. R. Skjoldal, and M. E. Huntley (London: Academic Press), 223–259.

Friedland, K. D., Stock, C., Drinkwater, K. F., Link, J. S., Leaf, R. T., Shank, B. V., et al. (2012). Pathways between primary production and fisheries yields of large marine ecosystems. *PLoS ONE* 7:e28945. doi: 10.1371/journal.pone.0028945

Frisch, A. J., Ireland, M., and Baker, R. (2014). Trophic ecology of large predatory reef fishes: energy pathways, trophic level, and implications for fisheries in a changing climate. *Mar. Biol.* 161, 61–73. doi: 10.1007/s00227-013-2315-4

Fulton, E. A., Fuller, M., Smith, A. D. M., and Punt, A. (2005). *Ecological Indicators of the Ecosystem Effects of Fishing: Final Report.* Australian Fisheries Management Authority. Report Number R99/1546.

Fulton, E. A., Smith, A. D. M., and Johnson, C. R. (2003). Mortality and predation in ecosystem models: is it important how these are expressed? *Ecol. Modell.* 169, 157–178. doi: 10.1016/S0304-3800(03)00268-0

Fulton, E. A., Smith, A. D. M., Smith, D. C., and van Putten, I. E. (2011). Human behaviour: the key source of uncertainty in fisheries management. *Fish Fish.* 12, 2–17. doi: 10.1111/j.1467-2979.2010.00371.x

Gaardsted, F., Tande, K. S., and Pedersen, O. P. (2011). Vertical distribution of overwintering *Calanus finmarchicus* in the NE Norwegian Sea in relation to hydrography. *J. Plankton Res.* 33, 1477–1486. doi: 10.1093/plankt/fbr042

Gerritsen, J., and Strickler, J. R. (1977). Encounter probabilities and community structure in zooplankton: a mathematical model. *J. Fish. Res. Board Can.* 34, 73–82. doi: 10.1139/f77-008

Godø, O. R., Handegard, N. O., Browman, H. I., Macaulay, G. J., Kaartvedt, S., Giske, J., et al. (2014). Marine ecosystem acoustics (MEA): quantifying processes in the sea at the spatio-temporal scales on which they occur. *ICES J. Mar. Sci.* 71, 2357–2369. doi: 10.1093/icesjms/fsu116

Greene, C., and Wiebe, P. (1990). Bioacoustical oceanography: new tools for zooplankton and micronekton research in the 1990s. *Oceanography* 3, 12–17. doi: 10.5670/oceanog.1990.15

Gregg, W. W. (2008). Assimilation of SeaWiFS ocean chlorophyll data into a three-dimensional global ocean model. *J. Mar. Syst.* 69, 205–225. doi: 10.1016/j.jmarsys.2006.02.015

Griffiths, S. P., Young, J. W., Lansdell, M. J., Campbell, R. A., Hampton, J., Hoyle, S. D., et al. (2010). Ecological effects of longline fishing and climate change on the pelagic ecosystem off eastern Australia. *Rev. Fish Biol. Fish.* 20, 239–272. doi: 10.1007/s11160-009-9157-7

Grosjean, P., Picheral, M., Warembourg, C., and Gorsky, G. (2004). Enumeration, measurement, and identification of net zooplankton samples using the ZOOSCAN digital imaging system. *ICES J. Mar. Sci.* 61, 518–525. doi: 10.1016/j.icesjms.2004.03.012

Grüss, A., Schirripa, M. J., Chagaris, D., Velez, L., Shin, Y.-J., Verley, P., et al. (2016). Estimating natural mortality rates and simulating fishing scenarios for Gulf of Mexico red grouper (*Epinephelus morio*) using the ecosystem model OSMOSE-WFS. *J. Mar. Syst.* 154, 264–279. doi: 10.1016/j.jmarsys.2015.10.014

Guiet, J., Poggiale, J.-C., and Maury, O. (2016). Modelling the community size-spectrum: recent developments and new directions. *Ecol. Modell.* 337, 4–14. doi: 10.1016/j.ecolmodel.2016.05.015

Hall, S. J., Collie, J. S., Duplisea, D. E., Jennings, S., Bravington, M., and Link, J. (2006). A length-based multispecies model for evaluating community responses to fishing. *Can. J. Fish. Aquat. Sci.* 63, 1344–1359. doi: 10.1139/f06-039

Hamner, W. M., Jones, M. S., Carleton, J. H., Hauri, I. R., and Williams, D. M. (1988). Zooplankton, planktivorous fish, and water currents on a windward reef face - great barrier-reef, Australia. *Bull. Mar. Sci.* 42, 459–479.

Handegard, N. O., Buisson, L. D., Brehmer, P., Chalmers, S. J., De Robertis, A., Huse, G., et al. (2012). Towards an acoustic-based coupled observation and modelling system for monitoring and predicting ecosystem dynamics of the open ocean. *Fish Fish.* 14, 605–615. doi: 10.1111/j.1467-2979.2012.00480.x

Hartvig, M., Andersen, K. H., and Beyer, J. E. (2011). Food web framework for size-structured populations. *J. Theor. Biol.* 272, 113–122. doi: 10.1016/j.jtbi.2010.12.006

Heneghan, R. F., Everett, J. D., Blanchard, J. L., and Richardson, A. J. (2016). Zooplankton are not fish: improving zooplankton realism in size-spectrum models mediates energy transfer in food webs. *Front. Mar. Sci.* 3:201. doi: 10.3389/fmars.2016.00201

Henschke, N., Bowden, D. A., Everett, J. D., Holmes, S. P., Kloser, R. J., Lee, R. W., et al. (2013). Salp-falls in the Tasman Sea: a major food input to deep-sea benthos. *Mar. Ecol. Prog. Ser.* 491, 165–175. doi: 10.3354/meps10450

Henschke, N., Everett, J. D., Richardson, A. J., and Suthers, I. M. (2016). Rethinking the role of salps in the ocean. *Trends Ecol. Evol.* 31, 720–733. doi: 10.1016/j.tree.2016.06.007

Herman, A. W. (1988). Simultaneous measurement of zooplankton and light attenuance with a new optical plankton counter. *Cont. Shelf Res.* 8, 205–221. doi: 10.1016/0278-4343(88)90054-4

Herman, A. W. (2004). The next generation of Optical Plankton Counter: the Laser-OPC. *J. Plankton Res.* 26, 1135–1145. doi: 10.1093/plankt/fbh095

Herman, A. W., and Harvey, M. (2006). Application of normalized biomass size spectra to laser optical plankton counter net intercomparisons of zooplankton distributions. *J. Geophys. Res. Oceans* 111:C05S05. doi: 10.1029/2005jc002948

Hjøllo, S. S., Huse, G., Skogen, M. D., and Melle, W. (2012). Modelling secondary production in the Norwegian Sea with a fully coupled physical/primary production/individual-based *Calanus finmarchicus*model system. *Mar. Biol. Res.* 8, 508–526. doi: 10.1080/17451000.2011.642805

Holliday, D. V., and Pieper, R. E. (1995). Bioacoustical oceanography at high frequencies. *ICES J. Mar. Sci.* 52, 279–296. doi: 10.1016/1054-3139(95)80044-1

Holliday, D. V., Donaghay, P. L., Greenlaw, C. F., Napp, J. M., and Sullivan, J. M. (2009). High-frequency acoustics and bio-optics in ecosystems research. *ICES J. Mar. Sci.* 66, 974–980. doi: 10.1093/icesjms/fsp127

Holzer, M., and Primeau, F. W. (2013). Global teleconnections in the oceanic phosphorus cycle: patterns, paths, and timescales. *J. Geophys. Res. Oceans* 118, 1775–1796. doi: 10.1002/jgrc.20072

Hunt, B. P. V., and Hosie, G. W. (2003). The Continuous Plankton Recorder in the Southern Ocean: a comparative analysis of zooplankton communities sampled by the CPR and vertical net hauls along 140°E. *J. Plankton Res.* 25, 1561–1579. doi: 10.1093/plankt/fbg108

Huo, Y., Sun, S., Zhang, F., Wang, M., Li, C., and Yang, B. (2012). Biomass and estimated production properties of size-fractionated zooplankton in the Yellow Sea, China. *J. Mar. Syst.* 94, 1–8. doi: 10.1016/j.jmarsys.2011.09.013

Irigoien, X., Klevjer, T. A., Røstad, A., and Martinez, U. (2014). Large mesopelagic fishes biomass and trophic efficiency in the open ocean. *Nat. Commun.* 5:3271. doi: 10.1038/ncomms4271

Jackson, G. A., and Checkley, D. M. Jr (2011). Particle size distributions in the upper 100m water column and their implications for animal feeding in the plankton. *Deep Sea Res. Part I Oceanogr. Res. Pap.* 58, 283–297. doi: 10.1016/j.dsr.2010.12.008

Jacobsen, N. S., Gislason, H., and Andersen, K. H. (2013). The consequences of balanced harvesting of fish communities. *Proc. R. Soc. B Biol. Sci.* 281:20132701. doi: 10.1098/rspb.2013.2701

Jennings, S., and Collingridge, K. (2015). Predicting consumer biomass, size-structure, production, catch potential, responses to fishing and associated uncertainties in the world's marine ecosystems. *PLoS ONE* 10:e0133794. doi: 10.1371/journal.pone.0133794

Jennings, S., and Mackinson, S. (2003). Abundance-body mass relationships in size-structured food webs. *Ecol. Lett.* 6, 971–974. doi: 10.1046/j.1461-0248.2003.00529.x

Jennings, S., Barnes, C., Sweeting, C. J., and Polunin, N. V. C. (2008a). Application of nitrogen stable isotope analysis in size-based marine food web and macroecological research. *Rapid Commun. Mass Spectrom.* 22, 1673–1680. doi: 10.1002/rcm.3497

Jennings, S., Melin, F., Blanchard, J. L., Forster, R. M., Dulvy, N. K., and Wilson, R. W. (2008b). Global-scale predictions of community and ecosystem properties from simple ecological theory. *Proc. R. Soc. B Biol. Sci.* 275, 1375–1383. doi: 10.1098/rspb.2008.0192

Jennings, S., Pinnegar, J. K., Polunin, N., and Boon, T. W. (2001). Weak cross-species relationships between body size and trophic level belie powerful size-based trophic structuring in fish communities. *J. Anim. Ecol.* 70, 934–944. doi: 10.1046/j.0021-8790.2001.00552.x

John, E. H., Batten, S. D., Harris, R. P., and Hays, G. C. (2001). Comparison between zooplankton data collected by the Continuous Plankton Recorder survey in the English Channel and by WP-2 nets at station L4, Plymouth (UK). *J. Sea Res.* 46, 223–232. doi: 10.1016/S1385-1101(01)00085-5

Jones, E. M., Baird, M. E., Mongin, M., Parslow, J., Skerratt, J., Lovell, J., et al. (2016). Use of remote-sensing reflectance to constrain a data assimilating marine biogeochemical model of the Great Barrier Reef. *Biogeosciences* 13, 6441–6469. doi: 10.5194/bg-13-6441-2016

Kaartvedt, S., Staby, A., and Aksnes, D. L. (2012). Efficient trawl avoidance by mesopelagic fishes causes large underestimation of their biomass. *Mar. Ecol. Prog. Ser.* 456, 1–6. doi: 10.3354/meps09785

Kandel, S., Heer, J., Plaisant, C., Kennedy, J., van Ham, F., Riche, N. H., et al. (2011). Research directions in data wrangling: visualizations and transformations for usable and credible data. *Inform. Vis. J.* 10, 271–288. doi: 10.1177/1473871611415994

Kidston, M., Matear, R. J., and Baird, M. E. (2011). Parameter optimisation of a marine ecosystem model at two contrasting stations in the Sub-Antarctic Zone. *Deep Sea Res. Part II Top. Stud. Oceanogr.* 58, 2301–2315. doi: 10.1016/j.dsr2.2011.05.018

Kidston, M., Matear, R., and Baird, M. E. (2013). Phytoplankton growth in the Australian sector of the Southern Ocean, examined by optimising ecosystem model parameters. *J. Mar. Syst.* 128, 123–137. doi: 10.1016/j.jmarsys.2013.04.011

Kingsford, M. J., and MacDiarmid, A. B. (1988). Interrelations Between Planktivorous Reef Fish and Zooplankton in Temperate Waters. *Mar. Ecol. Prog. Ser.* 48, 103–117. doi: 10.3354/meps048103

Kloser, R. J., Ryan, T. E., Young, J. W., and Lewis, M. E. (2009). Acoustic observations of micronekton fish on the scale of an ocean basin: potential and challenges. *ICES J. Mar. Sci.* 66, 998–1006. doi: 10.1093/icesjms/fsp077

Kruk, C., Huszar, V. L. M., Peeters, E. T. H. M., Bonilla, S., Costa, L., Lürling, M., et al. (2010). A morphological classification capturing functional variation in phytoplankton. *Freshw. Biol.* 55, 614–627. doi: 10.1111/j.1365-2427.2009.02298.x

Lacroix, G., Ruddick, K., Park, Y., Gypens, N., and Lancelot, C. (2007). Validation of the 3D biogeochemical model MIRO&CO with field nutrient and phytoplankton data and MERIS-derived surface chlorophyll a images. *J. Mar. Syst.* 64, 66–88. doi: 10.1016/j.jmarsys.2006.01.010

Lassalle, G., Lobry, J., Le Loc'h, F., Mackinson, S., Sanchez, F., Tomczak, M. T., et al. (2013). Ecosystem status and functioning: searching for rules of thumb using an intersite comparison of food-web models of Northeast Atlantic continental shelves. *ICES J. Mar. Sci.* 70, 135–149. doi: 10.1093/icesjms/fss168

Lavery, A. C., Wiebe, P. H., Stanton, T. K., Lawson, G. L., Benfield, M. C., and Copley, N. (2007). Determining dominant scatterers of sound in mixed zooplankton populations. *J. Acoust. Soc. Am.* 122, 3304–3323. doi: 10.1121/1.2793613

Le Mezo, P., Lefort, S., Seferian, R., Aurnont, O., Maury, O., Murtugudde, R., et al. (2016). Natural variability of marine ecosystems inferred from a coupled climate to ecosystem simulation. *J. Mar. Syst.* 153, 55–66. doi: 10.1016/j.jmarsys.2015.09.004

Le Quere, C., Buitenhuis, E. T., Moriarty, R., Alvain, S., Aumont, O., Bopp, L., et al. (2015). Role of zooplankton dynamics for Southern Ocean phytoplankton biomass and global biogeochemical cycles. *Biogeosci. Discuss.* 12, 11935–11985. doi: 10.5194/bgd-12-11935-2015

Le Quere, C., Harrison, S. P., Prentice, I. C., Buitenhuis, E. T., Aumont, O., Bopp, L., et al. (2005). Ecosystem dynamics based on plankton functional types for global ocean biogeochemistry models. *Glob. Chang. Biol.* 11, 2016–2040. doi: 10.1111/j.1365-2486.2005.1004.x

Lefort, S., Aumont, O., Bopp, L., Arsouze, T., Gehlen, M., and Maury, O. (2015). Spatial and body-size dependent response of marine pelagic communities to projected global climate change. *Glob. Chang. Biol.* 21, 154–164. doi: 10.1111/gcb.12679

Lehodey, P., Senina, I., and Dragon, A. C. (2014). Spatially explicit estimates of stock size, structure and biomass of North Atlantic albacore tuna (*Thunnus alalunga*). *Earth Syst. Sci. Data* 6, 317–329. doi: 10.5194/essd-6-317-2014

Lehodey, P., Senina, I., and Murtugudde, R. (2008). A spatial ecosystem and populations dynamics model (SEAPODYM) - Modeling of tuna and tuna-like populations. *Prog. Oceanogr.* 78, 304–318. doi: 10.1016/j.pocean.2008.06.004

Lenz, J. (2000). "Chapter 1: introduction," in *Zooplankton Methodology Manual*, eds R. P. Harris, P. H. Wiebe, J. Lenz, H. R. Skjoldal, and M. E. Huntley (London: Academic Press), 1–32.

Letcher, B. H., Rice, J. A., Crowder, L. B., and Rose, K. A. (1996). Variability in survival of larval fish: disentangling components with a generalized individual-based model. *Can. J. Fish. Aquat. Sci.* 53, 787–801. doi: 10.1139/f95-241

Lewis, K., Allen, J. I., Richardson, A. J., and Holt, J. T. (2006). Error quantification of a high resolution coupled hydrodynamic-ecosystem coastal-ocean model: Part3, validation with Continuous Plankton Recorder data. *J. Mar. Syst.* 63, 209–224. doi: 10.1016/j.jmarsys.2006.08.001

Libralato, S., Christensen, V., and Pauly, D. (2006). A method for identifying keystone species in food web models. *Ecol. Modell.* 195, 153–171. doi: 10.1016/j.ecolmodel.2005.11.029

Lindeman, R. L. (1942). The trophic-dynamic aspect of ecology. *Ecology* 23, 399–418. doi: 10.2307/1930126

Luo, J. G., and Brandt, S. B. (1993). Bay anchovy anchoa-mitchilli production and consumption in mid-chesapeake bay based on a bioenergetics model and acoustic measures of fish abundance. *Mar. Ecol. Prog. Ser.* 98, 223–236. doi: 10.3354/meps098223

Maier Reimer, E., Kriest, I., Segschneider, J., and Wetzel, P. (2005). *The HAMburg Ocean Carbon Cycle Model HAMOCC 5.1: Technical Description Release 1.1.* Max Planck Institute for Meteorology. Reports on Earth System Science.

Marcolin, C. R., Lopes, R. M., and Jackson, G. A. (2015). Estimating zooplankton vertical distribution from combined LOPC and ZooScan observations on the Brazilian Coast. *Mar. Biol.* 162, 2171–2186. doi: 10.1007/s00227-015-2753-2

Marcolin, C. R., Schultes, S., Jackson, G. A., and Lopes, R. M. (2013). Plankton and seston size spectra estimated by the LOPC and ZooScan in the Abrolhos Bank ecosystem (SE Atlantic). *Cont. Shelf Res.* 70, 74–87. doi: 10.1016/j.csr.2013.09.022

Marquis, E., Niquil, N., Vezina, A. F., Petitgas, P., and Dupuy, C. (2011). Influence of planktonic foodweb structure on a system's capacity to support pelagic production: an inverse analysis approach. *ICES J. Mar. Sci.* 68, 803–812. doi: 10.1093/icesjms/fsr027

Matear, R. J., and Lenton, A. (2014). Quantifying the impact of ocean acidification on our future climate. *Biogeosciences* 11, 3965–3983. doi: 10.5194/bg-11-3965-2014

Maury, O. (2010). An overview of APECOSM, a spatialized mass balanced "Apex Predators ECOSystem Model" to study physiologically structured tuna population dynamics in their ecosystem. *Prog. Oceanogr.* 84, 113–117. doi: 10.1016/j.pocean.2009.09.013

Maury, O., and Poggiale, J.-C. (2013). From individuals to populations to communities: a dynamic energy budget model of marine ecosystem

size-spectrum including life history diversity. *J. Theor. Biol.* 324, 52–71. doi: 10.1016/j.jtbi.2013.01.018

Megrey, B. A., Rose, K. A., Klumb, R. A., Hay, D. E., Werner, F. E., Eslinger, D. L., et al. (2007). A bioenergetics-based population dynamics model of Pacific herring (*Clupea harengus pallasi*) coupled to a lower trophic level nutrient–phytoplankton–zooplankton model: description, calibration, and sensitivity analysis. *Ecol. Modell.* 202, 144–164. doi: 10.1016/j.ecolmodel.2006.08.020

Melle, W. R., Runge, J., Head, E., Plourde, S., Castellani, C., Licandro, P., et al. (2014). The North Atlantic Ocean as habitat for *Calanus finmarchicus*: environmental factors and life history traits. *Prog. Oceanogr.* 129, 244–284. doi: 10.1016/j.pocean.2014.04.026

Mitra, A. (2009). Are closure terms appropriate or necessary descriptors of zooplankton loss in nutrient–phytoplankton–zooplankton type models? *Ecol. Modell.* 220, 611–620. doi: 10.1016/j.ecolmodel.2008.12.008

Mitra, A., and Flynn, K. J. (2006). Accounting for variation in prey selectivity by zooplankton. *Ecol. Modell.* 199, 82–92. doi: 10.1016/j.ecolmodel.2006.06.013

Mitra, A., Castellani, C., Gentleman, W. C., Jónasdóttir, S. H., Flynn, K. J., Bode, A., et al. (2014). Bridging the gap between marine biogeochemical and fisheries sciences; configuring the zooplankton link. *Prog. Oceanogr.* 129, 176–199. doi: 10.1016/j.pocean.2014.04.025

Moore, S. K., and Suthers, I. M. (2006). Evaluation and correction of subresolved particles by the optical plankton counter in three Australian estuaries with pristine to highly modified catchments. 111:C05SC04. doi: 10.1029/2005jc002920

Moriarty, R., and O'Brien, T. D. (2013). Distribution of mesozooplankton biomass in the global ocean. *Earth Syst. Sci. Data* 5, 45–55. doi: 10.5194/essd-5-45-2013

O'Brien, T. D. (2005). *COPEPOD: A Global Plankton Database*. US Dep. Commerce, NOAA Tech. Memo.

Oke, P. R., Griffin, D. A., Schiller, A., Matear, R. J., Fiedler, R., Mansbridge, J., et al. (2013). Evaluation of a near-global eddy-resolving ocean model. *Geosci. Model Dev.* 6, 591–615. doi: 10.5194/gmd-6-591-2013

Opdal, A. F., and Vikebø, F. B. (2016). Long-term stability in modelled zooplankton influx could uphold major fish spawning grounds on the Norwegian continental shelf 1. *Can. J. Fish. Aquat. Sci.* 73, 189–196. doi: 10.1139/cjfas-2014-0524

Oschlies, A. (2001). Model-derived estimates of new production: new results point towards lower values. *Deep Sea Res. Part II Top. Stud. Oceanogr.* 48, 2173–2197. doi: 10.1016/S0967-0645(00)00184-3

Oschlies, A., and Schartau, M. (2005). Basin-scale performance of a locally optimized marine ecosystem model. *J. Mar. Res.* 63, 335–358. doi: 10.1357/0022240053693680

Palmer, J. R., and Totterdell, I. J. (2001). Production and export in a global ocean ecosystem model. *Deep Sea Res. Part I Oceanogr. Res. Pap.* 48, 1169–1198. doi: 10.1016/S0967-0637(00)00080-7

Parada, C., Hinckley, S., Horne, J., Mazur, M., Hermann, A., and Curchister, E. (2016). Modeling connectivity of walleye pollock in the Gulf of Alaska: are there any linkages to the Bering Sea and Aleutian Islands? *Deep Sea Res. Part II Top. Stud. Oceanogr.* 132, 227–239. doi: 10.1016/j.dsr2.2015.12.010

Pavés, H. J., González, H. E., and Christensen, V. (2013). Structure and functioning of two pelagic communities in the North Chilean Patagonian coastal system. *Hydrobiologia* 717, 85–108. doi: 10.1007/s10750-013-1576-8

Pedersen, T., Ramsvatn, S., Nilssen, E. M., Nilsen, M., Morissette, L., Ivarjord, T., et al. (2016). Species diversity affects ecosystem structure and mass flows in fjords. *Reg. Stud. Mar. Sci.* 3, 205–215. doi: 10.1016/j.rsma.2015.10.007

Perhar, G., Kelly, N. E., Ni, F. J., Simpson, M. J., Simpson, A. J., and Arhonditsis, G. B. (2016). Using Daphnia physiology to drive food web dynamics: a theoretical revisit of Lotka-Volterra models. *Ecol. Inform.* 35, 29–42. doi: 10.1016/j.ecoinf.2016.07.001

Peters, R. H. (1983). *The Ecological Implications of Body Size*. Cambridge: Cambridge University Press.

Pinnegar, J. K., Blanchard, J. L., Mackinson, S., Scott, R. D., and Duplisea, D. E. (2005). Aggregation and removal of weak-links in food-web models: system stability and recovery from disturbance. *Ecol. Modell.* 184, 229–248. doi: 10.1016/j.ecolmodel.2004.09.003

Piroddi, C., Coll, M., Steenbeek, J., Moy, D. M., and Christensen, V. (2015). Modelling the Mediterranean marine ecosystem as a whole: addressing the challenge of complexity. *Mar. Ecol. Prog. Ser.* 533, 47–65. doi: 10.3354/meps11387

Platt, T., and Denman, K. (1977). Organisation in the pelagic ecosystem. *Helgoländer Wiss. Meeresuntersuchungen* 30, 575–581. doi: 10.1007/BF02207862

Pope, J. G., Rice, J. C., Daan, N., Jennings, S., and Gislason, H. (2006). Modelling an exploited marine fish community with 15 parameters–results from a simple size-based model. *ICES J. Mar. Sci.* 63, 1029–1044. doi: 10.1016/j.icesjms.2006.04.015

Postel, L. (1990). The mesozooplankton response to coastal upwelling off West Africa with particular regard to biomass. *Mar. Sci. Rep.* 1, 1–127.

Postel, L., Fock, H., and Hagen, W. (2000). "Biomass and abundance," in *ICES Zooplankton Methodology Manual,* eds R. Harris, P. Wiebe, J. Lenz, H. R. Skjoldal, and M. Huntley (Cambridge, MA: Academic Press), 83–192.

Reid, P. C., Colebrook, J. M., Matthews, J. B. L., and Aiken, J. (2003). The Continuous Plankton Recorder: concepts and history, from Plankton Indicator to undulating recorders. *Prog. Oceanogr.* 58, 117–173. doi: 10.1016/j.pocean.2003.08.002

Rice, J. A., Miller, T. J., Rose, K. A., Crowder, L. B., Marschall, E. A., Trebitz, A. S., et al. (1993). Growth-Rate Variation and Larval Survival - Inferences From an Individual-Based Size-Dependent Predation Model. *Can. J. Fish. Aquat. Sci.* 50, 133–142. doi: 10.1139/f93-015

Richardson, A. J., John, E. H., Irigoien, X., Harris, R. P., and Hays, G. C. (2004). How well does the continuous plankton recorder (CPR) sample zooplankton? A comparison with the Longhurst Hardy Plankton Recorder (LHPR) in the northeast Atlantic. *Deep Sea Res. Part I Oceanogr. Res. Pap.* 51, 1283–1294. doi: 10.1016/j.dsr.2004.04.002

Richardson, A. J., Walne, A. W., John, A. W. G., Jonas, T. D., Lindley, J. A., Sims, D. W., et al. (2006). Using continuous plankton recorder data. *Prog. Oceanogr.* 68, 27–74. doi: 10.1016/j.pocean.2005.09.011

Robson, B. J. (2014). State of the art in modelling of phosphorus in aquatic systems: review, criticisms and commentary. *Environ. Modell. Softw.* 61, 339–359. doi: 10.1016/j.envsoft.2014.01.012

Rose, K. A., Allen, J. I., Artioli, Y., Barange, M., Blackford, J., Carlotti, F., et al. (2010). End-to-end models for the analysis of marine ecosystems: challenges, issues, and next steps. *Mar. Coast. Fish.* 2, 115–130. doi: 10.1577/C09-059.1

Sameoto, D. D., Wiebe, P. H., Runge, J., Postel, L., Dunn, J., Miller, C. B., et al. (2000). "Chapter 3: collecting zooplankton," in *Zooplankton Methodology Manual*, eds R. P. Harris, P. H. Wiebe, J. Lenz, H. R. Skjoldal, and M. E. Huntley (London: Academic Press), 55–82.

Savina, M., Forrest, R. E., Fulton, E. A., and Condie, S. A. (2013). Ecological effects of trawling fisheries on the eastern Australian continental shelf: a modelling study. *Mar. Freshw. Res.* 64:1068. doi: 10.1071/MF12361

Schmid, M. S., Aubry, C., Grigor, J., and Fortier, L. (2016). The LOKI underwater imaging system and an automatic identification model for the detection of zooplankton taxa in the Arctic Ocean. *Methods Oceanogr.* 15–16, 129–160. doi: 10.1016/j.mio.2016.03.003

Schultes, S., and Lopes, R. M. (2009). Laser Optical Plankton Counter and Zooscan intercomparison in tropical and subtropical marine ecosystems. *Limnol. Oceanogr. Methods* 7, 771–784. doi: 10.4319/lom.2009.7.771

Scott, F., Blanchard, J. L., and Andersen, K. H. (2014). mizer: an R package for multispecies, trait-based and community size spectrum ecological modelling. *Methods Ecol. Evol.* 5, 1121–1125. doi: 10.1111/2041-210X.12256

Sheldon, R. W., and Parsons, T. R. (1967). A continuous size spectrum for particulate matter in the sea. *J. Fish. Res. Board Can.* 24, 909–915. doi: 10.1139/f67-081

Sheldon, R. W., Prakash, A., and Sutcliffe, W. H. Jr. (1972). The size distribution of particles in the ocean. *Limnol. Oceanogr.* 17, 327–340. doi: 10.4319/lo.1972.17.3.0327

Shin, Y. J., and Cury, P. (2004). Using an individual-based model of fish assemblages to study the response of size spectra to changes in fishing. *Can. J. Fish. Aquat. Sci.* 61, 414–431. doi: 10.1139/f03-154

Shin, Y.-J., Travers, M., and Maury, O. (2010). Coupling low and high trophic levels models: towards a pathways-orientated approach for end-to-end models. *Prog. Oceanogr.* 84, 105–112. doi: 10.1016/j.pocean.2009.09.012

Sieracki, C. K., Sieracki, M. E., and Yentsch, C. S. (1998). An imaging-in-flow system for automated analysis of marine microplankton. *Mar. Ecol. Prog. Ser.* 168, 285–296. doi: 10.3354/meps168285

Silvert, W., and Platt, T. (1978). Energy flux in the pelagic ecosystem: a time-dependent equation. *Limnol. Oceanogr.* 23, 813–816. doi: 10.4319/lo.1978.23.4.0813

Simmonds, J., and MacLennan, D. N. (2005). *Fisheries Acoustics: Theory and Practice*. Oxford: Blackwell Science Ltd.

Skaret, G., Dalpadado, P., Hjollo, S. S., Skogen, M. D., and Strand, E. (2014). *Calanus finmarchicus* abundance, production and population dynamics in the Barents Sea in a future climate. *Prog. Oceanogr.* 125, 26–39. doi: 10.1016/j.pocean.2014.04.008

Skjoldal, H. R., Wiebe, P. H., Postel, L., Knutsen, T., Kaartvedt, S., and Sameoto, D. D. (2013). Intercomparison of zooplankton (net) sampling systems: results from the ICES/GLOBEC sea-going workshop. *Prog. Oceanogr.* 108, 1–42. doi: 10.1016/j.pocean.2012.10.006

Smith, A. D. M., Brown, C. J., Bulman, C. M., Fulton, E. A., Johnson, P., Kaplan, I. C., et al. (2011). Impacts of fishing low-trophic level species on marine ecosystems. *Science* 333, 1147–1150. doi: 10.1126/science.1209395

Sprules, W. G., and Munawar, M. (1986). Plankton size spectra in relation to ecosystem productivity, size, and perturbation. *Can. J. Fish. Aquat. Sci.* 43, 1789–1794. doi: 10.1139/f86-222

Steele, J. H., and Henderson, E. W. (1992). The role of predation in plankton models. *J. Plankton Res.* 14, 157–172. doi: 10.1093/plankt/14.1.157

Stemmann, L., Picheral, M., and Gorsky, G. (2000). Diel variation in the vertical distribution of particulate matter (> 0.15 mm) in the NW Mediterranean Sea investigated with the Underwater Video Profiler. *Deep Sea Res. Part I Oceanogr. Res. Pap.* 47, 505–531. doi: 10.1016/S0967-0637(99)00100-4

Sun, S., Huo, Y., and Yang, B. (2010). Zooplankton functional groups on the continental shelf of the yellow sea. *Deep Sea Res. Part II Top. Stud. Oceanogr.* 57, 1006–1016. doi: 10.1016/j.dsr2.2010.02.002

Suthers, I. M., Taggart, C. T., Rissik, D., and Baird, M. E. (2006). Day and night ichthyoplankton assemblages and zooplankton biomass size spectrum in a deep ocean island wake. *Mar. Ecol. Prog. Ser.* 322, 225–238. doi: 10.3354/meps322225

Thorpe, R. B., Le Quesne, W. J. F., Luxford, F., Collie, J. S., and Jennings, S. (2015). Evaluation and management implications of uncertainty in a multispecies size-structured model of population and community responses to fishing. *Methods Ecol. Evol.* 6, 49–58. doi: 10.1111/2041-210X.12292

Tian, R. C. (2006). Toward standard parameterizations in marine biological modeling. *Ecol. Modell.* 193, 363–386. doi: 10.1016/j.ecolmodel.2005.09.003

Travers-Trolet, M., Shin, Y. J., and Field, J. G. (2014). An end-to-end coupled model ROMS-N2P2Z2D2-OSMOSE of the southern Benguela foodweb: parameterisation, calibration and pattern-oriented validation. *Afr. J. Mar. Sci.* 36, 11–29. doi: 10.2989/1814232X.2014.883326

Trebilco, R., Baum, J. K., Salomon, A. K., and Dulvy, N. K. (2013). Ecosystem ecology: size-based constraints on the pyramids of life. *Trends Ecol. Evol.* 28, 423–431. doi: 10.1016/j.tree.2013.03.008

Trevorrow, M. V., Mackas, D. L., and Benfield, M. C. (2005). Comparison of multifrequency acoustic and *in situ* measurements of zooplankton abundances in Knight Inlet, British Columbia. *J. Acoust. Soc. Am.* 117, 3574–3588. doi: 10.1121/1.1920087

Urmy, S. S., Horne, J. K., and Barbee, D. H. (2012). Measuring the vertical distributional variability of pelagic fauna in Monterey Bay. *ICES J. Mar. Sci.* 69, 184–196. doi: 10.1093/icesjms/fsr205

Vandromme, P., Nogueira, E., Huret, M., Lopez- Urrutia, Á., Gonzalez-Nuevo, G., Sourisseau, M., et al. (2014). Springtime zooplankton size structure over the continental shelf of the Bay of Biscay. *Ocean Sci.* 10, 821–835. doi: 10.5194/os-10-821-2014

Wallis, J. R., Swadling, K. M., Everett, J. D., Suthers, I. M., Jones, H. J., Buchanan, P. J., et al. (2016). Zooplankton abundance and biomass size spectra in the East Antarctic sea-ice zone during the winter–spring transition. *Deep Sea Res. Part II Top. Stud. Oceanogr.* 131, 170–181. doi: 10.1016/j.dsr2.2015.10.002

Ward, B. A., Dutkiewicz, S., and Follows, M. J. (2014). Modelling spatial and temporal patterns in size-structured marine plankton communities: top-down and bottom-up controls. *J. Plankton Res.* 36, 31–47. doi: 10.1093/plankt/fbt097

Ward, B. A., Dutkiewicz, S., Jahn, O., and Follows, M. J. (2012). A size-structured food-web model for the global ocean. *Limnol. Oceanogr.* 57, 1877–1891. doi: 10.4319/lo.2012.57.6.1877

Ward, T., and Staunton-Smith, J. (2002). Comparison of the spawning patterns and fisheries biology of the sardine, Sardinops sagax, in temperate South Australia and sub-tropical southern Queensland. *Fish. Res.* 56, 37–49. doi: 10.1016/S0165-7836(01)00314-9

Watanabe, S., Hajima, T., Sudo, K., Nagashima, T., Takemura, T., Okajima, H., et al. (2011). MIROC-ESM 2010: model description and basic results of CMIP5-20c3m experiments. *Geosci. Model Dev.* 4, 845–872. doi: 10.5194/gmd-4-845-2011

Watson, R. A., Nowara, G. B., Tracey, S. R., Fulton, E. A., Bulman, C. M., Edgar, G. J., et al. (2013). Ecosystem model of Tasmanian waters explores impacts of climate-change induced changes in primary productivity. *Ecol. Modell.* 264, 115–129. doi: 10.1016/j.ecolmodel.2012.05.008

Werner, F. E., Quinlan, J. A., Lough, R. G., and Lynch, D. R. (2001). Spatially-explicit individual based modeling of marine populations: a review of the advances in the 1990s. *Sarsia* 86, 411–421. doi: 10.1080/00364827.2001.10420483

Wiebe, P. H. (1988). Functional regression equations for zooplankton displacement volume, wet weight, dry weight, and carbon : a correction. *Fish. Bull* 86, 833–835.

Wiebe, P. H., and Benfield, M. C. (2003). From the Hensen net toward four-dimensional biological oceanography. *Prog. Oceanogr.* 56, 7–136. doi: 10.1016/S0079-6611(02)00140-4

Wiebe, P. H., and Holland, W. R. (1968). Plankton patchiness: effects on repeated net tows. *Limnol. Oceanogr.* 13, 315–321. doi: 10.4319/lo.1968.13.2.0315

Wiebe, P. H., Ashjian, C. J., Gallager, S. M., Davis, C. S., Lawson, G. L., and Copley, N. J. (2004). Using a high-powered strobe light to increase the catch of Antarctic krill. *Mar. Biol.* 144, 493–502. doi: 10.1007/s00227-003-1228-z

Wroblewski, J. S., Sarmiento, J. L., and Flierl, G. R. (1988). An Ocean Basin Scale Model of plankton dynamics in the North Atlantic: 1. Solutions For the climatological oceanographic conditions in May. *Global Biogeochem. Cycles* 2, 199–218. doi: 10.1029/GB002i003p00199

Yool, A., Popova, E. E., and Anderson, T. R. (2011). MEDUSA-1.0: a new intermediate complexity plankton ecosystem model for the global domain. *Geosci. Model Dev.* 4, 381–417. doi: 10.5194/gmd-4-381-2011

Zhao, J., Ramin, M., Cheng, V., and Arhonditsis, G. B. (2008). Plankton community patterns across a trophic gradient: the role of zooplankton functional groups. *Ecol. Modell.* 213, 417–436. doi: 10.1016/j.ecolmodel.2008.01.016

Zhou, M. (2006). What determines the slope of a plankton biomass spectrum? *J. Plankton Res.* 28, 437–448. doi: 10.1093/plankt/fbi119

Zhou, M., and Huntley, M. E. (1997). Population dynamics theory of plankton based on biomass spectra. *Mar. Ecol. Prog. Ser.* 159, 61–73. doi: 10.3354/meps159061

Zhou, M., Carlotti, F., and Zhu, Y. (2010). A size-spectrum zooplankton closure model for ecosystem modelling. *J. Plankton Res.* 32, 1147–1165. doi: 10.1093/plankt/fbq054

Zhou, M., Tande, K. S., Zhu, Y., and Basedow, S. (2009). Productivity, trophic levels and size spectra of zooplankton in northern Norwegian shelf regions. *Deep Sea Res. Part II Top. Stud. Oceanogr.* 56, 1934–1944. doi: 10.1016/j.dsr2.2008.11.018

**Conflict of Interest Statement:** The authors declare that the research was conducted in the absence of any commercial or financial relationships that could be construed as a potential conflict of interest.

frontiers in Marine Science

ORIGINAL RESEARCH
published: 19 October 2016
doi: 10.3389/fmars.2016.00201

# Zooplankton Are Not Fish: Improving Zooplankton Realism in Size-Spectrum Models Mediates Energy Transfer in Food Webs

*Ryan F. Heneghan*[1]*, *Jason D. Everett*[2,3], *Julia L. Blanchard*[4] and *Anthony J. Richardson*[1,5]

[1] Centre for Applications in Natural Resource Mathematics, School of Mathematics and Physics, University of Queensland, Brisbane, QLD, Australia, [2] School of Biological, Earth and Environmental Sciences, University of New South Wales, Sydney, NSW, Australia, [3] Sydney Institute of Marine Science, Sydney, NSW, Australia, [4] Institute of Marine and Antarctic Studies, University of Tasmania, Hobart, TAS, Australia, [5] Ecosciences Precinct, CSIRO Ocean and Atmosphere, Brisbane, QLD, Australia

The evidence for an equal distribution of biomass from bacteria to whales has led to development of size-spectrum models that represent the dynamics of the marine ecosystem using size rather than species identity. Recent advances have improved the realism of the fish component of the size-spectrum, but these often assume that small fish feed on an aggregated plankton size-spectrum, without any explicit representation of zooplankton dynamics. In these models, small zooplankton are grouped with phytoplankton as a resource for larval fish, and large zooplankton are parameterized as small fish. Here, we investigate the impact of resolving zooplankton and their feeding traits in a dynamic size-spectrum model. First, we compare a base model, where zooplankton are parameterized as smaller fish, to a model that includes zooplankton-specific feeding parameters. Second, we evaluate how the parameterization of zooplankton feeding characteristics, specifically the predator–prey mass ratio (PPMR), assimilation efficiency and feeding kernel width, affects the productivity and stability of the fish community. Finally, we compare how feeding characteristics of different zooplankton functional groups mediate increases in primary production and fishing pressure. Incorporating zooplankton-specific feeding parameters increased productivity of the fish community, but also changed the dynamics of the entire system from a stable to an oscillating steady-state. The inclusion of zooplankton feeding characteristics mediated a trade-off between the productivity and resilience of the fish community, and its stability. Fish communities with increased productivity and lower stability were supported by zooplankton with a larger PPMR and a narrower feeding kernel–specialized herbivores. In contrast, fish communities that were stable had lower productivity, and were supported by zooplankton with a lower PPMR and a wider feeding kernel—generalist carnivores. Herbivorous zooplankton communities were more efficient at mediating increases in primary production, and supported fish communities more resilient to fishing. Our results illustrate that zooplankton are not just a static food source for larger organisms,

OPEN ACCESS

***Edited by:***
*Christian Lindemann,*
*University of Bergen, Norway*

***Reviewed by:***
*Jan Marcin Weslawski,*
*Institute of Oceanology (PAN), Poland*
*Francis Poulin,*
*University of Waterloo, Canada*

***Correspondence:**
*Ryan F. Heneghan*
*ryan.heneghan@uqconnect.edu.au*

***Specialty section:***
*This article was submitted to Marine Ecosystem Ecology, a section of the journal Frontiers in Marine Science*

***Received:*** *03 August 2016*
***Accepted:*** *29 September 2016*
***Published:*** *19 October 2016*

***Citation:***
*Heneghan RF, Everett JD, Blanchard JL and Richardson AJ (2016) Zooplankton Are Not Fish: Improving Zooplankton Realism in Size-Spectrum Models Mediates Energy Transfer in Food Webs. Front. Mar. Sci. 3:201. doi: 10.3389/fmars.2016.00201*

nor can they be resolved as very small fish. The unique feeding characteristics of zooplankton have enormous implications for the dynamics of marine ecosystems, and their representation is of critical importance in size-spectrum models, and end-to-end ecosystem models more broadly.

**Keywords: zooplankton dynamics, marine size-spectrum, end-to-end modeling, fish productivity, ecosystem stability**

## INTRODUCTION

In the 50 years since Sheldon et al. (1967) first hypothesized an equal concentration of biomass from bacteria to whales, a range of size-spectrum models have been developed to explain this remarkable consistency (Andersen et al., 2015; Guiet et al., 2016b). Size-spectrum models represent the entire marine community as a size distribution, and traditionally do not resolve species identity. Their simplicity and parsimonious parameterization makes it possible for them to be used to investigate human impacts at the community level, including fishing (e.g., Andersen and Pedersen, 2010; Jacobsen et al., 2014; Law et al., 2016), climate change (e.g., Blanchard et al., 2012; Woodworth-Jefcoats et al., 2013; Barange et al., 2014; Dueri et al., 2014), and habitat loss (Rogers et al., 2014).

The focus of these models has been on higher trophic levels—primarily fish and fishing—and in recent years there has been considerable effort in improving their parameterization (Andersen et al., 2015; Guiet et al., 2016b). For example, recent theoretical developments now allow size-spectrum models to resolve different functional groups and even species by their traits, and this has been implemented for various fish (e.g., Blanchard et al., 2014; Dueri et al., 2014; Zhang et al., 2015). The focus on fish has meant that the dynamics of the plankton-dominated lower trophic levels has been neglected in model formulations. Zooplankton, as the main consumers of phytoplankton and prey of small fish are the chief intermediaries between primary production and higher trophic levels, and thus play a critical role in marine food web dynamics (Carlotti and Poggiale, 2010; Mitra and Davis, 2010).

In current dynamic size-spectrum models, the minimum size of the dynamic consumer spectrum extends to mesozooplankton. For smaller zooplankton, there are three common representations. First, phytoplankton and small zooplankton are represented as a fixed resource spectrum (with a varying intercept and a slope held at $-1$), and are considered only as a food source for the smallest fish size classes (Maury et al., 2007; Blanchard et al., 2009, 2011, 2012; Law et al., 2009; Datta et al., 2010; Guiet et al., 2016a). Second, the phytoplankton and small zooplankton spectrum is determined by an external nutrient–phytoplankton–zooplankton (NPZ) model, with no predation feedback from the larger dynamic size classes (Woodworth-Jefcoats et al., 2013; Lefort et al., 2015; Le Mézo et al., 2016). Third, phytoplankton and small zooplankton are modeled as a semi-chemostat system, with a fixed carrying capacity and predation feedback from higher trophic levels (Hartvig et al., 2011; Blanchard et al., 2014; Scott et al., 2014; Zhang et al., 2015, 2016). The latter approach is the only one in which the size-spectrum of fish dynamically interacts with phytoplankton and small zooplankton. These current representations essentially group smaller zooplankton and phytoplankton together as food for the smallest dynamic size classes, and resolve larger zooplankton as small fish.

Assuming zooplankton have the same dynamics as phytoplankton or small fish is not only incorrect, but could have considerable effects on energy transfer in food webs. Zooplankton have feeding characteristics distinctly different from fish. For instance, the average predator–prey mass ratio (PPMR; in grams of wet weight) for fish is typically around 100 (Jennings et al., 2001) but for zooplankton it is $>1000$ (Kiørboe, 2008; Wirtz, 2012). Additionally, zooplankton exhibit vast phylogenetic biodiversity, with at least eight phyla commonly present (crustaceans, chordates, chaetognaths, molluscs, cnidarians, echinoderms, ctenophores, and annelids), each with considerable differences in their feeding ecology, from passive suspension grazing of the water column to active ambushing and carnivory (Kiørboe, 2011). Further complicating their feeding, various species of jellyfish, copepods, and microzooplankton can switch between suspension and ambush feeding modes, and this is reflected in different optimal prey sizes realized by the same species (Landry, 1981; Goldman and Dennett, 1990; Saiz and Kiørboe, 1995).

Size-based predation is the key driver of dynamics in size-based ecosystems (Jennings et al., 2001; Woodward et al., 2005; Andersen et al., 2016) and is broadly defined by five key parameters: (1) PPMR; (2) search rate coefficient; (3) body-size exponent, which determines how the search rate scales with body-size; (4) assimilation efficiency; and (5) the width of the feeding kernel (the diet breadth around the preferred PPMR), and modeling studies of the size-spectra of fish have shown that these parameters have a large effect on food web dynamics (Law et al., 2009; Datta et al., 2011; Zhang et al., 2013). For instance, a wider feeding kernel and lower PPMR dampens traveling waves through the fish community size-spectrum (Blanchard, 2008; Law et al., 2009; Zhang et al., 2013). Further, there is evidence that higher assimilation efficiency has a similar effect on the steady state of the size-spectrum (Datta et al., 2011). The sensitivity of ecosystem dynamics to parameterization of fish feeding characteristics strongly suggests that zooplankton feeding characteristics could be important to energy transfer through the food web. Therefore, the first step toward including zooplankton in end-to-end size-spectrum models is to include an accurate representation of their feeding characteristics.

The extensive experimental work elucidating zooplankton feeding characteristics has formed the basis of several recent syntheses of size-based feeding (Fuchs and Franks, 2010;

Kiørboe, 2011; Wirtz, 2012, 2014) and provides an opportunity for improving zooplankton parameterization in size-spectrum models. Wirtz (2012) used the data collected by Hansen et al. (1994) and Fuchs and Franks (2010) to develop a mechanistic model that links zooplankton PPMR with their feeding characteristics. In another paper, Wirtz (2014) derived an ideal feeding kernel width for zooplankton from simple biomechanical laws, which agrees well with empirical data. Fuchs and Franks (2010) synthesized data from previous studies to investigate the relationship between zooplankton PPMR and the width of the feeding kernel. They found that the feeding kernel width decreased with decreasing PPMR, suggesting increasing selectivity amongst individuals who prey on individuals closer to their own size. Kiørboe (2011) found that the size-specific zooplankton search rate is independent of body size across seven different functional groups.

Here, we evaluate how the size-dependent feeding characteristics of zooplankton affect the dynamics of higher trophic levels in size-structured pelagic ecosystems. We extract feeding characteristics from a range of syntheses of size-based feeding (Fuchs and Franks, 2010; Kiørboe, 2011, 2013; Wirtz, 2012, 2014) and implement them in a dynamic size-spectrum model framework (Datta et al., 2010; Andersen et al., 2015; Guiet et al., 2016b). To our knowledge this is the first dynamic size-spectra model to resolve predation-based growth and mortality of zooplankton. The model has three components—a static phytoplankton resource spectrum and two dynamic spectra representing a general zooplankton and fish community, respectively. In our model, biomass flows from smaller to larger size classes as a consequence of larger organisms consuming smaller organisms, and growth at one size is balanced by mortality in smaller size classes. We separate our findings in three parts. In *Zooplankton Are Not Fish*, we provide a size-spectrum model using the best parameter estimates from the literature, and establish the individual effect each of the five key zooplankton feeding parameters has on the community size-spectrum, by comparing against a base model where zooplankton are parameterized as just another fish community. In *Sensitivity Analysis*, we assess how varying the feeding characteristics of the zooplankton community impact the stability and productivity of the fish community size-spectrum. Finally in *Mediating Primary Production and Fishing*, we evaluate how the feeding characteristics of different zooplankton functional groups—salps, chaetognaths, herbivorous copepods, flagellates, and carnivorous copepods—mediate changes in phytoplankton abundance and increased fishing mortality on the fish community size spectrum. The purpose of this study is not to give a quantitative evaluation of zooplankton or fish abundance, rather we wish to illustrate how incorporating zooplankton-specific feeding characteristics could affect the dynamics of size-structured ecosystems. Our ultimate aim is to investigate how zooplankton feeding characteristics influence energy transfer from phytoplankton and fish, and thus move toward a more realistic and consistent parameterization for the zooplankton component of size-spectrum models.

# METHODS

## The Model

We developed a size-spectrum model that consists of a size-spectrum comprised of three communities: phytoplankton, zooplankton, and fish (**Figure 1**; **Tables 1**,**2**). The phytoplankton component covers the smallest size classes $[w_p, w_z]$ and is held constant as a background resource spectrum for zooplankton. Size-dependent processes of growth and mortality drive the zooplankton and fish components. These two components are delineated by different size ranges and feeding characteristics. The zooplankton community covers the size range between phytoplankton and fish $[w_z, \overline{W}_z]$, and the fish community covers the largest size classes $[w_f, \overline{W}_f]$, although some of the smallest fish size classes extend into the zooplankton range (from $w_f = 0.1\,\mathrm{g}$ to $\overline{W}_z = 1\,\mathrm{g}$). Fish community size classes that extend into the zooplankton range represent larvae and very small fish that are smaller than the largest zooplankton. Predation is size-dependent, with big things eating smaller ones, so depending on their size, zooplankton can feed on phytoplankton, smaller zooplankton, and the smallest fish size classes. Similarly, fish feed on zooplankton and smaller fish. The temporal dynamics of the zooplankton and fish communities are governed by separate McKendrick–von Foerster equations with second-order diffusion terms (Datta et al., 2010),

$$\frac{\delta}{\delta t}N_i\left(w,t\right) = -\frac{\delta}{\delta w}\left(g_i\left(w,t\right)N_i\left(w,t\right)\right) - \mu_i\left(w,t\right)N_i\left(w,t\right) + \frac{1}{2}\frac{\partial^2}{\partial w^2}\left(f_i\left(w,t\right)N_i\left(w,t\right)\right). \quad (1)$$

The density of individuals in community $i$ (where $i$ is either zooplankton or fish) per unit mass per unit volume ($\mathrm{g}^{-1}\mathrm{m}^{-3}$) is denoted by $N_i(w, t)$. Growth, mortality, and diffusion rates of individuals of group $i$ at size $w$ and time $t$, are denoted by $g_i\,(w, t)$, $\mu_i\,(w, t)$ , and $f_i\,(w, t)$, respectively. In this context, the diffusion

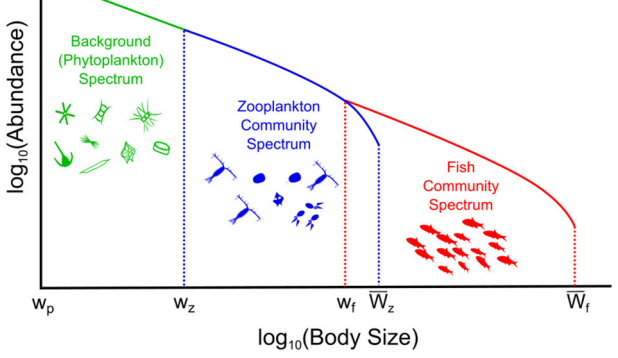


**FIGURE 1 | Conceptual illustration of the phytoplankton–zooplankton–fish system.** The background (phytoplankton) spectrum is held constant, the dynamic zooplankton, and fish community spectrums are governed by Equation (1) and the Equations in **Table 2**.

**TABLE 1 | Table of parameter values for the phytoplankton–zooplankton–fish dynamic size spectrum model.**

| Symbol | Definition | Value | Unit | Source |
|---|---|---|---|---|
| | Body mass ranges for: | | | |
| 1. $w_p, w_z$ | 1. Phytoplankton | 1. $10^{-15}, 10^{-5}$ | g | – |
| 2. $w_z, \overline{W}_z$ | 2. Zooplankton | 2. $10^{-5}, 10^{0}$ | | 1 |
| 3. $w_f, \overline{W}_f$ | 3. Fish | 3. $10^{-3}, 10^{6}$ | | 2, 3, 4 |
| $\beta_F$ | PPMR for fish | 100 | – | 5 |
| | Quantitative feeding mode for | | | |
| $m$ | 1. Salps and Doliolids | 1. −2.68 | – | 6 |
| | 2. Herbivorous copepods | 2. −0.48 | | |
| | 3. Chaetognaths | 3. −0.20 | | |
| | 4. General community | 4. 0.00 | | |
| | 5. Flagellates | 5. 0.53 | | |
| | 6. Carnivorous copepods | 6. 1.5 0 | | |
| $\sigma$ | Feeding kernel width for zooplankton and fish | $\sigma_Z = 0.75$ | – | 7 |
| | | $\sigma_F = 1$ | | 2, 3, 4 |
| $\alpha$ | Exponent of search rate for zooplankton and fish | $\alpha_Z = 1.01$ | – | 8 |
| | | $\alpha_F = 0.80$ | | 9 |
| $\gamma$ | Coefficient of search rate for zooplankton and fish | $\gamma_Z = 875$ | $g^{-\alpha} m^{-3}\ yr^{-1}$ | 8 |
| | | $\gamma_F = 640$ | | 9 |
| $K$ | Assimilation efficiency for zooplankton and fish | $K_Z = 0.7$ | – | See text |
| | | $K_F = 0.6$ | | 5 |
| $B_0$ | Coefficient for background mortality | 0.04 | $g^{-c}\ yr^{-1}$ | 2, 4 |
| $c$ | Exponent for background mortality | –0.25 | – | 2, 4, 11 |
| $S_0$ | Coefficient for senescence mortality | 0.2 | $g^{-s}\ yr^{-1}$ | 2, 4, 10 |
| $s$ | Exponent for senescence mortality | 1.2 | – | 2, 4, 10 |
| $w_s$ | Body size at which senescence mortality begins for zooplankton and fish | $w_{s_Z} = 10^{-2}$ | | – |
| | | $w_{s_F} = 10^{4}$ | g | – |
| $a$ | Coefficient for background size-spectrum | 0.017 | $g^{-1-b} m^{-3}$ | 12, 13 |
| $b$ | Exponent for background size-spectrum | −1 | – | 2, 3, 4 |

*Sources: 1. Zhou et al. (2010), 2. Blanchard et al. (2009), 3. Benoît and Rochet (2004), 4. Blanchard et al. (2011), 5. Andersen et al. (2015), 6. Wirtz (2012), 7. Wirtz (2014), 8. Kiørboe (2011), 9. Peters (1983), 10. Hall et al. (2006), 11. Brown et al. (2004), 12. Barnes et al. (2011), 13. Rousseaux and Gregg (2015).*

term allows the model to incorporate demographic variation in the growth rates of each community. That is, within each community two individuals of the same weight eating the same food will not grow by the same amount (Datta et al., 2010). This not only increases model realism, but the stability of the system steady state, over the traditional first-order McKendrick–von Foerster equation (Datta et al., 2011).

Phytoplankton dynamics in the background resource spectrum are not explicitly modeled, with the density of individuals held constant through time:

$$N_P(w,t) = aw^{-b}, \tag{E11}$$

Equations are also found in **Table 2**. We use an exponent of −1 for the background spectrum, implying equal biomass over logarithmically equal body–mass intervals in keeping with past dynamic size-spectrum models Benoît and Rochet, 2004; Law et al., 2009, 2016; Blanchard et al., 2012). The coefficient $a$ for the background spectrum (Equation 11) was calculated using the empirical equation from Barnes et al. (2011) and annual median chlorophyll-$a$ concentrations for different ocean basins between 2005 and 2010 (Rousseaux and Gregg, 2015). Unless specified otherwise, we use the global median chlorophyll-$a$ value (0.16 mg $m^{-3}$) to give a value of 0.017 for $a$.

From the predator's perspective, total consumption depends on the total biomass of suitable prey. For an individual of size $w$ at time $t$ from community $i$, this is determined by the predator's search rate:

$$V_i(w) = \gamma_i w^{\alpha_i}, \tag{E5}$$

and the density of suitable prey:

$$D_i(w,t) = \int_{w_p}^{w} \phi_i\left(w, w'\right) \sum_j N_j\left(w', t\right) w' dw'. \tag{E6}$$

The growth rate of an individual of size $w$ at time $t$ is fuelled by consumption of prey from smaller size classes:

$$g_i(w_i, t) = K_i V_i(w) D_i(w, t), \tag{E7}$$

where $K_i$ is the assimilation efficiency of community $i$.

**TABLE 2 | Model equations with their units.**

| Description | Equation | Units | Equation number |
|---|---|---|---|
| **ZOOPLANKTON CHARACTERISTICS** | | | |
| Zooplankton size in ESD | $D_w = 2\sqrt[3]{3w \times 10^{12}/4\pi}$ | μm | (E1) |
| PPMR | $\beta_Z(w) = \left(\exp\left(0.02\ln\left(D_w/D_0\right)^2 - m + 1.832\right)\right)^3$ | – | (E2) |
| Feeding kernel width | $\sigma_Z = 3(0.05\log_{10}(\beta_Z) + 0.11)$ | – | (E3) |
| **CONSUMPTION AND GROWTH** | | | |
| Size selection | $\phi_i(w, w') = \exp\left[-\left(ln\left(\beta_i(w)w'/w\right)\right)^2/2\sigma_i^2\right]/\left(\sigma_i\sqrt{2\pi}\right)$ | – | (E4) |
| Search rate | $V_i(w) = \gamma_i w^{\alpha_i}$ | $m^{-3}\ yr^{-1}$ | (E5) |
| Density of suitable prey | $D_i(w,t) = \int_{w_p}^{w} \phi_i(w,w') \sum_j N_j(w',t)\, w' dw'$ | $g\ m^{-3}$ | (E6) |
| Growth rate | $g_i(w_i, t) = K_i V_i(w) D_i(w,t)$ | $g\ yr^{-1}$ | (E7) |
| **MORTALITY** | | | |
| Predation | $\mu_P(w,t) = \sum_j \mathbb{I}_{\{w<\bar{W}_j\}} \int_w^{\bar{W}_j} \phi_j(w',w) V_j(w) N_j(w',t)\, dw'$ | $yr^{-1}$ | (E8) |
| Intrinsic mortality | $\mu_{0_i}(w,t) = B_0 w^C + S_{0_i} w^S$ | $yr^{-1}$ | (E9) |
| Total mortality | $\mu_i(w,t) = \mu_P(w,t) + \mu_{0_i}(w,t)$ | $yr^{-1}$ | (E10) |
| **OTHER EQUATIONS** | | | |
| Background (Phytoplankton) Spectrum | $N_P(w,t) = aw^{-b}$ | $g^{-1}m^{-3}$ | (E11) |
| Zooplankton boundary condition | $N_Z(w_Z) = aw_Z^{-b}$ | $g^{-1}m^{-3}$ | (E12) |
| Fish boundary condition | $N_F(w_F, t) = N_Z(w_F, t)$ | $g^{-1}m^{-3}$ | (E13) |
| Diffusion term | $f_i(w,t) = \gamma_i w^{\alpha_i} \sum_j K_{ij}^2 \int_{w_p}^{w} (w')^2 \phi_i(w,w') N_j(w',t) dw'$ | $g^2\ yr^{-1}$ | (E14) |
| **COMMUNITY CHARACTERISTICS:** | | | |
| Total biomass | $B_i(t) = \int_{w_i}^{\overline{W_i}} wN_i(w,t)dw$ | $g\ m^{-3}$ | (E15) |
| Total throughput | $T_i(t) = \int_{w_i}^{\overline{W_i}} wV_i(w) D_i(w,t) N_i(w,t)dw$ | $g\ m^{-3}\ yr^{-1}$ | (E16) |
| Production–biomass ratio | $PB_i(t) = \int_{w_i}^{\overline{W_i}} w\mu_i(w,t) N_i(w,t)dw / \int_{w_i}^{\overline{W_i}} wN_i(w,t)dw$ | $yr^{-1}$ | (E17) |
| Fish–zooplankton biomass ratio | $FZ(t) = B_F(t)/B_Z(t)$ | – | (E18) |

*An equation number is given that is used in the main text.*

Kiørboe (2011) found that the search rate (Equation 5) for zooplankton, across a wide range of taxa is largely independent of organism size ($\alpha_Z = 1.01$). This stands in contrast to the scaling for fish ($\alpha_F = 0.8$; Peters, 1983) that implies the specific search-rate per unit mass declines with increasing body size. Further, the search rate coefficient is higher for zooplankton $\gamma_Z = 875 g^{-\alpha_Z} m^{-3}\ year^{-1}$ (Kiørboe, 2011), compared to fish $\gamma_F = 640 g^{-\alpha_F} m^{-3}\ year^{-1}$ (Peters, 1983). The probability that a predator of size $w$ will consume an individual of size $w'$ is given by the log-normal function (Equation 4), where $\beta_i$ and $\sigma_i$ are community $i$ 's PPMR and feeding kernel width.

In previous size-spectrum models the PPMR is held constant across the entire size range of the community (Andersen et al., 2015). For zooplankton, the wide variation in observed PPMR across phyla suggests a constant value across all zooplankton size classes is inappropriate (Wirtz, 2012). We have thus used the mechanistic formulation from Wirtz (2012) who argues that for zooplankton, PPMR will increase non-linearly as predator size increases, due to the non-isometric scaling of feeding-related apparatus with body size (**Figure 2**):

$$\beta_Z(w) = \left(\exp\left(0.02\ln\left(D_w/D_0\right)^2 - m + 1.832\right)\right)^3, \quad \text{(E2)}$$

where $D_w$ is the predator equivalent spherical diameter (ESD) in μm:

$$D_w = 2\sqrt[3]{3w \times 10^{12}/4\pi}. \quad \text{(E1)}$$

The mechanistic model from Wirtz (2012) also allows the range of feeding modes across different zooplankton functional groups to be quantitatively incorporated. The feeding mode of the zooplankton community is denoted by $m$, and ranges from $-3$ to 2. A larger, positive $m$-value (say $m = 2$) suggests a more raptorial, carnivorous feeding strategy with a lower PPMR (**Figure 1**). Alternatively, a negative $m$-value (say $m = -3$) implies a more passive, herbivorous feeding strategy. For the fish community, we set $\beta_F = 100$ (Andersen et al., 2015).

A wider feeding kernel means an individual feeds over a wider range of size classes, implying a more generalist feeding strategy. Wirtz (2014) obtained a general feeding kernel width for zooplankton of 0.75 $\log_{10}$ grams body-size from simple biomechanical laws, and found this value agreed well with measured values from different species. Fuchs and Franks derived an empirical equation that links zooplankton PPMR $\beta_Z$ with the feeding kernel width:

$$\sigma_Z = 3\left(0.05\log_{10}(\beta_Z) + 0.11\right). \quad \text{(E3)}$$

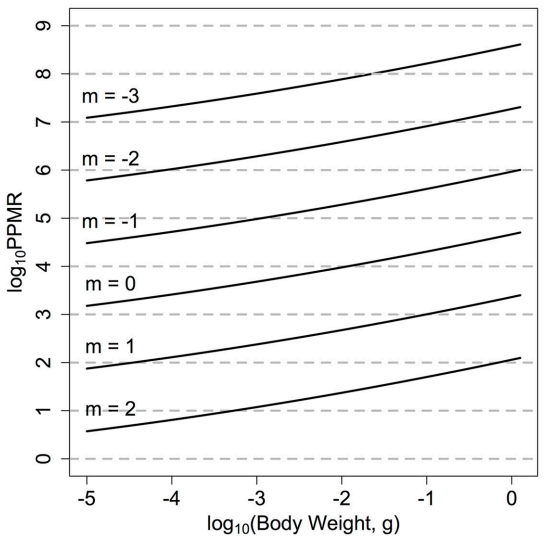


**FIGURE 2 | $\log_{10}$PPMR for the range of quantitative feeding modes from carnivores to herbivores.** Wirtz (2012), across the zooplankton size classes. The solid lines indicate the realized $\log_{10}$PPMR for different feeding modes, across the size range of the zooplankton community.

This equation suggests a positive relationship between the width of the feeding kernel and the PPMR. In other words, more active, carnivorous groups ($m > 0$), have a narrower, more selective prey size range compared to passive, filter feeding groups ($m < 0$) that have a wider, more generalist prey size range. For the fish community, we set $\sigma_F = 1$ (Andersen et al., 2015).

For individuals in community $i$, a fraction $K_i$ of consumed biomass, the assimilation efficiency, is assimilated into new biomass. Observational and experimental work across different zooplankton functional groups show that assimilation efficiency of ingested food into new biomass ranges from 0.3 to 0.9 (Landry et al., 1984; Kiørboe, 2008; Montagnes and Fenton, 2012; Abe et al., 2013). Assimilation efficiency of copepods (Landry et al., 1984), dinoflagellates and larval fish (Kiørboe, 2008) depends on whether they were acclimated to low or high food environments; those from low food environments have a higher assimilation efficiency compared to those from high food environments. Similarly, the density and type or prey available had a significant effect on zooplankton assimilation efficiency—higher density and higher carbon content of prey gave lower assimilation efficiencies (Montagnes and Fenton, 2012; Abe et al., 2013). In previous models, assimilation efficiency for zooplankton is usually held constant at 0.70 (e.g., Zhou, 2006; Fuchs and Franks, 2010; Ward et al., 2012, 2014). Unless specified otherwise, we keep $K_Z = 0.7$ to follow previous size-based plankton-focused models (Baird and Suthers, 2006; Zhou, 2006; Stock et al., 2008; Fuchs and Franks, 2010; Banas, 2011). For the fish community, we set $K_F = 0.6$, as this is a common values given in previous dynamic size-spectrum models (Andersen et al., 2015).

From the prey's perspective, the total predation pressure from all larger size classes gives the predation mortality rate:

$$\mu_p(w,t) = \sum\nolimits_j \mathbb{I}_{\{w<\overline{W}_j\}} \int_w^{\overline{W}_j} \phi_j\left(w', w\right) V_j(w) N_j\left(w', t\right) dw'. \tag{E8}$$

To account for other sources of mortality (e.g., disease), we include a U-shaped intrinsic mortality term:

$$\mu_{0_i}(w,t) = B_0 w^c + S_{0_i} w^s \tag{E9}$$

that covers non-predation sources of mortality such as disease and senescence (Brown et al., 2004; Hall et al., 2006; Blanchard et al., 2009, 2011). Since individuals grow through time, the background mortality term describes rapidly decreasing background mortality in the early stages of life, a constant mortality for middle-age individuals, and an increasing mortality with senescence. The increase in senescence mortality with body size acts as a closure term for the largest size classes, by preventing a buildup of very large individuals (Andersen et al., 2015).

## Community Characteristics

To evaluate effects of feeding characteristics of the zooplankton community on the fish community, we calculated several community-level measures. The total biomass of community $i$ was obtained by integrating the abundance in all size classes:

$$B_i(t) = \int_{w_i}^{\overline{W_i}} w N_i(w,t)\, dw. \tag{E15}$$

Similar to Blanchard et al. (2011), we defined the total throughput of community $i$ as the total consumption rate:

$$T_i(t) = \int_{w_i}^{\overline{W_i}} w V_i(w) D_i(w,t) N_i(w,t)\, dw. \tag{E16}$$

The production to biomass ratio of a community $i$ —where production was defined as the total flux out of the community from all sources of mortality (Brown et al., 2004)—was used to evaluate the total energy flux through a community:

$$PB_i(t) = \left(\int_{w_i}^{\overline{W_i}} w \mu_i(w,t) N_i(w,t) dw\right) / \left(\int_{w_i}^{\overline{W_i}} w N_i(w,t) dw\right). \tag{E17}$$

Total throughput is a measure of how energy moves internally through the system from predation processes, whereas the production to biomass ratio is an indicator of how much new biomass is produced to replace biomass lost to mortality, per unit of existing biomass. To evaluate the transfer efficiency from zooplankton to the fish community, we calculate the ratio of total fish biomass to total zooplankton biomass:

$$FZ(t) = B_F(t) / B_Z(t). \tag{E18}$$

This is similar to the approach taken in previous studies evaluating the transfer efficiency of phytoplankton to zooplankton (Friedland et al., 2012; Havens and Beaver, 2013).

We use two measures to evaluate the stability and total variability of the system. First, the nature of the system steady state was determined using the Newton–Raphson multidimensional root-finding method (Press et al., 2007). For each configuration of zooplankton feeding characteristics in this study, the abundance of the zooplankton and fish communities was taken after 20 years. The stability of this abundance was determined by the maximum real part ($\lambda_{max}$) of the eigenvalues of the Jacobian matrix calculated with the Newton–Raphson method. If $\lambda_{max} < 0$, the entire system will settle into a stable equilibrium over time where the abundance in each size-class does not fluctuate. The more negative $\lambda_{max}$ is, the faster the system will recover from local perturbations to the steady state. Alternatively, if $\lambda_{max} > 0$, over time the system will settle into a repeating, periodic traveling wave of abundance from smaller to larger size-classes. In this case, the more positive $\lambda_{max}$ is, the faster the traveling wave moves through the size classes. Second, we measured the total variability of the system by calculating the coefficient of variation (CV) of the time-series of biomass over the last 10 years of the simulation. The Newton–Raphson stability analysis and the CV work together; the first will identify if the steady state is stable or oscillating, and the CV gives a measure of the magnitude of these oscillations through time.

### Numerical Implementation

Dynamics of the zooplankton and fish communities are modeled with Equation (1), which we solve numerically using a second-order semi-implicit upwind finite difference scheme (Press et al., 2007). We present the results in $\log_{10}$ space for ease of interpretation, mathematical convenience and comparison with previous work. For the numerical implementation we discretize the dynamic size range $[10^{-5}, 10^{6}]$ into equal 0.1 $\log_{10}$ size intervals (on a $\log_{10}$ gram scale), and use a daily-time step for the time interval. We chose these values to discretize the time and weight ranges to ensure convergence in our numerical implementation without requiring unnecessary computational effort, in keeping with past studies (Press et al., 2007; Plank and Law, 2012; Zhang et al., 2013; Law et al., 2016). For simplicity we are not explicitly modeling reproduction, thus the abundances of the smallest size classes in the zooplankton and fish communities are held constant. This implies that we are assuming constant recruitment for zooplankton and fish (Law et al., 2009; Blanchard et al., 2012). The assumption of constant recruitment permits a clearer evaluation of how the feeding characteristics of the zooplankton affect the dynamics of a fish community, in keeping with previous community size-spectrum models (e.g., Benoît and Rochet, 2004; Maury et al., 2007; Law et al., 2009; Zhang et al., 2013). For the zooplankton community, the density of individuals in the smallest size class is determined from the continuation of the phytoplankton size-spectrum:

$$N_Z(w_z) = a w_z^{-b}, \tag{E12}$$

and the density of the smallest size class in the fish community is held equal to the equivalent zooplankton size class:

$$N_F(w_f, t) = N_Z(w_f, t). \tag{E13}$$

We ran each simulation for a 20-year period. In each simulation, our initial condition starts the zooplankton and fish community spectra as a continuation of the resource spectrum (Equation 11). If the solution was stable ($\lambda_{max} < 0$), there would initially be some oscillations around the steady state that would diminish over time. For a stable solution, the closer $\lambda_{max}$ was to zero the greater the initial variance and the longer it took for the system to stabilize. When the solution was a traveling wave ($\lambda_{max} > 0$), the variance of the system and magnitude of the oscillations would increase over time until the steady state was achieved. In this situation, the closer $\lambda_{max}$ was to zero, the longer the system took to find the unstable steady state. In all simulations the system achieved steady state within the first 5 years, therefore we discarded the first 10 years as a burn-in period.

## Zooplankton Are Not Fish

To establish the individual effect each of the five zooplankton feeding parameters has on the fish community, we begin with a base model where zooplankton are parameterized as another general fish community. From the base model, we build up to a model where the zooplankton community feeding characteristics are parameterized to represent a general, mixed zooplankton community. To do this, we use $m = 0$ to represent the average PPMR of a zooplankton community characterized equally by herbivorous and carnivorous feeding behavior, and set $\sigma_Z = 0.75$, $K_Z = 0.7$, $\gamma_Z = 875 \mathrm{g}^{-\alpha_Z}\mathrm{m}^{-3}\ \mathrm{year}^{-1}$, and $\alpha_Z = 1.01$ to reflect the average feeding characteristics of zooplankton across multiple functional groups.

We change each zooplankton feeding parameter one at a time, then all together, and evaluate their individual relative impact on fish community measures against the base model, by calculating the change in the measure against the base model. For example, the relative fish biomass (rFB) for a new parameterization of the zooplankton community is obtained by dividing the fish biomass from the new model by the fish biomass from the base model.

## Sensitivity Analysis

In this section, we assess how variation in the feeding characteristics of the zooplankton community affects the productivity and stability of the fish community. We focus on zooplankton feeding mode ($m$), feeding kernel width ($\sigma_Z$), and assimilation efficiency ($K_z$), since these parameters vary across different zooplankton functional groups and environmental conditions. We vary $m$ between $-3$ and 2, $\sigma_Z$ between 0.4 and 2.2, and $K_Z$ between 0.3 and 0.9.

## Mediating Primary Production and Fishing

In our final section, we assess how the feeding characteristics of different zooplankton functional groups affect the productivity and stability of the fish community, and mediate increased primary production and fishing pressure, by evaluating the effect of these changes on the average total biomass of the fish community. We use the $m$-values from Wirtz (2012) for five different zooplankton functional groups (salps, chaetognaths, herbivorous copepods, flagellates, and carnivorous copepods) and a general zooplankton community (**Table 1**). The width of the feeding kernel for each of the six groups was determined

with Fuchs and Franks' (2010) empirical Equation (Equation 3), which links the average zooplankton community PPMR with the feeding kernel width. For all groups, we hold the search rate and assimilation efficiency constant (see **Table 1**).

We used chlorophyll-*a* concentrations from two ocean basins—the North Central Pacific (0.06 mg $m^{-3}$) and the North Atlantic (high concentration, 0.28 mg $m^{-3}$)—to give a range of coefficient values (intercept of the spectrum; *a*) between 0.010 and 0.024, which corresponds to a total phytoplankton abundance in the background resource spectrum of between 0.23 and 0.55 $g^{-1}m^{-3}$. To include fishing pressure, we incorporate an additive fishing mortality term with a value between 0 and 2 $year^{-1}$, for all individuals in the fish community > 200 g.

# RESULTS

## Zooplankton Are Not Fish

The base model (denoted as the dashed line in each of the sub-plots in **Figure 3**) was a stable spectrum ($\lambda_{max}$ of −0.58), with the dynamic zooplankton and fish communities essentially a continuation of the static background spectrum in the base model.

Individually changing the zooplankton assimilation efficiency $K_Z$ from 0.6 and 0.7 (**Figure 3A**) increased the total throughput and production to biomass ratio of the fish community, in comparison to the base model (**Table 3**), and increased resilience of the entire system to local perturbations, with $\lambda_{max} = -0.71$. Increasing the zooplankton community search rate coefficient ($\gamma_Z$) from 640 to 875 ($g^{-\alpha_Z}m^{-3}\,yr^{-1}$) (**Figure 3B**), had a negligible effect on the total biomass or productivity of the fish community, compared to the based model (**Table 3**), however it did increase the stability of the system, with $\lambda_{max} = -0.76$. Changing the search rate exponent for the zooplankton community ($\alpha_Z$; **Figure 3C**) from 0.82 to 1.01 reduced the total fish biomass by almost 70%, and reduced the relative production to biomass ratio (45% decrease) and relative total throughput (87% decrease), against the base model. Updating $\gamma_Z$ decreased the resilience of the system, with $\lambda_{max} = -0.04$, however the steady state remained a stable spectrum.

Individually reducing the zooplankton feeding kernel ($\sigma_Z$; **Figure 3D**) from 1 to 0.75, and changing the PPMR (**Figure 3E**) of the zooplankton component increased the total biomass, throughput and production to biomass ratio of the fish community, in comparison to the base model (**Table 3**). Changing the PPMR of the zooplankton gave the most significant increase in relative production to biomass (75% increase) and relative total throughput (335% increase) of the fish community. Only changing the zooplankton PPMR affected the relative fish to zooplankton biomass significantly, with a 22% increase against the base model. Changing the feeding kernel width and the PPMR for the zooplankton community changed the steady state from a stable spectrum to an oscillating system. Between the two parameters, changing PPMR gave the fastest oscillations, with

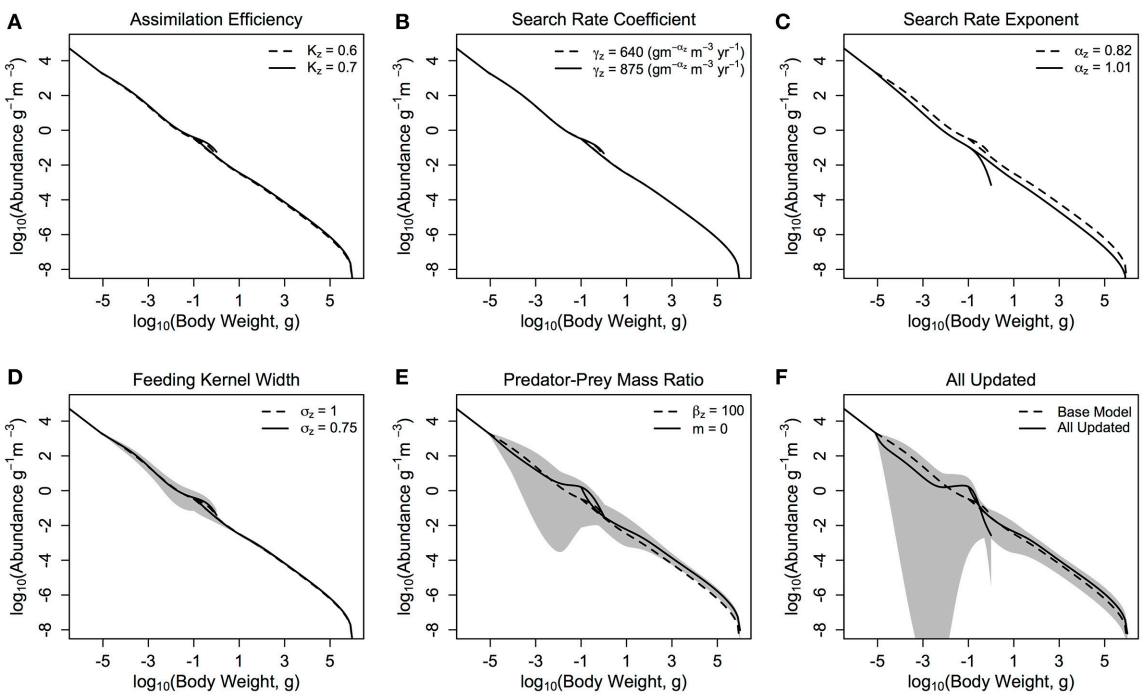


**FIGURE 3 | The zooplankton and fish community size-spectra when various parameters are updated (A–E) one at a time and (F) all together.** The dashed lines in each plot represent the zooplankton and fish communities in the base model parameterization, and the solid lines denotes the average abundance of the fish and zooplankton communities over 10 years in the modified model. The shaded areas show the regions of the traveling wave solutions over 10 years if the steady state is unstable.

**TABLE 3 | Fish community biomass (FB), fish to zooplankton biomass ratio (F:Z), fish community production to biomass ratio (P:B), and throughput (TP) relative to the base model (r), the variation in fish community biomass (coefficient of variation; CV) and the maxmium real part of the Jacobian ($\lambda_{max}$) when the zooplankton community feeding parameters are updated one at a time, and all-together.**

| | rFB | rF:Z | rP:B (Fish) | rTP (Fish) | CV (Fish) | $\lambda_{max}$ |
|---|---|---|---|---|---|---|
| Base model | 1.00 | 1.00 | 1.00 | 1.00 | 0.00 | −0.58 |
| $K_Z = 0.7$ | 1.17 | 1.00 | 1.11 | 1.35 | 0.00 | −0.71 |
| $\gamma_Z = 875$ | 0.99 | 0.96 | 1.00 | 0.99 | 0.00 | −0.76 |
| $\alpha_Z = 1.01$ | 0.34 | 0.96 | 0.55 | 0.13 | 0.00 | −0.04 |
| $\sigma_Z = 0.75$ | 1.06 | 0.95 | 1.04 | 1.13 | 0.07 | 0.24 |
| $m = 0$ | 2.27 | 1.22 | 1.75 | 4.35 | 0.28 | 0.65 |
| All changed | 1.69 | 1.44 | 1.42 | 2.40 | 0.62 | 0.47 |

*The system has a stable steady state when $\lambda_{max} < 0$, and an unstable, oscillating steady state when $\lambda_{max} > 0$.*

$\lambda_{\max} = 0.65$ compared to $\lambda_{\max} = 0.24$ for $\sigma_Z$. Further, the magnitude of the oscillations was larger when the zooplankton community PPMR was updated ($CV = 0.28$), compared to $\sigma_Z$ ($CV = 0.07$, **Table 3**, **Figures 3D,E**).

When all parameters were changed for the zooplankton community (**Figure 3F**) there were significant increases against the base model in total fish biomass (69%), the fish to zooplankton biomass ratio (44%), and the fish community production to biomass ratio and total throughput (44 and 140%, respectively). Except for the relative fish to zooplankton biomass ratio, the increase in the total fish biomass and productivity measures were lower when all the parameters were updated, compared to just updating the zooplankton PPMR. (**Table 3**) The overall system was not stable ($\lambda_{\max} = 0.47$), and the magnitude of the oscillations through the system were higher than any seen in a system with a single parameter updated, with $CV = 0.62$. However, oscillations were slower compared to the system where only zooplankton PPMR was updated.

## Sensitivity Analysis

The total biomass of the fish community increases exponentially as $m$ decreases (**Figure 4A**). From $m = 2$ to $-3$ (corresponding to an average zooplankton community PPMR range of 1—7.5), total fish biomass increases over 3 orders of magnitude (0.3 g $m^{-3}$ for $m = 2$ to 620 g $m^{-3}$ for m $= -3$). The exponential increase in fish biomass and productivity measures with respect to zooplankton PPMR starts at around $m = -0.5$, which corresponds to an average zooplankton community PPMR of 4.5. Similarly, a smaller feeding kernel width ($\sigma_Z$)—indicating a predator that feeds on a narrower size range of prey—results in an almost exponential increase in total fish community biomass (**Figure 4B**). From $\sigma_Z = 0.4$ to 1.1, total fish biomass increases from 0.25 g $m^{-3}$ to 2.9 g $m^{-3}$. There is a roughly linear, positive relationship between total fish biomass and the assimilation efficiency $K_Z$ of the zooplankton community (**Figure 4C**). As $K_Z$ increases from 0.3 to 0.9, total fish biomass increases from 0.20 to 0.65 g $m^{-3}$. Similar patterns can be seen in the relationship between zooplankton PPMR, feeding kernel width and assimilation efficiency and the fish community productivity measures (Supplementary Figure 1).

The fish to zooplankton biomass ratio peaks at around $m = 0$ (3.60), and stays around 2.9 for $m < -1$, and decreases for $m > 0.5$ to settle around 2.1 (**Figure 4D**). For $\sigma_Z$, the fish to zooplankton biomass ratio peaks at $\sigma_Z = 0.5$ around 4.8, before uniformly declining as $\sigma_Z$ increases (**Figure 4E**). There is minimal change in fish to zooplankton biomass ratio with increasing $K_Z$, which suggests zooplankton biomass and fish biomass increase at the same rate (**Figure 4F**). Except for $m > 0.5$, the fish to zooplankton biomass ratio was higher than the base model (dashed line in **Figures 4 D–F**) across the ranges of $m$, $\sigma_Z$ and $K_Z$.

With $\sigma_Z = 0.75$, the CV is zero for $m$-values above 1 (**Figure 5A**) which corresponds to a stable steady state region (**Figure 5D**). The CV increases as $m$ decreases from 0.5 to −0.5, which implies increasing variability in total fish biomass as the zooplankton community shifts from carnivorous to herbivorous feeding behavior. The CV stabilizes between 1 and 1.5 for $m < 0$. This suggests that even though the total fish community biomass is still exponentially increasing as $m$ becomes more negative, the relative variation in fish biomass through time does not increase. There is a negative relationship between increasing $\sigma_Z$ and CV, indicating increasing stability with a wider feeding kernel (**Figure 5B**). A similar pattern is observed in **Figure 5D**; the range of $m$-values that enable a stable system is larger, as $\sigma_Z$ increases. The CV of the fish community varies across the range of $K_Z$-values but within a much smaller range than the other two parameters (**Figure 5C**). Increasing $K_Z$ slightly increases the minimum $\sigma_Z$, and decreases the minimum $m$ required for a stable steady state (**Figures 5E,F**).

## Mediating Primary Production and Fishing

Our results suggest a trade-off between the stability of the overall system and the total average fish productivity and biomass for most zooplankton groups (**Figure 6** and **Table 4**). The herbivorous salp community ($m = -2.68$, PPMR $\approx 7$) is an exception (**Figure 6A**). It supports the most abundant and productive fish community, yet it is a more stable system overall than the one dominated by herbivorous copepods and chaetognaths (**Figures 6B,C**; **Table 4**). The salp community has the widest feeding kernel ($\sigma_Z = 0.70$), which suggests a wider feeding kernel gives a more stable system without sacrificing the productivity of the fish community.

A lower, increasingly negative $m$-value results in a zooplankton community with a flatter abundance spectrum. In other words, increasing herbivory results in a higher abundance in the larger zooplankton size classes. For the fish community, a shallower zooplankton spectrum leads to a higher abundance in the smallest fish size classes. The overall average slope of the fish community spectrum is similar across the 6 plots (**Figure 6**). This suggests the average slope of the fish community spectrum depends more on the feeding characteristics of the fish, over the dynamics of the zooplankton community. The total average fish biomass increases with increasing phytoplankton

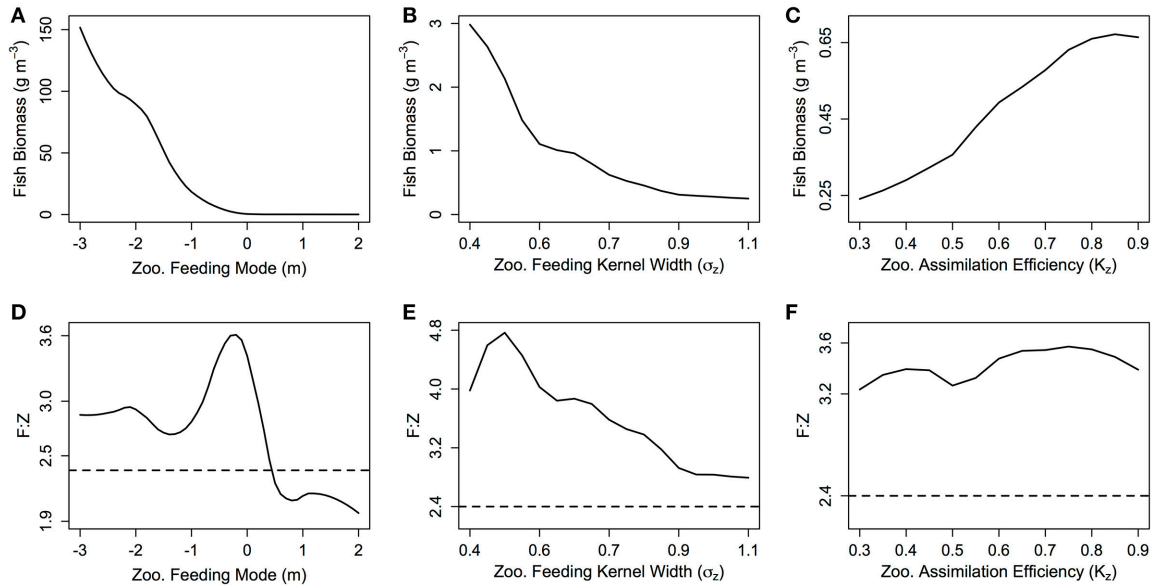


**FIGURE 4 | (A–C)** The total fish community biomass (g m$^{-3}$) and **(D–F)** the fish to zooplankton biomass ratio (F:Z) for different values of zooplankton feeding mode ($m$) , feeding kernel width ($\sigma_Z$) and assimilation efficiency ($K_Z$). In each plot, the other feeding parameters not specified are held constant at $m = 0$, $\sigma_Z = 0.75$ and $K_Z = 0.7$. The dashed line in **(D–F)** indicates the F:Z in the base model, where the zooplankton community are parameterized as fish.

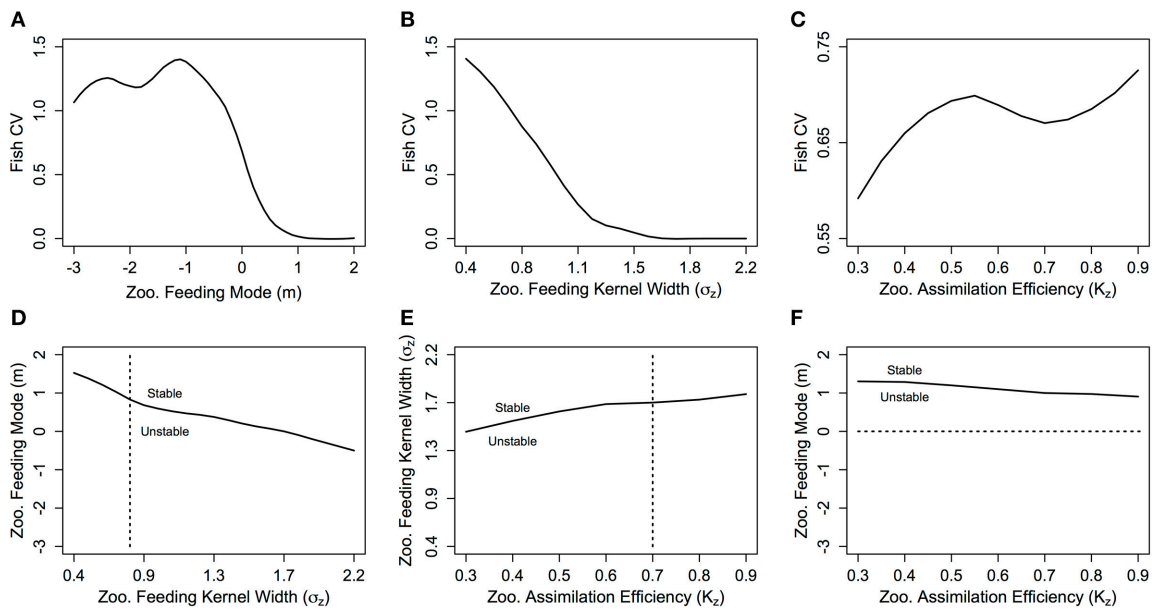


**FIGURE 5 | The fish community biomass coefficient of variation (CV) against zooplankton (A) feeding mode ($m$), (B) feeding kernel width ($\sigma_Z$) and (C) assimilation efficiency ($K_Z$), and the stability regions of (D) $m$ against $\sigma_Z$, (E) $\sigma_Z$ against $K_Z$ and (F) $m$ against $K_Z$.** In **(D–F)** the dashed lines indicate the transect over which the CV in the plot above is taken. In each plot, the other feeding parameters not specified are held constant at $m = 0$, $\sigma_Z = 0.75$ and $K_Z = 0.7$.

abundance, across all six systems (**Figure 7A**). The magnitude of the increase in fish biomass correlated with the F:Z and CV of the system (**Table 4**). More fish were associated with a higher F:Z, and lower CV. The general zooplankton community system had the highest fish to zooplankton biomass ratio (4.43) and had the largest increase in total fish abundance: an 800% increase in fish. In contrast, the herbivorous copepod and chaetognath systems had similar fish to zooplankton biomass ratios to the general community (4.40 and 3.78), but higher CV's (1.26 and 1.27). These systems' fish biomass

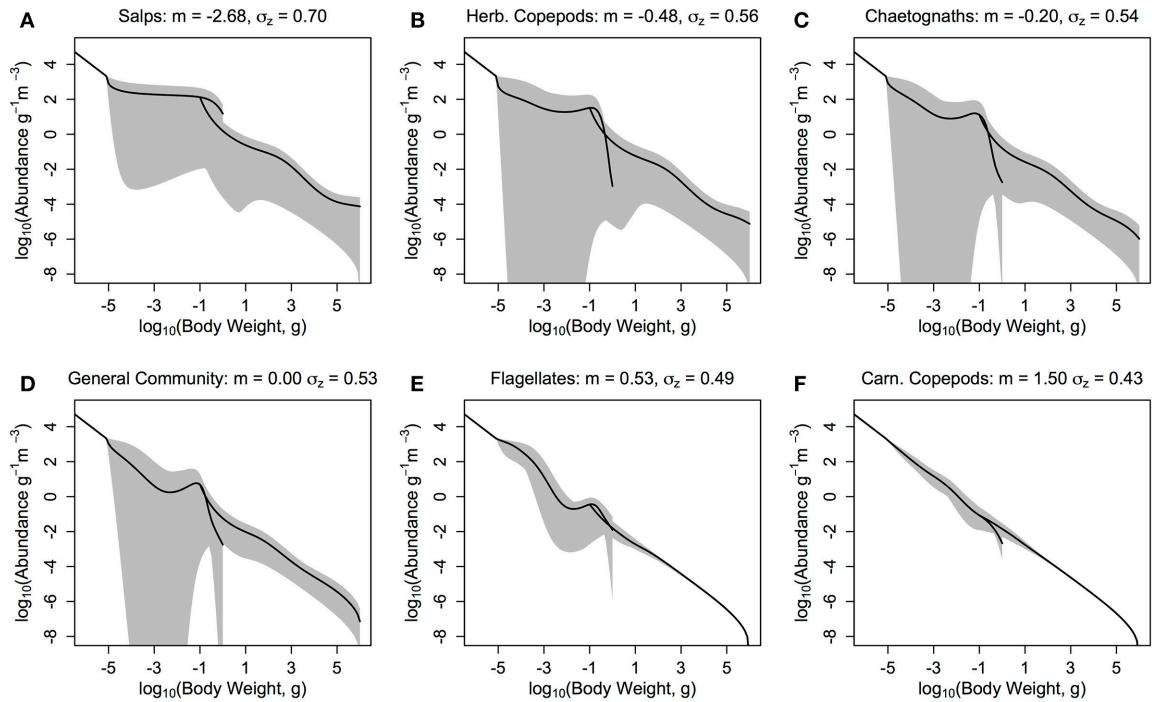


**FIGURE 6 | The zooplankton and fish community size-spectra when the zooplankton community is defined by the feeding characteristics (here, quantitative feeding mode *m*; Wirtz, 2012, and feeding kernel width $\sigma_Z$; Fuchs and Franks, 2010) of a single functional group. (A)** Salps ($m = -2.68$, $\sigma_Z = 0.70$), **(B)** Herbivorous Copepods ($m = -0.48$, $\sigma_Z = 0.56$), **(C)** Chaetognaths ($m = -0.20$, $\sigma_Z = 0.54$), **(D)** General Community ($m = 0.00$, $\sigma_Z = 0.53$), **(E)** Flagellates ($m = 0.53$, $\sigma_Z = 0.49$), and **(F)** Carnivorous Copepods ($m = 1.50$, $\sigma_Z = 0.43$). The solid lines denotes the average abundance slope of the zooplankton and fish communities over 10 years. The shaded areas show the regions of the travelling wave solutions over 10 years if the steady state is unstable.

**TABLE 4 | Fish community biomass (FB), fish to zooplankton biomass ratio (F:Z), fish community production to biomass ratio (P:B) and throughput (TP), the variation in fish community biomass (coefficient of variation; CV) and the maxmium real part of the Jacobian ($\lambda_{max}$) when the zooplankton community is defined by the feeding characteristics of different functional groups.**

| | FB | F:Z | P:B (Fish) | TP (Fish) | CV (Fish) | $\lambda_{max}$ |
|---|---|---|---|---|---|---|
| Salps and Doliolids | 133.02 | 2.86 | 366.38 | 5402.88 | 1.11 | 0.25 |
| Herb. Copepods | 13.43 | 3.79 | 73.76 | 586.25 | 1.26 | 0.67 |
| Chaetognaths | 4.33 | 4.40 | 29.77 | 69.61 | 1.27 | 0.59 |
| General | 1.40 | 4.43 | 11.84 | 8.06 | 0.97 | 0.51 |
| Flagellates | 0.20 | 1.73 | 3.13 | 0.27 | 0.11 | 0.53 |
| Carn. Copepods | 0.13 | 2.15 | 2.42 | 0.11 | 0.01 | 0.20 |

*The system has a stable steady state when $\lambda_{max} < 0$, and an unstable, oscillating steady state when $\lambda_{max} > 0$.*

increased by 340 and 410%, respectively. The flagellate system had the lowest fish to zooplankton biomass ratio (1.73), the second lowest CV (0.11) and the lowest increase in total fish biomass (170%).

Fish communities supported by herbivorous zooplankton communities were more resilient to fishing pressure, compared to fish supported by more carnivorous zooplankton (**Figure 7B**). The salp system had a negligible decline in average fish biomass, and chaetognath, herbivorous copepod and general community systems declined by up to 1, 2, 5%, respectively, with increasing fishing pressure. The two systems with carnivorous zooplankton communities (flagellates and carnivorous copepods) had an almost identical relationship between total rFB and fishing pressure, with both losing up to 15% of their average unfished biomass.

## DISCUSSION

This study is the first qualitative assessment of how zooplankton feeding characteristics mediate the transfer of energy from phytoplankton to higher trophic levels with a dynamic size-spectrum model. Improving the realism of the zooplankton community with zooplankton-specific feeding parameters increased the transfer efficiency of the system and the total mean biomass of the fish community, but changed the steady state of the system from a stable linear spectrum, to a series of traveling waves of abundance from smaller to larger size classes (**Table 3**; **Figure 3**). The change in steady state came from updating the zooplankton community PPMR and feeding kernel width ($\sigma_Z$). The general zooplankton community had a *m*-value of 0, which corresponds to a $\log_{10}$ PPMR of between 3 and 5 across the size range of the zooplankton community, and $\sigma_Z$ of 0.75. This is in contrast to the fish community $\log_{10}$ PPMR of 2, and feeding

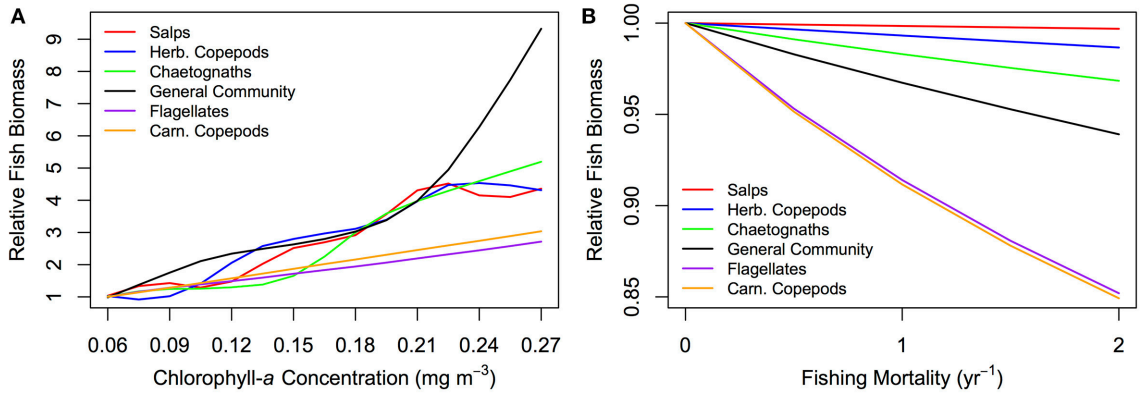


**FIGURE 7 | Relative fish biomass against (A) total phytoplankton abundance (chlorophyll-*a* concentration mg m$^{-3}$) and (B) fishing mortality (yr$^{-1}$) for fish communities supported by a zooplankton community with the feeding characteristics of different functional groups.** The relative fish biomass is calculated from the total fish biomass divided by the total fish biomass at **(A)** the lowest phytoplankton abundance (0.06 mg m$^{-3}$ chlorophyll-*a*) and **(B)** no fishing mortality (0 yr$^{-1}$).

kernel width of 1. This observed change in the steady state agrees with the observed effects of increasing PPMR and decreasing $\sigma_Z$ for fish communities (Blanchard, 2008; Law et al., 2009; Datta et al., 2011; Zhang et al., 2013).

Our results suggest a trade-off mediated by the zooplankton community, between the stability of the overall system and the total biomass and productivity of the fish community. A zooplankton community with a more generalist, carnivorous feeding strategy—defined by a lower PPMR (larger, positive $m$) and a wider feeding kernel—stabilized the steady state of the system (**Figure 5**), but the fish community was less abundant and productive (**Figure 4**). In contrast, a zooplankton community characterized by specialized, herbivorous behavior—defined by a higher PPMR (larger, negative $m$) and a narrower feeding kernel—increased the total average biomass and productivity of the fish community (**Figure 4**), but destabilized the system steady state (**Figure 5**). Herbivorous and mixed communities ($m \leq 0$) with a narrower $\sigma_Z$ had a higher ratio of fish to zooplankton biomass (**Figures 4D,E**), indicating a more efficient transfer of biomass from zooplankton to fish. This positive relationship between the zooplankton community PPMR and transfer efficiency corroborates with previous theoretical (Andersen et al., 2009) and empirical work (Jennings et al., 2002; Barnes et al., 2010); a higher PPMR yields a higher transfer efficiency between trophic levels, and fewer trophic levels separating phytoplankton from fish.

Zooplankton communities with a higher PPMR and narrower $\sigma_Z$ had more variance in their abundance (**Figure 5**). These results suggest the abundance of zooplankton communities characterized by specialized herbivorous feeding behavior could exhibit more variation in their abundance than carnivorous communities. A similar relationship for fish species was found by Blanchard (2008), who established a link between the variation in fisheries catch of certain species of fish with their PPMR and $\sigma$; species with a higher PPMR and narrower feeding kernel had greater variability in their fishing catch through time. Further, Jennings and Warr (2003) identified a link between environmental stability and a smaller ecosystem average PPMR, which in this context means increasing herbivory amongst zooplankton in unstable environments. Such a relationship has been observed in marine ecosystems; herbivorous zooplankton dominate in unstable coastal and upwelling regions, whereas more carnivorous zooplankton are abundant in the open ocean (Raymont, 1980).

The resilience of the fish community to fishing pressure increased, and ecosystems became more efficient in mediating energy from phytoplankton to fish, when zooplankton communities had a larger $\sigma_Z$ and higher PPMR characteristic of more herbivorous functional groups (**Figure 7**). The relationship between zooplankton community feeding characteristics, and the resilience of the fish community and ecosystem transfer efficiency, has potential implications for the marine environment under climate change. The world ocean's oligotrophic regions are expected to expand as a result of climate change (Doney et al., 2012; Sarmiento et al., 2004; Polovina et al., 2008). Food chains in warmer, oligotrophic oceans are traditionally believed to be longer than other regions, as a result of the dominance of smaller phytoplankton (Sprules and Munawar, 1986; Irwin et al., 2006; Morán et al., 2010), which would result in lower rates of energy transfer from primary producers to higher trophic levels. Further, recent studies suggest possible climate-driven shifts in the dominance of certain zooplankton functional groups, such as salps or jellyfish (Atkinson et al., 2004; Richardson et al., 2009; Schofield et al., 2010). Our results indicate that, everything else being equal, an increase in the dominance of carnivorous zooplankton groups could further decrease the transfer efficiency of expanding oligotrophic regions. Conversely, an increase in the abundance of herbivorous groups with a large PPMR, such as salps or herbivorous copepods, could decrease the number of trophic levels between phytoplankton and fish and thereby increase the transfer efficiency of these future oligotrophic regions.

Overall, increasing the zooplankton community PPMR had the greatest effect on increasing the total abundance, productivity and resilience of the fish community (**Figures 4**, **7**), and increasing $\sigma_Z$ had the greatest stabilizing effect on the steady state of the system (**Figure 5**). Zooplankton have a higher average PPMR and smaller $\sigma_Z$ in comparison to average observed values for fish and this difference has enormous implications for ecosystem transfer efficiency and stability (Barnes et al., 2010). This means that zooplankton feeding characteristics—in particular PPMR and feeding kernel width—are a critical component to consider moving forward in how the transfer of energy from primary production to higher trophic levels is resolved in marine ecosystem models. This agrees with Jennings and Collingridge (2015), who suggest that a poor understanding of energy transfer in lower trophic levels is a potential cause for the order of magnitude discrepancy between model predictions and observed mesopelagic fish biomass over large spatial scales (Davison et al., 2013; Irigoien et al., 2014).

The large changes in fish biomass and productivity as a result of changes in the zooplankton community lead us to assess the implications of assuming a constant phytoplankton abundance spectrum within the model. In this study, we assume no feedbacks on the phytoplankton community from zooplankton (i.e., predation), however we know from empirical studies that the slope of the phytoplankton spectrum does change. The phytoplankton spectrum is shallower in eutrophic, upwelling systems—indicating a higher abundance of larger individuals such as diatoms—and steeper in oligotrophic systems where small-celled phytoplankton dominate (Sprules and Munawar, 1986; Irwin et al., 2006). The effects of eutrophy or oligotrophy on higher trophic levels could be investigated by varying not only the intercept, but also the slope of the phytoplankton community and incorporating feedback from zooplankton predation.

Our model did not investigate how changes in the body composition of different zooplankton functional groups affects energy transfer from phytoplankton to fish. Gelatinous zooplankton have around one-tenth of the carbon content per unit of live mass compared to non-gelatinous plankton (Kiørboe, 2013) and carbon content as a proportion of weight scales isometrically with increasing body size for carnivorous zooplankton (e.g., ctenophores and cnidarians), but decreases for filter feeders such as salps (Molina-Ramírez et al., 2015). This would have implications for the nutritional value of different zooplankton groups for the fish community, and the fish community's resultant growth rates. Future work could investigate the effect zooplankton body composition might have on energy transfer, by varying the assimilation efficiency of the fish community for different zooplankton functional groups.

Looking forward, theoretical studies have shown that including more traits than just individual body size increases the stability of the size-spectrum (Datta et al., 2011; Zhang et al., 2013) and improves the realism of modeled predator-prey dynamics (Boukal, 2014). Recent developments in dynamic size-spectrum theory now allow multiple functional groups and even species to be resolved within the community spectrum (Maury, 2010; Hartvig et al., 2011; Scott et al., 2014) and have been used to represent actual fish communities with increasing realism (e.g., Blanchard et al., 2014; Dueri et al., 2014; Spence et al., 2016; Zhang et al., 2016). The instabilities in our single-spectrum zooplankton community indicate that more complexity is needed if we are to represent realistic zooplankton communities within a dynamic size-spectrum framework. We envision the next steps toward this goal would involve a functional group approach, where the unique size-based characteristics of multiple size-based zooplankton communities are represented, and the model is calibrated and compared with real-world data. The growing literature on the size-based behavior of zooplankton functional groups—coupled with the recent theoretical developments in dynamic size-spectrum modeling—means size-spectrum models that realistically resolve both zooplankton and fish may now be within reach.

## CONCLUDING REMARKS

In present size-spectrum model formulations focused on fish, small zooplankton are lumped together with phytoplankton in a background resource spectrum, and large zooplankton are represented as fish. The results of this study clearly demonstrate what we already know to be true: zooplankton are not fish, and nor are they phytoplankton. Current formulations that do not resolve the unique feeding characteristics of zooplankton are neglecting a significant factor in how energy is transferred from phytoplankton to fish. The results of this study motivate further work toward increasing the realism of zooplankton processes in size-spectrum models, and end-to-end marine ecosystem models more broadly.

## AUTHOR CONTRIBUTIONS

All authors were involved in conceiving the original idea for this study. JB provided code from past size-spectrum modeling studies. RH undertook the literature review to obtain zooplankton-specific feeding parameters, constructed the model, conducted the analysis, and wrote the manuscript, with input from AR, JB, and JE.

## ACKNOWLEDGMENTS

We thank Kai Wirtz for being available to answer questions about his mechanistic zooplankton feeding equations. We also thank Iain Suthers for helpful comments about the assumptions underlying our model, from a biological perspective. This study was supported by an Australian Research Council Discovery Grant (DP150102656).

## SUPPLEMENTARY MATERIAL

The Supplementary Material for this article can be found online at: http://journal.frontiersin.org/article/10.3389/fmars.2016.00201

## REFERENCES


Abe, Y., Natsuike, M., Matsuno, K., Terui, T., Yamaguchi, A., and Imai, I. (2013). Variation in assimilation efficiencies of dominant Neocalanus and Eucalanus copepods in the subarctic Pacific: consequences for population structure models. *J. Exp. Mar. Biol. Ecol.* 449, 321–329. doi: 10.1016/j.jembe.2013.10.023

Andersen, K. H., Berge, T., Gonçalves, R. J., Hartvig, M., Heuschele, J., Hylander, S., et al. (2016). Characteristic sizes of life in the oceans, from bacteria to whales. *Ann. Rev. Mar. Sci.* 8, 1–25. doi: 10.1146/annurev-marine-122414-034144

Andersen, K. H., Beyer, J. E., and Lundberg, P. (2009). Trophic and individual efficiencies of size-structured communities. *Proc. Biol. Sci.* 276, 109–114. doi: 10.1098/rspb.2008.0951

Andersen, K. H., Jacobsen, N. S., Life, O., Resources, A., Castle, C., Security, G. F., et al. (2015). The theoretical foundations for size-spectrum models of fish communities. *Can. J. Fish. Aquat. Sci.* 588, 1–47. doi: 10.1139/cjfas-2015-0230

Andersen, K. H., and Pedersen, M. (2010). Damped trophic cascades driven by fishing in model marine ecosystems. *Proc. R. Soc. B Biol. Sci.* 277, 795–802. doi: 10.1098/rspb.2009.1512

Atkinson, A., Siegel, V., Pakhomov, E. and Rothery, P. (2004). Long-term decline in krill stock and increase in salps within the Southern Ocean. *Nature* 432, 100–103. doi: 10.1038/nature02950.1

Baird, M. E., and Suthers, I. M. (2006). A size-resolved pelagic ecosystem model. *Ecol. Model.* 3, 185–203. doi: 10.1016/j.ecolmodel.2006.11.025

Banas, N. S. (2011). Adding complex trophic interactions to a size-spectral plankton model: emergent diversity patterns and limits on predictability. *Ecol. Model.* 222, 2663–2675. doi: 10.1016/j.ecolmodel.2011.05.018

Barange, M., Merino, G., Blanchard, J. L., Scholtens, J., Harle, J., Allison, E. H., et al. (2014). Impacts of climate change on marine ecosystem production in societies dependent on fisheries. *Nat. Clim. Change* 4, 211–216. doi: 10.1038/nclimate2119

Barnes, C., Irigoien, X., De Oliveira, J. A. A., Maxwell, D., and Jennings, S. (2011). Predicting marine phytoplankton community size structure from empirical relationships with remotely sensed variables. *J. Plankton Res.* 33, 13–24. doi: 10.1093/plankt/fbq088

Barnes, C., Maxwell, D., Reuman, D. C., and Jennings, S. (2010). Global patterns in predator-prey size relationships reveal size dependency of trophic transfer efficiency. *Ecology* 91, 222–232. doi: 10.1890/08-2061.1

Benoît, E., and Rochet, M.-J. (2004). A continuous model of biomass size-spectra governed by predation and the effects of fishing on them. *J. Theor. Biol.* 226, 9–21. doi: 10.1016/S0022-5193(03)00290-X

Blanchard, J. L. (2008). *The Dynamics of Size-Structured Ecosystems*. Ph.D. dissertation, University of York.

Blanchard, J. L., Andersen, K. H., Scott, F., Hintzen, N. T., Piet, G., and Jennings, S. (2014). Evaluating targets and trade-offs among fisheries and conservation objectives using a multispecies size-spectrum model. *J. Appl. Ecol.* 51, 612–622. doi: 10.1111/1365-2664.12238

Blanchard, J. L., Jennings, S., Holmes, R., Harle, J., Merino, G., Allen, J. I., et al. (2012). Potential consequences of climate change for primary production and fish production in large marine ecosystems. *Philos. Trans. R. Soc. B Biol. Sci.* 367, 2979–2989. doi: 10.1098/rstb.2012.0231

Blanchard, J. L., Jennings, S., Law, R., Castle, M. D., McCloghrie, P., Rochet, M. J., et al. (2009). How does abundance scale with body size in coupled size-structured food webs? *J. Anim. Ecol.* 78, 270–280. doi: 10.1111/j.1365-2656.2008.01466.x

Blanchard, J. L., Law, R., Castle, M. D., and Jennings, S. (2011). Coupled energy pathways and the resilience of size-structured food webs. *Theor. Ecol.* 4, 289–300. doi: 10.1007/s12080-010-0078-9

Boukal, D. S. (2014). Trait- and size-based descriptions of trophic links in freshwater food webs: current status and perspectives. *J. Limnol.* 73, 171–185. doi:10.4081/jlimnol.2014.826

Brown, J. H., Gillooly, J. F., Allen, A. P., Savage, V. M., and West, G. B. (2004). Toward a metabolic theory of ecology. *Ecology* 85, 1771–1789. doi: 10.1890/03-9000

Carlotti, F., and Poggiale, J. C. (2010). Towards methodological approaches to implement the zooplankton component in "end to end" food-web models. *Prog. Oceanogr.* 84, 20–38. doi: 10.1016/j.pocean.2009.09.003

Datta, S., Delius, G. W., and Law, R. (2010). A jump-growth model for predator-prey dynamics: derivation and application to marine ecosystems. *Bull. Math. Biol.* 72, 1361–1382. doi: 10.1007/s11538-009-9496-5

Datta, S., Delius, G. W., Law, R., and Plank, M. J. (2011). A stability analysis of the power-law steady state of marine size-spectra. *J. Math. Biol.* 63, 779–799. doi: 10.1007/s00285-010-0387-z

Davison, P. C., Checkley, D. M., Koslow, J. A., and Barlow, J. (2013). Carbon export mediated by mesopelagic fishes in the northeast Pacific Ocean. *Prog. Oceanogr.* 116, 14–30. doi: 10.1016/j.pocean.2013.05.013

Doney, S. C., Ruckelshaus, M., Duffy E. J., Barry, J. P., Chan, F., English, C. A., et al. (2012). Climate change impacts on marine ecosystems. *Estuaries* 25, 149–164. doi: 10.1146/annurev-marine-041911-111611

Dueri, S., Bopp, L., and Maury, O. (2014). Projecting the impacts of climate change on skipjack tuna abundance and spatial distribution. *Glob. Chang. Biol.* 20, 742–753. doi: 10.1111/gcb.12460

Friedland, K. D., Stock, C., Drinkwater, K. F., Link, J. S., Leaf, R. T., Shank, B. V., et al. (2012). Pathways between primary production and fisheries yields of large marine ecosystems. *PLoS ONE* 7:e28945. doi: 10.1371/journal.pone.0028945

Fuchs, H. L., and Franks, P. J. S. (2010). Plankton community properties determined by nutrients and size-selective feeding. *Mar. Ecol. Prog. Ser.* 413, 1–15. doi: 10.3354/meps08716

Goldman, J. C., and Dennett, M. R. (1990). Dynamics of prey selection by an omnivorous flagellate. *Mar. Ecol. Prog. Ser.* 59, 183–194. doi: 10.3354/meps059183

Guiet, J., Aumont, O., Poggiale, J.-C., and Maury, O. (2016a). Effects of lower trophic level biomass and water temperature on fish communities: a modeling study. *Prog. Oceanogr.* 146, 22–37. doi: 10.1016/j.pocean.2016.04.003

Guiet, J., Poggiale, J.-C., and Maury, O. (2016b). Modelling the community size-spectrum: recent developments and new directions. *Ecol. Model.* 337, 4–14. doi: 10.1016/j.ecolmodel.2016.05.015

Hall, S. J., Collie, J. S., Duplisea, D. E., Jennings, S., Bravington, M., and Link, J. (2006). A length-based multispecies model for evaluating community responses to fishing. *Can. J. Fish. Aquat. Sci.* 63, 1344–1359. doi: 10.1139/f06-039

Hansen, B., Bjørnsen, P. K., and Hansen, P. J. (1994). The size ratio between planktonic predators and their prey. *Limnol. Oceanogr.* 39, 395–403. doi: 10.4319/lo.1994.39.2.0395

Hartvig, M., Andersen, K. H., and Beyer, J. E. (2011). Food web framework for size-structured populations. *J. Theor. Biol.* 272, 113–122. doi: 10.1016/j.jtbi.2010.12.006

Havens, K. E., and Beaver, J. R. (2013). Zooplankton to phytoplankton biomass ratios in shallow Florida lakes: an evaluation of seasonality and hypotheses about factors controlling variability. *Hydrobiologia* 703, 177–187. doi: 10.1007/s10750-012-1357-9

Irigoien, X., Klevjer, T. A., Røstad, A., Martinez, U., Boyra, G., Acuña, J. L., et al. (2014). Large mesopelagic fishes biomass and trophic efficiency in the open ocean. *Nat. Commun.* 5, 3271. doi: 10.1038/ncomms4271

Irwin, A. J., Finkel, Z. V., Schofield, O. M. E., and Falkowski, P. G. (2006). Scaling-up from nutrient physiology to the size-structure of phytoplankton communities. *J. Plankton Res.* 28, 459–471. doi: 10.1093/plankt/fbi148

Jacobsen, N. S., Gislason, H., and Andersen, K. H. (2014). The consequences of balanced harvesting of fish communities. *Proc. Biol. Sci.* 281:20132701. doi: 10.1098/rspb.2013.2701

Jennings, S., and Collingridge, K. (2015). Predicting consumer biomass, size-structure, production, catch potential, responses to fishing and associated uncertainties in the world's marine ecosystems. *PLoS ONE* 10:e0133794. doi: 10.1371/journal.pone.0133794

Jennings, S., Pinnegar, J. K., Polunin, N. V. C., and Boon, T. W. (2001). Weak cross-species relationships between body size and trophic level belie powerful size-based trophic structuring in fish communities. *J. Anim. Ecol.* 70, 934–944. doi: 10.1046/j.0021-8790.2001.00552.x

Jennings, S., and Warr, K. J. (2003). Smaller predator-prey body size ratios in longer food chains. *Proc. Biol. Sci.* 270, 1413–1417. doi: 10.1098/rspb.2003.2392

Jennings, S., Warr, K. J., and Mackinson, S. (2002). Use of size-based production and stable isotope analyses to predict trophic transfer efficiencies and predator-prey body mass ratios in food webs. *Mar. Ecol. Prog. Ser.* 240, 11–20. doi: 10.3354/meps240011

Kiørboe, T. (2008). *A Mechanistic Approach to Plankton Ecology*. Princeton, NJ: Princeton University Press.

Kiørboe, T. (2011). How zooplankton feed: mechanisms, traits and trade-offs. *Biol. Rev.* 86, 311–339. doi: 10.1111/j.1469-185X.2010.00148.x

Kiørboe, T. (2013). Zooplankton body composition. *Limnol. Oceanogr.* 58, 1843–1850. doi: 10.4319/lo.2013.58.5.1843

Landry, M. R. (1981). Switching between herbivory and carnivory by the planktonic marine copepod *Calanus pacificus*. *Mar. Biol.* 65, 77–82. doi: 10.1007/BF00397070

Landry, M. R., Hassett, R. P., Fagerness, V., Downs, J., and Lorenzen, C. J. (1984). Effect of food acclimation on assimilation efficiency of *Calanus pacificus*. *Limnol. Oceanogr.* 29, 361–364. doi: 10.4319/lo.1984.29.2.0361

Law, R., Plank, M. J., James, A., and Blanchard, J. L. (2009). Size-spectra dynamics from stochastic predation and growth of individuals. *Ecology* 90, 802–811. doi: 10.1890/07-1900.1

Law, R., Plank, M. J., and Kolding, J. (2016). Balanced exploitation and coexistence of interacting, size-structured, fish species. *Fish Fish.* 17, 281–302. doi: 10.1111/faf.12098

Lefort, S., Aumont, O., Bopp, L., Arsouze, T., Gehlen, M., and Maury, O. (2015). Spatial and body-size dependent response of marine pelagic communities to projected global climate change. *Glob. Chang. Biol.* 21, 154–164. doi: 10.1111/gcb.12679

Le Mézo, P., Lefort, S., Séférian, R., Aumont, O., Maury, O., Murtugudde, R., et al. (2016). Natural variability of marine ecosystems inferred from a coupled climate to ecosystem simulation. *J. Mar. Syst.* 153, 55–66. doi: 10.1016/j.jmarsys.2015.09.004

Maury, O. (2010). An overview of APECOSM, a spatialized mass balanced "Apex Predators ECOSystem Model" to study physiologically structured tuna population dynamics in their ecosystem. *Prog. Oceanogr.* 84, 113–117. doi:10.1016/j.pocean.2009.09.013

Maury, O., Faugeras, B., Shin, Y.-J., Poggiale, J.-C., Ari, T. B., and Marsac, F. (2007). Modeling environmental effects on the size-structured energy flow through marine ecosystems. Part 1: the model. *Prog. Oceanogr.* 74, 479–499. doi: 10.1016/j.pocean.2007.05.002

Mitra, A., and Davis, C. (2010). Defining the 'to' in end-to-end models. *Prog. Oceanog.* 84, 39–42. doi: 10.1016/j.pocean.2009.09.004

Montagnes, D. J. S., and Fenton, A. (2012). Prey-abundance affects zooplankton assimilation efficiency and the outcome of biogeochemical models. *Ecol. Model.* 243, 1–7. doi: 10.1016/j.ecolmodel.2012.05.006

Molina-Ramírez, A., Cáceres, C., Romero-Romero, S., Bueno, J., González-Gordillo, J. I., Irigoien, X., et al. (2015). Functional differences in the allometry of the water, carbon and nitrogen content of gelatinous organisms. *J. Plankton Res.* 37, 989–1000. doi: 10.1093/plankt/fbv037

Morán, X. A. G., López-Urrutia, Á., Calvo-Díaz, A., and Li, W. K. W. (2010). Increasing importance of small phytoplankton in a warmer ocean. *Glob. Change Biol.* 16, 1137–1144. doi: 10.1111/j.1365-2486.2009.01960.x

Peters, R. H. (1983). *The Ecological Implications of Body Size*. Cambridge: Cambridge University Press.

Plank, M. J., and Law, R. (2012). Ecological drivers of stability and instability in marine ecosystems. *Theor. Ecol.* 5, 465–480. doi: 10.1007/s12080-011-0137-x

Polovina, J. J., Howell, E. A., and Abecassis, M. (2008). Ocean's least productive waters are expanding. *Geophys. Res. Lett.* 35, 2–6. doi: 10.1029/2007GL031745

Press, W. H., Teukolsky, S. A., Vetterling, W. T., and Flannery, B. P. (2007). *Numerical Recipes: The Art of Scientific Computing, 3rd Edn*. New York, NY: Cambridge University Press.

Raymont, J. E. G. (1980). *Plankton and Productivity in the Oceans: Vol. 1, Phytoplankton, 2nd End.* Oxford, UK: Pergamon Press Ltd.

Richardson, A. J., Bakun, A., Hays, G. C., and Gibbons, M. J. (2009). The jellyfish joyride: causes, consequences and management responses to a more gelatinous future. *Trends Ecol. Evol.* 24, 312–322. doi: 10.1016/j.tree.2009.01.010

Rogers, A., Blanchard, J. L., and Mumby, P. J. (2014). Vulnerability of coral reef fisheries to a loss of structural complexity. *Curr. Biol.* 24, 1000–1005. doi: 10.1016/j.cub.2014.03.026

Rousseaux, C. S., and Gregg, W. W. (2015). Recent decadal trends in global phytoplankton composition. *Glob. Biogeochem. Cycles* 29, 1674–1688. doi: 10.1002/2015GB005139

Saiz, E., and Kiørboe, T. (1995). Predatory and suspension feeding of the copepod *Acartia tonsa* in turbulent environments. *Mar. Ecol. Prog. Ser.* 122, 147–158. doi: 10.3354/meps122147

Sarmiento, J. L., Slater, R., Barber, R., Bopp, L., Doney, S. C., Hirst, A. C., et al. (2004). Response of ocean ecosystems to climate warming. *Glob. Biogeochem. Cycles* 18:GB3003. doi: 10.1029/2003GB002134

Schofield, O., Ducklow, H. W., Martinson, D. G., Meredith, M. P., Moline, M. A., and Fraser, W. R. (2010). How do polar marine ecosystems respond to rapid climate change? *Science* 328, 1520–1523. doi: 10.1126/science.1185779

Scott, F., Blanchard, J. L., and Andersen, K. H. (2014). mizer: an R package for multispecies, trait-based and community size-spectrum ecological modelling. *Methods Ecol. Evol.* 5, 1121–1125. doi: 10.1111/2041-210X.12256

Sheldon, R. W., Evelen, T. P. T., and Parsons, T. R. (1967). On the occurrence and formation of small particles in seawater. *Limnol. Oceanogr.* 7, 367–375.

Spence, M. A., Blackwell, P. G., and Blanchard, J. L. (2016). Parameter uncertainty of a dynamic multi-species size-spectrum model. *Can. J. Fish. Aquat. Sci.* 9, 1–9. doi: 10.1139/cjfas-2015-0022

Sprules, W. G., and Munawar, M. (1986). Plankton size-spectra in relation to ecosystem productivity, size, and perturbation. *Can. J. Fish. Aquat. Sci.* 43, 1789–1794. doi: 10.1139/f86-222

Stock, C. A., Powell, T. M., and Levin, S. A. (2008). Bottom-up and top-down forcing in a simple size-structured plankton dynamics model. *J. Mar. Syst.* 74, 134–152. doi: 10.1016/j.jmarsys.2007.12.004

Ward, B. A., Dutkiewicz, S., and Follows, M. J. (2014). Modelling spatial and temporal patterns in size-structured marine plankton communities: top-down and bottom-up controls. *J. Plankton Res.* 36, 31–47. doi: 10.1093/plankt/fbt097

Ward, B. A., Dutkiewicz, S., Jahn, O., and Follows, M. J. (2012). A size-structured food-web model for the global ocean. *Limnol. Oceanogr.* 57, 1877–1891. doi: 10.4319/lo.2012.57.6.1877

Wirtz, K. W. (2012). Who is eating whom? Morphology and feeding type determine the size relation between planktonic predators and their ideal prey. *Mar. Ecol. Prog. Ser.* 445, 1–12. doi: 10.3354/meps09502

Wirtz, K. W. (2014). A biomechanical and optimality-based derivation of prey-size dependencies in planktonic prey selection and ingestion rates. *Mar. Ecol. Prog. Ser.* 507, 81–94. doi: 10.3354/meps10894

Woodward, G., Ebenman, B., Emmerson, M., Montoya, J. M., Olesen, J. M., Valido, A., et al. (2005). Body size in ecological networks. *Trends Ecol. Evol.* 20, 402–409. doi: 10.1016/j.tree.2005.04.005

Woodworth-Jefcoats, P. A., Polovina, J. J., Dunne, J. P., and Blanchard, J. L. (2013). Ecosystem size structure response to 21st century climate projection: large fish abundance decreases in the central North Pacific and increases in the California Current. *Glob. Chang. Biol.* 19, 724–733. doi: 10.1111/gcb.12076

Zhang, C., Chen, Y., and Ren, Y. (2015). Assessing uncertainty of a multispecies size-spectrum model resulting from process and observation errors. *ICES J. Mar. Sci.* 72, 2223–2233. doi: 10.1093/icesjms/fsv086

Zhang, C., Chen, Y., and Ren, Y. (2016). An evaluation of implementing long-term MSY in ecosystem-based fisheries management: incorporating trophic interaction, bycatch and uncertainty. *Fish. Res.* 174, 179–189. doi: 10.1016/j.fishres.2015.10.007

Zhang, L., Thygesen, U. H., Knudsen, K., and Andersen, K. H. (2013). Trait diversity promotes stability of community dynamics. *Theor. Ecol.* 6, 57–69. doi: 10.1007/s12080-012-0160-6

Zhou, M. (2006). What determines the slope of a plankton biomass spectrum? *J. Plankton Res.* 28, 437–448. doi: 10.1093/plankt/fbi119

Zhou, M., Carlotti, F., and Zhu, Y. (2010). A size-spectrum zooplankton closure model for ecosystem modelling. *J. Plankton Res.* 32, 1147–1165. doi: 10.1093/plankt/fbq054

**Conflict of Interest Statement:** The authors declare that the research was conducted in the absence of any commercial or financial relationships that could be construed as a potential conflict of interest.

frontiers in Marine Science

ORIGINAL RESEARCH
published: 23 September 2016
doi: 10.3389/fmars.2016.00185

# Impacts of Intraguild Predation on Arctic Copepod Communities

*Karolane Dufour[1]*, Frédéric Maps[1], Stéphane Plourde[2], Pierre Joly[2] and Frédéric Cyr[3]*

*[1] Takuvik Joint International Laboratory, Université Laval (Canada) – Centre National de la Recherche Scientifique (France), Québec-Océan and Département de Biologie at Université Laval, Québec, QC, Canada, [2] Institut Maurice-Lamontagne, Department of Fisheries and Oceans Canada, Mont-Joli, QC, Canada, [3] Aix-Marseille Université, Université de Toulon, Centre National de la Recherche Scientifique/INSU, IRD, Mediterranean Institute of Oceanography, UM 110, Marseille, France*

Communities of large copepods form an essential hub of matter and energy fluxes in Arctic marine food webs. Intraguild predation on eggs and early larval stages occurs among the different species of those communities and it has been hypothesized to impact its structure and function. In order to better understand the interactions between dominant copepod species in the Arctic, we conducted laboratory experiments that quantified intraguild predation between the conspicuous and omnivorous *Metridia longa* and the dominant *Calanus hyperboreus*. We recorded individual egg ingestion rates for several conditions of temperature, egg concentration, and alternative food presence. In each of these experiments, at least some females ingested eggs but individual ingestion rates were highly variable. The global mean ingestion rate of *M. longa* on *C. hyperboreus* eggs was 5.8 eggs ind$^{-1}$ d$^{-1}$, or an estimated 37% of *M. longa* daily metabolic need. Among the different factors tested and the various individual traits considered (prosome length, condition index), only the egg concentration had a significant and positive effect on ingestion rates. We further explored the potential ecological impacts of intraguild predation in a simple 1D numerical model of *C. hyperboreus* eggs vertical distribution in the Amundsen Gulf. Our modeling results showed an asymmetric relationship in that *M. longa* has little potential impact on the recruitment of *C. hyperboreus* (<3% egg standing stock removed by IGP at most) whereas the eggs intercepted by the former can account for a significant portion of its metabolic requirement during winter (up to a third).

**Keywords: intraguild predation, copepods, *Metridia longa*, *Calanus hyperboreus*, Arctic regions, numerical modeling**

OPEN ACCESS

***Edited by:***
*Susanne Menden-Deuer, University of Rhode Island, USA*

***Reviewed by:***
*Jose M. Riascos, Universidad del Valle, Colombia*
*Øyvind Fiksen, University of Bergen, Norway*

****Correspondence:***
*Karolane Dufour*
*karolane.dufour@gmail.com*

***Specialty section:***
*This article was submitted to Marine Ecosystem Ecology, a section of the journal Frontiers in Marine Science*

***Received:*** *29 July 2016*
***Accepted:*** *09 September 2016*
***Published:*** *23 September 2016*

***Citation:***
*Dufour K, Maps F, Plourde S, Joly P and Cyr F (2016) Impacts of Intraguild Predation on Arctic Copepod Communities. Front. Mar. Sci. 3:185. doi: 10.3389/fmars.2016.00185*

## INTRODUCTION

Arctic and subarctic marine food webs are characterized by the presence of large calanoid copepods that channel primary production toward secondary consumers. Copepods have developed life cycle strategies that allow them to thrive in these highly seasonal environments. In the Arctic Ocean, several species of *Calanus* dominate the mesozooplankton biomass (Head et al., 2003; Hopcroft et al., 2010). During the short productive period in spring and summer, copepods feed on ice algae (when available in ice-covered regions) and phytoplankton and concentrate this energy into lipids, mostly stored as wax ester in hypertrophied oil sacs (Lee et al., 2006). In winter, they survive thanks to those lipid reserves that fuel their reduced metabolism during an extended period of dormancy

(the diapause). All year long, copepods are an essential food source for many predators such as bowhead whale, little auk, and above all Arctic cod, a cornerstone component of the Arctic food web (Fort et al., 2010; Falardeau et al., 2013; Pomerleau et al., 2014). Thus, communities of large copepods form a critical hub of matter and energy fluxes in Arctic and subarctic marine food webs.

In the Arctic, copepod community biomass is mainly composed of the large species *Calanus hyperboreus* and *Calanus glacialis* (adult female median prosome length of 6.7 and 4.1 mm, respectively), the medium-sized *Metridia longa* (2.8 mm) and the small *Pseudocalanus* spp. (1.1 mm) (Darnis et al., 2012). Following the current dynamics, the boreal species *C. finmarchicus* is also regularly found in marginal Arctic seas, especially in the eastern Greenland Sea and Barents Sea (Conover and Huntley, 1991). Moreover, *C. finmarchicus*' biogeographic distribution in the surface layer is projected to move even farther northward in response to surface circulation and temperature forcing induced by climate change (Reygondeau and Beaugrand, 2011). The structure and functions of copepod communities are critical from an energetic point of view for marine ecosystems and depend on the actual assemblage of species. From one species to the other, the oil sac size is different and therefore the energetic content differs. *C. hyperboreus* and *C. glacialis* are bigger and contain more lipids than the boreal *C. finmarchicus*. Consequently, many small visual predators such as fish larvae and juveniles, would reap a larger energetic reward for a similar harvesting effort, making these Arctic copepod species the preys of choice. Hence, changes in the assemblage of copepods communities could impact marine predators' recruitment, resulting in a form of bottom-up control (Mills et al., 2013; Greene and Pershing, 2014). For example, along the West coast of the Spitsbergen island in the Svalbard archipelago, the increase of warm Atlantic water masses that bring along abundant *C. finmarchicus* may have a negative impact on the reproductive success of little auks by reducing the relative abundance of its preferred prey, *C. glacialis* (Kwasniewski et al., 2010). In order to understand and predict impacts of environmental changes on Arctic marine ecosystems, it is necessary to better understand the mechanisms responsible for the specific assemblages of copepod communities.

In addition to physical forcing, relationships occurring within copepod communities can influence their structures and functions. Species that follow each other and co-occur in a community not only share food and space resources, but also develop complex interactions between them. Intraguild predation (IGP) has been proposed as an ecological strategy that could structure copepod communities (Irigoien and Harris, 2006; Plourde et al., 2009; Darnis, 2013; Melle et al., 2014). This particular type of predation occurs between members of a group of species that share the same food resources (Polis et al., 1989). This phenomenon is widespread across a variety of marine and terrestrial ecosystems and through all taxonomic and trophic levels (Polis et al., 1989; Holt and Polis, 1997; Arim and Marquet, 2004). This complex interaction is particularly interesting since it results in an immediate energy gain for the predator as well as a long term reduction of its competition (Hiltunen et al., 2013).

In copepod populations, survival rate to adulthood is strongly influenced by egg and nauplii mortality (Davis, 1984; Plourde et al., 2009). Egg mortality is particularly high in broadcast spawning species that release their eggs in the water column (Ohman et al., 2004), such as *Calanus* spp and *M. longa*. Although predominantly considered to be herbivorous, most calanoid copepod species have a flexible diet and can be omnivorous or even cannibalistic (Landry, 1981; Ohman and Hirche, 2001; Bonnet, 2004; Basedow and Tande, 2006). These species usually generate a filtration current to obtain small prey, essentially phytoplankton and micro-zooplankton, or cruise through the water and attack when a prey is detected (Kiørboe, 2013). Thus, they can consume eggs and young nauplii stages with limited mobility.

Cannibalism on eggs and nauplii can control the phenology of *C. finmarchicus* recruitment (Ohman and Hirche, 2001). It is therefore likely that IGP can impact recruitment as well as influencing the temporal succession of dominant species (Irigoien and Harris, 2006). In environments as contrasted as the Beaufort Sea and the St-Lawrence estuary, reduced *C. hyperboreus* recruitment and abundance co-occurred with an increase in *M. longa* abundance (Plourde et al., 2002; Darnis, 2013). During the time of peak egg production by *C. hyperboreus*, the gut of individual *M. longa* is often observed to be orange, a particularity linked to the probable ingestion of lipid-rich *C. hyperboreus* eggs (Conover and Huntley, 1991). Hence it has been hypothesized that *M. longa* individuals that remain active at intermediate depths throughout winter (no diapause) could intercept and ingest buoyant *C. hyperboreus* eggs that are spawned in deep waters (Plourde et al., 2003; Darnis, 2013). Given that *M. longa* population dynamics resources are scarce in winter, lipid-rich eggs could represent an important energy source for such an omnivorous (opportunistic) species. Later in early spring, numerous *C. hyperboreus* and *C. glacialis* that emerge from diapause and ascend toward the surface ahead of the phytoplankton bloom could also be feeding on eggs and young nauplii stages. Consequently, IGP could impact the recruitment of the true Arctic *C. hyperboreus*.

Surprisingly, only few studies have been conducted on predation within calanoid copepod communities (Landry, 1981; Huntley and Escritor, 1992; Bonnet, 2004; Basedow and Tande, 2006; Vestheim et al., 2013). The majority of the studies targeted cannibalism and while none was focused on IGP between the dominant Arctic species *M. longa* and *C. hyperboreus*, Huntley and Escritor (1992) reported ingestion rates of the vicariant species *M. gerlachei* on eggs of the dominant Antarctic *Calanoides acutus* in the Austral Ocean. In all experiments, ingestion rates on eggs (and nauplii) vary according to their concentration. The influence of alternative food source on ingestion produced ambiguous experimental results. On one hand, experiments with female *C. pacificus* suggest a switch between herbivorous and carnivorous behavior that depends on the relative abundances of phytoplankton and their own nauplii (Landry, 1981). On the other hand, experiments with *C. finmarchicus* have shown that ingestion rates on its own

nauplii are independent of the ambient algae concentration (Basedow and Tande, 2006).

Copepod community models have been developed with a focus on development, growth and competition for food resources (Record et al., 2012, 2013). However, community level processes involving interspecific interactions such as IGP have not yet been implemented into these models. In order to provide a better understanding of IGP and to provide a better parameterization for models of copepod communities, we conducted laboratory experiments that quantified the ingestion of copepod eggs by some of the dominant Arctic copepod species, *M. longa* and *C. hyperboreus*. We further conducted a simple numerical experiment in order to assess the potential ecological implications of our findings in Arctic marine ecosystems. Copepods were sampled in the Lower St-Lawrence estuary (LSLE) and feeding experiments on eggs were conducted under different conditions of temperature, egg concentration, and alternative food availability.

# METHODS

## Area of Study and Sampling

The LSLE is the southernmost sea directly influenced by Arctic water masses and that presents Arctic features in the North Atlantic (**Figure 1**). Arctic water masses enter in the Gulf of St-Lawrence (GSL) by the Strait of Belle Isle in the North, transporting Arctic copepods species such as *C. hyperboreus, C. glacialis*, and *M. longa*. Warmer North Atlantic water masses enter the system by Cabot Strait in the South and carry along boreal species such as *C. finmarchicus*. Both Arctic and temperate species thrive in the GSL system where cold and warm water masses are segregated vertically between the thin seasonal surface layer, the cold intermediate layer renewed locally each winter (core temperatures can be negative) and the deep Atlantic layer (between 4 and 5°C). Colder water masses dominate the eastern and northern parts of the Gulf and the deep lower Estuary where upstream tidal pumping brings cold and nutrient-rich waters to the surface, whereas warm surface waters (up to 20°C) develop throughout the summer over the shallow southern half of the Gulf (Saucier et al., 2003; Le Fouest et al., 2005). These particular water masses and species mix make the LSLE an exceptional experimental model to study IGP in the context of the rapid environmental changes that the Arctic is currently facing. Zooplankton was sampled in the LSLE (48°40′N, 68°35′W) in October 2014 with a vertical plankton net (158 μm mesh size, 1 m diameter) at 125 or 200 m from the surface at a towing speed of 0.5 m $s^{-1}$. The catch was diluted into 4 L jars filled with filtered seawater and maintained close to ambient temperature at 5 to 6°C in coolers during transport to the laboratory (less than an hour).

In a subsequent numerical experiment, we applied our observations to a truly Arctic environment, the Amundsen Gulf. The Amundsen Gulf is located in the Canadian territory of Nunavut at about 71°N and bordered by Banks Island and Victoria Island. It connects south-eastern Beaufort Sea to the Canadian archipelago (**Figure 1**). The Amundsen Gulf water masses are generally cold (around 0°C) and are mainly discriminated by their different salinities: the Polar-Mixed Layer from the surface to c.a. 50 m ($S \sim 31.6$), the Pacific Halocline below until 200 m ($32.4 < S < 33.1$) and the slightly warmer Atlantic Layer below 200 m ($S \sim 34$) (Carmack and Macdonald, 2002). The Gulf covers about 60,000 $km^2$ and the maximum

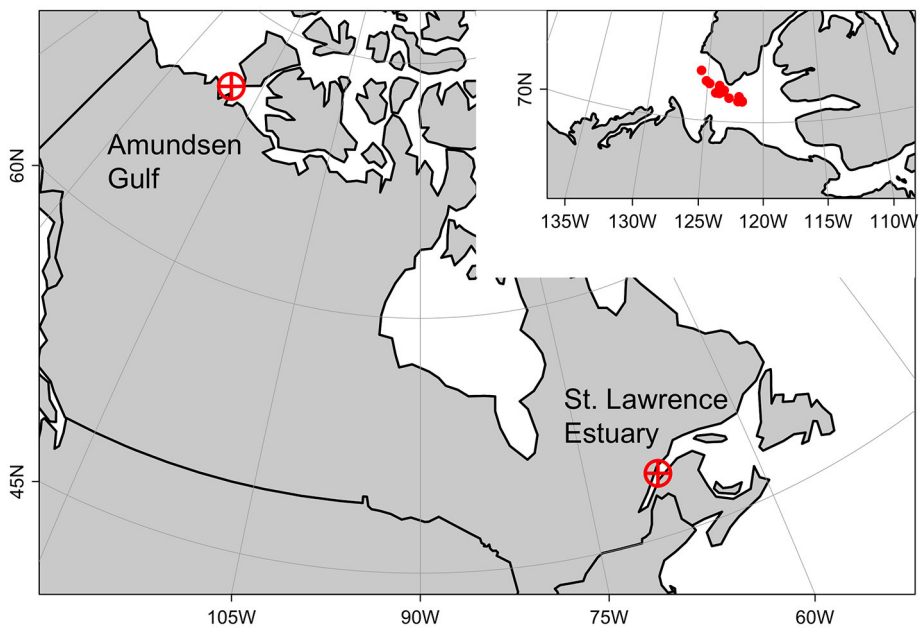


**FIGURE 1 | Studied area.** Arctic copepod species used in incubation experiments were sampled from the St. Lawrence Estuary. Environmental and biological forcing used in numerical experiments came from the Amundsen Gulf. Position of mean individual profiles shown in inset, upper-right corner.

depth of this large channel is 630 m. In winter, it is entirely ice-covered except for sporadic polynyas and flaw leads and the spring ice-breakup his highly variable (Galley et al., 2008).

## Live Animal Sorting

Owing to the harsh conditions at sea during winter over the LSLE, copepods were sampled at the end of October 2014 prior to the beginning of *C. hyperboreus* reproduction and the formation of dense sea ice. Plourde et al. (2003) have previously shown, for a similar experimental setup, that capture and handling of *C. hyperboreus* females triggered gonad maturation, leading to egg production a few weeks after collection and approximately a month earlier than expected according to the *in situ* timing. A visual inspection of appendages and behavior under a binocular microscope allowed us to select adult female *M. longa* and *C. hyperboreus* in good condition from the live samples, within 48 h of the catch. Animals were kept in the dark between 3 and 5°C in groups of 25 to 50 in 1 L beakers equipped with egg separators (mesh size = 333 μm) and filled with filtered seawater. Female *M. longa* were fed with solutions of concentrated diatoms *Thalassiosira weissflogii* (Instant Algae® *TW 1200*), whereas female *C. hyperboreus* where not fed since egg production is entirely fuelled by internal lipids during the dormant part of their life cycle. The beakers were inspected daily for egg production for about a month until female *C. hyperboreus* spawned enough eggs to start the experiments.

## Predation Experiments

Within 48 h of the start of the experiment, individuals used as predators were photographed laterally using a PixeLINK camera of 5 Mb (PL-E425CU) mounted on a LEICA MZ6 stereoscope. In order to minimize stress, individuals were kept in cooled seawater until the very moment that the picture was taken and gently manipulated with handling needles. Prosome length (distance between the tip of the cephalosome and the tip of the last thoracic segment), prosome area, oil sac length, and area were measured with the software ImageJ v. 1.49. The condition index was estimated as the oil sac area divided by the prosome area of the individual in order to give an indication of its lipid content. Predators' carbon content was estimated from species and stage-specific seasonal relationships between individual carbon mass and prosome length (Forest et al., 2010). The photographed animals were then placed individually in 45 mL Petri dishes filled with filtered seawater and equipped with egg separator (mesh size = 333 μm) for acclimation at the experimental temperatures.

Experiments were carried in an atmosphere-controlled chamber in November 2014 with female *M. longa* fed with *C. hyperboreus* eggs. Predators were placed individually in a bottle (1.35 or 2.37 L) filled with filtered seawater containing a precise number of eggs spawned within the previous 48 h. Bottles were turned upside down once per minute on a rotating wheel in order to maintain the eggs in suspension. Manipulations were conducted under a dimmed red light and the experiments were carried in the dark. Incubation time was kept relatively short (less than 24 h) in order to avoid a complete consumption of the eggs and hence a failure to accurately estimate ingestion rates. It also varied according to incubation conditions, with longer incubation times for lower egg concentration (lower encounter probability between eggs and the predator). After 4 to 22 h, the contents of the bottles were filtered with a 73 μm sieve and the remaining eggs were counted. A minimum of two controls without predator for each treatment was set up in order to check the accuracy of the egg recovery method. The status of each individual was verified at the end of the experiment. Ingestion rates were discarded for the few dead individuals, and the sluggish or unhealthy-looking ones as well.

We tested the effect of temperature on *M. longa* ingestion of *C. hyperboreus* eggs. Incubations were carried at 1, 4, and 8°C to reflect the potential range of *in situ* water temperature encountered by this species between the Arctic and subarctic regions. Unfortunately, we could not test for negative water temperatures. In order to characterize functional responses, we tested the effect of *C. hyperboreus* egg concentration on *M. longa* ingestion rate. We were not aware of actual data about *in situ C. hyperboreus* egg concentrations in the water column, but we estimated it to be low (Huntley and Escritor, 1992). Hence we chose concentrations of 5, 10, 20, and 30 egg $L^{-1}$. Finally, we checked whether there was an influence of alternative food availability, by adding an additional food source in the form of concentrated diatoms *T. weissflogii* (Instant Algae® *TW 1200*) in half of our replicates. Algae were offered at about 50 μg C $L^{-1}$ according to cell concentration determined with a Hausser Bright-Line Hemacytomer (couting chamber) and carbon to volume relationships for diatoms (Menden-Deuer and Lessard, 2000).

## Estimation of Ingestion Rates

The instantaneous feeding rate on eggs $g$ ($h^{-1}$) was derived from an exponential equation (Båmstedt et al., 2000):

$$g = \frac{ln\left(\frac{E_f}{E_0}\right)}{t} \quad (1)$$

where $E_0$ and $E_f$ are respectively the egg concentration at beginning and the end of experiment (egg $L^{-1}$) and $t$ is incubation time (h). The number of *C. hyperboreus* eggs obviously did not increase during the experiments, and experiment duration was not long enough for hatching to occur (no nauplii was ever found in any of the control or experiment bottles).

We deduced the clearance rate $F$ (L $ind^{-1}$ $h^{-1}$), which corresponds to the volume of water processed assuming 100% capture efficiency and a homogeneous food concentration, from both $g$ and the volume of the incubation bottle $V$ (L):

$$F = g \times V \quad (2)$$

Finally, we obtained the ingestion rate $I$ (egg $ind^{-1}$ $h^{-1}$) with:

$$I = F \times [E] \quad (3)$$

where $[E]$ is the average egg concentration as given by:

$$[E] = (E_0 \times \frac{1 - e^{(-g \times t)}}{g \times t}) \quad (4)$$

Daily ingestion rates where assumed to be 24 times the hourly rates since *M. longa* is known to be active and swimming almost continuously (Hirche, 1987). Egg ingestion rates were then converted in carbon units using an egg carbon content of 0.84 ($\mu$g C egg$^{-1}$; Plourde et al., 2003). The proportion of daily metabolic needs (%) satisfied by egg ingestion was estimated from the ratio of carbon ingestion rate $I_C = 0.84 * I$ ($\mu$g C ind$^{-1}$ d$^{-1}$) and a mean and constant respiration rate ($\mu$g C ind$^{-1}$ d$^{-1}$) measured by Seuthe et al. (2006).

## Data Analysis

The number of ingested eggs followed a Poisson distribution (an asymmetric right-skewed distribution of discrete values). Hence, in order to minimize estimating errors, a generalized linear model (GLM) for Poisson distribution was used to predict the number of eggs ingested (*EI*) (the raw data) according to temperature (*T*), egg concentration (*E*), presence of additional food source (*AC*), prosome length (*PL*), and condition index (*CI*) of the predator. Bottle volume (*V*) and duration of experiment (*D*) were taken into account by using them in an offset term. Several models were tested (with and without interactions) and we computed Akaike's information criterion corrected for overdispersion (QAIC) as a decision-support metric. The GLMs formulae were of the form (here is the one with all the independent variables but no interactions):

$$\log\left(\frac{EI}{D \times V}\right) = \beta_0 + (\beta_T \times T) + (\beta_E \times E) + (\beta_{AC} \times AC) + (\beta_{PL} \times PL) + (\beta_{CI} \times CI) \quad (5)$$

where $\beta_i$ are the coefficient estimates for each variable. The number of eggs ingested per unit of time and volume can easily be obtained from this model results.

## Model of Egg Vertical Distribution

In order to assess the implications of our findings in the context of Arctic marine ecosystems, we developed a simple water column (1D) model of the vertical distribution of *C. hyperboreus* eggs in the Amundsen Gulf. The model computed the time evolution of egg concentration at a given depth according to advection and diffusion, gains by egg production and losses by development and predation (**Figure 4**). The rate of change of egg concentration followed the classical advection-diffusion-reaction formulation (Soetaert and Herman, 2009):

$$\frac{\partial E}{\partial t} = -w\frac{\partial E}{\partial z} + K\frac{\partial^2 E}{\partial z^2} + P_z - I * M + 1/H * E \quad (6)$$

where the first right-hand side term represents the effect of egg vertical velocity, the second the effect of diffusion and the others several biological reaction terms. More specifically, *E* was the egg concentration (egg m$^{-3}$), *t* the time (h), *w* the egg velocity (m h$^{-1}$) defined positive downward, *z* the depth (m), *K* the vertical eddy diffusivity coefficient (m$^2$ h$^{-1}$), $P_Z$ the depth-dependent egg production rate (egg m$^{-3}$ h$^{-1}$), *H* the egg hatching time (h), M the females *M. longa* concentration (ind m$^{-3}$) and *I* the ingestion rate by other copepods (egg ind$^{-1}$ h$^{-1}$). The egg velocity *w* was given by Stokes' law (Visser and Jónasdóttir, 1999):

$$w = 3600 \times \frac{g \times d^2 \times (\rho_{egg} - \rho_{water})}{18 \times \mu} \quad (7)$$

where *g* is the gravitational constant (9.81 m s$^{-2}$), *d* is the egg diameter (m), $\rho_{egg}$ is the egg density (g m$^{-3}$), $\rho_{water}$ is the water density (g m$^{-3}$) and $\mu$ is the dynamic viscosity of the seawater (1.85 g m$^{-1}$ s$^{-1}$), here taken as a constant (**Table 1**).

The source term for eggs ($P_Z$) came from the average daily production of *C. hyperboreus* population (30,000 eggs m$^{-2}$) observed between February and April 2008 in the Amundsen Gulf (Darnis, 2013). *C. hyperboreus* females released more than 90% of their eggs during this 3 month-period, while remaining at depths between 200 and 300 m (Darnis, 2013). As a result, we computed the vertical profile of egg production rate $P_Z$ according to a normal distribution whose mean was centered at 250 m, its standard deviation 15 m and its integral equal to 30,000 eggs m$^{-2}$ (99.9% of the eggs were released between 200 and 300 m).

The IGP rate *I* (h$^{-1}$) exerted on *C. hyperboreus* eggs was simply the product of *M. longa* females' abundance (ind m$^{-3}$) and the individual filtration rate (m$^3$ ind$^{-1}$ h$^{-1}$) found in our grazing experiments.

Egg hatching time *H* (h) followed an empirical Bělehrádek's function obtained from observed hatching times of *C. hyperboreus* eggs (Jung-Madsen et al., 2013):

$$H = a \times (T - \alpha)^{-b} \quad (8)$$

where *T* was water temperature (°C), *a* (d °C$^{-1}$), $\alpha$ (°C) and *b* constants.

A simple ordinary differential equation framework was not optimal for the modeling of developing eggs because of the "numerical diffusivity" caused by the hatching rate (Gentleman et al., 2008). Simply put, with a development (hatching) rate, the progression through development stages is treated as a continuous process within the population, instead of a discrete event highly synchronized among many individuals. This can

**TABLE 1 | Model parameters and references.**

| Parameter | Unit | Value | References |
|---|---|---|---|
| *H*, egg hatching time | | | JM2013 |
| *a* | d °C$^{-1}$ | 1196 | JM2013 |
| $\alpha$ | °C | 12.7 | JM2013 |
| *b* | – | −2.05 | JM2013 |
| *d*, egg diameter | m | $1.92 \times 10^{-4}$ | JM2013 |
| *P*, egg production | egg m$^{-2}$ d$^{-1}$ | 30,000 | D2013 |
| $\rho_{egg}$, egg density | g m$^{-3}$ | $0.6 \times 10^3$ (min) | JM2013 |
| | | $19.4 \times 10^3$ (mean) | JM2013 |
| | | $26.8 \times 10^3$ (max) | JM2013 |
| $\mu$, dynamic viscosity | g m$^{-1}$ s$^{-1}$ | 1.9 | VJ1999 |

*VJ1999, Visser and Jónasdóttir (1999); D2013, Darnis (2013); JM2013, Jung-Madsen et al. (2013)*

lead to unrealistic and spurious results, such as a small fraction of the simulated egg population that has already hatched after the first time step! In order to prevent this, we used the simple approach of spreading the egg development over 20 numerical stages of equal length (Gentleman et al., 2008) and we further integrated the development throughout theses stages with a flux limiting numerical scheme (Record and Pershing, 2008).

## Simulations

The 1D water column model was split into 5 m vertical layers between 0 and 300 m, and the time step of integration was 12 h. For the model forcing, we used physical and biological datasets from the Circumpolar Flaw Lead System Study (CFL; Barber et al., 2011). We only selected profiles from stations that were at least 300 m deep and located within the Amundsen Gulf. As a result, the physical forcing came from mean vertical profiles of eddy diffusivity coefficient ($K$), temperature ($T$), and water density ($\rho_{water}$) obtained at 20 different stations. These stations were sampled in November and December 2007 under dense sea-ice cover with a vertical microstructure profiler (VMP500, Rockland Scientific International). For two long-term stations the number of casts used in the average profile were respectively 24 and 25, whereas at least 5 profiles were used to build the 18 other mean profiles. Missing values in averaged profiles (e.g., near the surface or below 250 m) were dealt with according to Equation (1) from Bourgault et al. (2011). Further details about this dataset can be found in their study.

We also used 18 vertical profiles of *M. longa* female abundance obtained with a Hydrobios ® multinet sampler. Details of the sampling procedure can be found in Darnis and Fortier (2014). We selected the stations sampled between February and April 2008, during the peak of *C. hyperboreus* reproduction. The layer thickness for the vertical sampling ranged from 10 to 144 m, with a median of 20 m.

In order to test the sensitivity of the model to both the physical properties of the water column and the vertical distribution of the predators (*M. longa*) we ran 360 simulations, one for each possible combination of the physical and biological forcing fields. In addition, we ran this ensemble of simulations for three different scenarios of egg density in order to verify the impacts of different egg velocities: the mean (scenario $D_0$), minimum ($D_{min}$) and maximum ($D_{max}$) egg densities observed by Jung-Madsen et al. (2013). Simulations ran for 15 days in order to reach a quasi-steady state where the maximum local rate of change in egg concentration $\delta E/\delta t$ was less than $10^{-6}$.

# RESULTS

## Egg Ingestion Rates

Predation of *C. hyperboreus* eggs by female *M. longa* occurred in each of the incubation experiments. However, in each experiment there was high individual variability and several individual incubations showed no egg ingestion. After discarding incubations within which dead or unhealthy individuals were found at the end of the experiment, for each treatment approximately 8 individual replicates out of the initial 10 were used for further analyses. The frequency distribution of ingestion rates was positively skewed, i.e., the median value was lower than the mean. The global mean ingestion rate of *C. hyperboreus* eggs by *M. longa* was 5.8 eggs $ind^{-1}$ $d^{-1}$ ($SE = 0.57$, $n = 141$) and the median was 3.7 eggs $ind^{-1}$ $d^{-1}$ (**Figure 2**). In terms of carbon, the mean ingestion rate was 4.9 μg C $ind^{-1}$ $d^{-1}$ and the median 3.1 μg C $ind^{-1}$ $d^{-1}$ ($SE = 0.48$, $n = 141$; **Figure 2**). *C. hyperboreus* eggs constituted an energy-rich food source (0.84 μg C $egg^{-1}$; (Plourde et al., 2003) and the average daily ration of *M. longa* females feeding on *C. hyperboreus* eggs was 37% of their estimated metabolic needs based on respiration rates ($SE = 4$, $n = 141$). Individual variability resulted in a contrasted pattern where about a quarter of *M. longa* did not ingest any eggs, while an equivalent proportion filled more than 50% of their daily energetic requirements through egg ingestion. Some individuals actually largely exceeded their daily metabolic needs (i.e., over 100%, **Figure 2**), even when eggs were offered at low concentrations.

## Influence of Incubation Conditions

According to the GLM analysis, presence of additional food source, prosome length, or condition index of the individuals had no discernable effect on egg ingestion (**Table 2**). The only predictor that improved the model and that significantly affected the number of eggs ingested by *M. longa* was egg concentration (**Figure 3**). In the full model with no interactions, temperature seemed to have a significant negative effect on ingestion rates (**Table 2**). However, in the model that only kept egg concentration and temperature as independent variables, the influence of temperature and the interaction term between them did not remain significant. Moreover, the size effect of the temperature and interaction term coefficients was small compared to the impact of egg concentration and the QAIC values were very close between the models. Hence, we decided to use the simplest model with only egg concentration as predictor of egg ingestion (**Figure 3**). We did not observe any feeding saturation for the range of egg concentrations offered.

## Simulated Egg Vertical Distribution

The velocity of *C. hyperboreus* eggs estimated with Equation (7) ranged between −9 and −4.1 m $d^{-1}$ for the mean egg density scenario ($D_0$) over the 20 physical forcing profiles. Negative velocities meant that eggs were positively buoyant, from the bottom of the water column up to the surface. Egg velocity was dependent on the water density profile and it decreased slowly with decreasing depth (**Figure 4**). This pattern was conserved among the 20 physical forcing profiles whose overall variability was low. Egg velocity was strongly influenced by egg density itself. *C. hyperboreus* egg density is highly variable, both between individual females and within clutches of the same female (Jung-Madsen et al., 2013). When we used the minimal egg density (scenario $D_{min}$) the velocity tripled to range between −26.2 and −21.3 m $d^{-1}$, whereas for maximal egg density (scenario $D_{max}$) the associated velocity was not negative throughout the water column. The egg velocity ranged between −2.3 and 2.6 m $d^{-1}$ with a converging depth of neutral buoyancy around 100 m.

Egg velocity was critical for egg vertical distribution. In the ensemble of simulations for scenario $D_0$, egg vertical

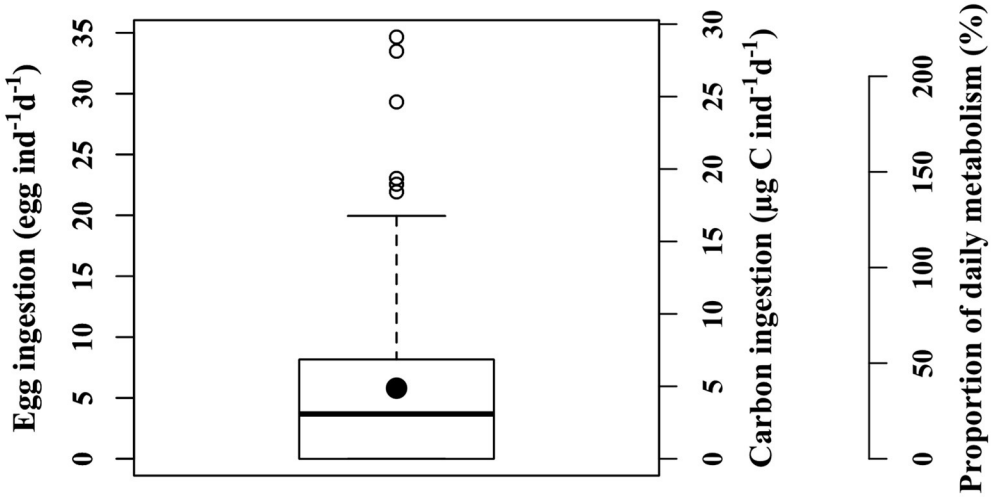


**FIGURE 2 | Ingestion rates of female *M. longa* on *C. hyperboreus* eggs from all experiments according to different units: number of eggs, carbon content, and proportion of daily metabolic needs (see text).** Thick black line: median; black circle: mean; box: range between the first and third quartiles (IQR); whiskers: ±1.5 IQR; open circles: outliers.

distributions showed higher concentrations between 150 and 275 m and peaked around 225 m to reach about 3000 eggs $m^{-3}$ (or 3 eggs $L^{-1}$) once the simulation reached its steady state (**Figure 4**). For scenario $D_{max}$, the denser eggs ascend only slightly in the water column before hatching. They remained concentrated between 200 and 300 m with a maximum egg concentration a little less than 4000 eggs $m^{-3}$ near 250 m (**Figure 4**). Contrarily, in the $D_{min}$ scenario, eggs moved rapidly upward and some even managed to reach the first 5 m of the water column to attain a concentration of a little less than 300 eggs $m^{-3}$ (**Figure 4**). Eggs where spread over the entire column and concentration peaked above 160 m at about 1200 eggs $m^{-3}$.

## Impact of *M. longa* Predation on *C. hyperboreus* Eggs

For each egg density scenario tested, the proportion of egg biomass eaten by *M. longa* was more sensitive to the profiles of *M. longa* abundance than to the physical forcing (see **Figure 5** for scenario $D_0$). Over the ensemble of 360 simulations of the $D_0$ scenario, the percentage of *C. hyperboreus* egg standing stock ingested by *M. longa* ranged between 0.1 and 1.1% with most of the values being in the low end (**Figure 6**). The percentage of egg standing stock ingested by *M. longa* varied between 0.2 and 3.2% for scenario $D_{min}$ and between 0 and 0.8% for maximal egg density (scenario $D_{max}$; **Figure 6**).

This modest impact of *M. longa* IGP is hardly noticeable between the egg concentration profiles simulated with and without egg predation, even for the combination of physical conditions and *M. longa* profiles that lead to the maximum difference (**Figure 7**). The corresponding daily egg ingestion of the whole population of *M. longa* ranged between a little more than 1 to almost 20 eggs $m^{-3}$ $d^{-1}$ (**Figure 7**). It is noticeable, though, that such egg ingestion values could allow *M. longa* individuals to satisfy almost 10% of their metabolic needs according to respiration rates from Seuthe et al. (2006), or up to 37% if we consider the lower respiration rates reported by Hirche (1987).

**TABLE 2 | Results from the generalized linear models (GLM) fitted to predict the number of *C. hyperboreus* eggs ingested by female *M. longa* according to egg concentration (*E*), temperature (*T*), alternative food source (*AC*), condition index (*CI*), prosome length (*PL*), and interactions between the terms.**

| GLM | Predictor | *β* | *SE* | *P-value* | QAIC |
|---|---|---|---|---|---|
| *E, T, AC, CI, PL* | *Intercept* | −1.870 | 3.340 | *ns* | 215 |
| | *E* | 0.068 | 0.012 | *** | |
| | *T* | −0.093 | 0.040 | * | |
| | *AC* | 0.0007 | 0.004 | *ns* | |
| | *CI* | −0.927 | 1.118 | *ns* | |
| | *PL* | −0.300 | 1.165 | *ns* | |
| *E, T, E×T* | *Intercept* | −3.365 | 0.379 | *** | 208 |
| | *E* | 0.111 | 0.024 | *** | |
| | *T* | 0.031 | 0.078 | *ns* | |
| | *E×T* | −0.008 | 0.004 | *ns* | |
| ***E*** | ***Intercept*** | **−2.944** | **0.199** | *** | **215** |
| | ***E*** | **0.053** | **0.009** | *** | |

*Estimated coefficients b, standard error SE, P-values (***P < 0.001;**P< 0.01; *P < 0.1; ns not significant) and Akaike's information criterion corrected for overdispersion QAIC. Model entry in bold indicates the one selected for further numerical experiments.*

# DISCUSSION

## Individual Variability

Our results show high individual variability of egg ingestion rates, with a quarter of all the individuals not ingesting any eggs and about the same proportion satisfying more than half of

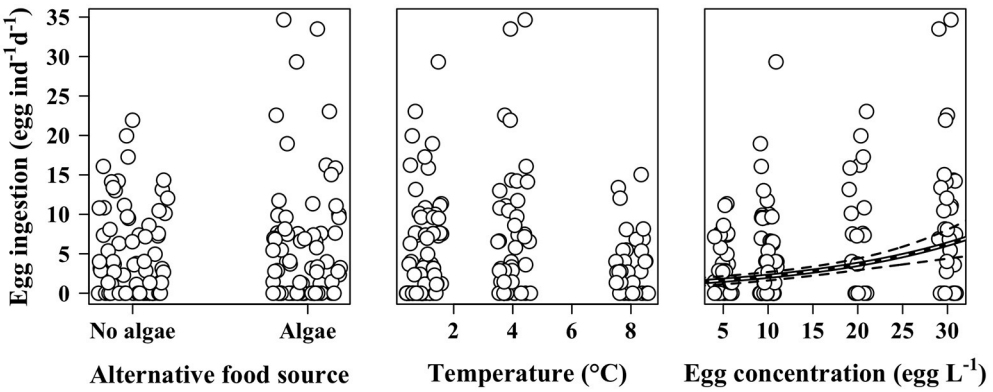


**FIGURE 3 | Ingestion rates of female *M. longa* on *C. hyperboreus* eggs according to the presence of alternative food source (left panel), temperature (middle panel), and egg concentration (right panel).** Points are jittered to reduce overlap. Black and white line is the prediction of the mean from the selected generalized linear model (see text); dotted black lines are the corresponding 95% confidence intervals.

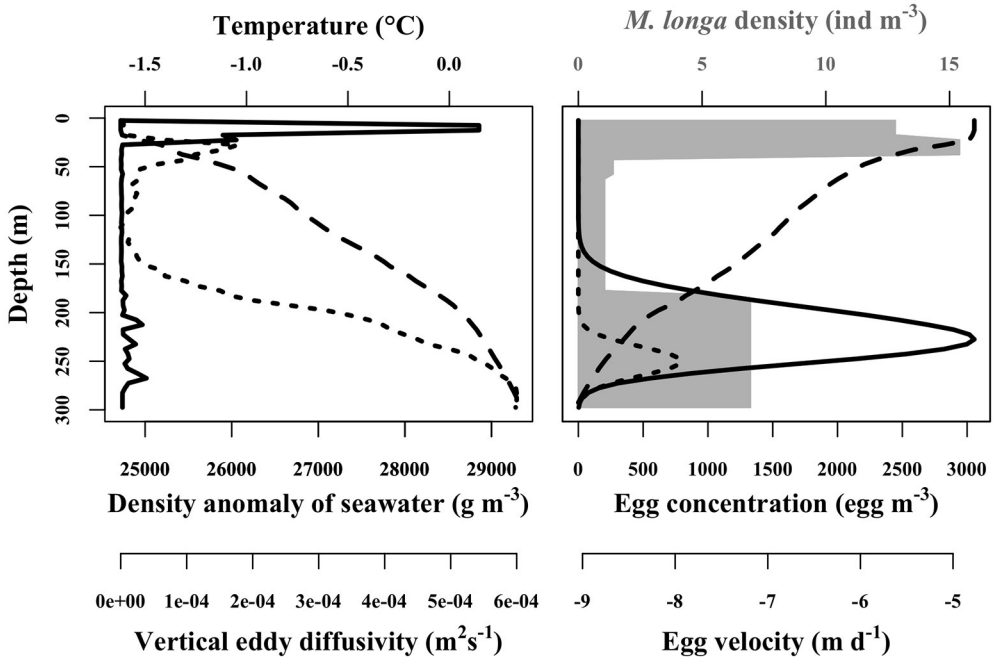


**FIGURE 4 | Example of *in situ* physical forcing profiles from Amundsen Gulf used in the egg vertical distribution simulation (left panel).** Solid line is the vertical eddy diffusivity (m$^2$ s$^{-1}$), dashed line is the density anomaly of seawater (g m$^{-3}$) and dotted line is the temperature (°C). Corresponding egg concentrations simulated for mean egg density (scenario $D_0$) of 19.4 kg m$^{-3}$ are presented in the right panel. Dashed line is the egg velocity (m d$^{-1}$) computed according to Stokes' law. Dotted line is at the initial condition corresponding to the spawned eggs profile. Solid line is the egg concentration distribution after 15 days of simulation. Gray area is the female *M. longa* abundance (ind m$^{-3}$).

their daily metabolic needs from egg grazing. This asymmetric and widely spread distribution has a geometric coefficient of variation of 149%. This pattern is consistent across the range of incubation conditions we tested, and this level of variability is common in any experimental setting measuring individual biological features (size, structural or storage weight, swimming behavior, etc.) and physiological rates (respiration, ingestion, growth, etc.) (e.g., Basedow and Tande, 2006). We do not have clear explanations for the level of variability we observed, but it is a useful observation to report (see Supplementary Material for a spreadsheet of individual observations). Individual variability has long been recognized as a key property of plankton ecology since population dynamics and trophic interactions (that are of primary interest for marine ecologists) are emerging properties of individual characteristics and behaviors (Båmstedt, 1988). Modern experimental and *in situ* observation methods

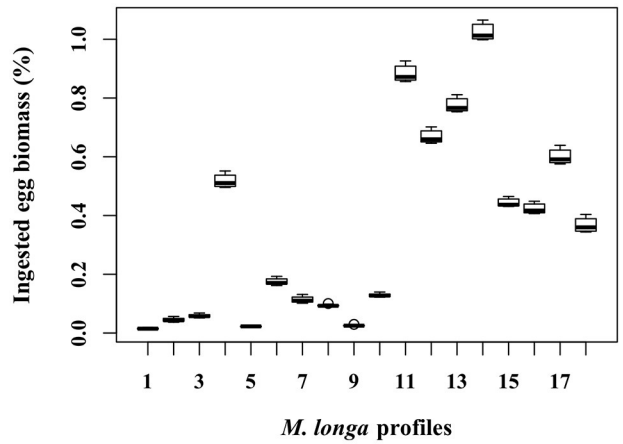


**FIGURE 5 | Proportion of *C. hyperboreus* egg standing stock (%) ingested by female *M. longa* for all the 360 simulations with mean egg density (scenario $D_0$) and grouped according to each of the 18 *in situ* female *M. longa* abundance profiles.**

are providing increasingly detailed and abundant individual-level data (e.g., Schmid et al., 2016), while current numerical approaches allow for testing how and how well individual-based models can effectively represent emerging properties at higher organizational levels (Neuheimer et al., 2010; Morozov et al., 2013).

## Dynamical Interactions in the Water Column

This modeling exercise provided insight on the physical and biological dynamical processes interacting in the water column and their relative importance for the vertical distribution of *C. hyperboreus* eggs.

We first performed a scale analysis of the two first terms on the right-hand side of Equation (7), i.e., egg buoyancy and vertical turbulence. For the simulation scenario illustrated in **Figure 4**, we can estimate the vertical gradient in egg concentration $\frac{\partial E}{\partial z} \approx 15$ egg $m^{-4}$ near the maximum egg concentration at 250 m (an approximate increase of 750 egg $m^{-3}$ over 50 m) and $\frac{\partial^2 E}{\partial z^2} \approx 1$ egg $m^{-5}$ ( $\frac{\partial E}{\partial z}$ varies between $\pm$ 15 egg $m^{-3}$ over about 30 m from both sides of the maximum concentration), simple arithmetic suggests that

$$w\frac{\partial E}{\partial z} \approx [1, 3] \times 10^{-3} \text{egg m}^{-3}\ \text{s}^{-1}$$

and

$$K\frac{\partial^2 E}{\partial z^2} \approx 10^{-5} \text{egg m}^{-3}\ \text{s}^{-1}$$

with $w$ ε [4, 9.3] m $d^{-1}$ (see Results) and $K = 3.4\times10$ $m^{-6}$ $s^{-1}$ (background turbulent diffusivity) from (Bourgault et al., 2011). This suggest that from a physical point of view, the buoyant vertical displacement of eggs is dominant over the turbulent diffusion mechanism, and only turbulent events about a 100 times above the background value could effectively influence their distribution. The role of turbulent mixing in egg distribution (aggregation or spreading) is likely minimal and the use of a parameterization such as the one presented in Bourgault et al. (2011) could have been sufficient here. The effect of turbulence may only become important for denser eggs rising very slowly toward the surface or directly after the spawning if it occurs in a thin layer pattern, hence producing a high concentration gradient. This effect could be studied more efficiently with new *in situ* sampling devices such as the LOKI underwater imaging system that can provide highly resolved vertical distribution of adult females *C. hyperboreus*, their eggs, a whole suite of potential other intraguild predators beyond *M. longa* and the physical properties of the water column as well (Schmid et al., 2016).

From a biological point of view, egg density had an overwhelming impact on egg vertical distribution patterns (**Figure 7**). Egg density defined their vertical velocity $w$ and as a result both the range of depth they could reach before hatching and their corresponding concentration. For two out of three egg density scenarios, eggs laid at depth did not manage to reach and accumulate within the surface layer. Even for the minimum density scenario $D_{min}$, the amount of eggs reaching the surface remained marginal. This is coherent with the generally accepted idea that *C. hyperboreus* nauplii, rather than eggs, accumulate under the ice in advance of the phytoplankton bloom (Conover and Huntley, 1991). Meanwhile, the maximum egg concentration reached was about 4 eggs $L^{-1}$, close the minimal egg concentration used in our grazing experiments. Depth and concentration were crucial for the interaction with female *M. longa* whose vertical position and abundance vary a lot, and whose ingestion rate depends on the surrounding egg concentration. As a result, it appeared that the probability of encounter between a predator and an egg of *C. hyperboreus* was determined essentially by the density of the latter.

## Impact of Intraguild Predation on *C. hyperboreus* Recruitment

If we consider thin layer effects to remain marginal, our results suggest that impacts on *C. hyperboreus* population dynamics may remain limited in space and time since *M. longa* IGP was limited to a little more than 3% of *C. hyperboreus* egg biomass. However, young nauplii stages could also be preyed upon by *M. longa* and thus our figures could underestimate the actual impact of *M. longa* on *C. hyperboreus* recruitment. *M. longa* is a cruising feeder, i.e., it cruises through water searching for food and prey and captures them upon detection. Moreover, motile preys such as nauplii can generate a hydrodynamic trail while swimming that could render them be easier to detect by *M. longa* than non-motile preys such as eggs (Kiørboe, 2011). This assumption is supported by feeding experiments with *M. lucens* and *M. longa* in which phytoplankton and much larger nauplii *Artemia* were offered together, illustrating selective feeding on *Artemia* nauplii (Haq, 1967).

In addition to females *M. longa*, other development stages of this species and other copepod species could also exert IGP on

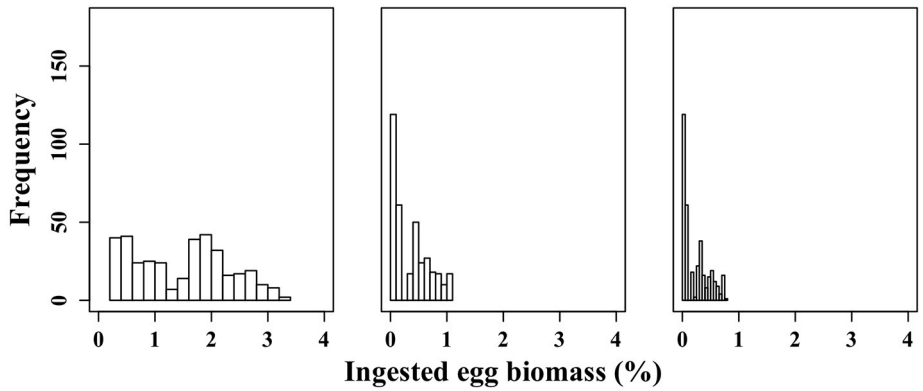


**FIGURE 6 | Frequency distribution of the proportion of *C. hyperboreus* eggs standing stock ingested by female *M. longa* according to the minimal (0.6 kg $m^{-3}$) (scenario $D_{min}$) (left panel), mean (19.4 kg $m^{-3}$) (scenario $D_0$) (middle panel) and maximal *C. hyperboreus* egg density (26.8 kg $m^{-3}$) (scenario $D_{max}$) (right panel).**

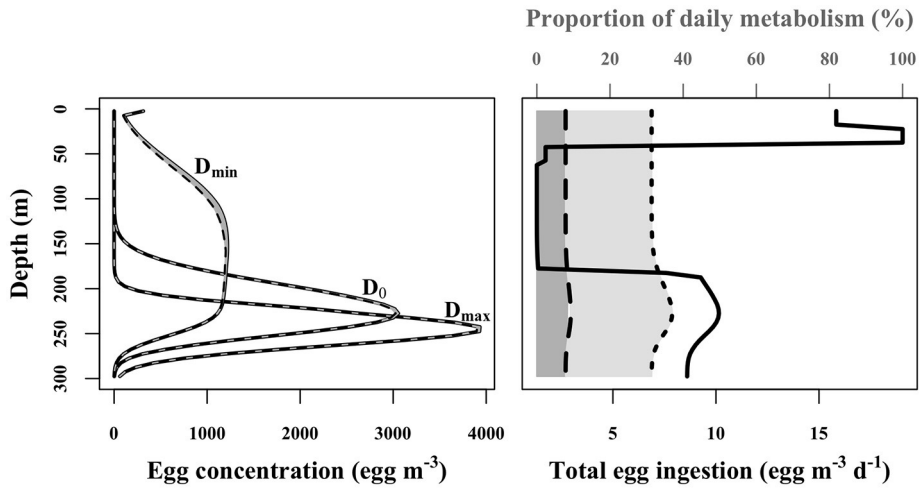


**FIGURE 7 | Simulated egg concentration profiles for three different scenarios (scenario $D_{min}$, $D_0$, and $D_{max}$; left panel).** Solid line is without female *M. longa* intraguild predation, dashed line is with intraguild predation and the gray area is the difference between both. On the right panel, solid line is the *C. hyperboreus* egg biomass ingested by the population of female *M. longa* (egg $m^{-3}$ $d^{-1}$) according to the simulated egg concentration with scenario $D_0$ and *M. longa* abundance profile presented in **Figure 4**. Proportion of individual daily metabolic needs satisfied by egg ingestion (%) according to respiration rates from Seuthe et al. (2006; Dashed line) and Hirche (1987; Dotted line).

*C. hyperboreus* eggs. As already mentioned, adults and advanced copepodite stages of the large *C. glacialis* emerge from diapause and initiate ascent to surface layers prior the spring bloom to feed on ice algae (Daase et al., 2013). Therefore, they could also benefit from the energy rich *C. hyperboreus* eggs (and potentially the nauplii) and add to the predation pressure. Thus, we likely have underestimated IGP pressure on *C. hyperboreus* and its impact on its recruitment in several ways. However, it may remain very dependent on the seasonal timing of the feeding activity of these potential predators, as well as their vertical position in the water column as already demonstrated.

It seems that there is actually an ecological trade-off for *C. hyperboreus* females to lay low (lipid-rich) or high-density (lipid-poor) eggs. On one hand the obvious metabolic advantage for lipid-rich eggs is that the offspring can rely on abundant reserves to develop. The downside however could be that low-density eggs reach faster and "en masse" the layer where *M. longa* and other species are abundant, hence increasing their mortality risk. On the other hand, dense eggs ascend very slowly and actually hatch before having reached these dangerous depths. The wide range in egg density that has been observed among eggs from different *C. hyperboreus* females but also within the same egg clutch (Jung-Madsen et al., 2013) could actually be part of a strategy that mitigates predation risk by spreading the eggs across a range of ascent speeds. However, the delicate balance of both opposing effects on offspring fitness could only be assessed in a more detailed modeling study supported by finely resolved and

concurrent observation of the zooplankton community vertical distribution.

### *C. hyperboreus* Importance in the Arctic System

Our results could offer an interesting contrast with the earlier study of Huntley and Escritor (1992) on a couple of homologous species from Antarctica, *M. gerlachei* and *C. acutus*. They showed from incubations of a group of individuals that *M. gerlachei* could reach daily rations ranging between 4 to 11% of its body weight when offered 1000 egg $L^{-1}$. The authors further estimated that this concentration was about three orders of magnitude higher than what it could be *in situ* (1 egg $L^{-1}$) and thus concluded that this type of predation is likely insignificant. However, our experimental results showed that *M. longa* individuals could meet up to 75% of their daily metabolic requirements on eggs of *C. hyperboreus* offered at a concentration of 5 $L^{-1}$, based on respiration rates observed in Amundsen Gulf (Seuthe et al., 2006). We also simulated that the mean *in situ* ration of eggs for *M. longa* females should vary between 8 and 37% of their metabolic needs, depending on the respiration rate. The lower boundary is based on Seuthe et al. (2006), whereas the upper boundary is based on lower respiration rates (Hirche, 1987). Neither value is sufficient to ensure complete metabolic maintenance, but during wintertime it could be combined to some level of lipid stores to cope with the otherwise scarce food background available to these copepods. Lipid-rich *C. hyperboreus* eggs (and potentially nauplii) are a reliable and valuable food source that at least some *M. longa* individuals seem prone to take advantage of during several months of the year.

Our study stresses the importance of *C. hyperboreus* as a linchpin of Arctic marine trophic network. This key species has adapted to the extreme environment by evolving its ability to store considerable amounts of lipids. *C. hyperboreus* efficiently concentrate the energy from the short-lived primary production bloom and supports the entire marine trophic network. Higher trophic levels rely heavily on its large copepodite and adult development stages, while zooplankton species from a similar trophic level (from the same guild) also benefit from the smaller packaging of the bounty within its eggs. Moreover, since *C. hyperboreus* reproduction occurs for several months during a period of the polar year when primary production has shut down, it likely provides a precious and unparalleled resource for several species of planktonic predators that remain active in the dead of winter. Hence, IGP should not only be considered as an extra mortality source that could affect recruitment of the species that is preyed upon, but also as a crucial survival strategy that could shape the life cycle strategies of some opportunistic species.

IGP needs to be studied further as we move toward an integrated approach of marine ecology that recognizes the influence of both individual variability and community-level interactions. Other implications of IGP than those evoked in our study could be important. In the North Atlantic for example, the survival of *C. finmarchicus* early stages follows different seasonal patterns in areas where it is the dominant *Calanus* species than in areas where its larger congeners, *C. glacialis* and *C. hyperboreus,* co-occur. In such areas where all three species live together, the *C. finmarchicus* recruitment peak can occur several weeks after the spring bloom, much later than it usually does (Melle et al., 2014). In early spring, *C. hyperboreus* and *C. glacialis,* that are already active when *C. finmarchicus* initiates its reproduction fuelled by the phytoplankton bloom, could ingest *C. finmarchicus* eggs and affect its recruitment. Interestingly, IGP could contribute to the resistance of marginal Arctic marine ecosystems to the northward advance of the boreal *C. finmarchicus* under the pressure of climate change.

## AUTHOR CONTRIBUTIONS

KD designed and ran the laboratory experiments, participated to the *in situ* sampling, did the statistical analysis, ran the modeling experiment, and wrote most of the paper. FM contributed to the design of the laboratory experiment, contributed to the data analysis, designed, and executed most of the modeling experiment and contributed to the writing. SP contributed to the design of the laboratory experiment, provided access to the laboratory facility, and contributed to the writing. PJ contributed to the design and the execution of the laboratory experiment, and ran the *in situ* sampling. FC contributed to the design of the numerical experiment, provided data from Amundsen Gulf, and contributed to the writing.

## FUNDING

This work has been supported by an NSERC Discovery grant to FM, DFO, and Québec-Océan.

## ACKNOWLEDGMENTS

KD is grateful to PJ for his invaluable help in the field and in the laboratory, Geneviève Parent for her help with image analysis, Michel Starr and Liliane St-Amand for their help with laboratory analysis, David Levasseur for his assistance in the laboratory experiments and Daniel Bourgault for the Amundsen Gulf physical data. KD also thanks FM, SP, and Maurice Levasseur for the stimulating and constructive discussions and finally FC and Jeffrey Runge for their help on the manuscript. This is a contribution to the research programs of Québec-Océan, ArcticNet and UMI Takuvik.

## SUPPLEMENTARY MATERIAL

The Supplementary Material for this article can be found online at: http://journal.frontiersin.org/article/10.3389/fmars.2016.00185

The R code and forcing fields for the model can be found online at: https://github.com/NEOLab-Git/Chyp_Egg_1D.git

The detailed table of individual observations is provided.

## REFERENCES


Arim, M., and Marquet, P. A. (2004). Intraguild predation: a widespread interaction related to species biology. *Ecol. Lett.* 7, 557–564. doi: 10.1111/j.1461-0248.2004.00613.x

Båmstedt, U. (1988). Ecological significance of individual variability in copepod bioenergetics. *Hydrobiologia* 167–168, 43–59. doi: 10.1007/BF00026293

Båmstedt, U., Gifford, D. J., Irigoien, X., Atkinson, A., and Roman, M. (2000). "Feeding", in *ICES Zooplankton Methodology Manual*, eds R. Harris, P. Wiebe, J. Lenz, H.-R. Skjoldal, and M. Huntley (Plymouth: Academic Press), 297–399.

Barber, D. G., Asplin, M. G., Gratton, Y., Lukovich, J. V., Galley, R. J., Raddatz, R. L., et al. (2011). The International polar year (IPY) circumpolar flaw lead (CFL) system study: overview and the physical system. *Atmosphere Ocean* 48, 225–243. doi: 10.3137/OC317.2010

Basedow, S., and Tande, K. (2006). Cannibalism by female *Calanus finmarchicus* on naupliar stages. *Mar. Ecol. Prog. Ser.* 327, 247–255. doi: 10.3354/meps327247

Bonnet, D. (2004). *Calanus* the cannibal. *J. Plankton Res.* 26, 937–948. doi: 10.1093/plankt/fbh087

Bourgault, D., Hamel, C., Cyr, F., Tremblay, J. É., Galbraith, P. S., Dumont, D., et al. (2011). Turbulent nitrate fluxes in the Amundsen Gulf during ice-covered conditions. *Geophys. Res. Lett.* 38, L15602. doi: 10.1029/2011GL047936

Carmack, E. C., and Macdonald, R. W. (2002). Oceanography of the Canadian Shelf of the Beaufort Sea: a setting for marine life. *Arctic* 55, 29–45. doi: 10.14430/arctic733

Conover, R. J., and Huntley, M. (1991). Copepods in ice-covered seas - distribution, adaptations to seasonally limited food, metabolism, growth patterns and life cycle strategies in polar seas. *J. Mar. Syst.* 2, 1–41. doi: 10.1016/0924-7963(91)90011-I

Daase, M., Falk-Petersen, S., Varpe, Ø., Darnis, G., Søreide, J. E., Wold, A., et al. (2013). Timing of reproductive events in the marine copepod *Calanus glacialis*: a Pan-Arctic perspective. *Can. J. Fish. Aqua. Sci.* 14, 1–14. doi: 10.1139/cjfas-2012-0401

Darnis, G. (2013). *Migration Verticale du Zooplancton et flux Respiratoire de Carbone en mer de Beaufort (Arctique Canadien)*. Thesis, Université Laval, Québec, QC.

Darnis, G., and Fortier, L. (2014). Temperature, food and the seasonal vertical migration of key arctic copepods in the thermally stratified Amundsen Gulf (Beaufort Sea, Arctic Ocean). *J. Plankton Res.* 36, 1092–1168. doi: 10.1093/plankt/fbu035

Darnis, G., Robert, D., Pomerleau, C., Link, H., Archambault, P., Nelson, R. J., et al. (2012). Current state and trends in Canadian Arctic marine ecosystems: II. Heterotrophic food web, pelagic-benthic coupling, and biodiversity. *Clim. Change* 115, 179–205. doi: 10.1007/s10584-012-0483-8

Davis, C. S. (1984). Predatory control of copepod seasonal cycles on Georges Bank. *Mar. Biol.* 82, 31–40. doi: 10.1007/BF00392761

Falardeau, M., Robert, D., and Fortier, L. (2013). Could the planktonic stages of polar cod and Pacific sand lance compete for food in the warming Beaufort Sea? *ICES J. Mar. Sci.* 71, 1956–1965. doi: 10.1093/icesjms/fst221

Forest, A., Galindo, V., Darnis, G., Pineault, S., Lalande, C., Tremblay, J. E., et al. (2010). Carbon biomass, elemental ratios (C:N) and stable isotopic composition ($^{13}$C, $^{15}$N) of dominant calanoid copepods during the winter-to-summer transition in the Amundsen Gulf (Arctic Ocean). *J. Plankton Res.* 33, 161–178. doi: 10.1093/plankt/fbq103

Fort, J., Cherel, Y., Harding, A. M. A., Welcker, J., Jakubas, D., Steen, H., et al. (2010). Geographic and seasonal variability in the isotopic niche of little auks. *Mar. Ecol. Prog. Ser.* 414, 293–302. doi: 10.3354/meps08721

Galley, R. J., Key, E., Barber, D. G., Hwang, B. J., and Ehn, J. K. (2008). Spatial and temporal variability of sea ice in the southern Beaufort Sea and Amundsen Gulf: 1980-2004. *J. Geophys. Res. Oceans* 113, 1–18. doi: 10.1029/2007jc004553

Gentleman, W. C., Neuheimer, A. B., and Campbell, R. G. (2008). Modelling copepod development: current limitations and a new realistic approach. *ICES J. Mar. Sci.* 65, 399–413. doi: 10.1093/icesjms/fsn047

Greene, C. H., and Pershing, A. J. (2014). The flip-side of the North Atlantic Oscillation and modal shifts in slope-water circulation patterns. *Limnol. Oceanogr.* 48, 319–322. doi: 10.4319/lo.2003.48.1.0319

Haq, S. M. (1967). Nutritional physiology of *Metridia lucens* and *M. longa* from the Gulf of Maine. *Limnol. Oceanogr.* 12, 40–51. doi: 10.4319/lo.1967.12.1.0040

Head, E. J. H., Harris, L. R., and Yashayaev, I. (2003). Distributions of *Calanus* spp. and other mesozooplankton in the Labrador Sea in relation to hydrography in spring and summer (1995–2000). *Prog. Oceanogr.* 59, 1–30. doi: 10.1016/S0079-6611(03)00111-3

Hiltunen, T., Jones, L. E., Ellner, S. P., and Hairston, N. G. (2013). Temporal dynamics of a simple community with intraguild predation: an experimental test. *Ecology* 94, 773–779. doi: 10.1890/12-0786.1

Hirche, H. J. (1987). Temperature and plankton II. Effect on respiration and swimming activity in copepods from the Greenland Sea. *Mar. Biol.* 94, 347–356. doi: 10.1007/BF00428240

Holt, R. D., and Polis, G. A. (1997). A theoretical framework for intraguild predation. *Am. Nat.* 149, 745–764. doi: 10.1086/286018

Hopcroft, R. R., Kosobokova, K. N., and Pinchuk, A. I. (2010). Zooplankton community patterns in the Chukchi Sea during summer 2004. *Deep Sea Res. Part II: Top. Stud. Oceanogr.* 57, 27–39. doi: 10.1016/j.dsr2.2009.08.003

Huntley, M. E., and Escritor, F. (1992). Ecology of *Metridia gerlachei* Giesbrecht in the western Bransfield Strait, Antarctica. *Deep Sea Res. Part A Oceanogr. Res. Pap.* 39, 1027–1055. doi: 10.1016/0198-0149(92)90038-U

Irigoien, X., and Harris, R. P. (2006). Comparative population structure, abundance and vertical distribution of six copepod species in the North Atlantic: evidence for intraguild predation? *Mar. Biol. Res.* 2, 276–290. doi: 10.1080/17451000600865321

Jung-Madsen, S., Nielsen, T. G., Grønkjaer, P., Hansen, B. W., and Møller, E. F. (2013). Early development of *Calanus hyperboreus* nauplii: response to a changing ocean. *Limnol. Oceanogr.* 58, 2109–2121. doi: 10.4319/lo.2013.58.6.2109

Kiørboe, T. (2011). How zooplankton feed: mechanisms, traits and trade-offs. *Biol. Rev. Camb. Philos. Soc.* 86, 311–339. doi: 10.1111/j.1469-185X.2010.00148.x

Kiørboe, T. (2013). Attack or attacked: the sensory and fluid mechanical constraints of copepods' predator-prey interactions. *Integr. Comp. Biol.* 53, 821–831. doi: 10.1093/icb/ict021

Kwasniewski, S., Gluchowska, M., Jakubas, D., Wojczulanis-Jakubas, K., Walkusz, W., Karnovsky, N., et al. (2010). The impact of different hydrographic conditions and zooplankton communities on provisioning Little Auks along the West coast of Spitsbergen. *Prog. Oceanogr.* 87, 72–82. doi: 10.1016/j.pocean.2010.06.004

Landry, M. R. (1981). Switching Between Herbivory and Carnivory by the Planktonic Marine Copepod *Calanus pacificus*. *Mar. Biol.* 65, 77–82. doi: 10.1007/BF00397070

Lee, R. F., Hagen, W., and Kattner, G. (2006). Lipid storage in marine zooplankton. *Mar. Ecol. Prog. Ser.* 307, 273–306. doi: 10.3354/meps307273

Le Fouest, V., Lefouest, V., Zakardjian, B., Saucier, F. J., and Starr, M. (2005). Seasonal versus synoptic variability in planktonic production in a high-latitude marginal sea: The Gulf of St. Lawrence (Canada). *J. Geophys. Res. C Oceans* 110, 1–21. doi: 10.1029/2004JC002423

Melle, W., Runge, J., Head, E., Plourde, S., Castellani, C., Licandro, P., et al. (2014). The North Atlantic Ocean as habitat for *Calanus finmarchicus*: environmental factors and life history traits. *Prog. Oceanogr.* 129, 244–284. doi: 10.1016/j.pocean.2014.04.026

Menden-Deuer, S., and Lessard, E. J. (2000). Carbon to volume relationships for dinoflagellates, diatoms, and other protist plankton. *Limnol. Oceanogr.* 45, 569–579. doi: 10.4319/lo.2000.45.3.0569

Mills, K. E., Pershing, A. J., Sheehan, T. F., and Mountain, D. (2013). Climate and ecosystem linkages explain widespread declines in North American Atlantic salmon populations. *Glob. Chang. Biol.* 19, 3046–3061. doi: 10.1111/gcb.12298

Morozov, A., Pasternak, A. F., and Arashkevich, E. G. (2013). Revisiting the role of individual variability in population persistence and stability. *PLoS ONE* 8:e70576. doi: 10.1371/journal.pone.0070576

Neuheimer, A. B., Gentleman, W. C., Pepin, P., and Head, E. J. H. (2010). How to build and use individual-based models (IBMs) as hypothesis testing tools. *J. Mar. Syst.* 81, 122–133. doi: 10.1016/j.jmarsys.2009.12.009

Ohman, M. D., and Hirche, H. J. (2001). Density-dependent mortality in an oceanic copepod population. *Nature* 412, 638–641. doi: 10.1038/35088068

Ohman, M., Eiane, K., Durbin, E., Runge, J., and Hirche, H. (2004). A comparative study of *Calanus finmarchicus* mortality patterns at five localities in the North Atlantic. *ICES J. Mar. Sci.* 61, 687–697. doi: 10.1016/j.icesjms.2004.03.016

Plourde, S., Dodson, J. J., Runge, J. A., and Therriault, J. C. (2002). Spatial and temporal variations in copepod community structure in the lower St. Lawrence Estuary, Canada. *Mar. Ecol. Prog. Ser.* 230, 211–224. doi: 10.3354/meps230211

Plourde, S., Joly, P., Runge, J. A., Dodson, J., and Zakardjian, B. (2003). Life cycle of *Calanus hyperboreus* in the lower St. Lawrence Estuary and its relationship to local environmental conditions. *Mar. Ecol. Prog. Ser.* 255, 219–233. doi: 10.3354/meps255219

Plourde, S., Maps, F., and Joly, P. (2009). Mortality and survival in early stages control recruitment in *Calanus finmarchicus*. *J. Plankton Res.* 31, 371–388. doi: 10.1093/plankt/fbn126

Polis, G. A., Myers, C. A., and Holt, R. D. (1989). The ecology and evolution of intraguild: potential competitors that eat each other. *Annu. Rev. Ecol. Syst.* 20, 297–330. doi: 10.1146/annurev.es.20.110189.001501

Pomerleau, C., Lesage, V., Winkler, G., Rosenberg, B., and Ferguson, S. H. (2014). Contemporary diet of bowhead whales (*Balaena mysticetus*) from the Eastern Canadian Arctic inferred from fatty acid biomarkers. *Arctic* 67, 84. doi: 10.14430/arctic4366

Record, N. R., and Pershing, A. J. (2008). Modeling zooplankton development using the monotonic upstream scheme for conservation laws. *Limnol. Oceanogr. Methods* 6, 364–372. doi: 10.4319/lom.2008.6.364

Record, N. R., Pershing, A. J., and Maps, F. (2012). First principles of copepod development help explain global marine diversity patterns. *Oecologia* 170, 289–295. doi: 10.1007/s00442-012-2313-0

Record, N. R., Pershing, A. J., and Maps, F. (2013). Emergent copepod communities in an adaptive trait-structured model. *Ecol. Model.* 260, 11–24. doi: 10.1016/j.ecolmodel.2013.03.018

Reygondeau, G., and Beaugrand, G. (2011). Future climate-driven shifts in distribution of *Calanus finmarchicus*. *Glob. Chang. Biol.* 17, 756–766. doi: 10.1111/j.1365-2486.2010.02310.x

Saucier, F. J., Roy, F., and Gilbert, D. (2003). Modeling the formation and circulation processes of water masses and sea ice in the Gulf of St. Lawrence, Canada. *J. Geophys. Res.* 3269, 2501–2520. doi: 10.1029/2000jc000686

Schmid, M. S., Aubry, C., Grigor, J., and Fortier, L. (2016). The LOKI underwater imaging system and an automatic identification model for the detection of zooplankton taxa in the Arctic Ocean. *Methods Oceanogr.* 160, 129–160. doi: 10.1016/j.mio.2016.03.003

Seuthe, L., Darnis, G., Riser, C. W., Wassmann, P., and Fortier, L. (2006). Winter–spring feeding and metabolism of Arctic copepods: insights from faecal pellet production and respiration measurements in the southeastern Beaufort Sea. *Polar Biology* 30, 427–436. doi: 10.1007/s00300-006-0199-1

Soetaert, K., and Herman, P. M. J. (2009). *A Practical Guide to Ecological Modelling*. Dordrecht: Springer.

Vestheim, H., Brucet, S., and Kaartvedt, S. (2013). Vertical distribution, feeding and vulnerability to tactile predation in *Metridia longa* (Copepoda, Calanoida). *Mar. Biol. Res.* 9, 949–957. doi: 10.1080/17451000.2013.793806

Visser, A. W. W., and Jónasdóttir, S. H. (1999). Lipids, buoyancy and the seasonal vertical migration of *Calanus finmarchicus*. *Fish. Oceanogr.* 8, 100–106. doi: 10.1046/j.1365-2419.1999.00001.x

**Conflict of Interest Statement:** The authors declare that the research was conducted in the absence of any commercial or financial relationships that could be construed as a potential conflict of interest.

frontiers in Ecology and Evolution

ORIGINAL RESEARCH
published: 18 July 2017
doi: 10.3389/fevo.2017.00078

# Modeling Plankton Mixotrophy: A Mechanistic Model Consistent with the Shuter-Type Biochemical Approach

*Caroline Ghyoot*[1]*, *Kevin J. Flynn*[2], *Aditee Mitra*[2], *Christiane Lancelot*[1] and *Nathalie Gypens*[1]

[1] Ecologie des Systèmes Aquatiques, Université libre de Bruxelles, Brussels, Belgium, [2] Biosciences, Swansea University, Swansea, United Kingdom

Mixotrophy, i.e., the ability to combine phototrophy and phagotrophy in one organism, is now recognized to be widespread among photic-zone protists and to potentially modify the structure and functioning of planktonic ecosystems. However, few biogeochemical/ecological models explicitly include this mode of nutrition, owing to the large diversity of observed mixotrophic types, the few data allowing the parameterization of physiological processes, and the need to make the addition of mixotrophy into existing ecosystem models as simple as possible. We here propose and discuss a flexible model that depicts the main observed behaviors of mixotrophy in microplankton. A first model version describes constitutive mixotrophy (the organism photosynthesizes by use of its own chloroplasts). This model version offers two possible configurations, allowing the description of constitutive mixotrophs (CMs) that favor either phototrophy or heterotrophy. A second version describes non-constitutive mixotrophy (the organism performs phototrophy by use of chloroplasts acquired from its prey). The model variants were described so as to be consistent with a plankton conceptualization in which the biomass is divided into separate components on the basis of their biochemical function (Shuter-approach; Shuter, 1979). The two model variants of mixotrophy can easily be implemented in ecological models that adopt the Shuter-approach, such as the MIRO model (Lancelot et al., 2005), and address the challenges associated with modeling mixotrophy.

**Keywords: constitutive mixotroph (CM), non-constitutive mixotroph (NCM), modeling, phytoplankton, zooplankton**

OPEN ACCESS

***Edited by:***
*Michael Arthur St. John, Institute for Aquatic Resources, Danish Technical University, Denmark*

***Reviewed by:***
*Peter Allan Thompson, Commonwealth Scientific Industrial Research Organisation, Australia*
*Alberto Basset, University of Salento, Italy*

***Correspondence:**
*Caroline Ghyoot*
*cghyoot@ulb.ac.be*

***Specialty section:***
*This article was submitted to Marine Ecosystem Ecology, a section of the journal Frontiers in Ecology and Evolution*

***Received:*** *21 June 2016*
***Accepted:*** *30 June 2017*
***Published:*** *18 July 2017*

***Citation:***
*Ghyoot C, Flynn KJ, Mitra A, Lancelot C and Gypens N (2017) Modeling Plankton Mixotrophy: A Mechanistic Model Consistent with the Shuter-Type Biochemical Approach. Front. Ecol. Evol. 5:78. doi: 10.3389/fevo.2017.00078*

## INTRODUCTION

Traditionally, planktonic protists are separated into two distinct functional groups: the phototrophic phytoplankton and the phago-heterotrophic microzooplankton. However, many protists assigned to these two groups are recognized as capable of combining phototrophy and phago-heterotrophy (Flynn et al., 2013). These mixotrophic protists have been reported in all planktonic functional groups (with the notable exception of the diatoms) and they include a large diversity of mixotrophic types (Flynn et al., 2013). In some mixotrophs, growth is mainly supported by phototrophy (e.g., *Cryptomonas ovata*; Tranvik et al., 1989) while in others, growth

is mainly supported by phagotrophy (e.g., *Poterioochromonas malhamensis*; Sanders, 1991). Some mixotrophs are forced to use both trophic modes to grow and survive because some essential metabolites come specifically from one of the two metabolic pathways (e.g., the ciliate *Laboea strobila*; Stoecker et al., 1988); others are facultative mixotrophs (e.g., the dinoflagellate *Fragilidium duplocampanaeforme*; Park et al., 2015). Some mixotrophs use their second trophic mode to fulfill carbon requirements (e.g., the haptophyte *Chrysochromulina brevifilum*; Stoecker, 1998); for others, it is a means to fulfill nutrient requirements (e.g., the dinoglagellate *Prorocentrum minimum*; Stoecker, 1998); and for others yet, it is a mechanism to get specific metabolites (as phospholipids; Kimura and Ishida, 1989).

Among this large diversity of mixotrophic types, a major distinction can be made between mixotrophs depending on whether they photosynthesize using their own chloroplasts or using chloroplasts acquired from their phototrophic prey (Mitra et al., 2016). Mixotrophs that actively synthesize and maintain their own chloroplasts are called constitutive mixotrophs (CMs). Mixotrophs that do not constitutively synthesize chloroplasts but photosynthesize using chloroplasts acquired from their phototrophic prey are called non-constitutive mixotrophs (NCMs). The acquired chloroplasts in NCMs remain functional for periods ranging from hours to days, depending on the type of NCM (Mitra et al., 2016). Generalist NCMs, i.e., those that acquire chloroplasts from a broad range of phototrophic prey, have a poor ability to maintain functional chloroplasts (Dolan and Pérez, 2000). By contrast, specialist NCMs, i.e., those that need to acquire chloroplasts from specific phototrophic prey, can maintain a photosynthetic activity for long periods (Stoecker et al., 2009; Hansen et al., 2013). Specialist NCMs can further be divided into those that retain the entire photosynthetic prey (endosymbiosis) and those that only retain the chloroplasts (kleptochloroplasty; Mitra et al., 2016). In a functional capacity, the CMs are closer to the strict phototrophs while the NCMs are closer to the strict phago-heterotrophs.

While mixotrophy has been reported for a long time, it is now appreciated as being much more widespread in aquatic ecosystems than initially thought. Previously, the mixotrophic status was only accorded to some dinoflagellates, forams, radiolarian, and acantheria while now, mixotrophy has been acknowledged in all eukaryote planktonic microorganism groups, except diatoms (Sanders and Porter, 1988; Burkholder et al., 2008; Flynn et al., 2013). In addition, these species are not limited to a specific habitat: mixotrophs are observed in both freshwater and marine (Sanders, 1991; Stoecker et al., 2009), oligotrophic and eutrophic systems (Burkholder et al., 2008), and from polar to equatorial regions (Zubkov and Tarran, 2008; Stoecker et al., 2009; Sanders and Gast, 2012). In coastal areas, mixotrophic flagellates can account for some 50% of the pigmented biomass (Havskum and Riemann, 1996) and chloroplast-containing ciliates can account for 40–>60% of the planktonic ciliates in summer (Stoecker et al., 1987; Bernard and Rassoulzadegan, 1994). In oceanic waters, mixotrophs account for 40–95% of the bacterivory in the euphotic layer (Zubkov and Tarran, 2008).

Constitutive mixotrophy is suggested to play an important ecological role when inorganic nutrients are low (e.g., in oligotrophic systems; e.g., Arenovski et al., 1995) or unbalanced (e.g., in eutrophied systems; e.g., Nygaard and Tobiesen, 1993; Burkholder et al., 2008), and when light is limiting (e.g., during the polar night or occasionally in eutrophied systems; e.g., Bird and Kalff, 1986; Roberts and Laybourn-Parry, 1999; Jones et al., 2009). In such systems, prey ingestion provides nutrients and energy. Similarly, non-constitutive mixotrophy may be advantageous in "high light–low prey" ecosystems (e.g., in oligotrophic systems; e.g., Skovgaard, 1998; Hansen et al., 2013) because acquired phototrophy supplies carbon by photosynthesis. Finally, mixotrophy is worthy of interest in an environmental perspective because most marine harmful algae have been reported as mixotrophs (Stoecker et al., 2006; Burkholder et al., 2008; Jeong et al., 2010).

Several models have been developed with the specific aims of exploring planktonic mixotrophy from an ecophysiological or ecological (species competition) perspective. Most interest has been leveled at the potential impact of mixotrophs on the microbial food web structure and functioning, and the conditions under which mixotrophs may likely coexist with strict phototrophs and heterotrophs (Thingstad et al., 1996; Baretta-Bekker et al., 1998; Stickney et al., 2000; Jost et al., 2004; Hammer and Pitchford, 2005; Hood et al., 2006; Flynn and Mitra, 2009; Crane and Grover, 2010; Ward et al., 2011; Våge et al., 2013). By far the greater effort has been applied to CM organisms. The complexity of the model structure varies widely among such studies. The simplest models describe mixotrophy as the ability to combine both phototrophy and heterotrophy without any feedbacks or trade-offs between the two nutritional modes and organisms have a fixed stoichiometry (e.g., Hammer and Pitchford, 2005). At the other extreme, the most complex model explicitly describes the main regulative processes that occur between phototrophy and heterotrophy in the mixotroph and allows for a variation of the cellular stoichiometry (Flynn and Mitra, 2009).

Despite the potential significance of mixotrophy in aquatic systems and the existence of mathematical models describing this trophic mode, few ecological/biogeochemical models consider it explicitly (e.g., Mitra et al., 2014). Those models that do include mixotrophs demonstrate the potential for mixotrophy to significantly impact the flow of energy and nutrients in the system. In particular, primary production can potentially be increased by a factor 2 compared to a system in which mixotrophy is not considered, thanks to a shortened and more effective chain from nutrient regeneration to primary production (Mitra et al., 2014).

Considering mixotrophy in biogeochemical/ecological models is however challenging due to the large diversity of mixotrophic types, the scarcity of data allowing the parameterization of physiological processes, and the need to make the inclusion of mixotrophy into existing ecosystem models as simple as possible. Indeed, the addition of a mixotroph functional type description into ecosystem models will inevitably be tempered by the structure of the extant ecosystem model.

Regarding the diversity of mixotrophic types, this paper proposes a flexible mechanistic model featuring the two main types of mixotrophy: constitutive and non-constitutive. The two mixotrophic types have indeed different ecophysiology and different relation to their prey (the NCM being strictly dependent on the presence of prey); therefore, they affect differently the ecosystem dynamics (Mitra et al., 2016). In addition, the version describing constitutive mixotrophy can be configured to represent either CMs that favor either phototrophy or heterotrophy. Simulations have been performed to compare each mixotrophic type with the strict trophic type it most closely resembles from a functional perspective (the CM with the strict phototroph and the NCM with the strict heterotroph) in order to explore the competitive advantage of mixotrophy over strict forms.

As for the explicit inclusion of mixotrophy into existing biogeochemical/ecological models, we were mainly interested in introducing mixotrophy in a form consistent with the mechanistic structure of the AQUAPHY model (Lancelot et al., 1991); this model has been used to describe primary production via phytoplankton growth physiology within several biogeochemical models (Billen et al., 1994; Lancelot et al., 2000, 2005). A feature of AQUAPHY is that the total cellular carbon is divided into separate classes of components on the basis of their function: these comprise synthetic and structural material (i.e., photosynthetic apparatus, ribosomes, genetic material, membranes, etc.), stored carbon (i.e., carbohydrates, lipids), and carbon monomers (i.e., photosynthetic products and precursors of complex molecules). This mechanistic approach was suggested by Shuter (1979) as a means to successfully describe the observed behavior of a variety of unicellular algal species, qualitatively and quantitatively. The work is thus a first step in the implementation of mixotrophy in the biogeochemical models that adopt a "Shuter mechanistic approach" to describe the phytoplankton physiology.

# METHODS

## Constitutive Mixotrophy

The model of constitutive mixotrophy was constructed on the basis of the following hypotheses, summarizing the main qualitative observations related to CMs : (i) the CM is preferentially phototrophic but it can supplement its nutrient requirements (under inorganic nutrient limitation) or its carbon requirements (under light limitation) by ingesting prey (e.g., in Jones et al., 1995; Carvalho and Granéli, 2010; McKie-Krisberg et al., 2015); (ii) the maximum mixotrophic growth is not allowed to exceed the maximum phototrophic growth; (iii) the phototrophic growth has to account for at least 10% of the mixotrophic growth, such that we describe an obligate phototroph (Caron et al., 1993; Brutemark and Granéli, 2011); (iv) the nutrients regenerated by heterotrophic activity ($PO_4^{3-}$, $NH_4^+$) are re-assimilated to sustaining phototrophic growth with any surplus being excreted (Flynn and Mitra, 2009).

The model combines an adaptation of the AQUAPHY model (Lancelot et al., 1991; Ghyoot et al., 2015) for the phototrophic pathway, coupled to a simple zooplankton model (Lancelot et al., 2005) for the phago-heterotrophic path. It is important to note that, in keeping with the formulation of the AQUAPHY model, the description of mixotrophy given here describes biomass growth (i.e., molC $m^{-3}$ $time^{-1}$) rather than per capita growth (i.e., C $C^{-1}$ $time^{-1}$) as in some other models (e.g., Flynn and Mitra, 2009). **Figure 1A** shows the schematic representation of the CM growth physiology, linking the phototrophic (dark gray) and heterotrophic (light gray) components. The CM model contains six state variables (**Table 1**) describing intracellular components on the basis of their function: the functional and structural metabolites (e.g., nucleic acids, proteins) synthesized by phototrophic and heterotrophic activities ($F^{phot}$ and $F^{het}$, respectively), soluble carbon monomers (i.e., early products of photosynthesis; $S_C$), carbon reserves (i.e., carbohydrates, fatty acids; $R_C$), intracellular soluble phosphate ($S_P$), and intracellular soluble inorganic nitrogen ($S_N$). The total C-cell biomass (mmolC $m^{-3}$) is given by the sum of $F^{phot}$, $F^{het}$, $S_C$, and $R_C$. The $F^{phot}$ and $F^{het}$ pools are assumed to have a fixed C:N:P stoichiometry, based on biochemical constraints (Geider and Laroche, 2002). Variable cellular stoichiometry is enabled by considering the additional C, P, and N accumulated as carbon monomers ($S_C$), carbohydrates and fatty acids ($R_C$), soluble inorganic phosphorus ($S_P$), and soluble inorganic nitrogen ($S_N$). The model of constitutive mixotrophy is linked to three state variables describing external inorganic nutrients—dissolved inorganic nitrogen (DIN $= NO_3^- + NH_4^+$) and phosphate ($PO_4^{3-}$)—and also the prey which in reality expresses a variable C:N:P stoichiometry (though here prey stoichiometry is fixed as the emphasis is on the description of the autecology of the mixotrophs, rather than system ecology).

**Tables 2**, **3** show, respectively, the nine conservation equations related to the state variables and the associated processes. Phototrophic growth ($\mu^{phot}$; Equation 17) is controlled by the concentration of the structural and functional metabolites related to phototrophic activity ($F^{phot}$), by the limitation in carbon monomers $S_C$—either directly produced by photosynthesis ($\varphi$; Equation 20) or indirectly by $R_C$ catabolism ($cat_{RC}$; Equation 10)—and by the limitation in internal soluble inorganic nutrients ($S_N$ and $S_P$). The $S_C$ limitation is formulated by a Michaelis–Menten equation in which the substrate concentration is expressed by $X_{S_C} - k_{S_C}$, with $X_{S_C} = \frac{S_C}{F^{phot}}$ and $k_{S_C}$, which is the minimum value for $X_{S_C}$ (assumed to be equal to the half-saturation constant for $S_C$ assimilation). The inorganic nutrient limitation is formulated by the Liebig's minimum law in which the limitation for each nutrient is expressed by a hyperbolic function depending on $X_{S_{N,P}}$ (the ratio between $S_{N,P}$ and the N,P contained in $F^{phot}$). The uptake of inorganic nutrients ($upt_{DIN}$ and $upt_{PO4}$; Equations 26 and 27) depends on the external nutrient concentration and the status of the internal nutrient reserve. The phototrophic respiration ($resp^{phot}$; Equation 22) includes costs for cellular maintenance and for synthesis of new $F^{phot}$.

Prey ingestion ($graz$; Equation 14) is controlled by the concentration of the structural and functional metabolites related to heterotrophic activity ($F^{het}$) and by prey availability; the latter

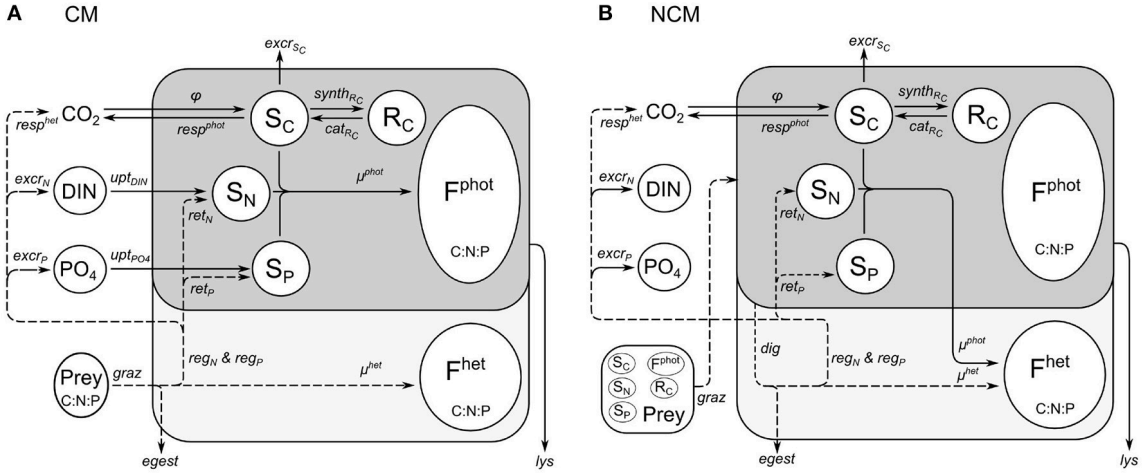


**FIGURE 1 |** Schematic representation of functioning of constitutive mixotroph (CM; **A**) and non-constitutive mixotroph (NCM; **B**). Total mixotroph biomass is divided into six components: structural and functional metabolites related to phototrophic activity ($F^{phot}$) and heterotrophic activity ($F^{het}$), carbon monomers ($S_C$), carbon reserves ($R_C$), soluble inorganic nitrogen ($S_N$), and soluble inorganic phosphorus ($S_P$). The "dark gray part/solid lines" is the phototrophic part and the "light gray part/dashed lines" is the heterotrophic part.

**TABLE 1 |** Model state variables (all expressed as a concentration in water).

| State variable | Description | Units |
|---|---|---|
| **MIXOTROPH** | | |
| $F^{phot}$ | Functional and structural metabolites related to phototrophy | mmolC $m^{-3}$ |
| $F^{het}$ | Functional and structural metabolites related to heterotrophy | mmolC $m^{-3}$ |
| $S_C$ | Soluble carbon monomers (early products of photosynthesis) | mmolC $m^{-3}$ |
| $R_C$ | Carbon reserves (carbohydrates, fatty acids) | mmolC $m^{-3}$ |
| $S_N$ | Intracellular soluble inorganic nitrogen | mmolN $m^{-3}$ |
| $S_P$ | Intracellular soluble phosphate | mmolP $m^{-3}$ |
| **EXTERNAL NUTRIENTS** | | |
| DIN ($NO_3 + NH_4$) | Dissolved inorganic nitrogen | mmolN $m^{-3}$ |
| $PO_4$ | Phosphate | mmolP $m^{-3}$ |
| Prey | Prey | mmolC $m^{-3}$ |

**TABLE 2 |** Conservation equations for the constitutive mixotroph (CM).

| Eq. | Conservation equations | Units |
|---|---|---|
| 1 | $\frac{dF^{phot}}{dt} = \mu^{phot} - lys_{F^{phot}}$ | mmolC $m^{-3}$ $h^{-1}$ |
| 2 | $\frac{dF^{het}}{dt} = \mu^{het} - lys_{F^{het}}$ | mmolC $m^{-3}$ $h^{-1}$ |
| 3 | $\frac{dS_C}{dt} = \varphi - excr_{S_C} - synth_{R_C} + cat_{R_C} - \mu^{phot} - resp^{phot} - lys_{S_C}$ | mmolC $m^{-3}$ $h^{-1}$ |
| 4 | $\frac{dR_C}{dt} = synth_{R_C} - cat_{R_C} - lys_{R_C}$ | mmolC $m^{-3}$ $h^{-1}$ |
| 5 | $\frac{dS_N}{dt} = upt_{DIN} - \frac{\mu^{phot}}{CN^{F^{phot}}} + ret_N - lys_{S_N}$ | mmolN $m^{-3}$ $h^{-1}$ |
| 6 | $\frac{dS_P}{dt} = upt_{PO4} - \frac{\mu^{phot}}{CP^{F^{phot}}} + ret_P - lys_{S_P}$ | mmolP $m^{-3}$ $h^{-1}$ |
| 7 | $\frac{dDIN}{dt} = -upt_{DIN} + excr_N + lys_{S_N}$ | mmolN $m^{-3}$ $h^{-1}$ |
| 8 | $\frac{dPO_4}{dt} = -upt_{PO4} + excr_P + lys_{S_P}$ | mmolP $m^{-3}$ $h^{-1}$ |
| 9 | $\frac{dPrey}{dt} = -graz$ | mmolC $m^{-3}$ $h^{-1}$ |

is controlled by a sigmoid (type III) function. From the ingested prey, a non-assimilated fraction is egested (*egest*; Equation 11) as dissolved and particulate organic matter (loss terms), a fraction is respired to meet the heterotrophic metabolic costs and is released as carbon dioxyde ($resp^{het}$; Equation 21), and the last fraction is assimilated and contributes directly to the heterotrophic growth ($\mu^{het}$; Equation 16). If the nutrient content of the prey is higher than the nutrient required by $F_{het}$, the surplus is regenerated as $NH_4^+$ and $PO_4^{3-}$ ($reg_i$ with $i$ = N, P; Equation 23). These regenerated nutrients can be retained up to a maximum level in the inorganic nutrient reserves $S_N$ and $S_P$ ($ret_i$; Equation 24), contributing to the phototrophic growth. If the reserve capacity is full, the surplus is excreted to the environment ($excr_i$; Equation 12).

Mixotrophic growth is computed as the sum of the phototrophic and the heterotrophic growth rate, but limited by the maximum mixotrophic growth. The latter is computed differently according to whether phagotrophy is used to offset a lack of carbon or a lack of nutrients. When the 24 h-average $S_C$ limitation is below a threshold value ($thresh^{S_C lim}$) set here as 0.15, we assumed that the mixotroph switches to perform increasing levels of phagotrophy to acquire carbon (in addition to nutrients if also nutrients limited) and, therefore, the maximum mixotrophic growth is equal to the phototrophic growth obtained with no limitation ($\mu^{mix}_{\max}$; Equation 18). When the 24 h-average $S_C$ limitation is above this threshold value, we assumed that the CM undertakes phagotrophy to acquire nutrients and, therefore, the maximum mixotrophic growth is equal to the phototrophic growth obtained with no nutrient limitation ($\mu^{mix}_{max}$; Equation 19). If the sum of the phototrophic and the heterotrophic growth is higher than the maximum mixotrophic growth, either the grazing or the photosynthesis rate is regulated to

**TABLE 3 |** Equations that describe the processes occurring in the constitutive mixotroph (CM).

| Eq. | Process | Value | Units | Explanation |
|---|---|---|---|---|
| 10 | $cat_{R_C}$ | $k_{cR} \cdot R_C$ | mmolC $m^{-3}$ $h^{-1}$ | Catabolism of carbon reserves |
| 11 | *egest* | $fp \cdot graz$ | mmolC $m^{-3}$ $h^{-1}$ | Egestion of non-assimilated prey |
| 12 | $excr_{S_C}$ | $k^{excr} \cdot S_C$ | mmolC $m^{-3}$ $h^{-1}$ | Excretion of soluble C monomers |
| 13 | $excr_i$ ($i$ = N, P) | $reg_i - ret_i$ ($i$ = N, P) | mmol $i$ $m^{-3}$ $h^{-1}$ ($i$ = N, P) | Excretion of $NH_4^+$ and $PO_4^{3-}$ which are regenerated by the heterotrophic activity but are not retained in the reserves $S_N$ and $S_P$ |
| 14 | *graz* | $g_{max} \cdot \frac{prey^2}{prey^2+k_g^2} \cdot F^{het}$ | mmolC $m^{-3}$ $h^{-1}$ | Grazing |
| 15 | $lys_i$ ($i$ = $F^{phot}$, $F^{het}$, $S_C$, $R_C$, $S_N$, $S_P$) | $k^{lys} \cdot i$ ($i$ = $F^{phot}$, $F^{het}$, $S_C$, $R_C$, $S_N$, $S_P$) | mmol $i$ $m^{-3}$ $h^{-1}$ ($i$ = C, N, P) | Biomass lysis; $k^{lys}$ depends on the nutrient limitation such as lysis is higher when nutrient limitation is strong |
| 16 | $\mu^{het}$ | $y \cdot graz$ | mmolC $m^{-3}$ $h^{-1}$ | Heterotrophic growth |
| 17 | $\mu^{phot}$ | $\mu_{max}^{phot} \cdot \frac{X_{S_C}-k_{S_C}}{\left(X_{S_C}-k_{S_C}\right)+k_{S_C}} \cdot min\left[\frac{X_{S_N}}{X_{S_N}+k_{S_N}}, \frac{X_{S_P}}{X_{S_P}+k_{S_P}}\right] \cdot F^{phot}$ | mmolC $m^{-3}$ $h^{-1}$ | Phototrophic growth depending on $S_C$ limitation ($XS_C = S_C/F_{phot}$) and nutrient limitation: $X_{S_N} = S_N/\left(F^{phot}/CN^{F^{phot}}\right)$ and $X_{S_P} = S_P/\left(F^{phot}/CP^{F^{phot}}\right)$ |
| 18 | $\mu_{max}^{mix}$ | $\mu_{max}^{phot} \cdot \left(F^{phot} + F^{het}\right)$ | mmolC $m^{-3}$ $h^{-1}$ | Maximum mixotrophic growth under light (and nutrient) limitation |
| 19 | $\mu_{max}^{mix}$ | $\mu_{max}^{phot} \cdot \frac{X_{S_C}-k_{S_C}}{\left(X_{S_C}-k_{S_C}\right)+k_{S_C}} \cdot \left(F^{phot} + F^{het}\right)$ | mmolC $m^{-3}$ $h^{-1}$ | Maximum mixotrophic growth under nutrient limitation only |
| 20 | $\varphi$ | $k_{max} \cdot \left(1 - e^{-\frac{\alpha \cdot PAR}{k_{max}}}\right) \cdot F^{phot}$ with $PAR = PAR_0 \cdot e^{-\eta \cdot dpth}$ | mmolC $m^{-3}$ $h^{-1}$ | Photosynthesis depending on light intensity (PAR) in the water column. The shading ($\eta$) is controlled by the concentration of photosynthetic plankton: $\eta = \eta_{self} \cdot \left(\frac{1}{CChl^{F^{phot}}}\right) \cdot F^{phot}$ |
| 21 | $resp^{het}$ | $(1 - fp - y) \cdot graz$ | mmolC $m^{-3}$ $h^{-1}$ | Heterotrophic respiration, which is the carbon part of the prey that is not egested and not assimilated in $F^{het}$ |
| 22 | $resp^{phot}$ | $k^{maint} \cdot F^{phot} + \xi \cdot \mu^{phot}$ | mmolC $m^{-3}$ $h^{-1}$ | Phototrophic respiration including costs for cellular maintenance and synthesis of new $F^{phot}$. The cost for $F^{phot}$ synthesis depends on a metabolic cost function ($\xi$) varying as a function of the N source, $NO_3$ or $NH_4$ |
| 23 | $reg_i$ ($i$ = N, P) | $(1 - fp) \cdot \frac{graz}{Ci^{prey}} - \frac{\mu^{het}}{Ci^{Fhet}}$ ($i$ = N, P) | mmol $i$ $m^{-3}$ $h^{-1}$ ($i$ = N, P) | Regeneration of $NH_4$ and $PO_4$ through heterotrophic activity (regeneration is then distributed between retention and excretion) |
| 24 | $ret_i$ ($i$ = N, P) | $min\left[ret_i^{max}, reg_i\right]$ ($i$ = N, P) | mmol $i$ $m^{-3}$ $h^{-1}$ ($i$ = N, P) | Retention of $NH_4$ and $PO_4$ in the $S_N$ and $S_P$ reserves. Retention stops when $S_N$ and $S_P$ are full |
| 25 | $synth_{R_C}$ | $sr_{max} \cdot \frac{X_{S_C}}{\left(X_{S_C}-k_{S_C}\right)} \cdot F^{phot}$ | mmolC $m^{-3}$ $h^{-1}$ | Synthesis of carbon reserves |
| 26 | $upt_{DIN}$ | $upt_{max}^{DIN} \cdot \frac{DIN}{DIN+k_N} \cdot \frac{\left(1-X_{S_N}/X_{S_N}^{max}\right)^4}{\left(1-X_{S_N}/X_{S_N}^{max}\right)^4+k^{uptNreg}} \cdot \frac{F^{phot}}{CN^{Fphot}}$ | mmolN $m^{-3}$ $h^{-1}$ | Uptake of DIN depending on the external DIN concentration and restricted by $X_{S_N}\left(= S_N\Big/\left(F^{phot}\Big/CN^{F^{phot}}\right)\right)$ |
| 27 | $upt_{PO4}$ | $upt_{max}^{PO4} \cdot \frac{PO4}{PO4+k_P} \cdot \frac{\left(1-X_{S_P}/X_{S_P}^{max}\right)^4}{\left(1-X_{S_P}/X_{S_P}^{max}\right)^4+k^{uptPreg}} \cdot \frac{F^{phot}}{CP^{Fphot}}$ | mmolP $m^{-3}$ $h^{-1}$ | Uptake of $PO_4$ depending on the external $PO_4$ concentration and restricted by $X_{S_P}\left(= S_P\Big/\left(F^{phot}\Big/CP^{F^{phot}}\right)\right)$ |

limit the mixotrophic growth to its maximum. In other terms, the mixotroph can favor either phototrophic or heterotrophic growth. The model offers the possibility to test either of these two configurations: the CM that regulates its grazing rate (i.e., tends to grow phototrophically) hereafter referred to as "$Reg^{graz}$" and the CM that regulates its photosynthesis (i.e., tends to grow heterotrophically) hereafter referred to as "$Reg^{phot}$." In either case, we assumed that phototrophic growth has to represent at least 10% of the mixotrophic growth. This implies that phagotrophy cannot sustain growth under prolonged dark conditions because of an obligatory demand for products of photosynthesis.

Parameter values were selected here to describe constitutive mixotrophic nanoflagellates that graze on bacteria to fulfill nutrient or energy requirements (**Table 4**). Parameters related to phototrophic carbon pathways are those of phototrophic nanoflagellates as used in the MIRO model (the MIRO model being a biogeochemical model that uses AQUAPHY to represent phytoplankton growth and that describes the planktonic ecosystem of the Southern North Sea; Lancelot et al., 2005). Parameters related to phototrophic P-pathways are similar to those presented in Ghyoot et al. (2015). Parameters related to phototrophic N-pathways and parameters related to heterotrophic activity were estimated by implementing the mixotrophy model into the MIRO model and by tuning the model against observations reported in the Belgian coastal zone (Ghyoot et al., submitted). Observations used in that tuning included plankton biomass (bacteria, nanoflagellates, diatoms, *Phaeocystis* colonies, microzooplankton, and copepods) and nutrient concentrations [$NO_3^-$, $NH_4^+$, $PO_4^{3-}$, and dissolved silica (DSi)].

Single parameter steady-state model sensitivity to parameters values was studied with the method of Haefner (1996). The model was run under "low DIN–high prey" chemostat-type conditions and a normalized sensitivity index (*SI*; Equation 28) based on steady-state biomass was calculated for each parameter:

$$SI = \frac{(R - R_{ref})/R_{ref}}{(p - p_{ref})/p_{ref}} \tag{28}$$

Where $R_{ref}$ is the value of CM biomass reached at steady-state with the reference parameter value $p_{ref}$ (**Table 4**) and $R$ is the value of CM biomass reached at steady-state with $p$, the reference parameter increased/decreased by 25%. The *SI*-value is thus a measure of the relative variation of CM biomass compared to the relative variation of the parameter.

## Non-constitutive Mixotrophy

We constructed the model of non-constitutive mixotrophy on the basis of available qualitative observations specific to this type of mixotrophy: (i) the photosynthetic capacity of the ingested phototrophic prey is retained for some time in the food vacuole so that it provides carbon to the mixotroph (Skovgaard, 1998); (ii) in the food vacuole, there is no replication of the functional metabolites related to phototrophy; they are only supplied by phagotrophy on phototrophic prey; (iii) the digestion rate of the ingested phototrophic prey is constant; (iv) nutrients regenerated through heterotrophic activity ($PO_4^{3-}$, $NH_4^+$) can be retained for the phototrophic activity while the excess is excreted outside the cell; (v) there is no inorganic nutrient uptake (we assume these NCMs are generalist rather than specialist NCMs; the latter, such as *Mesodinium* and *Dinophysis*, are capable of using externally supplied inorganic nutrients; Hansen et al., 2013); (vi) the organism does not require some level of phototrophy to grow, meaning that we describe a facultative mixotroph (but a minimum level of phagotrophy is required for obtaining chloroplasts).

As for the model of constitutive mixotrophy, the model of non-constitutive mixotrophy combines the AQUAPHY model for the phototrophic path and a simple zooplankton model for the heterotrophic path. **Figure 1B** shows the schematic representation of the NCM growth physiology, showing the heterotrophic (light gray) and phototrophic (dark gray) components. While the model of non-constitutive mixotrophy deploys the same six state variables as the model of constitutive mixotrophy and operates with the same external factors (**Table 1**), some conservation equations (**Table 5**) and processes (**Table 6**) differ. The differences mainly rely on the fact that NCMs acquire their phototrophic capacity by ingesting phototrophic prey and they are not able to permanently maintain this capacity.

The phototrophic prey biomass (*prey*) is characterized by the five phototrophic compounds usually used within AQUAPHY: $F^{phot}$, $S_C$, $R_C$, $S_N$, and $S_P$ (we have therefore: $prey_{F^{phot}}$, $prey_{S_C}$, $prey_{R_C}$, $prey_{S_N}$, and $prey_{S_P}$). The grazing on each of these five compounds ($graz_i$ with $i = F^{phot}$, $S_C$, $R_C$, $S_N$, $S_P$; Equation 41) is computed as the grazing on the total prey biomass ($prey = prey_{F^{phot}} + prey_{S_C} + prey_{R_C}$) relative to the compound concentration. Once ingested by the NCM, the five compounds are distributed to their corresponding pools. As there is no mechanism for synthesis or maintenance of $F^{phot}$ in the NCM configuration, $F^{phot}$ is exclusively supplied via grazing on photrophic $prey_{F^{phot}}$ (Equation 30). $S_C$, $R_C$, $S_N$, and $S_P$ are supplied by the grazing but also by other (phototrophic and heterotrophic) processes (Equations 31–34). Photosynthesis and $R_C$ catabolism supply $S_C$ in the same way as in the model of constitutive mixotrophy ($\varphi$; cf. Equation 20 and $cat_{Rc}$; cf. Equation 10). $R_C$ synthesis supplies $R_C$, as in the model of constitutive mixotrophy ($synth_{Rc}$; cf. Equation 25), while nutrient retention supplies $S_N$ and $S_P$ ($ret_i$ with $i = N, P$; cf. Equation 24).

The phototrophic components obtained by grazing enables phototrophic growth to be computed as for the model of constitutive mixotrophy ($\mu^{phot}$; cf. Equation 17) but now the phototrophic growth supports the production of $F^{het}$ instead of $F^{phot}$ (Equation 29). As there is no synthesis and maintenance of $F^{phot}$, phototrophic respiration includes only costs for the synthesis of $F^{het}$ ($resp^{phot}$; Equation 44).

The phototrophic components in NCMs ($F^{phot}$, $S_C$, $R_C$, $S_N$, $S_P$) are continuously degraded (de facto digested) at a constant rate ($dig_i$ with $i = F^{phot}$, $S_C$, $R_C$, $S_N$, $S_P$; Equation 39). The digested material has three possible fates: the non-assimilated material is egested outside the cell (*egest*; Equation 40) as dissolved and particulate organic matter, a fraction of the assimilated material is respired ($resp^{het}$; Equation 43) to meet the heterotrophic metabolic costs, and the remaining fraction is used for heterotrophic growth ($\mu^{het}$; Equation 42). If the C:N:P stoichiometry of the digested prey is higher than the C:N:P stoichiometry of $F^{het}$, $NH_4^+$, and $PO_4^{3-}$ are regenerated ($reg_i$ with $i = N, P$; Equation 45). These nutrients can be retained in $S_N$ and $S_P$ and contribute to the phototrophic growth ($ret_i$ with $i = N, P$ calculated as in CM; cf. Equation 24). As we assumed that inorganic nutrient uptake does not occur in NCMs, these retained inorganic nutrients are the only ones that allow phototrophic growth. If the reserves $S_N$ and $S_P$ are full, the regenerated nutrients are excreted outside the cell ($excr_i$ with $i = N, P$ calculated as in CMs; cf. Equation 13).

**TABLE 4 |** Constant parameters used in the constitutive mixotroph (CM) and non-constitutive mixotroph (NCM) models.

| Parameters | CM | NCM | Units | Explanation |
|---|---|---|---|---|
| $\alpha$ | 0.002 | 0.002 | $h^{-1}$ $\mu mol^{-1}$ $m^2$ s | Parameter of light adaptation |
| $CChlF^{phot}$ | 2.083 | 2.083 | mmolC $mgChl^{-1}$ | C:Chl ratio for $F^{phot}$ |
| $CNF^{het}$ | 5.25 | 5.25 | molC $molN^{-1}$ | C:N ratio for $F^{het}$ |
| $CNF^{phot}$ | 4.1 | 4.1 | molC $molN^{-1}$ | C:N ratio for $F^{phot}$ |
| $CN^{prey}$ | 4.67 | variable | molC $molN^{-1}$ | C:N ratio for prey |
| $CPF^{het}$ | 84 | 84 | molC $molP^{-1}$ | C:P ratio for $F^{het}$ |
| $CPF^{phot}$ | 65 | 65 | molC $molP^{-1}$ | C:P ratio for $F^{phot}$ |
| $CP^{prey}$ | 74.67 | variable | molC $molP^{-1}$ | C:P ratio for prey |
| $\eta_{self}$ | 0.02 | 0.02 | $m^{-1}$ | Light extinction coeff. related to chl. |
| $fp$ | 0.25 | 0.25 | - | Egested fraction of ingestion |
| $g_{max}$ | 0.07 | 0.052 | $h^{-1}$ | Maximum grazing rate (at optimal T) |
| $k_{cR}$ | 0.06 | 0.06 | $h^{-1}$ | Constant of $R_C$ catabolism (at optimal T) |
| $k^{dig}$ | – | 0.03 | $h^{-1}$ | Constant digestion of ingested prey (at opt. T) |
| $k^{excr}$ | 0.001 | 0.001 | $h^{-1}$ | Constant of $S_C$ excretion |
| $k_g$ | 1.25 | 1.75 | mmolC $m^{-3}$ | Half-saturation constant of grazing |
| $k^{lys}$ | 0.0025 | 0.002 | $h^{-1}$ | Constant of cell autolysis (at optimal T) |
| $k^{maint}$ | 0.00081 | – | $h^{-1}$ | Constant of cellular maintenance (at opt. T) |
| $k_{max}$ | 0.1 | 0.1 | $h^{-1}$ | Maximum photosynthesis rate (at opt. T) |
| $k_N$ | 0.2 | – | mmolN $m^{-3}$ | Half-saturation constant for DIN uptake |
| $k_P$ | 0.25 | – | mmolP $m^{-3}$ | Half-saturation constant for $PO_4$ uptake |
| $k_{S_C}$ | 0.06 | 0.06 | – | Half-saturation constant for $S_C$ assimilation |
| $k_{S_N}$ | 0.014 | 0.014 | – | Half-saturation constant for $S_N$ assimilation |
| $k_{S_P}$ | 0.02 | 0.02 | – | Half-saturation constant for $S_P$ assimilation |
| $k^{uptNreg}$ | 0.0055 | – | – | Half-saturation constant for DIN uptake regulation |
| $k^{uptPreg}$ | 0.01 | – | – | Half-saturation constant for $PO_4$ uptake regulation |
| $\mu_{max}^{phot}$ | 0.09 | 0.09 | $h^{-1}$ | Maximum phototrophic growth rate (at opt. T) |
| $sr_{max}$ | 0.1 | 0.1 | $h^{-1}$ | Maximum $R_C$ synthesis rate (at optimal T) |
| $thresh^{S_C lim}$ | 0.15 | – | – | Threshold value of 24 h-average $S_C$ limitation under which the organism ingests prey for its C requirements |
| $upt_{max}^{DIN}$ | 0.2 | – | $h^{-1}$ | Maximum DIN uptake rate (at optimal T) |
| $upt_{max}^{PO4}$ | 0.22 | – | $h^{-1}$ | Maximum $PO_4$ uptake rate (at optimal T) |
| $X_{S_N}^{max}$ | 0.14 | 0.14 | – | Maximum $S_N/(F^{phot}/CN^{Fphot})$ ratio |
| $X_{S_P}^{max}$ | 0.2 | 0.2 | – | Maximum $S_P/(F^{phot}/CP^{Fphot})$ ratio |
| $y$ | 0.35 | 0.35 | – | Heterotrophic growth yield |

*Values were taken from Lancelot et al. (2005), Ghyoot et al. (2015) and Ghyoot et al. (submitted).*

**TABLE 5 |** Conservation equations for the non-constitutive mixotroph (NCM).

| Eq. | Conservation equations | Units |
|---|---|---|
| 29 | $\frac{dF^{het}}{dt} = \mu^{het} + \mu^{phot} - lys_{F^{het}}$ | mmolC $m^{-3}$ $h^{-1}$ |
| 30 | $\frac{dF^{phot}}{dt} = graz_{F^{phot}} - dig_{F^{phot}} - lys_{F^{phot}}$ | mmolC $m^{-3}$ $h^{-1}$ |
| 31 | $\frac{dS_C}{dt} = graz_{S_C} - dig_{S_C} + \varphi - excr_{S_C} - synth_{R_C} + cat_{R_C} - \mu^{phot} - resp^{phot} - lys_{S_C}$ | mmolC $m^{-3}$ $h^{-1}$ |
| 32 | $\frac{dR_C}{dt} = graz_{R_C} - dig_{R_C} + synth_{R_C} - cat_{R_C} - lys_{R_C}$ | mmolC $m^{-3}$ $h^{-1}$ |
| 33 | $\frac{dS_N}{dt} = graz_{S_N} - dig_{S_N} - \frac{\mu^{phot}}{CN^{F^{het}}} + ret_N - lys_{S_N}$ | mmolN $m^{-3}$ $h^{-1}$ |
| 34 | $\frac{dS_P}{dt} = graz_{S_P} - dig_{S_P} - \frac{\mu^{phot}}{CP^{F^{het}}} + ret_P - lys_{S_P}$ | mmolP $m^{-3}$ $h^{-1}$ |
| 35 | $\frac{dDIN}{dt} = excr_N + lys_{S_N}$ | mmolN $m^{-3}$ $h^{-1}$ |
| 36 | $\frac{dPO_4}{dt} = excr_P + lys_{S_P}$ | mmolP $m^{-3}$ $h^{-1}$ |
| 37 | $\frac{dprey_i}{dt} = -graz_i$ ($i = F^{phot}, S_C, R_C, S_N, S_P$) | mmol$i$ $m^{-3}$ $h^{-1}$ |

With the selected parameters values (**Table 4**), the model describes a generalist non-constitutive mixotrophic microzooplankton (ciliate) that feeds on phototrophic nanoflagellates and uses their chloroplasts to photosynthesize. The value of the constant rate of degradation of acquired photosystems is 0.03 $h^{-1}$, the same as in Flynn and Hansen (2013). The other parameters related to heterotrophic processes were estimated by implementing the mixotrophy models into the MIRO model that describes the planktonic ecosystem of the Southern North Sea and by tuning the model against observations reported in this area (Ghyoot et al., submitted). Parameters values involved in phototrophic processes are those of the phototrophic prey, i.e., the nanoflagellates, as in the model of constitutive mixotrophy.

**TABLE 6 |** Equations that describe the processes occurring in the non-constitutive mixotroph (NCM).

| Eq. | Process | Value | Units | Explanation |
|---|---|---|---|---|
| 38 | $dig$ | $k^{dig} \cdot \left(F^{phot} + S_C + R_C\right)$ | mmolC $m^{-3}$ $h^{-1}$ | Digestion of the ingested prey at a constant rate |
| 39 | $dig_i (i = F^{\text{phot}}, S_C, R_C, S_N, S_P)$ | $k^{dig} \cdot i$ ($i$ = $F^{\text{phot}}$, $S_C$, $R_C$, $S_N$, $S_P$) | mmol $i$ $m^{-3}$ $h^{-1}$ ($i$ = C, N, P) | Digestion of the ingestion prey according to the cellular component |
| 40 | $egest$ | $fp \cdot dig$ | mmolC $m^{-3}$ $h^{-1}$ | Egestion of non-assimilated prey |
| 41 | $graz_i (i = F^{\text{phot}}, S_C, R_C, S_N, S_P)$ | $g_{max} \cdot \frac{prey^2}{prey^2 + k_g^2} \cdot \frac{prey_i}{prey} \cdot F^{het}(i = F^{\text{phot}}, S_C, R_C, S_N, S_P)$ | mmol $i$ $m^{-3}$ $h^{-1}$ ($i$ = C, N, P) | Grazing |
| 42 | $\mu^{het}$ | $y \cdot dig$ | mmolC $m^{-3}$ $h^{-1}$ | Heterotrophic growth |
| 43 | $resp^{het}$ | $(1 - fp - y) \cdot dig$ | mmolC $m^{-3}$ $h^{-1}$ | Heterotrophic respiration which is the carbon part of the prey that is not egested and not assimilated in $F^{het}$ |
| 44 | $resp^{phot}$ | $\xi \cdot \mu^{phot}$ | mmolC $m^{-3}$ $h^{-1}$ | Phototrophic respiration including only costs for synthesis of new $F^{het}$ |
| 45 | $reg_i$ ($i$ = N, P) | $(1 - fp) \cdot \frac{dig}{Ci^{IngPrey}} - \frac{\mu^{het}}{Ci^{Fhet}}$ ($i$ = N, P) | mmol $i$ $m^{-3}$ $h^{-1}$ ($i$ = N, P) | Regeneration of $NH_4$ and $PO_4$ through heterotrophic activity (regeneration is then distributed between retention and excretion). The Ci of the ingested prey ($Ci^{IngPrey}$) is computed as: $Ci = \frac{F^{phot} + S_C + R_C}{\left(F^{phot}/Ci^{Fphot}\right) + S_i}$ with $i$ = N,P |

Model sensitivity to the parameter values was studied with the method of Haefner (1996) as described above for the model of constitutive mixotrophy (Equation 28).

# RESULTS

## Constitutive Mixotrophy

In order to explore the qualitative behavior of the CM under different environmental conditions, we ran the model of constitutive mixotrophy under steady-state conditions with various values of DIN (ranging from 0 to 20 mmolN $m^{-3}$) and prey (bacteria) biomass (ranging from 0 to 20 mmolC $m^{-3}$). These simulations were run under two contrasting photon flux densities (30 and 200 μmol quanta $m^{-2}$ $s^{-1}$). Conditions are such that P never limits the growth and the prey is considered as "inert" (i.e., bacteria growth and metabolism is not described). The two possible regulation mechanisms (photosynthesis "$Reg^{phot}$" vs. grazing "$Reg^{graz}$") limiting the mixotrophic growth to its maximum were tested. The performance of the two CMs ("$Reg^{graz}$" and "$Reg^{phot}$") is compared with that of the strict phototrophic nanoflagellate when growing under the same growth conditions.

Under high photon flux density (**Figure 2**), the growth rate of the strict phototroph decreases to zero as DIN decreases to zero because phototrophic growth is prevented by the lack of DIN (**Figure 2A**). By contrast, when prey concentration is higher than 4 mmolC $m^{-3}$, the growth rate of the two CM configurations ("$Reg^{graz}$" and "$Reg^{phot}$") does not vary as a function of DIN because the lack of DIN is offset by bacteria ingestion (**Figures 2F,K**). De facto, the model captures correctly the competitive advantage of the mixotrophs at low inorganic nutrient concentration and high prey concentration. The grazing rate of the two CMs varies in function of the external conditions: it increases when prey concentration increases and when DIN decreases (**Figures 2H,M**). Thanks to their grazing activity, at low DIN, the photosynthesis rate of the two CMs decreases less than the photosynthesis rate of the strict phototroph (**Figures 2B,G,L**). When mixotrophs ingest prey under high photon flux density, the entire part of the regenerated DIN is retained inside the cell to sustain phototrophic activity (**Figures 2J,O**); there is no $NH_4$ excretion (**Figures 2I,N**). Under this photon flux density, there is no noticeable difference between the two mixotrophic configurations (CM "$Reg^{graz}$" vs. CM "$Reg^{phot}$").

Under low photon flux density (**Figure 3**), the strict phototroph cannot grow in any nutrient conditions because the carbon monomers ($S_C$) limitation (which is controlled by the light limitation) is too high to allow steady-state growth rates above zero (**Figure 3A**). In function of its configuration, the CM behaves differently: the CM "$Reg^{graz}$" is able to grow under specific DIN and prey conditions (**Figure 3F**) while the CM "$Reg^{phot}$" has a zero steady-state growth in all conditions (**Figure 3K**). This different behavior is explained by the initial hypothesis used to construct the model, i.e., a minimum level of phototrophic growth (involving inorganic nutrient assimilation) is needed to allow prey ingestion. When the "$Reg^{phot}$" configuration is used, the CM down-regulates its photosynthesis when the maximum mixotrophic growth is attained, instead of its grazing. Therefore, phototrophy is more constrained in this "$Reg^{phot}$" configuration and the minimum level of phototrophic growth required to allow prey ingestion is not attained. The hypothesis of a minimum level of phototrophy also explains that the CM "$Reg^{graz}$" cannot take advantage of its ability to ingest prey at low DIN, as phototrophy involves inorganic nutrient assimilation (**Figure 3F**). By comparison with the high photon flux density conditions, the regenerated DIN related to phagotrophic activity is not entirely retained inside the cell; a significant part is

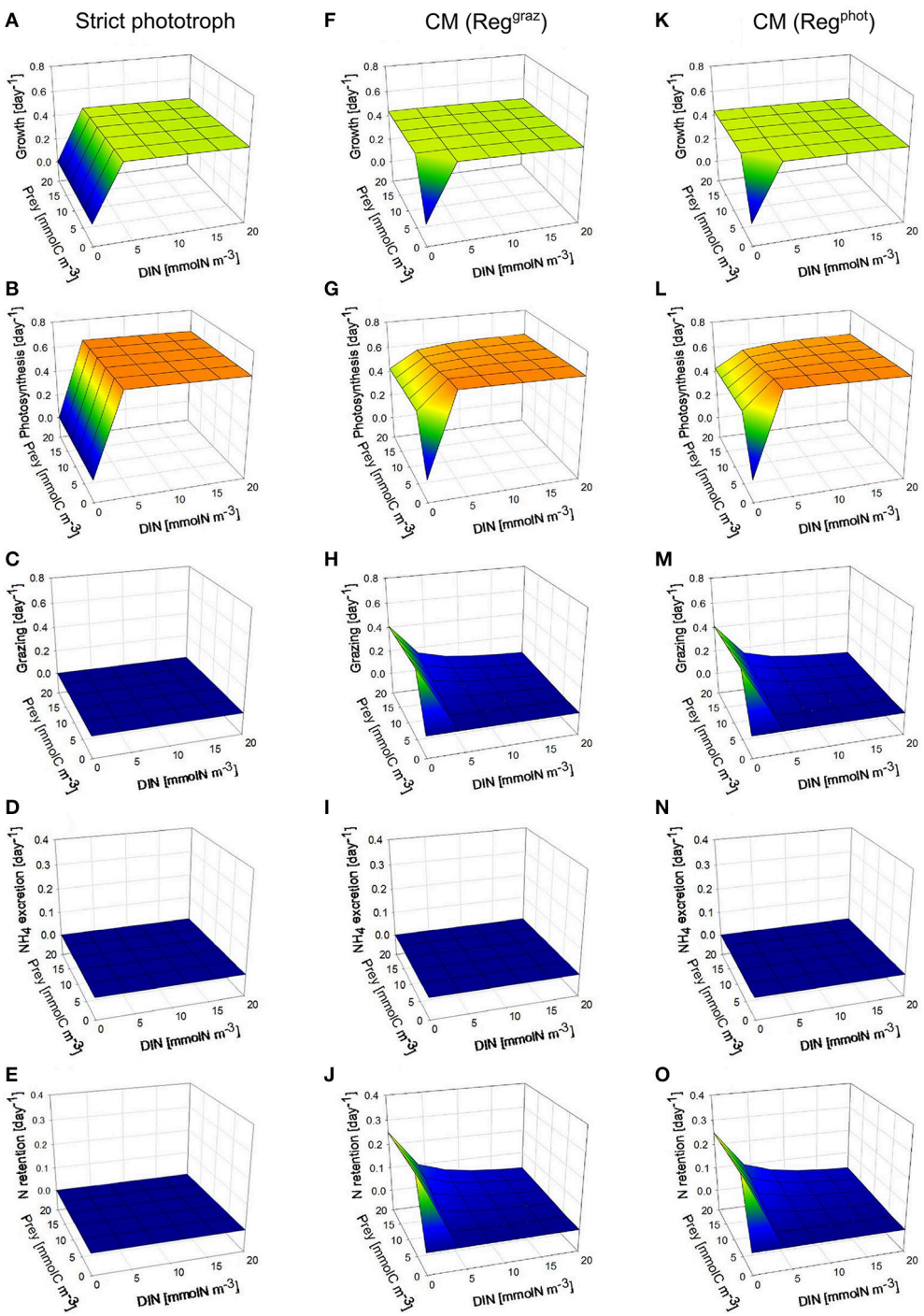


**FIGURE 2 |** Comparison between steady-state behaviors of two different types of constitutive mixotrophs (CMs; middle and right column) and a strict phototroph (left column, **A–E**), under constant high photon flux density (200 μmol quanta $m^{-2}$ $s^{-1}$) and under different DIN and prey biomass. The two CMs differ by their propensity to use either phototrophy or heterotrophy to grow: CM "$Reg^{graz}$" (middle column, **F–J**) tends to down-regulate its grazing rate while CM "$Reg^{phot}$" (right column, **K–O**) tends to down-regulate its photosynthesis. With the physiological parameters used, the model describes a phototrophic nanoflagellate and mixotrophic nanoflagellates grazing on bacteria. Growth, photosynthesis and grazing rates are expressed in C $C^{-1}$ $day^{-1}$ while $NH_4$ excretion and N retention rates are expressed in N $N^{-1}$ $day^{-1}$.

excreted outside the cell (**Figure 3I**) because the demand is lower due to the low photosynthesis rate (**Figure 3G**). Without the hypothesis of a minimum level of phototrophic growth, the behavior of the two CMs is similar a steady-state growth rate is reached around 0.3 $day^{-1}$ when prey is available (not shown).

The sensitivity analysis conducted on the physiological parameters involved in the model of constitutive mixotrophy shows that parameter rankings constructed on the basis of the sensitivity index (*SI*; Equation 28) differ according to the model configuration selected, i.e., "$Reg^{graz}$" or "$Reg^{phot}$" (**Figures 4A,B**). Because grazing is the process that is regulated when the configuration "$Reg^{graz}$" is selected, the parameters related to phago-heterotrophy have proportionally a higher impact on the model response (as shown on the left part of the ranking; **Figure 4A**). By contrast, if the configuration "$Reg^{phot}$" is selected, the parameters related to phago-heterotrophy are located on the right part of the ranking, indicating that they have a lower impact than parameters related to phototrophic processes (**Figure 4B**). Despite the difference of parameter appearance in the ranking, the two model configurations are generally low-sensitive to most of parameters in the range of the tested values; 17 out of 22 parameters have a $SI < 0.4$ for "$Reg^{graz}$" and 15 out of 22 parameters have a $SI < 0.4$ for "$Reg^{phot}$", meaning that a 25% change of their reference value induces <10% change of the mixotroph biomass reached at steady-state.

## Non-constitutive Mixotrophy

To study the behavior of the NCM, we ran the model under steady-state conditions for various prey (a phototrophic nanoflagellate) biomass (ranging from 0 to 20 mmolC $m^{-3}$) and for various DIN-values (ranging from 0 to 20 mmolN $m^{-3}$). These simulations were run under two contrasting photon flux densities (30 and 200 μmol quanta $m^{-2}$ $s^{-1}$). As for the model of constitutive mixotrophy, we considered the prey as inert, meaning that the metabolism of the phototrophic prey is not active. The behavior of the NCM is compared with that of a strict heterotrophic microzooplankton under the same growth conditions.

Under high photon flux density (**Figure 5**), the NCM can grow at lower prey concentrations than the strict heterotroph (**Figures 5A,F**) because the NCM takes advantage of the photosynthetic capacity of the prey retained in the food vacuole for C supply (**Figures 5B,G**) and of inorganic nutrient retention from heterotrophic regeneration (**Figures 5E,J**). DIN concentration has no impact on the NCM growth rate because we assumed that the NCM is not able to take up inorganic nutrients; the inorganic nutrients required for phototrophic growth are only provided by nutrient recycling from prey digestion. As photosynthesis in the NCM relies exclusively on the acquired prey chloroplasts, when prey concentration is lower than 5 mmolC $m^{-3}$, the NCM cannot grow so well because the grazing is limited by the low prey availability (**Figures 5F–H**). With the model configuration used, the grazing rate of the NCM is lower than the grazing rate of the strict heterotroph at prey concentration higher than 8 mmolC $m^{-3}$ (**Figures 5C,H**). The difference is explained by the phototrophic growth that contributes to the mixotrophic growth by providing photo-assimilated C (**Figure 5G**) and inorganic nutrient from nutrient retention (**Figure 5J**). This illustrates the benefit of the close interactions that occur between phototrophy and heterotrophy inside the mixotrophic cell. At high prey concentrations, $NH_4$ excretion is substantially lower for the NCM than for the strict heterotroph (**Figures 5D,I**). Given the low N retention observed for the NCM (**Figure 5J**), the difference cannot be only explained by the ability of the NCM to retain a part of the regenerated N for its phototrophic growth. The difference is actually due to a different N regeneration for the strict heterotroph and the NCM (N regeneration being defined here as the sum of $NH_4$ excretion and N retention). As the grazing rate of the NCM is lower than that of the strict heterotroph at high prey concentration, N regeneration is lower for the NCM. In addition, when the NCM photosynthesizes thanks to the chloroplasts acquired from its prey, it can use a part of the N inorganic pool ($S_N$) of the prey to grow phototrophically. This process tends to increase the C/N stoichiometry of the prey so that N regeneration issued from prey digestion is lower (Equation 45). The latter effect is particularly important at high photon flux density because the nutrient demand for phototrophic growth is higher.

Under low photon flux density (**Figure 6**), the growth rates of the NCM are the same as those obtained under high photon flux density (**Figures 6A,F**) because the decrease of photosynthesis rate in the NCM (**Figure 6G**) associated with the lower photon flux density is offset by an increase of grazing rate (**Figure 6H**). As we assumed that the NCM was a facultative mixotroph (i.e., does not require some level of photosynthesis to grow), it is not impacted by the low light. Due to its higher grazing rate, $NH_4$ excretion and N retention by the NCM are slightly higher than under high photon flux density (**Figures 6I,J**).

The sensitivity analysis conducted on the physiological parameters involved in the model of non-constitutive mixotrophy (**Table 4**) shows that the parameters that have the highest impact on the model response (here, in terms of steady-state biomass) are those related to heterotrophic activity (**Figure 4C**). As the grazing directly controls the heterotrophic growth as well as the phototrophic growth, it is not surprising to observe that the half-saturation constant for grazing ($k_g$) and the maximum grazing rate ($g_{max}$) are the two first parameters in the ranking. Among parameters related to heterotrophic activity, the half-saturation constant for prey digestion ($k^{dig}$) is the most problematic to measure experimentally. Further, it is an important parameter because it directly controls the extent to which the organism is able to use phototrophy, as a low $k^{dig}$ means that the organism maintains the kleptochloroplasts active during a long period while a high $k^{dig}$ means that the organism rapidly digests the kleptochloroplasts and thus, approaches the strict heterotrophic organism. However, the model is rather robust against $k^{dig}$ changes because $SI = 0.4$, meaning that a 25% change of its reference value only induces a 10% change of the mixotroph biomass reached at steady-state.

Parameters related to phototrophic activity are generally of lower importance as most of them have a $SI < 0.003$, meaning that a 25% change of the parameter value induces a 0.075% change of the mixotroph biomass reached at steady-state. The parameter of light adaptation (α) and the maximum photosynthesis rate ($k_{max}$), i.e., the two parameters directly involved in the photosynthesis (Equation 20), are the only parameters related to phototrophy that have a visible impact on the model response. However, their impact is minor as the *SIs* are, respectively, 0.33 and 0.19.

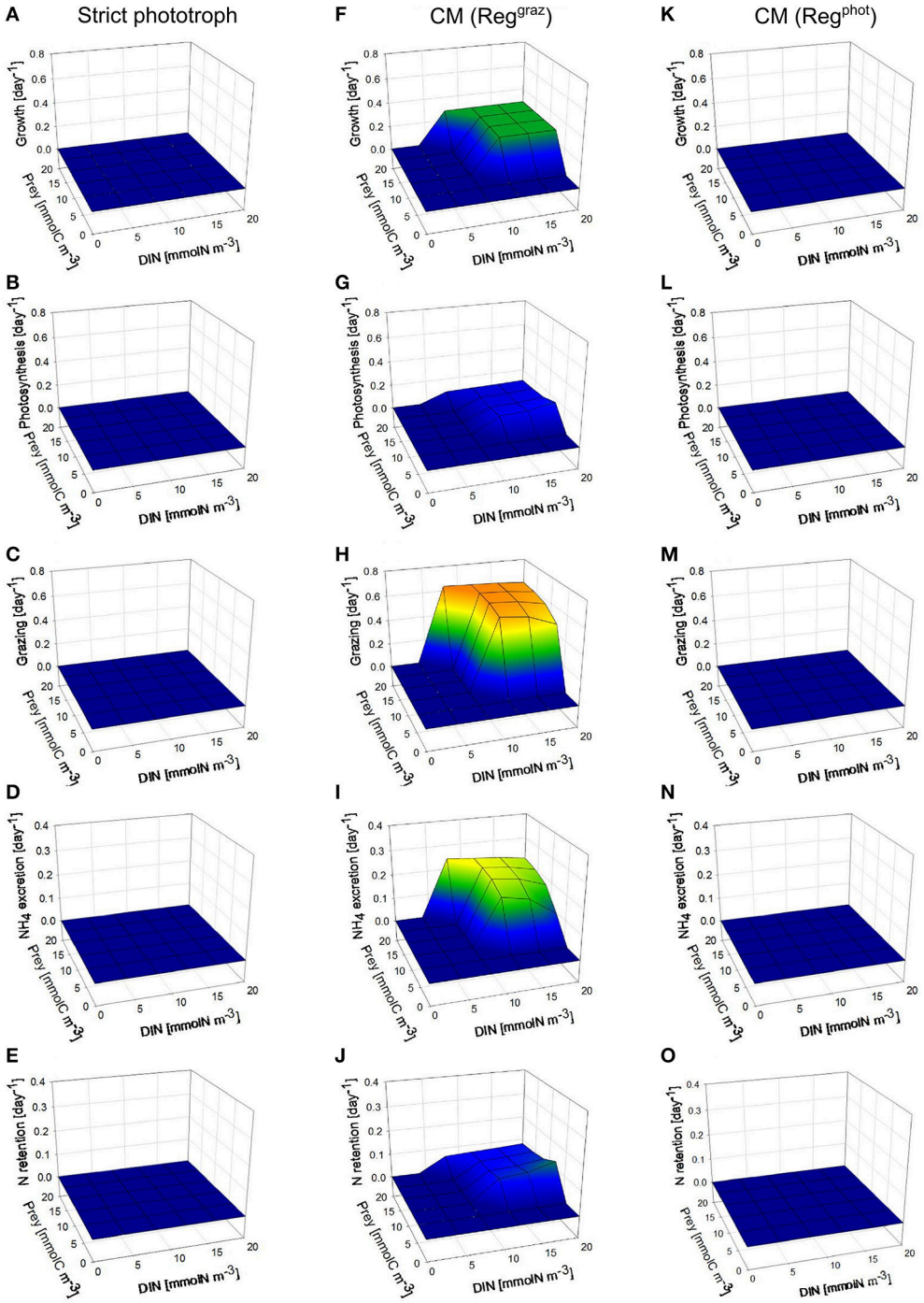


**FIGURE 3 |** As **Figure 2** except under constant low photon flux density (30 μmol quanta $m^{-2}$ $s^{-1}$).

## DISCUSSION

Many field, experimental and modeling studies have highlighted the potential, if not real significance, of planktonic mixotrophy in aquatic systems (e.g., Bird and Kalff, 1986; Estep et al., 1986; Bockstahler and Coats, 1993; Hall et al., 1993; Nygaard and Tobiesen, 1993; Arenovski et al., 1995; Havskum and Riemann, 1996; Stoecker et al., 1997; Stickney et al., 2000; Carvalho and Granéli, 2010; Hartmann et al., 2012; Mitra et al., 2014). In addition, experimental studies have shown that there is a large diversity among mixotrophs, in terms of (i) planktonic groups in which mixotrophic species have been observed, (ii) prey

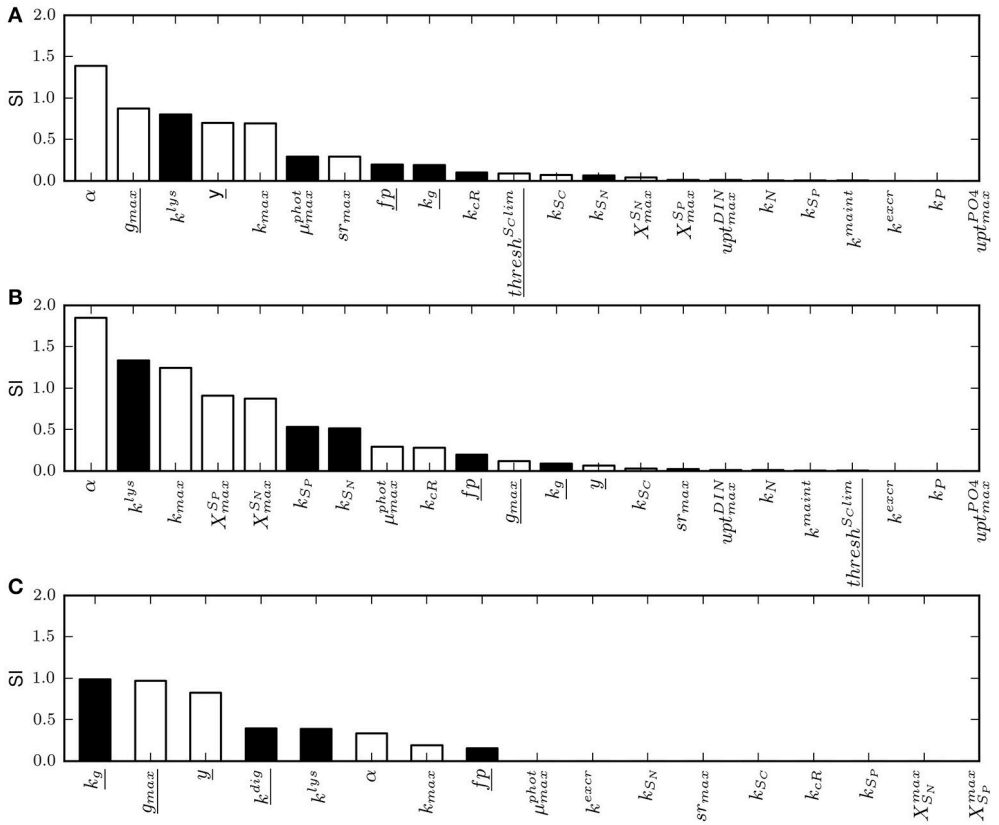


**FIGURE 4 |** Ranking of model parameters based on their normalized sensitivity index (*SI*) calculated as in Equation (28) for a 25% change of the parameter value. White bars are parameters for which the model response (the mixotroph biomass) is positive when the parameter value is increased. Inversely, black bars are parameters for which the model response is negative when the parameter value is increased. **(A)** *SI* obtained with the model of constitutive mixotrophy for the configuration "Reg$^{graz}$", **(B)** *SI* obtained with the model of constitutive mixotrophy for the configuration "Reg$^{phot}$," **(C)** *SI* obtained with the model of non-constitutive mixotrophy. Underlined parameters are those related to heterotrophic processes. See **Table 4** for full description of parameters.

ingested, (iii) obligation to feed on a specific prey (specialist or generalist mixotroph), (iv) obligation to use the two trophic modes (obligate or facultative mixotrophy), (v) proportion of phototrophy and heterotrophy involved in growth, and (vi) factors inducing the use of the additional trophic mode (carbon limitation or nutrient limitation). However, despite the large diversity, a major distinction can be made among mixotrophs according to the origin of their chloroplasts: either constitutive or acquired from ingested phototrophic prey (Mitra et al., 2016). All mixotrophic protists can, therefore, be divided between being CMs or NCMs. The aim of this work is thus to offer a model able to represent the two contrasting forms of mixotrophy and that can be easily implemented in biogeochemical/ecological models. Specifically, the offering here facilitates the implementation of these groups into the AQUAPHY model that deploys the Shuter (1979) concept. The aim was not to develop descriptions for specific organisms, but rather to provide flexible constructs in which key parameters could be safely varied (as demonstrated by sensitivity analyses, **Figure 4**) to enable applications as appropriate for different ecosystem scenarios.

We adopted a model structure in which the organism biomass is divided into different components (on the basis of their function in the cell, i.e., structure, synthesis, or reserve) that interact and explain the main features related to microalgae metabolism (as in Shuter, 1979). This kind of model structure offers the advantage to be particularly appropriate to represent the main interactions that occur between phototrophic and heterotrophic activities in a mixotroph. Mitra and Flynn (2010) have indeed shown that descriptions integrating physiological processes, with some degree of feedback to modulate the processes of phototrophy and heterotrophy, are needed to properly represent the qualitative behavior of mixotrophs. Among existing mixotrophic models, only those of Stickney et al. (2000) and the "perfect beast" of Flynn and Mitra (2009) take the interactions between the two trophic modes into account; the others rely on additive descriptions of phototrophy and heterotrophy (Thingstad et al., 1996; Baretta-Bekker et al., 1998; Jost et al., 2004; Hammer and Pitchford, 2005; Crane and Grover, 2010; Ward et al., 2011; Våge et al., 2013).

In this work we presented descriptions of the two mixotroph forms: the CMs and NCMs. The two versions, describing

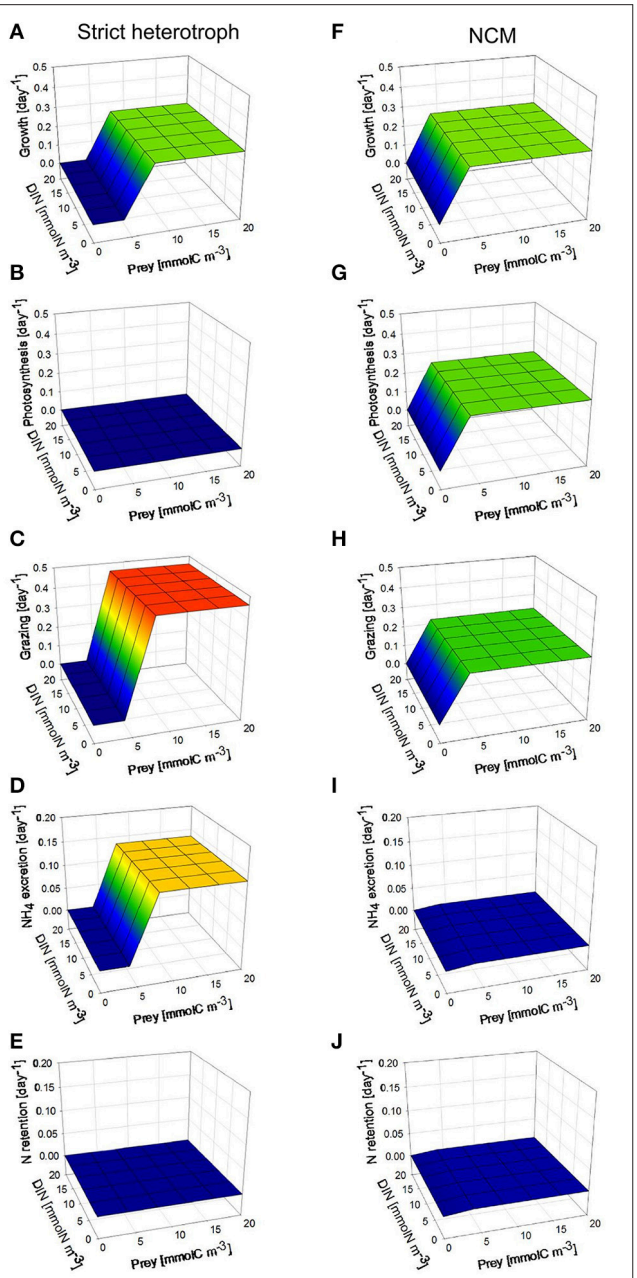


**FIGURE 5 |** Comparison between steady-state behaviors of a non-constitutive mixotroph (NCM; right column, **F–J**) and a strict heterotroph (left column, **A–E**), under constant high photon flux density (200 μmol quanta m$^{-2}$ s$^{-1}$) and under different prey biomass. With the physiological parameters used, the model describes a strict phago-heterotrophic microzooplankton (ciliate) and a mixotrophic ciliate that both graze on a phototrophic nanoflagellate. Growth, photosynthesis, and grazing rates are expressed in C C$^{-1}$ day$^{-1}$ while $NH_4$ excretion and N retention rates are expressed in N N$^{-1}$ day$^{-1}$.

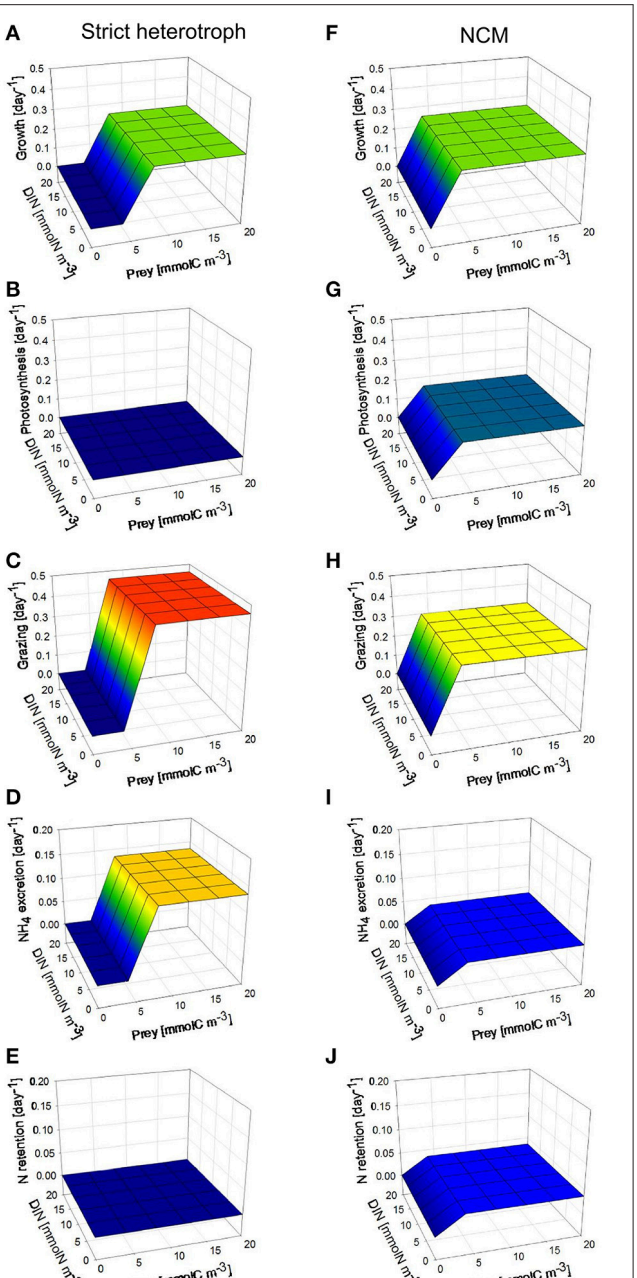


**FIGURE 6 |** As for **Figure 5** but under constant low photon flux density (30 μmol quanta m$^{-2}$ s$^{-1}$).

fundamentally different mixotroph functional types, differ in the models by the processes linking the different components (i.e., the state variables) though they do share a common structure, with similar components in most respects. In the tested conditions, the model of constitutive mixotrophy was able to reproduce the expected observed behaviors of CMs: under light limitation or nutrient limitation (here, DIN), the CM has a growth rate substantially higher than its equivalent strictly autotroph (**Figures 2**, **3**). This is consistent with field and experimental observations showing that mixotrophs are generally dominants under these conditions (Nygaard and Tobiesen, 1993; McKie-Krisberg et al., 2015). Regarding the model of non-constitutive mixotrophy, it properly captures the competitive advantage of NCMs over the strict heterotrophs

under light conditions, when prey are limiting (**Figure 5**), in accordance with the observations (Skovgaard, 1998).

In this work, we configured the CM as a nanoflagellate able to feed on bacteria while the NCM was illustrated by a microzooplankton (ciliate) that feeds on autotrophic nanoflagellates. However, parameters values can easily be adapted to describe other planktonic group or other prey. To consider another prey, the only parameter that has to be changed in the CM model is the prey C:N:P ratio (if assumed fixed). In the NCM model, all parameters values related to phototrophy have to be changed in order to be the same as those of the prey. The type of prey will have an impact on the amount of inorganic nutrients that is retained inside the cell or excreted outside the cell (for the CM and the NCM), and also impacts on the phototrophic capacity for the NCM. We did not consider the fact that some specialists NCMs (i.e., acquiring photosynthetic capabilities from a specific prey) are capable of replicating their acquired photosystems (Hansen et al., 2013). It has been reported, for instance, that *Mesodinium rubrum* had the potential to synthesize and replicate new chloroplasts at least 3–5 times when starved of prey (Hansen et al., 2013). To take this specificity into account, the constant degradation rate of ingested prey ($k^{dig}$) can be lowered to maintain the kleptochloroplasts for a longer period.

By imposing a minimum level of phototrophy to mixotrophic growth, we assumed that the CM is an obligate phototroph, but a facultative mixotroph. The fact that our CM cannot maintain a positive growth rate when both light and DIN are limiting, despite the high prey concentration, stems directly from the assigned 10% minimum level of phototrophic growth in the mixotrophic growth. However, to describe an obligate mixotroph, the only thing to do is imposing a minimum level of heterotrophy in the mixotrophic growth, in addition to the minimum level of phototrophy. A similar approach was enacted by Flynn and Mitra (2009). In the NCM configuration, we also assumed that mixotrophy is facultative but we assumed that phototrophy is facultative too (in contrast to the CM configuration). The NCM configuration could, however, be modified to match that of the CM in respect of the minimum level phototrophic growth required in the mixotrophic growth.

To take account that the proportion of phototrophy and heterotrophy involved in mixotrophic growth is not the same for all mixotrophs, we distinguished two model configurations for the model of constitutive mixotrophy: one that describes CMs using phototrophy as a priority (e.g., *C. ovata;* Tranvik et al., 1989) and another that describes CMs using heterotrophy as a priority (e.g., *P. malhamensis;* Sanders, 1991). The appropriate configuration can therefore be selected as appropriate for the application. When comparing the two CM model configurations (i.e., "$Reg^{graz}$" vs. "$Reg^{phot}$") results show that they behave similarly under high photon flux density. The different behaviors under low photon flux density are more explained by a combination of the model configuration and the hypothesis of a minimum level of phototrophy, than by the configuration controlling the dominance of heterotrophy vs. phototrophy itself.

When constructing the model of constitutive mixotrophy, we assumed that both carbon and nutrient limitations could induce phagotrophy. If only one of these factors was to be considered, the formulation of $\mu_{max}^{mix}$ (**Table 3**, Equations 18–19) can be changed to take only account of the factor inducing phagotrophy. For instance, if only nutrient limitation is assumed to induce phagotrophy, the formulation of $\mu_{\max}^{mix}$ would be restricted to Equation (19).

In conclusion, the model structure presented in this work is able to take account of the main features and interactions between phototrophy and phago-heterotrophy in mixotrophs, and has enough flexibility to represent the observed diversity among mixotrophs. The mechanistic model of mixotrophy developed by Flynn and Mitra (2009)—the "perfect beast"—has these two characteristics as well. The main difference between the two models lies in the model structure; the "perfect beast" of Flynn and Mitra (2009) is based on cell quotas and results from the merging between C:N:P zooplankton and photoacclimative models, while the models presented here are based on the Shuter approach of a division of the biomass between components chosen on the basis of their function in the cell. The type of biogeochemical/ecological model in which mixotrophy will be implemented could guide the choice between either of these model structures; the models presented in this work are particularly adapted to be implemented in those biogeochemical models that use the "Shuter" mechanistic approach to describe the phytoplankton compartment but that do not take mixotrophy into account yet.

## AUTHOR CONTRIBUTIONS

All five authors contributed to the model conception and test design. CG conducted the model analyses and prepared the manuscript while AM, CL, KF, and NG revised it.

## FUNDING

CG was supported by a Ph.D. scholarship funded through the Fonds de la Recherche Scientifique (F.R.S.-FNRS, Belgium). This work was partly enabled by support for an International Network grant from the Leverhulme Trust (UK) to KF and AM.

## REFERENCES

Arenovski, A. L., Lim, E. L., and Caron, D. A. (1995). Mixotrophic nanoplankton in oligotrophic surface waters of the Sargasso Sea may employ phagotrophy to obtain major nutrients. *J. Plankton Res.* 17, 801–820. doi: 10.1093/plankt/17.4.801

Baretta-Bekker, J. G., Baretta, J. W., Hansen, A. S., and Riemann, B. (1998). An improved model of carbon and nutrient dynamics in the microbial food web in marine enclosures. *Aquat. Microb. Ecol.* 14, 91–108. doi: 10.3354/ame014091

Bernard, C., and Rassoulzadegan, F. (1994). Seasonal variations of mixotrophic ciliates in the northwest mediterranean sea. *Mar. Ecol. Prog. Ser.* 108, 295–301. doi: 10.3354/meps108295

Billen, G., Garnier, J., and Hanset, P. (1994). Modelling phytoplankton development in whole drainage networks: the RIVERSTRAHLER model applied to the Seine river system. *Hydrobiologia* 289, 119–137. doi: 10.1007/BF00007414

Bird, D. F., and Kalff, J. (1986). Bacterial grazing by planktonic lake algae. *Science* 231, 493–495. doi: 10.1126/science.231.4737.493

Bockstahler, K. R., and Coats, D. W. (1993). Grazing of the mixotrophic dinoflagellate *Gymnodinium sanguineum* on ciliate populations of Chesapeake Bay. *Mar. Biol.* 116, 477–487. doi: 10.1007/BF00350065

Brutemark, A., and Granéli, E. (2011). Role of mixotrophy and light for growth and survival of the toxic haptophyte *Prymnesium parvum*. *Harm. Algae* 10, 388–394. doi: 10.1016/j.hal.2011.01.005

Burkholder, J. M., Glibert, P. M., and Skelton, H. M. (2008). Mixotrophy, a major mode of nutrition for harmful algal species in eutrophic waters. *Harm. Algae* 8, 77–93. doi: 10.1016/j.hal.2008.08.010

Caron, D. A., Sanders, R. W., Lim, E. L., Marrasé, C., Amaral, L. A., Whitney, S., et al. (1993). Light-dependent phagotrophy in the freshwater mixotrophic chrysophyte *Dinobryon cylindricum*. *Microb. Ecol.* 25, 93–111. doi: 10.1007/BF00182132

Carvalho, W. F., and Granéli, E. (2010). Contribution of phagotrophy versus autotrophy to *Prymnesium parvum* growth under nitrogen and phosphorus sufficiency and deficiency. *Harm. Algae* 9, 105–115. doi: 10.1016/j.hal.2009.08.007

Crane, K. W., and Grover, J. P. (2010). Coexistence of mixotrophs, autotrophs, and heterotrophs in planktonic microbial communities. *J. Theor. Biol.* 262, 517–527. doi: 10.1016/j.jtbi.2009.10.027

Dolan, J. R., and Pérez, M. T. (2000). Costs, benefits and characteristics of mixotrophy in marine oligotrichs. *Freshwater Biol.* 45, 227–238. doi: 10.1046/j.1365-2427.2000.00659.x

Estep, K. W., Davis, P. G., Keller, M. D., Sieburth, J., and Mc, N. (1986). How important are oceanic algal nanoflagellates in bacterivory? *Limnol. Oceanogr.* 31, 646–650. doi: 10.4319/lo.1986.31.3.0646

Flynn, K. J., and Hansen, P. J. (2013). Cutting the canopy to defeat the "selfish gene"; conflicting selection pressures for the integration of phototrophy in mixotrophic protists. *Protist* 164, 811–823. doi: 10.1016/j.protis.2013.09.002

Flynn, K. J., and Mitra, A. (2009). Building the "perfect beast": modelling mixotrophic plankton. *J. Plankton Res.* 31, 965–992. doi: 10.1093/plankt/fbp044

Flynn, K. J., Stoecker, D. K., Mitra, A., Raven, J. A., Glibert, P. M., Hansen, P. J., et al. (2013). Misuse of the phytoplankton – zooplankton dichotomy: the need to assign organisms as mixotrophs within plankton functional types. *J. Plankton Res.* 35, 3–11. doi: 10.1093/plankt/fbs062

Geider, R., and Laroche, J. (2002). Redfield revisited: variability of C:N:P in marine microalgae and its biochemical basis. *Eur. J. Phycol.* 37, 1–17. doi: 10.1017/s0967026201003456

Ghyoot, C., Gypens, N., Flynn, K. J., and Lancelot, C. (2015). Modelling alkaline phosphatase activity in microalgae under orthophosphate limitation: the case of *Phaeocystis globosa*. *J. Plankton Res.* 37, 869–885. doi: 10.1093/plankt/fbv062

Haefner, J. W. (1996). *Modelling Biological Systems: Principles and Applications*. New York, NY: Chapman & Hall. doi: 10.1007/978-1-4615-4119-6

Hall, J. A., Barrett, D. P., and James, M. R. (1993). The importance of phytoflagellate, heterotrophic flagellate and ciliate grazing on bacteria and picophytoplankton sized prey in a coastal marine environment. *J. Plankton Res.* 15, 1075–1086. doi: 10.1093/plankt/15.9.1075

Hammer, A. C., and Pitchford, J. W. (2005). The role of mixotrophy in plankton bloom dynamics, and the consequences for productivity. *ICES J. Mar. Sci.* 62, 833–840. doi: 10.1016/j.icesjms.2005.03.001

Hansen, P. J., Nielsen, L. T., Johnson, M., Berge, T., and Flynn, K. J. (2013). Acquired phototrophy in *Mesodinium* and *Dinophysis* – a review of cellular organization, prey selectivity, nutrient uptake and bioenergetics. *Harm. Algae* 28, 126–139. doi: 10.1016/j.hal.2013.06.004

Hartmann, M., Grob, C., Tarran, G. A., Martin, A. P., Burkill, P. H., Scanlan, D. J., et al. (2012). Mixotrophic basis of Atlantic oligotrophic ecosystems. *Proc. Natl. Acad. Sci. U.S.A.* 109, 5756–5760. doi: 10.1073/pnas.1118179109

Havskum, H., and Riemann, B. (1996). Ecological importance of bacterivorous, pigmented flagellates (mixotrophs) in the Bay of Aarhus, Denmark. *Mar. Ecol. Prog. Ser.* 137, 251–263. doi: 10.3354/meps137251

Hood, R. R., Zhang, X., Glibert, P. M., Roman, M. R., and Stoecker, D. K. (2006). Modeling the influence of nutrients, turbulence and grazing on *Pfiesteria* population dynamics. *Harm. Algae* 5, 459–479. doi: 10.1016/j.hal.2006.04.014

Jeong, H. J., Yoo, Y. D., Kim, J. S., Seong, K. A., Kang, N. S., and Kim, T. H. (2010). Growth, feeding and ecological roles of the mixotrophic and heterotrophic dinoflagellates in marine planktonic food webs. *Ocean Sci. J.* 45, 65–91. doi: 10.1007/s12601-010-0007-2

Jones, H., Cockell, C. S., Goodson, C., Price, N., Simpson, A., and Thomas, B. (2009). Experiments on mixotrophic protists and catastrophic darkness. *Astrobiology* 9, 563–571. doi: 10.1089/ast.2008.0283

Jones, H., Durjun, P., Leadbeater, B. S. C., and Green, J. C. (1995). The relationship between photoacclimation and phagotrophy with respect to chlorophyll a, carbon and nitrogen content, and cell size of *Chrysochromulina brevifilum* (Prymnesiophyceae). *Phycologia* 34, 128–134. doi: 10.2216/i0031-8884-34-2-128.1

Jost, C., Lawrence, C. A., Campolongo, F., van de Bund, W., Hill, S., and DeAngelis, D. L. (2004). The effects of mixotrophy on the stability and dynamics of a simple planktonic food web model. *Theor. Popul. Biol.* 66, 37–51. doi: 10.1016/j.tpb.2004.02.001

Kimura, B., and Ishida, Y. (1989). Phospholipid as a growth factor of *Uroglena americana*, a red tide Chrysophyceae in lake Biwa. *Nippon Suisan Gakkaishi* 55, 799–804. doi: 10.2331/suisan.55.799

Lancelot, C., Hannon, E., Becquevort, S., Veth, C., and De Baar, H. J. W. (2000). Modeling phytoplankton blooms and carbon export production in the Southern Ocean: dominant controls by light and iron in the Atlantic sector in Austral spring 1992. *Deep-Sea Res.* 47(Pt I), 1621–1662. doi: 10.1016/S0967-0637(00)00005-4

Lancelot, C., Spitz, Y., Gypens, N., Ruddick, K., Becquevort, S., Rousseau, V., et al. (2005). Modelling diatom and *Phaeocystis* blooms and nutrient cycles in the Southern bight of the North Sea: the MIRO model. *Mar. Ecol. Prog. Ser.* 289, 63–78. doi: 10.3354/meps289063

Lancelot, C., Veth, C., and Mathot, S. (1991). Modelling ice-edge phytoplankton bloom in the Scotia-Weddell sea sector of the Southern Ocean during spring 1988. *J. Mar. Syst.* 2, 333–346. doi: 10.1016/0924-7963(91)90040-2

McKie-Krisberg, Z. M., Gast, R. J., and Sanders, R. W. (2015). Physiological responses of three species of Antarctic mixotrophic phytoflagellates to changes in light and dissolved nutrients. *Microb. Ecol.* 70, 21–29. doi: 10.1007/s00248-014-0543-x

Mitra, A., and Flynn, K. J. (2010). Modelling mixotrophy in harmful algal blooms: more or less the sum of the parts? *J. Mar. Syst.* 83, 158–169. doi: 10.1016/j.jmarsys.2010.04.006

Mitra, A., Flynn, K. J., Burkholder, J. M., Berge, T., Calbet, A., Raven, J. A., et al. (2014). The role of mixotrophic protists in the biological carbon pump. *Biogeosciences* 11, 1–11. doi: 10.5194/bg-11-995-2014

Mitra, A., Flynn, K. J., Tillmann, U., Raven, J. A., Caron, D., Stoecker, D. K., et al. (2016). Defining planktonic protist functional groups on mechanisms for energy and nutrient acquisition: incorporation of diverse mixotrophic strategies. *Protists* 167, 106–120. doi: 10.1016/j.protis.2016.01.003

Nygaard, K., and Tobiesen, A. (1993). Bacterivory in algae: a survival strategy during nutrient limitation. *Limnol. Oceanogr.* 38, 273–279. doi: 10.4319/lo.1993.38.2.0273

Park, M. G., Kim, M., and Kim, S. (2015). Phased cell division and facultative mixotrophy of the marine dinoflagellate *Fragilidium duplocampanaeforme* and its trophic interactions with the dinoflagellates *Dinophysis* spp. and a ciliate *Mesodinium rubrum*. *Harm. Algae* 43, 20–30. doi: 10.1016/j.hal.2015.02.001

Roberts, E. C., and Laybourn-Parry, J. (1999). Mixotrophic cryptophytes and their predators in the dry valley lakes of Antarctica. *Freshwater Biol.* 41, 737–746. doi: 10.1046/j.1365-2427.1999.00401.x

Sanders, R. W. (1991). Mixotrophic protists in marine and freshwater ecosystems. *J. Protozool.* 38, 76–81. doi: 10.1111/j.1550-7408.1991.tb04805.x

Sanders, R. W., and Gast, R. J. (2012). Bacterivory by phototrophic picoplankton and nanoplankton in Arctic waters. *FEMS Microbiol. Ecol.* 82, 242–253. doi: 10.1111/j.1574-6941.2011.01253.x

Sanders, R. W., and Porter, K. G. (1988). "Phagotrophic phytoflagellates," in *Advances in Microbial Ecology,* Vol. 10, ed K. C. Marshall (Boston, MA: Springer), 167–192.

Shuter, B. (1979). A model of physiological adaptation in unicellular algae. *J. Theor. Biol.* 78, 519–552.

Skovgaard, A. (1998). Role of chloroplast retention in a marine dinoflagellate. *Aquat. Microb. Ecol.* 15, 293–301.

Stickney, H. L., Hood, R. R., and Stoecker, D. K. (2000). The impact of mixotrophy on planktonic marine ecosystems. *Ecol. Model.* 125, 203–230. doi: 10.1016/S0304-3800(99)00181-7

Stoecker, D. K. (1998). Conceptual models of mixotrophy in planktonic protists and some ecological and evolutionary implications. *Eur. J. Protistol.* 34, 281–290.

Stoecker, D. K., Johnson, M. D., de Vargas, C., and Not, F. (2009). Acquired phototrophy in aquatic protists. *Aquat. Microb. Ecol.* 57, 279–310. doi: 10.1016/S0304-3800(99)00181-7

Stoecker, D. K., Li, A., Coats, D. W., Gustafson, D. E., and Nannen, M. K. (1997). Mixotrophy in the dinoflagellate *Prorocentrum minimum*. *Mar. Ecol. Prog. Ser.* 152, 1–12.

Stoecker, D. K., Michaels, A. E., and Davis, L. H. (1987). Large proportion of marine planktonic ciliates found to contain functional chloroplasts. *Nature* 326, 790–792. doi: 10.1038/326790a0

Stoecker, D. K., Silver, M. W., Michaels, A. E., and Davis, L. H. (1988). Obligate mixotrophy in *Laboea strobila*, a ciliate which retains chloroplasts. *Mar. Biol.* 99, 415–423.

Stoecker, D., Tillmann, U., and Granéli, E. (2006). "Phagotrophy in harmful algae," in *Ecology of Harmful Algae*, Vol. 189, eds G. Granéli and J. T. Turner (Berlin; Heidelberg: Springer), 177–187.

Thingstad, T. F., Havskum, H., Garde, K., and Riemann, B. (1996). On the strategy of "eating your competitor": a mathematical analysis of algal mixotrophy. *Ecology* 77, 2108–2118.

Tranvik, L. J., Porter, K. G., Sieburth, J., and Mc, N. (1989). Occurrence of bacterivory in *Cryptomonas*, a common freshwater phytoplankter. *Oecologia 78*, 473–476.

Våge, S., Castellani, M., Giske, J., and Thingstad, T. F. (2013). Successful strategies in size structured mixotrophic food webs. *Aquat. Ecol.* 47, 329–347. doi: 10.1007/s10452-013-9447-y

Ward, B. A., Dutkiewicz, S., Barton, A. D., and Follows, M. J. (2011). Biophysical aspects of resource acquisition and competition in algal mixotrophs. *Am. Nat.* 178, 98–112. doi: 10.1086/660284

Zubkov, M. V., and Tarran, G. A. (2008). High bacterivory by the smallest phytoplankton in the north atlantic ocean. *Nature* 455, 224–226. doi: 10.1038/nature07236

**Conflict of Interest Statement:** The authors declare that the research was conducted in the absence of any commercial or financial relationships that could be construed as a potential conflict of interest.

frontiers in Marine Science

ORIGINAL RESEARCH
published: 30 August 2016
doi: 10.3389/fmars.2016.00155

# Key Drivers of Seasonal Plankton Dynamics in Cyclonic and Anticyclonic Eddies off East Australia

*Leonardo Laiolo*[1,2]*, *Allison S. McInnes*[1], *Richard Matear*[2] and *Martina A. Doblin*[1]

[1] Climate Change Cluster, University of Technology Sydney, Ultimo, NSW, Australia, [2] Oceans and Atmosphere, CSIRO, Hobart, TAS, Australia

Mesoscale eddies in the south west Pacific region are prominent ocean features that represent distinctive environments for phytoplankton. Here, we examine the seasonal plankton dynamics associated with averaged cyclonic and anticyclonic eddies (CE and ACE, respectively) off eastern Australia. We do this through building seasonal climatologies of mixed layer depth (MLD) and surface chlorophyll-a for both CE and ACE by combining remotely sensed sea surface height (TOPEX/Poseidon, Envisat, Jason-1, and OSTM/Jason-2), remotely sensed ocean color (GlobColour) and *in situ* profiles of temperature, salinity and pressure from Argo floats. Using the CE and ACE seasonal climatologies, we assimilate the surface chlorophyll-a data into both a single (WOMBAT), and multi-phytoplankton class (EMS) biogeochemical model to investigate the level of complexity required to simulate the phytoplankton chlorophyll-a. For the two eddy types, the data assimilation showed both biogeochemical models only needed one set of parameters to represent phytoplankton but needed different parameters for zooplankton. To assess the simulated phytoplankton behavior we compared EMS model simulations with a ship-based experiment that involved incubating a winter phytoplankton community sampled from below the mixed layer under ambient and two higher light intensities with and without nutrient enrichment. By the end of the 5-day field experiment, large diatom abundance was four times greater in all treatments compared to the initial community, with a corresponding decline in pico-cyanobacteria. The experimental results were consistent with the simulated behavior in CE and ACE, where the seasonal deepening of the mixed layer during winter produced a rapid increase in large phytoplankton. Our model simulations suggest that CE off East Australia are not only characterized by a higher chlorophyll-a concentration compared to ACE, but also by a higher concentration of large phytoplankton (i.e., diatoms) due to the shallower CE mixed layer. The model simulations also suggest the zooplankton community is different in the two eddy types and this behavior needs further investigation.

**Keywords: data assimilation, mesoscale features, phytoplankton dynamics, zooplankton dynamics, biological oceanography, size based model**

OPEN ACCESS

***Edited by:***
*Christian Lindemann, University of Bergen, Norway*

***Reviewed by:***
*Kemal Can Bizsel, Institute of Marine Sciences and Technology, Turkey*
*Bruno Buongiorno Nardelli, National Research Council, Italy*

***Correspondence:**
*Leonardo Laiolo*
*Leonardo.Laiolo@gmail.com*

***Specialty section:***
*This article was submitted to Marine Ecosystem Ecology, a section of the journal Frontiers in Marine Science*

***Received:*** *10 June 2016*
***Accepted:*** *16 August 2016*
***Published:*** *30 August 2016*

***Citation:***
*Laiolo L, McInnes AS, Matear R and Doblin MA (2016) Key Drivers of Seasonal Plankton Dynamics in Cyclonic and Anticyclonic Eddies off East Australia. Front. Mar. Sci. 3:155. doi: 10.3389/fmars.2016.00155*

## INTRODUCTION

Mesoscale eddies play crucial roles in ocean circulation and dynamics, stimulating phytoplankton growth and enhancing the global primary production by ∼20% (Falkowski et al., 1991; McWilliams, 2008). Usually, eddies occur where there are strong currents and oceanic fronts (Robinson, 1983) and hence are a common feature of western boundary currents (Chelton et al., 2011). The direction and resulting temperature of an eddy circulation can be categorized as either cyclonic cold core or anticyclonic warm-core (Robinson, 1983). The cyclonic eddies (CE) are associated with low sea level anomalies, doming of the isopycnals and shoaling of the nutricline (Falkowski et al., 1991; McGillicuddy, 2015). The shoaling of the nutricline helps supply nutrient-rich waters to the euphotic zone when mixed layer depth (MLD) undergoes seasonal deepening (Dufois et al., 2014; McGillicuddy, 2015) and, thereby stimulating phytoplankton growth (Jenkins, 1988; Falkowski et al., 1991; McGillicuddy and Robinson, 1997). In contrast, anticyclonic eddies (ACE) are associated with high sea level anomalies, depression of the isopycnals and deepening of the nutricline (McGillicuddy, 2015). The MLD of ACEs is generally deeper than CEs (Dufois et al., 2014) and this changes the supply of nutrients to the euphotic zone when the eddy undergoes seasonal deepening of the MLD with additional impacts to light levels (Dufois et al., 2014; McGillicuddy, 2015). While representing different physical and nutrient conditions, the characteristics of CE and ACE can also differ because of differences in how these eddies form. The process called "eddy trapping" (McGillicuddy, 2015) was used to describe how composition of the water trapped in an eddy depends on the process of eddy formation as well as on the local gradients in physical, chemical, and biological properties. One example is the formation of eddies off Western Australian where the Leeuwin Current generates ACE initialized with high Chl-a derived from the coastal water (Moore et al., 2007).

CE and ACE represent two distinct environments because of differences in their physical properties and in the physical processes that form them, which can lead to different phytoplankton abundance, biomass, and composition (Angel and Fasham, 1983; Arístegui et al., 1997; Arístegui and Montero, 2005; Moore et al., 2007; Everett et al., 2012, **Table 1**). In addition, sub-mesoscale processes can affect phytoplankton dynamics in mesoscale eddies (Klein and Lapeyre, 2009); in particular small-scale upwellings and downwellings seem to have a significant impact on phytoplankton subduction and primary production (Levy et al., 2001).

Multiple processes can impact phytoplankton composition and growth in mesoscale eddies. Oceanographic studies show that large photosynthetic eukaryotes (>3 μm, diatoms in particular) appear confined to the center of CE (Rodriguez et al., 2003; Brown et al., 2008). In comparison, higher concentrations of cyanobacteria (<3 μm) are located in the surrounding oligotrophic waters (Olaizola et al., 1993; Rodriguez et al., 2003; Vaillancourt et al., 2003; Brown et al., 2008) and in adjacent ACEs (e.g., Haury, 1984; Huang et al., 2010). However, we still have very limited understanding about the phytoplankton communities that characterize eddy environments because they remain largely under-sampled.

**TABLE 1 | Schematic representation of main physical and biological differences between CE and ACE off East Australia.**

| Eddy properties | Eddy type | |
|---|---|---|
| | ACE (warm core) | CE (cold core) |
| Direction of circulation | Counter clockwise | Clockwise |
| Vertical structure | Downwelling | Upwelling |
| Sea surface height anomalies | Positive | Negative |
| Dissolved nutrient concentration | Lower | Higher |
| Mixed layer depth | Deeper | Shallower |
| Chlorophyll a concentration | Lower | Higher |

Phytoplankton are limited by two primary resources in marine environments: light and nutrients (Behrenfeld and Boss, 2014). Eddies represent an interesting resource paradox because, through physical processes, they influence light and nutrient concentrations simultaneously. Indeed, the seasonal deepening of the MLD can bring nutrient-rich water from depth into the euphotic zone but decrease the total photon flux to cells. Due to the differing nutrient requirements of phytoplankton, the water mass below the MLD could therefore play an important role in determining eddy phytoplankton concentration and composition (Bibby and Moore, 2011; Dufois et al., 2016). Furthermore, the shallower MLD that characterizes CE leads to higher light levels in the surface mixed layer, while ACE have lower light levels (Tilburg et al., 2002). Understanding what the primary driver of phytoplankton dynamics in these two environments is an important question, given the uncertainty in regional predictions of primary production under projected ocean change (Bopp et al., 2013).

Floristic shifts in phytoplankton at a regional level will play an important role in determining the marine ecosystem response to future climate change (Boyd and Doney, 2002). Representation of phytoplankton in biogeochemical models ranges in complexity from a single phytoplankton compartment to multi-phytoplankton compartments that can be separated into different functional groups and/or sizes (Fennel and Neumann, 2004). To advance knowledge about the physical-biological interactions in mesoscale features and reduce uncertainty, McGillicuddy (2015) suggests coupling *in situ* observations, remote sensing, and modeling. Here, we follow such an inter-disciplinary approach.

Our study area is eastern Australia (**Figure 1**), a region strongly influenced by the southward flowing Eastern Australian Current (EAC), which forms both CE and ACE (Hamon, 1965; Tranter et al., 1986). EAC waters are low in nutrients and any subsurface nutrients are rarely upwelled to the euphotic zone (Oke and Griffin, 2011). However, increases in phytoplankton biomass occur in this region as a response to occasional upwelling-favorable wind events, the separation of the EAC from the shelf or the formation of CE (Tranter et al., 1986; Cresswell, 1994; Roughan and Middleton, 2002). Both eddy types form from meanders in the EAC and move into adjacent water with different

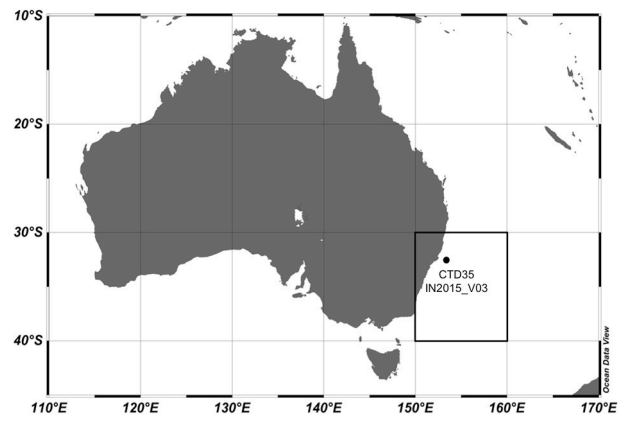


**FIGURE 1 | Map showing the study area, including the location of the where water was collected for the shipboard manipulation experiment (CTD35 IN2015_V03).**

physical, chemical, and biological characteristics (Lochte and Pfannkuche, 1987).

Here, we characterize phytoplankton dynamics in CE and ACE off East Australia using a combination of *in situ* observations, remote sensing, and modeling. We firstly explore the level of phytoplankton complexity required to estimate the phytoplankton chlorophyll-a (Chl-a) for eddies in the East Australian system, using a single (WOMBAT) and a multi-phytoplankton class model (EMS). Models were used to simulate the observed Chl-a concentrations obtained from satellites (MERIS, SeaWiFS, and MODIS-Aqua). Shifts in phytoplankton composition and size distribution were also examined using a manipulative ship-board experiment and comparing outcomes with simulations. Results show that CE and ACE off eastern Australia are not only characterized by a different Chl-a concentration but also by different phytoplankton composition. Both models suggest these differences are related to distinct zooplankton dynamics. Furthermore, simulation results are consistent with the ship-based experiment, highlighting the important role of MLD and irradiance in driving eddy phytoplankton dynamics off eastern Australia.

# MATERIALS AND METHODS

## Study Region and Location of Voyage Experiment

The eastern Australian ocean region is significant for Australia's economy and marine ecology (Hobday and Hartmann, 2006). This area is adjacent to capital cities, major shipping lanes and regions of environmental significance (e.g., Great Barrier Reef World Heritage area). Pelagic offshore fisheries, including the valuable Bluefin tuna, are strongly influenced by the EAC, the major western boundary current of the South Pacific sub-tropical gyre (Mata et al., 2000; Ridgway and Dunn, 2003; Hobday and Hartmann, 2006; Brieva et al., 2015). Furthermore, the ocean circulation of this region has a crucial role in removing heat from the tropics and releasing it to the mid-latitude atmosphere (Roemmich et al., 2005). In this region, climate change is projected to increase eddy activity and hence primary productivity (Matear et al., 2013). Due to its importance, the area selected for this study is located between 30° and 40°S, and 150° and 160°E (**Figure 1**).

## Description of Biogeochemical Models

To explore the level of complexity required to represent seasonal phytoplankton dynamics associated with mean MLD variations in CE and ACE within the domain, two biogeochemical models were used. The first model, "WOMBAT" (Whole Ocean Model of Biogeochemistry And Trophic-dynamics) is a Nutrient, Phytoplankton, Zooplankton and Detritus (NPZD) model, with one zooplankton and one phytoplankton class (i.e., total Chl-a concentration) characterized by a fixed C:Chl-a ratio (Kidston et al., 2011, **Figure 2A**). WOMBAT has a total of 14 different parameters. The second NPZD biogeochemical model, Environmental Modeling Suite (EMS), is a more complex size-dependent model characterized by a total of 104 parameters (CSIRO Coastal Environmental Modelling Team, 2014). EMS has been developed to model coupled physical, chemical, and biological processes in marine and estuarine environments (CSIRO Coastal Environmental Modelling Team, 2014) and can be implemented in a wide range of configurations. We set it up with two phytoplankton and two zooplankton classes, characterized by different sizes, growth, mortality, and grazing rates (zooplankton only; **Figure 2B**). The two EMS phytoplankton classes can adjust their C:Chl-a ratio daily, to attain the ratio that allows optimal phytoplankton growth (Baird et al., 2013).

Both biogeochemical models are configured as 0D to represent a well-mixed MLD with a prescribed seasonal cycle of nutrient levels below the MLD. Phytoplankton and zooplankton concentrations are uniformly distributed in the MLD. The MLD climatology was the only environmental factor differing between the CE and ACE systems. The time series of temperature in the MLD and nutrients below the MLD from the CSIRO Atlas of Regional Seas dataset (CARS; http://www.marine.csiro.au/~dunn/cars2009/; Ridgway et al., 2002) were used in the simulations, with no distinction between the eddy environments. The surface incident irradiance comes from seasonal climatology of the region (Large and Yeager, 2008). Because other physical phenomena, such as upwelling or downwelling were not explicitly represented, the only supply of nutrients to the MLD occurs with the deepening of the MLD (i.e., when the MLD is shoaling there is no new supply of nutrients to the MLD). In both models, when the MLD is deepening from a time step to the next one, the nutrient concentration (calculated from the nitrate dataset below the MLD obtained from CARS; Ridgway et al., 2002) is added to the MLD. Following Matear (1995) approach the nutrients concentration added in the MLD is calculated as:

$$N_{t+1} = \frac{\delta h \cdot N_b + h \cdot N_m}{h + \delta h}$$

where $h$ represents the MLD, $\delta$h the difference in the MLD between the time $t$ and $t$+1, $N_b$ represent the nutrient

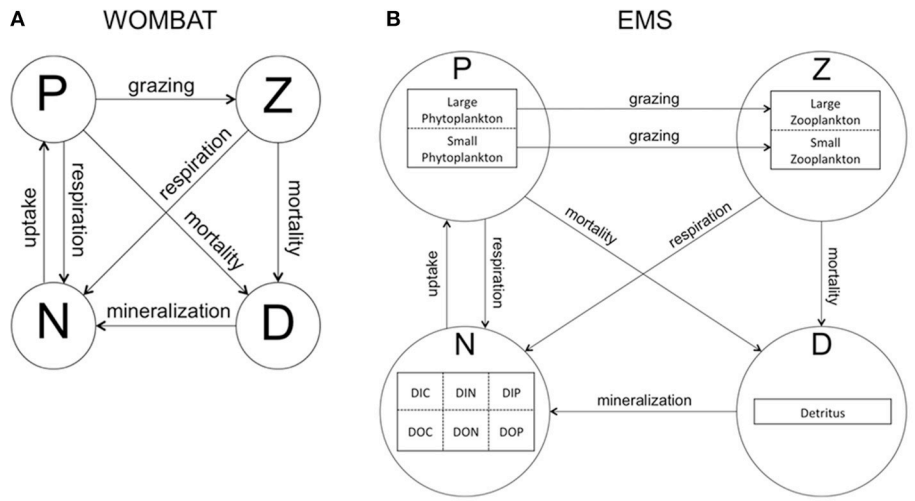


**FIGURE 2 | Structure of biogeochemical models used in this study.** Arrows represent interactions and links between model compartments. **(A)** WOMBAT (Whole Ocean Model of Biogeochemistry And Trophic-dynamics), which has one phytoplankton (P) and one zooplankton (Z) class, detritus (D), and one nutrient compartment (N). **(B)** EMS (Environmental Modeling Suite), characterized by two phytoplankton (P) and zooplankton (Z) sized-based classes, detritus (D) and one nutrient compartment divided into dissolved inorganic carbon, nitrogen, phosphate (DIC, DIN, DIP), and dissolved organic carbon, nitrogen, phosphate (DOC, DON, DOP).

concentration below the MLD, $N_m$ the nutrient concentration in the MLD.

To evaluate the sensitivity of the model to higher-frequency variations in the MLD, we added Gaussian random noise to the CE and ACE daily MLD dataset, where the standard deviation of the random noise was estimated from the standard error of the CE and ACE MLDs (i.e., ACE 1.3 m; CE 1.2 m).

## Input Data and Implementation to Biogeochemical Models

Because of their different dynamical balances, ACE and CE can be identified through sea surface height anomalies (SSH) detected by satellites (Lee-Lueng et al., 2010). A 17 year, 8-day composite dataset of SSH anomalies (2 September, 1997–26 September, 2014), was downloaded from AVISO (Delayed-Time Reference Mean Sea-Level Anomaly; http://www.aviso.altimetry.fr/en/data/products/sea-surface-height-products.html). Eddies were identified by prescribing ±0.2 m SSH anomaly threshold that characterizes ACE and CE, respectively (Pilo et al., 2015). Satellite-derived Chl-a measurements (25 km spatial resolution, 8-day average) were downloaded from GlobColour (an ocean color product that combines output from MERIS, SeaWIFS, and MODIS; http://hermes.acri.fr/index.php?class=archive). Using this kind of product ensures data continuity, improves spatial and temporal coverage and reduces noise (ACRI-ST GlobColour Team et al., 2015). To obtain MLD measurements, Argo data (temperature, salinity, time, pressure, location for every Argo Float) were downloaded from the GODAE (Global Ocean Data Assimilation Experiment; http://www.usgodae.org/cgi-bin/argo_select.pl). The MLD value was defined as the depth where temperature changed by 1°C and density by 0.05 kg $m^{-3}$ from the surface value (Brainerd and Gregg, 1995; de Boyer Montegut et al., 2004; Dong et al., 2008). The climatology of surface water (5 m) temperature and nitrate concentration below the MLD was obtained from CARS (**Figure 3**; Ridgway et al., 2002); while we obtained the irradiance from the seasonal climatology of the downward short wave radiation at the surface of the ocean (Large and Yeager, 2008). Before inputting to the models, all data were filtered to exclude locations shallower than 1000 m, to avoid including data from coastal systems.

The Chl-a and MLD datasets obtained from GlobColour and GODAE were mapped in time and space onto the 8-day averaged CE and ACE SSH fields. Thus, we obtained surface Chl-a concentrations and MLDs for CE and ACE off East Australia occurring from 1 December 2002 to 1 December 2014 in an 8-day averaged dataset (Argo data are not available before 2002 in our domain). Chl-a concentration and MLD were averaged over time periods ($n = 546$) at their original resolution, obtaining a Chl-a and a MLD 8-day averaged seasonal climatology for an idealized CE an ACE of the selected East Australia region (**Figure 4**). The datasets extracted from CARS (nitrogen, temperature, and light) were used in the two biogeochemical models without any distinction between CE and ACE, as the available data from CARS are an average of the whole area of study.

## Statistical Analysis and Goodness of the Fit

The student *t*-test was performed to assess statistical differences between the CE and ACE Chl-a climatologies, calculated from the GlobColour dataset. The same approach was applied to the MLD climatology derived from the GODAE Argo dataset. The same test was used to asses if there were statistical differences between the average of the observed and modeled data (i.e., GlobColour Chl-a climatology vs. simulated Chl-a), with significance for all tests defined as $p < 0.05$.

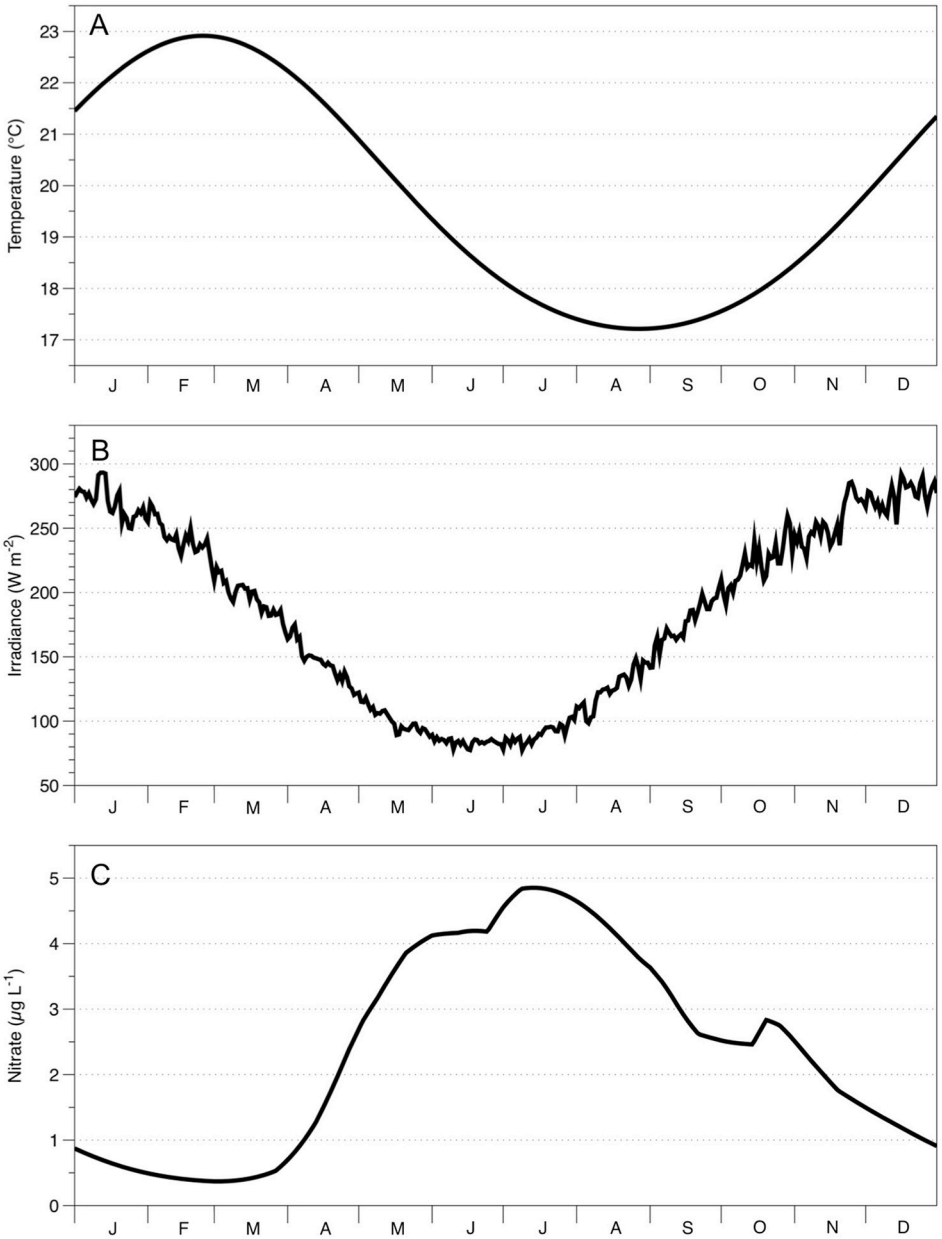


**FIGURE 3 | Seasonal climatology of the study area (30°S to 40°S, 150°E to 160°E) for (A) surface temperature; (B) surface irradiance; (C) nitrate concentration 5 m below seasonal mixed layer depth.** Data for **(A,C)** come from the CSIRO Atlas of Regional Seas (CARS) available at http://www.marine.csiro.au/~dunn/cars2009/. Data for **(B)** comes from seasonal climatology of the downward short wave radiation at the surface of the ocean (Large and Yeager, 2008).

The goodness of the fit between simulated and observed seasonal climatology of Chl-a was assessed through the Chi-squared misfit ($\chi^2$):

$$\chi^2 = \frac{1}{\nu}\sum_{t=1}^{T}\frac{(Q_m^t - Q_o^t)^2}{\sigma^t}$$

where $Q_m^t$ is the value of the modeled data at time $t$ and $Q_o^t$ is the observed value of Chl-a at time $t$, while $\sigma^t$ is the variance at time $t$ of the Chl-a climatology. The degrees of freedom are represented by $\nu$:

$$\nu = n_o - n_p$$

where $n_o$ is the number of observations, and $n_p$ is the number of fitted parameters. A $\chi^2$ value of $\sim$1 represents an acceptable model fit to the observations.

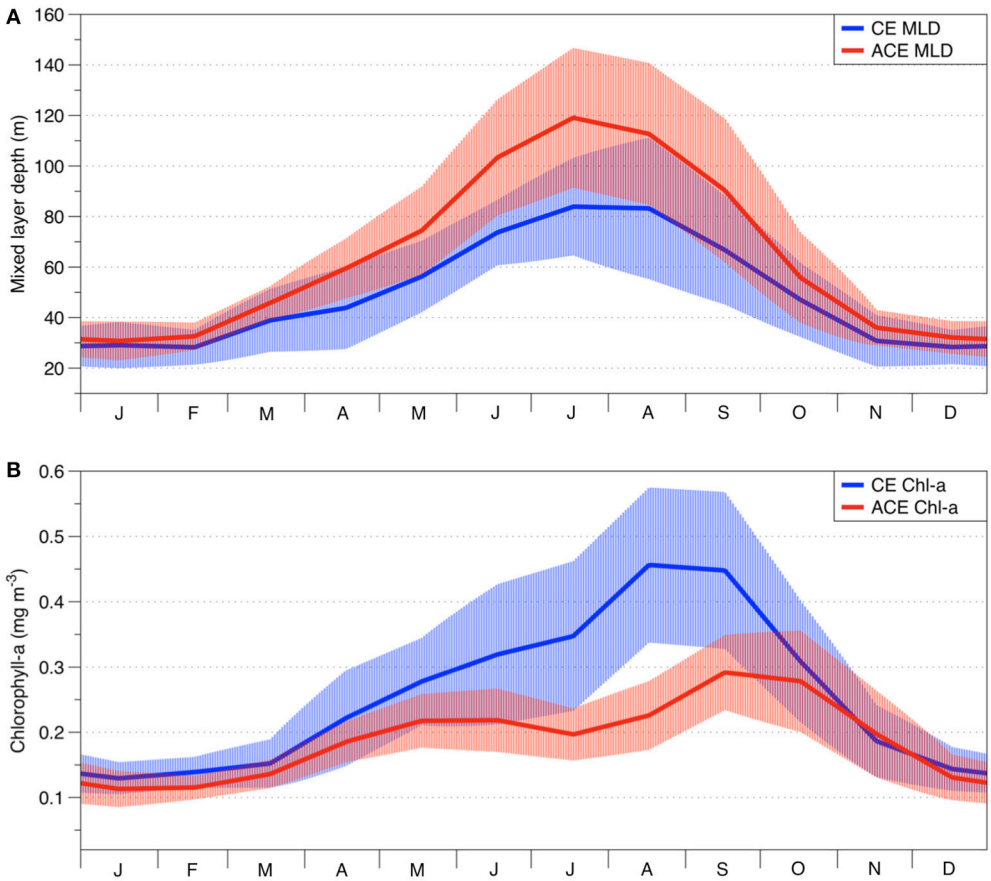


**FIGURE 4 | Seasonal climatology of cold core CE (solid blue lines) and warm core ACE (solid red lines) eddies for: (A) mixed layer depth (MLD) (GODAE); (B) surface chlorophyll-a concentration (GlobColour).** The light blue and light red areas represent standard deviation for CE and ACE, respectively.

## Data Assimilation

The observed CE and ACE Chl-a seasonal climatologies were used for the data assimilation, with the purpose of finding parameter sets that best fitted the observations from the two environments (e.g., Matear, 1995). The observed Chl-a climatology was assumed to represent the Chl-a concentration in the MLD (i.e., Chl-a uniformly distributed in the MLD). Although this assumption is commonly made, caution needs to be used when interpreting results because a chlorophyll maximum below the surface mixed layer may be not be detected by satellites (e.g., Sallée et al., 2015). To quantify the difference between the simulated and observed Chl-a concentrations we used a cost function ($x$) defined as:

$$x = \sum_{t=1}^{T} \frac{(\ln Q_m^t - \ln Q_o^t)^2}{n}$$

where $Q_m^t$ is the value of the modeled data (total Chl-a concentration) at time $t$, $Q_o^t$ is the observed value of Chl-a at time t and n is the number of samples over time. The "ln" transformation was applied to achieve normal distribution of the Chl-a concentrations around the mean seasonal value, thus allowing us to employ statistical parametric methods.

To estimate the optimized parameter set for WOMBAT, we used a simulated annealing algorithm based on the likelihood cost metric ($x$). This approach has been previously used in marine ecosystem models and can solve optimization problems with a small number of unknown parameters (e.g., Matear, 1995; Kidston et al., 2013). The simulated annealing algorithm was run for 200 iterations to allow the algorithm to converge to the minimum cost function value. The data assimilation was performed with WOMBAT, fitting CE and ACE seasonal climatology independently by allowing eight parameters that controlled plankton growth to vary (**Table 3**). Data assimilation was also used to fit both the environments with one parameter set to determine if the one-phytoplankton class model was sufficiently complex to represent both eddy types.

The data assimilation was then performed with EMS, fitting the CE and ACE Chl-a seasonal climatology independently and fitting both the environments with one parameter set. Because the simulated annealing algorithm computational requirements are large and EMS is a much more complex model than WOMBAT, we estimated EMS parameters with the conjugate-gradient algorithm because it was more computationally efficient. Although this algorithm is sensitive to the choice of the initial model parameters, it is used to solve optimization problems with

**TABLE 2 | Results of the statistical comparisons (student *t*-test): Chl-a means (observed vs. simulated, ACE observed vs. CE observed) and MLD means (ACE observed vs. CE observed).**

| | | Chl-a concentration | |
|---|---|---|---|
| | **ACE observed vs. CE observed** | **ACE model vs. ACE observed** | **CE model. vs. CE observed** |
| Chl-a climatology | *** $p = 0.0002$ | | |
| MLD climatology | ** $p = 0.006$ | | |
| WOMBAT (CE and ACE, 2 distinct parameter set) | | N.S. $0.12 < p < 0.49$ $0.8 < \chi^2 < 1.6$ | N.S. $0.22 < p < 0.42$ $0.88 < \chi^2 < 1.1$ |
| WOMBAT (CE and ACE, 1 equal parameter set) | | *** $p = 0.001$ $\chi^2 = 1.8$ | ** $p = 0.003$ $\chi^2 = 1.7$ |
| EMS (CE and ACE, 2 distinct parameter set) | | N.S. $0.13 < p < 0.27$ $1.5 < \chi^2 < 2.2$ | N.S. $0.24 < p < 0.43$ $0.6 < \chi^2 < 1.6$ |
| EMS (CE and ACE, 1 equal parameter set) | | *** $p = 0.0003$ $\chi^2 = 2.8$ | ** $p = 0.002$ $\chi^2 = 1.9$ |

*Results at significance values are highlighted: N.S, indicates not significant ($p > 0.05$); *indicates $p < 0.05$; **$p < 0.01$; and ***$p < 0.001$. $\chi^2$ indicates the Chi-squared misfit value: the closer $\chi^2$ is to 1, the more accurate the simulation. In this table, "p" and "$\chi^2$ intervals represent the minimum and the maximum value obtained from acceptable solutions. Simulations were considered acceptable when both $p > 0.05$ and $\chi^2 > 2.5$.*

marine biogeochemical models as well (e.g., Fasham et al., 1995; Evans, 1999). Advantages and disadvantages of using simulated annealing or conjugate-gradient algorithms are discussed in Matear (1995). The phytoplankton size classes in EMS were fixed, with the purpose of representing two distinct phytoplankton types to examine if their abundance was different between CE and ACE: 2 μm diameter for small phytoplankton cells and 40 μm diameter for large phytoplankton cells. With EMS, the data assimilation was allowed to vary 12 parameters—like WOMBAT, they were the parameters controlling plankton growth (**Table 4**).

To recognize that there was not one unique solution, rather a range of parameter values could produce acceptable solutions, we show a range of simulated behavior to reflect the non-uniqueness of the solution. From data assimilation results, only acceptable solutions are shown, which were simulations where both $0 < \chi^2 < 2.5$ and there was no significant difference between the annual mean simulated and observed Chl-a concentration (with 95% confidence in the equivalence test; Wellek, 2010).

## Shipboard Manipulation Experiment

To investigate the potential shift in phytoplankton size and abundance in a CE we examined phytoplankton responses to increased light and nutrients by performing an experiment during an oceanographic research voyage. The experiment was carried out on board the *RV Investigator* (voyage IN2015_V03), with water sampled from a station located in the EAC (32.7°S and 153.6°E), inside the modeling domain (**Figure 1**). This site was representative of potential source water for eddies, allowing us to evaluate the effect of light and nutrients on the phytoplankton community prior to the seasonal shoaling of the MLD. Water was sampled a few meters below the MLD (∼110 m, water temperature ∼20.9°C) and exposed to increased light and nutrients. Sampled seawater was transferred directly from the CTD-rosette into 15 acid-cleaned 4 L polycarbonate vessels. Vessels were sealed, randomly assigned to three light treatments, with half the bottles being amended with inorganic nutrients and the other half remaining unamended, before they were all placed in a deck-board incubator which had continuous flow of surface seawater of ∼21.5°C. The nutrient enrichment consisted of daily nutrient addition of dissolved inorganic Fe III 0.005 μmol $L^{-1}$, N as nitrate 1.2 μmol $L^{-1}$, Si as silicate 1.2 μmol $L^{-1}$, P as phosphate 0.075 μmol $L^{-1}$, in Redfield proportion (McAndrew et al., 2007; Ellwood et al., 2013). The experimental treatments included control (CON; ambient light i.e., ∼1% incident light, no nutrient amendment), low light (LL; 20% incident light), high light (HL; 40% incident light), low light and nutrients (LL+N), high light and nutrients (HL+N), and were made in triplicate. Incident light was attenuated using shade cloth. Pigment samples for Ultra-High Performance Liquid Chromatography (UPLC) analysis were collected from each bottle at the end of the 5-day experiment, as well as the initial phytoplankton community.

Samples for UPLC analysis were filtered through 25 mm glass fiber filters (Whatman GF/F), filters were placed in cryotubes, flash frozen in liquid nitrogen, and stored in a −80°C freezer. The pigment extraction was carried out following a modified method used by Van Heukelem and Thomas (2001). Each filter was placed into an individual 15 mL falcon tube with 1.5 mL of chilled 90% acetone. Each filter was then disrupted using a 40 W ultrasonic probe for ∼30 s, keeping the tube in ice; then the samples were stored at 4°C overnight. The sample slurry was vortexed for 10 s and clarified by passing through a 0.2 μm PTFE 13 mm syringe filter before storage in UPLC glass vials, followed by analysis. The dataset obtained from the UPLC analyses was analyzed following Barlow et al. (2004) formulae and Thompson et al. (2011) for the pigment quality control.

# RESULTS

## Characterization of CE and ACE

The physical environment of the CE and ACE show important differences in their seasonal climatologies. For ACE, the MLD is deeper than CE throughout the seasonal cycle (**Figure 4A**; $n = 365$, $p<0.01$, **Table 2**). Conversely, the surface Chl-a concentrations are higher in CE than ACE for most of the year (**Figure 4B**, $n = 365$, $p < 0.001$, **Table 2**). Both Chl-a and MLD show the greatest differences between CE and ACE in the May and October period (austral winter/spring); while for the rest of the year (November to April) Chl-a concentrations and MLD are similar (**Figure 4**).

## WOMBAT and EMS Simulations

Data assimilation to independently determine WOMBAT parameter sets for the CE and ACE environments produced acceptable simulations of the Chl-a seasonal climatology

**TABLE 3 | WOMBAT parameter set for CE and ACE fitted independently, and the optimized parameter set fitting the two environments simultaneously (CE + ACE).**

| Parameter | CE | ACE | CE + ACE | Unit |
|---|---|---|---|---|
| Photosynthetic efficiency (initial slope of P–I curve) | 0.020 ± 0.003 | 0.024 ± 0.006 | 0.024 | $day^{-1}$ ($W\ m^{-2}$) |
| Shortwave fraction of photosynthetically active radiation | 0.43 | 0.43 | 0.43 | |
| Half saturation constant for N uptake | 1.2 ± 0.1 | 1.2 ± 0.1 | 1.23 | $mmol\ m^{-3}$ |
| Phytoplankton maximum growth rate parameters | a) 1.6 ± 0.2 | 1.7 ± 0.1 | 1.8 | $day^{-1}$ |
| | b) 1.066 | 1.066 | 1.066 | |
| | c) 1.0 | 1.0 | 1.0 | |
| Phytoplankton mortality | 0.02 ± 0.01 | 0.02 ± 0.01 | 0.03 | $day^{-1}$ |
| Zooplankton assimilation efficiency | 0.75 ± 0.1 | 0.6 ± 0.25 | 0.85 | |
| Zooplankton maximum grazing rate | 2.55 ± 1.05 | 2.0 ± 0.5 | 1.70 | $day^{-1}$ |
| Zooplankton prey capture rate | 2.9 ± 1.1 | 3.1 ± 0.8 | 2.86 | $(mmol\ N/m^2)^{-1}\ day^{-1}$ |
| Zooplankton (quadratic) mortality | 0.8 ± 0.1 | 0.3 ± 0.2 | 0.64 | $(mmol\ N/m^3)^{-1}\ day^{-1}$ |
| Zooplankton excretion | 0.01 | 0.01 | 0.01 | $day^{-1}$ |
| Remineralization rate | 0.10 | 0.10 | 0.10 | $day^{-1}$ |
| Sinking velocity | 5.00 | 5.00 | 5.00 | $m\ day^{-1}$ |

**TABLE 4 | EMS parameter set for CE and ACE.**

| Parameter | CE | ACE | CE + ACE | Unit |
|---|---|---|---|---|
| Large zooplankton growth efficiency | 0.37 ± 0.03 | 0.29 ± 0.05 | 0.34 | |
| Small zooplankton growth efficiency | 0.33 ± 0.03 | 0.27 ± 0.02 | 0.30 | |
| Large phytoplankton natural (linear) mortality rate | 0.01 ± 0.003 | 0.01 ± 0.003 | 0.01 | $day^{-1}$ |
| Small phytoplankton natural (linear) mortality rate | 0.02 ± 0.008 | 0.02 ± 0.01 | 0.02 | $day^{-1}$ |
| Large zooplankton natural (quadratic) mortality rate | 0.76 ± 0.15 | 0.42 ± 0.08 | 0.55 | $(mmol\ N/m^3)^{-1}\ day^{-1}$ |
| Small zooplankton natural (quadratic) mortality rate | 0.35 ± 0.02 | 0.42 ± 0.08 | 0.36 | $(mmol\ N/m^3)^{-1}\ day^{-1}$ |
| Large phytoplankton maximum growth rate at Tref | 1.85 ± 0.25 | 1.7 ± 0.2 | 2.0 | $day^{-1}$ |
| Large phytoplankton cells diameter | 40.0 | 40.0 | 40.0 | μm |
| Small phytoplankton maximum growth rate at Tref | 1.1 ± 0.1 | 1.1 ± 0.1 | 1.1 | $day^{-1}$ |
| Small phytoplankton cells diameter | 2.0 | 2.0 | 2.0 | μm |
| Small zooplankton maximum growth rate of at Tref | 0.38 ± 0.02 | 0.4 ± 0.03 | 0.41 | $day^{-1}$ |
| Small zooplankton swimming velocity | 0.002 ± 0.0005 | 0.0015 ± 0.0003 | 0.0022 | m/s |
| Large zooplankton maximum growth rate at Tref | 0.85 ± 0.25 | 0.4 ± 0.1 | 0.62 | $day^{-1}$ |
| Large zooplankton swimming velocity | 0.052 ± 0.003 | 0.06 ± 0.005 | 0.058 | m/s |
| Remineralization rate | 0.10 | 0.10 | 0.10 | $day^{-1}$ |
| Sinking velocity | 5.00 | 5.00 | 5.00 | $m\ day^{-1}$ |

*EMS contains a total of 104 different parameters, in this table are shown only the parameters that were allowed to vary during the data assimilation analyses (except large and small phytoplankton cells diameter, remineralization rate, and sinking velocity).*

(**Figures 5A,B**). Acceptable simulations are demonstrated by the $\chi^2$ values and the non-significant *t*-student test (ACE $p > 0.12$; CE $p > 0.22$, 95% confidence that the two dataset are equivalent), confirming that there are no significant differences between the average of the modeled and observed data (**Table 2**).

The data assimilation carried out with the single phytoplankton model WOMBAT for the two eddy environments yielded distinct parameter sets (**Table 3**). For acceptable solutions, the main difference between the parameter sets relate to zooplankton (quadratic) mortality, where CE shows ∼130% greater values than ACE (**Table 3**). From the acceptable solutions, we show the primary production and zooplankton concentrations for the two types of eddies (**Figures 5C–F**). When the data assimilation tries to fit both the environments with a single parameter set there is a significant probability (ACE $p = 0.003$; CE $p = 0.005$, **Table 2**) the annual mean Chl-a differs between the observed and simulated value.

The data assimilation carried out with EMS for the two environments leads to acceptable simulation of Chl-a (**Table 2**), with the simulated annual mean Chl-a consistent with the observed value (ACE $p > 0.13$; CE $p > 0.24$, 95% confidence that the two dataset are equivalent; **Figure 6**, **Table 2**). However, no acceptable solutions were found fitting both the environments with one parameter set (**Table 2**). The data assimilation with EMS produced distinct parameter sets for the CE and ACE environments, with main differences

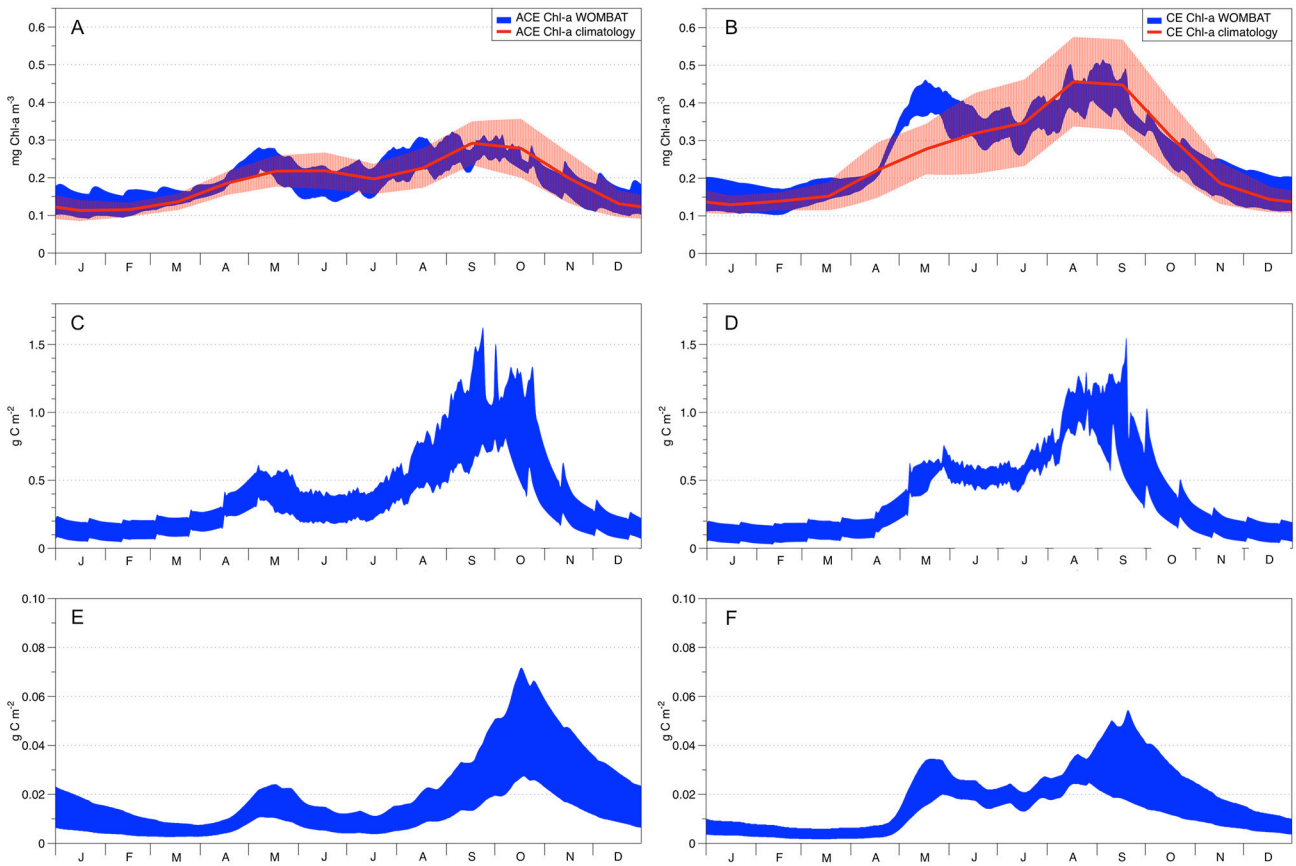


**FIGURE 5 | WOMBAT's acceptable solutions obtained from data assimilation.** Left column shows ACE seasonality and right column CE seasonality. The red solid lines in plots **(A,B)** show the Chl-a observed seasonal climatology with the red shading denoting the standard deviation variability. In all remaining plots, the blue areas represent WOMBAT acceptable solutions. Plots (**C**; ACE) and (**D**; CE) represent primary production (g C $m^{-2}$) while plots **(E,F)** represent the zooplankton dynamics for the ACE and CE systems, respectively.

related to the large zooplankton parameters: large zooplankton quadratic mortality rate is ∼1.8 times greater in CE and large zooplankton maximum growth rate is ∼2.1 times greater in CE (**Table 4**). For the acceptable EMS solutions we show the primary production for large and small phytoplankton and the seasonal evolution of the small and large zooplankton concentrations (**Figures 6C–H**). The development of the winter/spring (May–October) phytoplankton bloom is driven by increased production of large phytoplankton, that is considerably greater in the CEs than the ACEs.

Simulations carried out to evaluate higher-frequency variations in the MLD (i.e., with the inclusion of random noise), produce plankton dynamics within the range of the acceptable solutions (**Figures 5**, **6**).

## Shipboard Manipulation Experiment

The initial phytoplankton community sampled below the EAC MLD, at ∼110 m in June was composed mainly of picophytoplankton (<2 μm) and nanophytoplankton (2-20 μm) while the microphytoplankton (>20 μm) was the least abundant phytoplankton size class (**Figure 7A**). *Prochlorococcus* (as indicated by the concentration of divinyl chlorophyll-a) and haptophytes (hex-fucoxanthin) were the dominant phytoplankton classes in the initial community (**Figure 7B**). At the end of the shipboard experiment, the phytoplankton composition (as determined by pigment analyses) was similar in all treatments (**Figure 7**). By the end of the experiment, there was a large change in the phytoplankton community, highlighting a shift from nano and picophytoplankton to the larger microphytoplankton (**Figure 7A**) and from *Prochlorococcus* and haptophytes to diatoms (**Figure 7B**). The pigment concentrations in the control vessels at the end of the experiment were below detection (>0.004 μg $L^{-1}$), and are hence shown as zero in **Figure 7**.

# DISCUSSION

## The Role of Mixed Layer Depth and Light on Phytoplankton

Statistical analysis of the MLD and Chl-a seasonal climatologies clearly shows that CE and ACE off eastern Australia are two distinct environments (**Figure 4**, **Table 2**). Similarities in

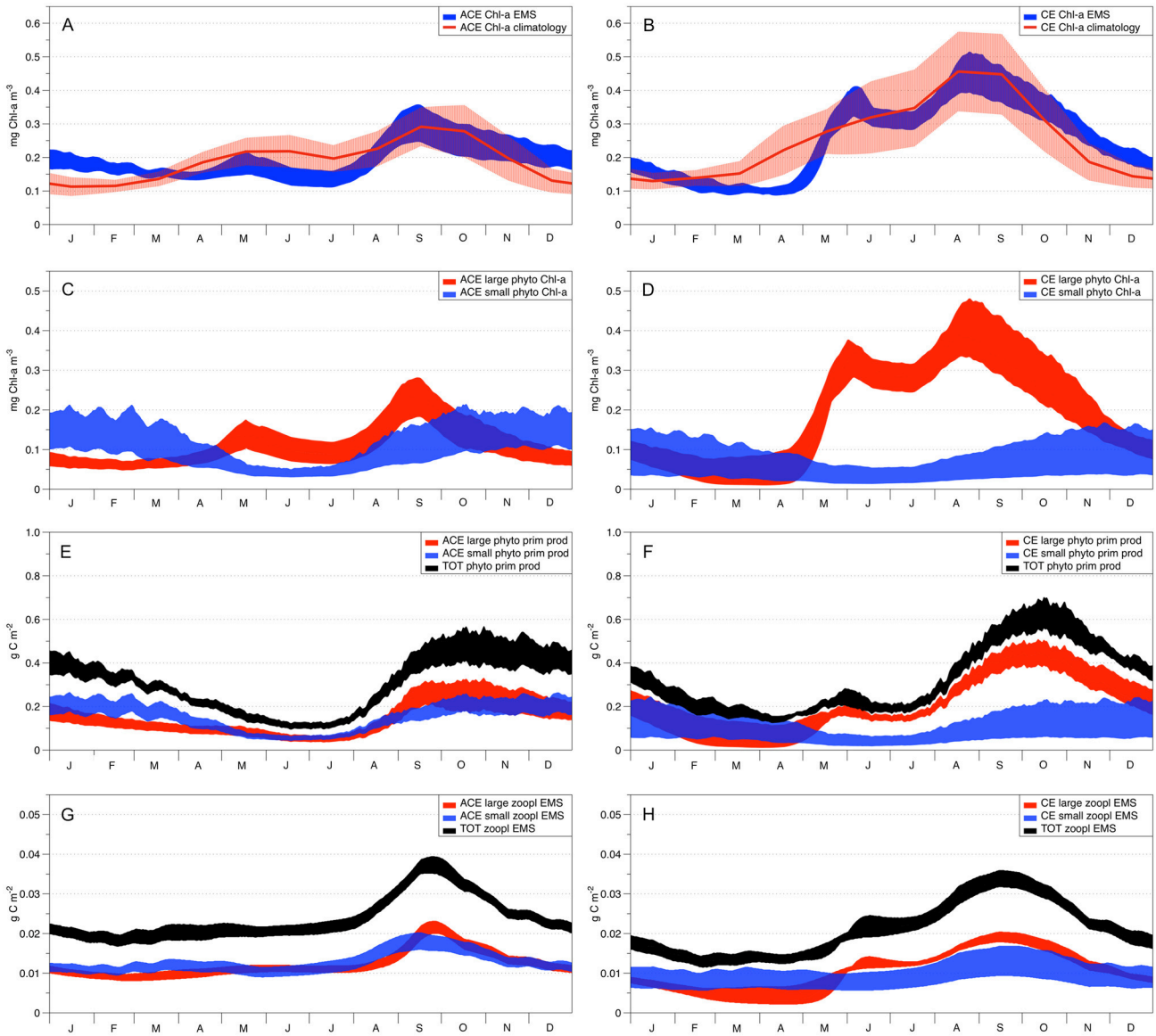


**FIGURE 6 | EMS acceptable solutions from the data assimilation.** Left column shows ACE seasonality and right column CE seasonality. The red solid lines in plots **(A,B)** show the Chl-a observed seasonal climatology with the red shading denoting the standard deviation variability. Patterns of the two EMS phytoplankton classes (Chl-a) are represented in plot (**C**; ACE) and (**D**; CE), where red areas represent the large phytoplankton class (40 μm diameter) and blue areas represent the small phytoplankton class (2 μm diameter). Plots (**E**; ACE) and (**F**; CE) represent the total primary production (g C $m^{-2}$) in black and the primary production for small (blue) and large phytoplankton (red). The total zooplankton biomass (g C $m^{-2}$) is represented in black on plots (**G**; ACE) and (**H**; CE), while the small and large zooplankton biomass is represented in blue and red, respectively.

the MLD and Chl-a seasonal climatology dynamics (**Figure 4**) suggest the MLD could be a key environmental driver of differences in Chl-a between these two environments. The importance of MLD deepening to Chl-a seasonality in subtropical water is consistent with a recent study of Chl-a variability in eddies of the Indian Ocean (Dufois et al., 2016).

In both the single and multiple box phytoplankton models, the MLD seasonal climatology was enough to drive the phytoplankton dynamics and reflect the observed differences between the CE and ACE environments (**Figures 5A,B**, **6A,B**). Although our simulations did not take physical dynamics (i.e., sub-mesoscale events) directly into account, these processes are indirectly accounted for by the implementation of observed CE and ACE MLD.

WOMBAT and EMS simulations confirm that MLD dynamics play an important role in driving the Chl-a concentration in both eddy types. The evolution of the MLD leads to a change in both the nutrient concentration and the light available for photosynthesis, which in turn influences the phytoplankton abundance and community composition (Officier

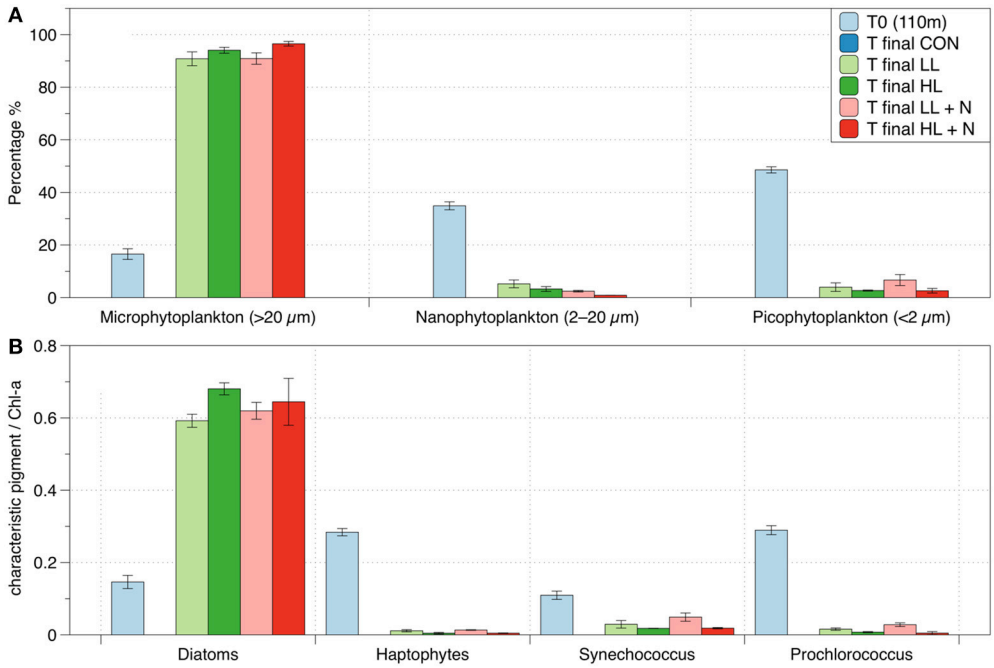


**FIGURE 7 | Pigment analysis of phytoplankton in different treatments (shipboard incubation experiment): (A) size distribution at the initial and final time of the experiment; (B) ratio between characteristic phytoplankton classes pigment and total Chl-a (Diatoms: Fucoxanthin, Haptophytes: 19-Hex-fucoxanthin, Synechococcus: Zeaxanthin, Prochlorococcus: DV Chlorophyll a, Barlow et al., 2004).** In all panels it is represented the "T0 (110m)" showing the initial condition and the "T final" showing the last day of the experiment (6th day). The treatments are labeled as: LL (20% surface irradiance), HL (40% surface irradiance), N (daily nutrients addition). The control (CON, ∼1% incident light, no nutrient amendment). The CON is not represented at the end of the experiment (T final) because the pigment concentrations were below detection (>0.004 μg/L).

and Ryther, 1980; Pitcher et al., 1991; Tilburg et al., 2002). The differences in Chl-a and MLD between CE and ACE are greatest in the austral winter/spring when surface light irradiance are near their seasonal minimum (**Figure 3B**). During the winter/spring period the MLD is deep and it has been shown to cause strong light limitation of phytoplankton growth (Behrenfeld and Boss, 2014). McGillicuddy (2015) hypothesized that in such a light-limited regime, the shallower MLD of the CE than ACE could lead to higher Chl-a concentration in CE.

The shipboard manipulation experiment clarifies the effect of light and nutrients on the phytoplankton community sampled in the same area as our modeling study. The water collected in austral winter from below the MLD (110 m) originally contained a low abundance of phytoplankton (total Chl-a concentration $0.068 \pm 0.003$ μg $L^{-1}$, mean ± standard deviation). After being exposed to 1% surface light (ambient irradiance at the sampling depth) for 6 days, phytoplankton were undetectable (<0.004 μg Chl-a $L^{-1}$), confirming they did not have enough light to remain viable. The same phytoplankton community exposed to 20 and 40% surface irradiance resulted in growth and showed a similar shift in community structure whether nutrients were added or not (**Figure 7A**). The shipboard experiment reveals that, in this region, during winter while the MLD is still deepening (**Figure 4A**), the phytoplankton growth is limited by light rather than by nutrients.

## Phytoplankton Composition and Size Structure

During the shipboard experiment with elevated light, the phytoplankton community shifted from picophytoplankton (<2 μm; ∼49% of the initial community) and nanophytoplankton (2–20 μm; ∼35% of the initial community) to microphytoplankton (>20 μm; ∼90% of the final community; **Figure 7A**). The microphytoplankton appear most light-limited because they are initially in lowest abundance and then dominate the community when exposed to elevated light. The microphytoplankton are almost totally composed of fucoxanthin-containing cells, most likely reflecting diatoms (**Figure 7B**).

Data assimilation with WOMBAT and EMS showed that both models could represent the seasonal evolution of Chl-a in the two types of eddies if the two environments had different parameter values (**Table 2**). The physical and chemical environment that characterizes the CE in oligotrophic oceans, generally drives the accumulation of large phytoplankton species such as diatoms, while small phytoplankton species and cyanobacteria are more characteristic of the surrounding waters and ACE (Jeffrey and Hallegraeff, 1980; Olaizola et al., 1993; Rodriguez et al., 2003; Vaillancourt et al., 2003; Brown et al., 2008). EMS simulations are consistent with such behavior where different phytoplankton dominate CE and ACE (**Figure 6**). In particular, EMS simulations show the differences between CE and ACE Chl-a concentrations are attributed to the large

phytoplankton class, while the small phytoplankton class has similar dynamics in both the systems (**Figures 6C,D**). The greatest difference in the EMS simulated large phytoplankton occurs between May and October when observed Chl-a shows the greatest differences between the ACE and CE Chl-a (**Figure 6**).

Trying to get WOMBAT to use one parameter set to represent both CE and ACE failed to satisfactorily represent Chl-a observations (**Table 2**). WOMBAT's failure to represent the two environments with a unique parameter set may be expected for a model that does not resolve different plankton sizes. However, the parameter values from fitting the two environments separately are very similar. Furthermore, EMS with its two sizes of phytoplankton shows a similar pattern to WOMBAT, where model simulations are unable to produce an acceptable Chl-a simulation using one parameter set to represent both ACE and CE. This suggests that it is more than phytoplankton size that is driving differences between Chl-a in CEs and ACEs.

### Zooplankton

For both WOMBAT and EMS, the optimized parameter sets suggest that the zooplankton in CE have twice the mortality rate and nearly double the growth rate compared to the ACE (**Tables 3**, **4**). Hence, in both models, the phytoplankton grow better in CE than in ACE, because of the higher mortality of their grazers which reduces top-down grazing pressure. Bakun (2006) suggests that an enhanced primary production (typical of CEs) improves zooplankton growth but comes at a cost of increased zooplankton predator abundance; this concept is consistent with the higher zooplankton mortality and growth rate obtained from the parameter optimization in the CE system (**Tables 3**, **4**). Another possible explanation is that two distinct zooplankton communities characterize CE and ACE, with higher grazing pressure in CE environments. Such behavior is consistent with the water in CEs from this region tending to have more coastal organisms than ACEs (Macdonald et al., 2016). However, the interpretation of the difference in zooplankton behavior requires some caution because it may be related to eddy dynamics not directly considered in our simulations (i.e., sub-mesoscale interactions). While the differences in zooplankton properties between CE and ACE is a robust feature of the model simulations, additional observations are needed to confirm this result, and determine the mechanism responsible.

## CONCLUSION

Biogeochemical models are increasingly considering phytoplankton composition to characterize elemental cycles in the contemporary and future ocean (Finkel et al., 2009; Follows and Dutkiewicz, 2011). This study shows that inclusion of multiple phytoplankton groups provides useful, and potentially unexpected, insights about ecosystem dynamics, demonstrating divergent accumulation of biomass in different phytoplankton and zooplankton size classes in CE and ACE.

To put the impact and relevance of these mesoscale features in eastern Australian waters into perspective, an average of 13 CE and 15 ACE with a lifetime $\geq$10 weeks occur annually in the study region (obtained from Chelton et al., 2011 eddy database, yearly average from 1 December 2002 to 4 April 2012). Given that the primary productivity in East Australia is projected to increase 10% by the 2060s due to an increase in eddy activity (Matear et al., 2013), it is therefore critical to quantify plankton concentration, composition, and functioning within eddies and adjacent water masses to advance our understanding of their ecological and trophic roles and impacts to regional fisheries and biogeochemical cycling.

## AUTHOR CONTRIBUTIONS

LL, AM, RM, and MD conceived and designed the experiment. LL and RM acquired the data, performed the modeling work, and analyse the data. LL, AM, and MD performed the ship-based experiment. LL drafted the work, prepared figures, and tables; all authors critically revised the work.

## FUNDING

This research was supported by the Australian Research Council Discovery Projects funding scheme (DP140101340), the Marine National Facility, and the School of Life Science, University of Technology Sydney (postgraduate scholarship to LL), and the Climate Change Cluster research institute (operational support).

## ACKNOWLEDGMENTS

We would like to acknowledge the valuable reviews provided by the two reviewers, which has helped improve the clarity and focus of the manuscript. LL would like to thank Mark Baird, Farhan Rizwi, and Mathieu Mongin (CSIRO) for their useful suggestions and explanations about the Environmental Modeling Suite (EMS), Olivier Laczka (UTS) for his assistance with setting up the experiment aboard the RV Investigator and Gabriela Semolini Pilo (UTAS) for the useful conversations about eddy dynamics. This research was supported by the Australian Research Council Discovery Projects funding scheme (DP140101340 awarded to MD and RM), the Marine National Facility, and the School of Life Science, University of Technology Sydney (postgraduate scholarship to LL) and the Climate Change Cluster research institute (operational support). The authors would like to acknowledge the captain and crew of the IN2015_V03 voyage, as well as the chief scientist, Prof. Iain Suthers. Furthermore, we would like to thank GlobColour, AVISO and the International Argo Program for the production and distribution of the dataset used in this study.

## REFERENCES


ACRI-ST GlobColour Team, Mangin, A., and Fanton d'Andon, O. (2015). *GlobColour Product User Guide, GC-UM-ACR-PUG-01, Version* 3.2. Sophia-Antipolis.

Angel, M. V., and Fasham, M. J. R. (1983). "Eddies and biological processes," in *Eddies in Marine Science*, *Chap*. 22, ed A. R. Robinson (Berlin: Springer), 492–524.

Arístegui, J., and Montero, M. F. (2005). Temporal and spatial changes in plankton respiration and biomass in the Canary Islands region: the effect of mesoscale variability. *J. Mar. Syst.* 54, 65–82. doi: 10.1016/j.jmarsys.2004.07.004

Arístegui, J., Tett, P., Hernandez-Guerra, A., Basterretxea, G., Montero, M. F., Wild, K., et al. (1997). The influence of island-generated eddies on chlorophyll distribution: a study of mesoscale variation around Gran Canaria. *Deep Sea Res.* 44, 71–96. doi: 10.1016/S0967-0637(96)00093-3

Baird, M. E., Ralph, P. J., Rizwi, F., Wild-Allen, K. A., and Steven, A. D. L. (2013). A dynamic model of the cellular carbon to chlorophyll ratio applied to a batch culture and a continental shelf ecosystem. *Limnol. Oceanogr.* 58, 1215–1226. doi: 10.4319/lo.2013.58.4.1215

Bakun, A. (2006). Fronts and eddies as key structures in the habitat of marine fish larvae: opportunity, adaptive response and competitive advantage. *Sci. Mar.* 70S2, 105–122. doi: 10.3989/scimar.2006.70s2105

Barlow, R., Aiken, J., Moore, G. F., Holligan, P. M., and Lavender, S. (2004). Pigment adaptations in surface phytoplankton along the eastern boundary of the Atlantic Ocean. *Mar. Ecol. Prog. Ser.* 281, 13–26. doi: 10.3354/meps281013

Behrenfeld, M. J., and Boss, E. S. (2014). Resurrecting the ecological underpinnings of ocean plankton blooms. *Ann. Rev. Mar. Sci.* 6, 167–194. doi: 10.1146/annurev-marine-052913-021325

Bibby, T. S., and Moore, C. M. (2011). Silicate:nitrate ratios of upwelled waters control the phytoplankton community sustained by mesoscale eddies in sub-tropical North Atlantic and Pacific. *Biogeosciences* 8, 657–666. doi: 10.5194/bg-8-657-2011

Bopp, L., Resplandy, L., Orr, J. C., Doney, S. C., Dunne, J. P., Gehlen, M., et al. (2013). Multiple stressors of ocean ecosystems in the 21st century: projections with CMIP5 models. *Biogeosciences* 10, 6225–6245. doi: 10.5194/bg-10-6225-2013

Boyd, P. W., and Doney, S. C. (2002). Modelling regional responses by marine pelagic ecosystems to global climate change. *Geophys. Res. Lett.* 29, 53-1–53-4. doi: 10.1029/2001GL014130

Brainerd, K. E., and Gregg, M. C. (1995). Surface mixed and mixing layer depths. *Deep Sea Res.* 42, 1521–1543. doi: 10.1016/0967-0637(95)00068-H

Brieva, D., Ribbe, J., and Lemckert, C. (2015). Is the East Australian Current causing a marine ecological hot-spot and an important fisheries near Fraser Island, Australia? *Estuar. Coast. Shelf Sci.* 153, 121–134. doi:10.1016/j.ecss.2014.12.012

Brown, S. L., Landry, M. R., Selph, K. E., Jin Yang, E., Rii, Y. M., and Bidigare, R. R. (2008). Diatoms in the desert: plankton community response to a mesoscale eddy in the subtropical North Pacific. *Deep Sea Res. II Top. Stud. Oceanogr.* 55, 1321–1333. doi: 10.1016/j.dsr2.2008.02.012

Chelton, D. B., Schlax, M. G., and Samelson, R. M. (2011). Global observations of nonlinear mesoscale eddies. *Prog. Oceanogr.* 91, 167–216. doi:10.1016/j.pocean.2011.01.002

Cresswell, G. R. (1994). Nutrient enrichment of the Sydney continental shelf. *Aust. J. Mar. Freshw. Res.* 45, 677–691. doi: 10.1071/MF9940677

CSIRO Coastal Environmental Modelling Team, (2014). *CSIRO Environmental Modelling Suite: Scientific Description of the Optical, Carbon Chemistry and Biogeochemical Models Parameterised for the Great Barrier Reef.* Hobart, TAS: Commonwealth Scientific and Industrial Research Organisation Marine and Atmospheric Research.

de Boyer Montegut, C., Madec, G., Fischer, A. S., Lazar, A., and Iudicone, D. (2004). Mixed layer depth over the global ocean: an examination of profile data and a profile-based climatology. *J. Geophys. Res.* 109, C12003. doi: 10.1029/2004jc002378

Dong, S., Sprintall, J., Gille, S. T., and Talley, L. (2008). Southern ocean mixed-layer depth from argo float profiles. *J. Geophys. Res.* 113:C06013 doi: 10.1029/2006jc004051

Dufois, F., Hardman-Mountford, N. J., Greenwood, J., Richardson, A. J., Feng, M., Herbette, S., et al. (2014). Impact of eddies on surface chlorophyll in the South Indian Ocean. *J. Geophys. Res. Oceans* 119, 8061–8077. doi: 10.1002/2014jc010164

Dufois, F., Hardman-Mountford, N. J., Greenwood, J., Richardson, A. J., Feng, M., and Matear, R. J. (2016). Anticyclonic eddies are more productive than cyclonic eddies in subtropical gyres because of winter mixing. *Sci. Adv.* 2:e1600282. doi: 10.1126/sciadv.1600282

Ellwood, M. J., Law, C. S., Hall, J., Woodward, E. M. S., Strzepek, R., Kuparinen, J., et al. (2013). Relationships between nutrient stocks and inventories and phytoplankton physiological status along an oligotrophic meridional transect in the Tasman Sea. *Deep Sea Res. I* 72, 102–120. doi: 10.1016/j.dsr.2012.11.001

Evans, G. T. (1999). The role of local models and data sets in the joint global ocean flux study. *Deep Sea Res. I* 46, 1369–1389. doi: 10.1016/S0967-0637(99)00010-2

Everett, J. D., Baird, M. E., Oke, P. R., and Suthers, I. M. (2012). An avenue of eddies: Quantifying the biophysical properties of mesoscale eddies in the Tasman Sea. *Geophys. Res. Lett.* 39:L16608. doi: 10.1029/2012GL053091

Falkowski, P. G., Ziemann, D., Kolber, Z., and Bienfang, P. (1991). Role of eddy pumping in enhancing primary production in the ocean. *Nature* 352, 55–58. doi: 10.1038/352055a0

Fasham, M. J., Evans, G. T., Kiefer, D. A., Creasey, M., and Leach, H. (1995). The use of optimization techniques to model marine ecosystem dynamics at the JGOFS station at 47 degrees N 20 degrees W. *Philos. Trans. R. Soc. Lond. B Biol. Sci.* 348, 203–209. doi: 10.1098/rstb.1995.0062

Fennel, W., and Neumann, T. (2004). *Introduction to the Modelling of Marine Ecosystems.* Amsterdam: Elsevier Oceanography Series.

Finkel, Z. V., Beardall, J., Flynn, K. J., Quigg, A., Rees, T. A. V., and Raven, J. A. (2009). Phytoplankton in a changing world: cell size and elemental stoichiometry. *J. Plankton Res.* 32, 119–137. doi: 10.1093/plankt/fbp098

Follows, M. J., and Dutkiewicz, S. (2011). Modeling diverse communities of marine microbes. *Ann. Rev. Mar. Sci.* 3, 427–451. doi: 10.1146/annurev-marine-120709-142848

Hamon, B. V. (1965). The East Australian Current, 1960-1964. *Deep Sea Res.* 12, 889–921. doi: 10.1016/0011-7471(65)90813-2

Haury, L. R. (1984). An offshore eddy in the california current system part IV: plankton distributions. *Prog. Oceanogr.* 13, 95–111. doi: 10.1016/0079-6611(84)90007-7

Hobday, A. J., and Hartmann, K. (2006). Near real-time spatial management based on habitat predictions for a longline bycatch species. *Fish. Manag. Ecol.* 13, 365–380. doi: 10.1111/j.1365-2400.2006.00515.x

Huang, B., Hu, J., Xu, H., Cao, Z., and Wang, D. (2010). Phytoplankton community at warm eddies in the northern South China Sea in winter 2003/2004. *Deep Sea Res. II* 57, 1792–1798. doi: 10.1016/j.dsr2.2010.04.005

Jeffrey, S. W., and Hallegraeff, G. M. (1980). Studies of phytoplankton species and photosynthetic pigments in a warm core eddy of the East Australian Current. I. Summer populations. *Mar. Ecol. Prog. Ser.* 3, 285–294.

Jenkins, W. (1988). Nitrate flux into the euphotic zone near Bermuda. *Nature* 331, 521–523. doi: 10.1038/331521a0

Kidston, M., Matear, R., and Baird, M. E. (2011). Parameter optimisation of a marine ecosystem model at two contrasting stations in the Sub-Antarctic Zone. *Deep Sea Res. II* 58, 2301–2315. doi: 10.1016/j.dsr2.2011.05.018

Kidston, M., Matear, R., and Baird, M. E. (2013). Phytoplankton growth in the Australian sector of the Southern Ocean, examined by optimising ecosystem model parameters. *J. Mar. Syst.* 128, 123–137. doi: 10.1016/j.jmarsys.2013.04.01

Klein, P., and Lapeyre, G. (2009). The oceanic vertical pump induced by mesoscale and submesoscale turbulence. *Ann. Rev. Mar. Sci.* 1, 351–375. doi: 10.1146/annurev.marine.010908.163704

Large, W. G., and Yeager, S. G. (2008). The global climatology of an interannually varying air–sea flux data set. *Clim. Dyn.* 33, 341–364. doi: 10.1007/s00382-008-0441-3

Lee-Lueng, F., Chelton, D. B., Le Traon, P., and Morrow, R. (2010). Eddy dynamics from satellite altimetry. *Oceanography* 23, 14–25. doi: 10.5670/oceanog.2010.02

Levy, M., Klein, P., and Treguier, A.-M. (2001). Impact of sub-mesoscale physics on production and subduction of phytoplankton in an oligotrophic regime. *J. Mar. Res.* 59, 535–565. doi: 10.1357/002224001762842181

Lochte, K., and Pfannkuche, O. (1987). Cyclonic cold-core eddy in the eastern North Atlantic. II. Nutrients, phytoplankton and bacterioplankton. *Mar. Ecol. Prog. Ser.* 39, 153–164.

Macdonald, H. S., Roughan, M., Baird, M. E., and Wilkin, J. (2016). The formation of a cold-core eddy in the East Australian Current. *Cont. Shelf Res.* 114, 72–84. doi: 10.1016/j.csr.2016.01.002

Mata, M. M., Tomczak, M., Wijffels, S., and Church, J. A. (2000). East Australian Current volume transports at 30 degrees S: estimates from the World ocean circulation experiment hydrographic sections PR11/P6 and the PCM3 current meter array. *J. Geophys. Res. Oceans* 105, 28509–28526. doi: 10.1029/1999JC000121

Matear, R. (1995). Parameter optimization and analysis of ecosystem models using simulated annealing: a case study at Station P. *J. Mar. Res.* 53, 571–607. doi: 10.1357/0022240953213098

Matear, R. J., Chamberlain, M. A., Sun, C., and Feng, M. (2013). Climate change projection of the Tasman Sea from an Eddy-resolving Ocean Model. *J. Geophys. Res. Oceans* 118, 2961–2976. doi: 10.1002/jgrc.20202

McAndrew, P. M., Bjorkman, K. M., Church, M. J., Morris, P. J., Jachowski, N., Williams, P. J. B., et al. (2007). Metabolic response of oligotrophic plankton communities to deep water nutrient enrichment. *Mar. Ecol. Prog. Ser.* 332, 63–75. doi: 10.3354/meps332063

McGillicuddy, D. (2015). Mechanisms of Physical - Biological - Biogeochemical Interaction at the Oceanic Mesoscale. *Ann. Rev. Mar. Sci.* 8, 13.1-13.36. doi: 10.1146/annurev-marine-010814-015606

McGillicuddy, D., and Robinson, A. (1997). Eddy-induced nutrient supply and new production in the Sargasso Sea. *Deep Sea Res. I* 44, 1427–1450. doi: 10.1016/S0967-0637(97)00024-1

McWilliams, J. C. (2008). The nature and consequences of oceanic eddies. Ocean Modeling in an Eddying Regime. *Am. Geophys. Union* 177, 5–15. doi: 10.1029/177GM03

Moore, T. S. I. I., Matear, R. J., Marra, J., and Clementson, L. (2007). Phytoplankton variability off the Western Australian Coast: mesoscale eddies and their role in cross-shelf exchange. *Deep Sea Res. II Top. Stud. Oceanogr.* 54, 943–960. doi: 10.1016/j.dsr2.2007.02.006

Officier, C. B., and Ryther, J. H. (1980). The possible importance of silicon in marine eutrophication. *Mar. Ecol. Prog. Ser.* 3, 83–91. doi: 10.3354/meps003083

Oke, P. R., and Griffin, D. A. (2011). The cold-core eddy and strong upwelling off the coast of New South Wales in early 2007. *Deep Sea Res. II* 58, 574–591. doi: 10.1016/j.dsr2.2010.06.006

Olaizola, M., Ziemann, D. A., Bienfang, P. K., Walsh, W. A., and Conquest, L. D. (1993). Eddy-induced oscillations of the pycnocline affect the floristic composition and depth distribution of phytoplankton in the subtropical Pacific. *Mar. Biol.* 116, 533–542. doi: 10.1007/BF00355471

Pilo, G. S., Mata, M. M., and Azevedo, J. L. L. (2015). Eddy surface properties and propagation at Southern Hemisphere western boundary current systems. *Ocean Sci.* 11, 629–641. doi: 10.5194/os-11-629-2015

Pitcher, G. C., Walker, D. R., Mitchell-Innes, B. A., and Moloney, C. L. (1991). Short-term variability during an anchor station study in the southern Benguela upwelling system: phytoplankton dynamics. *Prog. Oceanogr.* 28, 39–64. doi: 10.1016/0079-6611(91)90020-M

Ridgway, K. R., and Dunn, J. R. (2003). Mesoscale structure of the mean East Australian Current System and its relationship with topography. *Prog. Oceanogr.* 56, 189–222. doi: 10.1016/S0079-6611(03)00004-1

Ridgway, K. R., Dunn, J. R., and Wilkin, J. L. (2002). Ocean interpolation by four-dimensional least squares -Application to the waters around Australia. *J. Atmos. Ocean. Technol.* 19, 1357–1375. doi: 10.1175/1520-0426(2002)019<1357:OIBFDW>2.0.CO;2

Robinson, A. R. (Ed.). (1983). *Eddies in Marine Science.* New York, NY: Springer, 609.

Rodriguez, F., Varela, M., Fernandez, E., and Zapata, M. (2003). Phytoplankton and pigment distributions in an anticyclonic slope water oceanic eddy (SWODDY) in the southern Bay of Biscay. *Mar. Biol.* 143, 995–1011. doi: 10.1007/s00227-003-1129-1

Roemmich, D., Gilson, J., Willis, J., Sutton, P., and Ridgway, K. (2005). Closing the time-varying mass and heat budgets for large ocean areas: the Tasman box. *J. Clim.* 18, 2330–2343. doi: 10.1175/JCLI3409.1

Roughan, M., and Middleton, J. H. (2002). A comparison of observed upwelling mechanisms off the east coast of Australia. *Cont. Shelf Res.* 22, 2551–2572. doi: 10.1016/S0278-4343(02)00101-2

Sallée, J. B., Llort, J., Tagliabue, A., and Levy, M. (2015). Characterization of distinct bloom phenology regimes in the Southern Ocean. *ICES J. Mar. Sci.* 72, 1985–1998. doi: 10.1093/icesjms/fsv069

Thompson, P. A., Bonham, P., Waite, A. M., Clementson, L. A., Cherukuru, N., Hassler, C., et al. (2011). Contrasting oceanographic conditions and phytoplankton communities on the east and west coasts of Australia. *Deep Sea Res. II* 58, 645–663. doi: 10.1016/j.dsr2.2010.10.003

Tilburg, C., Subrahmanyam, B., and O'Brien, J. (2002). Ocean color variability in the Tasman sea. *Geophys. Res. Lett.* 29, 1487–1490. doi: 10.1029/2001GL014071

Tranter, D. J., Carpenter, D. J., and Leech, G. S. (1986). The coastal enrichment effect of the East Australian Current eddy field. *Deep Sea Res.* 33, 1705–1721. doi: 10.1016/0198-0149(86)90075-0

Vaillancourt, R. D., Marra, J., Seki, M. P., Parsons, M. L., and Bidigare, R. R. (2003). Impact of a cyclonic eddy on phytoplankton community structure and photosynthetic competency in the subtropical North Pacific Ocean. *Deep Sea Res. I* 50, 829–847. doi: 10.1016/S0967-0637(03)00059-1

Van Heukelem, L., and Thomas, C. S. (2001). Computer-assisted high-performance liquid chromatography method development with applications to the isolation and analysis of phytoplankton pigments. *J. Chromatogr. A* 910, 31–49. doi: 10.1016/S0378-4347(00)00603-4

Wellek, S. (2010). *Testing Statistical Hypotheses of Equivalence.* Boca Raton, FL: Chapman and Hall/CRC, 431.

**Conflict of Interest Statement:** The authors declare that the research was conducted in the absence of any commercial or financial relationships that could be construed as a potential conflict of interest.

frontiers in Marine Science

ORIGINAL RESEARCH
published: 13 April 2017
doi: 10.3389/fmars.2017.00092

# Modeling Larval Connectivity of Coral Reef Organisms in the Kenya-Tanzania Region

*C. Gabriela Mayorga-Adame*[1,2]*, *Harold P. Batchelder*[1,3] *and Yvette. H. Spitz*[1]

[1] College of Earth, Ocean, and Atmospheric Sciences, Oregon State University, Corvallis, OR, USA, [2] National Oceanography Centre, Liverpool, UK, [3] North Pacific Marine Science Organization, Sidney, BC, Canada

Most coral reef organisms have a bipartite life-cycle; they are site attached to reefs as adults but have pelagic larval stages that allow them to disperse to other reefs. Connectivity among coral reef patches is critical to the survival of local populations of reef organisms, and requires movement across gaps that are not suitable habitat for recruitment. Knowledge of population connectivity among individual reef habitats within a broader geographic region of coral reefs has been identified as key to developing efficient spatial management strategies to protect marine ecosystems. The study of larval connectivity of marine organisms is a complex multidisciplinary challenge that is difficult to address by direct observation alone. An approach that couples ocean circulation models with individual based models (IBMs) of larvae with different degrees of life-history complexity has been previously used to assess connectivity patterns in several coral reef regions [e.g., the Great Barrier Reef (GBR) and the Caribbean]. We applied the IBM particle tracking approach to the Kenya-Tanzania region, which exhibits strong seasonality in the alongshore currents due to the influence of the monsoon. A 3-dimensional (3D) ocean circulation model with 2 km horizontal resolution was coupled to IBMs that track virtual larvae released from each of 661 reef habitats, associated with 15 distinct regions. Given that reefs provide homes to numerous species, each with distinctive, and in aggregate very diverse life-histories, several life-history scenarios were modeled to examine the variety of dispersal and connectivity patterns possible. We characterize virtual larvae of *Acropora* corals and *Acanthurus* surgeonfish, two coral reef inhabitants with greatly differing pelagic life-histories, to examine the effects of short (<12 days) and long (>50 days) pelagic larval durations (PLD), differences in swimming abilities (implemented as reef perception distances), and active depth keeping in reef connectivity. *Acropora* virtual larvae were modeled as 3D passive particles with a precompetency period of 4 days, a total PLD of 12 days and a perception distance of 10 m. *Acanthurus* virtual larvae were characterized by 50 days precompetency period, a total PLD of 72 days and a perception distance of 4 km. *Acanthurus* virtual larvae were modeled in two ways—as 3D passive particles and including an idealized ontogenetic vertical migration behavior. A range of distances within which larvae were able to perceive reefs and directionally swim to settle on them during the competency period were evaluated. The influence of interannual environmental variations was assessed for 2 years (2000, 2005) of contrasting physics. The spatial scale of connectivity is much smaller for the short

OPEN ACCESS

**Edited by:**
*Christian Lindemann, University of Bergen, Norway*

**Reviewed by:**
*Louis Worth Botsford, University of California, Davis, USA*
*Anne Chenuil, Centre National de la Recherche Scientifique (CNRS), France*
*Guillem Chust, AZTI-Tecnalia, Spain*

***Correspondence:**
*C. Gabriela Mayorga-Adame*
*gmaya@noc.ac.uk*

**Specialty section:**
*This article was submitted to Marine Ecosystem Ecology, a section of the journal Frontiers in Marine Science*

**Received:** *05 August 2016*
**Accepted:** *15 March 2017*
**Published:** *13 April 2017*

**Citation:**
*Mayorga-Adame CG, Batchelder HP and Spitz YH (2017) Modeling Larval Connectivity of Coral Reef Organisms in the Kenya-Tanzania Region. Front. Mar. Sci. 4:92. doi: 10.3389/fmars.2017.00092*

PLD coral, with successful connections restricted to a 1° radius (~100 km) around source reefs. In contrast, long distance connections from the southern to the northernmost reefs (~950 km) are common for virtual *Acanthurids.* Successful settlement for virtual *Acropora* larvae was <0.3%, and within region settlement (local retention) was 0.38%, substantially greater than inter-region settlement (ca. 0.2%). Settlement of *Acanthurus* virtual larvae was >20% overall, with cross-region recruitment much increased compared to the coral larvae. Approximately 8% of *Acropora* larvae that successfully settled, recruited to their source reef (self-recruitment), an important proportion compared to only 1–2% self-recruitment for *Acanthurus.* These rates and dispersal distances are similar to previous modeling studies of similar species in other coral reef regions and agree well with the few observational studies within the Kenya-Tanzania region.

**Keywords: larval connectivity, coral reefs, Western Indian Ocean, individual based modeling, particle tracking, ocean modeling**

## INTRODUCTION

Tropical coral reef ecosystems are very important from both the ecological and economical points of view (Spalding et al., 2001). However, they are also particularly fragile, and have been declining in recent years in most regions of the world (Hughes et al., 2003; Pandolfi et al., 2003; Melbourne-Thomas et al., 2011), since they are highly susceptible to anthropogenic stressors operating at global scales (e.g., global warming and ocean acidification) and local scales (e.g., pollution/eutrophication, fishing, over-commercialization for recreation). Coral reef ecosystems are complex communities with very high species diversity. Most reef species have bipartite life histories with a planktonic larval stage and a benthos associated adult life. As adults, coral reef organisms exhibit various degrees of site attachment ranging from completely sessile, like corals and sponges, to highly mobile, like fish and crustaceans. Generally, even fish capable of swimming several kilometers in a few hours have restricted home ranges, since they are relatively territorial and are associated with specific reef habitats that are patchily distributed (Sale, 2006). Most adult reef organisms are distributed in metapopulations connected by pelagic larvae that disperse subject to the ocean currents (Bode et al., 2006; Cowen and Sponaugle, 2009).

Coral reefs extend along the coast of East Africa from the equator to ~14°S, being absent only at major river outflows or Pleistocene river valleys. Fringing reefs are the most common type, but complex formations occur around islands and other regions where the continental shelf extends more than a few kilometers from shore. Reefs are absent on the Somali coast north of the equator due to seasonal upwelling of cold water associated with the monsoon winds. The southernmost reef is found in Mozambique at 26°S; but scattered colonies of scleractinian corals occur as far south as 34°S, in South Africa (Day, 1974 cited in Hamilton and Brakel, 1984). Western Indian Ocean coral reef communities are characterized by high levels of species diversity and may be centers of biodiversity (Spalding et al., 2001). Coastal communities of Kenya and Tanzania depend on the reef for food. Since there is little regulation on the use of these resources through formal resource management strategies, reef areas in Kenya and Tanzania have been degraded due to overfishing, destructive fishing techniques, coastal pollution and other activities affecting the coastal environment (Hamilton and Brakel, 1984; Spalding et al., 2001). Increasing interest in coral reef tourism is simultaneously leading to increased pressure on some coral reefs while providing a powerful local incentive for conservation (Spalding et al., 2001). There are 26 Marine Protected Areas (MPAs) in Kenya and Tanzania reported in the Protected Planet Database (http://www.protectedplanet.net/; accessed July 2016) that encompass coral reef habitat; some of these were established as recently as 2010. Eight of the 26 MPAs are no-take areas, while 18 of them allow extraction using traditional fishing methods like handlines and traps (Muthiga et al., 2008). The benefits of MPAs for biodiversity conservation and fisheries management are well known (McClanahan and Mangi, 2000; Gell and Roberts, 2003; Roberts et al., 2005; Lester et al., 2009; Micheli et al., 2012); however, the design (spacing, size and separation distance) of effective MPA networks is not trivial (e.g., Botsford et al., 2003; McLeod et al., 2009; Edgar et al., 2014). Many studies (e.g., Botsford et al., 2009; McCook et al., 2009; Hogan et al., 2011; Rossi et al., 2014) emphasize the importance of larval connectivity on the performance of MPA spatial management for meeting conservation and fisheries yield objectives.

Larval connectivity is vital to the survival of marine metapopulations, both at ecological and evolutionary time scales (James et al., 2002; Cowen and Sponaugle, 2009; Burgess et al., 2014). Population connectivity plays a fundamental role in local and metapopulation dynamics, community dynamics and structure, genetic diversity, ecosystem responses to environmental changes, and the resiliency of populations to human exploitation (Cowen et al., 2007). Connectivity among marine metapopulations is controlled by physical transport and dispersion, temperature, and biological processes such as the timing of spawning, pelagic larval duration (PLD), larval behavior, and mortality. The net combined effect of these processes determines the spatial scales over which a population is connected (Gawarkiewicz et al., 2007). Connectivity is therefore

a function of several interacting variables including species, geographical area, and ocean conditions, and is highly variable in both time and space (e.g., Cowen and Sponaugle, 2009; Christie et al., 2010b; Domingues et al., 2012). Often, little is known about the connections among different coral reef regions (Cowen et al., 2000; Mora and Sale, 2002; Sponaugle et al., 2002) and the degree to which local populations are open (dependent on recruits from external sources) (e.g., Saenz-Agudelo et al., 2011) or closed (self-replenishing) (e.g., Schultz and Cowen, 1994).

Observational approaches for studying connectivity use genetic techniques (Baums et al., 2005; Jones et al., 2005; Christie et al., 2010a,b; Hogan et al., 2011; Harrison et al., 2012), spatially varying natural bio-markers leaving a geochemical signature in calcified structures (i.e., otoliths and statoliths) (Thorrold et al., 1998, 2007) or tagging otoliths of larvae (Jones et al., 1999; Almany et al., 2007). These techniques are limited in the spatio-temporal scales they can resolve and some of them are restricted to specific species or environments (Gawarkiewicz et al., 2007; Hedgecock et al., 2007; Thorrold et al., 2007). Challenges of applying observational techniques to larval connectivity in the Kenya-Tanzania (KT) region are that these methods are expensive, time-consuming and require highly specialized equipment and expertise (Thorrold et al., 2007). Individual based Lagrangian particle tracking models (IBM) coupled to realistic ocean circulation models are a less limiting method to study potential connectivity among East-African coral reefs. So long as the ocean circulation model reasonably depicts the time-varying flows, IBMs can resolve time varying 3-dimensional (3D) potential dispersion of planktonic larvae over large spatial scales with high spatio-temporal resolution (Werner et al., 2007). Results of numerical simulations can only provide estimates of potential connectivity, that need to be validated with empirical measurements (i.e., Foster et al., 2012; Soria et al., 2012) and scaled by observed reproductive input (Watson et al., 2010) and settlement (i.e., Sponaugle et al., 2012). Even in the absence of empirical confirmations, estimates of potential connectivity from modeling studies provide a comprehensive understanding of the spatial-temporal dynamics of marine populations, that inform the design of more efficient MPAs (Willis et al., 2003; Sale et al., 2005). With the exception of a few studies (McClanahan, 1994; McClanahan et al., 1994; Mangubhai, 2008; Yahya et al., 2011; Kruse et al., 2016), knowledge of reef biota ecology is lacking for much of the Western Indian Ocean region, due to the lack of infrastructure and local expertise, combined with problems of national security in some areas (Spalding et al., 2001). Few studies have examined larval supply and connectivity in coral reefs in the Western Indian Ocean (Kaunda-Arara et al., 2009; Crochelet et al., 2013, 2016). Genetic techniques have been used to study connectivity at evolutionary time scales of several reef fish (Dorenbosch et al., 2006, *Lutjanus fulviamma*; Visram et al., 2010, *Scarus ghobban*; and Muths et al., 2012, *Lutjanus kasmira*). High gene flow and weak genetic structure were found in these fish, even among sites as distant as 4000 km (Muths et al., 2012). Recently, van der Ven et al. (2016) used genetic techniques to examine connectivity at evolutionary time scales of the branching coral *Acropora tenuis* in the Kenya-Tanzania region. They report high but variable connectivity among sample sites spanning 900 km along the coast. These studies do not address ecologically significant timescales of a few generations, and are in general concerned with large spatial scales (∼1000 s of km), therefore they cannot provide insights on population demography at temporal and spatial scales relevant to the implementation of management and conservation strategies at national and regional levels. Only Souter et al. (2009) used genetic techniques to examine both evolutionary and ecological connectivity of the coral *Pocillopora damicornis* in the MPAs of the KT region. They identified the Mnemba Conservation area northeast of Zanzibar Island as a potential source for the *P. damicornis* population, and Malindi Marine National Park and Reserve in north Kenya as a genetically isolated reef.

For decades the spatial connectivity of larval fish and invertebrates was thought to be a passive process governed primarily by the ocean physics and the duration of the larval period (e.g., Shanks, 2009). The PLD of coral reef organisms varies greatly; from a few hours for some coral species to a few months for some fish and crustaceans (Shanks, 2009). Recent studies (i.e., Leis and Carson-Ewart, 2003; Paris and Cowen, 2004; Shanks, 2009; Pineda et al., 2010) have shown that larval transport of most marine organisms is not strictly passive and that there is an uncoupling between dispersal distance and PLD due to larval behavior, such as active depth selection and directional swimming. Discrepancies between the passive transport hypothesis and observed patterns of recruitment point to the importance of biological factors (i.e., behavior, predation, starvation, etc.) in the control of larval dispersal and connectivity (Paris and Cowen, 2004; Cowen et al., 2006; Leis et al., 2007; Cowen and Sponaugle, 2009; Sponaugle et al., 2012). Even excluding mortality, the degree to which biological factors influence connectivity is greater than originally hypothesized (Shanks, 2009). Recent studies have shown the importance of physiological and behavioral characteristics of larvae on influencing the connectivity and dispersal of species with a planktonic larval stage (i.e., Kingsford et al., 2002). Growth rates (e.g., Bergenius et al., 2002), ontogenetic and diel vertical migrations (Paris et al., 2007; Drake et al., 2013), swimming ability (e.g., Stobutzki and Bellwood, 1997; Wolanski et al., 1997; Leis and Carson-Ewart, 2003; Leis et al., 2007), orientation through olfaction (Atema et al., 2002, 2015; Gerlach et al., 2007; Paris et al., 2013) and audition (Tolimieri et al., 2000; Leis et al., 2003; Simpson et al., 2005; Heenan et al., 2009; Vermeij et al., 2010), and settlement strategies (Leis and Carson-Ewart, 1999; Lecchini, 2005) are important in controlling connectivity of coral reef organisms. Observational studies suggest that marked ontogenetic vertical zonation is important for larval transport (Boehlert and Mundy, 1993; Cowen and Castro, 1994). In modeling studies, vertical migration often promotes local retention and recruitment of pelagic larvae to suitable habitat. A modeling study of the California Current System (CCS) by Drake et al. (2013) showed that larvae that remained below the surface boundary layer were 500 times more likely to be retained within 5 km of the coast after 30 days than larvae that remained near the surface. Settlement in the CCS increased by an order of magnitude when larvae remained at 30 m depth. Similarly,

settlement success in different regions of the Caribbean increased when a shallow ontogenetic vertical migration (OVM) behavior was added to the virtual larvae (Paris et al., 2007). Potential settlement estimates increased up to 190% in the southern Florida Keys with the OVM (Paris et al., 2007). The influence of larval physiology and behavior on connectivity and dispersal of coral reef species is now well established (Kingsford et al., 2002; Paris et al., 2007; Wolanski and Kingsford, 2014). However, biological characteristics are known with certainty only for a handful of species.

The hydrodynamics of the KT coastal ocean is highly variable at seasonal and subseasonal time scales, due to the influence of the monsoons and complex tidal interactions. The coastal circulation is mainly influenced by: (1) the northward flowing East African Coastal Current (EACC) fed by (2) the regionally westward flowing North East Madagascar Current (NEMC), (3) the seasonally reversing Somali Current (SC), (4) tides and (5) local winds (see Figure 1 of Mayorga-Adame et al., 2016). SW monsoon conditions are characterized by strong continuous northward flow along the coast and relatively cool (∼24°C) sea surface temperatures (SST) that prevail from May to October. During the NE monsoon, from January to March, a strong north-south SST gradient is caused by the intrusion of the shallow, southward flowing, cold and salty Somali Current that meets the slow northward flowing, warm and fresh EACC. The convergence of the two currents forms the eastward flowing South Equatorial Counter Current. The inter-monsoon seasons, in between these two periods, are characterized by strong mixing and slow currents.

The relative lack of physiological and behavioral data for larvae of coral reef species in the Kenya-Tanzania region led us to examine connectivity among coral reefs using idealized particle tracking experiments that simulate larvae with characteristics of two ubiquitous and ecologically important species groups: the *Acropora* branching corals with short PLD (ca. 12 days; Babcock and Heyward, 1986; Nishikawa et al., 2003; Nozawa and Harrison, 2008) and the *Acanthurus* surgeon fish with long PLD (72 days; Rocha et al., 2002) (See Mayorga-Adame, 2015 for a review of the genus life histories). Particle tracking of individual organisms using the output of ocean circulation models is a suitable, cost effective tool to examine larval connectivity among coral reefs in large areas and at fine spatio-temporal scales relevant to the population ecology of coral reef species (Werner et al., 2001, 2007; Cowen and Sponaugle, 2009). Insight developed from connectivity matrices generated from this study could aid local managers and decision makers tasked with regulating the use of marine resources in the Kenya-Tanzania region. Hindcasting the connections among reefs in the strongly dynamical Kenya-Tanzania region is challenging and the level of uncertainty is high. The results presented are a first attempt at assessing connectivity in the region and should be treated as a regional result suitable for comparison with similar studies in other coral reef regions [Great Barrier Reef (GBR); Mesoamerican Caribbean Reef]. In addition, these model results should be useful for developing hypotheses and designing observational campaigns aimed at validating or improving the described connectivity patterns.

# METHODS

## Hydrodynamic Model

A 2 km horizontal resolution Regional Ocean Model System (ROMS) (Haidvogel et al., 2008) that includes tides, the 2 km Kenyan-Tanzanian Coastal Model (hereafter 2KTCM), was used to generate (3D) ocean velocity fields. This model is an enhanced resolution version of the 4 km Kenyan-Tanzanian Coastal Model (KTCM) (Mayorga-Adame et al., 2016). The model domain is a rectangular grid extending from 38° to 47°E and from the equator to 10°S (**Figure 1**). It has 31 terrain following vertical levels. The model bathymetry comes from the 30 s global GEBCO product (http://www.gebco.net/data_and_products/gridded_bathymetry_data/; accessed April 2011). The model coastline was manually edited to retain as many features as the 2 km resolution allowed. Only Pate Island in north Kenya, and Pemba, Zanzibar and Mafia Islands in Tanzania are included as dry cells in the land mask. The atmospheric forcing (wind stress, heat and freshwater fluxes) is calculated by ROMS bulk formulation using atmospheric variables from the daily NCEP/NCAR reanalysis (Kalnay et al., 1996). The model is initialized and forced at the boundaries by monthly fields of T, S and velocity from the KTCM (Mayorga-Adame et al., 2016) and tides are provided by the TPXO6 global tidal model (Egbert et al., 1994; Egbert and Erofeeva, 2002). Freshwater runoff and diurnal wind variability are not included in the model. The ocean model was run continuously for 8.25 years from October 1999 to December 2007. Three-hourly averages of the velocity fields

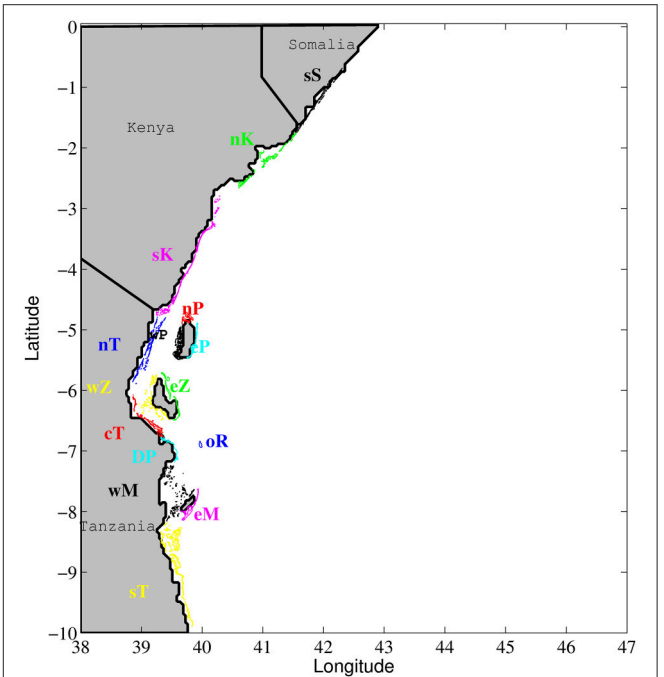


**FIGURE 1 | Study area with coral reefs grouped by color into 15 regions.** sS, south Somalia; nK, north Kenya; sK, south Kenya; wP, west Pemba; eP, east Pemba; nP, north Pemba; nT, north Tanzania; wZ, west Zanzibar; eZ, east Zanzibar; cT, central Tanzania; DP, Dar es Salaam Peninsula; oR, offshore Reef; wM, west Mafia; eM, east Mafia; sT, south Tanzania.

for 2000 and 2005 were stored and used for the particle tracking experiments.

## Lagrangian Particle Tracking

An Individual Based Model (IBM) (Batchelder, 2006) was run offline using previously stored 3-h averages of the 3D-2KTCM velocity fields. The IBM interpolates tri-linearly in space and linearly in time the velocity fields from the ROMS simulation. Particle trajectories are computed using a 4th order Runge-Kutta algorithm. No explicit diffusion (e.g., random walk applied to the individual's position) is invoked since the 2 km horizontal resolution of the ocean circulation model is enough for significant eddy formation and horizontal mixing to occur around reefs, and the terrain following coordinates provide very high vertical resolution (<15 cm) in the shallow regions. A 3D advection-only version of the IBM was used to track forward in time the dispersal of particles (virtual larvae) originating from all reef polygons. The tracking was done using a 30 min time step. Coral larvae were tracked using the 3D passive advection scenario only. For surgeonfish, with longer PLDs and greater ability to control depth in the water column, an idealized ontogenetic vertical migration scenario was implemented.

## Biological Assumptions

In the model experiments all reefs were seeded randomly with a density of 50 particles per square kilometer of reef. Reefs smaller than 1 $km^2$ were seeded with 50 particles. A total of 129 184 particles were released for each modeled spawning day, using identical seeding locations for all simulations. Spawning was assumed to take place at 5:30 p.m. local time (∼sunset) during February and March, the months of peak spawning for coral reef species in the Western Indian Ocean (Mangubhai, 2008; Mangubhai and Harrison, 2008). All particles were released at 3 m depth. For the 3D passive experiments (reference experiments) virtual larvae were spawned at the release locations at 3 day intervals starting on February 2nd for a total of 20 releases. PLD for Caribbean species of *Acanthurus* range from 45 to 70 days (Rocha et al., 2002). The Indo-Pacific species *A. triostegus* has a mean PLD of 54 days (range of 44–83 days) (Randall, 1961; McCormick, 1999; Longenecker et al., 2008). *Acanthurus* virtual larva were tracked for 72 days and considered competent to settle 50 days after their release, giving them a competency period of 22 days. *Acropora* virtual larvae were tracked for 12 days and considered competent after 4 days giving them a competency period of 8 days. These assumptions were made considering the results of laboratory rearing studies that reported a minimum pre-competency period of 3 to 4 days for *A. muricata, A. valida* (Nozawa and Harrison, 2008), and *A. tenuis* (Nishikawa et al., 2003), and up to 97% settlement 10 days after spawning (Babcock and Heyward, 1986; Nishikawa et al., 2003; Nozawa and Harrison, 2008). The ability of reef larvae to sense nearby reefs and swim toward settlement habitat is often represented in models as a sensory zone based on perception distance (Paris et al., 2007; Sponaugle et al., 2012), a buffer distance around suitable habitat that defines how far away from a reef larvae are able to successfully settle. Based on observational studies of sensing, swimming and settling ability (Leis and Carson-Ewart, 1999; Leis and Fisher, 2006; Atema et al., 2015), perception distance for competent *Acanthurus* larvae was assumed to be 4 km, which is consistent with the distance used to model other coral reef fish (Paris et al., 2007; Sponaugle et al., 2012). Perception distance for competent *Acropora* larvae was assumed to be much shorter, only 10 m, because despite their ability to perceive sounds (Vermeij et al., 2010) and chemical cues (Dixson et al., 2014) emanating from reefs they have very limited swimming ability and are unlikely to overcome water speeds (Baird et al., 2014). Virtual larvae were evaluated each night during their competency period to determine if reefs were within their perception distance. If so, they were assumed to settle on the first reef they encountered. Sensitivity analysis to evaluate whether the destination reef of settled larvae was affected by the time of evaluation during the dark hours indicated little temporal variation within a night. Therefore, settlement of virtual larvae was evaluated once per night at 11:30 p.m. local time. The *Acanthurus* ontogenetic vertical migration (OVM) experiment included passive dispersal for 20 days, then larvae were shifted to 50 m (or 3 m above the bottom at locations shallower than 50 m). Virtual larvae at 50 m continued to be passive in their horizontal movement but were kept at fixed depth for 20 days. At day 40, the larvae migrated back to 3 m depth to find suitable reef habitat when reaching competency (50 days after spawning). After the upward migration, larvae are advected passively in three dimensions until day 72, when the trajectory was terminated. Successful settlement was assessed as described in the reference experiment. OVM experiments were run for the February to March period as the passive experiments, but with larvae released only every sixth day (for a total of 10 release dates).

## Seascape Analysis

Kenya and Tanzania have very narrow continental shelves, with the 200 m isobath only 12 km offshore, except at the Mafia and Zanzibar Channels. The shores of Kenya and Tanzania are bordered by a virtually continuous chain of fringing coral reefs that stretches along the coast, only breaking at river mouths and estuaries. The coral reef polygons in the model domain were extracted from the Global Distribution of Coral Reefs 2010 database available at the Ocean Data Viewer webpage (http://data.unep-wcmc.org/). After simplifying the polygons using ArcGIS, by merging adjacent reefs (separated by <20 m), and discarding individual reefs smaller than 25 $m^2$, a total of 661 individual reef polygons identified reef habitat for larval settlement (**Figure 1**). A connectivity matrix showing the origin locations on one axis and destination locations on the other axis is used to visualize the geographic connections among habitat patches for simple alongshore linear systems. However, the two dimensional nature of the reef systems bordering East Africa, with multiple reefs at the same latitude (e.g., mainland fringing reefs, atolls or patch reefs in the channels between the islands and mainland, fringing reefs on the west and east coast of the islands), make the reef to reef connectivity matrices organized by the latitude of the centroid of the reef polygons insufficiently informative regarding inshore-offshore connections. Due to the spatial complexity of the reef habitat, we simplified the connectivity matrices by assigning individual reefs

to one of fifteen geographic subregions (**Figure 1**). Geographic regions considered mainland continuity of reefs, but also national borders and offshore island masses, many of which have both shoreward facing and offshore facing fringing reefs (**Figure 1**). This allowed a more meaningful visualization of the results. Based on the number of particles released within a region, the percentage of particles that successfully connect from region to region was calculated. Summing the percentages in the horizontal direction (all destination regions) on the connectivity matrices shows the percent of successful recruits from each region of origin.

The term local retention refers to the ratio of virtual larvae settling at their released location and the total number of virtual larvae released at that location, while self-recruitment is the ratio of virtual larvae settling at their released location and the total number of larvae settling at that location. In the results section the comparatives "weaker" and "stronger" are used to refer to the magnitude of connections between two specific sites, indicating the proportion of particles connecting from one reef or region to another. Strong connections appear as large color-coded circles in the connectivity matrices, while weak connections are small black circles. Conversely "few" and "more/lots" are used to refer to the number of sites that are connecting to a reef or region. The number of connections for a region will be represented by the number of circles on each row or column for origin and destination regions, respectively.

We use the terms "source" and "origin" interchangeably to refer to reefs or regions from which virtual larvae are released. Similarly, we use the terms "sinks" and "destinations" interchangeably to refer to reefs or regions into which virtual larvae successfully settle. We are not referring to population source/sinks according to the classical population ecology definition, since we do not consider spatially variable reproductive input nor variable mortality during the settlement phase. In this case we are referring only to source/sinks of the planktonic pool of successful virtual larvae, and therefore the terms only refer to the diversity of origins/destinations of the virtual larvae that are assumed to successfully settle.

## Sensitivity Analysis

Complementary analysis and "in silico" experiments were carried out to determine the sensitivity of the resulting connectivity matrices linking origins and destinations to the perception distance assumption and to the inclusion of vertical diffusion. To investigate the sensitivity of settlement success to perception distance, the coral and surgeonfish reference runs of 2000 were re-analyzed with perception distances of 10, 500, and 4000 m. This analysis was performed for particle releases every sixth day for a total of 10 spawning days within February and March. The percent of larvae that successfully settled on reef habitat and the standard deviation among the 10 release dates was calculated.

In order to assess the effects of vertical diffusion on connectivity, and to investigate if an important proportion of reef-to-reef connections is being missed by considering advective only experiments, additional experiments similar to the advective only *Acanthurus* reference runs, but with the addition of vertical diffusion processes, were carried out for 26 selected reefs (Supplementary Figure 5). In order to perform these simulations with the same computer resources used for the advective only simulations the number of release locations had to be greatly reduced; we subsampled 10% (a total of 2694 release locations) from the 26938 release locations used for the advection only scenario for these 26 reefs. For each advection-diffusion release location 100 replicate particles were released on each of 3 release dates; at the beginning, middle and end of the presumed spawning season (February 2nd, March 1st, and March 31st, respectively) of 2000 and 2005. Vertical diffusion was implemented as a vertical random walk scaled by the vertical viscosity coefficient of the ocean model according to the model detailed by Batchelder et al. (2002). The connectivity provided by the advection-diffusion simulations was compared to advection only results from the same 26 reefs to investigate the potential role of vertical diffusion in either enhancing or reducing connectivity and modifying the general patterns observed in the advective only experiments. Comparisons were done at the reef scale. Magnitude of the connections was calculated as the percentage of particles released per reef that settled. The number of particles released was an order of magnitude higher in the experiments with diffusion, while the number of release locations was 10 times greater in the advective only experiments (e.g., 1 particle from each of 50 different locations from a 1 $km^2$ reef in the advection only case vs. 500 particles from each of only 5 release locations within the same reef in experiments including vertical diffusion). The results of all 6 release dates (three in each of 2000 and 2005) were aggregated on a binary reef to reef connectivity matrix, which neglects the magnitude of the connections, and compared to the advective only counterpart. The subtraction of the matrices eliminates connections present in both scenarios and provides an estimate of how many connections were missed by one or the other experimental set ups. Trajectories and connectivity patterns were also visualized and compared to gain understanding of the observed differences, but are not shown.

# RESULTS

## *Acanthurus* and *Acropora* 3-D Passive Advective Experiments

### Settlement Success

Larvae that find a reef within their perception distance during their competency period are assumed to successfully settle. The percentage of successful settlers differs greatly between the two modeled genera. For virtual larvae characterized as *Acanthurus* surgeonfish the mean settlement success of the 40 releases during February and March of 2000 and 2005 is 24.4 $\pm$ 4.7% while for the *Acropora* coral virtual larvae the mean is 0.28 $\pm$ 0.04% (**Figure 2**). Settlement success variability around the mean is similar between the two species groups. Changes in yearly mean settlement success are opposite for the two modeled genera (*Acanthurus* 25.5% in 2000 and 23.3% in 2005, *Acropora* 0.27% in 2000 and 0.28% in 2005).

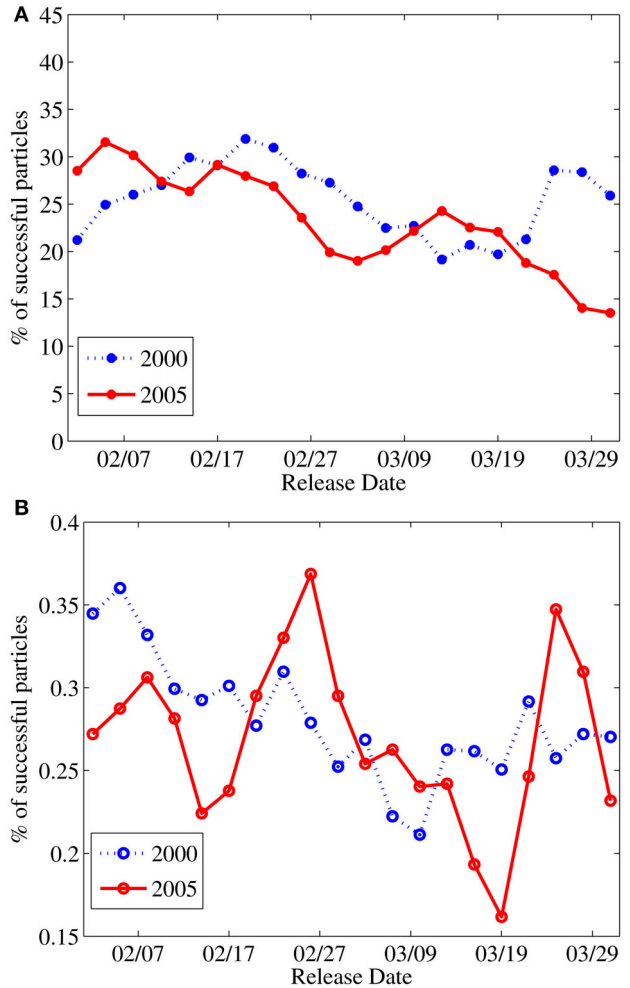


**FIGURE 2 | Percentage of settlement success per each simulated release date during 2000 and 2005 for the (A)** *Acanthurus* and **(B)** *Acropora* genera.

## Region to Region Connectivity Matrices

The region to region connectivity matrices allow an easier visualization of the main connectivity patterns, synthesizing the information of reef to reef connectivity matrices (Supplementary Figure 6). Regional connectivity matrices with reefs grouped into 15 regions (**Figure 1**) show a dominant South to North connectivity pattern along the Kenya-Tanzania coast (**Figure 3**), as represented by the predominance of circles below the 1:1 diagonal line, which indicates sites where local retention occurred (larvae released in a region settled in the same region). This pattern is prevalent in both modeled years (2000 and 2005) for both larvae types (*Acanthurus* and *Acropora*) (**Figure 3**), and reflects the strong south to north flows that prevail along most of the Kenya-Tanzania region, which is influenced by the northward flowing EACC year round. Most of the small number of circles above the 1:1 line of the connectivity matrices indicate north to south connections [a few of them represent west to east connections, for example west Zanzibar (wZ) to east Zanzibar (eZ)], which are much less common but occur in the northern part of the domain due to the influence of the southward flowing Somali Current during the Northeast monsoon (December-March), or to small scale recirculation features, such as eddies, in a few other locations. The magnitude and location of north to south connections is particularly variable interannually. For the 2000 *Acanthurus* simulation (**Figure 3A**) small proportions of north to south connections occur in most regions, but mainly at the northern-most (Somalia [sS], Kenya regions [nK, sK]) and southern-most regions (east Mafia [eM]) and in some central regions (Dar es Salaam Peninsula [DP] and central Tanzania [cT]). In 2005 (**Figure 3C**) north to south connections are weak at the northern and southern limits of the domain, but somewhat stronger in the central region (Dar es Salaam Peninsula [DP], western Zanzibar [wZ] and central Tanzania [cT]).

In *Acropora* corals (**Figures 3B,D**) most of the connections are due to within region recruitment, and strong connections are restricted to a 1 degree (∼100 km) radius around the reef of origin. The reef offshore of Dar es Salaam (oR), east Mafia (eM) and south Tanzania (sT) regions show the longest distance connections. Interannual variability in north to south connections is similar to that of *Acanthurus* virtual larvae.

Regional connectivity matrices enable differentiation among across-shore reefs at the same latitude, and yield insights about well-connected and isolated reef regions. At a regional scale, the Kenya (sK, nK) and Somali (SS) reefs receive *Acanthurus* virtual larvae from all other reef regions in both modeled years. In contrast reef regions adjacent to Pemba Island (eP, nP, wP) receive very few *Acanthurus* larvae from any other reef habitats within the model domain (**Figures 3A,C**). The reef offshore of the Dar es Salaam peninsula (oR at ca. 7°S), due to its oceanic location and exposure to the strong northward flowing EACC, has potential for long distance connections. Settlement of *Acanthurus* from oR was very different in the two modeled years. In 2000 it was a source for larvae settling on distant Kenyan (sK, nK) and Somali (sS) reefs only; in 2005 it exported larvae to Kenyan (sK, nK) and Somali (sS) reefs, but also to some nearer Tanzania regions (central and north Tanzania and east Zanzibar regions; cT, nT, eZ). This offshore reef (oR) is not a large sink reef for *Acanthurus* larvae, but the origin of its arriving larvae is diverse, coming from reefs to the south of it in 2000 and from all regions except east Zanzibar (eZ) in 2005. The Somalia (sS) and Kenya (sK, nK) regions are the sink regions with the greatest diversity of source reefs, followed by the north Tanzania (nT) region. Larvae from Dar es Salaam Peninsula (DP) region settling in the north Tanzania region represented the strongest connection in 2000, followed in magnitude by the connection from the east Zanzibar (eZ) region to the south Kenya (sK) region. In 2005 the strongest connection remains the same but the second strongest connection was between east Zanzibar (eZ) and the north Tanzania (nT) region. During 2005 source reefs around Zanzibar Island (eZ, wZ) and the central Tanzania (cT) region had more connections to southern destination reefs. However, local retention of *Acanthurus* surgeonfish virtual larvae at the regional scale was larger in 2000.

For *Acropora* corals (**Figures 3B,D**) the highest proportion of recruitment is due to local within region recruitment at the

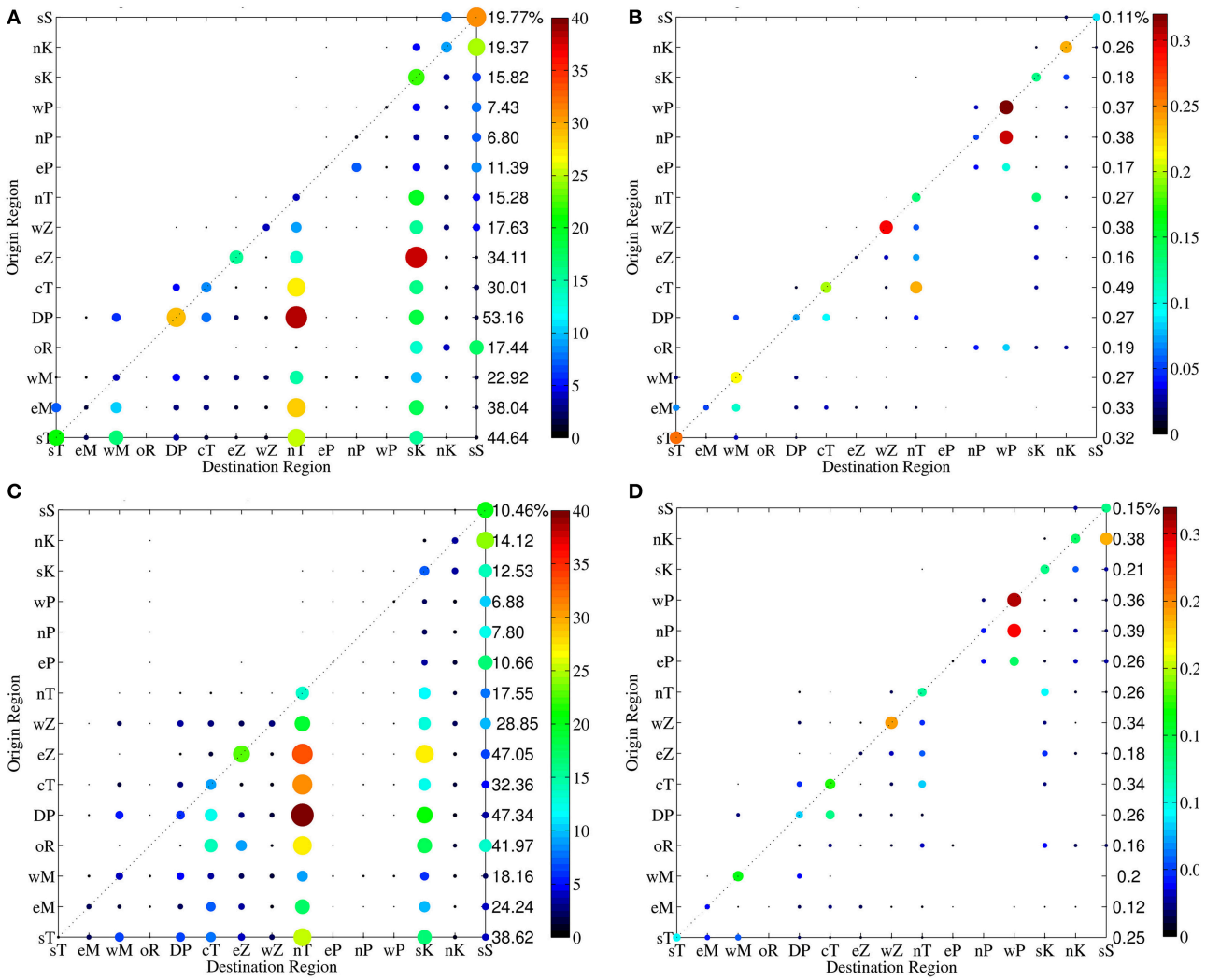


**FIGURE 3 | Region to region connectivity matrices for Acanthurus in 2000 (A)**, 2005 **(C)**, Acropora in 2000 **(B)**, 2005 **(D)**, with reefs grouped into 15 regions marked with different colors in **Figure 1** and identified as sS, south Somalia; nK, north Kenya; sK, south Kenya; wP, west Pemba; nP, north Pemba; eP, east Pemba; nT, north Tanzania; wZ, west Zanzibar; eZ, east Zanzibar; cT, central Tanzania; DP, Dar es Salaam Peninsula; oR, offshore Reef; wM, west Mafia; eM, east Mafia, and sT, south Tanzania. Color and size of the circles are proportional to the percentage of successful connections from source (origin) to sink (destination) reefs according to the colorbars to the right of the panels.

west Zanzibar (wZ) and west Pemba (wP) regions in both 2000 and 2005. In all regions except east Pemba (eP) and the offshore reef (oR), the probability of recruiting locally is higher than the probability of connecting to another reef region. Similar to *Acanthurus*, more north to south connections of *Acropora* are observed in the regions between north Tanzania (nT) and the Dar es Salaam Peninsula (DP) in 2005 than in 2000, when substantial north to south connection occurred only between Dar es Salaam (DP) and west Mafia (wM). In 2000, the offshore reef (oR) connects to all Pemba regions (eP, wP, nP) and north Kenya (nK), while in 2005 it connects to all regions north of Dar es Salam except north and west Pemba (nP, wP). This offshore reef is the only source of *Acropora* larvae for the east Pemba (eP) region. North and west Pemba get recruits from all Pemba regions in both years.

The variable number of north to south connections between the two modeled years is explained by the influence of the mesoscale circulation on the shelf circulation pattern. In 2000 the northward flowing East African Coastal Current (EACC) was weak during the spawning months ($<0.5\,m\ s^{-1}$) as is typical during the NE monsoon season. The Somali Current (SC) that flows southward at this time of the year was strong in February ($\sim 0.68\,m\ s^{-1}$) and its subsurface influence prevailed until April (Supplementary Figure 1). The strong influence of the southward flowing SC current in the northern part of the domain is responsible for the north to south connections in that region. In the rest of the domain the weak EACC generates slower northward velocities on the shelf during the spawning months, especially February (Supplementary Figure 2), allowing for some north to south connections at most latitudes, more

evident in the reef to reef connectivity matrices (Supplementary Figure 6).

In contrast, in 2005, the SC was weaker and only present during February and March since the transition to SW monsoon conditions happened very early in the year, with strong northward flow ($>1$ m $s^{-1}$) established in March and already re-established in the upper 300 m by April (Supplementary Figure 3). The weak SC only promotes a few north to south connections in the northern part of the domain. The strong EACC intensifies the flow reversal north of the Mafia and Zanzibar Channels, which is generated as the northward flow overshoots and turns southward into the channels when trying to follow the curved bathymetric contours past the islands (Supplementary Figure 4). This small scale circulation pattern is responsible for the north to south connections observed on regions around the north and south entrances of the Zanzibar Channel in 2000 for both *Acanthurus* and *Acropora* virtual larvae (Supplementary Figure 6).

## *Acanthurus* Ontogenetic Vertical Migration (OVM) Experiments

### *Acanthurus* OVM Settlement Success

Experiments that include an idealized OVM exhibit greater variability in *Acanthurus* settlement success among release dates within a year and between the two modeled years compared to the passive larvae experiments (**Figures 2A**, **4**). Mean settlement success is 34.5% ± 14.6 for 2000 and 17.7% ± 8.3 in 2005, but due to the large variability among release dates, the year to year difference is not statistically significant. There is a marked decrease in settlement success from earlier to later spawning dates in the OVM scenario, going from 46.8% for particles released in February 2nd to 7.2% for those released on March 31th in 2000 and from 34.0 to 15.9% for those same dates in 2005. The decrease in settlement success occurred earlier in 2005 than during 2000, associated with the rapid transition to SW monsoon conditions in 2005 (Supplementary Figure 4). In the northern part of the model domain the core of the northward flowing EACC is subsurface (below 70 m depth) at the beginning of the spawning season (NE monsoon), but it re-establishes in the upper 300 m by May in 2000 and April in 2005 (Supplementary Figures 2, 4). This implied that 2005 larvae migrating down to 50 m are affected longer by the strong northward flow than the 2000 larvae. Three-dimensional passive larvae tend to stay near the surface and are therefore less likely to be carried away from suitable habitat by the strong northward flowing EACC core transitioning from deep to shallow waters during the second half of the spawning season.

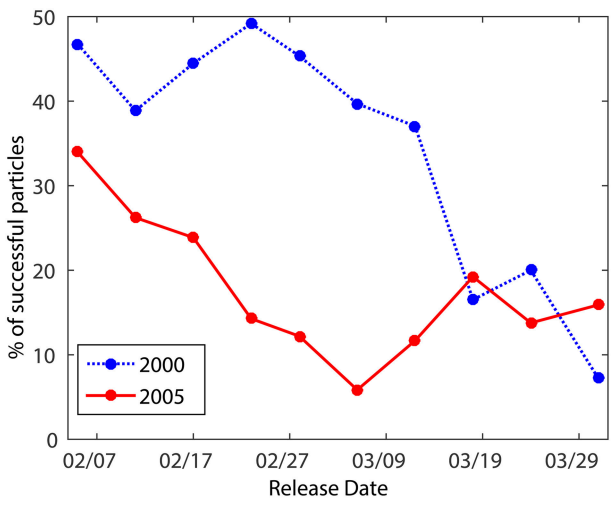


**FIGURE 4 | Percentage of settlement success per each simulated release date during 2000 and 2005 for *Acanthurus* virtual larvae with an idealized Ontogenetic Vertical Migration (OVM).**

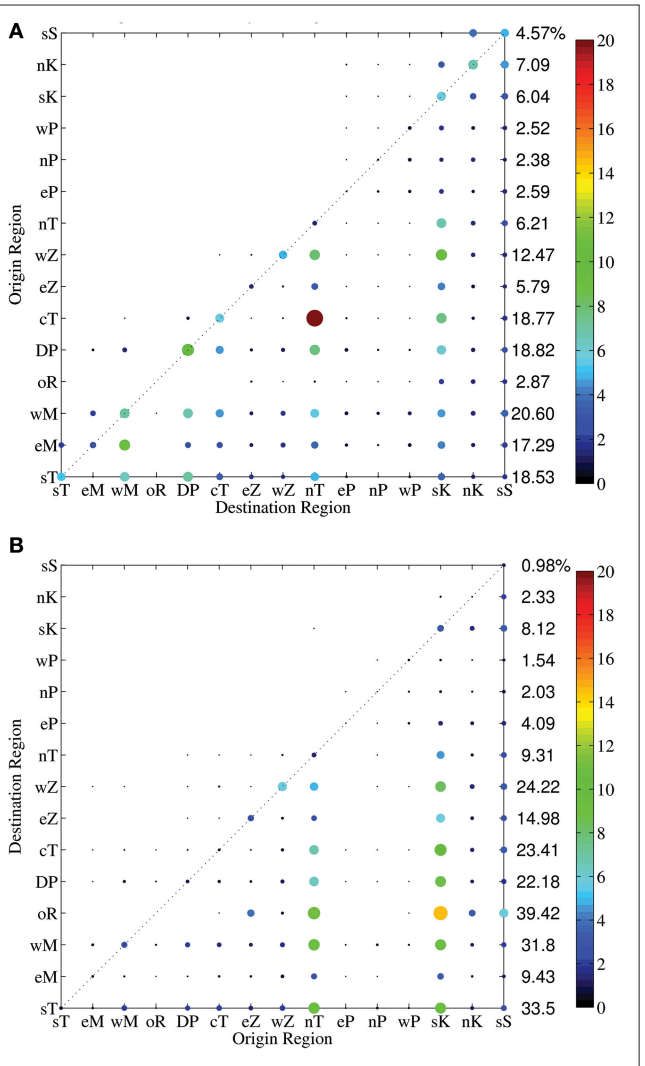


**FIGURE 5 | Region to region connectivity matrices for *Acanthurus* virtual larvae with OVM for 2000 (A)** and 2005 **(B)**. Reefs were grouped into 15 regions identified by two letters in **Figure 1**. Color and size of the circles are proportional to the percentage of successful connections from source (origin) to sink (destination) reefs according to the colorbar.

### *Acanthurus* OVM Region to Region Connectivity Matrices

When grouped at the regional level the *Acanthurus* OVM numerical experiments showed that in 2000 (**Figure 5A**) the strongest connection was between central Tanzania (cT) and north Tanzania (nT). The north Tanzania (nT) region received virtual larvae from all southward reefs. The south and north Kenya regions (sK, nK) and the south Somalia (sS) region receive recruitments from all other regions. Southern Tanzania (sT), east and west Mafia (eM, wM) and the Dar es Salaam Peninsula (DP) regions provide larvae to most other regions except the offshore reef (oR), but their probabilities of connecting to the Pemba regions are very low. The main sinks for larvae coming from the offshore reef (oR) in 2000 are the distant Kenya (sK, nK) and Somalia (sS) regions. Minimal north to south connections occur with larvae originating at east and west Mafia (eM, wM) and the Dar es Salam Peninsula regions (DP) in Tanzania, the south and north Kenya (sK, nK) regions and south Somalia (sS), connecting to southward regions. Across shore connections are observed mainly from west Zanzibar (wZ) to north Tanzania (nT) and from east to west Mafia (eM to wM).

In 2005 (**Figure 5B**), the offshore Dar es Salaam reef (oR) has strong connections with both Zanzibar (eZ, wZ) and north Tanzania (nT) regions as well as distant Kenya and Somalia regions. The strongest connection of 2005 occurred between the offshore reef (oR) and the south Kenya (sK) region. Most regions successfully connect to northward regions, except to the three Pemba Island reef regions, which get few recruits in both years modeled. Small proportions of the larvae spawned at the Dar es Salaam Peninsula (DP) and north Tanzania (nT) regions connect southward to the west Mafia and west Zanzibar regions, respectively. Across shore connections are weaker.

Interannual variability in the general patterns of reef connectivity for *Acanthurus* is enhanced when the ontogenetic vertical migration behavior is included, especially regarding the magnitude of the connections. Weaker and fewer connections are observed in 2005 in comparison to 2000 (**Figure 5**). As in the passive scenario, a strong interannual difference is observed in the number and location of south to north connections, with stronger north to south connectivity in the southern and northern most regions in 2000, and uniformly weak north to south connections in 2005. Overall, spatial connectivity of OVM *Acanthurus* in each of 2000 and 2005 are remarkably similar to the patterns observed for 3D passive *Acanthurus*, although the overall connectivity is lower with OVM than the passive, particularly in 2005.

## Sensitivity Analysis

### Sensitivity to Perception Distance

The analysis with increased (reduced) perception distance for *Acropora* (*Acanthurus*) is presented to provide insight on one of the processes responsible for the large difference in settlement success between the modeled species groups, and to illustrate the variability that might be expected among coral reef species with different life-history strategies. The percentage of settlement success increased with greater perception distance for both the *Acanthurus* surgeonfish and the *Acropora* coral simulations (**Figure 6**). However, the increase in settlement success for the short PLD coral was always much higher than that of the surgeonfish for the same increase in perception distance, with the coral reaching 95% settlement success with a 4 km perception distance. The difference in settlement success between the two genera was significant for all perception distance scenarios (**Figure 6**), indicating that with the same perception distance short PLD virtual larvae will always be more successful. Perception distance scenarios alternative to the reference run experiments are not appropriate for the specific genera used here, but might be appropriate for other coral reef organisms with different life-history traits. *Acropora* coral larvae perceive reefs through sound (Visram et al., 2010) and chemical cues (Heyward and Negri, 1999; Dixson et al., 2014), but their perception capabilities are unlikely to exceed 100 m. Laboratory experiments have shown that coral larvae are able to detect reef sounds 0–1 m from the source and move toward them (Visram et al., 2010). If planulae are capable of detecting particle motions anticipated perception distances are on the 10–100 m range (Visram et al., 2010). Despite their sensing abilities, the swimming ability of coral larvae is very limited and usually negligible in comparison to ocean currents (Kingsford et al., 2002; Baird et al., 2014). To the contrary, *Acanthurus* late larvae are one of the strongest swimmers among coral reef fish larvae, with reported *in situ* swimming speeds ranging from 8.7 to 65.3 cm $s^{-1}$ (Leis and Carson-Ewart, 1999; Leis and Fisher, 2006). They have been observed to navigate *in situ* disregarding current direction, perhaps guided by a sun compass (Leis and Carson-Ewart, 2003). Navigational capabilities exceeding 1 km are therefore expected for *Acanthurus*.

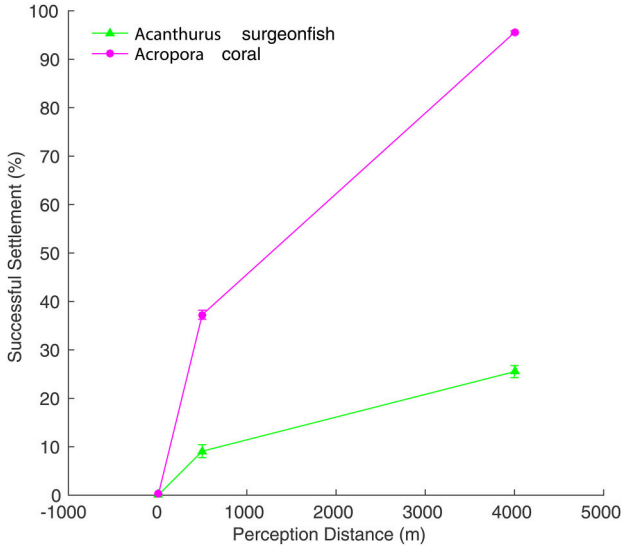


**FIGURE 6 | Settlement success for *Acropora* (magenta circles) and *Acanthurus* (green triangles) larvae with different perception distances (10, 500, and 4000 m).** Shown is the mean (±1 standard error) from 10 release dates during 2000.

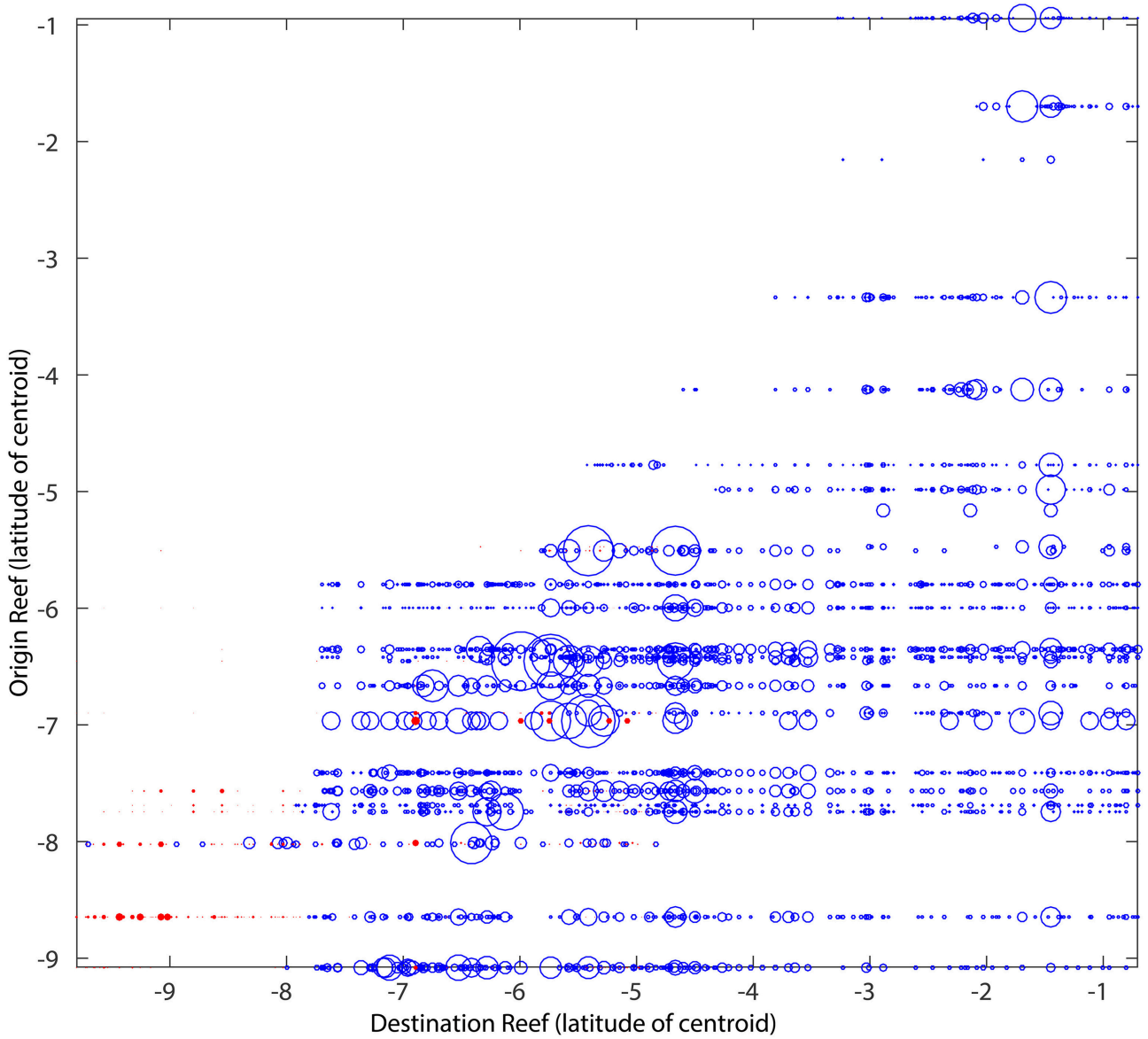


**FIGURE 7 | *Acanthurus* connectivity matrix for the 26 origin reefs selected for the experiments including vertical diffusion (Supplementary Figure 5), showing only the unique connections present in either the advective only experiments (blue) or the advection-diffusion experiments (red).** The figure is the cumulative result of 3 release dates in each modeled year (2000 and 2005). The size of the bubbles is proportional to the percentage of particles exchanged with the biggest bubble representing 11%.

## Diffusion Effect

The inclusion of vertical diffusion greatly increased the vertical spread of the virtual larvae and distributed them throughout the water column over the shelf. This, in turn, increased the horizontal spread of virtual larvae. The main connectivity patterns of the *Acanthurus* advective only experiments were also represented in the experiments with diffusion, including the interannual differences (not shown). The strength of the connections on the *Acanthurus* diffusive scenario was, however, an order of magnitude smaller than in the advective only scenario, indicating that the vertical spread of particles released at the same location leads to the majority of them dispersing away from suitable habitat. The extent to which the inclusion of vertical diffusion generated new connections, not represented in the advective only scenario was modest (**Figure 7**). From the 100% represented by the total number of connections found only in one of the two scenarios, 12.4% came from the scenario that included vertical diffusion, whereas 87.6% came from the advective only scenario. Thus, it is clear that including diffusion to the advection scenario produces relatively few new connections to the matrix, and that, for this particular case, the inclusion of a vertical random walk component may not be essential to providing a representative connectivity matrix.

## DISCUSSION

The dominant pattern of connectivity for both *Acanthurus* and *Acropora* in the KT region is southern reefs providing virtual larvae to northern reefs. The spatial scale of connectivity is much smaller for the short PLD coral group; successful connections are restricted to a 1° radius (∼100 km) around source reefs. 8.2% of *Acropora* larvae that successfully settle, recruited to their source reef (self-), an important proportion compared to only 1–2% for *Acanthurus*. Some *Acropora* were capable of long distance dispersal, particularly larvae spawned at the reef offshore of Dar es Salaam peninsula. This indicates that they can take advantage of the strong offshore EACC to reach distant northern reefs, and that even for short PLD, latitudinal isolation may be minimal, especially at longer (i.e., evolutionary) timescales.

In contrast to the generally short dispersal distances of *Acropora*, long distance connections from the southern to the northern most reefs (∼950 km) are common for virtual *Acanthurus*. Their longer pelagic durations lead to greater transport distances and reduced local retention. Overall settlement success was significantly greater in *Acanthurus* (24%) than in *Acropora* (<0.5%). This is due to several factors that enhance *Acanthurus* successful settlement probabilities: longer competency period, greater reef perception distance and swimming ability.

While south to north connections predominate in the connectivity matrices, some north to south connections occur, mostly in inshore regions that experience substantial eddy flows and topographically steered flow reversals. Examples of these are (1) the northern region that is seasonally influenced by the southward flowing Somali current (SC) (**Figure 3**), and (2) the northern entrance of the Zanzibar Channel and the region south of the Dar es Salaam peninsula where nearshore flow reversal is promoted by strong northward offshore currents (Mayorga-Adame et al., 2016). Therefore, there is strong interannual variability in the amount and location of north to south connections depending on the strength of the offshore mesoscale currents. When the Somali Current is strong (e.g., in 2000), short distance north to south connections are common at most latitudes, but are most prevalent near the northern and southern edges of the study region. When northward offshore flow is strong and the SC disappears early in the year (e.g., 2005), north to south connections are restricted to reefs in the wider shelf region between Pemba and Mafia Islands (due to enhanced small scale flow reversals) and the region north of 3°S where the Somali Current has a direct effect.

Interannual variability is also evident in the strength of the connections among reefs and the proportion of local retention. Thirteen reef regions (all but oR, eP) experience local retention in 2000, however in 2005 five regions (sT, oR, eP, nP, wP) had no or minimal local retention. In several cases the strong connections among regions are not consistent between 2000 and 2005; analysis of simulations for other years is needed to assess the persistence of connectivity patterns. Multi-year simulations [e.g., James et al. (2002), 20 years' model of reef fish connectivity in a section of the (GBR); Dorman et al. (2015), 46 years' model of *Acropora millepora* connectivity in the South China Sea] would give further insight on the variability and robustness of the connectivity patterns and help to identify connections that are vital to maintaining regional metapopulations of different species groups.

The different connectivity patterns and scales of dispersal for the two genera characterized in these modeling experiments show that it is important to consider interspecies life-history variability when implementing conservation strategies to ecosystems as diverse as coral reefs, since ideal spatial management strategies would enhance settlement success for a wide suite of species with different perception and dispersal capabilities. Our results indicate, for example, that *Acanthurus* virtual larvae settling to coral reefs around Pemba Island come from relatively few source reefs, which highlights the need for strong local protection since the resilience, (e.g., potential recolonization of Pemba's *Acanthurus* populations from more distant reefs), is minimal, despite their relatively lengthy larval pelagic phase. Pemba Island *Acropora* coral populations are less vulnerable since they show stronger and more variable connections. This seems counter intuitive given the smaller scale of connectivity and higher local retention rates of *Acropora*, however the local oceanographic regime around Pemba Island, including a strong return flow on the western side of the island, promotes retention at short time scales, favoring *Acropora* connections, while the much longer PLD of *Acanthurus* favors transport away from Pemba's suitable habitat.

The level of connectivity of a reef is a component of its resilience and the extent of its ecological impact in the region. For example, strong sink reefs, those receiving settlers from many different source reefs, are more resilient to local and global stresses, since having multiple sources increases the probability of receiving recruits in any given year. The diversity of sources providing potential recruits would enhance resilience to short term local detrimental phenomena such as bleaching events and overfishing. On the other hand, important source reefs, those with potential of providing settlers to many other reefs, could have a disproportionately large ecological impact for many other reefs. Reefs that provide larvae to many other sites are important to protect from a larger ecosystem conservation perspective, since an increase of the local spawning population would likely impact recruitment to a large number of reefs elsewhere, therefore increasing the impacts of spatially limited conservation measures (e.g., MPA) beyond their boundaries (Bode et al., 2006; Figueira, 2009). "Source and sink" maps are useful for identifying ecologically important areas based on the number and type of connections present. Source and sink maps for *Acanthurus* are shown in **Figures 8A,C**, and for *Acropora* virtual larvae in **Figures 8B,D**. The passive and OVM scenarios (not shown) for *Acanthurus* yielded similar source and sink maps. In general reefs south of Mafia Island (8°S) provide larvae of both species groups to the greatest number of reefs. In the case of *Acanthurus* larvae (**Figure 8A**) these reefs connect to more than 350 different reefs, and for *Acropora* (**Figure 8B**) to more than 70 reefs. Reefs in the northern half of Tanzania are good sources of *Acropora* larvae, connecting to more than 50 reefs, while Kenyan reefs connect to ∼30 different reefs. Local conservation efforts in these areas are likely to have an important

ecological impact beyond their local ecosystem, since they can help maintain and replenish multiple other metapopulations at various destination reefs. Somali reefs to the contrary provide *Acanthurus* virtual larvae to <50 reefs and *Acropora* virtual larvae to <10 different reefs. While this may be an artifact of these reefs being near the northern border outflow, the role of Somali reefs in providing recruits of reef species further north is minimal as there are few coral reefs within the immediate north region. Kenyan and Somali reefs are however the most common sink reefs, receiving larvae from many reefs to their south (**Figure 8D**). These northern reefs may be more resilient to local threats. The source and sink patterns reflect the strong, mostly unidirectional south to north flow along the coast. For *Acropora* larvae, the source and sink maps are much more patchy (**Figures 8B,D**, respectively), reflecting the effects of the smaller dispersal scale of *Acropora* larvae.

A recent genetic study of *Acropora tenuis* connectivity in the KT region, reports high but variable connectivity between sample sites, which cluster in 3 different groups: (1) Kenya and northern-Tanzania, (2) southern Tanzania, and (3) sample sites located in the Zanzibar and Pemba channels (van der Ven et al., 2016). No clear genetic break on samples collected along 900 km of coral reefs was observed. Also, no genetic differentiation with increasing geographical separation was found, in contrast to similar studies in the (GBR) and Japan. They associate the genetic uniformity in the KT region with uniform oceanographic conditions promoted by the continuous south to north linear flow of the EACC. The highest differentiation observed in group 3 is associated with local oceanographic conditions causing larval retention. The connectivity patterns of our modeling study agree with their findings, despite the different time scales assessed. The north to south connectivity we report is expected to minimize genetic differences along the KT coast. Our model also corroborates the isolation they infer for their highly differentiated Pemba and Zanzibar Channel sites. Our model results indicate that west Pemba (wP) and west Zanzibar regions, receive the majority of their *Acropora* virtual larvae through within region recruitment. The circulation patterns depicted by our ROMS model included flow reversals at the northern entrance of the channels and eddy blockage in the southern entrance of the Zanzibar Channel (Mayorga-Adame et al., 2016); these might provide sufficient isolation to upstream sources to produce genetically different *Acropora* populations in the channel sites.

Genetic connectivity patterns for *Pocillopora damicornis* (a brooding coral species) based on contemporary gene flow (Souter et al., 2009) can be compared with our modeling results for the longer PLD, broadcast spawner *Acropora* corals. Souter et al. (2009) identified first generation migrants of *P. damicornis* at 29 reefs sites in the Kenya-Tanzania region, and therefore determined the degree of isolation of the different reefs sampled. They found patchiness in the degree of isolation at very small scales, with marked differences even between lagoon and fringing reefs within the Malindi Marine National Park and Reserve in south Kenya. The patchiness observed in our *Acropora* source and sink maps is consistent with their results, indicating strong small-scale spatial variability in the number of connections (degree of isolation) among nearby reefs. Souter et al. (2009) identified isolated reefs, highly dependent on local retention for population renewal, in south Kenya, west Pemba, and south Mafia. In the *Acropora* simulations these regions receive virtual larvae from <10 different source reefs (**Figure 8D**). The regional *Acropora* connectivity matrices (**Figures 3B,D**) show that local retention is important for these regions. In our regional connectivity results, however, only west Pemba, east Mafia and south Tanzania show relative isolation, receiving *Acropora* larvae from only three and two other regions respectively; south Kenya in contrast receives settlers from many regions further south. This discrepancy between our model results and Souter et al.'s (2009) genetic study may reflect the different spatial scales considered, since our regional grouping aggregates connections for several reefs that might have different degrees of isolation. Souter et al. (2009) identify Mnemba Conservation Area (in the east Zanzibar region) as a strong source for other sampled sites. This site shows the highest genetic diversity and is similar only to one site in the Dar es Salaam Peninsula and one site in southeast Mafia Island. In the simulation *Acropora* larvae that settle in the east Zanzibar region, which includes Mnemba Island, come from few origin reefs (mainly Dar es Salaam Peninsula and east Mafia regions; **Figures 3B,D**). The number of regions that receive *Acropora* larvae from east Zanzibar ranges between 3 and 5 in the 2000 and 2005 simulations. The source map for *Acropora* (**Figure 8B**) shows that most reefs around Mnemba (east Zanzibar) provide larvae to ∼30 to 60 different reefs. Our model results identify specific reefs in the west Mafia and southern Tanzania regions as the main providers of *Acropora* larvae while the genetic results of Souter et al. (2009) do not identify their south Mafia and Mtwara (south of our model domain) sites as important sources. This could be due to the high reef to reef patchiness on the level of isolation identified by both their observational and our modeling study, the uncertainty of which specific reefs were actually sampled for the genetic study, and the shorter PLD of *Pocillopora damicornis*. To the extent allowed by the comparison of this model with the genetic sampling of specific reefs results of Souter et al. (2009), the main connectivity patterns elucidated by their genetic study for an ecologically similar coral species are well represented in the connectivity results provided by the coupled biophysical model for *Acropora*. This comparison is limited to the regional level, since the exact location of the reefs sampled by Souter et al. (2009) is not reported.

Only at the beginning of the spawning season did the ontogenetic vertical migration "*in silico*" experiments of *Acanthurus* virtual larvae generate more successful settlers than the 3D passive scenario (**Figures 2A**, **5**). This is inconsistent with prior reports in the literature for various larvae in the Caribbean (Paris et al., 2007) and the California Current System (Drake et al., 2013), where OVM consistently increased settlement success. Differences in shear and stratification of the water column of each region may be responsible for this marked difference among oceanographically distinct regions. The shelf circulation of Kenya and Tanzania is dominated by strong alongshore flows with an increased magnitude offshore, a shallow (i.e., <50–100 m) wind driven mixed layer is not common. Northward flow velocities dominate the coastal

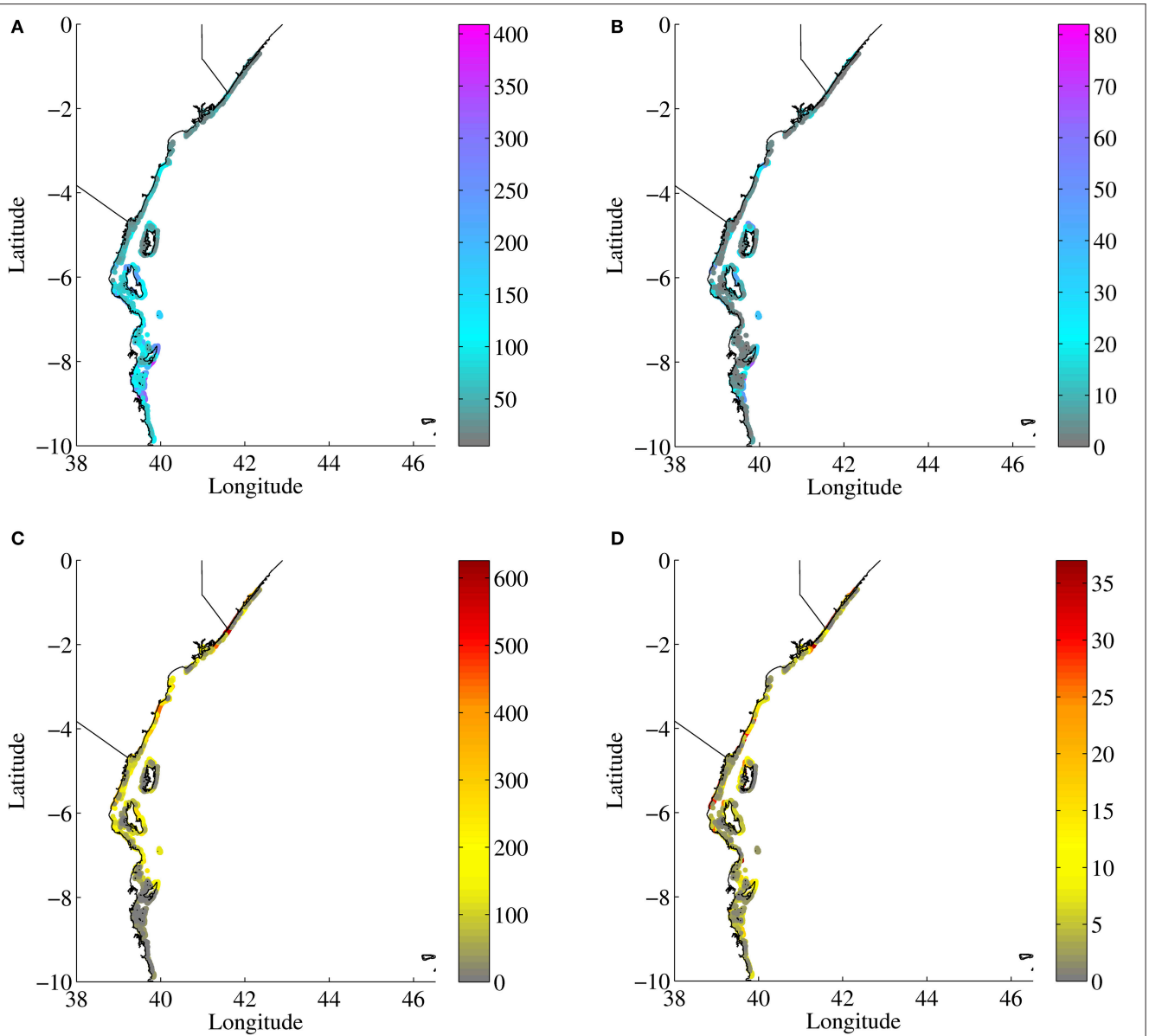


**FIGURE 8 | Top row, reefs color coded by the number of different destination reefs reached by virtual larvae originated from them, in both simulated years, to identify the best source reefs for *Acanthurus* (A)** and Acropora **(B)**. Bottom row, reefs color coded by the number of different source reefs it received virtual larvae from, in both simulated years, to identify the best sink reefs for *Acanthurus* **(C)** and Acropora **(D)**.

circulation off Kenya and Tanzania down to 300 m depth during most of the year. Therefore, a vertical migration down to 50 m depth would have little effect on transport pathways. During the SE monsoon (Dec-Mar) the Somali Current flows southward in the upper 100 m north of 3°S. During this period, which encompasses part of the spawning period, staying near the surface, instead of migrating to deeper waters, would facilitate north to south connections and retention if the duration of the pelagic phase includes the seasonal reversal to northward flow. Only during the transition between NE to SE monsoon conditions would a shallow migration result in significantly shorter horizontal displacements for *Acanthurus* larvae. Intraseasonal and interannual variability increased when the simple ontogenetic vertical migration behavior was implemented because the evolution of the vertical structure of alongshore velocities was markedly different in the two modeled years (Supplementary Figures 2, 4). The ontogenetic vertical migration pattern modeled here is based on the increased depth of the *Acanthurus* larvae during ontogeny observed by Irisson et al. (2010). The depth of the migration is not well defined and could be site dependent. For example, Irisson et al. (2010) reported post-flexion *Acanthurus* larvae in the 25–60 m

depth range near reefs in French Polynesia, while Oxenford et al. (2008) found aggregations of late *Acanthurus* larvae to be more abundant at 120 m in the eastern Caribbean Sea. No observations for the East-African coast exist. Observations of vertical distribution and abundance of pelagic larvae concurrent with hydrographic conditions are needed to design more realistic vertical migration experiments, and to assess larval fish responses to temperature, light, or velocity. The implementation of vertical migration in these numerical experiments was highly idealized, shifting all particles to 50 m depth 20 days after release, ignoring their vertical position at that time. This meant that some larvae that had passively advected deeper than the 50 m fixed migration depth were actually displaced upward with this vertical migrating behavior. The number of particles that advected below 50 m depth was not an important fraction of the successful larvae since most larvae stayed in the upper 5 m when passively advected; a small proportion, however, reached depths below 100 m. Migrating only shallow particles downward would be a more realistic scenario as well as distributing the particles within a broader depth range rather than fixing them to a single specific depth. Many other, perhaps more realistic scenarios are possible next steps. However, in-situ data of larvae depth distributions would be required to properly parameterize more realistic scenarios. The aim of the simple scenario modeled here was to illustrate the potential effects on connectivity of an ontogenetic vertical migration to 50 m (with depth keeping) in a rapidly evolving water column with deep stratification and strong shear.

The numerical experiments presented here are deterministic and represent a population where all larvae develop and behave identically, without actively responding to its environment. Real larvae are complex organisms, with strong inter-specific and potentially intra-individual variability in physiology and behavior, constantly reacting to their environment. Complex models with behavior cueing on the environmental conditions experienced by the virtual larvae have been developed (e.g., Armsworth, 2001; Staaterman et al., 2012; Wolanski and Kingsford, 2014). Assuming that larvae are well adapted to the pelagic phase, larval behavior, particularly sensing, orientation and swimming abilities would enhance their probability of finding suitable settlement habitat, which might reduce interannual variability in settlement success. However, when challenged by increased environmental variability due to climate change effects, their strategies may not be guaranteed to work. The numerical experiments presented here, although idealized, serve as an initial effort to develop hypotheses that might be examined using more complex models and empirical studies. Monitoring recruitment of coral reef organisms is basic to assessing the effects of environmental variability on settlement success. Having long term time series of recruitment of coral reef dependent species in the Kenya-Tanzania region would be valuable for "tuning" models, as has been done for other coral reef regions (i.e., Sponaugle et al., 2012).

The fraction of released larvae that settle on suitable habitat is highly sensitive to the individual's habitat perception and swimming abilities; further knowledge regarding the capabilities of coral reef larvae to perceive, navigate and settle on suitable habitat is a very important and a challenging piece of information to obtain. Both in-situ and laboratory observations of larval development and behavior are needed to further increase the realism of modeling experiments. The dependence of PLD on temperature is well established for aquatic organisms (O'Connor et al., 2007) but observations for the studied genera are insufficient to adequately parameterize the functional response between temperature and PLD. The inclusion of temperature dependent PLD in bio-physical models is essential for examining climate change effects on connectivity and settlement success of marine larvae (Lett et al., 2010; Figueiredo et al., 2014). Changes in ocean circulation will alter connectivity patterns, but physiological effects due to the increased temperature will also have an important effect (Munday et al., 2009; Lett et al., 2010; Kendall et al., 2016). Reduced pelagic larval durations are expected under faster developmental rates, which could lead to a reduction in dispersal distances and the spatial scale of connectivity (Munday et al., 2009; Lett et al., 2010). Bio-physical modeling connectivity studies including temperature dependent PLD report increased local retention (Figueiredo et al., 2014; Andrello et al., 2015) and significant changes in Marine Protected Area network interconnectivity (Andrello et al., 2015) under climate change scenarios. Well-informed idealized experiments that include temperature dependent PLD of virtual larvae are a future direction for assessing the effects of climate change scenarios on connectivity and recruitment of coral reef organisms in the East-African coast.

Larvae in the ocean are subject to mixing at scales smaller than those represented in the ocean circulation model. In particle tracking models these unresolved motions are often implemented as a random walk scaled by the model diffusivity. Simulations that implement a random walk to mimic diffusion are considered more realistic but computationally expensive. We conducted a few sensitivity experiments that included (3D) variable vertical diffusion. Simulations that included vertical diffusion (not shown) reproduced the main connectivity patterns produced by the 3D advective only experiments, but with smaller connectivities—mostly due to greater vertical dispersion that subjected larvae to greater horizontal flow variation. These results are probably more realistic for early or weakly swimming larvae (e.g., coral species) that are unable to maintain their vertical position in the water column in the presence of vigorous vertical mixing.

While reef-to-reef connectivity is important in metapopulation ecology, regional connectivity is expected to be more robust to the uncertainty introduced by the oceanographic and biological assumptions made in these models. Region to region connectivity matrices synthesize the information of reef to reef connectivity matrices, making it more manageable and easier to interpret. The regional summary could assist managers, policy makers and the general public to understand the interconnections among coral reef regions due to pelagic larval dispersion of their local populations. Previous bio-physical connectivity studies highlight the importance of considering larval connectivity at regional levels when trying to prioritize the implementation of management strategies for both conservation and fisheries enhancement goals. One of the insights of examining connectivity at a regional scale is that the importance of international connections becomes obvious, as has been shown by Kough et al. (2013) for the Mesoamerican

reefs and by Rossi et al. (2014) for the Mediterranean Sea. In all numerical experiments Tanzanian reefs were an important source of settlers to Kenyan reefs; this provides insight and guidance on the spatial scale at which management strategies are required and points to the need for regional international collaborations in order to provide enduring conservation measures and protection to the east African coral reef ecosystem.

This modeling study is a first approach to understanding the connectivity among coral reef populations in a data poor region. The information provided, even though preliminary, presents a general pattern of the potential regional connectivity and identifies particularly resilient and vulnerable areas as well as the hydrodynamic features driving the connections. Spatial scales of connectivity and settlement success rates are within the ranges reported by other bio-physical modeling studies for similar genera in other coral reef regions (Paris et al., 2007; Dorman et al., 2015). However, the robustness of the connectivity patterns presented needs to be further evaluated by performing experiments for more years and longer spawning seasons, and carrying out more extensive sensitivity analysis to the model assumptions. After gaining more confidence in the modeled connectivity patterns, the information provided by this modeling study could be carefully and critically evaluated, in order to be applied to optimize the effectiveness of marine protected area management and other marine protection efforts. Further modeling experiments similar to those presented here, but better informed by empirical data, and including the capability of larvae to respond to the ocean conditions will provide greater detail on the complex biophysical interactions that occur in the sea, and will provide a more realistic, and less uncertain, representation of connectivity patterns. These results will aid in understanding how a range of species specific individual responses influence the distribution and connectivity patterns and should enable more specific guidelines for spatial management that provide better resource resiliency and protection throughout the Kenya-Tanzania coastal region.

## AUTHOR CONTRIBUTIONS

CGMA, HB, and YS designed the experiments, analysis and paper. CGMA Carried out the numerical modeling experiments and analysis and wrote initial draft of the paper. HB and YS revised and improved the initial manuscript.

## FUNDING

CGMA was partially funded by CONACYT Mexico.

## ACKNOWLEDGMENTS

Thanks to Dr. Ted Strub for access to computing resources. To CEOAS-OSU technicians Eric Beals and Tom Leach for technical support. To CONACYT Mexico for scholarship funding for CGMA, and to the UK National Oceanography Centre (NOC) for allowing her time to finalize and review this paper. HB thanks the North Pacific Marine Science Organization (PICES) for allowing time for him to contribute to this paper, and for payment of the article processing fee.

## SUPPLEMENTARY MATERIAL

The Supplementary Material for this article can be found online at: http://journal.frontiersin.org/article/10.3389/fmars.2017.00092/full#supplementary-material

## REFERENCES

Almany, G. R., Berumen, L. M., Thorrold, R. S., Planes, S., and Jones, G. P. (2007). Local replenishment of coral reef fish populations in a marine reserve. *Science* 316, 742–744. doi: 10.1126/science.1140597

Andrello, M., Mouillot, D., Somot, S., Thuiller, W., and Manel, S. (2015). Additive effects of climate change on connectivity between marine protected areas and larval supply to fished areas. *Divers. Distributions* 21, 139–150. doi: 10.1111/ddi.12250

Armsworth, P. R. (2001). Directed motion in the sea: efficient swimming by reef fish larvae. *J. Theor. Biol.* 210, 81–91. doi: 10.1006/jtbi.2001.2299

Atema, J., Gerlach, G., and, Paris, C. B. (2015). "Sensory biology and navigation behavior of reef fish larvae," in *Ecology of Fishes on Coral Reefs*, ed C. Mora (Cambridge: Cambridge University Press), 3–15.

Atema, J., Kingsford, M. J., and Gerlach, G. (2002). Larval reef fish could use odour for detection, retention and orientation to reefs. *Mar. Ecol. Prog. Ser.* 241, 151–160. doi: 10.3354/meps241151

Babcock, R. C., and Heyward, A. J. (1986). Larval development of certain gamete-spawning scleractinian corals. *Coral Reefs* 5, 111–116. doi: 10.1007/BF00298178

Baird, A. H., Cumbo, V. R., Figueiredo, J., Harii, S., Hata, T., and Madin, J. S. (2014). Comment on "Chemically mediated behavior of recruiting corals and fishes: a tipping point that may limit reef recovery." *PeerJ PrePrints* 2:e628v1. doi: 10.7287/peerj.preprints.628v1

Batchelder, H. P. (2006). Forward-in-Time-/Backward-in-Time-Trajectory (FITT/BITT) modeling of particles and organisms in the coastal ocean∗. *J. Atmos. Oceanic Technol.* 23, 727–741. doi: 10.1175/JTECH1874.1

Batchelder, H. P., Edwards, C. A., and Powell, T. M. (2002). Individual-based models of copepod populations in coastal upwelling regions: implications of physiologically and environmentally influenced diel vertical migration on demographic success and nearshore retention. *Progr. Oceanogr.* 53, 307–333. doi: 10.1016/S0079-6611(02)00035-6

Baums, I. B., Miller, M. W., and Hellberg, M. E. (2005). Regionally isolated populations of an imperiled caribbean coral, *Acropora Palmata*. *Mol. Ecol.* 14, 1377–1390. doi: 10.1111/j.1365-294X.2005.02489.x

Bergenius, M. A., Meekan, M. G., Robertson, R. D., and McCormick, M. I. (2002). Larval growth predicts the recruitment success of a coral reef fish. *Oecologia* 131, 521–525. doi: 10.1007/s00442-002-0918-4

Bode, M., Lance, B., and Paul Armsworth, R. (2006). Larval dispersal reveals regional sources and sinks in the great barrier reef. *Mar. Ecol. Prog. Ser.* 308, 17–25. doi: 10.3354/meps308017

Boehlert, G. W., and Mundy, B. C. (1993). Ichthyoplankton assemblages at seamounts and oceanic islands. *Bull. Mar. Sci.* 53, 336–361.

Botsford, L. W., Micheli, F., and Hastings, A. (2003). Principles for the design of marine reserves. *Ecol. Appl.* 13, 25–31. doi: 10.1890/1051-0761(2003)013[0025:PFTDOM]2.0.CO;2

Botsford, L. W., White, J. W., Coffroth, M. A., Paris, C. B., Planes, S., Shearer, T. L., et al. (2009). Connectivity and resilience of coral reef metapopulations in marine protected areas: matching empirical efforts to predictive needs. *Coral Reefs* 28, 327–337. doi: 10.1007/s00338-009-0466-z

Burgess, S. C., Nickols, K. J., Griesemer, C. D., Barnett, L. A. K., Dedrick, A. G., Satterthwaite, E. V., et al. (2014). Beyond connectivity: how empirical methods

can quantify population persistence to improve marine protected-area design. *Ecol. Appl.* 24, 257–270. doi: 10.1890/13-0710.1

Christie, M. R., Johnson, D. W., Stallings, C. D., and Hixon, M. A. (2010a). Self-recruitment and sweepstakes reproduction amid extensive gene flow in a coral-reef fish. *Mol. Ecol.* 19, 1042–1057. doi: 10.1111/j.1365-294X.2010.04524.x

Christie, M. R., Tissot, B. N., Albins, A. A., Beets, P., Jia, Y., Ortiz, D. M., et al. (2010b). Larval connectivity in an effective network of marine protected areas. *PLoS ONE* 5:e15715. doi: 10.1371/journal.pone.0015715

Cowen, R. K., and Castro, L. R. (1994). Relation of coral reef fish larval distributions to island scale circulation around barbados, west indies. *Bull. Mar. Sci.* 54, 228–244.

Cowen, R., Gawarkiewicz, G., Pineda, J., Thorrold, S., and Werner, F. (2007). Population connectivity in marine systems: an overview. *Oceanography* 20, 14–21. doi: 10.5670/oceanog.2007.26

Cowen, R. K., Lwiza, K. M. M., Sponaugle, S., Paris, C. B., and Olson, D., B. (2000). Connectivity of marine populations: open or closed? *Science* 287, 857–859. doi: 10.1126/science.287.5454.857

Cowen, R. K., Paris, C. B., and Srinivasan, A. (2006). Scaling of connectivity in marine populations. *Science* 311, 522–527. doi: 10.1126/science.1122039

Cowen, R. K., and Sponaugle, S. (2009). Larval dispersal and marine population connectivity. *Ann. Rev. Mar. Sci.* 1, 443–466. doi: 10.1146/annurev.marine.010908.163757

Crochelet, E., Chabanet, P., Pothin, K., Lagabrielle, E., Roberts, J., Pennober, G., et al. (2013). Validation of a fish larvae dispersal model with otolith data in the Western Indian Ocean and implications for marine spatial planning in data-poor regions. *Ocean Coast. Manage.* 86, 13–21. doi: 10.1016/j.ocecoaman.2013.10.002

Crochelet, E., Roberts, J., Lagabrielle, E., Obura, D., Petit, M., and Chabanet, P. (2016). A model-based assessment of reef larvae dispersal in the Western Indian Ocean reveals regional connectivity patterns—potential implications for conservation policies. *Reg. Stud. Mar. Sci.* 7, 159–167. doi: 10.1016/j.rsma.2016.06.007

Day, J. H. (1974). *A Guide to Marine Life of South African Shores, 2nd Edn*. Cape Town: Balkema.

Dixson, D. L., Abrego, D., and Hay, M. E. (2014). Chemically mediated behavior of recruiting corals and fishes: a tipping point that may limit reef recovery. *Science* 345, 892–897. doi: 10.1126/science.1255057

Domingues, C. P., Nolasco, R., Dubert, J., and Queiroga, H. (2012). Model-derived dispersal pathways from multiple source populations explain variability of invertebrate larval supply. *PLoS ONE* 7:e35794. doi: 10.1371/journal.pone.0035794

Dorenbosch, M., Pollux, B. J. A., Pustjens, A., Rajagopal, Z., Nagelkerken, S., van der Velde, G., et al. (2006). Population structure of the dory snapper, lutjanus fulviflamma, in the Western Indian Ocean revealed by means of AFLP fingerprinting. *Hydrobiologia* 568, 43–53. doi: 10.1007/s10750-006-0020-8

Dorman, J. G., Frederic Castruccio, S., Enrique Curchitser, N., Joan Kleypas, A., and Thomas Powell, M. (2015). Modeled connectivity of acropora millepora populations from reefs of the spratly islands and the greater South China Sea. *Coral Reefs* 35, 169–179. doi: 10.1007/s00338-015-1354-3

Drake, P. T., Edwards, C. A., Morgan, S. G., and Dever, E. P. (2013). Influence of larval behavior on transport and population connectivity in a realistic simulation of the california current system. *J. Mar. Res.* 71, 317–350. doi: 10.1357/002224013808877099

Edgar, G. J., Stuart-Smith, R. D., Willis, T. J., Kininmonth, S., Baker, S. C., Banks, S., et al. (2014). Global conservation outcomes depend on marine protected areas with five key features. *Nature* 506, 216–220. doi: 10.1038/nature13022

Egbert, G. D., Bennett, A. F., and Foreman, M. G. G. (1994). TOPEX/POSEIDON tides estimated using a global inverse model. *J. Geophys. Res. Oceans* 99, 24821–24852. doi: 10.1029/94JC01894

Egbert, G. D., and Erofeeva, S. Y. (2002). Efficient inverse modeling of barotropic ocean tides. *J. Atmos. Oceanic Technol.* 19, 183–204. doi: 10.1175/1520-0426(2002)019<0183:EIMOBO>2.0.CO;2

Figueira, W. F. (2009). Connectivity or demography: defining sources and sinks in coral reef fish metapopulations. *Ecol. Modell.* 220, 1126–1137. doi: 10.1016/j.ecolmodel.2009.01.021

Figueiredo, J., Baird, A. H., Harii, S., and Connolly, S. R. (2014). Increased local retention of reef coral larvae as a result of ocean warming. *Nat. Clim. Chang* 4, 498–502. doi: 10.1038/nclimate2210

Foster, N. L., Paris, C. B., Kool, J. T., Baums, I. B., Stevens, J. R., Sanchez, J. A., et al. (2012). Connectivity of caribbean coral populations: complementary insights from empirical and modelled gene flow. *Mol. Ecol.* 21, 1143–1157. doi: 10.1111/j.1365-294X.2012.05455.x

Gawarkiewicz, G., Monismith, S., and Largier, J. (2007). Observing larval transport processes affecting population connectivity: progress and challenges. *Oceanography* 20, 40–53. doi: 10.5670/oceanog.2007.28

Gell, F. R., and Roberts, C. M. (2003). Benefits beyond boundaries: the fishery effects of marine reserves. *Trends Ecol. Evol.* 18, 448–455. doi: 10.1016/S0169-5347(03)00189-7

Gerlach, G., Atema, J., Kingsford, M. J., Black, K. P., and Miller-Sims, V. (2007). Smelling home can prevent dispersal of reef fish larvae. *Proc. Natl. Acad. Sci. U.S.A.* 104, 858–863. doi: 10.1073/pnas.0606777104

Haidvogel, D. B., Arango, H., Budgell, W. P., Cornuelle, B. D., Curchitser, E., Di Lorenzo, E., et al. (2008). Ocean forecasting in terrain-following coordinates: formulation and skill assessment of the regional ocean modeling system. *J. Comput. Phys.* 227, 3595–3624. doi: 10.1016/j.jcp.2007.06.016

Hamilton, H. G. H., and Brakel, W. H. (1984). Structure and Coral Fauna of East African Reefs. *Bull. Mar. Sci.* 34, 248–266.

Harrison, H. B., Williamson, D. H., Evans, R. D., Almany, G. R., Thorrold, S. R., Russ, G. R., et al. (2012). Larval export from marine reserves and the recruitment benefit for fish and fisheries. *Curr. Biol.* 22, 1023–1028. doi: 10.1016/j.cub.2012.04.008

Heenan, A., Simpson, S., D., and Braithwaite, V. A. (2009). "Testing the generality of acoustic cue use at settlement in larval coral reef fish," in *Proceedings of the 11th International Coral Reef Symposium, International Society for Reef Studies*. Available online at: http://research-information.bristol.ac.uk/en/publications/testing-the-generality-of-acoustic-cue-use-at-settlement-in-larval-coral-reef-fish(a6fce20c-2ee6-4898-a72c-766263aea453).html

Hedgecock, D., Barber, P. H., and Edmands, S. (2007). Genetic approaches to measuring connectivity. *Oceanography* 20, 70–79. doi: 10.5670/oceanog.2007.30

Heyward, A. J., and Negri, A. P. (1999). Natural inducers for coral larval metamorphosis. *Coral Reefs* 18, 273–279. doi: 10.1007/s003380050193

Hogan, J. D., Thiessen, R. J., Sale, P. F., and Heath, D. D. (2011). Local retention, dispersal and fluctuating connectivity among populations of a coral reef fish. *Oecologia* 168, 61–71. doi: 10.1007/s00442-011-2058-1

Hughes, T. P., Baird, A. H., Bellwood, D. R., Card, M., Connolly, S. R., Folke, C., et al. (2003). Climate change, human impacts, and the resilience of coral reefs. *Science* 301, 929–933. doi: 10.1126/science.1085046

Irisson, J., Paris, C. B., Guigand, C., and Planes, S. (2010). Vertical distribution and ontogenetic 'migration' in coral reef fish larvae. *Limnol. Oceanogr.* 55, 909–919. doi: 10.4319/lo.2009.55.2.0909

James, M. K., Armsworth, P. R., Mason, L. B., and Bode, L. (2002). The structure of reef fish metapopulations: modelling larval dispersal and retention patterns. *Proc. R. Soc. Lond. B Biol. Sci.* 269, 2079–2086. doi: 10.1098/rspb.2002.2128

Jones, G. P., Milicich, M. J., Emslie, M. J., and Lunow, C. (1999). Self-Recruitment in a coral reef fish population. *Nature* 402, 802–804. doi: 10.1038/45538

Jones, G. P., Planes, S., and Thorrold, S. R. (2005). Coral reef fish larvae settle close to home. *Curr. Biol.* 15, 1314–1318. doi: 10.1016/j.cub.2005.06.061

Kalnay, E., Kanamitsu, M., Kistler, R., Collins, W., Deaven, D., Gandin, L., et al. (1996). The NCEP/NCAR 40-Year reanalysis project. *Bull. Am. Meteorol. Soc.* 77, 437–471. doi: 10.1175/1520-0477(1996)077<0437:TNYRP>2.0.CO;2

Kaunda-Arara, B., James Mwaluma, M., Gamoe Locham, A., Vidar Øresland, and Melckzedeck Osore, K. (2009). Temporal variability in fish larval supply to malindi marine park, coastal Kenya. *Aquat. Conserv. Mar. Freshwater Ecosyst.* 19, S10–S18. doi: 10.1002/aqc.1038

Kendall, M. S., Poti, M., and Karnauskas, K. B. (2016). Climate change and larval transport in the ocean: fractional effects from physical and physiological factors. *Glob. Chang. Biol.* 22, 1532–1547. doi: 10.1111/gcb.13159

Kingsford, M. J., Leis, J. M., Shanks, A., Lindeman, K. C., Morgan, S. G., and Pineda, J. (2002). Sensory environments, larval abilities and local self-recruitment. *Bull. Mar. Sci.* 70, 309–340.

Kough, A. S., Paris, C. B., and Butler, M. J. IV. (2013). Larval connectivity and the international management of fisheries. *PLoS ONE* 8:e64970. doi: 10.1371/journal.pone.0064970

Kruse, M., Taylor, M., Muhando, C. A., and Reuter, H. (2016). Lunar, diel, and tidal changes in fish assemblages in an East African marine reserve. *Reg. Stud. Mar. Sci.* 3, 49–57. doi: 10.1016/j.rsma.2015.05.001

Lecchini, D. (2005). Spatial and behavioural patterns of reef habitat settlement by fish larvae. *Mar. Ecol. Prog. Ser.* 301, 247–252. doi: 10.3354/meps301247

Leis, J. M., and Carson-Ewart, B. M. (1999). *In situ* swimming and settlement behaviour of larvae of an indo-pacific coral-reef fish, the coral trout plectropomus leopardus (Pisces: Serranidae). *Mar. Biol.* 134, 51–64. doi: 10.1007/s002270050524

Leis, J. M., and Carson-Ewart, B. M. (2003). Orientation of pelagic larvae of coral-reef fishes in the ocean. *Mar. Ecol. Prog. Ser.* 252, 239–253. doi: 10.3354/meps252239

Leis, J. M., Carson-Ewart, B. M., Hay, A. C., and Cato, D. H. (2003). Coral-reef sounds enable nocturnal navigation by some reef-fish larvae in some places and at some times. *J. Fish Biol.* 63, 724–737. doi: 10.1046/j.1095-8649.2003.00182.x

Leis, J. M., and Fisher, R. (2006). "Swimming speed of settlement-stage reef-fish larvae measured in the laboratory and in the field: a comparison of critical speed and in situ speed," in *Proceedings of the 10th International Coral Reef Symposium* (Okinawa).

Leis, J. M., Wright, K. J., and Johnson, R. N. (2007). Behaviour that influences dispersal and connectivity in the small, young larvae of a reef fish. *Mar. Biol.* 153, 103–117. doi: 10.1007/s00227-007-0794-x

Lester, S., Halpern, B., Grorud-Colvert, K., Lubchenco, J., Ruttenberg, B., Gaines, S., et al. (2009). Biological effects within no-take marine reserves: a global synthesis. *Mar. Ecol. Prog. Ser.* 384, 33–46. doi: 10.3354/meps08029

Lett, C., Ayata, S., Huret, M., and Irisson, J. (2010). Biophysical modelling to investigate the effects of climate change on marine population dispersal and connectivity. *Prog. Oceanogr.* 87, 106–113. doi: 10.1016/j.pocean.2010.09.005

Longenecker, K., Langston, R., and Barrett, B. (2008). *A Compendium of Live History Information for some Exploited Hawaiian Reef Fishes*. Bishop Museum Technical Report (No. 44). Fisheries Local Action Strategy, Honolulu, HI.

Mangubhai, S. (2008). "Spawning patterns of Acropora species in the Mombasa lagoon in Kenya," in *Ten Years after Bleaching - Facing the Consequences of Climate Change in the Indian Ocean, CORDIO Status Report 2008*, eds D. O. Obura, J. Tamelander, and O. Linden (Mombasa: Coastal Ocean Research and Development in the Indian Ocean/Sida-SAREC), 213–221.

Mangubhai, S., and Harrison, P. (2008). Asynchronous coral spawning patterns on equatorial reefs in Kenya. *Mar. Ecol. Prog. Ser.* 360, 85–96. doi: 10.3354/meps07385

Mayorga-Adame, C. G. (2015). *Modeled Larval Connectivity Patterns in Two Coral Reef Regions : The Western Caribbean and the Kenyan-Tanzanian Shelf*. PhD thesis, Oregon State University, Corvallis, OR. Available online at: http://ir.library.oregonstate.edu/xmlui/handle/1957/57502

Mayorga-Adame, C. G., Strub, P. T., Batchelder, H. P., and Spitz, Y. H. (2016). Characterizing the circulation off the kenyan-tanzanian coast using an ocean model. *J. Geophys. Res. Oceans* 121, 1377–1399. doi: 10.1002/2015jc010860

McClanahan, T. R. (1994). Kenyan coral reef lagoon fish: effects of fishing, substrate complexity, and sea urchins. *Coral Reefs* 13, 231–241. doi: 10.1007/BF00303637

McClanahan, T. R., and Mangi, S. (2000). Spillover of exploitable fishes from a marine park and its effect on the adjacent fishery. *Ecol. Appl.* 10, 1792–1805. doi: 10.1890/1051-0761(2000)010[1792:SOEFFA]2.0.CO;2

McClanahan, T. R., Nugues, M., and Mwachireya, S. (1994). Fish and sea urchin herbivory and competition in kenyan coral reef lagoons: the role of reef management. *J. Exp. Mar. Biol. Ecol.* 184, 237–254. doi: 10.1016/0022-0981(94)90007-8

McCook, L. J., Almany, G. R., Berumen, M. L., Day, J. C., Green, A. L., Jones, G. P., et al. (2009). Management under uncertainty: guide-lines for incorporating connectivity into the protection of coral reefs. *Coral Reefs* 28, 353–366. doi: 10.1007/s00338-008-0463-7

McCormick, M. I. (1999). Delayed metamorphosis of a tropical reef fish (Acanthurus Triostegus): a field experiment. *Mar. Ecol. Prog. Ser.* 176, 25–38. doi: 10.3354/meps176025

McLeod, E., Salm, R., Green, A., and Almany, J. (2009). Designing marine protected area networks to address the impacts of climate change. *Front. Ecol. Environ.* 7, 362–370. doi: 10.1890/070211

Melbourne-Thomas, J., Johnson, C. R., Aliño, P. M., Geronimo, R. C., Villanoy, C. L., and Gurney, G. G. (2011). A multi-scale biophysical model to inform regional management of coral reefs in the western Philippines and South China Sea. *Environ. Modell. Softw.* 26, 66–82. doi: 10.1016/j.envsoft.2010.03.033

Micheli, F., Saenz-Arroyo, A., Greenley, A., Vazquez, L., Espinoza Montes, J. A., Rossetto, M., et al. (2012). Evidence that marine reserves enhance resilience to climatic impacts. *PLoS ONE* 7:e40832. doi: 10.1371/journal.pone.0040832

Mora, C., and Sale, P. F. (2002). Are populations of coral reef fish open or closed? *Trends Ecol. Evol.* 17, 422–428. doi: 10.1016/S0169-5347(02)02584-3

Munday, P. L., Leis, J. M., Lough, J. M., Paris, C. B., Kingsford, M. J., Berumen, M. L., et al. (2009). Climate change and coral reef connectivity. *Coral Reefs* 28, 379–395. doi: 10.1007/s00338-008-0461-9

Muthiga, N., Costa, A., Motta, H., Muhando, C., Mwaipopo, R., and Schleyer, M. (2008). "Status of coral reefs in East Africa: Kenya, Tanzania, Mozambique and South Africa," in *Status of Coral Reefs of the World: 2008*, ed C. Wilkinson (Townsville, AU: Global Coral Reef Monitoring Network and Reef and Rainforest Research Centre), 91–104.

Muths, D., Gouws, G., Mwale, M., Tessier, E., and Bourjea, J. (2012). Genetic connectivity of the reef fish lutjanus kasmira at the scale of the Western Indian Ocean. *Can. J. Fish. Aquat. Sci.* 69, 842–853. doi: 10.1139/f2012-012

Nishikawa, A., Masaya, K., and Sakai, K. (2003). Larval settlement rates and gene flow of broadcast-spawning (*Acropora Tenuis*) and Planula-Brooding (*Stylophora Pistillata*) corals. *Mar. Ecol. Prog. Ser.* 256, 87–97. doi: 10.3354/meps256087

Nozawa, Y., and Harrison, P. L. (2008). Temporal patterns of larval settlement and survivorship of two broadcast-spawning acroporid corals. *Mar. Biol.* 155, 347–351. doi: 10.1007/s00227-008-1034-8

O'Connor, M. I., Bruno, J. F., Gaines, S. D., Halpern, B. S., Lester, S. E., Kinlan, B. P., et al. (2007). Temperature control of larval dispersal and the implications for marine ecology, evolution, and conservation. *Proc. Natl. Acad. Sci. U.S.A.* 104, 1266–1271. doi: 10.1073/pnas.0603422104

Oxenford, H. A., Fanning, P., and Cowen, R. K. (2008). "Spatial distribution of surgeonfish (*Acanthuridae*) pelagic larvae in the eastern caribbean," in *Proceedings of a Special Symposium, 9–11 November 2006, 59th Annual Meeting of the Gulf and Caribbean Fisheries Institute*, *Caribbean Connectivity: Implications Fo R Marine Protected Area Management*, *Vol. 195,* eds Rikki Grober-Dunsmore and D. Brian Keller (Belize City, Belize; Silver Spring, MD: Marine Sanctuaries Conservation Series ONMS-08-07. U.S. Department of Commerce, National Oceanic and Atmospheric Administration, Office of National Marine Sanctuaries), 42–51.

Pandolfi, J. M., Bradbury, R. H., Sala, E., Hughes, T. P., Bjorndal, K. A., Cooke, R. G., et al. (2003). Global trajectories of the long-term decline of coral reef ecosystems. *Science* 301, 955–958. doi: 10.1126/science.1085706

Paris, C. B., Atema, J., Irisson, J. O., Kingsford, M., Gerlach, G., and Guigand, C. M. (2013). Reef odor: a wake up call for navigation in reef fish larvae. *PLoS ONE* 8:e72808. doi: 10.1371/journal.pone.0072808

Paris, C. B., Chérubin, L., and Cowen, R. K. (2007). Surfing, spinning, or diving from reef to reef: effects on population connectivity. *Mar. Ecol. Prog. Ser.* 347, 285–300. doi: 10.3354/meps06985

Paris, C. B., and Cowen, R. K. (2004). Direct evidence of a biophysical retention mechanism for coral reef fish larvae. *Limnol. Oceanogr.* 49, 1964–1979. doi: 10.4319/lo.2004.49.6.1964

Pineda, J., Porri, F., Starczak, V., and Blythe, J. (2010). Causes of decoupling between larval supply and settlement and consequences for understanding recruitment and population connectivity. *J. Exp. Mar. Biol. Ecol.* 392, 9–21. doi: 10.1016/j.jembe.2010.04.008

Randall, J. E. (1961). A contribution to the biology of the convict surgeonfish of the hawaiian islands, Acanthurus triostegus sandvicensis. *Pac. Sci.* 15, 215–272.

Roberts, C. M., Hawkins, J. P., and Gell, F. R. (2005). The role of marine reserves in achieving sustainable fisheries. *Philos. Trans. R. Soc. Lond. B Biol. Sci.* 360, 123–132. doi: 10.1098/rstb.2004.1578

Rocha, L. A., Bass, A. L., Robertson, D. R., and Bowen, B. W. (2002). Adult habitat preferences, larval dispersal, and the comparative phylogeography of

three Atlantic surgeonfishes (Teleostei: Acanthuridae). *Mol. Ecol.* 11, 243–251. doi: 10.1046/j.0962-1083.2001.01431.x

Rossi, V., Ser-Giacomi, E., López, C., and Hernández-García, E. (2014). Hydrodynamic provinces and oceanic connectivity from a transport network help designing marine reserves. *Geophys. Res. Lett.* 41, 2883–2891. doi: 10.1002/2014GL059540

Saenz-Agudelo, P., Jones, G. P., Thorrold, S. R., and Planes, S. (2011). Connectivity dominates larval replenishment in a coastal reef fish metapopulation. *Proc. R. Soc. Lond. B Biol. Sci.* 278, 2954–2961. doi: 10.1098/rspb.2010.2780

Sale, P. F. (2006). *Coral Reef Fishes: Dynamics and Diversity in a Complex Ecosystem*. San Diego, CA: Gulf Professional Publishing.

Sale, P. F., Cowen, R. K., Danilowicz, B. S., Jones, G. P., Kritzer, J. P., Lindeman, K. C., et al. (2005). Critical science gaps impede use of no-take fishery reserves. *Trends Ecol. Evol.* 20, 74–80. doi: 10.1016/j.tree.2004.11.007

Schultz, E. T., and Cowen, R. K. (1994). Recruitment of coral reef fishes to bermuda: local retention or long-distance transport? *Mar. Ecol. Prog. Ser.* 109, 15–28.

Shanks, A. L. (2009). Pelagic larval duration and dispersal distance revisited. *Biol. Bull.* 216, 373–385. doi: 10.1086/BBLv216n3p373

Simpson, S. D., Meekan, M., Montgomery, J., McCauley, R., and Jeffs, A. (2005). Homeward sound. *Science* 308, 221–221. doi: 10.1126/science.1107406

Soria, G., MunguaVega, A., Marinone, S. G., MorenoBez, M., MartnezTovar, I., and CudneyBueno, R. (2012). Linking bio-oceanography and population genetics to assess larval connectivity. *Mar. Ecol. Prog. Ser.* 463, 159–175. doi: 10.3354/meps09866

Souter, P., Henriksson, O., Olsson, N., and Grahn, M. (2009). Patterns of genetic structuring in the coral pocillopora damicornis on reefs in East Africa. *BMC Ecol.* 9:19. doi: 10.1186/1472-6785-9-19

Spalding, M., Ravilious, C., and Green, E. P. (2001). *World Atlas of Coral Reefs*. Bekeley, CA: University of California Press.

Sponaugle, S., Cowen, R. K., Shanks, A., Morgan, S. G., Leis, J. M., Pineda, J., et al. (2002). Predicting self-recruitment in marine populations: biophysical correlates and mechanisms. *Bull. Mar. Sci.* 70(Suppl. 1), 341–375.

Sponaugle, S., Paris, C., Walter, K., Kourafalou, V., and D'Alessandro, E. (2012). Observed and modeled larval settlement of a reef fish to the florida keys. *Mar. Ecol. Prog. Ser.* 453, 201–212. doi: 10.3354/meps09641

Staaterman, E., Paris, C. B., and Helgers, J. (2012). Orientation behavior in fish larvae: a missing piece to Hjort's critical period hypothesis. *J. Theor. Biol.* 304, 188–196. doi: 10.1016/j.jtbi.2012.03.016

Stobutzki, I. C., and Bellwood, D. R. (1997). Sustained swimming abilities of the late pelagic stages of coral reef fishes. *Oceanogr. Lit. Rev.* 9:986. doi: 10.3354/meps149035

Thorrold, S. R., Jones, C. M., Campana, S. E., McLaren, J. W., and Lam, J. W. H. (1998). Trace element signatures in otoliths record natal river of juvenile American Shad (*Alosa Sapidissima*). *Limnol. Oceanogr.* 43, 1826–1835. doi: 10.4319/lo.1998.43.8.1826

Thorrold, S. R., Zacherl, D., and Levin, L. (2007). Population connectivity and larval dispersal using geochemical signatures in calcified structures. *Oceanography* 20, 80–89. doi: 10.5670/oceanog.2007.31

Tolimieri, N., Jeffs, A., and Montgomery, J. (2000). Ambient sound as a cue for navigation by the pelagic larvae of reef fishes. *Mar. Ecol. Prog. Ser.* 207, 219–224. doi: 10.3354/meps207219

van der Ven, R. M., Triest, L., De Ryck, D. J. R., Mwaura, J. M., Mohammed, M. S., and Kochzius, M. (2016). Population genetic structure of the stony coral *Acropora Tenuis* shows high but variable connectivity in East Africa. *J. Biogeogr.* 43, 510–519. doi: 10.1111/jbi.12643

Vermeij, M. J., Marhaver, K. L., Huijbers, C. M., Nagelkerken, I., and Simpson, S. D. (2010). Coral larvae move toward reef sounds. *PLoS ONE* 5:e10660. doi: 10.1371/journal.pone.0010660

Visram, S., Yang, M.-C, Pillay, R. M., Said, S., Henriksson, O., Grahn, M., et al. (2010). Genetic connectivity and historical demography of the blue barred parrotfish (*Scarus ghobban*) in the Western Indian Ocean. *Mar. Biol.* 157, 1475–1487. doi: 10.1007/s00227-010-1422-8

Watson, J. R., Mitarai, S., Siegel, D. A., Caselle, E., Dong, C., and McWilliams, J. C. (2010). Realized and Potential Larval Connectivity in the Southern California Bight. *Mar. Ecol. Prog. Ser.* 401, 31–48. doi: 10.3354/meps08376

Werner, F., Cowen, R. K., and Paris, C. (2007). Coupled biological and physical models: present capabilities and necessary developments for future studies of population connectivity. *Oceanography* 20, 54–69. doi: 10.5670/oceanog.2007.29

Werner, F. E., Quinlan, J. A., Lough, R. G., and Lynch, D. R. (2001). Spatially-explicit individual based modeling of marine populations: a review of the advances in the 1990s. *Sarsia* 86, 411–421. doi: 10.1080/00364827.2001.10420483

Willis, T. J., Millar, R. B., Babcock, R. C., and Tolimieri, N. (2003). Burdens of evidence and the benefits of marine reserves: putting descartes before des horse? *Environ. Conserv.* 97–103. doi: 10.1017/S0376892903000092

Wolanski, E., Doherty, P., and Carleton, J. (1997). Directional swimming of fish larvae determines connectivity of fish populations on the great barrier reef. *Naturwissenschaften* 84, 262–268. doi: 10.1007/s001140050394

Wolanski, E., and Kingsford, M. J. (2014). Oceanographic and behavioural assumptions in models of the fate of coral and coral reef fish larvae. *J. R. Soc. Interface* 11:20140209. doi: 10.1098/rsif.2014.0209

Yahya, S. A. S., Christopher, M., and Martin, G. (2011). *Fish and Sea Urchin Community Patterns and Habitat Effects on Tanzanian Coral Reefs*. Available online at: http://www.diva-portal.org/smash/record.jsf;jsessionid=nipyf9_yNdz7jOSnL4fD0CFn7-kTc3Qeqsy5MQ7I.diva2-search7-vm?pid=diva2%3A440148&dswid=-8234

**Conflict of Interest Statement:** The authors declare that the research was conducted in the absence of any commercial or financial relationships that could be construed as a potential conflict of interest.

# Advantages of publishing in Frontiers

**OPEN ACCESS**
Articles are free to read, for greatest visibility

**COLLABORATIVE PEER-REVIEW**
Designed to be rigorous – yet also collaborative, fair and constructive

**FAST PUBLICATION**
Average 85 days from submission to publication (across all journals)

**COPYRIGHT TO AUTHORS**
No limit to article distribution and re-use

**TRANSPARENT**
Editors and reviewers acknowledged by name on published articles

**SUPPORT**
By our Swiss-based editorial team

**IMPACT METRICS**
Advanced metrics track your article's impact

**GLOBAL SPREAD**
5'100'000+ monthly article views and downloads

**LOOP RESEARCH NETWORK**
Our network increases readership for your article

**Frontiers**
EPFL Innovation Park, Building I • 1015 Lausanne • Switzerland
Tel +41 21 510 17 00 • Fax +41 21 510 17 01 • info@frontiersin.org
**www.frontiersin.org**

**Find us on**